Heteroligomeric interactions of the Kv1.3 channelosome

Sara Raquel Roig Merino

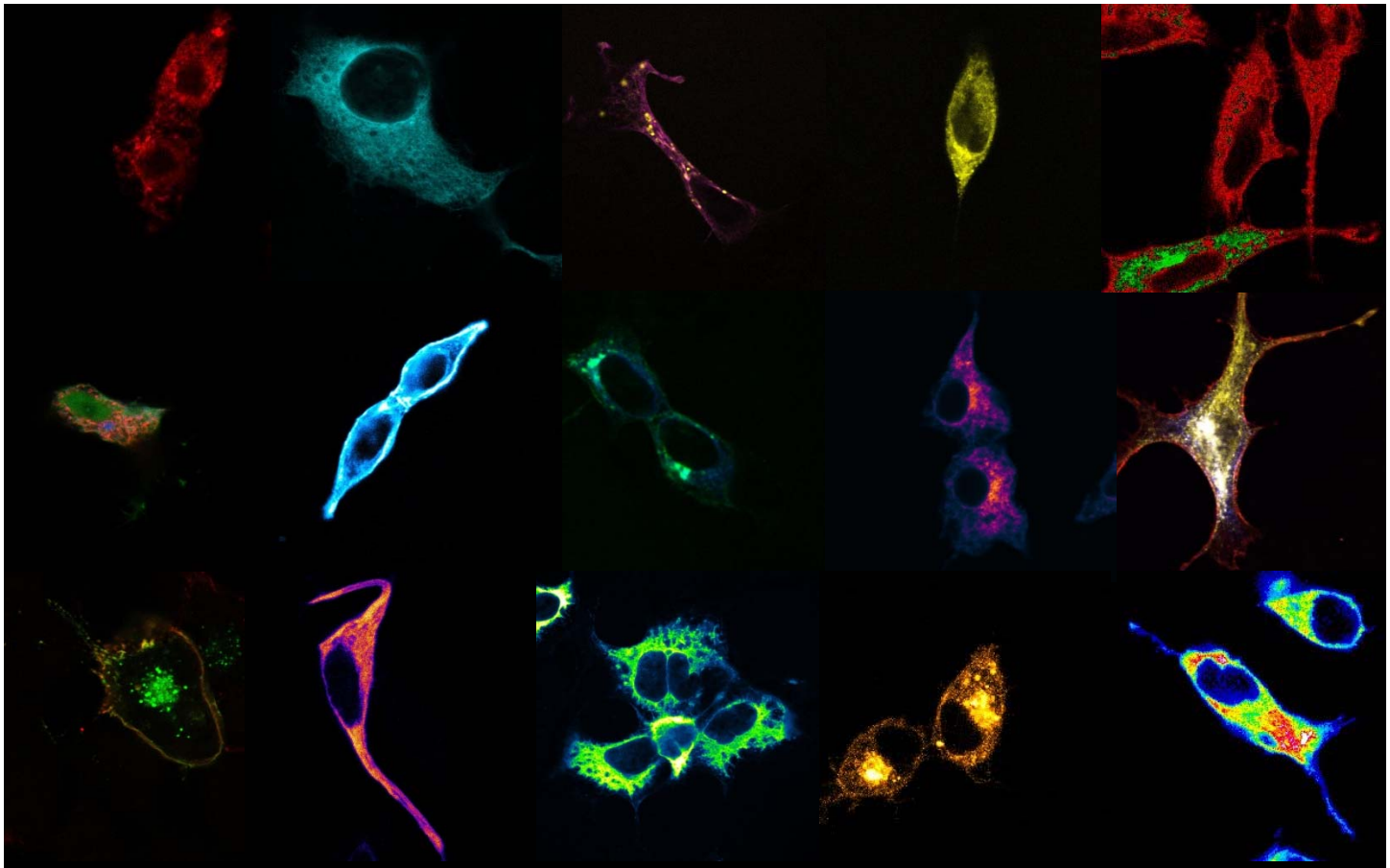

HETEROLIGOMERIC INTERACTIONS OF THE Kv1.3 CHANNELOSOME

Sara Raquel Roig Merino

Barcelona, 2017

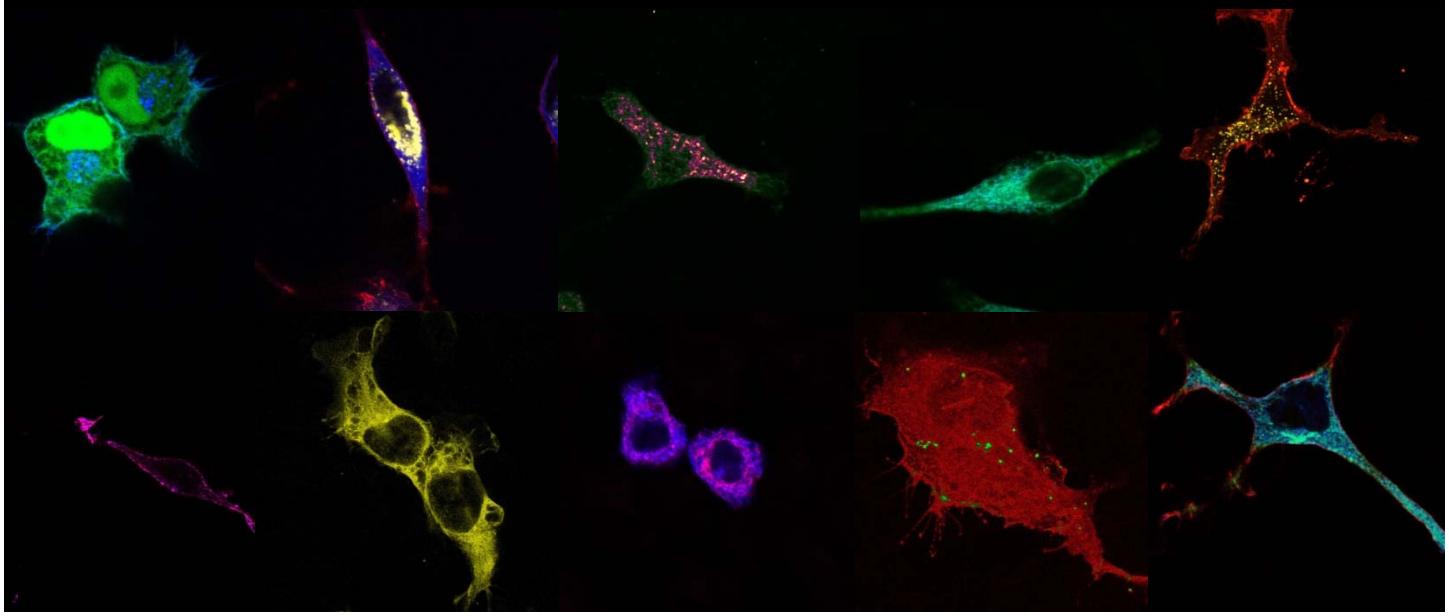

UNIVERSITAT DE BARCELONA

Heteroligomeric Interactions Of The Kv1.3 Channelosome

Sara Raquel Roig Merino

This PhD Thesis has been performed by **Sara Raquel Roig Merino** under the direction of Dr. **Antonio Felipe Campo** in the Molecular Physiology laboratory at the Department of Biochemistry and Molecular Biomedicine, Institute of Biomedicince (IBUB), Faculty of Biology, University of Barcelona, to opt to the Doctor degree in Biomedicine by the Univeristy of Barcelona.

Antonio Felipe Campo

PhD thesis director

Sara Raquel Roig Merino

PhD candidate

PhD Thesis
University of Barcelona, Faculty of Biology
Department of Biochemistry and Molecular Biomedicine
Doctoral programme in Biomedicine
Barcelona, 2017

A mi familia.

Pasada, presente y futura.

AKNOWLEDGEMENTS

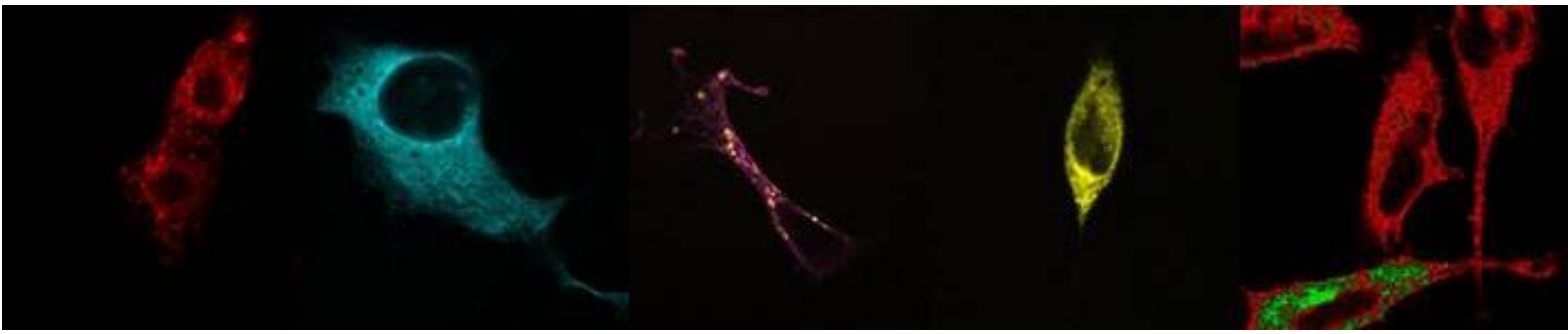

Por eso los mayores tienen menos miedo. Ellos hacen memoria de su juventud y lo recuerdan todo, el frío, los mutilados que pedían limosna por la calle, los silencios […]. Cuando se caía un trozo de pan al suelo, los adultos obligaban a los niños a recogerlo y darle un beso antes de devolverlo a la panera, tanta hambre habían pasado sus familias en aquellos años en los que murieron todas esas personas queridas cuyas historias nadie quiso contarles.

Porque hasta hace treinta años, los hijos heredaban la pobreza pero también la dignidad de sus padres, una manera de ser pobres sin sentirse humillados, sin dejar de ser dignos ni de luchar por un futuro. Vivían en un país donde la pobreza no era un motivo para avergonzarse y mucho menos para darse por vencido.

[Los besos en el pan – Almudena Grandes]

Por fin! Aquí estamos! Te lo has imaginado en mil ocasiones, te has leído tantas veces los agradecimientos de los MPs pasados que algunos pasajes te los sabes hasta de memoria. Tan esperado…! Y ahora la sensación de no estar a la altura es escandalosa. Estoy segura que no sabré decir todo lo que querría. Pero estoy también convencida que son éstas, y no otras, las palabras más importantes de la tesis para mí. Además, *es de bien nacido el ser agradecido* que dice mi madre. Así que, me siento en el laboratorio, sola, y pongo de fondo la voz de *Carlos Goñi* en *Básico 3* para que sea el momento perfecto.

Hará un par de meses entré en el despacho de **Antonio Felipe**, no recuerdo muy bien porqué, y acabamos hablando de la vida. Los derroteros de la conversación llevaron a que él dijera: es que tú, Sara, has sido muy feliz aquí. Y no podía ser más acertada la frase. Así que el primer gracias es para ti. Por llamarme un 11 de Julio de hará casi 10 años, por dejarme vivir la aventura que es la tesis en MP, por lo que proyectas de nosotros al mundo, por el aliento en momentos bajos y también en los más altos. Por todo ello, muchas gracias.

Y es que **MP** es mucho MP. A todos y cada uno de vosotros muchísimas gracias; al MP más antiguo y al más nuevo. A **Núria**, por tus clases de patch, tu humor y tu capacidad de saber estar en cualquier lugar. A la indispensable **Laurífor**. Creíamos que no sobreviviríamos cuando te fuiste! De ti aprendí todo lo que sé sobre un laboratorio: las deducciones críticas de los experimentos, la importancia del trabajo en equipo o la manía de nunca nunca cambiar un protocolo que funciona. Y me acabé llevando una amiga (sí, sí, aunque me vistieras de hawaiana en tu boda). A **Caveia**. Quién me hubiera dicho que iba a tener la inmensa suerte de encontrar a alguien que le gustara tanto discutir como a mí! Contigo he crecido, reflexionado, defendido, emocionado, y vuelto a discutir. Poníamos cualquier verdad en entredicho y elaborábamos argumentos mientras hablábamos. No sabes cómo te estoy echando de menos. A **Nana**. Por compartir conmigo las dudas de tus resultados, nuestras discusiones de ciencia han sido increíbles. Pero más aún todo lo que hemos compartido al margen de ella. Porqué la mayoría no las puedo escribir? Por cada confesión compartida, por cada broma recurrente. Por ser mi *marmoteta* y mi *cargol*. Por el: "per a tu Sara son 20 euros" con el que aún me río. En la principal, en las fiestas de gracia o las de sants, por las ladies night… somos invencibles. A **Berth**. Hace tiempo que sabemos que no hay uña sin carne ni carne sin uña. A mi inseparable pack de 2006 por seguir y dejar que siga la coña tonta del día. Por la música de los viernes, los jueves o el día que apetecía. Y sabemos que la calidad de la misma está sobrevalorada! Por la risa, el canto y el baile. Por el equilibrio entre ciencia y arte, A **Kash.** Your hugs and your smile come always when

needed without asking. For teaching me how to deal with staring people, for your minimal drinks and dances, for every coffee as my desperation partner. A **Antonio Jr.** Sabes que no puedo con tu cara post-broma, me encanta! Por cada risa y cada aclaración del mundo *freak* que tanto se me escapa. Aprovecho para confesar que yo también jugué al Pokemon. Sí! Sí! Pero si lo dices lo negaré! A **Jesusa** y a **Clara.** Por las conversaciones de la tele-basura pertinente, el checkeo de la compatibilidad de signos del zodíaco o la nueva colección de Rosa Clará. Porque así la ciencia siempre es más llevadera. A **Dani** y a **Irene.** Cuando entrasteis se nos cruzó una mirada cómplice con Albert: nuestro relevo! Y no podríamos haber estado más equivocados. Sois una versión mejorada! Mil gracias Dani porque no podría haber imaginado un mejor chaperón. Como dije una vez, enseñarte y verte desarrollarte como investigador en el laboratorio ha sido uno de los cometidos que más he disfrutado de estos años. Ahora solo queda que lo puedas hacer en la poyata E4! E Irene, acabo la tesis tranquila porque sé que el rosa y los tacones ya cuentan con sucesora, algo más diminutilla pero es que "en el pot petit hi ha la bona confitura". A **Sergi** y **Maria,** y a todos los MPs más recientes, desearos que estos años sean como han sido para mí. Que los disfrutéis y los exprimáis. Y que Antonio pueda deciros al acabar la misma frase que a mí. Ei! Y a **Vero.** Eres genuina. Eres una tía increíble. Lo único que me da rabia es que estés tan lejos. Pero dejemos que la vida teja sus planes!

A toda la gente del departamento que, con sus conversaciones, convierten los días en más llevaderos. A **Albert Viel** i **Xico Simoes.** El último día que compartí con ellos la sala de cultivo andaban cantando canciones en portugués! A **Enrica**, **Joana**, **Tonidillo**, **Raquel**, **Vanesa** y **David**. A **Anna Orozco** por el sentimiento que pones en todo lo que haces, eres un huracán! Aunque haya sido poco tiempo, estoy encantada de haberte conocido. A **Josep María** por contar conmigo para cada proyecto que le caía en las manos. Al *sempervirens* **Pere** que fue al final más MPL que nada. Por formar parte de cada plan a extraescolar de MP. Los vermuts o barbacoas en su terraza, las guitarras y ukeleles en el césped, las fiestas de gracia entre semana, las de sants para despedir a Anna, los cumpleaños de Albert, los míos o por participar en el corre-casas. Si es que… somos grandes! Qué de planazos estos años! Me llevo una familia conmigo. Muchas gracias!

A lo largo de este tiempo he tenido la inmensa suerte de poder ver y hacer ciencia en otros sitios distintos. En Elche, gracias al Dr. **González-Ros** por aceptar mi visita. A **Marcela** por enseñarme todo lo que sabe de geles blue-native, a **Miguel Ángel Poveda** por su ayuda. A las chicas por su apoyo y a **Robert** por ser un ánimo en las horas tardías. También tuve la suerte de desplazarme tres meses a Hannover. Gracias al Dr. **Ponimaskin** por aceptar la visita y al Dr. **Zeug** por la paciencia de enseñarme la técnica del lux-FRET. A **Tatiana** por ser una compañera de laboratorio amable y dulce, y a **Luisa** por ser mi *soul mate* en la experiencia. Con ella construimos el grupo que fuera del laboratorio fue nuestro apoyo. A **Pablo**, mi alicantino favorito, gracias porque tu humor mordaz siempre ha podido conmigo. A **Matthias**, por su enorme sonrisa mañanera y a **Laura** por su inquieta curiosidad. Vosotros fuisteis mis ganas y mis ánimos en aquel período. Danke schön!

Pero no todo el apoyo proviene del mundo de la ciencia. Ni hablar! La mayor parte me la he encontrado fuera. Y es que lo que más hace que una tesis avance es el apoyo incondicional de tu gente. Entonces no hay IP que se resista ni plasma membrane loan que no se quede bien pegadita al cristal.

Un gracias enorme a los compañeros del master de educación. En un año que fue más difícil de lo que me gustaría reconocer, ellos fueron motores de salida adelante. A **Esther**, la que no necesita que le diga el porqué. Seguro que lo sabe mejor ella! Sabes que sin ti, no lo hubiera sacado igual. Vas a ser una súper teacher. A **Anna Febrero**, mi tutora. Gracias a ti me di cuenta que no soy la única *iluminada* de este planeta. A **David** por su bondad y a **Andreu** por sus conversaciones de política. Y como no, a **Gloria** y a **Clara**, por los autoanálisis de conducta, las charlas de feminismo y las cervezas discutiendo sobre un mundo sin diferencias sociales. A los compañeros de salsa, que sí o sí siempre te sacan una sonrisa. Que nunca perdamos la alegría del baile.

Querría agradecer también a **Nyon** y **Natalia**. La vida nos ha ido llevando por caminos muy distintos y ahora incluso hasta el otro lado del planeta! Aun así, Nyon, gracias por ese ejemplo de valentía al cruzar el mundo siguiendo un sueño. Y mil gracias también a mi Nati. Siempre te lo he dicho: eres mi pierna, y sin ti no puedo avanzar. Si los días que nos sentábamos en la Gioconda, o en el Dinno con 16, 19 o 22 años, nos hubieran dicho todo lo que íbamos a pasar no nos lo creeríamos. Y sin embargo aquí estamos! Y juntas! Gracias por estar siempre.

Y como no, mis **Ángeles**: **Carla** y **Jenny**. Os llevo muy dentro del corazón. A mi **Carla** por sus verdades sin complejos, su humor rápido y su alegría de tenernos cerca. Ella es la supuesta chica de hielo que nunca lo fue. A mi **Jenny** por su ternura, su carácter, su alegría y achuchones mañaneros, sus locuras por audio. Ella es el ángel más tierno pero con su lado fuerte. Éste año hace diez que nos conocimos! Trío de viejillas que somos ya… Que nunca se acaben nuestros planes. Que se multipliquen por diez los años juntas! Gracias porque me apoyasteis desde el minuto 1 después de la llamada de Antonio. Gracias por decirme con sinceridad lo que hecho bien y lo que hecho mal. Gracias por acudir a una llamada de socorro. Gracias por todo. Cada rato con vosotras ha sido una bocanada de ánimo para seguir. Por Malta, Londres, Milán, Amsterdam, Florencia y Salou. Por nuestros pinchos, pizzas, kebabs y baile. Mil gracias por cuidar de mí!

Quisiera dar las gracias a **Pepi**, **Antonio**, **Laura**, **Juanjo** y el pequeño **Eric**. Uno a veces no se da cuenta de las acciones sobre los demás, pero cada vez que hemos hablado de la tesis y del trabajo, me habéis dado fuerzas y energías para tirar adelante. Muchísimas gracias! Y gracias también al pequeño Eric, que con sólo mirarle se le quitan a uno todos los males. Gracias por hacerme sentir tan a gusto.

A mis abuelos. A la yaya **Elisa** por su ejemplo. El hecho de nunca conocerla generó que absorbiera cada palabra sobre ella y cada imagen a mi disposición. Poco a poco se fue volviendo una figura de ternura, cariño y desparpajo; y con ello un referente para mí. Gracias a ella y al yayo **José** por cuidar de mi hermana en un momento *vital*. Al yayo **Ángel** por la dedicación a sus nietos. Él será siempre mi referente del valor de lo que es justo. Del valor del esfuerzo y del orgullo por la familia. A la yaya **Puri**, porque de su relación con mamá he aprendido la importancia de ser comedido y del perdón. A todos vosotros, mil gracias.

Todos los que me conocéis bien sabéis que no soy nadie sin mi familia más cercana. Siempre he pensado en ella como en un faro. Siempre presente, constante, recordándote donde están e iluminándote el camino. Y es que soy una persona muy afortunada porque tengo la mejor familia del mundo. Sí, así, tal cual. La verdad sin alardeo.

Quiero darle las gracias a mi hermana **Elisa**. En su eterna humildad, posiblemente crea haberme ayudado poco. Pero es en ella donde yo hallo la razón y la obviedad más claras. A ella las verdades que yo no veo. La evidente importancia de que la felicidad está el camino y no en el destino. La bondad sin límites. El orgullo por ausencia. La belleza de las cosas sencillas. A ti, portadora de un nombre con tanto significado para nosotros, gracias. A ti también **Marcel**, gracias por dejarme ver como miras a Elisa. Gracias por tu serenidad y tu sentido del humor.

Quiero darles las gracias a mis padres: **José** y **Puri**. Su fe en mis capacidades y la conciencia clara de mis virtudes y mis defectos han conseguido que llegue hasta donde estoy. La mayor parte de esta tesis es gracias a vuestra presencia. Pero de lo que más agradecida me siento es de haber crecido con todo aquello que emanaba de vosotros. De mi padre su firmeza, su constancia, su capacidad de trabajo y su curiosidad por el mundo. De mi madre su velocidad de pensamiento, su memoria y su ironía, su incansable empatía y la capacidad de disfrutar de todo aquello que la rodea y transmitirlo. A él la pregunta constante de qué podría mejorar. A ella la espontaneidad y sinceridad. A él mi inagotable análisis de conflictos (menudo eufemismo). A ella el disfrute con *David Copperfield,* la indignación con *Madame Bovary*, el sufrimiento con Mariam en *Mil Soles Espléndidos* y la desconcertante sensación de placer en *Nos vemos allá arriba*. A él el acercamiento a un mundo interior y el valor de lo que el hombre ha hecho para el hombre. A ella la emoción de entender que la *Balsa de la medusa* o la *Virgen de las rocas* son composiciones triangulares; o que es Klimt uno de mis pintores favoritos. A él sus viajes relámpagos a Barcelona tan precisos y necesarios. A ella su eterna capacidad de perdón y la imposibilidad de no seguir lo que siente. A él, que no nos escogió y nos quiere como si lo hubiera hecho. A ella por ser la más leona de las madres. A vosotros, por quereros. Porque el ejemplo que dais de lo que ello significa me ha traído hoy hasta aquí. Con todo mi corazón, gracias,

Y, deliberadamente para el final, a mi **Dani**. Eres mi alegría, mi felicidad diaria. Mi tranquilidad y serenidad. La recompensa al llegar a casa después de un día duro eres tú. No hubiera podido pensar en una vida más feliz y amable que la que tengo. Eres capaz de entender lo que aún no he dicho y cuando lo dices tú todo toma sentido. Gracias porque, ésta época, que no está siendo fácil, tú la conviertes en maravillosa. Sólo porque estamos juntos, ya merece la pena. Gracias por estar, por ser, por querer, por los planes, las risas con el humor absurdo, por seguirnos mutuamente las tonterías y por Runny. Y sobretodo, sobretodo, por el **Nosotros** del futuro. Que todo cambie para que todo siga igual. Mil gracias mi vida.

Este adiós, no maquilla un "hasta luego",
este nunca no esconde un ojalá
estas cenizas, no juegan con fuego,
este ciego, no mira para atrás.
Este notario firma lo que escribo,
esta letra no la protestaré.
Ahórrate el acuse de recibo,
estas vísperas, son las de después.
A este ruido, tan huérfano de padre
no voy a permitirle que taladre
un corazón, podrido de latir.
Este pez ya no muere por tu boca.
Este loco se va con otra loca.
Estos ojos, no lloran más por ti.

[Nos sobran los motivos – Joaquín Sabina]

TABLE OF CONTENTS

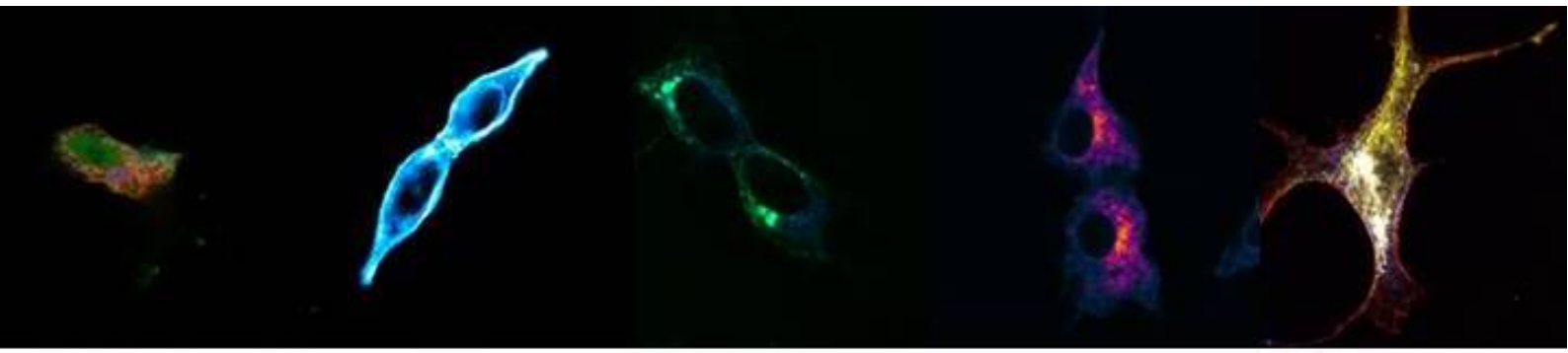

LIST OF ABBREVIATIONS **22**

1. INTRODUCTION **26**

1.1. Voltage-gated potassium channels (Kv) **26**
1.1.1. Structure 28
1.1.1.1. Selectivity 29
1.1.1.2. Voltage sensor 29
1.1.1.3. Gating machinery 30
1.1.1.4. Inactivation 30
1.1.2. Cell biology of Kv channels 31
1.1.2.1. Biogenesis and protein folding 31
1.1.2.2. Trafficking pathways 33
1.1.3. Subcellular localization of Kv channels: membrane distribution 36
1.1.3.1. Scaffolding proteins 36
1.1.3.2. Membrane compartmentalization: lipid raft microdomains 37
1.1.3.2.1. Caveolae 38
1.1.3.2.2. Palmitoylation modification 39

1.2. Kv1.3 **40**
1.2.1. Electrophysiological properties of Kv1.3 41
1.2.2. Functions of Kv1.3 42
1.2.3. Trafficking and subcellular location of Kv1.3 43
1.2.4. Regulation of Kv1.3 activity 44

1.3. Regulatory subunits **45**
1.3.1. Kvβs 45
1.3.1.1. Aldoketoreductase activity 48
1.3.1.2. Subunits 52
1.3.1.2.1. Kvβ1 53
1.3.1.2.2. Kvβ2 58
1.3.1.2.3. Kvβ3 61
1.3.2. KCNEs 61
1.3.2.1. KCNE1 64
1.3.2.2. KCNE2 65
1.3.2.3. KCNE3 65
1.3.2.4. KCNE4 66
1.3.2.5. KCNE5 68

2. AIMS **72**

3. RESULTS **76**

3.1. Chapter 1: New insights on Kvβ physiology and Kv1.3 modulation **78**
3.1.1. Contribution 1: Kvβ1.1 and Kvβ2.1 differential membrane targeting 80
3.1.2. Contribution 2: Oligomerization, affinity and location of Kvβ subfamily 116

3.1.3. Contribution 3: Kv1.3 lipid raft location and endocytosis modulation by Kvβ subfamily 140

3.2. Chapter 2: KCNE4 regulation mechanism of Kv1.3 traffic 162

3.2.1. Contribution 4: A non-canonical di-acidic signal at the C-terminus of Kv1.3 determines anterograde trafficking and surface expression. 164

3.2.2. Contribution 5: The C-terminal domain of Kv1.3 regulates functional interactions with the KCNE4 subunit. 191

3.2.3. Contribution 6: Competence for KCNE4 C-terminus: molecular determinants of a multiprotein binding site 213

3.3. Chapter 3: Heteroligomeric formation of Kv1.3 channelosome 247

3.3.1. Contribution 1: KCNE4 effects are dominant on Kv1.3-Kvβ2.1 complexes. 249

4. SUMMARY 265

5. GENERAL DISCUSSION 271

6. CONCLUSIONS 283

7. REFERENCES 287

LIST OF ABBREVIATIONS

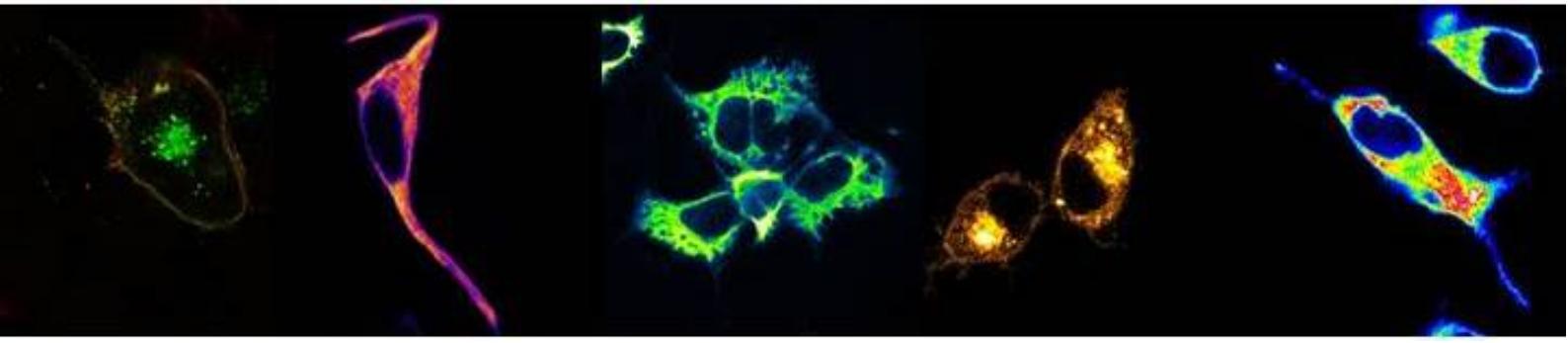

LIST OF ABBREVIATIONS

2-BP	2-Bromopalmitate
βBD	Kvβ Binding Domain
AFM	Atomic Force Microscopy
CBD	Caveolin Binding Domain
C-terminus	Carboxi Terminal End
EM	Elextron Microscopy
FBS	Fetal Bovine Serum
KCNE-S	KCNE Short Form
KCNE-L	KCNE Long Form
LPS	Lipopolysaccharide
MAGUK	Membrane-associate Guanilate Kinase
NFAT	Nuclear Factor of Activated T-cells
NK	Natural Killer Cells
N-terminus	Amino Terminal End
P	Porus
PBS	Phosphate-buffered Saline
PKA	Protein Kinase A
PKC	Protein Kinase C
PSD95	Postsynaptic Density Protein 95
SAP97	Synapse-associated Protein 97
TBS	Tris-buffered Saline
TM	Trasmembrane domain

1.INTRODUCTION

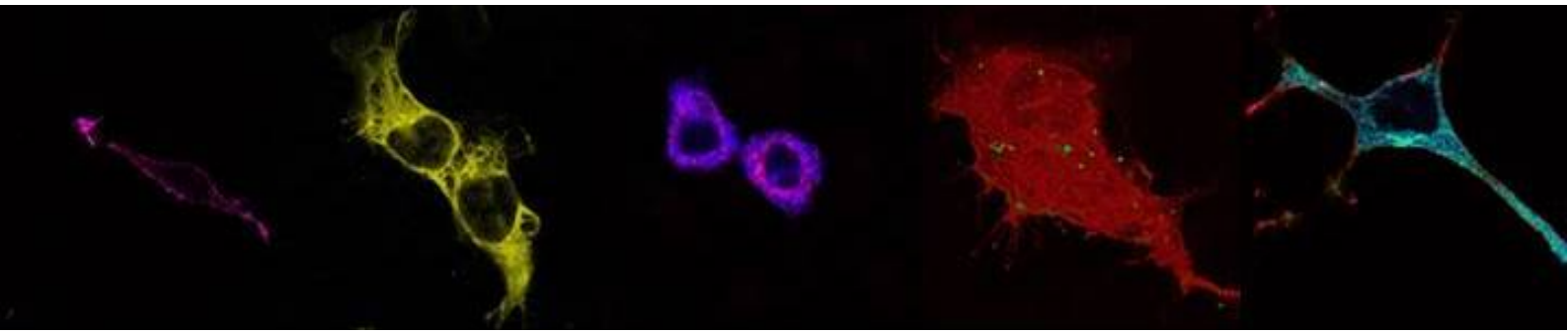

1. INTRODUCTION

1.1. *Voltage-gated potassium channels*

Ion channels are transmembrane proteins that conduct the movement of ions from one side of a membrane to the other. The resultant changes in local ion concentrations and electrical field play pivotal roles in physiological processes such as generation and propagation of the nerve impulse and the cardiac action potential. They can be classified according to the main ion conducted (Na^+, K^+, Cl^-, Ca^{2+} channels) and to their activation mechanism (voltage, ligands, mechanic stimuli, temperature, pH or second messenger activation) (Kew and Davies 2009).

Potassium-selective channels are the largest and most diverse group of ion channels, encoded by more than 70 genes in mammalians. According to their structure, potassium channels can be divided into:

- 2TM/1P: two transmembrane domains and one pore channel. They are also known as inwardly-rectifying potassium channels (K_{ir}). Those are mediating the transport of ions in order to stabilize the resting potential near the potassium equilibrium potential.
- 4TM/2P: four transmembrane domains and two pores channel (K_{2P}). It is believed that undergoes many leak currents in native cells. They tend to be opened at a range of voltage potentials and are widely regulated by neurotransmitters and other biochemical regulators.
- 6TM: six transmembrane domains. They are including the voltage-gated potassium channels (Kv) and the calcium-activated potassium channels (K_{Ca}) BK and SK.

The first cloned potassium channel was the *Drosophila* voltage-gated *shaker* channel. It was isolated due to the analysis of flies with natural mutations exhibiting a shaking phenotype. Three more related genes where cloned from this animal model: *ShaI, Shaw* and *Shab*. All of them were classified as voltage-gated potassium channels. Up to 40 human genes were cloned and were classified as members of this family thus, in turn, becoming the largest potassium channel subgroup.

Voltage-gated potassium channels were classified based on amino acid sequence alignments of the entire hydrophobic core of the proteins (figure 1). Resulting from the analysis, two different groups were determined: one comprising Kv1-9 and the second comprising Kv10-12. Within the first group there are the mammalian homologs to the previous specified *Drosophila* genes are Kv1 (Shaker), Kv2(Shab), Kv3 (Shaw) and Kv4 (ShaI). They are outward rectifiers because those channels allow current to flow out of the cell, but not in. The families Kv5, Kv6, Kv8 and Kv9 are not able to form functional homomeric channels and they are conducting when association with Kv2 and Kv3 families occurs. Kv7, also classified in this phylogenetic group and classically known as KCNQ1-5, are a further studied delayed rectifiers' family since they do not undergo fast inactivation. On the other hand, within the second group we find the Kv10 (eag1-2), Kv11 (erg1-3) and Kv12 (elk1-3). Those channels present two unique features: a specific sequence in the P loop different from the rest of the channels and a cyclic nucleotide binding sequence at the C-terminus (Gutman et al., 2005).

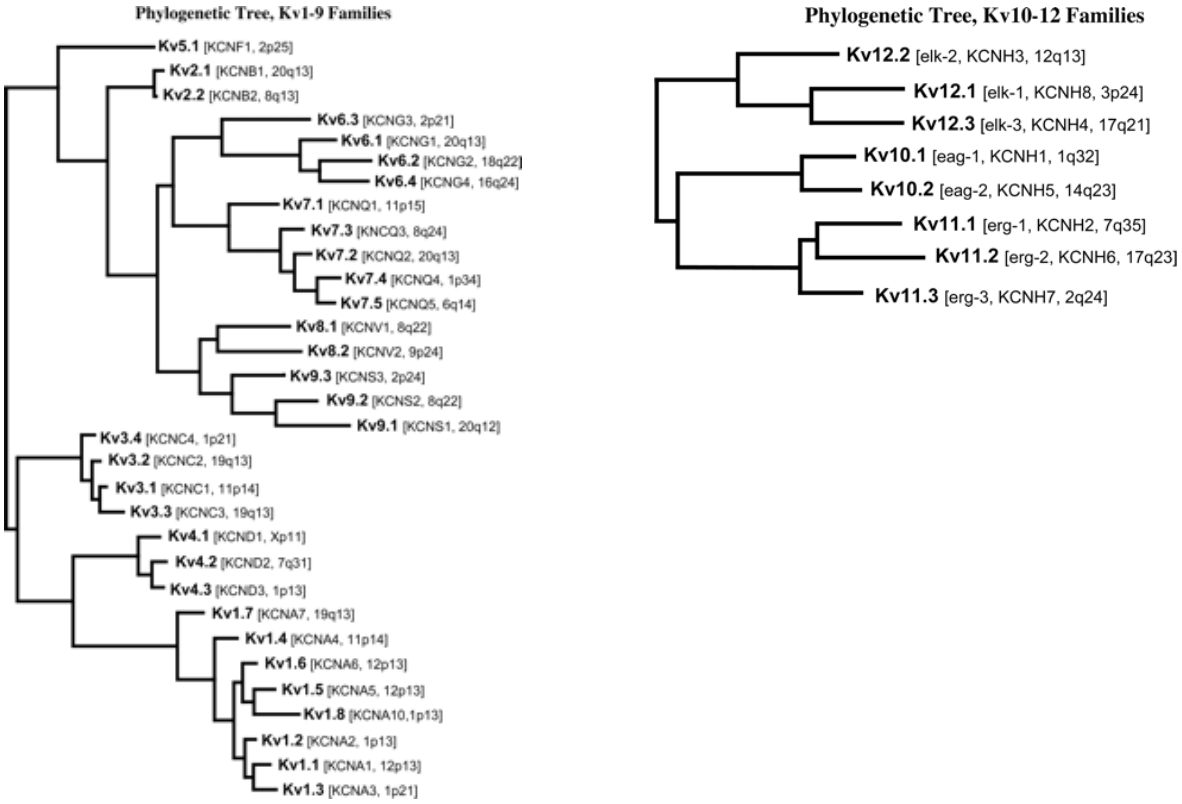

Figure 1. Phylogenetic trees of Kv1-9 and Kv10-12. Amino acid sequence alignments of the human channel Kc proteins were created using CLUSTALW, and analysis by maximum parsimony using PAUP. Only the hydrophobic cores (S1-S6) were used for analysis (Gutman et al., 2005).

The diversity detected from those molecules exceeds the gene diversity described, belonging to some different causes.

- Heteromultimerization: functional voltage-gated potassium channels are formed by four peptides encoded for one Kv gene. Thus, they can build up conducting pores as homotetramers or heterotetramers consisting in different subunits within the same family. The heterotetramers express properties different to those exhibited by homotetramers, for instance Kv1.1-Kv1.4 or Kv1.3–Kv1.5 combinations (Vicente et al., 2006, Villalonga et al., 2007).
- Modifier subunits: as mentioned before, Kv5, Kv6, Kv8 and Kv9 can not form functional homomeric channels and, by interacting with Kv2 or Kv3 families, transfer some different features to the resultant current.
- Accessory subunits: several families of regulating proteins have been determined to interact with those channels and alter the traffic and the electrophysiological properties. Called β-subunits generally, are Kvβs, KCNEs, KChIPs, KChAPs and calmodulin among others (Pongs and Schwarz, 2010).
- Alternative mRNA *splicing*: while the majority of Kv1 channel genes are intronless, various members of the Kv3, Kv4, Kv6, Kv7, Kv9, Kv10 and Kv11 gene families have coding regions made up of several exons that are alternately spliced, providing another significant source of channel diversity.

- Post-translational modification: many Kv channels can suffer modifications in their aminoacidic sequences. Those might comprise phosphorylation, ubiquitination, palmitoylation, sumoylation, nitrosylation, etc that in turn modify the channel functions or localizations.

1.1.1. *Structure*

Kv channels are formed by the tetramerization of four α or conducting subunits. Each of those subunits are formed by six transmembrane domains called S1 – S6 connected by intra or extracellular loops and with a re-entrant loop (P-loop) placed between the S5 and S6. Both N and C terminus are soluble located in the intracellular space (Hille, 2001). From the crystal structures of both bacterial and mammalian channels, a 3D composition of those channels was solved at a high resolution (figure 2A). Two clear different domains were presented: the ion conducting domain at the centre (S5-P-S6) and the voltage-sensing domain (S1-S4) located at the periphery of the channel. The pore domain of each integrating subunit is arranged with four-fold symmetry around the ion conducting pathway (figure 2B) (Doyle et al., 1998, Long et al., 2005). Within the voltage-sensing domain, at the S4 transmembrane part, there are some repeated motifs integrated by positively charged amino acid followed by two hydrophobic amino acids that has been widely accepted to act as the main voltage sensible component (Hille, 2001).

Less structural information is available about the N and C terminus, due to tis difficulty to achieve crystal structures. However, the addition of the auxiliary subunit Kvβ2 allowed this process on Kv1.2 (Long et al., 2005). It revealed the closed proximity between the amino and carboxiterminal domains. Moreover, the T1 domain of Kv1.3 has been recently solved (Kremer et al., 2013). The structure of the KcsA C-terminal domain was obtained also but accompanied with antigen-binding fragments (Fabs) for achieving the proper crystallization environment (Uysal et al., 2009).

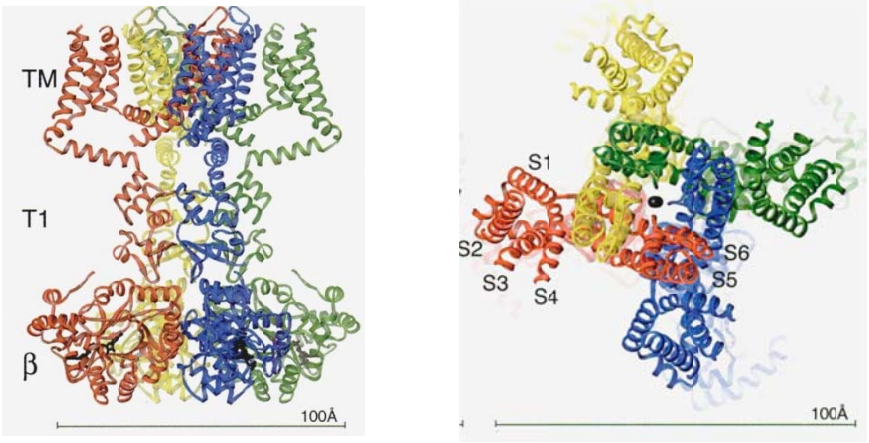

Figure 2. Crystal structure of Kv1.2 together with Kvβ2.1. A. Stereoview from the side. Each α and β subunit is coloured differently. B. Stereoview from the extracellular side. A potassium ion is depicted in black.(Long et al., 2005).

1.1.1.1. *Selectivity*

The pore domain of the α-subunit is located at S5 and S6 transmembrane segments, and a tilted pore helix (P-loop) that runs half way through the membrane. Closer to the membrane portion, the helixes S5 and S6 create a water-filled cavity in order to increase the potassium availability at the channel entrance. This is built by directing the C-terminal negative end-charge of α-helixes toward the ion pathway (MacKinnon, 2003).

Potassium selectivity occurs at the selectivity filter, located in the P-loop. It was there identified a sequence that exerts the function on selectivity: TVGYGG (figure 3, yellow at panel a). In fact, mutations in this sequence lead to a lack of K^+ ion selectivity (Heginbotham et al., 1994). This is highly conserved in potassium channels throughout the tree of life. Here, conducting K^+ ions encounter four evenly spaced layers of carbonyl oxygen atoms and a single layer of threonine hydroxyl oxygen atoms, which create four K^+ ion binding sites from the extracellular to the intracellular space. At these sites, K^+ ions are attached dehydrated and surrounded by eight oxygen atoms (figure 3, red in panel b), four above and four below. Thus, potassium ions are therefore able to diffuse from water into the selectivity filter where the energetic cost of dehydratation is compensated. It is accepted that the selectivity filter is occupied by two K^+ ions alternating between two configurations. Even Na^+ ions has a smaller ionic radius, the fixed filter structure is fine-tunned to coordinate a K^+ better than the smaller dehydratated Na^+ (MacKinnon, 2003).

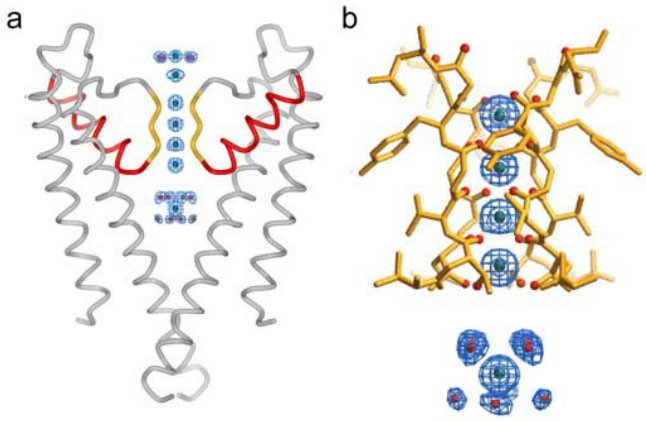

Figure 3. Structural model of the KcsA pore. A. Structure adopted by S5-S6 loops of two subunits. The selectivity filter is highlighted in yellow. The P-loop, in red. B. Conformation acquired for the selectivity filter. Oxygen atoms, in red (MacKinnon, 2003).

1.1.1.2. *The voltage sensor*

For voltage-gated channels the membrane voltage determines whether they are open and therefore they provide a way for the membrane voltage to feed back onto itself. The voltage sensing domain comprises the S1-S4 α-helixes. When a voltage-gated channel opens, charged amino acids called gating charges move through the membrane electric field, coupling electrical work to the opening process. The gating charge has been measured and is mostly attributable to four arginine residues per α-subunit. Even highly conserved sequences throughout S1, S2 and S3 are also involved in voltage-dependent

conformational changes, S4 plays the major role (MacKinnon, 2003). The S4 sequences contain a positive charged amino acid (Arg or Lys) every two hydrophobic amino acids, repetitively, 4-8 times: those are the main gating charges mentioned before. The S1-S3 segments complete the voltage-sensing domain by stabilising the positively charged S4 segment with their negatively charged amino acids and defining the pathway for the movement through the electric field (Hille, 2001).

1.1.1.3. *Gating machinery*

The X-ray crystallographic studies of different potassium channels in open or closed states, leaded to the discussion on the movement upon a voltage stimulus. Three main models were proposed:

- Helix screw: rotational movement of the gating charges at the S4 across the electric field (Larsson et al., 1996, Keynes and Elinder, 1999).
- Transporter: implies also a rotational movement of S4 charges from one site to the other but no translocation through the lipid bilayer is performed (Chanda et al., 2005).
- Paddle: movement of a rigid S3-S4 complex to a closer proximity of S1-S2 (Jiang et al., 2003).

However, thanks to the molecular simulations, all those theories come to converge in a single consensus model. The voltage sensor domain is connected to the pore domain because of the linker between S4 and S5, which in turn makes contact with S6. At the cytoplasmic end of this later one has a super flexible domain, the hinge PxP, very well conserved, that occludes the pore. Upon voltage stimulation, S4 is suffering a combination of movements that includes a rotation on its axis (180º), a tildation (30º) and vertical and radial translations (about 7Ă). This may create tension and displacement of the S4-S5 linker affecting its interaction with S6. It moves the hindge of the S6 and, in turn, dilates the inner opening of the pore allowing the ions to enter the conduction pathway (Bezanilla, 2008, Long et al., 2005, Jensen et al., 2012).

It was generally assumed that the transference of the S1-S4 movement to the S5-S6 pore domain was due to a mechanical stretching exerted at the S4-S5 linker. However, it has been recently described that the physical dissociation of the voltage domain and the pore conducting domain, does not prevent a functional voltage-gated potassium channel. Thus, the authors proposed that instead of an electromechanical mechanism underlying the activation, it would be based in electrical interactions through the end of S4 and/or the beginning of the S4/S5 linker with the proximal S6 COOH-terminal region (Lorinczi et al., 2015).

1.1.1.4. *Inactivation*

The inactivation of channels is a conjunct of processes that lead to the closure in a voltage independent manner. Thus, even the depolarization of the cell remains; the channels cease the potassium conduction. Different kinds of inactivation have been described.

- N-type inactivation: it occurs in the range of few milliseconds and it is due to the occlusion of the pore by a cytoplasmic particle. This entity can be placed at the N-terminus of the channel coding sequence, for instance in the case of Kv1.4, Kv3.3, Kv3.4 and Kv4 channels. However, other auxiliary subunits can supply this particle to the channelosomes via its oligomerization. It is the case of Kvβ1 and Kvβ3 subfamily members. Classically has been referred as the "ball-and-chain" inactivation (figure 4, left) (Rettig et al., 1994).
- C-type inactivation: slower than the previous one, the speed can range from tens of milliseconds to seconds. Even many Kv channels undergo this kind of inactivation process, it remains not completely well understood. It is thought to involve a constriction of the external mouth of the pore that occludes the ion flow, exerting a role of a second gate (figure 4, right) (Blunck et al., 2006).

In addition, it is important to mention the existence of another type of inactivation in certain types of K^+ channels termed cumulative or use-dependent. It is present on Kv1.3. This phenomenon consists on a reduction of the number of channels that opens during repetitive depolarizing pulses, due to the incomplete recovery in the interpulse interval. The amount of current elicited is fewer in the last pulse than in the previous one (Barros et al., 2012, Yellen, 2002).

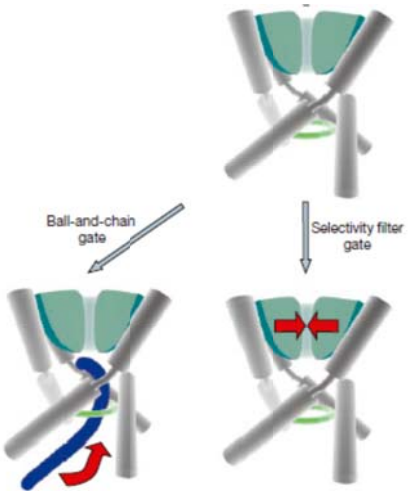

Figure 4. Representation of the inactivation of Kv channels. At the upper part, it is showed the opened conformation of the channel. Left down image represents the N-type inactivation. Left right image shows the C-type inactivation (Yellen, 2002).

1.1.2. *Cell biology of Kv channels*

1.1.2.1. *Biogenesis and protein folding*

Kv channels are synthesized from the mRNA transcript at the ribosomes close to the ER membrane, even they lack the membrane-protein signal. Multi-spanning membrane proteins drive this localization thanks to the presence of specific transmembrane domains that resemble to the signal sequence. For Kv1.3 it was detected at S2 transmembrane domain (Tu et al., 2000). Once translocated to the ER membrane while the translation

undergoes, the extracellular domains of the nascent protein are going to face the ER lumen.

In the case of some Kv family members, the tetramerization domain is placed at the N-terminus of the protein and it is properly folded very early in the biosynthesis. It is thought that the oligomerization of this domain among the different subunits is stablished even before the translation is ended (Kosolapov and Deutsch, 2003). The final configuration would follow some stablished steps. Two monomers are assembled into dimers, and the final tetramerization occurs by a dimer dimerization (Tu and Deutsch, 1999).

While the protein is synthesized, folded and assembled as tetramers, transference of oligosaccharides to the structure can come about in some specific residues. Those modifications are different in nature:

- N-glycosylation: attachment of a glycan to an asparagine (N) which is forming part of the consensus sequence NxS/T.
- O-glycosylation: started at the ER and followed at Golgi, it consists in the addition of a single sugar to a serine or a threonine.

Those modifications have folding promoting effects. At the ER compartment, they assist nascent polypeptides increasing their solubility on intermediate structures. The presence of those modifications leads to interaction with ER lectins such as calnexin or calreticulin. Those proteins exert a dual function consisting on folding enhancement or impairment of the ER exit for non-proper built proteins. If the protein fails to fold, it must be degraded following ER associated degradation (ERAD). This process implies a retro-translocation to the cytoplasm and subsequently ubiquitin-dependent degradation at the proteasome. The modification of the N-glycan is a driver for this degradation process to happen. Thus, sugar additions are enhancing protein folding, ER exiting or degradation dictating the Kv abundance at the cell surface (Peroz et al., 2009, Mihic et al., 2011).

Kv1 and Kv3 families are known to undergo massive glycosylation at the S1-S2 extracellular loop, while other members are not carrying any post-translational added sugar (Baycin-Hizal et al., 2014). Some β subunits are bearing those modifications, such as the KCNE family. KCNE1 is known to wear two different N-glycan trees as well as O-modifications. Those are controlling the physiological distribution of the protein (Bas et al., 2011).

Moreover, also at the ER compartment, it takes place the association to some β- subunits such as Kvβ or KChAP. Both have been described to enhance the proper protein folding and the traffic to the plasma membrane (Pongs and Schwarz, 2010). The KCNE family is also thought to interact at the ER compartment with the modulated ion channel. Although the stoichiometry of β subunits is under an intense debate in some cases, different functional stoichiometries are mediating distinct effects on the ion channels expression and function (Nakajo et al., 2010, Sole et al., 2009).

Main functions of Kv channels are membrane-location dependent. Several different mechanisms are defining and controlling the traffic to the membrane of proper-folded channels where they are exerting those major functions.

1.1.2.2. *Trafficking pathways*

As previously mentioned, the biogenesis of transmembrane proteins was classically described to happen at the ER compartment and to follow the ER-to-Golgi pathway. However, recent publications point out that other possible pathways are held within the cell physiology. To differentiate them, the former it is called the conventional while the rest are included in the pool of unconventional secretory pathways.

The *conventional secretory pathway* includes the traffic starting at the ER compartment, through the ER-to-Golgi intermediate compartment (ERGIC), the Golgi apparatus and trans-Golgi network (TGN) (figure 5).

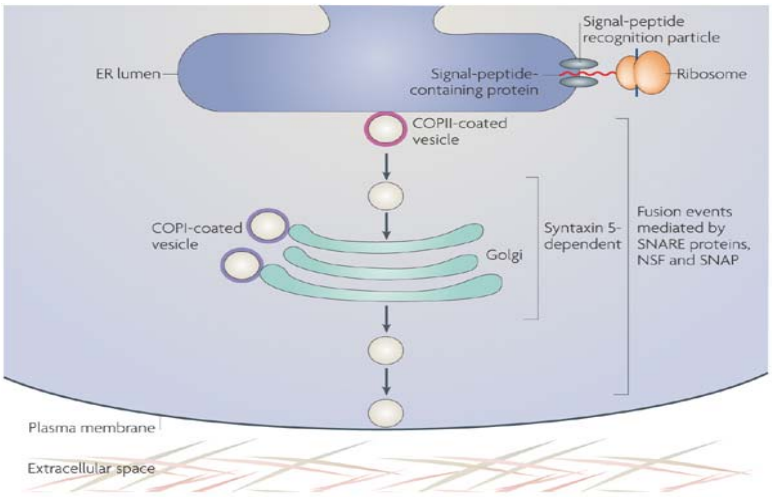

Figure 5. Conventional secretory pathway: schematic representation of the main steps of this traffic (Nickel and Rabouille, 2009).

Correctly folded and assembled proteins are packaged into COPII (coat associated protein II) vesicles and transported to Golgi via ERGIC compartment. The COPII mechanism mediates the recruitment of the cargo proteins, the curvature and cleavage from the ER membrane, and the delivery to the proper target. This event is taking place in specific ER membrane domains in which the surrounding cytoplasm is enriched in COPII soluble components (ER exiting sites: ERES). The machinery is formed by: Sar1, Sec23, Sec24, Sec13 and Sec31. The process starts by the insertion of the amphipathic helix of Sar1 upon GDP/GTP exchange (figure 6-1). This member is recognised by Sec23 which heterodimerises with Sec24. Both form the inner COPII coat. Sec24 is in charge to identify and interact with cargo proteins (figure 6-2,3). The process is followed by the recruitment of Sec13/Sec31 heterotetramers as the external coat, enhancing the membrane curvature (figure 6-5). Releasing the vesicle depends on the Sec23 GTPase activation of Sar1, which leads to the excision (figure 6-6) (Szul and Sztul, 2011, Jensen and Schekman, 2011).

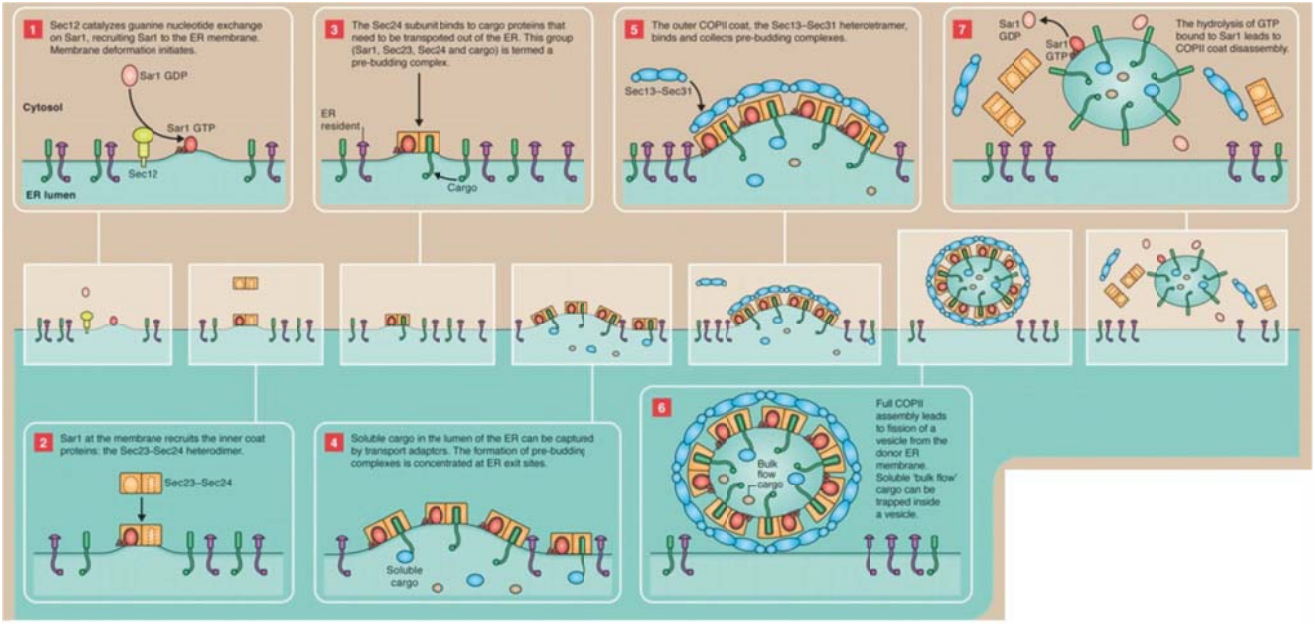

Figure 6. COPII dependent ER-to-Golgi mechanism. 1. Sar1 GDP exchange for GTP and anchor of it to the ER outer membrane. 2. Recruitment of Sec23 and Sec24. 3. Sec24 selects cargo proteins to be traffic to Golgi. 4. Repetition of the process at ERES domains. 5. Recruitment of Sec13 and Sec31 and budding of the vesicle. 6. Coated vesicle with COPII mediators. 7. Uncoating of COPII vesicles posterior to the excision (Jensen and Schekman, 2011).

Sec24 cargo recognition is basic for the conventional Kv export to the plasma membrane. It is selecting proteins exhibiting export signals: protein domains that will interact with Sec24 to be exported. Those include di-hydrophobic motifs such as di-phenylalanines (FF) or di-leucines (LL), di-acidic motifs (DxE) and aromatic motifs (Barlowe, 2003). More complex signatures such as VxxSL signatures have been identified as export potentiating domains in Kv physiology (Li et al., 2000). Not all the proteins present them, but by interacting with transmembrane sorting receptors, such as Erv14 in *Saccharomices cerevisiae*, they can also follow this via. Cargo receptors are also fundamental for the export of intra-luminal soluble proteins (Budnik and Stephens, 2009).

The next step in the pathway is the ERGIC compartment. It is considered as an autonomous organelle separated from ER and Golgi presenting a differential biochemical composition (Szul and Sztul, 2011). Typically located close to the ERES domains, it works as a stationary compartment at which the decision between conventional or unconventional route is taken. Vesicles from this compartment would travel to Golgi apparatus when conventional path is undertaken. The alternative would imply the direct communication with the endosomal recycling compartment undergoing then a by-pass of the Golgi (Saraste et al., 2009, Appenzeller-Herzog and Hauri, 2006).

After leaving this compartment, the next step is to fuse with the Golgi apparatus. This is organized in stacked cisterns with defined polarity: *cis*-Golgi facing the ER, *trans*-Golgi in the opposite site and *medial* in between. Multiple models have been considered about the progressive formation of this compartment and the one gaining more recognition is the cisternal maduration model. The newly formed *cis*-cisterns are travelling toward a *trans*

position by incorporating enzymes typically from this final target and loosing those from previous stages. This remodelling occurs by packaging the Golgi enzymes into coats formed by the COPI system and travelling in a retrograde manner: from *trans* to *cis.* Moreover, it is the main mechanism to traffic back vesicles to the ER. Actually, ER resident proteins are retained in the ER by a continual retrieval from Golgi (Szul and Sztul, 2011). Thus, there are two different kinds of signals:

- Anterograde signals: as mentioned before, are those recognised by Sec24 to traffic to ERGIC and Golgi. It has been described di-acidic signals for ion channels trafficking (K_{ir}, CFTR, K_{ATP}) as well as non-canonical motifs: DDxDxxxI for BK_{Ca} and VxxSL in Kv1.4 (Barlowe, 2003, Chen et al., 2010, Li et al., 2000).
- Retention signals: basically di-lysine motifs, KKxx/KxKxx as well as arginine repeats such as RxR. Those are recognised by COPI mechanism and brought back to the ER. It is thought to be exposed when the proteins are not properly folded in order not to reach the plasma membrane . Soluble proteins are thought to recycle back by interacting with the KDEL receptor (Jackson, 2014).

Anterograde and retention signals can coexist and the balance among those is a control of the proper folding and the possible ticket out to exit direction the plasma membrane. Retention signals, thus, act as an additional control to ensure that there are no misfolded channels at the cell surface. In addition, the exposure of them will be also modulated by the presence of β-subunits, scaffolding proteins or the heteroligomerization with other Kv members .

The most *trans*-cisternae are followed by another compartment: the Trans Golgi Network (TGN). This appears as a tubular, branching and reticular network. Apart from the direct traffic to the plasma membrane, there is also the possibility to target the vesicles from the TGN to the endosomal system, before the surface delivery. Along with the coat proteins, there are several different machineries involved in the process of cargo sorting. For instance, APs (Heteromeric Adaptor Protein complexes) can bind tyrosine-based domains, Yxxϕ (being ϕ an aromatic aminoacid) and di-leucine motifs. Another example are the GGAs (Golgi-localized γ-ear-containing ARF-binding proteins) which specifically recognize acidic clusters of di-leucine motifs: DxxLL. Concomitantly with the previous data, there are also some transmembrane cargo receptors that will interact with soluble proteins to be secreted (Kim, 2016).

The *unconventional secretory pathway* is, nowadays, under intense research to define the mechanisms and molecular components involved. Thus, they are not completely understood. To date, two different pathways have been identified:

- Transmembrane proteins such as CFTR or CD45 are inserted into the ER but reach the cell surface in a COPII and/or Golgi independent mechanism
- Cytoplasmic and nuclear proteins that lack the ER-signal peptide, such as FGF2, have been shown to exit the cell to the extracellular media avoiding both ER and Golgi compartments (figure 7).

Regarding ion channels physiology, Kv4.2 is known to by-pass COPII trafficking and to use a COPI mechanism when it iss coexpressed with KChIP1. However, conventional routes are driving the complex when the association is with KChIP2. The best-documented

example of by-passing Golgi is, indeed, CFTR. It has been shown that it is depending on COPII mechanism but the vesicles budded from the ER are directly associated to the endosomal system previous to the membrane targeting.

It has been reported that both secretory mechanisms can coexist inside the cell and used by a unique protein. Moreover, under some stress conditions has been observed that the *unconventional* can be potentiated to overcome the *conventional* blockage. Further investigations need to be performed to clarify all the possible routes followed by each studied protein (Nickel and Rabouille, 2009).

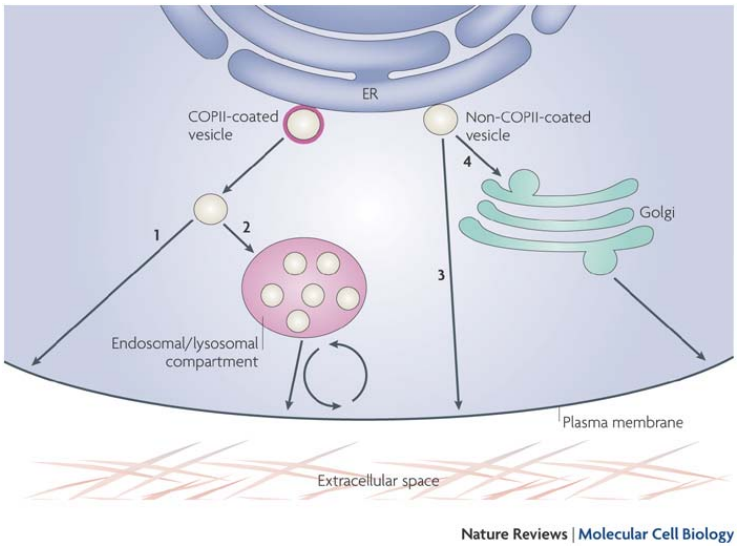

Figure 7. Unconventional secretory putative pathways. Representation of different mechanism of membrane targeting that have been inferred besides the conventional mechanism for signal-peptide-containing proteins (Nickel and Rabouille, 2009).

1.1.3. *Subcellular localization of Kv channels: membrane distribution.*

Posterior to the traffic by either conventional or unconventional pathways, Kv channels reach the membrane. Upon delivery, proteins can freely diffuse throughout the lipid bilayer. However, the expected physiology of Kv channels, as well as several other proteins, can depend on their localization, being imperative the control of their position. Various different mechanisms have been identified, in turn highly different in nature.

1.1.3.1. *Scaffolding proteins*

One possibility is to anchor molecular complexes by interacting with scaffolding proteins. Kv1 channels, for instance, present a C-terminal PDZ-binding domain able to complex with PDZ domain proteins. Classified within the MAGUK family, those are characterised by several interacting domains to cluster membrane-associated proteins. To do so, they present one or more PDZ domains, a SH3 domain (another protein-protein interaction domain) and an active guanylate kinase domain. Thus, since they can interact with basic

proteins of the cytoskeleton, it is promoting the immobility of their partners (Oliva et al., 2012).

PSD-95, a member from this family has been reported to interact with the PDZ-interacting domain of the Kv1 family which is present at the C-terminal domain. This complexation impairs the lateral movement and the recycling of the channels, inducing then a longer membrane expression. This protein has been identified as the responsible of the channel clusterization at the post-sinaptic membrane of Kv channels (Ogawa et al., 2008). SAP-97, another member of the family, is known to retain and stabilise channels in muscle physiology enhancing the signalosome's formation (Balse et al., 2012).

Apart from the direct interaction with scaffolding proteins that interact with cytoskeleton members, other space controlling mechanisms have been reported. Structural proteins of the membrane cytoskeleton are thought to form corrals: defined fences of space that limit the lateral diffusion of membrane proteins. This mechanism has been reported to confine Kv2.1 without any putative protein-cytoskeleton interaction (Tamkun et al., 2007).

1.1.3.2. *Membrane compartmentalization: lipid raft microdomains*

Even considered for a long time as a homogeneous lipid environment, the plasma membrane presents some differentiable areas characterised by a distinct lipid composition. In this context, lipid raft microdomains are defined as small and transitory structures of about 10-200mm. There is an enrichment of both sphingolipids, with highly saturated acyl chains, and cholesterol mainly in the outer leaflet that leads to a highly packed and ordered composition compared with the general membrane fluidity (figure 8). Because of their composition, those structures are characterised by low density and resistance to non-ionic detergent solubility at low temperatures (Brown and London, 1998, Schroeder et al., 1998). The targeting of membrane proteins to those specific domains is not completely understood. However, post-translational modifications such as palmitoylation and glycophoshatidilinositol addition have been related to the lipid raft presence of some proteins. Moreover, the composition and length of some transmembrane sequences can influence this specific localization (Paulick and Bertozzi, 2008, Melkonian et al., 1999, Diaz-Rohrer et al., 2014).

Entities involved in the same signalling pathway need to remain located closely in order to work in coordination and transmit the specific signal. Actually, lipid raft are considered platforms where this distance step can be overcome. Furthermore, it has been reported that lipid raft are implicated in highly different cellular processes such as endocytosis, exocytosis, internalization of toxins and viruses, cell migration and cell proliferation (Sonnino and Prinetti, 2013).

Kv channels are known to target those specific membrane subdomains. The localization into or out of these dynamic location has been related to control their activity and, therefore, the cell physiology. Lipid rafts are controlling Kv channels not only by aggregating them with signalling proteins but also by surrounding them of specific lipid environments. It is widely accepted that interactions between lipids and ion channels can

alter their functions (Dart, 2010). For instance, the activation of Kv1.3, in high presence of cholesterol, is shifted towards more positive potentials (Hajdu et al., 2003).

The association of specific Kv channels to those specific domains seems to be specific for Kv member and cell-type. Moreover, the molecular mechanisms underlying this final localization are not extrapolable, and retain channel specificity. Kv1.3 is present in lipid raft domains at T-lymphocytes, Kv1.4 and Kv4.2 in neurons and Kv1.5 in cardiomyocytes, together with Kv7.1 and Kv11.1 (Dart, 2010) .

1.1.3.2.1. *Caveolae*

Multiple kinds of lipid rafts have been identified with differences in lipid and protein composition. The only morphologically identifiable are caveolae, characterised by a Ώ-shaped membrane invagination (figure 8). Caveolin is the major structural protein of those structures and it is responsible for this highly specific membrane pattern. It is a small protein (18-20kDa) with three submembers in the family: caveolin 1 and caveolin 2, that are ubiquitous, and caveolin 3 that is specifically expressed at musculature. Attached to the membrane, rather than a spanning protein, it presents a hydrophobic sequence in the middle of the protein that hairpin-like is inserted in the inner leaflet of the membrane. At the N-terminus domain it presents the Caveolin Scaffolding Domain (CSD) which is related to the caveolin oligomerization, protein-protein interactions and cholesterol binding. However, the α-helix formed at the C-terminus it is thought to be intimately related with the membrane by holding palmytoilated cysteines (Williams and Lisanti, 2004).

Caveolae are involved in different functions such as the response to plasma membrane stretching, cholesterol homeostasis or vesicular trafficking. Moreover, several signalling proteins have been detected in those domains due to the interaction with caveolin at the CSD: PKC, eNOS, tyrosine kinases, H-Ras or MAPK (Patel et al., 2008). It was described that the recognition of an interactor would be through of a Caveolin Binding Domain (CBD) which is an enriched sequence on aromatic aminoacids. Three main signatures have been identified as potential CBD: ϕx ϕxxxx ϕ, ϕxxxx ϕxx ϕ or ϕx ϕxxxx ϕxx ϕ (where ϕ is an aromatic residue: Phe, Trp, Tyr, and X is any aminoacid) (Couet et al., 1997). However, there is some controversy with this CBD signal since there is not a common structure adopted by this domain and it is over represented at the mouse genome: >30% of proteins exhibited a similar sequence. Thus, the importance of testing the caveolin-protein interaction and study deeply the consequences are highly convenient (Collins et al., 2012).

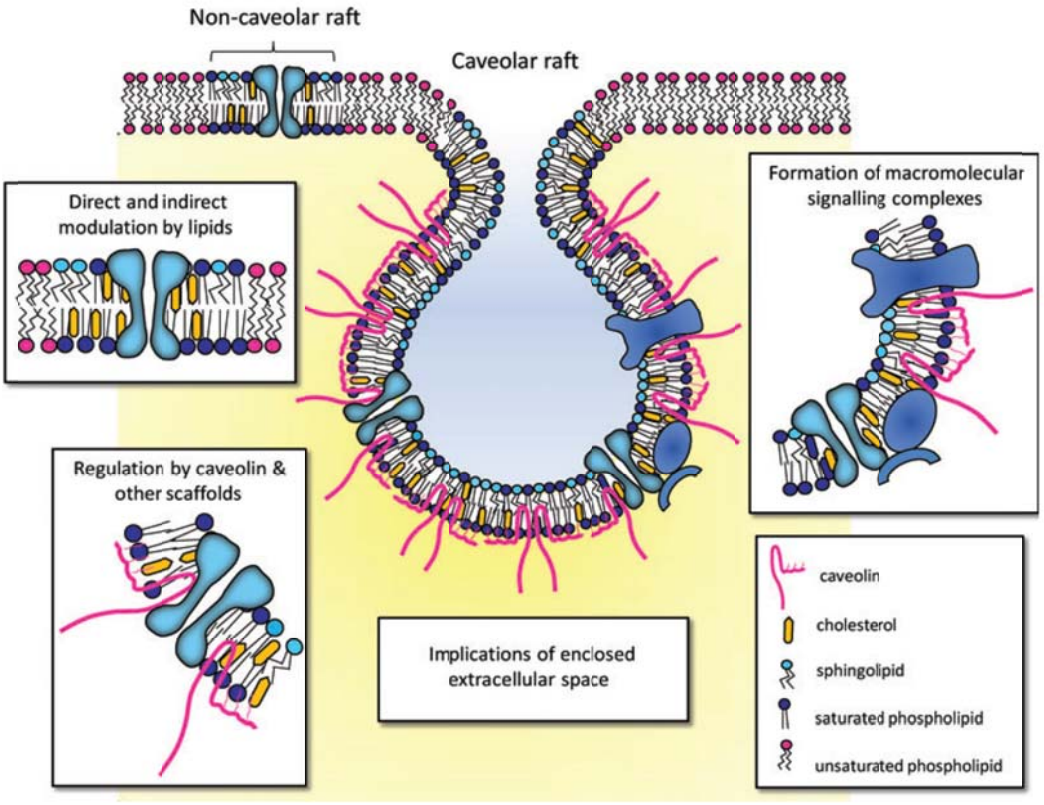

Figure 8. Representation of the plasma membrane with different lipid raft. Centrally represented a caveolae and at the upper left part a non-caveolae lipid raft microdomain. Different channels and receptors are detailed in the specified regions (Dart, 2010).

Regarding the ion channels physiology, recently, our laboratory have published that Kv1.3 putative caveolin binding domain is, indeed, responsible for the interaction with the caveolin and, in turn, provoking the localization of Kv1.3 at lipid raft microdomains (Perez-Verdaguer et al., 2016a). Moreover, Kv1.5 is also targeted to *lipid raft* microdomains by interacting with the third member of the family (Folco et al., 2004).

Not only interactions with scaffolding proteins are driving the targeting to those domains but also specific post-translational modifications such as palmitoylation, myristoylation or GPI.

1.1.3.2.2. *Palmitoylation modification*

Posttranslational modifications allow the cell to modulate rapidly protein function, localization and stability. Particularly, lipid additions have been related to the lipid raft targeting. Saturated fatty chains extended conformation are suitable to interact with the highly packed lipid raft structures (for instance palmitoylation or myristoylation), contrary to branched unsaturated acid chains (for instance prenylation) (Melkonian et al., 1999).

Opposite to other modifications, palmitoylation is a reversible modification which increases the fine–tunned protein regulation depending on the cellular conditions. It consists on the transference of a long-chain fatty acid to a cysteine, mainly. Two different kinds of palmitoylation are possible: (I) S-acylation is the transference of a palmitate through a thioester linkage or (ii) N-acylation which implies the transference to the N-terminus of a cysteine. It is known that most of the studied cases, palmitoylation happened in proteins already myristoylated or prenylated.

The addition of the palmitate is exerted by acyltranferases (PATs). Those enzymes are highly conserved from yeast to humans and more than 20 members have been identified in mammals. PATs are defined by the presence of the DHHC domain (Asp-His-His-Cys) involved in the catalytic function. The reverse reaction is held by acylthioesterases, and just two members have been identified: one placed in the cytosol and the other at the lysosomal lumen (Nadolski and Linder, 2007, Linder and Deschenes, 2007).

Research about palmitic effects on posttranslational modified proteins is exponentially increasing. The most commonly described function is to increase the affinity for membranes of a soluble protein, which can thereby affect not only its localization but also function. This is the case for both solely palmitoylated proteins and dually lipidated proteins. It is thought that myristoylation and prenylation promote transient interactions with membranes. The addition of a palmitate yields a long-lived association with the membrane of the dually lipidated protein. Thus, the PAT substrate can then move to different compartments but will do so by vesicle-mediated transfer (Nadolski and Linder, 2007). H-Ras and N-Ras are the example further studied of soluble proteins trafficking by the conventional secretory pathway to the plasma membrane (Linder and Deschenes, 2007). Several studies have been designed also on deciphering the role of lipidation in transmembrane proteins. Considering ion channels, upon palmitate addition, BK and Kv1.5 alter the membrane targeting, while Kv1.1 modifies its biophysical properties (Jindal et al., 2008, Gubitosi-Klug et al., 2005, Jeffries et al., 2010).

1.2. *Kv1.3*

Kv1.3 is the third member of the *Shaker* related human Kv1 subfamily (Gutman et al., 2005). It is encoded by the *kcna3* gene located in humans at the chromosome 1: 1p13.3. It was cloned, almost simultaneously, in brain of different species and T-lymphocytes (Grissmer et al., 1990, Grupe et al., 1990, Swanson et al., 1990). The gene sequence is intronless, and variations observed at the mRNA level are due to non-translated regions. Considering the protein, the α-subunit presents 575 aminoacids in humans and four subunits are forming a conducting entity. Kv1.3, as a voltage-gated potassium channel, is classified within the subgroup of outward delayed rectifiers (Hille, 2001).

This channel is expressed in several tissues, but the major intensity is located at the nervous and the immune system. In brain, ordered from higher to lower expression, is located at inferior colliculus, olfactory bulb, pons, medulla, midbrain, superior colliculus, corpus striatum, hippocampus and cerebral cortex. Considering the immune system, it has been detected in T and B-lymphocytes, pre-B cells, microglia, dendritic cells and macrophages. Moreover, Kv1.3 is also expressed at lung, islets, thymus, spleen, lymph

node, fibroblasts, tonsils, oligodendrocytes, osteoclasts, platelets, megakaryocytes and testis (Gutman et al., 2005). The presence is notably, also, in many cancers (Comes et al., 2013).

1.2.1. *Electrophysiological and pharmacological properties of Kv1.3*

Kv channels can increase the variability of their properties by associating with α-subunits from other Kv families like so interacting with β-subunits. However, when built up as a homomer, they present some specific biophysical features.

Kv1.3 is activated posterior to a cell depolarization of about -35mV. The channels are rapidly opened, reaching the maximum peak conductance about 10ms after a stimulus. The single-channel conductance was calculated around 13pS.

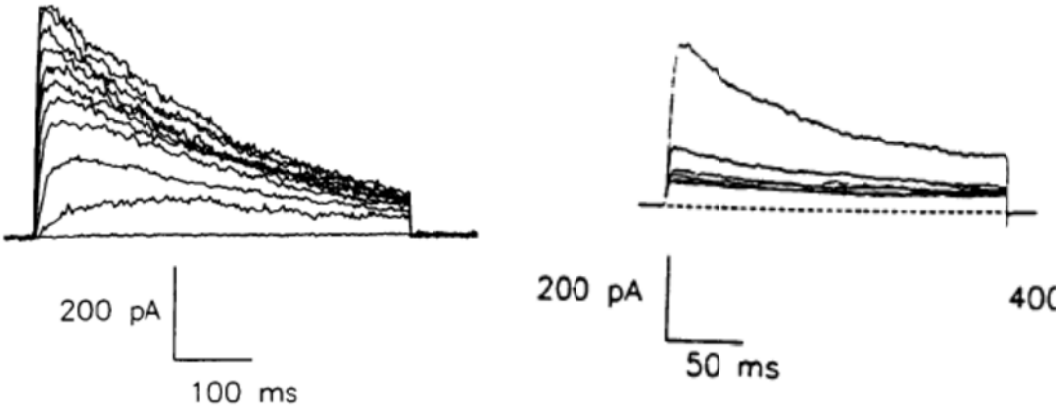

Figure 9. Electrophysiological classical Kv1.3 features. A. Potassium currents evoked by Kv1.3 in a voltage dependent manner. Currents elicited showed C-type inactivation. B. Cumulative inactivation of Kv1.3 currents upon repetitive pulses. (Grissmer et al., 1990)

Once the channels are opened, if the depolarization is kept, the current suffers a slow decay. So, Kv1.3 is presenting a C-type inactivation with a $\tau_{inactivation}$ around 250ms when measured at 40mV (figure 9A). There is no presence of rapid or N-type inactivation on the channel. Another typical feature described on Kv1.3 currents is the cumulative inactivation. Thus, there is a decrease in the potassium current after repetitive depolarising pulses (figure 9B) (Grissmer et al., 1990). The inactivation kinetics of the channel can be modulated by several inputs such as phosphorylation, temperature, pH or extracellular ionic composition (Panyi, 2005).

Several different compounds are known to suppress Kv1.3 such as quinine, TEA, 4-aminopiridine or Psora-4. However, the most effective inhibitors are derivative from natural venoms. Margatoxin, which exhibits a IC_{50} in the picomolar range, charybtoxin, Pi2 and Pi3 are scorpion venoms that can impair channel conductance. α-dendrotoxin presents also this ability but also blocks Kv1.1, Kv1.2 and Kv1.6. ShK toxin is one of the most specific for Kv1.3, even some effects have been reported on Kv1.1, Kv1.4 and Kv1.6 (Gutman et al., 2005). Produced by a sea anemone, a considerable effort has been invested

to test derivatives as a future treatment for autoimmune diseases (Beeton et al., 2011, Chi et al., 2012). Even though the amount of inhibitors is substantial, no activator has been identified yet.

1.2.2. *Functions of Kv1.3*

Kv1.3 is mainly expressed in nervous and immune system. In a nervous cell is mainly located at the axon. At the brain regions where it is expressed, Kv1.3 modulates the firing rate. It has been described functional heteromeric complexes of Kv1.3 with Kv1.1, Kv1.2 and Kv1.4 at the brain grey matter while in bovine cortex its accompanied by Kv1.2, Kv1.4 and Kv1.6 (Coleman et al., 1999, Shamotienko et al., 1997). The KO mice presented a *supersmeller* phenotype, with a higher ability for stimuli discrimination and a detection threshold 1000 to 10000 times smaller. Those are exhibiting abnormal firing at olfactory bulb neurons. Several other proteins have been detected to increase upon impaired Kv1.3 expression, such as odorant receptors or K_{Na} which explains this phenotype, and PSD95 or 14-3-3 among others (Fadool et al., 2004). Moreover, after a stimulation of insulin receptor expressed at the olfactory bulb, which inhibits Kv1.3 by phosphorylation, the obtained phenotype resembles the *supersmeller* Kv1.3 KO mice (Tucker et al., 2010).

Kv1.3 plays a pivotal role in the activation and (Szabo et al., 2008, Beeton and Chandy, 2005). After TCR activation, calcium release from the endoplasmic reticulum is mediated by the PLCγ effects. The sustained calcium signalling is necessary for the induction of the gene expression involved in activation and proliferation. Kv1.3, together with $K_{Ca}3.1$, is generating enough driving force to enhance the entrance of extracellular calcium through Orai1. Mediated by calcineurin, NFAT will be translocated to the nuclei in order to transcribe those previously mentioned genes (figure 10). So, Kv1.3 is necessary to achieve the proper threshold to the activation to happen (Cahalan and Chandy, 2009). The channel has been related to several autoimmune diseases such as type-I diabetes, multiple sclerosis or arthritis rheumatoid. Moreover, from patients suffering those illnesses Kv1.3 overreactive T_{EM} were isolated, and blocking of the channel ameliorates the effects of the multiple sclerosis (Varga et al., 2010).

Upon activation, it is known that Kv1.3 is translocated to the immunological synapse where colocalise with TCR, CD3 or PSD95 (Panyi et al., 2004). The nature of those signalling platforms has been related with lipid raft microdomains. Moreover, alteration of the lipid raft formation has been related to the also autoimmune disease Sistemic Lupus Erythematous (SLE)(Nicolaou et al., 2007, Nicolaou et al., 2010).

While activation of the channel is involved in activation and proliferation of the immune system cells, the inhibition could be related to apoptosis. The dual role of Kv1.3 in lymphocyte physiology highlights the importance of fine-tunning its localization and function. It is worthy to mention that Kv1.3 KO mice do not present alteration in the immune system functions due to the compensation by the increased role of chloride channels (Koni et al., 2003). However, it was reported a decreased incidence and severity to the development of the related multiple sclerosis mice experimental phenotype (Gocke et al., 2012).

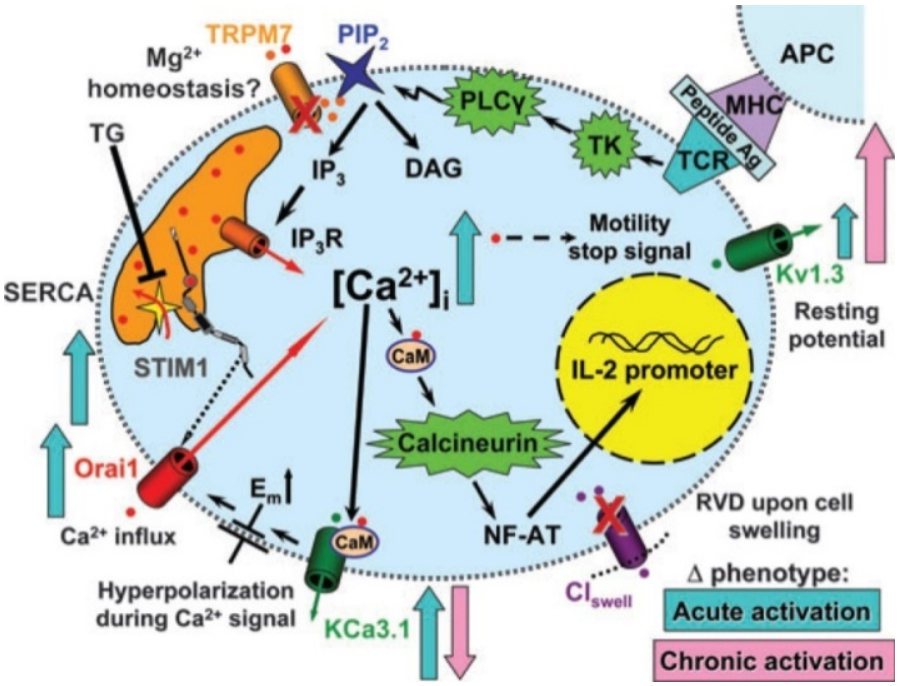

Figure 10. Signaling cascade initiated upon T-lymphocyte activation. Pathway of gene expression enhancement implies Kv1.3 activity. Blue and pink arrows point out the roles of the different proteins in acute or chronic activation respectively (Cahalan and Chandy, 2009).

Several other tissues present this channel, but in a lower extend. Kv1.3 has been proposed as a mediator for the glucose uptake in insulin-sensitive cells. The blocking of the channel would lead to a release of calcium from the internal stores, due to the hyperpolarization generated. Due to this increase, Glut4 receptor would be translocated to the membrane (Choi and Hahn, 2010). Moreover, Kv1.3 depleted expression leads also to a decreased body mass, as well as in the number of fat bodies. This phenotype was reported to be also diet-induced obesity resistant (Upadhyay et al., 2013).

1.2.3. *Trafficking and subcellular location of Kv1.3*

As determined for other Kv channels, Kv1.3 is translated by the ribosomes at the rough endoplasmic reticulum, even they do not present the typical signal that directs the channel to this compartment. Specifically for Kv1.3, S2 was reported to enhance the target to this localization (Tu et al., 2000). Some glycosylation are performed in the structure along the secretory pathway placing a N-glycosylation in the S1-S2 loop (Baycin-Hizal et al., 2014). It is while travelling through the secretory compartments that some other interactions will take place, for instance with Kvβ subunits or KCNE4 (Shi et al., 1996, Sole et al., 2009).

In heterologous systems, Kv1.3 homomers present a good traffic to the plasma membrane. Specifically, it has been found to be present at lipid raft microdomains when expressed in HEK cells (Vicente et al., 2008). The mobility of the channel is altered upon changes on the cholesterol levels in this cell line as well as its electrophysiological properties in T-lymphocytes (O'Connell and Tamkun, 2005, Hajdu et al., 2003). Moreover, the induction of

the apoptosis in T-lymphocytes promotes the mobilization to some ceramide enriched rafts (Bock et al., 2003).

Even though the majority of its expression is located at the cell surface, Kv1.3 has been detected at the inner mitochondrial membrane of lymphocytes (Szabo et al., 2005). Molecular determinants underlying this targeting remain unclear. Kv1.3 could reach this specific location straight from the biogenesis, travelling through MAM domains (mitochondria associated ER membranes). However, it cannot be discarded that recycled channels from the membrane are delivered at the mitochondria or any other non-determined yet pathway. Some theories propose that the length of transmembrane domains is the clue for their final targeting (Szabo et al., 2010). At the mitochondria physiology, upon apoptosis signal, Bax would change the membrane potential by blocking the channel conductance and provoking the release of the cytochrome C (figure 11) (Szabo et al., 2008).

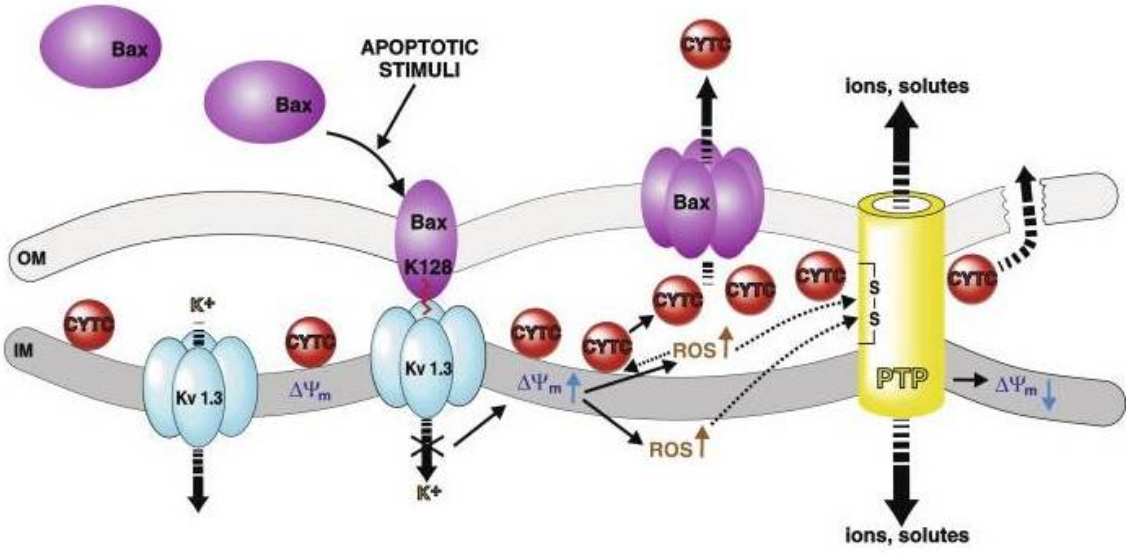

Figure 11. Schematic representation of mitochondrial Kv1.3 role in apoptosis. Inhibition of the channel by Bax would lead to an increase in ROS(Szabo et al., 2008) .

1.2.4. *Regulation of Kv1.3 activity*

The modulation of Kv1.3 can be exerted by different types of inputs. The heteroligomerization, as mentioned before, can fine-tune the final current and localization of the channels (Gutman et al., 2005). Not only at the nervous system, as mentioned before, but also at the immune system is forming heteroligomeric complexes . Kv1.3 is forming functional channels with Kv1.5 in macrophages (Vicente et al., 2006, Villalonga et al., 2007). Moreover, in dendritic cells are involved in the production of inflammatory cytokines (Matzner et al., 2008).

The interaction with auxiliary subunits such as KCNE4 and Kvβ2.1 is analyzed deeper in next sections. Further associations that control and modulate the channel function and localization were reported such as with MAGUK proteins SAP97 and PSD95 (Marks and

Fadool, 2007). Disruption of the PSD95 interaction is known to impair the Kv1.3 presence at immunological synapse (Szilagyi et al., 2013). Furthermore, those not only localize the channel at the plasma membrane by interacting with PDZ domains, but also served as platforms for other regulators, for instance Lck (Hanada et al., 1997). Kv1.3 can be modulated by several kinases with different effects: PKA, PKC, Src kinases or tyrosine kinase-activity receptors (EGF and Insulin receptors) (Payet and Dupuis, 1992, Gulbins et al., 1997, Fadool, 1998, Bowlby et al., 1997, Marks and Fadool, 2007). It was also demonstrated a calcium mediated regulation by the association with CaM kinase II but in the absence of calmodulin direct association (Chang et al., 2001, Fanger et al., 1999). Recently, a reduction on Kv1.3 currents dependent on calcium has been proposed for megakaryocytes (Martínez-Pinna et al., 2012). Previous results had been published on the Kv1.3-calcium relationship. Those were focused on the extracellular level of it showing an enhanced inactivation of Kv1.3 when it arises (Douglass et al., 1990). Finally, a direct interaction between the channel and β-integrins was detected, suggesting a putative new role by an intimate relationship with the cellular adhesion (Levite et al., 2000).

1.3 . *Regulatory subunits*

The in vivo expression of voltage-gated potassium channels is mainly forming channelosomes: multi-subunit complexes formed by Kv subunits (α subunits) and accessory subunits (β subunits). Those regulatory subunits influence a wide range of Kv channel properties; not only gating and pharmacology but also trafficking, subcellular localisation, post-translational modifications, etc. Among the different accessory subunits described, some of them are citoplasmatic (Kvβ, KChIP and KChAP) and others are integral membrane proteins (KCNE or DPPLs). Different insults have been reported to control the expression or the subcellular localization of them, fine-tuning the variability of channelosomes at different cell moments (Pongs and Schwarz, 2010, Li et al., 2006).

1.3.1. *Kvβ family*

Kvβ subfamily was the first accessory subunits identified. Attached to the purified glycosylated Kv channels employing the α-dendrotoxin, the determination of the proteolityc Kvβ polypeptides yielded partial sequences of Kvβ1 and Kvβ2 protein (Scott et al., 1990, Scott et al., 1994). This information was used to clone the mammalian Kvβ family. Three gene sequences are encoding for the family: Kvβ1, Kvβ2 and Kvβ3 (figure 12)(Heinemann et al., 1995, Leicher et al., 1996, Pongs et al., 1999, Schultz et al., 1996). Each of them presents alternative splicing variants with different protein sequence and varies upon the specie. In the human genome there are three gene products of the Kvβ1 coding sequence: Kvβ1.1, Kvβ1.2 and Kvβ1.3. Kvβ2 exhibits two protein isoforms but up to seven splice variants are obtainable from the human genome. However, human, mouse and rat present only one peptide confirmed encoded by Kvβ3 (figure 12)(Kilfoil et al., 2013).

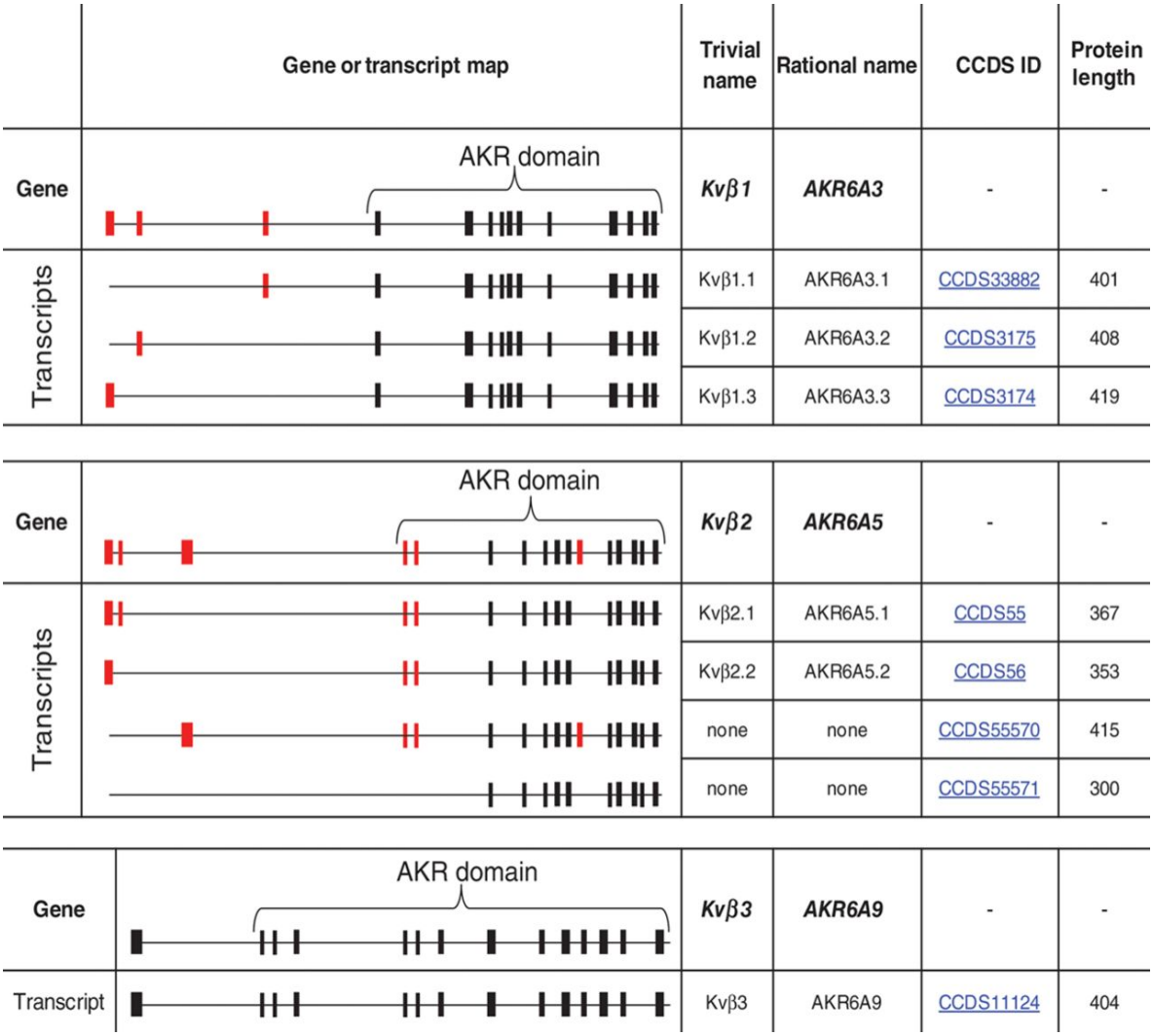

Figure 12. Schematic representation of Kvβ subfamilies gene and protein products. Kvβ1 at the top, Kvβ2 in the middle, and Kvβ3 at the bottom part (Kilfoil et al., 2013).

This regulatory subunit family is known to modulate gating and trafficking properties of the Kv1 subfamily. The interaction interfaces are placed at C-terminus domain of Kvβ (also known as core region) and the N-terminus of Kv1 or Kv4 subfamily (Li et al., 2006). Previous to the crystal structure, biochemical studies on Kv1 N-terminus domain elucidated that the specific region implicated is the one shown in figure 13 (Sewing et al., 1996). This protein region is well conserved in all Kv1 members, providing the molecular explanation for the specificity of Kvβs for this Kv subtype.

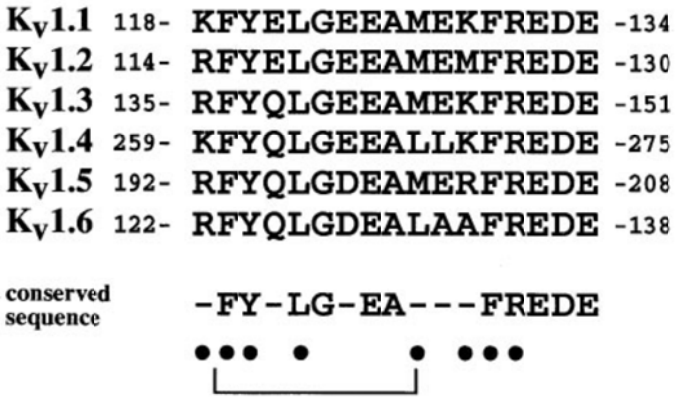

Figure 13. Experimentally determined region of interaction among Kv1 channels and Kvβ members. High conservation among the Kv1 family (Sewing et al., 1996).

However, the analysis of the crystal structure revealed some different results. The complex between the four T1 domains of a complete channel and the Kvβ tetramer is formed by the contact of four loops (figure 14A). The position of the interaction domain is located among M-70 and Y-80 of rKv1.1 T1 domain (figure 14B) (Long et al., 2005, Pongs and Schwarz, 2010, Gulbis et al., 2000).

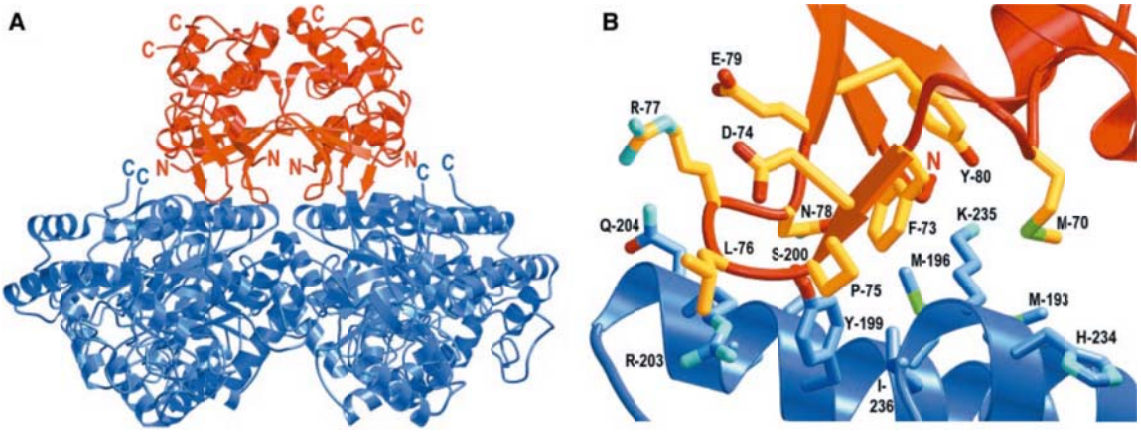

Figure 14. Structure of the T1 domain – Kvβ subunits. A. Lateral view exhibitin four contact loops that form the primary interface between T1 and Kvβ tetramers. T1 is shown in red. Kvβ, in blue. B. Molecular detail of a T1 contact loop touching the β subunit surface (Gulbis et al., 2000).

The members of Kvβ family present a 70% of similarity. Protein sequence alignment revealed a variable N-terminus giving diversity to the different peptides followed by a high conserved sequence, also called core region (Pongs and Schwarz, 2010, Li et al., 2006). This region is formed by 330 aminoacids and presents some features that allow us to classify the Kvβ family within the oxidoreductase family (Kilfoil et al., 2013).

Bioinformatics was confirmed by the low micromolar affinity for the oxidoreductase cofactors (NADPH and $NADP^+$) when Kvβ subunits were isolated (Liu et al., 2001).

1.3.1.1. Aldoketoreductase activity

The aldoketoreductase superfamily contains 190 annotated proteins in 16 different subfamilies. Each enzyme is characterised by the same protein fold, a triose-phosphate isomerase TIM barrel or $(\alpha/\beta)_8$-barrel with the insertion of several additional helixes (figure 15) (Hoog et al., 1994, Wilson et al., 1992).

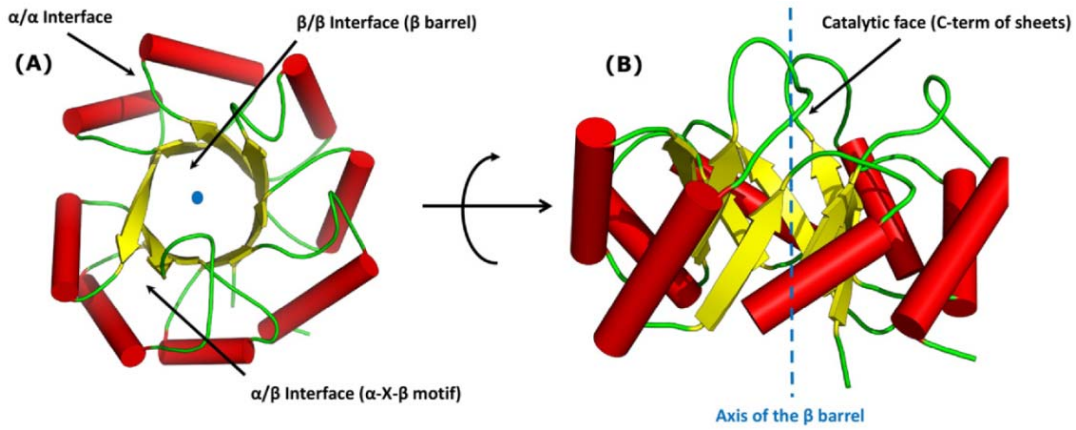

Figure 15. Schematic representation of the TIM barrel structure. A. Top view. It shows α-helixes depicted in red, loops in green and β-sheets in yellow arrows. B. Lateral view of the TIM barrel (Vijayabaskar and Vishveshwara, 2012).

Sequence alignment identifies a common cofactor binding domain which permits pro-R-hydride transfer to the acceptor group, and a conserved catalytic tetrad of Tyr, Lys, His and Asp(Jez et al., 1997). For the nomenclature, if the sequence presents a value lower than 40% identity, it becomes a new family (AKR1, AKR2, etc). Greater than 60% similarity between members, groups them within the same family. (Penning, 2015)

AKR family catalyse the reduction of an aldehyde to an alcohol by oxidizing and NADPH cofactor. The reaction follows a kinetic mechanism shown in figure 16. An AKR (E in figure 16) binds sequentially an NADPH and an aldehyde substrate to form a ternary complex. The redox reaction occurs, then, when AKR helps a hydride to be transferred from the cofactor to the aldehyde. The product, an alcohol, dissociates from the AKR and so the oxidized cofactor $NADP^+$ (figure 16). The hydride transfer step is usually a fast step, and nucleotide exchanges steps, or the protein conformational changes associated with them, are slow and rate-limiting (Weng et al., 2006).

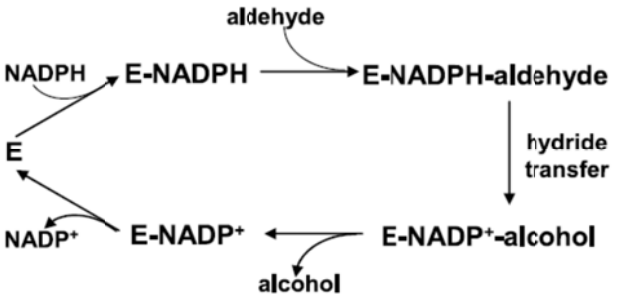

Figure 16. General enzymatic cycle of aldoketoreductases. Reduction and oxidation of NAPDH are also specified (Weng et al., 2006).

AKRs display nanomolar affinity for NADPH with Kd values in the range of 10-120nM but exhibit a micromolar affinity for NADH with Kd values between 100-250uM. Thus, the enzymes are thought to use the prevailing concentrations of NADPH and NAD^+ in cells. However, the high affinity for NADPH ensures that there is potent product inhibition of NAD^+ dependent oxidation reactions (Penning, 2015). Stable and transiently transfected mammalian cell lines show that when AKRs are forced to use the prevailing cofactor concentration in cells they catalyse reduction reactions only (Kilfoil et al., 2013).

The crystal structure of Kvβ2 revealed that, similar to the already described AKR topology, each subunit consists in a TIM barrel: $\alpha_8\beta_8$ arrangement of α-helixes and β-strands (figure 17) (Gulbis et al., 1999, Torres et al., 2007).

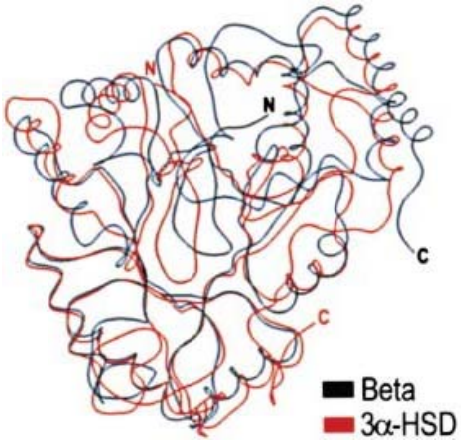

Figure 17. Comparison between Kvβ subunit and 3α-HSD aldoketoreductase by structural overlapping. Kvβ is represented in black, 3α-HSD in red .

The conserved residues for the catalytic site are conserved but the histidine is changed into an asparagine residue. Kvβ belongs to the AKR6A family and the nomenclature for Kvβ1, Kvβ2 and Kvβ3 is AKR6A3, AKR6A5 and AKR6A9 respectively (Kilfoil et al., 2013, Penning, 2015).

From a purified Kvβ2 protein it was measured that indeed, there was a NADPH oxidation, depending on its concentration. Corresponding to physiological pH ranges, its maximal

functionality was stablished between pH=7,2 – 7,4. Kvβ2 presented an aldehyde reduction not limited or affected by product inhibition and *in vitro* models showed that there was no observable cooperativity due to the tetramerization form. (Tipparaju et al., 2008)

Some aldehydes and ketones were identified as Kvβ2 substrates, not only chemical compounds but also natural ligands (Tipparaju et al., 2008, Xie et al., 2011, Alka et al., 2010, Weng et al., 2006). For instance, it was described that Kvβ2 can reduce aldehydes and ketones in enzymatic or nonenzymatic oxidized phospholipids (such as lipid peroxidation products), linking this family of proteins to the oxidative stress state. Some of these compounds can affect a variety of signalling pathways, leading to changes in vasodilatation, myocyte excitability and cell adhesion (Tsakadze et al., 2003, Bhatnagar, 1995, Leitinger et al., 1997). By mutating some residues in the Kvβ2 active site (tyrosine, lysine and aspartate) it was proved the specificity of those reactions. Specifically, tyrosine in the 90 position is clue to the acid-base catalysis which acts as a proton donor, already identified for other AKRs. Analysis of the opposite reaction (from alcohol to aldehyde) revealed a difficulty for the release of the cofactor once it's oxidized. This enzimatis characterisation proved that Kvβ2 is a slow enzyme to complete the entire turnover, but the rate for the hydride transfer is fast enough to consider it as a sensor of the redox state in the cell (Tipparaju et al., 2008, Xie et al., 2011).

Even the crystal structure was pointing to this interaction, Kvβ2-NADPH dynamic complex, as well as for Kvβ1.3, was determined and some residues involved in the interaction were characterised (Gulbis et al., 1999). The ability to interact with the cofactor is localised in the C-terminus of the protein, independently from the variable N-terminus. So, suggesting that probably is a general feature for all Kvβ family. However, the affinity of Kvβ2 for the cofactor is far higher than the Kvβ1.3, exhibiting that this parameter would be variable among the different members (Tipparaju et al., 2007). The avidity for pyridine nucleotides is similar to that observed for other enzymes of the AKR superfamily. Interestingly, and in contrast to others, the cofactor is attached to a deep cleft in the protein and covered by the β1-αG loop (yellow loop in figure 18) (Weng et al., 2006).

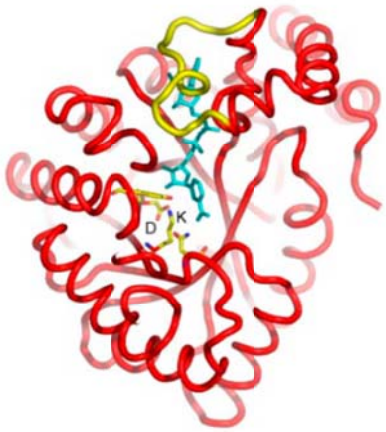

Figure 18. Structure of Kvβ together with NADPH. NADPH, showed in light blue, is placed in a cleft. Loop covering this space in yellow (Weng et al., 2006).

The testing for the recognition of different cofactors showed that Kvβ detects the ribose 2' phosphate of NADPH in detriment of NADH and so exhibiting a higher affinity. When compared, the avidity for NADPH is three fold higher than for the oxidized form of the cofactor. However, the oxidized form is preferred when NADH cofactor is analysed (Liu et al., 2001). Considering on one hand the preference for NADPH/NAD and on the other hand the major affinity for NADPH, authors speculate that in normal physiological conditions, where NADPH and NAD are the prevalent forms, Kvβ would be interacting with NADPH (Kilfoil et al., 2013). However, conditions leading to a decrease in the concentration of NADPH and an increase in NAD (e.g. hypoxia and oxidative stress) may result in changes in the nature of the Kvβ-nucleotide binary complex (Coppock et al., 2001, Ishii et al., 2013). All this data is strongly concomitant with the studies developed on other AKR members..

- ***AKR activity regulation of Kv channels***

Upon oligomerization with the channel Kvβs form tetrameric structures with four-fold symmetry (figure 14) matching the one seen for the conducting complex Kv channel. (Long et al., 2005). In those compositions, the active centre of their aldoketoreductase activity is facing out of the axis. The analysis of the crystal structure leads to detect a NADPH nucleotide in the Kvβ structure while its interacting with the α subunit (Gulbis et al., 1999).

Considering the specificity of this enzymatic function, the putative effects on the channels were analysed. Several different modulations derived from Kvβ AKR function were discovered. It was determined that $NADP^+$ impairs the inactivation of Kvβ1 on Kv1.1 as well as Kvβ3 on Kv1.5 (Pan et al., 2008a, Tipparaju et al., 2012). It is also impeding the Kvβ2-hyperpolarizing shift on Kv1.5 activation. And, concomitantly, in single channel experiments, the mean open time and the open probability was increased for Kv1.5+Kvβ1.3 and Kv1.1+Kvβ1.1 (Tipparaju et al., 2005, Pan et al., 2008a). Different mutants were generated on Kvβ1.3 wild type sequence with gradable effects on its affinity for NADPH. It was seen that the higher the impairment of the interaction, the fewer the inactivation effect on Kv1.5. The addition of NAD^+ to the intracellular solution in COS cells expressing both Kv1.5 and Kvβ1.3 exert the same phenotype. The mutants that are exerting the stronger change in NADPH affinity, modified also the expression pattern: lesser extend of colocalization with Kv1.5 was observed (Tipparaju et al., 2005). So, those results indicated that pyridine nucleotides can bind directly to Kvβ active site and that $NADP^+$ attachment induces conformational modifications that reduce the inactivating or the hyperpolarising effect, while NADPH preserves or promotes inactivation. Because NAD^+/NADPH ratio is sensitive to oxygen concentration, Kvβ-mediated effects on Kv channels could represent an oxygen-sensing mechanism (Chapalamadugu et al., 2015, Ishii et al., 2013). Considering the Kv distribution, Kvβ subunits can enhance the traffic of Kv1.2, but none of the mutants for the cofactor binding site are able to exert this function anymore. Concomitantly, the Kv1.2 axonal traffic its impaired when Kvβ1 or Kvβ2 cofactor binding mutants are coexpressed(Campomanes et al., 2002).

Both Kvβ1 and Kvβ2 display measurable catalytic activity with model and endogenous aldehydes. Enzyme kinetic studies have shown that like other AKRs, Kvβ uses the active

site tyrosine residues (Tyr-90) for acid-base catalysis and that the catalytic cycle follows an ordered reaction scheme in with the bond-breaking step is rate-limit. Thereby, it was proved that 4-CY (Kvβ substrate) is able to decrease the rate of channel inactivation of Kv1.4+ Kvβ2.1 and also Kv1.1+Kvβ1 (Weng et al., 2006, Pan et al., 2008a). Concomitantly, when catalytic residues were mutated, they were not conferring rapid inactivation on Kv1.5 at the same wild type's extension (Bahring et al., 2001). Upon traffic analysis, Kvβ2, is not exerting its trafficking modulation on Kv1.4 when this residue is substituted for a phenylalanine. However, neither this change in Kvβ2 nor in Kvβ1 is modifying the traffic control on Kv1.2. Only when switched for alanine, the effect is completely abolished. This was shown to be important also for the proper axonal targeting of Kv1.2 (Campomanes et al., 2002).

By mutating the lysine, also placed at the active site, which diminishes the catalytic rate, slows inactivation of Kv1.1+Kvβ1currents. This effect could be due to the production of $NADP^+$ from NADPH in the reaction (Pan et al., 2008a). However, other authors defend that neither some residues involved in the orientation of the nicotinaminic ring nor the catalytic site are changing the extension of inactivation of Kvβ2 on Kv1.4 (Peri et al., 2001).

Even the Kvβ molecular determinants involved in the interaction with Kv channels are placed in the N-terminus, the electron microscopy single particle analysis of the Shaker channel bound to Kvβ2 shows that the C-terminus domain is in close contact with the Kvβ active site (Sokolova et al., 2003). The removal of this channel end in Kv1.5 leads to a prevention of the Kvβ2 and Kvβ3 regulation. It presents a higher affinity for interacting with NADPH-bound Kvβ2 rather than NADP-bound one (Tipparaju et al., 2012, Pan et al., 2008a). However, unlike Kv1.5, the C-terminal domain of Kv1.1 doesn't affect the Kvβ1 modulation (Pan et al., 2008).

Far from the typical domains of the aldoketoreductases, at the N-terminus, it was described that the cysteine in position 7 of Kvβ1.1 sequence leads to an insensibilization of the inactivation to the redox state of the cell(Rettig et al., 1994).

Collecting all the results, coupling of Kv channels to oxidoreductases subunits can conduct to two different situations yet to be completely deciphered. On one hand, Kvβ proteins would confer redox sensitivity coupling the intracellular redox state with the membrane excitability. On the other hand, voltage-dependent changes in the Kv channel could regulate Kvβ catalysis by affecting the configuration of the Kvβ active site (Kilfoil et al., 2013).

1.3.1.2 Kvβ subunits

From the crystal structure, as we mentioned before, Kvβ family forms a fourfold symmetric tetramer of TIM barrels, each comprising eight parallel β-strands that build a central core with α-helices surrounding the perimeter of the barrel (Gulbis et al., 1999).

The Kvβ structure shows some other properties similar to those previously observed in the T1 tetramer structure: both have intersubunit interfaces that are mediated

predominantly by polar interaction, and both have a central water-filled cavity that is line with positively charged residues. The sizes of these cavities indicate that ions probably do not pass through these regions, but the ion-conducting pathway should reside between the T1 tetramer and the inner leaflet of the membrane (Biggin et al., 2000).

The oligomeric structure of Kvβs was under debate for some years. On one hand it was described that Kvβ2, but not Kvβ1 subfamily members, had the ability to form homo and heteroligomeric structures. The theory behind this hypothesis implied that the N-terminus domain of Kvβ2 was necessary, and absent in Kvβ1, to interact with the core domain (Xu et al., 1998). Thereby, Kvβ2 was presumably able to inhibit the Kvβ1 modulation on different Kv channels due to its ability to form homo and heteroligomers. This condition leads to a dose-independent control of their effects (Xu and Li, 1997). The tetrameric structure of Kvβ2 was then confirmed by atomic force and electron microscopy. They also detected some trimeric structures that assume to be intermediate stages of the complexation (van Huizen et al., 1999). However, implementing the same technique, another laboratory could detect oligomeric formations of the Kvβ1.2 member (Accili et al., 1997a) . The theory was confirmed by a detection of intermediate inactivating currents when Kvβ1.2 and Kvβ1.2 mutant for the inactivating ball were mixed. The different results obtained at the two laboratories could be due to differences in the affinity for forming each homoligomer (of Kvβ1 and Kvβ2) or to different Kvβ stoichiometry. However, no more investigation was addressed to solve this disjunctive.

The interaction with Kv channels is thought to happen early in the biosynthesis pathway. Some evidences point out to a coimunoprecipitation with mature and immature Kv forms (Nagaya and Papazian, 1997). Some specific combinations of Kvβ-Kv channels are enhancing the traffic to the plasma membrane, observed in an increase on the maturation form and inferring an early complex formation (Shi et al., 1996).

Three members are included in this family: Kvβ1, Kvβ2 and Kvβ3. Each of them conserve a core domain at the C-terminus (>85% of similarity) and a variable N-terminus (Pongs and Schwarz, 2010).

1.3.1.2.1. Kvβ1

This subfamily presents three different alternative splicing variants: Kvβ1.1, Kvβ1.2 and Kvβ1.3. All of them share an N-terminus with a sequence similar to that of the α- subunit N-terminal inactivation ball, which folds up into a compact domain by itself (figure 19). The Kv-Kvβ combination will determine the final current exhibited (Pongs and Schwarz, 2010).

It is widely and heterogeneously expressed an adult rat brain. By analysing the mRNA, a very high density of Kvβ1 expression was observed in the striatum, nucleus accumbens, olfactory tubercle, CA1 subfield of the hippocampus, and entorhinal and posterior cingulate cortices, and in several midbrain and brainstem motor nuclei. Intermediate levels of Kvβ1 were detected in the piriform cortex; neocortex; medial septal-diagonal band complex; anterior, mediodorsal, and ventral tier thalamic nuclei; and the cerebellar cortex and deep nuclei. Low levels of Kvβ1 expression were observed in the globus

pallidus and hypothalamus. At a cellular level, we can find them in cell bodies, dendrites, juxtaparanodal regions of myelinated axons, and terminal fields of several major projection systems (Rhodes et al., 1996). They are also expressed in immune system cells, such as T- and B-lymphocytes as well as macrophages (Autieri et al., 1997). Upon different stimuli, Kvβ1.1, Kvβ1.2 and Kvβ1.3 are regulated in the later one. While M-CSF is increasing the expression of all of them, LPS and TNFα lead to different Kvβ expression. LPS elevates Kvβ1.1 and Kvβ1.3 expression with a major pic at 6h while Kvβ1.2 is decreasing. TNFα decreased Kvβ1.2 in a similar extension, and increase the other two subunits with a pic at 24h (Vicente et al., 2005).

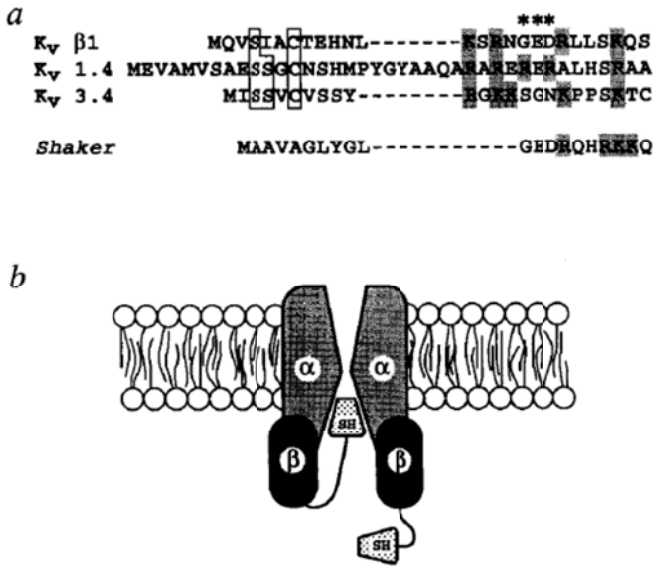

Figure 19. Inactivating ball-and-chain determined at Kvβ N-terminus. A. Sequence alignment of inactivating regions on Kvβ1, Kv1.4 and Kv3.4. B. Blocking mechanism exerted by Kvβ1 on Kv channels (Rettig et al., 1994).

The **Kvβ1.1** is the shortest member of the Kvβ1 subfamily and it was the first member identified (together with Kvβ2) when isolating DTX-sensible channels (Scott et al., 1990, Scott et al., 1994). It is widely expressed at the nervous and cardiac system (Pongs and Schwarz, 2010). It has been described that Kvβ1.1 could increase its expression upon development in the nervous system, enhancing inactivating currents in mature hippocampal neurons (Falk et al., 2003, Butler et al., 1998). However, other laboratories found a decrease in the adult hippocampus compared with post-natal day 9(Downen et al., 1999). Its expression is regulated in macrophages, as previously described, but also in T- and B- lymphocytes. Upon IL2 treatment, there is an increase in T-lymphocytes around the 6h, and the exposure of B-lymphocytes to LPS enhances a similar incremented expression (Autieri et al., 1997).

It confers rapid inactivation to Kv1.1, Kv1.2 and Kv1.5, but not to Kv1.3 and Kv1.6. The inhibition on Kv1.5 was almost complete, while on Kv1.1 and Kv1.2 a significant steady-

state current remained. Its observable a small initial inactivation component on Kv1.3 current (Heinemann et al., 1996). Other laboratories suggest that this is not even present (McCormack et al., 1999). It generates a faster inactivation on Kv1.4, and upon coexpression both closing domains compete for the interaction site (Leicher et al., 1996). It is also affecting the recovery from inactivation, increased under coexpression in a twofold level of Kv1.4 (Rettig et al., 1994). No effects on C-type inactivation were reported for this channel (McIntosh et al., 1997). The absence of N-type inactivating effect on Kv1.6 it's due to the presence of a region called N-type inactivation-prevention that impairs, acting as a dominant negative, this Kvβ1.1 effect (Roeper et al., 1998).

The analysis of the ball-and-chain domain of Kvβ1.1 has elucidated that inactivation occurs through the interaction of the Kv channel with the fully extended N-terminal peptide. The occlusion gate would be formed by two regions: one hydrophobic and another hydrophilic. The hydrophobic region of the peptide would extend from the cavity to the intracellular entryway, while the hydrophilic peptide region would emerge from the pore and interact with the aqueous protein surfaces lining the cage formed above the T1 domain.

By this mechanism, the A-type channels would move from open (O) to inactivated (I) passing through one different state (O'), when the hydrophilic region is contacting its receptor zone (figure 20) (Zhou et al., 2001).

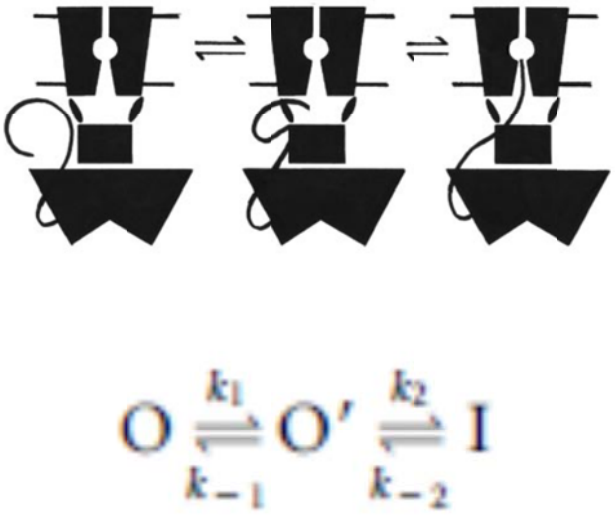

Figure 20. Two step model for Kvβ1 subfamily members' Kv blocking. A. Schematic representation of both parts involved in the inactivation. B. Equilibrium of the three putative Kv-Kvβ complex"s states (Zhou et al., 2001)

Even inactivation is the most popular function, some other effects can be observed from the mixture Kvβ1.1/Kv channels. Some laboratories have found that Kvβ1.1 can exert a shift in the activation to more depolarizing voltages when coexpressed with Kv1.5, while others defend that there is not such an effect (Leicher et al., 1996, Heinemann et al., 1995). The coassociation with Kv1.4 can accelerate the activation time constant up to two fold;

however the voltage dependence of Kv1.4 is not appreciably altered (McIntosh et al., 1997).

It has been proposed that it can increase the expression of Kv1.2, Kv1.3, Kv1.4 and Kv4.3 at the cell surface (McCormack et al., 1999, Shi et al., 1996, McIntosh et al., 1997). But, on Kv1.5 is demonstrated the contrary effect: the current density is decreased upon coexpression with Kvβ1 core (Accili et al., 1997b). For Kv4.3, as well as on Kv4.1 and Kv4.2, no major inactivating events are exerted by Kvβ1.1 and the interaction among them is placed in the C-terminus of the Kv4 channels (Yang et al., 2001, Perez-Garcia et al., 1999, Heinemann et al., 1996).

Kv channels modulation by this accessory subunit can, at the same time, be controlled by other insults. It has been demonstrated that PKC and PKA can influence the current evoked by some Kv alpha and Kvβ combinations. Thus, activation of PKA leads to a Kv1.1 phosphorylation that enhances Kvβ1.1 effect, while PKC would reduce its extent by dephosphorisation of the same residue (Levin et al., 1996b, Levy et al., 1998, Martens et al., 1999).

Not only phosphorylation has been demonstrated to present an effect on Kvβ1.1 function, but also lipid interaction. PIP_2 has the ability to immobilize the ball-and-chain domain of Kvβ1.1 and thus preventing the block of the Kv1.1 channel. Neither the activation nor the C-type inactivation was modified by the presence of this lipidic compound (Oliver et al., 2004). Moreover, it has been proved that Kvβ1.1 effect on Kv1.1 is mitigated by the increase of calcium intracellularly. The calcium-sensing domain is placed in the N-terminus of Kvβ1.1 but the specific determinants remain unkown. Both PIP_2 and Ca^{2+} are stimulus that can disappear restoring the effect of Kvβ1.1 on the Kv channels, and thus allowing a sporadic plasticity of the Kv currents (Jow et al., 2004).

It was predicted and widely accepted that Kvβs are a cytoplasmic family due to the absence of putative transmembrane domains and possible glycosylation residues. However, Kvβ1.1, but not Kvβ2.1, can interact with actin-based citoeskeleton driving this protein close to membrane regions (Nakahira et al., 1998). The disruption of microfilament results in increased Kvβ1.1-induced inactivation, probably due to the release of the N-terminus inactivating domain (Levin et al., 1996a).

The knock-out mice for Kvβ1.1 revealed a milder effect compared with the previous expectations. Upon spike trains, hippocampal neurons exhibit a broadening on the response spikes. The $Kv\beta1.1^{-/-}$ revealed a reduction on the recorded broadening. This effect leads to a smaller amplitude of the slow hyperpolarization, and this links with fewer Ca2+ dependent processes. The learning was, actually, affected, but not all types of it. The $Kv\beta1.1^{-/-}$ mice could learn but there is an absence of implementation of the learning to a new situation. It was called: the flexible learning (Giese et al., 1998).

The **Kvβ1.2** is the member with a medium size. Its expression has been detected in nervous and cardiac system as well as Kvβ1.1. It is present at atrium and ventricle, skeletal muscle, lung and kidney.

Kvβ1.2 interacts with Kv1.2, Kv1.4 and Kv1.5 at cardiac tissue. It confers rapid-inactivation to Kv1.5, but with less potency that Kvβ1.1 (Leicher et al., 1996), comparable

to the effect on Kv1.2 (Accili et al., 1997b). On Kv1.4, increases the voltage-dependent component of inactivation, reduces the peak current and shifted steady-state inactivation towards hyperpolarized potentials (Accili et al., 1998). The inactivation observed for Kvβ1.2 is not only N- but also C-type. This phenomena was detected also in Shaker channels and it is paradigmatically exerted by Kvβ1.2 N-terminus domain, linking to the proposed relationship between N and C-type domains for the A-type channels (Morales et al., 1996).

Similar to Kvβ1.1, Kvβ1.2 can increase the current density of Kv1.2 but it does not affect the activation parameters. However, the deactivation of this channel was slowed (Accili et al., 1997b).

PKC can also modulate Kvβ1.2 effects. It can lead to a specific decrease of Kv1.5 current only when it was coexpressed with Kvβ1.2 and not with Kvβ1.3 (Williams et al., 2002). On the other hand, those currents were not modulated by PKA (Kwak et al., 1999). Kvβ1.2 has been described to interact with KChAP through its C-terminus domain, and both can interfere in the other's function. KChAP impairs the inactivation on Kv1.5 by Kvβ1.2, and the later can reduce the chaperon effects on Kv4.3 and Kv2.1 of the former (Kuryshev et al., 2001).

The **Kvβ1.3** is the longest member of Kvβ1 subfamily and it was the latest identified (England et al., 1995a). Its expression has been detected in nervous system and cardiac tissue. It is thought to form a hairpin structure at the N-terminus that will occlude the pore interacting with amino acids deep on it.

It exerts a rapid but incomplete inactivation on Kv1.5, as well as Kv1.1, and it also modifies the voltage dependence of Kv1.5 channel opening by shifting the midpoint of activation 8-20mV in the hyperpolarizing direction. In addition, deactivation is slowed (by 2.4-fold) and peak current is depressed five-fold by what may be an ultrafast inactivation mechanism, without a decrease in cell surface channel protein (England et al., 1995a, Uebele et al., 1998) Moreover, upon coexpression, Kvβ1.3 changes its distribution to exhibit a more membrane-like phenotype (Tipparaju et al., 2007). Kvβ1.3 has been described to modify Kv1.5 in different ways under pharmacological treatments. It generates a diminution in the sensitivity of the channel to the block induced by antiarrhythmic drugs and local anesthesics, and a decrease in the degree of stereoselective blockage (Gonzalez et al., 2002, Decher et al., 2005, Arias et al., 2007)

Some phosphorilation events on them have been reported. While all the Kvβ1 subfamily members possess a conserved PKA phosphorilation predicted site, Kvβ1.3 shows two more in the variable N-terminus. Upon Kvβ1.3+Kv1.5 coexpression, PKA activation slowed fast inactivation with a small peak of K+ current. This effect leads to an increase in total Kv1.5 currents (Kwak et al., 1999). On the other hand, the Kvβ1.3 requires the phosphorilation of PKC to exert its inactivating function on Kv1.5. The inhibition of PKC leads to some Kv1.5-like currents without the loss of the complete complex (David et al., 2012).

Moreover, Kvβ1.3 has a molecular determinant that allows it to couple with PIP_2. Similar to Kvβ1.1, the interaction abolishes the inactivating properties on Kv1.5. PIP_2 is, then,

immobilizing and preventing the ball-and-chain domain from entering the central cavity to induce N-type inactivation (Decher et al., 2008).

1.3.1.2.2. Kvβ2

This subfamily present two different members: Kvβ2.1 and Kvβ2.2. Unlike Kvβ1.1 family, those two members differ from very few aminoacids. The member Kvβ2.1 presents 14 more aminoacids (STRYGSPKRQLQFY) at position 25 that are missing in Kvβ2.2 (figure 21). The first member discovered was Kvβ2.1, along with Kvβ1.1, and the main research performed has been about this member or the common core of all the Kvβs, assuming similar effects to Kvβ2.2. Unlike Kvβ1 family, it does not present any ball-and-chain inactivation domain (Pongs and Schwarz, 2010).

```
Kvβ2.1   MYPESTTGSPARLSLRQTGSPGMIYSTRYGSPKRQLQFYRNLGKSGLRVSCLGLGTWVTF  60
Kvβ2.2   MYPESTTGSPARLSLRQTGSPGMIY-------------RNLGKSGLRVSCLGLGTWVTF  46

Kvβ2.1   GGQITDEMAEQLMTLAYDNGINLFDTAEVYAAGKAEVVLGNIIKKKGWRRSSLVITTKIF  120
Kvβ2.2   GGQITDEMAEQLMTLAYDNGINLFDTAEVYAAGKAEVVLGNIIKKKGWRRSSLVITTKIF  106

Kvβ2.1   WGGKAETERGLSRKHIIEGLKASLERLQLEYVDVVFANRPDPNTPMEETVRAMTHVINQG  180
Kvβ2.2   WGGKAETERGLSRKHIIEGLKASLERLQLEYVDVVFANRPDPNTPMEETVRAMTHVINQG  166

Kvβ2.1   MAMYWGTSRWSSMEIMEAYSVARQFNLTPPICEQAEYHMFQREKVEVQLPELFHKIGVGA  240
Kvβ2.2   MAMYWGTSRWSSMEIMEAYSVARQFNLTPPICEQAEYHMFQREKVEVQLPELFHKIGVGA  226

Kvβ2.1   MTWSPLACGIVSGKYDSGIPPYSRASLKGYQWLKDKILSEEGRRQQAKLKELQAIAERLG  300
Kvβ2.2   MTWSPLACGIVSGKYDSGIPPYSRASLKGYQWLKDKILSEEGRRQQAKLKELQAIAERLG  286

Kvβ2.1   CTLPQLAIAWCLRNEGVSSVLLGASNADQLMENIGAIQVLPKLSSSIIHEIDSILGNKPY  360
Kvβ2.2   CTLPQLAIAWCLRNEGVSSVLLGASNADQLMENIGAIQVLPKLSSSIIHEIDSILGNKPY  346

Kvβ2.1   SKKDYRS  367
Kvβ2.2   SKKDYRS  353
```

Figure 21. Sequence alignment of human Kvβ2.1 and Kvβ2.2. The aminoacidic part highlighted in yellow is the only difference between them, missing at Kvβ2.2.

Kvβ2 is expressed in the nervous system, from where it was isolated. By mRNA expression it is known that the highest levels are presented in the piriform cortex, hippocampal formation, and in layer II of the entorhinal cortex. Somewhat lower levels are present in the neocortex, medial septal-diagonal band complex, and the anterior, VPM, and VPL nuclei of the thalamus. Low levels of Kvβ2 expression were observed in the remaining thalamic nuclei and in the striatum, globus pallidus and hypothalamus. The nervous intracellular distribution is the same than for Kvβ1.1 (Rhodes et al., 1996). During the development, Kvβ2 is increasing from low post-natal levels, to the achievement of adult brain levels at the third post-natal week (Downen et al., 1999). And not only is expressed

in the nervous system but also in immune system cells such as lymphocytes and macrophages. Similar to Kvβ1.1, upon stimulation with IL-2 on T-lymphocytes or LPS on B-lymphocytes, there is an increase in the expression of Kvβ2, reaching the maximum at 24h(Autieri et al., 1997). However, other authors cannot distinguish the Kvβ2 expression pre and post-activating treatment (McCormack et al., 1999). Regarding the macrophage physiology, Kvβ2 increases at 24h when treated with M-CSF and LPS, but no changes are taking place with TNF-α (Vicente et al., 2005). This subunit was also isolated from cardiac tissue (England et al., 1995b).

The absence of inactivating domain made forcedly Kvβ2 effects the more different from the Kvβ family. It presents moderate functions on Kv1.5: shifting the steady-state activation and inactivation without inducing rapid inactivation. It also enhances the degree of slow inactivation (Heinemann et al., 1996). The presence of this subunit in some cell lines was leading to confusion about the properties of the Kv1.5 (Uebele et al., 1996). No observable kinetic effects are detected when Kvβ2 is coexpressed with Kv1.1 or Kv1.3 (Heinemann et al., 1996, McCormack et al., 1999). However, Kvβ2 is surprisingly able to enhance N-type inactivation of Kv1.4 as well as it can accelerate the activation time constant (Accili et al., 1998). Unlike Kv1.5, there is not an appreciable shift in the voltage dependence of Kv1.4 activation when coassociated with Kvβ2. The slight tendency for inactivation of Kv1.4 to lengthen with depolarization was lost upon the subunit presence. In this specific case, Kvβ2 is as effective as Kvβ1.1 to enhance inactivation (McIntosh et al., 1997).

The interest on Kvβ2 increased when they observed that is the most expressed Kvβ member of the family, and no apparent function was attributable due to the missing inactivating domain (Rhodes et al., 1996). Some studies point to a chaperone activity helping on proper protein folding and/or alpha-subunit assembly and thus enhancing the transport from ER to Golgi and finally to cell surface. Kvβ2 is known to interact with unmature *Shaker* forms when the conventional pathway is blocked (Nagaya and Papazian, 1997). Concomitantly, when Kvβ2 and Kv1.2 or Kv1.1 are coexpressed, the channel exhibits a reduced turnover, a major efficiency of N-linked glycosylation and a higher presence of this one at the cell surface (Shi et al., 1996). Similar evidences were found for Kv1.3 and Kv1.4, were current density is increased when coexpressed with the subunit (McCormack et al., 1999, McIntosh et al., 1997). Kv4.3 cell surface expression is enhanced, without any other electrophysiological modification (Yang et al., 2001). And finally TREK1 and TRPV1 can interact also with Kvβ2 and both exhibit an increase membrane targeting upon coexpression (Bavassano et al., 2013, Kisselbach et al., 2012) .

Once the chaperone function was accepted, the knock-out mouse for Kvβ2 was produced. It was exhibiting occasional seizures, shortened life spans and cold swim-induced tremors. When effects on Kv1 were analysed, no major changes in the glycosylation of those proteins was observed, Concomitantly, Kv1.2 was properly concentrated in the cerebellar cortex. They did not observe any compensatory up-regulation of Kvβ1 sufamily. While it was clear that there were effects because of the absence of Kvβ2, it was unlikely to keep in a chaperone function theory (McCormack et al., 2002). Further experiments support the idea that the effect of a null mice for Kvβ2 depends on the genetic background. Combination of Kvβ2 and Kvβ1.1 null protein in a mice, exaggerates the Kvβ2 general phenotype. However, Kv1 distribution seemed to be unaltered (Connor et al., 2005).

Concomitantly, it was observed that neither *Shaker* channel nor Kv1.5 membrane expression presented any change upon coexpression with Kvβ2 (Nagaya and Papazian, 1997, Accili et al., 1997b).

Thus, the function of Kvβ2 is still controversial. Some patients with 1p36 deletion syndrome present a correlation between the absence of Kvβ2, and the presence of epilepsia or epileptic activity on electroencephalogram (Heilstedt et al., 2001). The absence of a proper membrane trafficking could give an explanation of this phenomena. Further evidences have been collected that support chaperone and trafficking helper theory. It was described that Kvβ2 cannot, unlike to Kvβ1.1, interact with the actin-based cytoskeleton (Nakahira et al., 1998). However, Kvβ2 was found to interact with EB1, a protein that specifically track the rapidly growing MT plus end and concentrate in distal axons, as well as with KIF3/Kinesin II. Thus, Kvβ2 can travel to the axonic end independently of Kv1.2 (Gu et al., 2006). Even this channel can traffic in the absence of Kvβ2, coexpression increases the velocity of the anterograde traffic (Gu and Gu, 2010). Moreover, CDK-mediated phosphorylation of Kvβ2 destabilises the interaction with EB1 protein, provoking a release of Kv1/Kvβ2 vesicles from their association to microtubules (Vacher and Trimmer, 2011, Vacher et al., 2011).

Kvβ2 is not only related to CDK, but also to members of the PKC family. It has been described that ZIP1, ZIP2 and ZIP3 can interact with Kvβ2. Those proteins are able to form homo and heterodimers and to interact with PKCζ, thus increasing the phosphorylation state of Kvβ2 (Gong et al., 1999, Croci et al., 2003, Martens et al., 1999). But it is not the only member able to enhance the phosphorylation: it was proposed a PKCα effect at the N-terminus of the Kvβ2 (Liu et al., 2003). However, other laboratories do not detect PKCα role on the subunit , but PKCγ, PKCδ and PKCε (Wang et al., 2004b). Upon coexpression with Kv1.5, the modulating effects of Kvβ2 are not altered when PKC activation is stimulated (Martens et al., 1999). Other posttranslational modifications are exerted on this subunit. It has been described that both GIP (gucose-dependent insulinotropic polypeptide) and GLP-1 (glucagon-like peptide-1) can enhance the phosphorylation and acetylation of Kvβ2 and Kv1.5, leading to an increase on protein-protein interactions between them (Kim et al., 2013).

As well as Kvβ1.2, Kvβ2 has the capability to interact with KChAP, thus the latter being able to counteract the effects of Kvβ2 on Kv1.4 (Kuryshev et al., 2001).

The interaction between K channels and Kvβs is placed at the N-terminus of the conducting proteins (Pongs and Schwarz, 2010). However, from the crystal structure it is detectable that the C-terminus domain is in close contact with those subunits (Gulbis et al., 1999). Actually, through electron microscopy there are detectable changes in the C-terminus of the *Shaker* channel (Sokolova et al., 2003). Similar to *Shaker*, Kv4.3 channels interact with Kvβ2 through the carboxy terminal domain (Yang et al., 2001). Concomitant results were found for the Kv1.5 in combination with Kvβ2, since the absence of C-terminus of the channel impairs the changes provoked by oxidoreduction modifications (Tipparaju et al., 2012).

The possible modulation of Kvβ effects on Kv channels through a pharmacological approach was thought to be important since the effects on them started to be reported.

Cortisone was showed to interact with Kvβ2 at two different localisations in the molecule: one close to the bound NADPH and another at the interface between Kvβ and Kv α-subunit. Thus, cortisone is able to dissociate the complexes that are already formed (Pan et al., 2008b). Posteriorly, 25 analogues were tested and fluticasone was identified as potential lead for designing more efficient small molecules that might influence channel function by dissociating the Kv1-Kvβ assembly (Pan et al., 2012). Further studies demonstrated that compounds like DOPAC (a neurotransmitter metabolite), rutin hydrate and resveratrol exhibited the highest inhibition effect on Kvβ2 reductase activity (Alka et al., 2014).

1.3.1.2.3. Kvβ3

Cloned from rat brain, it presents a unique member at the human genome. Similar to Kvβ1 subfamily its sequence codes for an inactivating domain (Pongs and Schwarz, 2010, Kilfoil et al., 2013). It is expressed mainly in the olfactory bulb and in thalamic nuclei, but not in hippocampal field, dentate gyrus and corpus striatum.

Originally Kvβ3 was supposed to increase Kv1.4 inactivation and recovery from the inactivation. No other effect was detected on Kv1.1, Kv1.5, Kv1.6 or Kv.2.1. This modulation observed was controlled by the redox changes in the medium. (Heinemann et al., 1995, Heinemann et al., 1996). They considered that Kvβ3 had a sequence of 27 amino acids that exert a NIP-like function on the rest of the channels. They would be impeding the ability of its own ball-and-chain inactivating domain to recognize the locus on the Kv channel (Pongs et al., 1999). However, when Kvβ3 was transfected in mammalian cells, Kv1.5 was modified by Kvβ3. The changes implied increment in the rate of inactivation, hyperpolarising shift activation and diminishing of the time-to-peak activation. As described for Kv1.4, this modulation was dependent in the redox state of Kvβ and dependent on the C-terminus of the channel (Tipparaju et al., 2012).

1.3.2. *KCNE family*

KCNE family is formed by small auxiliary subunits (14 – 20kDa) that are single spanned transmembrane proteins. The N terminus domain is extracellular and presents some glycosylation sites. Up to five members have been described to form the family encoded by the *kcne* gene. The sequences do not reveal a conserved specific protein end; sequence variations encompass the entire KCNE molecules (Pongs and Schwarz, 2010). The founding member, MinK for "minimal potassium channel", which is encoded by the *kcne1*, was initially reported to represent the minimal or smallest protein that could form a K channel (Takumi et al., 1988). Subsequent in vitro studies showed that the currents detected after KCNE1 transfection were due to the modulation of endogenous channels at *Xenopus laevis* (Blumenthal and Kaczmarek, 1994, Wang and Goldstein, 1995, Sanguinetti et al., 1996). Some years later, *kcne2, kcne3, kcne4* and finally, *kcne5* were described by using Basic Local Alignment Search Tool (BLAST) screening of online libraries of expressed sequence tags (figure 22) (Abbott and Goldstein, 1998, Piccini et al., 1999).

Initially, the proteins resulting from those genes were called MiRPs (MinK-related proteins) and finally KCNEs.

As a protein family is ubiquitously expressed, but each of its members will present a higher or lower expression depending on the tissue. Few comparative studies of KCNE expression are published. Since all KCNE members have been detected in myeloid and lymphoid lineages, our laboratory contributed recapitulating and analysing the abundance of those subunits in healthy and cancer tissue derived from the immune system. For instance, while KCNE1 expression increases in some cancers, KCNE2 and KCNE4 decrease (Sole and Felipe, 2010). Moreover, in further investigations, our laboratory demonstrated and compared the expression of this family in macrophages, T and B-lymphocytes. This study was developed analysing the expression throughout the cell cycle progression and upon some pharmacological treatments. We, thus, demonstrated that KCNE peptides are cell cycle dependent, and distinct specific insults differentially regulate their expression (Sole et al., 2013, Sole et al., 2009).

The most well-known described effects have been for KCNE on Kv7.1 channel gating. However, KCNE interaction with Kv channels is highly promiscuous: they are able to modulate a wide range of potassium channels. Kv1, Kv2, Kv3, Kv4, Kv7, HCN and HERG are described to interact with this family (Pongs and Schwarz, 2010). Each KCNE isoform is now known to have the capacity to regulate more than one type of Kvα subunit and many Kvα subunit can be regulated by more than one KCNE peptide (perhaps at the same time) (Abbott, 2015). Moreover, mutations in *kcne* genes are associated with hereditary, especially cardiac diseases. So, as evidenced by their role in health and disease, those subunits are considered important modulators of the final channelosomes behaviour and cell physiology (Abbott et al., 2001, Sole and Felipe, 2010, Lundquist et al., 2006).

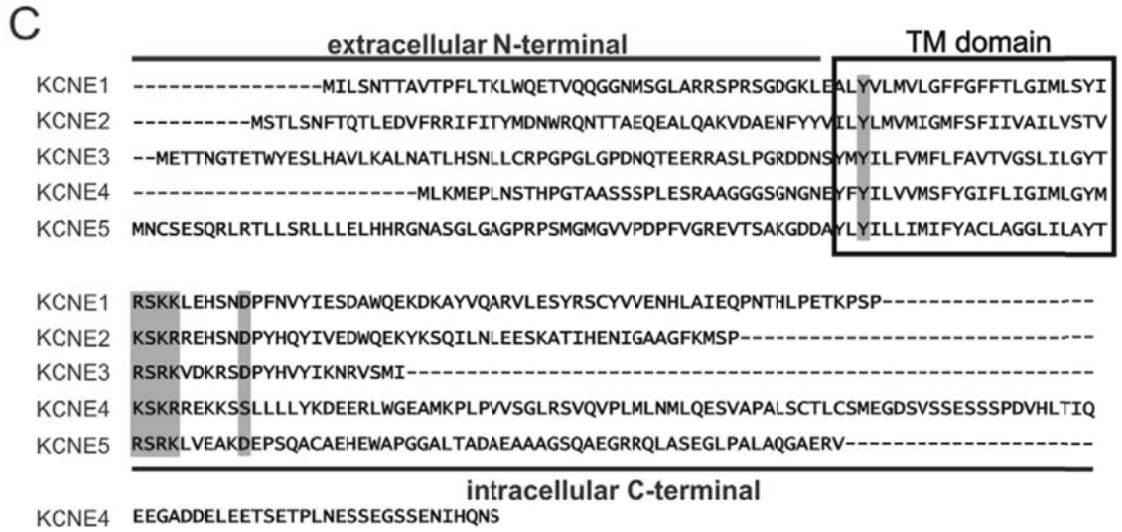

Figure 22. Sequence alignment of the five human KCNE members. Note that KCNE4 presents the largest intracellular domain (Abbott, 2016a).

Association and stoichiometry between channels and KCNE proteins has been under intense investigation and debate. Regarding the intracellular compartment where the complex was formed, some laboratories stablished an early endoplasmic reticulum association for those proteins (Chandrasekhar et al., 2006). However, delivery of KCNE subunits at the plasma membrane was found to modulate channels already present at the cell surface (Grunnet et al., 2002). It was shown that some KCNE members present the ability to traffic to the plasma membrane enforcing the lateral interaction of those proteins (Jiang et al., 2009). Moreover, stoichiometry of the complexes has been also under discussion. Two main theories were considered suggesting that (i) four α-subunits were assembled with two KCNE in a fixed composition or (ii) Variable number could be found in a complex depending on their total amount. Several evidences have been presented supporting both hypothesis, but lately the second supposition of a variable stoichiometry, up to 4 KCNEs/complex, is gaining more strength (Chen et al., 2003, Morin and Kobertz, 2008, Nakajo et al., 2010).

The molecular determinants governing the channel-KCNE interaction have been studied also mainly in the complexes formed by KCNE1 and Kv7.1. Several reports focus the attention on the C-terminal domain of KCNE as a possible player in this complexation. Initially it was described that it is necessary for the channel modulation, but not for the interaction (Tapper and George, 2000). However, other studies determined that it could be basic for the positioning and anchoring of this peptide to the channel (Melman et al., 2004). Finally, further investigations concluded that it is implied not only for the channel attachment but also for the open state destabilisation and kinetics of deactivation (Chen et al., 2009).

Residues at the transmembrane domain of both KCNE1 and KCNE3 have been mapped as modulator entities of the Kv7.1 channel (Melman et al., 2002). On the other hand, different parts of the channel are involved in the interaction with diverse KCNE peptides. Some evidences point out that the carboxi-terminal domain of the channel is in close proximity to the same domain in KCNEs. Moreover, anchoring functions are thought to lie in this domain (Melman et al., 2004). Different residues along the S5-S6 domain are required for modulation exerted by either KCNE1 or KCNE3 (Panaghie et al., 2006). A couple of residues placed at the C-terminal domain of the channel are needed for the inhibition induced by KCNE4 (Vanoye et al., 2009).

The localization of KCNE1 within the complex was initially placed on the pore, but deeper and further investigations revealed a more distal position (Wang et al., 1996, Tai and Goldstein, 1998, Chung et al., 2009, Tapper and George, 2000). Outside the pore, but in close proximity, is interacting with S1, S5 and S6 residues (Melman et al., 2004, Panaghie et al., 2006, Wu et al., 2010b). Actually, KCNE1 alters the coupling between the voltage sensor and the KV7.1 gate by constraining it (Wu et al., 2010b, Wu et al., 2010a). The obtainment of the NMR-based KCNE1 structure leaded the molecular dynamics model of Kv7.1 and KCNE1 in two states: open and closed. The analysis of the close state confirmed that KCNE1 restricts the movement of S4-S5 and is thought to press downward the cytosolic end of S6 domain to keep the non-conducting state. However, on the opened conformation, KCNE1 forms an interface with the domains already described: S1, S5 and S6 (Kang et al., 2008).

1.3.2.1 KCNE1

KCNE1 is an auxiliary subunit of 15kDa approximately with two splice variants identified: kcne1a and kcne1b. The latter is a specific cardiac isoform and the former is ubiquitously expressed (Lundquist et al., 2006). *Kcne1* transcripts can be found in kidney, eye, gastrointestinal tract, peripheral blood leukocytes and auditory epithelium. It was the first recognized member of the KCNE family, and it was identified as the responsible for the cardiac current $I_{ks.}$ However, as mentioned before, further studies confirmed that it was modulating the endogenous Kv7.1 currents expressed in *Xenopus oocytes*. The slow component of the delayed rectifier current (I_{ks}) is essential for the cardiac repolarization and was then stablished to be due to the combination of Kv7.1 and KCNE1 (Barhanin et al., 1996, Anantharam et al., 2003). This auxiliary subunit right-shifts the voltage dependence of Kv7.1 activation, slows its activation 5-10 fold, increases its unitary conductance 4-fold, slows its deactivation and eliminates its inactivation (Barhanin et al., 1996, Sanguinetti et al., 1996, Pusch, 1998, Tristani-Firouzi and Sanguinetti, 1998). As well as some mutations in this channel have been related to the LQTS, modifications on KCNE1 sequence are also related to these diseases. Those are raising the risk of ventricular arrhythmias and sudden death (Splawski et al., 2000). Biallelical mutations in human *kcne1 or kcnq1* (Kv7.1) can cause also congenital deafness (called Jervell and Lange-Nielsen syndrome) due to an impairment of the proper endolymph production at the cochlea (Jervell and Lange-Nielsen, 1957, Schulze-Bahr et al., 1997).

The KCNE1 knock-out mice exhibited alterations, as expected, in a cardiac level. Some spontaneous episodes of atrial fibrillation could be recorded (Temple et al., 2005). Moreover, it presents a disrupted K^+ secretion and degeneration of the inner ear (Nicolas et al., 2001).

As mentioned before, a three dimensional NMR-based structure of KCNE1 was solved in 2008. They argue that KCNE1 is a curved α-helix, flanked by intra and extracellular domains formed of α-helixes joined by flexible linkers (figure 23) (Kang et al., 2008).

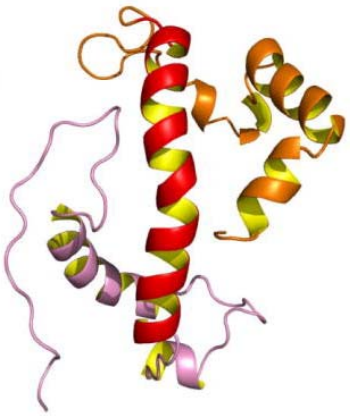

Figure 23. NMR-based structure of KCNE1. Curved trasmembrane domain in red. Partially structured N and C terminal α-helixes in orange and pink respectively (Kang et al., 2008).

1.3.2.2. KCNE2

KCNE2, originally named MiRP1, is also a 15kDa protein that, opposite to KCNE1 or KCNE3, is able to reach the membrane easily in the absence of any conducting subunit (Abbott, 2015). But upon coexpression with specific α subunits, such as Kv1.4, Kv3.3 and Kv3.4, prevents their anterograde trafficking to Golgi (Kanda et al., 2011). It is also able to mediate the internalization of some Kv partners, Kv11.1, enhancing the degradation of the channel provoking a diminution of the cell surface channel expression (Zhang et al., 2012). KCNE2 can interact with Kv1.5 and control its intercalated disks localization in murine ventricles (Roepke et al., 2008).

This subunit is also altering the electrophysiological properties of several channels. Major functions lead to a general decrease of the total current. The coexpression with Kv7.1 generates a smaller time-independent current (Tinel et al., 2000). When it is combined with Kv11.1, KCNE2 leads to a current that resembles the I_{KR} and with Kv4.2, the $I_{TO.}$ In both cases, there is a slower activation, but Kv11.1 presents a faster inactivation while Kv4.2 a slower one and shifts the voltage dependence to more depolarized voltages (Zhang et al., 2001, Abbott et al., 1999). This later modulation is similarly exerted on Kv3.1 and Kv3.2 (Lewis et al., 2004). It have been suggested an interaction between KCNE2 and Kv1.3 that would lead to a decrease of the current density without altering the voltage-dependence of the channel. Those complexes, located at the choroid plexus epithelium, would allow anion efflux in the cerebrospinal fluid (Roepke et al., 2011). However, other authors demonstrated that KCNE2 do not modulate Kv1.3 in *Xenopus oocytes* and HEK-293 cells (Grunnet et al., 2003).

Mutations in this peptide have been related to some alterations in the cardiac function, consistent with its involvement in repolarization. Cardiac arrhythmias, LQTS, drug-induced LQT, atrial fibrillation, sudden infant death syndrome or Brugada syndrome among others can be linked to some specific alterations in the gene sequence (Abbott et al., 1999, Splawski et al., 2000, Sesti et al., 2000, Arnestad et al., 2007, Wu et al., 2010c). Concomitantly, KCNE2 knock-out mice exhibited prolonged ventricular action potentials, suggesting a reduced repolarizing capacity (Roepke et al., 2008). Furthermore, animals presented achlorhydria, gastric hyperplasia, hypo-thyroidism, alopecia, stunted frowth and choroid plexus epithelia dysfunction, highlighting the diversity of the KCNE2 putative functions (Roepke et al., 2010).

1.3.2.3. KCNE3

KCNE3, also called MiRP2, is a 12kDa protein ubiquitously expressed throughout the body (Abbott, 2016a). Some authors have reported its expression in leukocytes, thymus and spleen, while some others report and absent RNA in leukocytes. (Lundquist et al., 2006, Abbott et al., 2001).

KCNE3 can modulate different channels, but it plays a major role in skeletal muscle upon its association with Kv3.4. This interaction is thought to contribute to the skeletal muscle resting membrane potential and, due to the acceleration exerted on the recovery from inactivation and de reduction on the cumulative inactivation; it facilitates the rapid trains

of action potentials (Abbott et al., 2001). Furthermore, the complex KCNE3-Kv3.4 is involved in proliferation of artery smooth muscle cells (Leblanc, 2010, Miguel-Velado et al., 2010).

Kv7.1 is also a target of KCNE3. It triggers an increase in current magnitude and in some drugs-sensitivity (Schroeder et al., 2000, MacVinish et al., 2001). Both proteins are present in the lateral membrane of crypt and surface cells, in distal colon and small intestine, where they control the chloride secretion by creating electrochemical driving forces (Liao et al., 2005, Dedek and Waldegger, 2001). They are also located in parietal stomach cells playing an important role in acid secretion. KCNE3 modulates by inhibition the Kv2.1, Kv3.1, Kv3.2, Kv4.2, Kv7.4 and Kv12.2 (McCrossan et al., 2003, Lewis et al., 2004, Clancy et al., 2009, Wang et al., 2014, Strutz-Seebohm et al., 2006).

KCNE3 gene disruption in mice impairs intestinal chloride secretion, predisposes to ventricular arrhytmogenesis and also impairs auditory function. Concomitantly, some mutations are associated with Méniere's disease, a disorder that can affect hearing and balancing (Doi et al., 2005). Regarding its complex with Kv3.4, a KCNE3 missense mutation is associated with periodic paralysis (Abbott et al., 2001).

Recently, it has been described the presence of coding regions at the first exon of the KCNE3 gene, as well as for KCNE4. Those lead to an increase on protein length of both KCNE3 and KCNE4 in 44 and 51 residues respectively. This work suggests that tissues in which KCNE3 is thought to be functionally important, KCNE3L (the new long version) constitutes the major isoform. Functional consequences of the extension where firstly analysed on Kv7.1 and Kv7.4. The amplitude modulation on Kv7.1 is comparable between both subtypes even the current dernsity recorded is fewer for KCNE3L-channel combination. Finally, no inhibition of the Kv7.4 current density was found with the new peptide analysed (Abbott, 2016c).

Considering the Kv4 family, as mentioned before, it was previously reported a strong inhibition of murine Kv4.2 by KCNE3 original short-form (KCNE3S) (Wang et al., 2014). However, KCNE3L is not able to exert the same function but it can slow the inactivation of the channel (Abbott, 2016c). Posteriorly, in further investigations, human Kv4.2 was evaluated and they obtained a moderately inhibition by both forms of KCNE3. Moreover, the coexpression of KChiP impairs this modulation of the current. Contrary, KCNE3L inhibition of Kv4.3, which is not observed when KCNE3S is coexpressed, is not altered by the presence of KChiP2. Inactivation of this channel can be regulated, also differently, by both subunits of KCNE3 (Abbott, 2016d).

1.3.2.4. KCNE4

KCNE4, also known as MiRP3, is a 20kDa protein and is the longer member of the family with the largest and most diverse C-terminal domain. It is expressed highly in heart, skeletal muscle, uterus and kidney. Also, even in a lower extend, in placenta, lungs, liver, brain and blood cells (Abbott, 2016b).

KCNE4 is able to control several channels and it mostly acts as a dominant-negative regulatory subunit. It exerts an inhibition of Kv1.1 and Kv1.3 in heterologous system

(Grunnet et al., 2003). Previously published results from our laboratory indicate that KCNE4 decreases Kv1.3 current density, slows activation, accelerates cumulative inactivation, retains the channel in the ER and impairs its targeting to lipid raft microdomains (figure 23). Moreover, KCNE4-Kv1.3 may play a role in regulation of immune responses, as both are expressed in macrophages, where they also colocalise. Activation of macrophages using LPS increased expression of both KCNE4 and Kv1.3 transcripts; in contract, dexamethasone was found to diminish Kv1.3 but not KCNE4 expression (Sole et al., 2009, Abbott, 2016b).

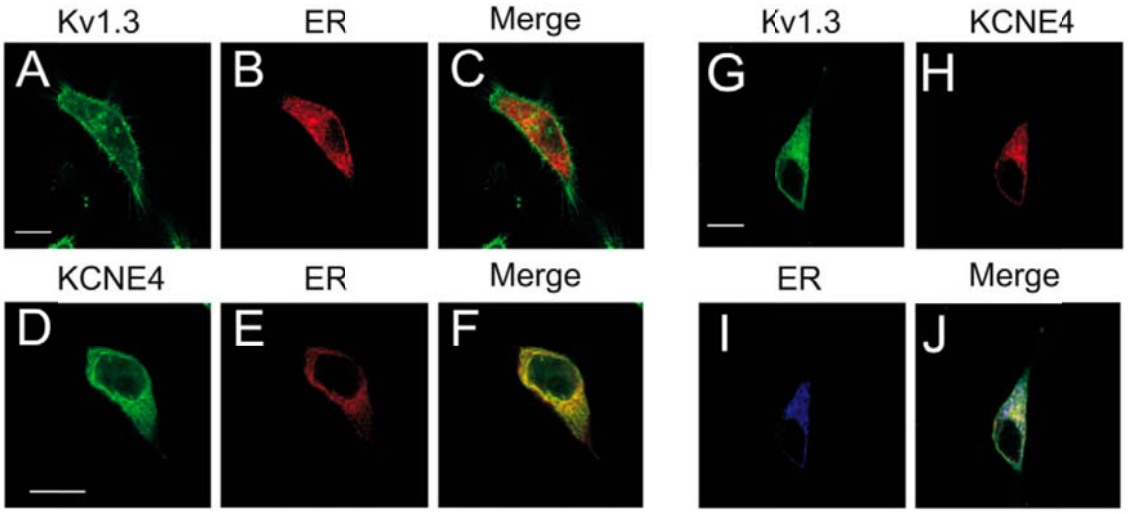

Figure 23. KCNE4 alteration of Kv1.3 cellular distribution. A-C. Kv1.3 does not colocalise with ER. D-F. KCNE4 exhibits a high merge with this marker. G-J. Kv1.3 is shifted to ER distribution upon coexpression with KCNE4 (Sole et al., 2009).

Studies on Kv1 family reported a negative interaction with Kv1.2, Kv1.4 and Kv1.5 (Grunnet et al., 2003). However, a recent publication suggests that KCNE4 forms complexes with Kv1.5 and enhances its membrane targeting and current density in CHO cells (Crump et al., 2016).

Moreover, it regulates Kv7.1, Kv2.1, Kv4.2 and $K_{Ca}1.1$. In heterologous expression, KCNE4 inhibits Kv7.1 currents (Teng et al., 2003, Grunnet et al., 2002). It has been described a SNP in the cytoplasmic end of KCNE4 which generates an increase in the amount of Kv7.1 current acting as a risk factor for atrial fibrillation in Han and Uygur Chinese populations (Ma et al., 2007). Moreover, recently it has been reported a calmodulin binding domain in the C-terminal region of KCNE4 (aminoacids 44 to 73). Depending on calcium presence, calmodulin is mediating the association of KCNE4 with Kv7.1 and allowing the heterotrimerisation with KCNE1 (Ciampa et al., 2011).

Up to 90% inhibition is exerted on Kv2.1 channels. However, it has little-to-no effect on the function of Kv2.1-Kv6.4 heteromers (David et al., 2015). Similar to KCNE2, it can regulate Kv4.2 and KChIP2 contributing to the cardiac transient outward potassium currents (I_{TO}) by slowing the channel's inactivation (Levy et al., 2010). It can also modulate the potassium urinary excretion through its interaction with $K_{Ca}1.1$ (Levy et al., 2008).

The knock out mice of KCNE4 showed high blood calcium, phosphor and cholesterol while glucose levels are reduced. They also exhibit a decrease in the body temperature as well as a shortening in the QT interval with possible implications for arrhythmia susceptibility; although the systolic blood pressure was similar to wild type animals. The deletion of *kcne4* reduced Kv currents in male mouse atrial myocytes by >45% (Crump et al., 2016). Regarding its presence in immune system cells, putative alterations where under investigation. No differences in the number of $CD4^+$ or $CD8^+$, NK, B cells or monocytes were observed. Moreover, the acute phase response or the ability to produce IgG_1 or IgG_2 antibodies following antigen challenge stayed unaltered (Ciampa 2011).

As previously mentioned, it has been proved the presence of new coding regions for KCNE4 generating an increase in the molecular weight at the N-terminus of the protein. They suggest that this new form could be the main subtype expressed at the tissues analysed: kidney, thymus, uterus, testis and prostate. Regarding the possible functional effects, the inhibition exerted on Kv7.1 is reduced compared with the shorter subtype. Concomitantly with KCNE3L, KCNE4L is no longer able to modulate Kv7.4 (Abbott, 2016c).

Further studies of the same laboratory contributed studying the role of this new peptide on Kv4 family. No major changes were detected on murine Kv4.2 channel between KCNE4S and KCNE4L. Both forms exerted a decreased inactivation, which was also observed for human Kv4.2 (Abbott, 2016c). However, KCNE4L decreased dramatically the current of the human isoform, while KCNE4S exerts half of this effect. They also described that KChIP2 coexpression is not able to impair this strong role on the channel, but the presence of this β-subunit do inhibits the slower inactivation exerted on the channel by both KCNE4S and L.

Concomitantly, the longer form is observed to strongly inhibit Kv4.3 current, while KCNE4S is not presenting this ability. However, in this specific situation, KChIP2 partially alleviates KCNE4L's effect (Abbott, 2016d).

1.3.2.5. KCNE5

KCNE5, originally called MiRP4, is a 11kDa protein and was the last member of the family discovered (Piccini et al., 1999). Expression studies locate KCNE5 in heart, skeletal muscle, brain, spinal cord, placenta, ovaries, spleen, testis and thymus. The *knce5* gene is placed in a gene-rich segment of DNA at the X chromosome, the deletion of which leads to the AMME syndrome. This is characterised by the Alport syndrome (that involves glomerulonephritis and sensorineural hearing loss), mental retardation, midface hypoplasia and alliptocytosis. (Lundquist et al., 2006, Abbott and Goldstein, 2001).

Few channels are known to be regulated by this member. Kv7.1 current is modulated by KCNE5, shifting the voltage activation curve to the positive direction in a high extend and decreasing the activation time constant, which leads to a suppression ok Kv7.1 currents (Bendahhou et al., 2005, Angelo et al., 2002).

Mutations in *kcne5* gene are related with cardiac pathologies such as non-familial forms of atrial fibrillation. It has been described the modulation of Kv4.3 + KChIP2 currents and

some variants appeared to cause idiopathic ventricular fibrillation, especially Brugada Syndrome, due to a gain of function of I_{TO} (Ohno et al., 2011).

It was thought that the expression of this member in several tissues where Kv7.1 or Kv4.3 are low or absent, suggest the potential interaction with other α-subunits or alternative functions channel-independent (Lundquist et al., 2006, Abbott and Goldstein, 2001). Even no effects were reported for the Kv1 family, a 50% inhibition is exerted on Kv2.1 current. Upon heteromeric formation with Kv6.4, KCNE5 speeded their activation and recovery from closed-state inactivation, as well as slowed their deactivation (David et al., 2015).

It is worthy to note that there are evidences of various KCNE at the same channelosomes. KCNE1, KCNE3 and Kv12.2 multimeric complexes have been isolated from mouse brain (Clancy et al., 2009). KCNE2, KCNE3, KCNE4 and KCNE5 are able to modulate the current generated by Kv7.1/KCNE1. However, the dominance of KCNE4 inhibition upon KCNE1 modulation presented some discrepancies (Lundquist et al., 2005, Wu et al., 2006). Also complexes formed by KCNE3, KCNE4 and Kv7.1 have been detected (Morin and Kobertz, 2007).

2. AIMS

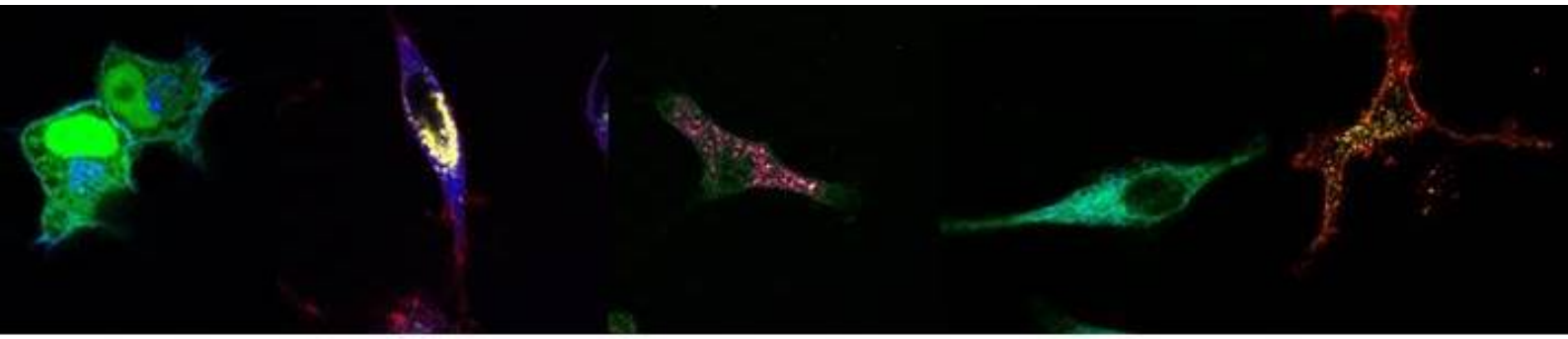

2. AIMS

Voltage-gated potassium channels are a group within the ion channel family that play a key role in maintenance of the resting potential and regulating the repolarization in excitable cells. However, several other functions have been related to those proteins: from adhesion, volume regulation or cell-cycle progression to mobility, homeostasis or apoptosis. Generally, Kv channels are exerting their functions not as solely conducting isles but as channelosomes built up with auxiliary subunits. Several classical repolarising currents from cardiac physiology have been reproduced on cell lines just when modulator proteins where coexpressed.

Kv1.3 is mainly expressed at nervous and immune system. Actually, it is one of the few channels expressed in leukocytes. The involvement of Kv1.3 on activation and proliferation is widely accepted. Upon those stimuli, it is recruited to the immunological synapse where it will keep the calcium signalling. However, apoptosis studies also pointed this channel as a player involved. Thus, fine-tunning of its properties will define the final cellular responses.

There are several auxiliary subunits that have been reported to modulate Kv1.3. Considering the immune system, Kvβ and KCNE subunits are also expressed. The former is a cytoplasmic family of proteins that modulates some electrophysiological properties as well as enhances the channel's surface expression. The latter family is a single-spanning protein group that presents a highest variability on functions exerted on conducting entities. Previous results from our laboratory showed that KCNE4 is acting as a dominant-negative particle on Kv1.3 traffic and surface expression.

The current dissertation aims to further the knowledge on Kv1.3 regulation by Kvβ1.1, Kvβ2.1 and KCNE4 proteins. To that end, we analyse the auxiliary subunits traffic properties and subcellular distribution. Moreover we linked those inner behaviours to the final effect on the channel trying to understand the molecular mechanisms behind them. Therefore, the specific objectives of the PhD dissertation are:

1. To dissect the localization of Kvβ1.1 and Kvβ2.1 and describe electrophysiology, traffic and subcellular distribution of the channelosomes formed with Kv1.3.

2. To identify the molecular determinants on Kv1.3 sequence for surface expression and KCNE4 interaction. Also KCNE4 mechanism to control final Kv1.3 localization.

3. To define heteroligomeric Kv1.3, Kvβs and KCNE complexes formation.

3. RESULTS

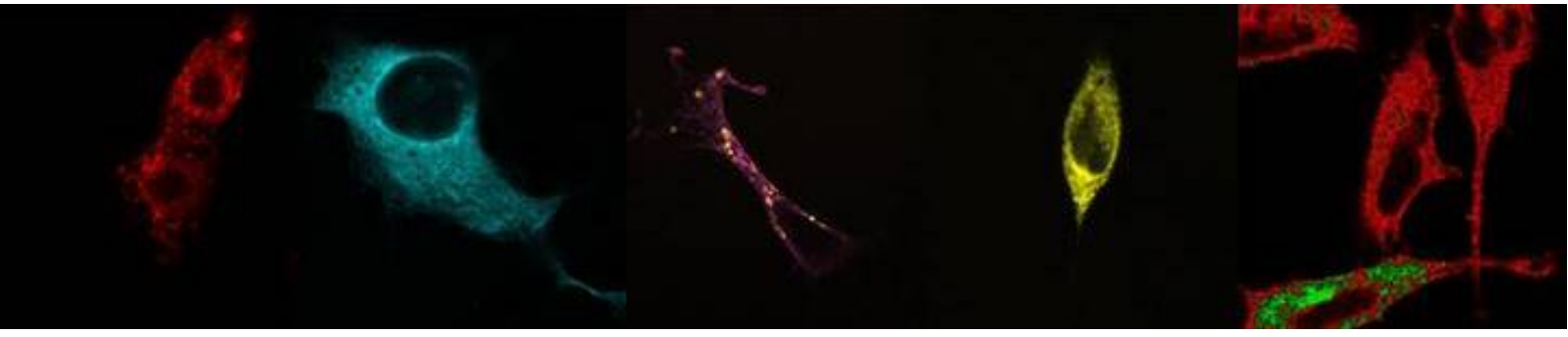

3.1. CHAPTER 1: NEW INSIGHTS ON Kvβ PHYSIOLOGY AND Kv1.3 MODULATION

3.1.1. Contribution 1

Kvß1.1 and Kvß2.1 differential membrane targeting

Roig SR[1], Pérez-Verdaguer M[1], Cassinelli S[2], Vicente R[3], Felipe A[1]

[1]Molecular Physiology Laboratory, Departament de Bioquímica i Biomedicina Molecular, Institut de Biomedicina (IBUB), Universitat de Barcelona, Avda. Diagonal 643, 08028 Barcelona, Spain
[2]Dipartamento scienze cliniche e biologiche
[3]Laboratory of Molecular Physiology and Channelopathies, Departament de Ciències Experimentals i de la Salut, Universitat Pompeu Fabra, Barcelona, Spain.

ABSTRACT

Members of the Kvß family were the first modulators characterised for Kv channels. Their function regulating the α-subunits has been under extensive study, as well as their aldoketoreductase activity. However, few is known about their own cellular distribution. Apart from their cytosolic presence, Kvß1 subunit was described to join actin filaments close to the plasma membrane, but not Kvß2 isoform. The latter was described to interact with microtubular related proteins at nervous system. The expression of this family is ubiquitous and, previous results from our laboratory demonstrated that its presence on macrophages is under specific control. Proliferative and activation stimuli lead to different effects depending on the isoform. The aim of this study was to dissect the possible locations of Kvß2.1 in the cellular space, as well as the possible implication of different insults as mechanisms that enhances its traffic. We have demonstrated the membrane targeting of Kvß2.1 and, moreover, its presence at lipid raft microdomains. Post traductional lipidic modifications are behind this new targeting. We have also determined that proliferative signalling enhances the membrane location for this protein, while PMA activation treatment diminishes the presence on those domains possibly by enhancing its endocytic internalization. This effect is counteracted by the presence of PSD95.

Report of the PhD student participation

Kvβ1.1 and Kvβ2.1 differential membrane targeting

Sara Raquel Roig Merino performed all the experiments and the data analysis of this article except the Kvß cloning and ABE palmitoylation assay.

Antonio Felipe

PhD thesis director

INTRODUCTION

Voltage-gated potassium channels are fundamental components in different cell types and tissues. They have been related to highly diverse functions such as proliferation, cell volume control or cell cycle progression. It is the largest family within the voltage-gated channels, but the functional diversity is even increased due to the existence of different modulators. Those can affect not only the electrophysiological properties of the channels, but also the localisation, traffic or turnover (Pongs and Schwarz, 2010).

Kvß was the first family identified as regulators of Kv channels. Three different genes are described to encode this family with different splicing variants: Kvß1, Kvß2 and Kvß3 (Kilfoil et al., 2013). Upon crystallization of the Kv1.2 channel in the presence of Kvß2.1, the suspected solubility of those proteins was confirmed (Gulbis et al., 1999). Typically cytoplasmic proteins, all three can modulate α-subunits once they interact with their C-terminus conserved region (Rettig et al., 1994). Some of the members have been reported to modulate the electrophysiological properties of Kv channels. However, the traffic has been also reported to be modified. Thus, it was proposed a chaperon-like effect of those proteins on the Kv channels enhancing its presents on the plasma membrane surface (Nagaya and Papazian, 1997, Shi et al., 1996).

While the modulation of Kv channels by Kvß subfamily has been under intensive investigation, their subcellular distribution has been poorly understood. Apart from its cytosolic distribution, Kvß1.1, but no Kvß2.1, has the ability of associating with the actin-based cytoskeleton (Rettig et al., 1994). This function is placed in its N-terminus, inducing a resistance to the extraction with non-ionic detergents (Nakahira et al., 1998). Since, the interaction with the cytoskeleton is placed in the ball-and-chain domain it gives the explanation why under depolymerisation, Kv1.1- Kvß1.1 current increases its inactivation (Levin et al., 1996a, Jing et al., 1997). However, Kvß2 was not completely absent in the non-soluble fractions. Further experiments demonstrate that it can be associated to microtubular cytoskeleton by its interaction with EB1 protein at neuronal cells (Gu and Gu, 2010, Gu et al., 2006). This fact generates that Kvß2 can be also polarised in some specific tissues.

Functionally, Kvß2, which lacks the inactivation ball-and-chain domain, has been described to enhance the folding, glycosylation, trafficking and axonal targeting of Kv1 proteins. However, this function is highly dependent on the α-subunit considered (Nagaya and Papazian, 1997, Accili et al., 1997b). It was also described that Kvß2 has the capability of reducing some substrates acting as an oxidoreductase (Tipparaju et al., 2008, Xie et al., 2011). The genetic ablation of Kvß2 lead to a reduced life spans, occasional seizures, and cold swim-induced tremors. Patients with 1p36 deletion syndrome where the *kcnab2* gene is lost were suffering from childhood seizures and/or exhibiting an electroencephalogram altered (Heilstedt et al., 2001). However, posterior to the analysis of Kv1 distribution, it was concluded that neither the chaperon-like function nor the AKR-like catalytic activity are the responsible for such a phenotype, so pointing to an unidentified property of Kvß2 not compensable by other family members (McCormack et al., 2002, Connor et al., 2005).

Both, PKA and PKC can phosphorylate Kvß2. While PKA just encounter a consensus site for its action, several others are present for PKC recognition and this family is the main responsible for *in vivo* modifications. PKC subtypes that can be involved are: PKCγ, PKCδ and PKCζ (Wang et al., 2004b). Some controversy is surrounding the combination

Kvß2/PKCα (Liu et al., 2003). The interaction of PKCζ and Kvß2 is mediated by the ZIP1, ZIP2 and ZIP3 proteins (Croci et al., 2003). The ratio ZIP1/ZIP2 can condition the PKCζ phosphorylation. While ZIP1 is able to promote a concentration-dependent Kvß2-phosphorilation, the presence of ZIP2 enhances a shift to lower levels of ZIP1 to achieve the same given amount. On the other hand, ZIP1 is four fold more potent to transfer phosphors to Kvß2. So, the final regulation is a confluence on ZIP1 and ZIP2 total amount as well as their ratio (Gong et al., 1999). Some other PKC subtypes cannot be discarded of the possible modulation on Kvß2 such as PKCγ, PKCδ (as mentioned above) or PKCθ which was not analysed in any publication. However, there has been no associated effect on Kv functionality consequence of the Kvß2 phosphorylation.

Despite the time and effort invested on the understanding the Kvß2 role in the cellular physiology, there are some non-solved doubts about its function and regulation (Connor et al., 2005, Giese et al., 1998). The present work stablishes the specific and unique presence of Kvß2 at lipid raft microdomains. This location, Kv-independent, is directly related on its lipidic post-traductional modification. We also describe that it can be modulated for some different insults: the proliferative stimulation induces its presence in those domains, while PMA-treatment decreases this new target. It is inferable that the most probable mechanism involved is an ubiquitination-dependent endocytic process.

MATERIAL AND METHODS

Expression plasmids and site-directed mutagenesis mKvβ1.1 and mKvβ2.1 were provided by M.M. Tamkun (Colorado State University). mKvβ1.1 and mKvβ2.1 were subcloned into pEYFP-N1 and pECFP-N1 (Clontech). mKvβ2.1CFP mutants were generated using the QuikChange and QuikChange lightning multi-site-directed mutagenesis kits (Stratagene). All constructs and mutants were verified using automated DNA sequencing.

Cell culture, *transfections and pharmacological treatments.* HEK-293 cells were cultured on DMEM (LONZA) containing 10% fetal bovine serum (FBS) supplemented with penicillin (10.000 U/ml), streptomycin (100 µg/ml) (GIBCO) and L-glutamine (4 mM).

For confocal imaging and co-immunoprecipitation experiments cells were seeded (70-80% of confluence), in 6-well dish containing poly-lysine-coated coverslips or 100mm dish, respectively, 24h before transfection. Lipotransfectina® (Attendbio Research) was used for transfection according to the supplier's instructions. The amount of transfected DNA was 4µg for a 100mm dish and 500ng for each well of a 6-well dish (for coverslip use). Next, 4-6h after transfection, the mixture was removed from the dishes and replaced with new fresh culture media. All the experiments were performed 24 h after transfection.

In some experiments, twenty-four hours HEK transfected cells were incubated with 1µM PMA for 30min at 37ºC. For 2-bromopalmitate treatment, HEK transfected cells were starved for 3h with DMEM supplemented with 1% of dialyzed FBS, and 60nM of 2-bromopalmitate is added 3 more hours all at 37ºC. The H_2O_2 addition was in a 400µM final concentration for 30 min at 37ºC.

Protein extraction, co-immunoprecipitation and western blotting. Cells were washed twice in cold PBS and lysed on ice with lysis buffer (5 mM HEPES, 150 mM NaCl, 1% Triton X-100, pH 7.5) supplemented with 1 µg/ml aprotinin, 1 µg/ml leupeptin, 1 µg/ml pepstatin and 1 mM phenylmethylsulfonyl fluoride as protease inhibitors. Cells were next scrapped and transferred to a 1.5 ml tube. Then they were incubated for 20 min at the orbital, and spun for 20 min at 14000 rpm. The supernatant was transferred to a new tube and protein contents were determined by using the Bio-Rad Protein Assay (Bio-Rad).

For co-immunoprecipitation, 1000 µg of protein of each condition were separated and brought up to a volume of 500 ml with Lysis Buffer for IPs (NaCl 150 mM, HEPES 50 mM, Titron X-100 1%, pH 7.4), supplemented with protease inhibitors. Preclean was performed with 40 µl of protein A sepharose beads (GE Healthcare), in an orbital 1 h at 4ºC. Next, each sample was incubated with a small chromatography column (BioRad Micro spin Cromaotgraphy Columns), which contained 2.5 µg of anti-GFP antibody (Genescript) previously crosslinked to protein A sepharose beads, for 2h at room temperature, with continuous mixing in an orbital. Next, columns were centrifuged 30s at 1000g. The supernatant (SN) was kept and stored at -20ºC. Columns were washed four times with 500µl of lysis buffer and centrifugations of 30sec at 1000 g. Finally, elution was performed by incubation of the columns with 100µl of 0.2M glycine pH 2.5, and spun 30sec at 1000g. The eluted proteins (IP) were prepared for western blot by adding 20µl of Loading Buffer (5x) and 5µl of 1M Tris-HCl pH 10.

Irreversible crosslinking of the antibody to the sepharose beads was performed after one hour of incubation at RT of the antibody with protein A sepharose beads, incubating the beads with 500ul of dimethyl pimelimidate (DMP, from Pierce) for 30 min at RT. Next columns, were washed four times with 500 µl of 1x TBS, four times with 500 µl of 0.2 M glycine pH 2.5 and three times more with 1x TBS. Once these steps are performed, the columns could be incubated with the protein lysates, in order to perform the immunoprecipitation, following the protocol described before.

Protein samples (50µg), supernatants and immunoprecipitates were boiled in Laemmli SDS loading buffer and separated on 10% SDS-PAGE. Next, they were transferred to nitrocellulose membranes (Immobilon-P, Millipore) and blocked in 0.2% Tween-20-PBS supplemented with 5% dry milk, before immunoreaction. Filters were immunoblotted with antibodies against Kvß1.1 (1/1000, Neuromab), Kvß2.1 (1/1000, Neuromab), Clathrin (1/1000, BD Transduction) or Caveolin (1/1000, BD transduction). Finally, filters were washed with 0.05% Tween-20-PBS and incubated with horseradish peroxidase conjugated secondary antibodies (BioRad).

Confocal microscopy and image analysis. For confocal image acquisition cells were seeded on poly-lysine-coated coverslips, and 24h later were transfected. The next day, cells were quickly washed twice, fixed with paraformaldehyde 4% for 10 min, washed three times for 5min with PBS-K+. Finally, coverslips were mounted on microscope slides (Acefesa) with house Mowiol mounting media. Coverslips were let dry at RT at least one day before imaging.

For membrane surface labelling, Wheat Germ Agglutinin-Texas Red (WGA) (from Invitrogen) was used. Live cells (on ice) were quickly washed with PBS at 4°C and stained

with a dilution of WGA-TexasRed (1/1500) in DMEM supplemented with 30 mM Hepes for 15min at 4°C. Subsequently, cells were quickly washed twice and fixed with 4% paraformaldehyde in PBS for 6 min. Next, cells were washed and mounted as described before. In order to detect EEA1 marker, after fixation, cells were further permeabilized with 0.1% Triton X-100 for 20min. After 60min incubation with blocking solution (10% goat serum, 5% non-fat powdered milk and 0.05% Triton X-100) primary mouse anti-EEA1 (1:500) antibody was added 2h at RT (BD Transduction Laboratories) in 10% goat serum and 0.05% Triton X-100. Next, fixed cells were incubated with secondary goat anti-mouse antibody conjugated with Cyanine 5, for 1 hour at room temperature. Mounting as previously described.

The Fluorescence Resonance Energy Transfer (FRET) via acceptor photobleaching technique was measured in discrete ROI (Region of Interest). Fluorescent proteins from fixed cells were excited with the 458 nm or the 514 nm lines using low excitation intensities. Next, 475 to 495 nm bandpass and >530 nm longpass emission filters were applied. The YFP protein was bleached using maximum laser power. We obtained approximately 80% of acceptor intensity bleaching. Posteriorly, images of the donors and acceptors were taken. The FRET efficiency was calculated using the equation $[(F_{CFPafter} - F_{CFPbefore})/F_{CFPbefore}]*100$, where $F_{CFPafter}$ was the fluorescence of the donor after bleaching and $F_{CFPbefore}$ was the fluorescence before bleaching. The loss of fluorescence as a result of the scans was corrected by measuring the CFP intensity in the unbleached part of the cell.

All images were acquired with a Leica TCS SL laser scanning confocal spectral microscope (Leica Microsystems), equipped with an Argon and Helium-Neon lasers. All experiments were done with a 63x oil-immersion objective lens NA 1.32. FRET and colocalization offline image analysis was done using Image J software. A pixel by pixel colocalization study by using JACoP (Just Another Colocalization Plugin) was used. Mander's split coefficients were obtained which are proportional to the amount of fluorescence of the colocalizing pixels in each color channel.

Plasma membrane lawns preparations. Plasma membrane lawns (PML) are membrane sheets obtained by an osmotic shock. HEK-293 cells were seeded in poli-D-lysine treated glass coverslips. Twenty-four hours after transfection they were cooled on ice for five minutes and washed twice in PBS. Next, incubated during five minutes in KHMgE buffer (70mM KCl, 30mM HEPES, 5mM MgCl2, 3mM EGTA, pH 7.5) diluted three times and then, gently washed with non-diluted KHMgE to induce the hypotonic shock. Bursted cells were removed from the coverslip by intensively pipetting up and down. After two washes with KHMgE buffer only membrane sheets remain attached. Preparations were fixed and mounted as previously described.

Lipid-raft isolation. Low density triton-insoluble complexes were isolated as previously described (Martens et al. 2000) from HEK293 cells transiently transfected with Kvß1.1CFP, Kvß2.1CFP or Kvß2.1CFP$^{C\text{-}lessA}$. Cells were homogenised in 1 ml of 1% Triton X-100, and sucrose was added to a final concentration of 40%. A 5-30% linear sucrose gradient was layered on top and further centrifuged (390.000g) for 20-22h at 4ºC in a

Beckman SW41 rotor. Gradient fractions (1ml) were collected from the top to the bottom and analysed by western blotting.

Ubiquitination assay. Cells were washed twice in cold PBS and frozen at -80ºC for at least one night. On ice, cells were lysed 20min on ice with 2mL of lysis buffer (50mM HEPES, 150mM NaCl, 1% Triton X-100, 10% Glicerol, pH 7.5) supplemented with 0.0125g NEM, 0.2mM MG132, 1mM EGTA 1mM EDTA, 20mM NaF, 1% NaOV, 2mM DTT, 1µg/ml aprotinin, 1µg/ml leupeptin, 1µg/ml pepstatin and 1mM phenylmethylsulfonyl fluoride as protease inhibitors. After scrapping the cells, they were centrifuge at 14.000gs for 15min. Immunoprecipitation assay was performed as previously described.

Membrane extraction. Twenty-four hour cells were washed twice in cold PBS. Scrapped in 1mL of HB buffer (20mM HEPES pH 7.4, 1mM EDTA, 255mM Succrose and 1µg/ml aprotinin, 1µg/ml leupeptin, 1µg/ml pepstatin and 1mM phenylmethylsulfonyl fluoride as protease inhibitors) and passed through a 25-gauge needle ten times. It was centrifuged at 4ºC 3000gs during 5min and the supernatant collected is diluted 1 to 3 with HB buffer. To isolate the membrane fraction, 1h and 30min of centrifugation at 150.000gs was performed, and the pellet was resuspended in 30uL HEPES 30mM.

ABE palmitoylation assay. HEK cells transfected with Kvß2.1 wild type and Kvß2.1 cysteine mutants were harvested in buffer A (150 mM NaCl, 50 mM Tris HCl, 0,2% Triton X-100, 5 mM EDTA, pH 7.4) containing 10mM NEM (Nethylmaleimide, Sigma) and lysates were collected by scraping on ice and passed through a 25-gauge needle. Samples were chloroform-methanol precipitated and the pellet was allowed to air dry for 2-3 minutes. The pellet was re-suspended in 300 µL of buffer B (4% sodium dodecyl sulfate, 50 mM Tris HCl, 5 mM EDTA, pH 7.4) and diluted four fold in lysis buffer containing 10mM NEM. The samples are incubated at 4°C overnight with gentle agitation. NEM was removed by performing 3 sequential chloroform-methanol precipitations and following the last precipitation, the pellet was re-suspended in 500 µL of buffer B. The sample was divided in two and one half was diluted with 950uL of the buffer C containing 0.7 M hydroxylamine (+HA) (50mM Tris-HCl, 1 mM HPDP-biotin, 0.2% Triton X-100, 100µM PMSF) and the other sample was diluted in buffer C without hydroxylamine (-HA). Samples were incubated at room temperature with gentle rocking for one hour. Three rounds of chloroform-methanol precipitation were performed and the final pellets were re-suspended in 250µL buffer B and diluted with 900 buffer D (150 mM NaCl, 50 mM Tris-HCl, 5 mM EDTA, 0.2 mM HPDP-biotin, 0.2% Triton X-100, pH 7.4). They were incubated at room temperature with gentle agitation for one hour prior to three sequential chloroform-methanol precipitations. The final pellet was re-suspended in 120 µL of buffer E (2% SDS, 50 mM Tris HCl, 0,2% Triton X-100, 5 mM EDTA, pH 7.4) and samples were diluted to 0.1% SDS in buffer A. Biotin-labeled proteins were captured with 50 µL of NeutrAvidin agarose beads. Those were previously whased with 400µL of buffer A and centrifuged 1 min at 2000gs. NeutrAvidine beads were pelleted by centrifugation of 2000gs for 30s. After washing the beads 4 times with 400µL of buffer A, captured proteins were boiled in

100µL Laemmli buffer 1x and 2% ß-mercaptoethanol. Samples were then analysed by SDS-PAGE and ImageJ quantification was performed.

RESULTS

Kvß2.1 is also localised in the plasma membrane

Few is known about other putative distributions of this auxiliary subunit family. However, they have been described to modulate some electrophysiological properties of potassium channels: typically membrane proteins. Some studies on the complex formation have point out to associated post-translationally, at the endoplasmic reticulum level (Nagaya and Papazian, 1997, Shi et al., 1996). Upon HEK transfection with Kvß1.1 (figure 1A) as well as Kvß2.1 (figure 1B), both subunits exhibited intracellular phenotypes, concomitant with a cytosolic distribution. However, coexpressed and analysed with a membrane marker, both Kvß1.1 (figura 1C-F) and Kvß2.1 (figure1G-J) can colocalize partially with this marker. The pixel-by-pixel graffics shows that the membrane marker, in blue, and the distribution of Kvβ1.1 (figure 1F) and Kvβ2.1 (figure 1J) share space fractions.

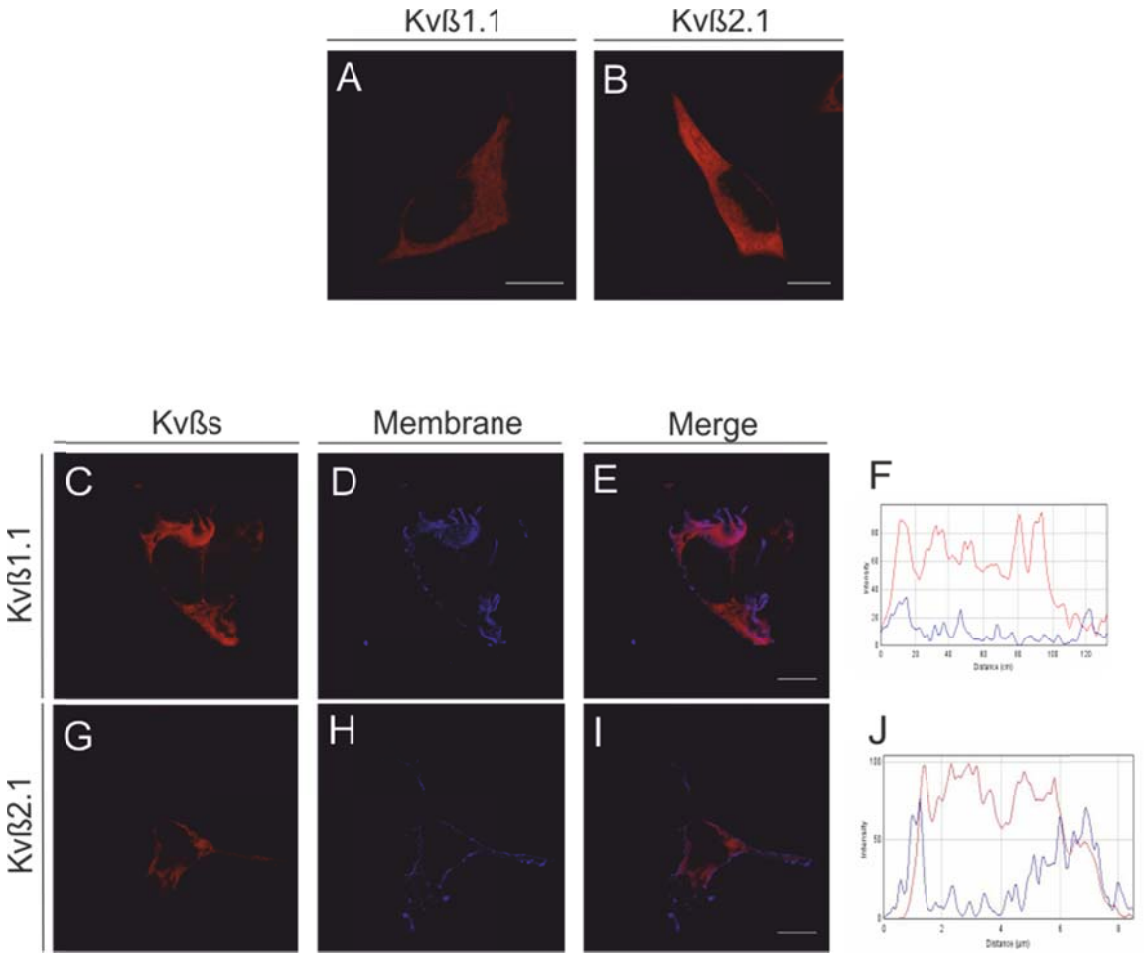

Figure 1. Kvß family presents not only an intracellular distribution but also a membrane targeting. A: Kvß2.1 representative distribution on HEK cells. B: Kvß1.1 representative distribution. C-F: Colocalisation of Kvß1.1 with a membrane marker. C: Kvß1.1. D: membrane marker. E: merge of channels, purple means colocalization. F: pixel-by-pixel analysis of ROI in E. G-J:

Colocalisation of Kvß1.1 with a membrane marker. G: Kvß2.1. H: membrane marker. E: merge of channels, purple means colocalization.

Kvß family has been typically described as cytosolic proteins. Their sequence analysis revealed the putative solubility of its structure since it was not presenting any hydrophobic alpha helix insertable in the plasma membrane. Mackinnon group's structure of Kv1.2 in the presence of Kvß2.1, as well as its crystal structure, it is appreciable that in deed it has a cytosolic distribution (Long et al., 2005, Gulbis et al., 1999).

In order to ensure the presence at the cell surface of those subunits, a membrane purification protocol was followed after Kvβ1.1 and Kvβ2.1 transfection on HEK cells (figure 2A). Following the extraction, samples were concentrated using the columns *Centrifugal Filter Units* (Amicon®). The efficiency of the concentration process is checkable bye the ratio supernatant(SN)/concentration(Conc) intensity bands. Both subunits separately or upon coexpression can be detected on membrane purifications (figure 2B).

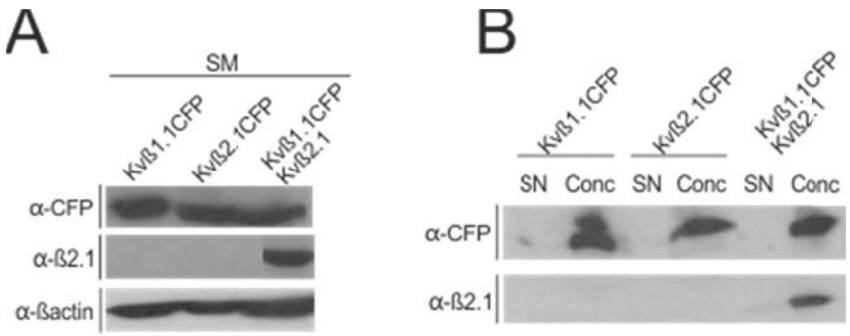

Figure 2. Kvß membrane targeting after a purification protocol. A: HEK cells expressing Kvß1.1CFP, Kvß2.1CFP or KvßCFP and Kvß2.1. B: Detection of Kvß1.1CFP, Kvß2.1CFP or Kvß1.1CFP and Kvß2.1. SN: Supernatant of an associated concentration protocol. Conc: Protein concentration on membrane portion purifications.

In 1998, Nakahira et al. described the association of Kvβ1.1 but not Kvβ2.1 with actin filaments. This interaction allowed the presence of one but not the other in subcellular localizations close to the plasma membrane (Nakahira et al., 1998). In order to ensure that Kvß2.1 membrane presence was, as stablished so many years ago, not due to actin interactions, Immunoprecipitations were performed of both subunits expressed separately in HEK cells. As we can detect in figure 3A, there is a molecular interaction between the Kvß1.1 with ß-actin. Thereby, stress fibres covering the membrane cytosolic face, can cause the presence of Kvß1.1 subunit at those fractions. On the other hand, Kvß2.1 had not the ability to interact with ß-actin (figure 3B). This result is pointing out that another mechanism is responsible for its membrane situation.

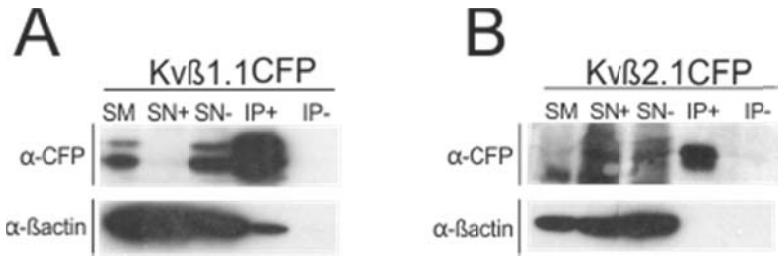

Figure 3. ß-actin association can partially explain Kvß membrane targeting. A: Coimmunoprecipitation of Kvß1.1CFP and ß-actin after a purification protocol. SM: staring material. SN+: supernatant collected after immunoprecipitation in presence of antibody. SN-: supernatant collected after immunoprecipitation in absence of antibody. IP+: immunoprecipitation in the presence of antibody. IP-: immunoprecipitation in the absence of antibody.

In order to understand if the membrane distribution for Kvß2.1 was a preferable localisation, a dose-dependent analysis of Kvß2.1 was performed, coexpressed with a membrane marker.

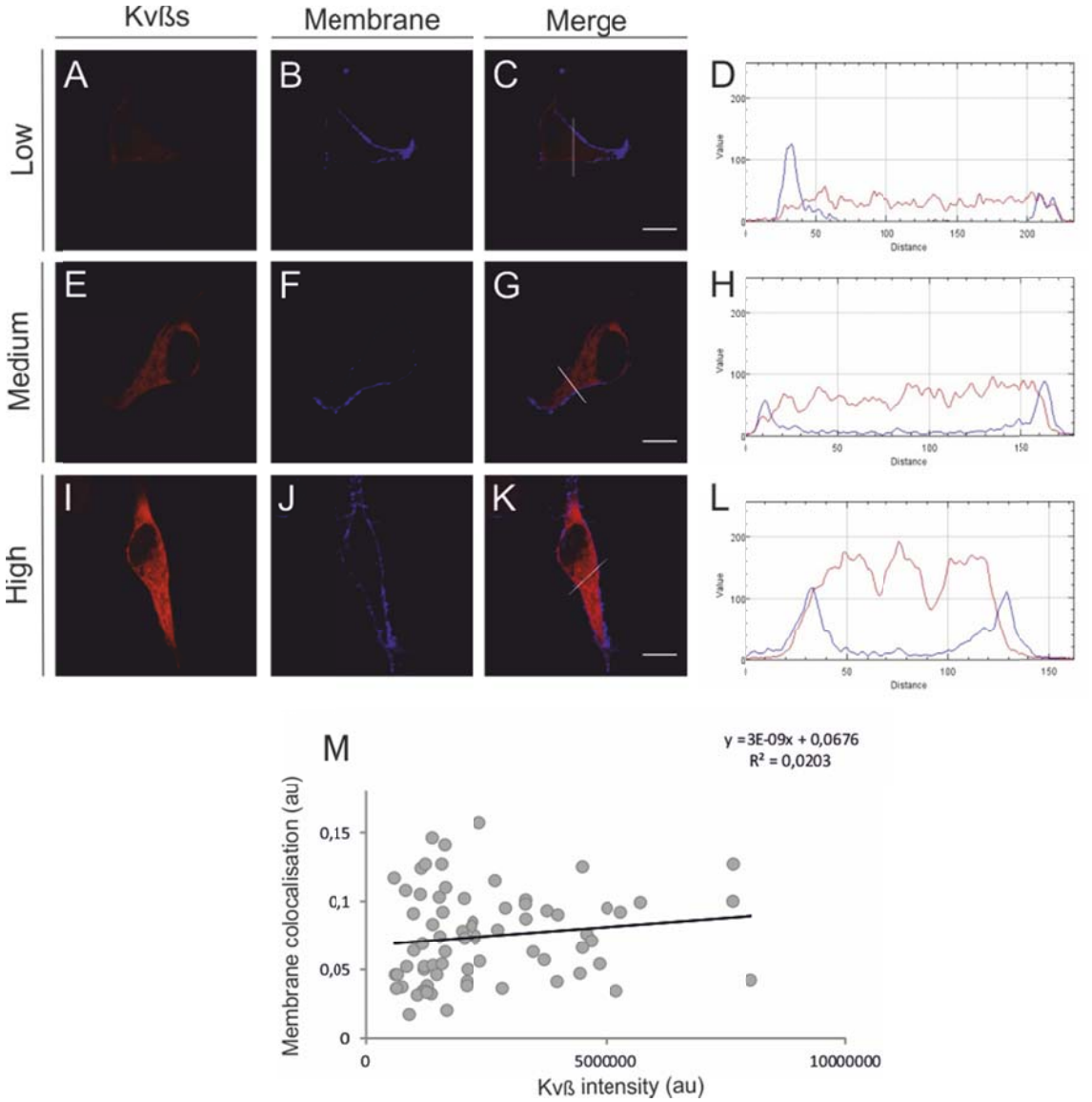

Figure 4. Kvß2.1 membrane targeting is dose-independent. A: Kvß2.1 representative distribution of low intensity HEK transfected cells. B: membrane marker. C: merge. D: pixel-by-pixel analysis of ROI in C. D: Kvß2.1 representative distribution

of medium intensity HEK transfected cells. E: membrane marker. G: merge. H: pixel-by-pixel analysis of ROI in G. I: Kvß2.1 representative distribution of high intensity HEK transfected cells. J: membrane marker. K: merge. L: pixel-by-pixel analysis of ROI in K. M: Plot of membrane colocalization versus intensity level of Kvß2.1.

By maintaining the settings of the confocal microscopy, several cells which were expressing different protein levels were processed and their membrane expression was explored and plotted (figure 4A-L). The analysis (figure 4M) revealed that Kvß2.1 presented a membrane targeting sustained and independent on concentration, turning unlikely to be an overexpression artefact.

Once stablished the presence dose-independent in the membrane and the absence of ß-actin interaction, this new distribution of Kvß2.1 was checked straight in single cells. In order to detect just the portion at this subcellular compartment, plasma membrane loans were prepared in HEK cells transfected with Kvß1.1, Kvß2.1, and both subunits. Kvß1.1 (figure 5A-C) as well as Kvß2.1 (figure 5D-F) are detectable in those preparations and colocalize partially with the membrane marker. The distribution observed in both preparations is not homogenous and appear to be limited to some spots. Upon coexpression, Kvß1.1 and Kvß2.1 can be situated in the same regions, colocalising also with the membrane marker (figure 4G-J). This punctuated pattern is kept in the last condition.

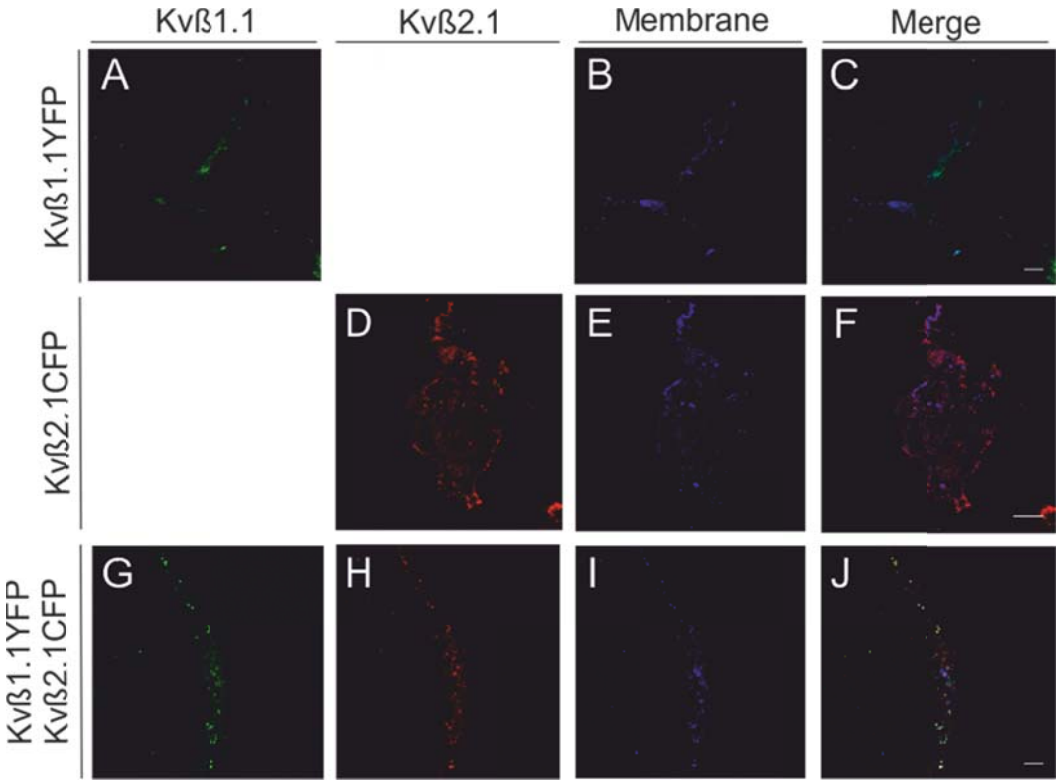

Figure 5. Kvß plasma membrane loan expression. A-C: Membrane preparations of Kvß1.1YFP and membrane marker. A: Kvß1.1CFP. B: Membrane marker. C: merge of channels, turquoise means colocalization. D-F: Membrane preparations of Kvß1.1CFP and membrane marker. D: Kvß2.1CFP. E: Membrane marker. F: merge of channels, purple means colocalization. G-J: Membrane preparations of Kvß1.1YFP, Kvß2.1CFP and membrane marker. G: Kvß1.1CFP. H: Kvß2.1CFP. I: Membrane marker. J: merge of channels, white means colocalization.

Several years ago, it was described that the plasma membrane is not a homogenous subcellular compartment. It is not considered anymore as a uniform lipid bilayer but a multiplatform structure by including the *lipid raft* domains in its structure (Brown and London, 1998). Since there were no evidences of interaction with ß-actin, but Kvß2.1 was present in the plasma membrane and showing a concrete pattern, the next step was to check the possible ability to traffic to lipid raft microdomains since it could explain the previous results. After the expression in HEK cells of both proteins (Kvß1.1 and Kvß2.1) extraction in the presence of a non-ionic detergent was applied. When immersed in a sucrose gradient, the *lipid raft* domains, which are non-soluble in this type of detergents, migrated to low sucrose concentrations. The rest of the membrane was dissolved and we detected them at the highest sucrose concentration fractions. The control parameters of this technique are two proteins mutually exclusive of the two membrane domains: caveolin as a marker for lipid raft fractions and clathrin as the opposite.

The western blotting of our conditions revealed that Kvß1.1 (figure 5A) exhibits a non-floating distribution, since the bands corresponding to the protein appear just in those fractions where chlatrin is also present. However, Kvß2.1 can be detected not only in chlatrin fractions but also partially in those marked by the presence of caveolin (figure 5B). Note that chlatrin and caveolin are not sharing any fraction of the gradient sucrose, ensuring the results.

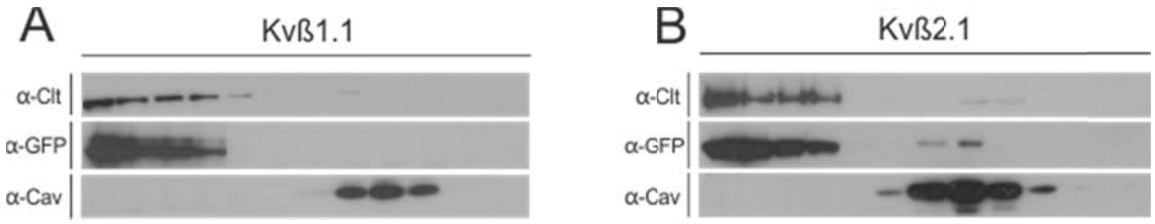

Figure 6. Lipid raft isolation of HEK cells transfected with Kvß1.1 or Kvß2.1. A: Western blotting of lipid raft fractions of Kvß1.1CFP. B: Western blotting of lipid raft fractions of Kvß2.1CFP.

Lipid raft structures can be widely diverse and integrate several different proteins that support and build them up. One type of those structures is characterised for the presence of the family protein of caveolins, our previous marker for the *lipid raft* extraction. Those subunits have been typically described as a chaperon-like family as well as helpers on the traffic to the membrane (Williams and Lisanti, 2004). A recent paper published by our laboratory confirm that the Kv1.3 channel present an aromatic sequence (previously described as a caveolin binding domain) able to interact with caveolin-1. Moreover, the direct interaction with this subunit enhances the traffic of the channel to *lipid raft* microdomains (Perez-Verdaguer et al., 2016a).

The analysis of the Kvß2.1 sequence revealed that, although it shows a high amount of aromatic aminoacids (figure 7), none of them kept the consensus sequences described: ϕxϕxxxxϕ, ϕxxxxϕxxϕ or ϕxϕxxxxϕxxϕ.

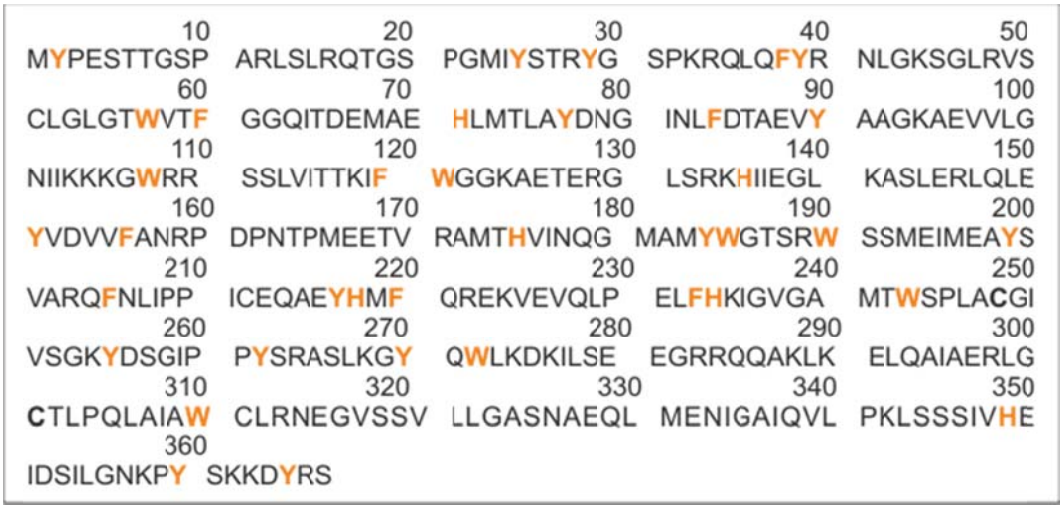

Figure 7. Kvß2.1 mouse aminoacid sequence. Aromatic residues are highlighted in orange.

However, several other proteins have been described to present a partially conserved CBD and a proper interaction with this subunit family. In some of those domains, the positions for aromatic amino acids in the consensus sequence have been substituted by hydrophobic ones. In this case, Kvß2.1 presents some putative sequences:

- Position 52: **L**GLGT**W**VT**F**
- Position 148: **L**E**Y**VDVV**F**
- Position 262: **Y**SRAS**L**KG**Y**
- Position 270: **Y**Q**W**LJDK**I**
-

Since the bioinformatics study revealed some possibilities, immunoprecipitations of Kvß1.1 (figure 8A) and Kvß2.1 (figure 8B) where performed to detect the hypothetical interaction. The western blotting revealed that there is not such interaction among those regulatory subunits.. Thereby, this was not the mechanism used for the traffic of Kvß to lipid raft.

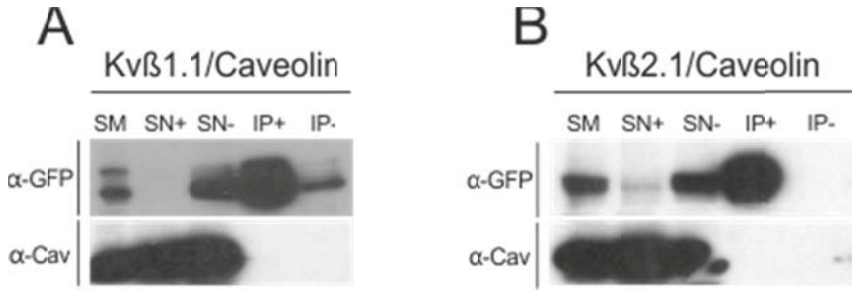

Figure 8. Kvß2.1 lipid raft targeting is not via caveolin interaction. A: Coimmunoprecipitation of Kvß1.1CFP in the presence of caveolin. B: Coimmunoprecipitation of Kvß2.1CFP in the presence of caveolin. SM: staring material. SN+: supernatant collected after immunoprecipitation in presence of antibody. SN-: supernatant collected after immunoprecipitation in absence of antibody. IP+: immunoprecipitation in the presence of antibody. IP-: immunoprecipitation in the absence of antibody.

Lipidic modifications are governing Kvß2.1 presence in the membrane

One kind of mechanism for soluble proteins to be attached to the membrane is lipidic post-translational modification. The most abundant variation on the protein sequence present in eukaryotic cell is the S-palmitoylation. The addition of this lipid to the aminoacid sequence is performed by the enzymes DHHC and it can be reverted by thiosterases. This modification has been related with several funcions such as protein-protein interactions or protein stability, but also with membrane association and protein trafficking. Those characteristics concerning to this modification have been described for membrane-bound proteins but also for soluble ones (Rocks et al., 2010).

Considering the presence of Kvß2.1 at membrane microdomains, we checked the possibility of founding a palmitate in the structure of the protein. The ABE assay, specifically designed for detection of post-traductional palmitic modification, was developed on HEK cells transfected with Kvß2.1.

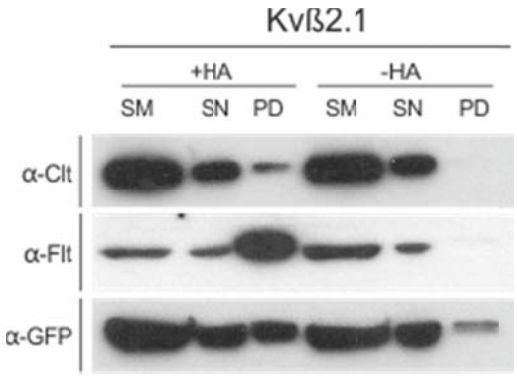

Figure 9. ABE palmitoilation assay on HEK cells transfected with Kvß2.1. +HA: Experiment developed in the presence of hydroxylamine. -HA: Experiment developed in the absence of hydroxylamine. SM: starting material. SN: supernatant collected after the pulldown. PD: pulldown of the palmitoilated proteins.

In figure 9, we can observe the positive pull down in the lines treated with hydroxylamine of the three analysed proteins: chlatrin and caveolin as positive controls and Kvß2.1. Regarding the negative control (absence of hydroxylamine), none or little presence of signal indicate that the result is valid. Kvß2.1 is undergoing palmitoylation at regular conditions in HEK transfected cells.

The presence of this modification does not imply a direct correlation with the membrane presence. In order to determine if the palmitoylation is explaining the flotability of this subunit, Kvß2.1 *lipid raft* presence was analysed posterior to the treatment using two different compounds: 2-bromopalmitate (2-BP) and H_2O_2. On one hand, 2-BP is a competitor of palmitate. It can interact with the palmitoyltransferase domain of PATs. Since palmitoylation is a reversible process, by treating with this compound during three hours, all the palmitoylated proteins undergo only the opposite reaction: deacylation. On the other hand, H_2O_2 is a powerful oxidant. The most common palmitoylation occurs on the S group present at the amino acid cysteine. The presence of an oxidant could impair this modification by the formation of cistine bounds. Moreover, Kvß family has been classified and studied as oxidoreductases. Those proteins are able to detect the redox state of the cell and convert the NADPH to NADP. This effect generates a buffer of the effect of oxidant

compounds. So, by combining both treatments we could infer if the presence into *lipid raft* domains is related to palmitoylation or stimuli of oxidation.

Kvß presence in lipid raft domains (figure 10A) is impaired posterior to the treatment not only with 2-BP (figure 10B), but also H_2O_2 (figure 10C). Those effects are significantly different from the absence of treatment but not between them (figure 9E). When applied a mixture of both treatments (figure 10D), there is a reduction on floatability significantly different compared with the absence of those. However, there are no changes when compared with the rest of the conditions. The effect of both does not appear to be neither synergic not summative. Those results point to the palmitoylation as the process to place Kvß in the lipid raft domains, independent of its oxidoreductase activity.

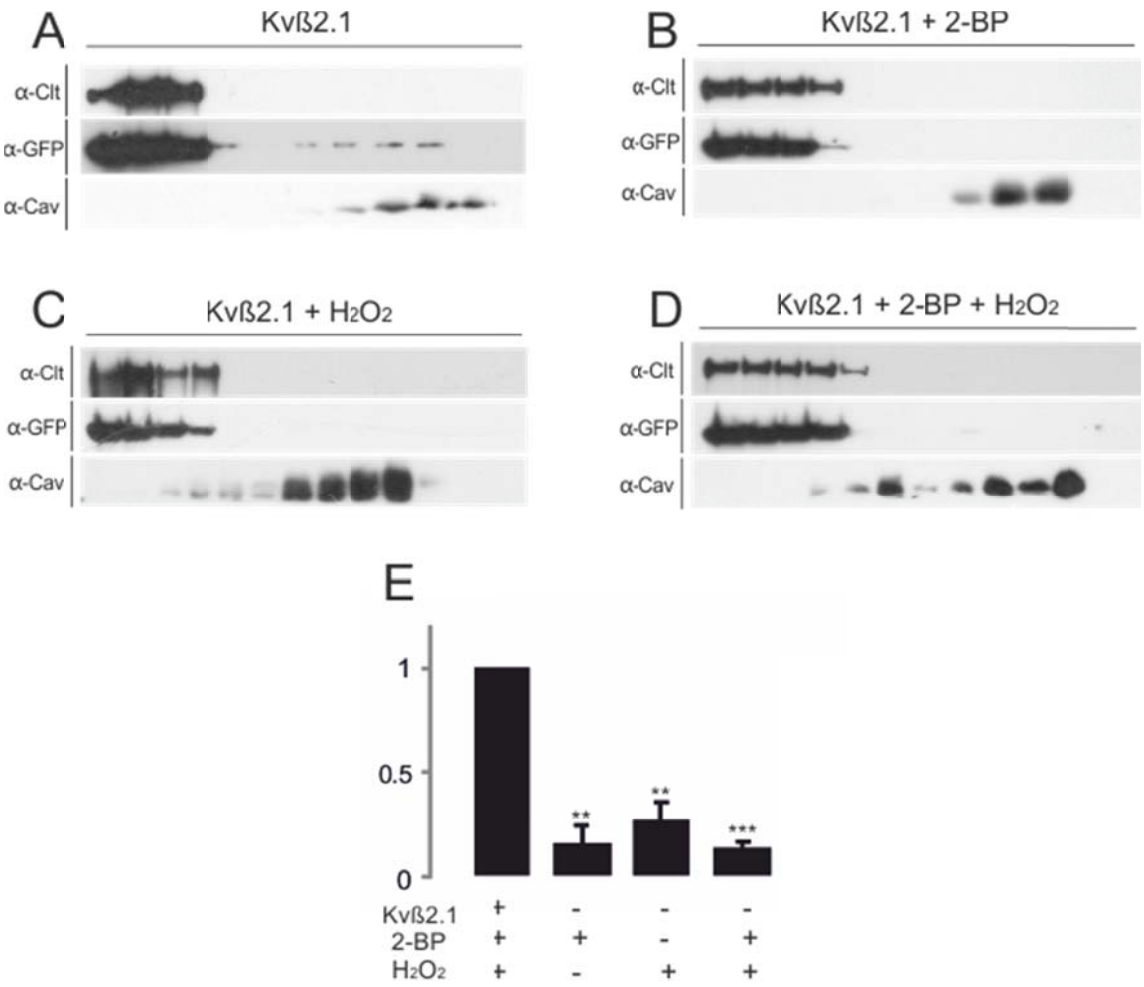

Figure 10. Lipid raft microdomains extraction in the presence of 2-Bromopalmitate (2-BP) and H_2O_2. A: Western blotting of lipid raft fractions of Kvß2.1CFP. B: Western blotting of lipid raft fractions of Kvß2.1CFP with 2-BP treatment. C: Western blotting of lipid raft fractions of Kvß2.1CFP with H_2O_2 treatment. D: Western blotting of lipid raft fractions of Kvß2.1CFP with 2-BP and H_2O_2 treatment. E. Quantification of the flotability in all conditions relativized by the total amount of expression.

To further support those results we analyse the membrane presence by confocal imaging of those conditions. This leaded us to check, qualitatively, that while Kvß2.1 (figure 11A) in the absence of any treatment is occupying the complete cell, when treated with 2-BP

(figure 11B) or H_2O_2 (figure 11C) it is observable a shift on its distribution: on the edge of the cells the presence of Kvß2.1 decreases.

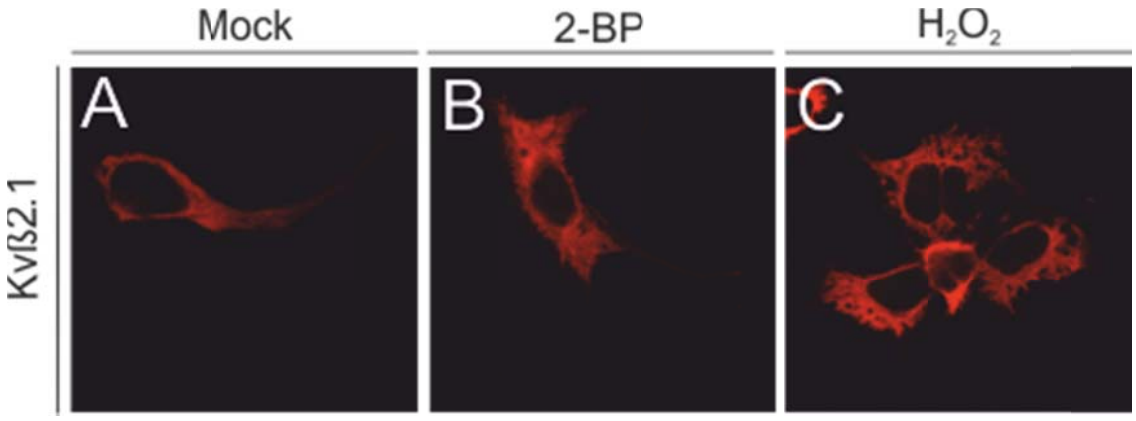

Figure 11. Representative Kvß2.1 distribution after different treatments. A: Kvß2.1 representative distribution. B: Kvß2.1 representative distribution after 2-BP treatment. B: Kvß2.1 representative distribution after H_2O_2 treatment.

Previous pharmacological treatments, 2-BP or H_2O_2, applied on our conditions can inhibit the palmitoylation of all the cellular proteins. Even proved the palmitoylation th Kvß2.1 subunit, and at this specific point, the results obtained can suggest two different situations:

- The palmitoylation that drives our subunit to lipid raft is taking place in its cysteines.
- The palmitoylation is performed in a Kvß2.1 interaction partner that traffics it until this location.

In order to distinguish which is the mechanism implied in this new targeting, the mutation of all Kvß2.1 cysteines was required. If the mutant was keeping the ability of travelling to *lipid raft* microdomains, it has a partner driving it.

```
                10                  20                  30                  40                  50
MYPESTTGSP  ARLSLRQTGS  PGMIYSTRYG  SPKRQLQFYR  NLGKSGLRVS
                60                  70                  80                  90                 100
CLGLGTWVTF  GGQITDEMAE  HLMTLAYDNG  INLFDTAEVY  AAGKAEVVLG
               110                 120                 130                 140                 150
NIIKKKGWRR  SSLVITTKIF  WGGKAETERG  LSRKHIIEGL  KASLERLQLE
               160                 170                 180                 190                 200
YVDVVFANRP  DPNTPMEETV  RAMTHVINQG  MAMYWGTSRW  SSMEIMEAYS
               210                 220                 230                 240                 250
VARQFNLIPP  ICEQAEYHMF  QREKVEVQLP  ELFHKIGVGA  MTWSPLACGI
               260                 270                 280                 290                 300
VSGKYDSGIP  PYSRASLKGY  QWLKDKILSE  EGRRQQAKLK  ELQAIAERLG
               310                 320                 330                 340                 350
CTLPQLAIAW  CLRNEGVSSV  LLGASNAEQL  MENIGAIQVL  PKLSSSIVHE
               360
IDSILGNKPY  SKKDYRS
```

Figure 12. Kvß2.1 mouse aminoacid sequence. Cysteines are highlighted in red.

Analysing the sequence of mouse Kvß2.1 (figure 12), it presents a total amount of five cysteines in the positions: 51, 212, 248, 301 and 311. By directed mutagenesis, some series of mutants were developed and classified. The strategy was to switch cysteine residues for serines. The choosing is done based on their similarity; actually, cysteine is often synthetized in animals from serine. The mutants obtained and analysed were the following.

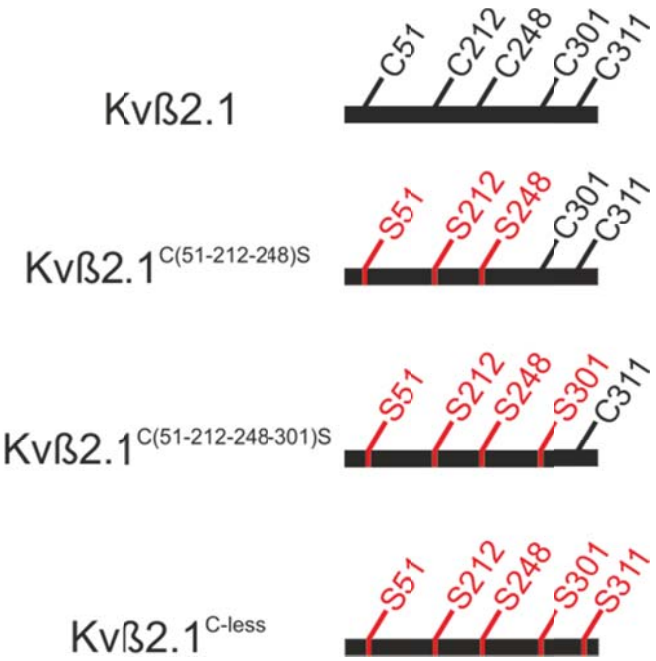

Figure 13. Schematic representation of the different mutants analysed.

In order to avoid the presence of deleterious mutants among our trials, the cellular distribution of them was checked by confocal microscopy. While the mutants Kvß2.1$^{c(52-212-248)S}$ (figure 14B) and Kvß2.1$^{c(52-212-248-301)S}$ (figure 14C) were presenting a comparable distribution with Kvß2.1 wild type (figure 14A), the Kvß2.1^{C-less} is exhibiting a totally different pattern of expression (figure 14D). Analysis of the colocalization with the membrane marker, while Kvß2.1 is mainly present in the intracellular space (figure 14E-H), Kvß2.1^{C-less} shows a profile coincident with the membrane marker (figure 14I-L). This mutant presents more than two-fold colocalization with the plasma membrane which is highly statistically different compared with the Kvß2.1 wild type (figure 14M).

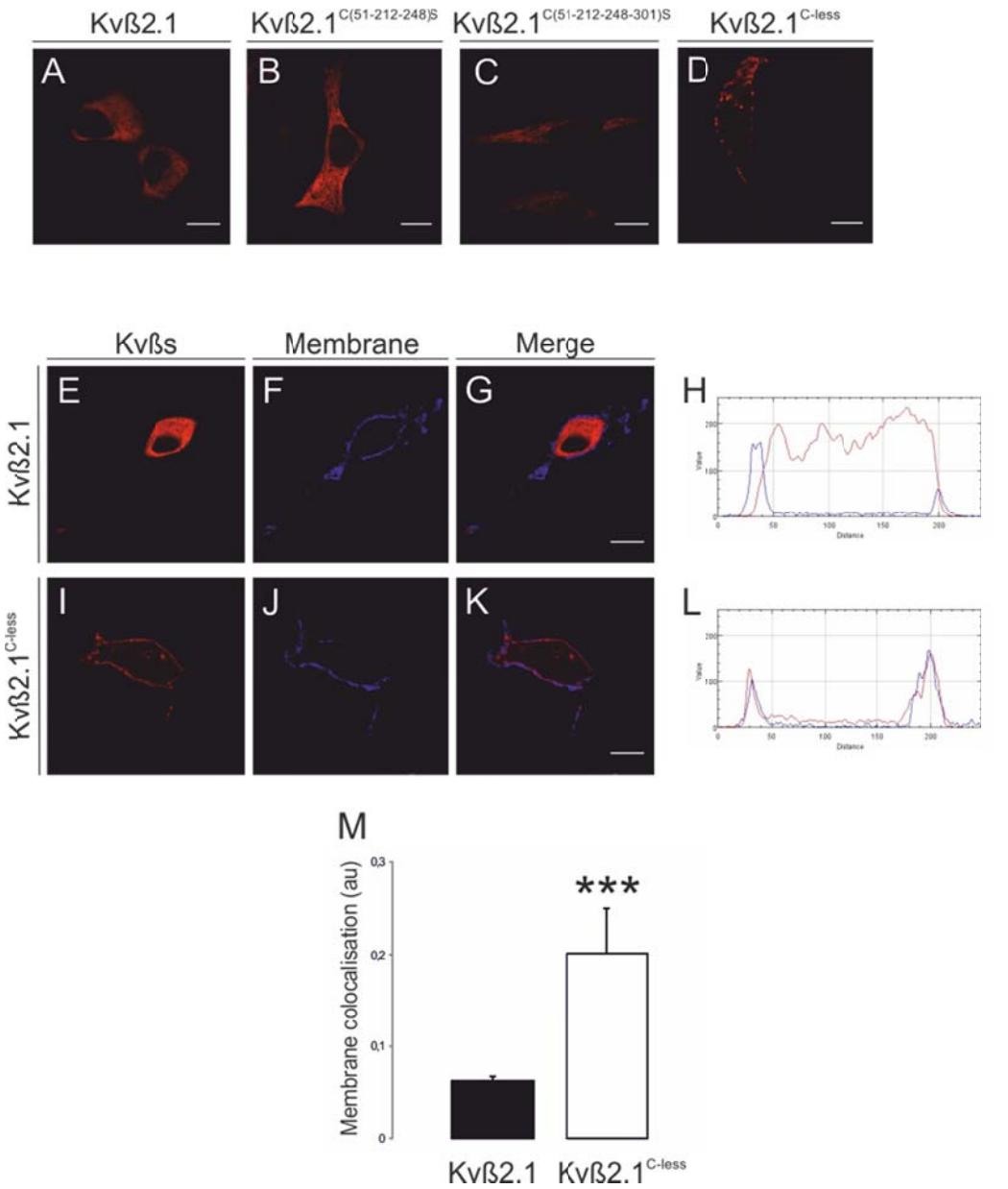

Figure 14. Representative Kvß2.1 mutants cellular distribution. A: Kvß2.1. B: Kvß2.1$^{c(52\text{-}212\text{-}248)S}$. C: Kvß2.1$^{c(52\text{-}212\text{-}248\text{-}301)S}$. D: Kvß2.1$^{C\text{-}less}$. E-H: membrane colocalization of Kvß2.1. **E**: Kvß2.1. F: membrane marker. G: merge of channels, purple means colocalization. H: pixel-by-pixel analysis of ROI in G. I-**L**: membrane colocalization of Kvß2.1$^{C\text{-}less}$. I: Kvß2.1$^{C\text{-}less}$. J: membrane marker. K: merge of channels, purple means colocalization. L: pixel-by-pixel analysis of ROI in K.

This highly different distribution of the mutant, possibly due to a new phosphorylation site insert by the mutagenesis of cysteine 311, forced us to build a new mutant. At this position we decided to alter the sequence in order to encode an alanine (figure 15).

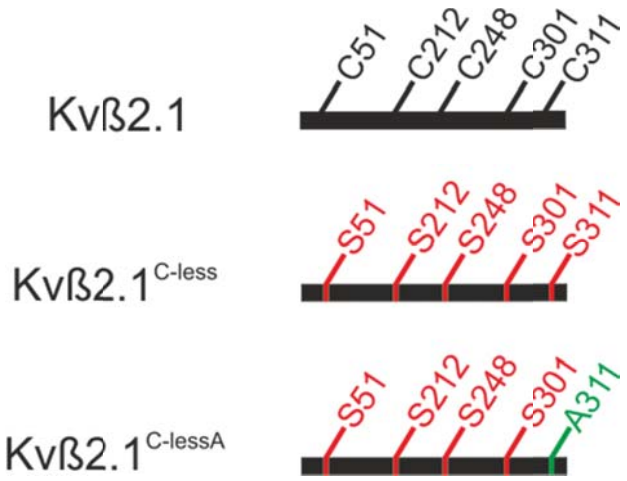

Figure 15. Schematic representation of the new mutant Kvβ2.1$^{C\text{-}lessA}$ generated.

Concomitantly, the cellular pattern of the new mutant was analysed. The expression of Kvβ2.1$^{C\text{-}lessA}$ (figure 16B) leads a distribution similar to the one showed by Kvβ2.1 wild type (figure 16A).

Once checked that there is a maintenance of the general protein physiology, the presence at the cell surface was analysed in the different mutants obtained. Kvβ2.1, as previously showed, exhibits a colocalisation (figure 16C-E) with the membrane marker patent in the overlap of pics at the pixel-by-pixel plot (figure 16F). This distribution is similar for the mutant Kvβ2.1$^{C(52\text{-}212\text{-}248)S}$ (figure 16G-I), the one which has three of its cysteines missing. It is detectable the fluorescence of this mutant under the pics of membrane marker showed at the plot (figure 16J). However, when analysed the Kvβ2.1$^{C(52\text{-}212\text{-}248\text{-}301)S}$ (figure 16K-M), it is detectable a shift to the cytoplasmic parts of the cell (figure 16N). Moreover, Kvβ2.1$^{C\text{-}lessA}$ (figure 16O-Q) exacerbates this effect: it decreases the distribution at the membrane and its closest regions. (figure 16R).

The quantification for the surface colocalisation reveals that, Kvβ2.1$^{C(52\text{-}212\text{-}248\text{-}301)S}$ and Kvβ2.1$^{C\text{-}lessA}$ are significantly different from the Kvβ2.1 wild type reaching just half of the distribution at the plasma membrane. However, there are no differences detected between this two conditions. The mutant lacking three cysteines, Kvβ2.1$^{C(52\text{-}212\text{-}248)S}$, presents a tendency of a reduction but not statistically relevant. However, its distribution is significantly different from this showed by the other two mutants (figure 16S). The tendency of the results obtained are pointing out that the more cysteines mutated, the less presence at the plasma membrane.

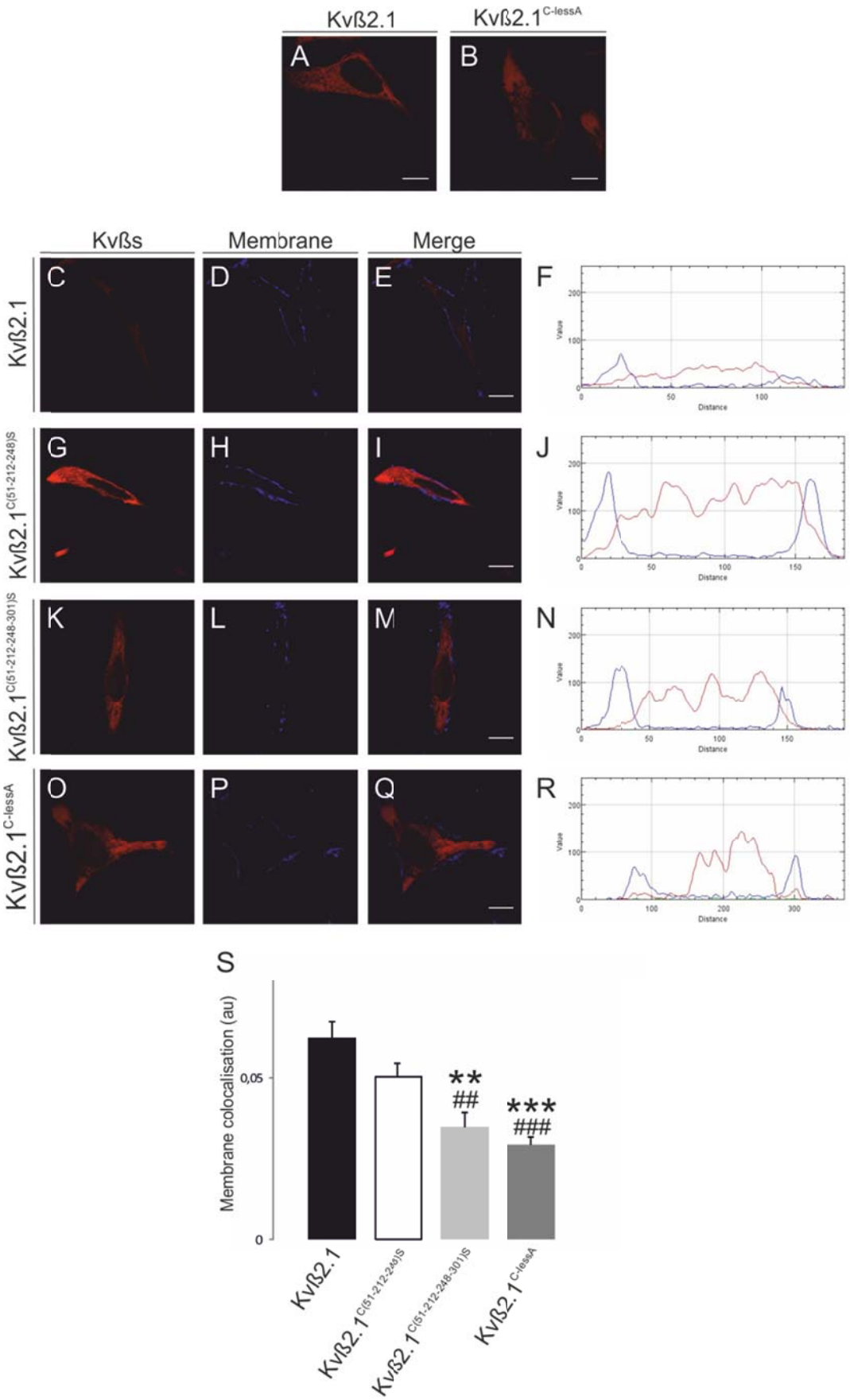

Figure 16. Representative Kvß2.1 and Kvß2.1$^{C\text{-}lessA}$ cellular distribution. A: Kvß2.1. B: Kvß2.1$^{C\text{-}lessS}$. C-F: Kvß2.1 membrane colocalisation. C: Kvß2.1. D: membrane marker. E: merge of channels, purple means colocalization. F: pixel-by-pixel analysis of ROI in E. G-J: Kvß2.1$^{c(51\text{-}212\text{-}248)S}$ membrane colocalisation. G: Kvß2.1$^{c(51\text{-}212\text{-}248)S}$. H: membrane marker. I: merge of channels,

purple means colocalization. J: pixel-by-pixel analysis of ROI in I. K-N: Kvß2.1$^{c(51\text{-}212\text{-}248\text{-}301)S}$ membrane colocalisation. K: Kvß2.1$^{c(51\text{-}212\text{-}248)S}$. L: membrane marker. M: merge of channels, purple means colocalization. N: pixel-by-pixel analysis of ROI in M. O-R: Kvß2.1$^{C\text{-}lessA}$ membrane colocalisation. O: Kvß2.1$^{C\text{-}lessA}$. P: membrane marker. Q: merge of channels, purple means colocalization. R: pixel-by-pixel analysis of ROI in Q. M: Quantification of membrane colocalisation using Mander's coefficiency. **p<0.01, ***p<0.001 compared with Kvß2.1. ##p<0.01, ###p<0.001 compared with Kvß2.1$^{c(51\text{-}212\text{-}248)S}$.

The surface expression seems to be related to the amount of cysteines remaining at the sequence. However, in order to ensure the previous results, ABE assay was performed on the mutants. Detecting a comparable starting material (figure 17A) for Kvβ2.1 and Kvβ2.1$^{C\text{-}lessA}$ conditions, the figure 17B shows that, unlike the wild type subunit, the *C-lessA mutant* exhibits an important reduction, almost completely, of the signal detectable for palmitoylation. The mutants tested for membrane targeting in figure 16, were showing intermediate and variable patterns of palmitoylation. However, as figure 17C shows, the mutant Kvβ2.1$^{C(52\text{-}212\text{-}248)S}$ presents a major acylation extent than Kvβ2.1$^{C(52\text{-}212\text{-}248\text{-}301)S}$, pointing the cysteine 301 as a target of palmitoylation.

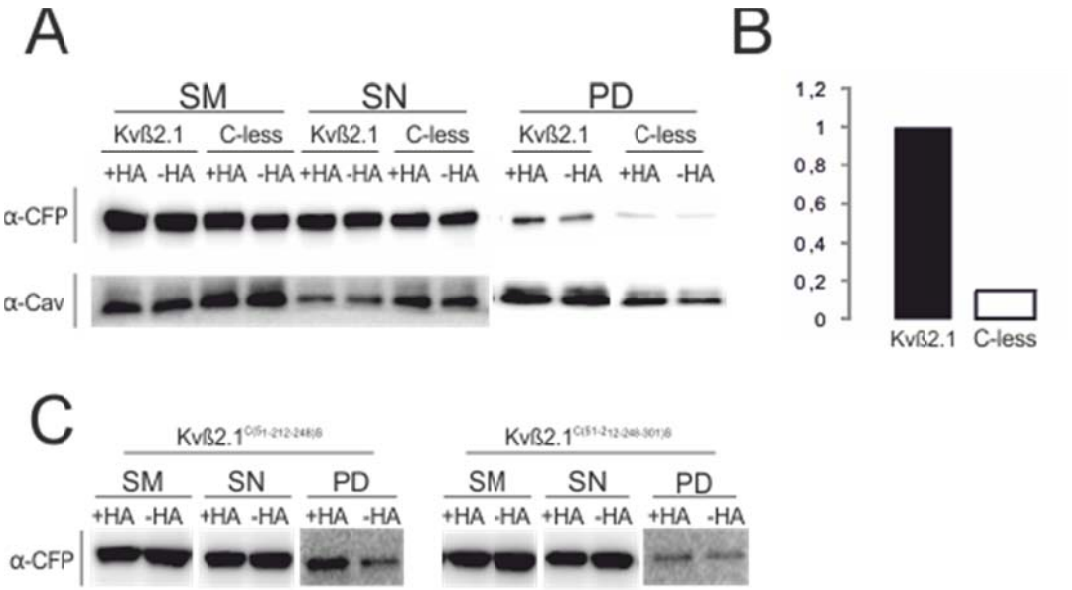

Figure 17. Kvß2.1 wild type and *C-less mutant* palmitoylation comparison. A. Representative ABE experiment of Kvß2.1 wild (Li et al., 2000)type and Kvß2.1$^{C\text{-}lessA}$. B. Quantification of pulldown amount in both conditions relative to the starting material. C. Representative ABE experiment of Kvß2.1$^{c(51\text{-}212\text{-}248)S}$ and Kvß2.1$^{c(51\text{-}212\text{-}248)S}$. +HA: Experiment developed in the presence of hydroxylamine. -HA: Experiment developed in the absence of hydroxylamine. SM: starting material. SN: supernatant collected after the pulldown. PD: pulldown of the palmitoylated proteins.

Even though the previous results showed that the progressive absence of cysteines in the Kvβ2.1 sequence is related to the loose of the palmitoylation presence at the protein and positively correlated with the loose of its membrane presence, the relationship with its location at the *lipid raft* microdomains remained not concluded.

Testing the ability for the traffic to this subcellular environment, Kvβ2.1$^{C\text{-}lessA}$, unlike Kvβ2.1 (figure 18A), presented and impairment for reaching those domains (figure 18B). The quantification (figure 18C) demonstrated that there is a highly significant reduction (68.06% ± 1.23) in the capability for occupying this location. Thereby, is the palmitoylation on Kvβ2.1 sequence the process that govern its *lipid raft* localisation.

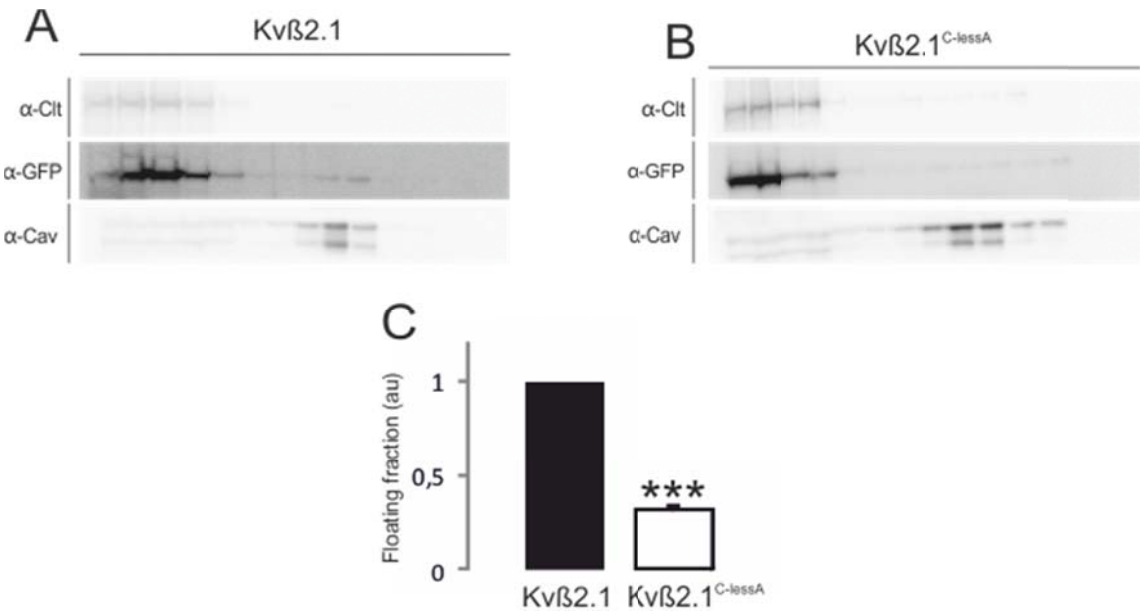

Figure 18. Lipid raft microdomains purification of Kvß2.1 and Kvß2.1$^{C\text{-}lessA}$. A: Western blotting of lipid raft fractions of Kvß2.1. B: Western blotting of lipid raft fractions of Kvß2.1$^{C\text{-}lessA}$. C. Quantification of the flotability relativized by the total amount of expression.

Although the reduction on the Kvβ2.1$^{C\text{-}lessA}$ floatability exhibited a high extent, this protein is still present at this emplacement (figure 18C). Thus, a part of its traffic to those domains is palmitoylation-independent.

Proliferative signalling and PMA interfere in Kvß2.1 localisation

Lipid raft microdomains are considered membrane platforms of signalling proteins. They allow to overcoming the spatial distance among proteins that need to be close. It can generate a spatial concentration for proteins that are involved in the same pathways (Dart, 2010). Considering its function as an oxidoreductase and as a Kv modulator, the positioning of Kvß2.1 in *lipid raft* microdomains is highly relevant. Palmitoylation, previously described as the mechanism for trafficking Kvß2.1 to those environments (figure 18), is a reversible process that can be modulated by different mechanisms. Actually, the research on this topic is taking off regarding the involvement of those processes in several different functions.

Considering that Kvß family exhibit a differential regulation upon proliferation or activation stimuli in some cells, such as macrophages, the ability of targeting *lipid raft* microdomains posterior to those insults was assessed (Vicente et al., 2005). Kvß2.1 was present in the floating fractions when the HEK cells were cultured in the presence of growth factors (figure 19A), but not when they are subjected to starvation (figure 19B). The quantification confirmed this reduction and it is significantly relevant (figure 19C).

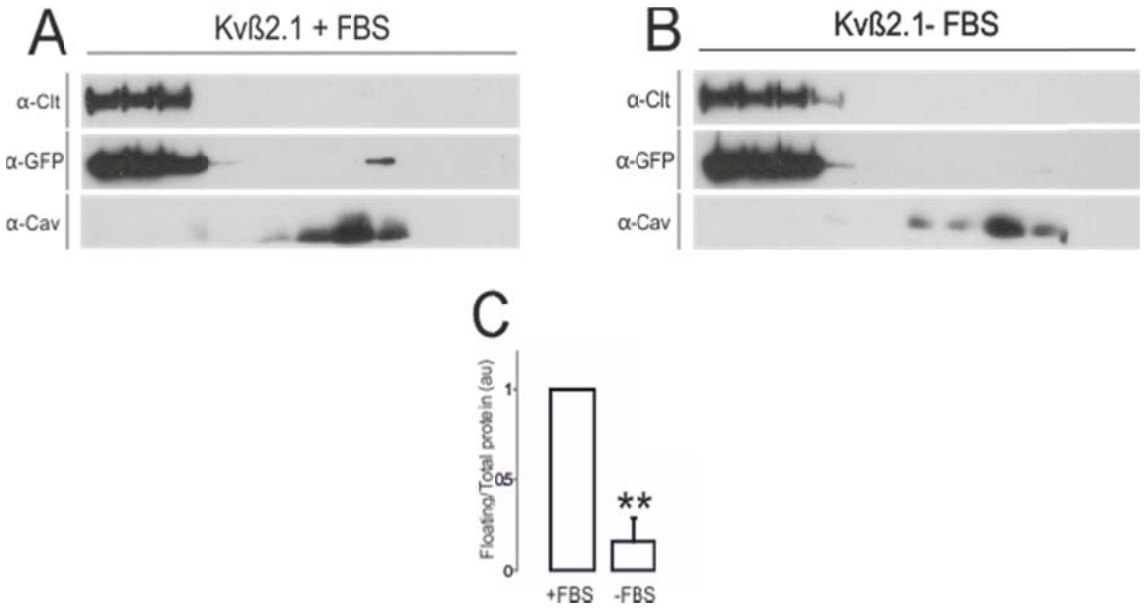

Figure 19. Lipid raft microdomains purification of Kvß2.1 under proliferative signalling. A. Western blotting of lipid raft fractions of Kvß2.1CFP in presence of FBS. B. Western blotting of lipid raft fractions of Kvß2.1CFP in the absence os FBS. C. Quantification of flotability in both conditions relativized by the total amount.

The effect on the lipid raft presence was also observable when analysed the membrane colocalisation by confocal microscopy.

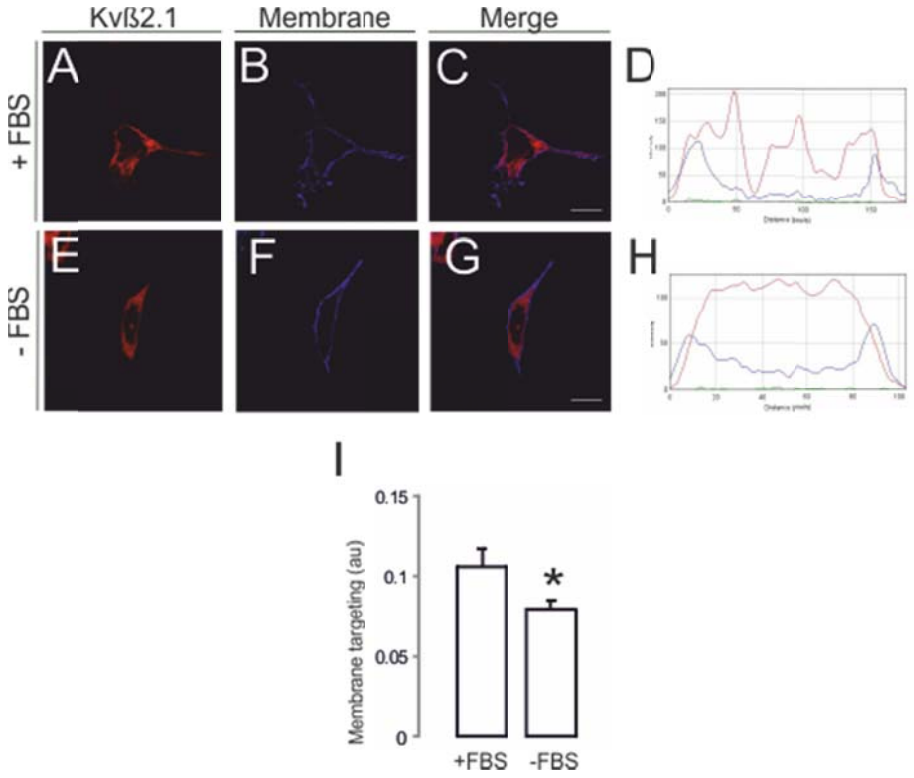

Figure 20. Differential Kvß2.1 membrane targeting. A-D: Cellular distribution of Kvß2.1 in the presence of FBS. A: Kvß2.1CFP. B: Membrane marker. C: merge, purple means colocalization. D: pixel-by-pixel analysis of ROI in C. E-H: Cellular

distribution of Kvß2.1 in absence of FBS. E: Kvß2.1CFP. D: membrane marker. E: merge of channels, purple means colocalization. H: pixel-by-pixel analysis of ROI in G. I: Quantification of membrane targeting in presence an absence of FBS. *p<0.05.

The effect of FBS on the membrane targeting was confirmed (Figure 20). While Kvß2.1 is detectable colocalising with the membrane marker in the presence of FBS (figure 20A-D), once the cells are subjected to starvation, the subunit loses partially this distribution (figure 20E-H). The impairment is slightly significant but confirms our previous results (figure 20I). Proliferating signals enhance the traffic of Kvß2.1 to *lipid raft* microdomains.

While FBS has the ability to target Kvß2.1 to specific domains of the plasma membrane, the mechanisms of recycling that will control the period of time it will remain in *lipid raft* are also highly relevant. Previous thesis from our laboratory reports the exit from those domains and endocytosis of Kv1.3 after a PMA treatment. Since Kvß2.1 is also present at *lipid raft* and it exerts the capability of modulate this channel, convergence of interests leads us to analyse how it is regulated by a PMA treatment.

In order to study deeply the putative effect, *lipid raft* microdomains extraction was performed in absence or presence of PMA. The experiment was developed also in the presence of the protein PSD95. Trying to approach the experimental conditions to a more physiological model, this MAGUK protein has been related strongly to the polarity of the neurons, acting as a platform in the post-synaptic membrane (Oliva et al., 2012). Not only in nervous system but also in immune cell physiology, a member of the protein family has been linked to pivotal roles such as: T-cell immunological synapse formation, NFAT activation, cytokine secretion or acting as a negative regulator of lymphocyte proliferation. Concretely, for PSD95, the inhibition has been related to a decrease in the T-cells uropod formation (Shaw and Filbert, 2009) .

Not only is present in the physiology of nervous system cells and immune system cells, where Kvß family is highly expressed, but also is expressed specifically in *lipid raft* domains in a palmitoylation-dependent manner (Cho et al., 1992, Wong and Schlichter, 2004). It has been also described the direct interaction between the PKCα and PSD95 (O'Neill et al., 2011). The possible modulation of Kvß2.1 by PSD95 addressed in the investigation was necessary to approach it to a more physiological model.

On one hand, the treatment with PMA clearly shifts the distribution of the protein to non-floating fractions (figure 21A-B), showing a 67,4%±7.5 reduction. On the other hand, the cotransfection of the protein PSD95, leads to two different effects: increases the presence of Kvß2.1 in *lipid raft* microdomains and impairs the decrease produced by PMA (figure 21C-E). This effect on Kvß2.1 subunit it might be exacerbated by the fact that PMA increases PSD95 presence in lipid raft domains under the presence of PMA treatment (figure 21F).

While proliferation signals and PSD95 presence enhance the traffic to those domains, the activation of PKC via PMA is inducing its diminution, and counteracted by the MAGUK subunit.

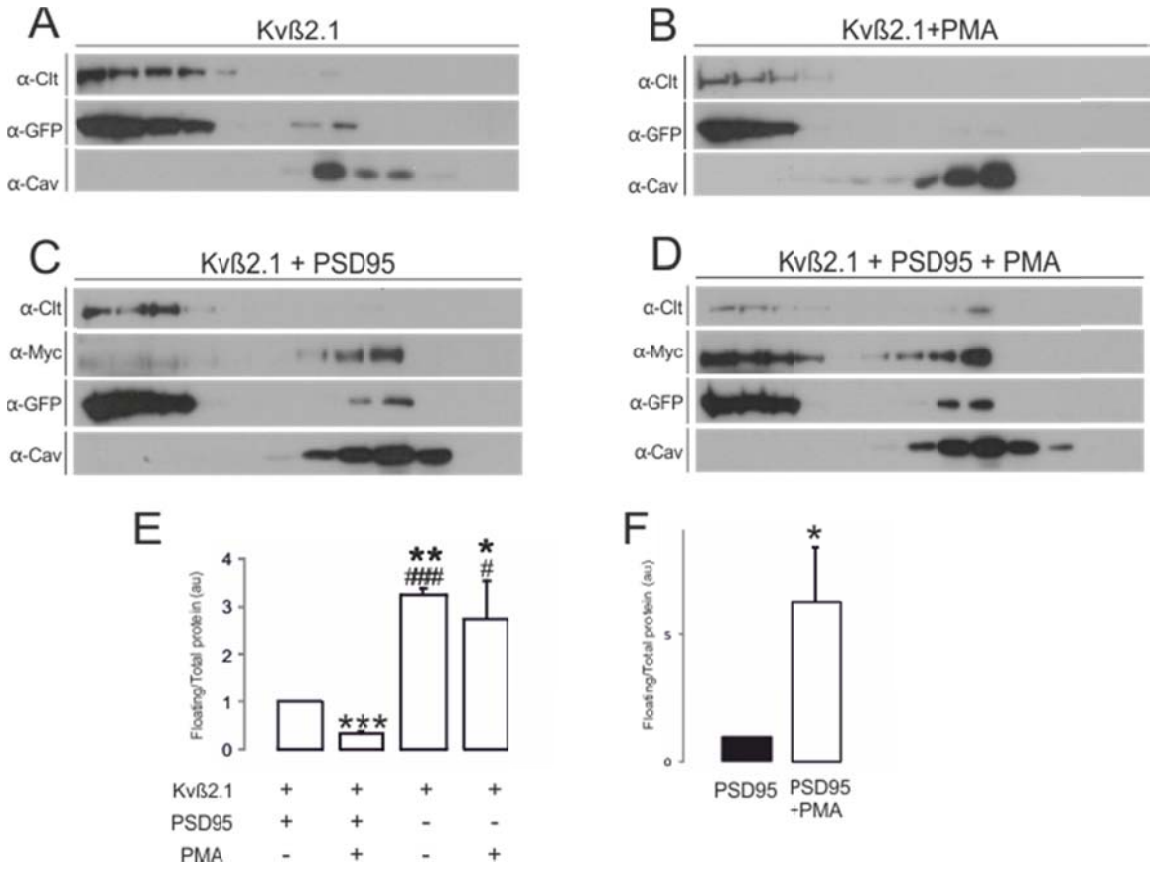

Figure 21. Lipid raft microdomains extraction of Kvß2.1CFP transfected cells in the presence of PMA and PSD95. A: Western blotting of lipid raft fractions of Kvß2.1CFP. B: Western blotting of lipid raft fractions of Kvß2.1CFP with PMA treatment C: Western blotting of lipid raft fractions of Kvß2.1CFP and PSD95. D: Western blotting of lipid raft fractions of Kvß2.1CFP and PSD95 with PMA treatment. E. Quantification of the Kvß2.1 flotability in all conditions relativized by the total amount of expression. F. Quantification of the PSD95 flotability in the presence and the absence of PMA. *p<0.05, **p<0.01, ***p<0.001 versus Kvß2.1 alone. #p<0.01, ###p<0.001 versus Kvß2.1 treated with PMA.

PSD95 exhibits three different PDZ domains and one SH_3 interacting motif. It has been typically described as a platform that can contact with several different protein families localising properly those in signalling regions. For instance, a previous thesis of our laboratory established that Kv1.3 interacts with PSD95 stabilising its presence in *lipid raft*, as well as avoiding the endocytic pathway enhanced by PMA. It has also been described that PSD95 can direct Kv1.4 to lipid raft, and depends on its own palmitoylation (Wong and Schlichter, 2004). However, it is also known that CaMKIIα can recruit PSD95 to those domains without a molecular interaction (Suzuki et al., 2008).

To decipher which is the PSD95 mechanism able to influence Kvß2.1 behaviour, and the putative modulation by PMA, the capability for interacting was tested. Not in the presence, neither in the absence of PMA (figure 22), there is PSD95 coimmunoprecipitation detected pulling-down Kvß2.1. Thereby, lipid raft stabilisation and PKC buffering could be the mechanisms involved in maintaining Kvß2.1 floatability.

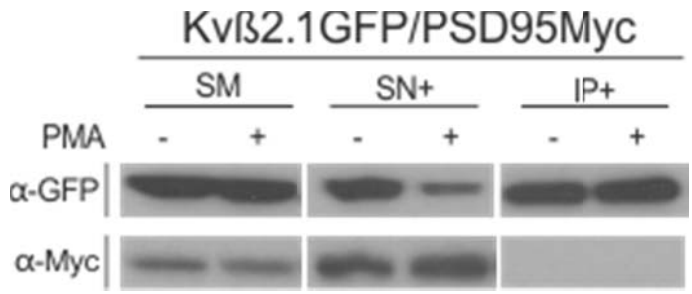

Figure 22. Kvß2.1 lipid raft stabilisation and PMA endocytosis impairment by PSD95 is not via direct interaction. Immunoprecipitation assay against GFP. Western blot using α-GFP antibody and α-Myc antibody. SM: starting material. SN+: supernatant of the precipitation. IP+: Immunoprecipitation in the presence of the antibody.

The PMA treatment could be enhancing the disappearance of Kvß2.1 by different mechanisms. In order to decipher if it is mediated by the endocytosis, the colocalisation with EEA-1 upon PMA treatment was analysed. Both conditions were exhibiting positive colocalisation since Kvß2.1 is mainly intracellular emplaced (figure 23A-F). However, when analysed (figure 23G) the level of coincidence in the presence of PMA treatment, the result was significantly positive.

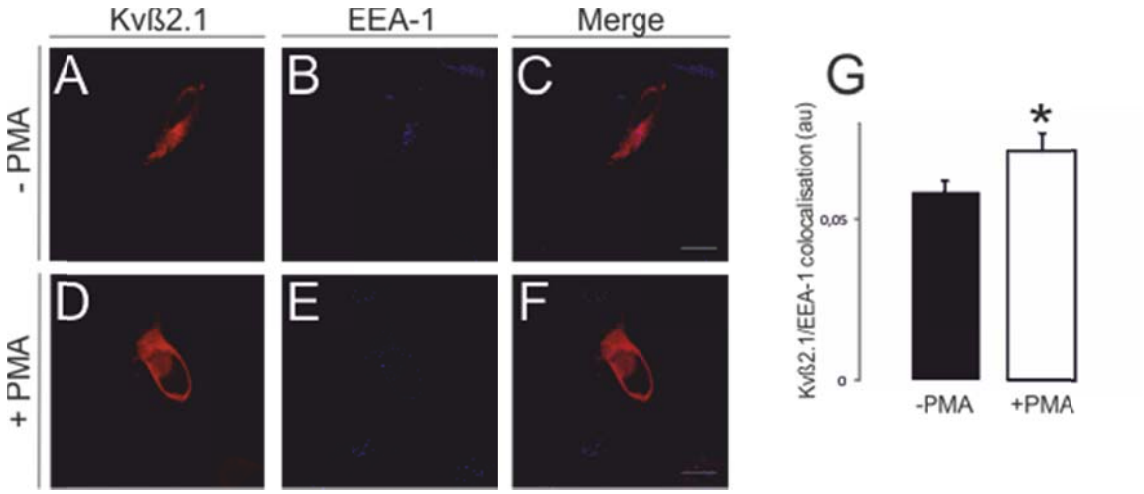

Figure 23. Colocalisation of Kvß2.1 with EEA-1 marker in with PMA treatment. A-D: Cellular distribution of Kvß2.1 in the absence of PMA. A: Kvß2.1CFP. B: Membrane marker. C: merge, purple means colocalization. E-H: Cellular distribution of Kvß2.1 in presence of PMA. E: Kvß2.1CFP. D: membrane marker. E: merge of channels, purple means colocalization. I: Quantification of EEA-1 colocalisation in presence an absence of PMA. *p<0.05.

Previous results from our laboratory stablished that the internalisation of Kv1.3 channel depending on PMA treatment was mediated by an ubiquitination process of some residues. Since the late result is pointing to an endocytosis of the Kvß2.1, the putative ubiquitination of this subunit was investigated. To proceed, an immunoprecipitation was performed to purify and isolate Kvß2.1 from the rest of the proteins. It is detectable the ubiquitination in the same weight of the Kvß2.1 and there is an increased smir in the PMA treated lane compared with the non-treated one (figure 24).

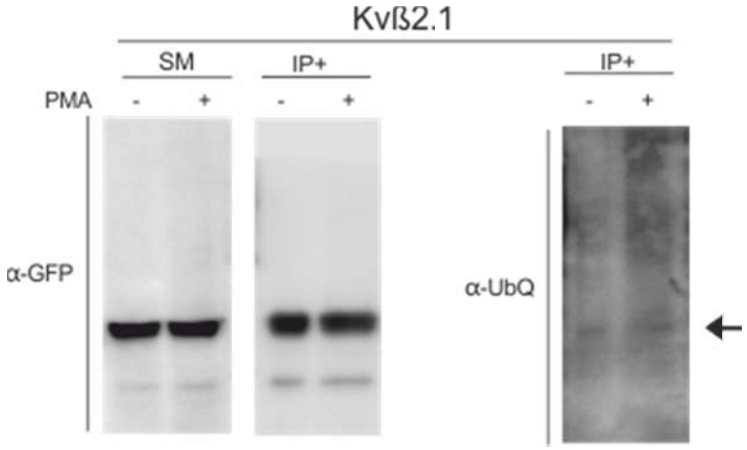

Figure 24. PMA treatment enhances slightly the Kvß2.1 ubiquitination. Immunoprecipitation of Kvß2.1 and immunoblotting against ubiquitin. SM: starting material. IP+: immunoprecipitation in the presence of GFP antibody. Arrow indicates Kvß2.1.

DISCUSSION

The present contribution described that Kvβ2, originally described as a cytoplasmic protein, is unexpectedly present at membrane fractions. We have demonstrated, pharmacologically and by Kvβ2.1 cysteine mutagenesis, that this localization is mediated principally by a post-traductional lipidic modification. Recently, effects of palmitoylation are under intense investigation not only in membrane but also in soluble proteins (Smotrys and Linder, 2004). In the first case, this modification has been related to determine lipid raft localization (Charollais and Van Der Goot, 2009). For soluble proteins, palmitoylation is also a mechanism to drive them to specific membrane locations where they can develop a specific function. SNAP-25 palmitoylation drives it to the plasma membrane where it will be forming finally the SNARE complex, a key process in membrane fusion (Greaves et al., 2010). Another example is the kinase DLK, critical for axon-to-soma retrograde signaling following nerve injury. Palmitoylation at DLK locates it in trafficking vesicles, it is required to assemble DLK signaling complexes and is essential for DLK kinase activity (Holland et al., 2016). So, which is the purpose of driving Kvβ2.1 to the plasma membrane?

The modification of Kvβ2.1 to control its location, as well as the control under specific stimulus, leads to think that some differential functions are performed when this target position is occupied. The most studied functions of Kvβ2.1 are related to its control of Kv1 and Kv4 families (Yang et al., 2001, Li et al., 2006). Even it does not present the ball-and-chain inactivation system, it has been published that Kvβ2.1 presents the ability of enhancing the surface expression of some channels. From those results it was hypothesized that Kvβ2.1 is a possible chaperone, helping them to achieve the proper functional conformation (Shi et al., 1996). It was also described that, upon specific combinations of Kvβ2.1/Kv channels, the half-voltage activation is switched to more negative values (Heinemann et al., 1996). Little is known about the role of this protein in the absence of pore-forming subunits. Computational analysis showed that Kvβ2.1 forms part of the AKR family and several studies were performed to demonstrate that is an

active enzyme with endogenous substrates (Kilfoil et al., 2013). Those results enhanced the analysis of the putative effect of Kvβ2.1-AKR activity on Kv currents. While the interaction with NADPH is required, most probably enhancing the proper folding of Kvβ2.1, the impairment of the enzymatic activity does not have major changes on Kvβ2.1 function (Campomanes et al., 2002, Weng et al., 2006).

Considering that Kvβ2.1 is undergoing a specific control of its location, palmitoylation-mediated, in the absence of α-subunits, and regarding that its aldoketoreductase activity is not highly coupled to their control on Kv channels, it is tempting to speculate that Kvβ2.1 could be acting as a sensor at specific domains at the plasma membrane. Even some studies revealed that it is a slow enzyme compared with other AKR; the measurement of the hydride transfer revealed that Kvβ2.1 is as fast as other members of the family (Liu et al., 2001). This made likely to think on Kvβ2.1 as a sensor for the redox state of the cell (Tipparaju et al., 2008, Weng et al., 2006). In the present work we demonstrate that Kvβ1.1 don't present lipid raft localization but it is placed at the plasma membrane depending on its actin interaction, as Trimmer group determined (Nakahira et al., 1998). For Kvβ1.3, closer to Kvβ1.1, it was measured a slower hydride transfer compared with Kvβ2.1 (Tipparaju et al., 2007). So, at the plasma membrane, the cell can place redox detectors with specific sensing rate. Concomitantly, it have been demonstrated that Kvβ2.1 can reduce aldehydes and ketones of membrane-derived oxidized lipids preferably, highlighting the importance for the Kvβ-membrane location (Xie et al., 2011, Tipparaju et al., 2008).

Moreover, we have shown that Kvβ2.1 lipid raft localization is controlled by different signals. Upon proliferative stimuli, we have demonstrated that the amount of Kvβ2.1 detected increased by membrane colocalization and lipid raft purification. However, posterior to a PMA treatment, an important decrease presence in those subcellular domains was observed counteracted by PSD95. This capability of PSD95 could be due to a direct interaction with PKC masking its region for detecting Kvβ2.1. By those mechanisms, it would be controllable the sensor position depending on the cellular time moment.

Moreover, several different partners have been related to Kvβ2.1, apart from Kv channels. ZIP1, ZIP2 and ZIP3 link this protein to the isoform PKCζ, and it can interact with PKA, EB1, KIF3/kinesin II, TRPV1, TREK among others (Gong et al., 1999, Croci et al., 2003, Gu et al., 2006, Bavassano et al., 2013, Kisselbach et al., 2012). Since Kvβ2.1 can be placed at lipid raft posterior to a palmitoylation process, their partners are possibly translocated to those domains. This idea leads us to consider that Kvβ family, in the absence of Kv channels, are exerting functions of signalling platforms. The control by FBS and PMA on its distribution could be, then, modifying the whole complex of proteins. Further experiments need to be performed to solve this hypothesis and to assess if there is redox control of those multicomplexes.

Since the Kvβ research started, several different groups have discussed the idea that there are some functions of this protein that are yet to be discovered. The expected effects on Kvβ2.1 null mice were considered mild compared with the range of consequences on Kv1.1 and Kv1.2 at the nervous system level (McCormack et al., 2002). The sensing in the hypoxia level can be transferred to Kv4.3 channel, by direct interaction, but also to a non-interacting partner: Kv2.1 (Coppock et al., 2001). So, this is inferring a different mechanism by which it could be able to transfer those detections. Finally, the fact that

Kvβ2.1 AKR activity do not exert major changes in the control of Kv channels, allow them to consider Kvβ2.1 as a moonlighting protein (Campomanes et al., 2002). This work stimulates even more this idea. A refined modulation of this accessory subunit, by palmitoylation, proliferation stimulus and PMA treatment in the absence of their principal partner, has to be considered as a functional protein entity by itself. Several studies need to be performed to finally elucidate their missing cellular role.

REFERENCES

ACCILI, E. A., KIEHN, J., YANG, Q., WANG, Z., BROWN, A. M. & WIBLE, B. A. 1997b. Separable Kvbeta subunit domains alter expression and gating of potassium channels. *J Biol Chem,* 272**,** 25824-31.

BAVASSANO, C., MARVALDI, L., LANGESLAG, M., SARG, B., LINDNER, H., KLIMASCHEWSKI, L., KRESS, M., FERRER-MONTIEL, A. & KNAUS, H. G. 2013. Identification of voltage-gated K(+) channel beta 2 (Kvbeta2) subunit as a novel interaction partner of the pain transducer Transient Receptor Potential Vanilloid 1 channel (TRPV1). *Biochim Biophys Acta,* 1833**,** 3166-75.

BROWN, D. A. & LONDON, E. 1998. Structure and origin of ordered lipid domains in biological membranes. *J Membr Biol,* 164**,** 103-14.

CAMPOMANES, C. R., CARROLL, K. I., MANGANAS, L. N., HERSHBERGER, M. E., GONG, B., ANTONUCCI, D. E., RHODES, K. J. & TRIMMER, J. S. 2002. Kv beta subunit oxidoreductase activity and Kv1 potassium channel trafficking. *J Biol Chem,* 277**,** 8298-305.

CHAROLLAIS, J. & VAN DER GOOT, F. G. 2009. Palmitoylation of membrane proteins (Review). *Mol Membr Biol,* 26**,** 55-66

CHO, K. O., HUNT, C. A. & KENNEDY, M. B. 1992. The rat brain postsynaptic density fraction contains a homolog of the Drosophila discs-large tumor suppressor protein. *Neuron,* 9**,** 929-42.

CONNOR, J. X., MCCORMACK, K., PLETSCH, A., GAETA, S., GANETZKY, B., CHIU, S. Y. & MESSING, A. 2005. Genetic modifiers of the Kv beta2-null phenotype in mice. *Genes Brain Behav,* 4**,** 77-88.

COPPOCK, E. A., MARTENS, J. R. & TAMKUN, M. M. 2001. Molecular basis of hypoxia-induced pulmonary vasoconstriction: role of voltage-gated K+ channels. *Am J Physiol Lung Cell Mol Physiol,* 281**,** L1-12.

CROCI, C., BRANDSTATTER, J. H. & ENZ, R. 2003. ZIP3, a new splice variant of the PKC-zeta-interacting protein family, binds to GABAC receptors, PKC-zeta, and Kv beta 2. *J Biol Chem,* 278**,** 6128-35.

DART, C. 2010. Lipid microdomains and the regulation of ion channel function. *J Physiol,* 588**,** 3169-78.

GIESE, K. P., STORM, J. F., REUTER, D., FEDOROV, N. B., SHAO, L. R., LEICHER, T., PONGS, O. & SILVA, A. J. 1998. Reduced K+ channel inactivation, spike broadening, and after-hyperpolarization in Kvbeta1.1-deficient mice with impaired learning. *Learn Mem,* 5**,** 257-73.

GONG, J., XU, J., BEZANILLA, M., VAN HUIZEN, R., DERIN, R. & LI, M. 1999. Differential stimulation of PKC phosphorylation of potassium channels by ZIP1 and ZIP2. *Science,* 285**,** 1565-9.

GREAVES, J., PRESCOTT, G. R., GORLEKU, O. A. & CHAMBERLAIN, L. H. 2010. Regulation of SNAP-25 trafficking and function by palmitoylation. *Biochem Soc Trans,* 38**,** 163-6.

GU, C., ZHOU, W., PUTHENVEEDU, M. A., XU, M., JAN, Y. N. & JAN, L. Y. 2006. The microtubule plus-end tracking protein EB1 is required for Kv1 voltage-gated K+ channel axonal targeting. *Neuron,* 52**,** 803-16.

GU, Y. & GU, C. 2010. Dynamics of Kv1 channel transport in axons. *PLoS One,* 5**,** e11931.

GULBIS, J. M., MANN, S. & MACKINNON, R. 1999. Structure of a voltage-dependent K+ channel beta subunit. *Cell,* 97**,** 943-52.

HEILSTEDT, H. A., BURGESS, D. L., ANDERSON, A. E., CHEDRAWI, A., THARP, B., LEE, O., KASHORK, C. D., STARKEY, D. E., WU, Y. Q., NOEBELS, J. L., SHAFFER, L. G. & SHAPIRA, S. K. 2001. Loss of the potassium channel beta-subunit gene, KCNAB2, is associated with epilepsy in patients with 1p36 deletion syndrome. *Epilepsia,* 42**,** 1103-11.

HEINEMANN, S. H., RETTIG, J., GRAACK, H. R. & PONGS, O. 1996. Functional characterization of Kv channel beta-subunits from rat brain. *J Physiol,* 493 (Pt 3)**,** 625-33.

HOLLAND, S. M., COLLURA, K. M., KETSCHEK, A., NOMA, K., FERGUSON, T. A., JIN, Y., GALLO, G. & THOMAS, G. M. 2016. Palmitoylation controls DLK localization, interactions and activity to ensure effective axonal injury signaling. *Proc Natl Acad Sci U S A,* 113**,** 763-8.

KISSELBACH, J., SCHWEIZER, P. A., GERSTBERGER, R., BECKER, R., KATUS, H. A. & THOMAS, D. 2012. Enhancement of K2P2.1 (TREK1) background currents expressed in Xenopus oocytes by voltage-gated K+ channel beta subunits. *Life Sci,* 91**,** 377-83.

LI, Y., UM, S. Y. & MCDONALD, T. V. 2006. Voltage-gated potassium channels: regulation by accessory subunits. *Neuroscientist,* 12**,** 199-210

LIU, S. Q., YIN, J. & BHATNAGAR, A. 2003. Protein kinase C-dependent phosphorylation of the beta-subunit of the voltage-sensitive potassium channels (Kvbeta2). *Chem Biol Interact,* 143-144**,** 597-604.

LIU, S. Q., JIN, H., ZACARIAS, A., SRIVASTAVA, S. & BHATNAGAR, A. 2001. Binding of pyridine coenzymes to the beta-subunit of the voltage sensitive potassium channels. *Chem Biol Interact,* 130-132**,** 955-62.

LONG, S. B., CAMPBELL, E. B. & MACKINNON, R. 2005. Crystal structure of a mammalian voltage-dependent Shaker family K+ channel. *Science,* 309**,** 897-903.

JING, J., PERETZ, T., SINGER-LAHAT, D., CHIKVASHVILI, D., THORNHILL, W. B. & LOTAN, I. 1997. Inactivation of a voltage-dependent K+ channel by beta subunit. Modulation by a phosphorylation-dependent interaction between the distal C terminus of alpha subunit and cytoskeleton. *J Biol Chem,* 272**,** 14021-4.

KILFOIL, P. J., TIPPARAJU, S. M., BARSKI, O. A. & BHATNAGAR, A. 2013. Regulation of ion channels by pyridine nucleotides. *Circ Res,* 112**,** 721-41.

LEVIN, G., CHIKVASHVILI, D., SINGER-LAHAT, D., PERETZ, T., THORNHILL, W. B. & LOTAN, I. 1996a. Phosphorylation of a K+ channel alpha subunit modulates the inactivation conferred by a beta subunit. Involvement of cytoskeleton. *J Biol Chem,* 271**,** 29321-8.

MCCORMACK, K., CONNOR, J. X., ZHOU, L., HO, L. L., GANETZKY, B., CHIU, S. Y. & MESSING, A. 2002. Genetic analysis of the mammalian K+ channel beta subunit Kvbeta 2 (Kcnab2). *J Biol Chem,* 277**,** 13219-28.

NAGAYA, N. & PAPAZIAN, D. M. 1997. Potassium channel alpha and beta subunits assemble in the endoplasmic reticulum. *J Biol Chem,* 272**,** 3022-7.

NAKAHIRA, K., MATOS, M. F. & TRIMMER, J. S. 1998. Differential interaction of voltage-gated K+ channel beta-subunits with cytoskeleton is mediated by unique amino terminal domains. *J Mol Neurosci,* 11**,** 199-208.

OLIVA, C., ESCOBEDO, P., ASTORGA, C., MOLINA, C. & SIERRALTA, J. 2012. Role of the MAGUK protein family in synapse formation and function. *Dev Neurobiol,* 72**,** 57-72.

O'NEILL, A. K., GALLEGOS, L. L., JUSTILIEN, V., GARCIA, E. L., LEITGES, M., FIELDS, A. P., HALL, R. A. & NEWTON, A. C. 2011. Protein kinase Calpha promotes cell migration through a PDZ-dependent interaction with its novel substrate discs large homolog 1 (DLG1). *J Biol Chem,* 286**,** 43559-68.

PEREZ-VERDAGUER, M., CAPERA, J., SERRANO-NOVILLO, C., ESTADELLA, I., SASTRE, D. & FELIPE, A. 2016b. The voltage-gated potassium channel Kv1.3 is a promising multitherapeutic target against human pathologies. *Expert Opin Ther Targets,* 20**,** 577-91.

PONGS, O., LEICHER, T., BERGER, M., ROEPER, J., BAHRING, R., WRAY, D., GIESE, K. P., SILVA, A. J. & STORM, J. F. 1999. Functional and molecular aspects of voltage-gated K+ channel beta subunits. *Ann N Y Acad Sci,* 868**,** 344-55.

RETTIG, J., HEINEMANN, S. H., WUNDER, F., LORRA, C., PARCEJ, D. N., DOLLY, J. O. & PONGS, O. 1994. Inactivation properties of voltage-gated K+ channels altered by presence of beta-subunit. *Nature,* 369**,** 289-94.

ROCKS, O., GERAUER, M., VARTAK, N., KOCH, S., HUANG, Z. P., PECHLIVANIS, M., KUHLMANN, J., BRUNSVELD, L., CHANDRA, A., ELLINGER, B., WALDMANN, H. & BASTIAENS, P. I. 2010. The palmitoylation machinery is a spatially organizing system for peripheral membrane proteins. *Cell,* 141**,** 458-71.

SHAW, A. S. & FILBERT, E. L. 2009. Scaffold proteins and immune-cell signalling. *Nat Rev Immunol,* 9**,** 47-56.

SHI, G., NAKAHIRA, K., HAMMOND, S., RHODES, K. J., SCHECHTER, L. E. & TRIMMER, J. S. 1996. Beta subunits promote K+ channel surface expression through effects early in biosynthesis. *Neuron,* 16**,** 843-52.

SMOTRYS, J. E. & LINDER, M. E. 2004. Palmitoylation of intracellular signaling proteins: regulation and function. *Annu Rev Biochem,* 73**,** 559-87.

SUZUKI, T., DU, F., TIAN, Q. B., ZHANG, J. & ENDO, S. 2008. Ca2+/calmodulin-dependent protein kinase IIalpha clusters are associated with stable lipid rafts and their formation traps PSD-95. *J Neurochem,* 104**,** 596-610.

TIPPARAJU, S. M., LIU, S. Q., BARSKI, O. A. & BHATNAGAR, A. 2007. NADPH binding to beta-subunit regulates inactivation of voltage-gated K(+) channels. *Biochem Biophys Res Commun,* 359**,** 269-76.

TIPPARAJU, S. M., BARSKI, O. A., SRIVASTAVA, S. & BHATNAGAR, A. 2008. Catalytic mechanism and substrate specificity of the beta-subunit of the voltage-gated potassium channel. *Biochemistry,* 47**,** 8840-54.

WANG, X., ZHANG, J., BERKOWSKI, S. M., KNOWLEG, H., CHANDRAMOULY, A. B., DOWNENS, M. & PRYSTOWSKY, M. B. 2004b. Protein kinase C-mediated phosphorylation of Kv beta 2 in adult rat brain. *Neurochem Res,* 29**,** 1879-86.

WENG, J., CAO, Y., MOSS, N. & ZHOU, M. 2006. Modulation of voltage-dependent Shaker family potassium channels by an aldo-keto reductase. *J Biol Chem,* 281**,** 15194-200.

WILLIAMS, T. M. & LISANTI, M. P. 2004. The caveolin proteins. *Genome Biol,* 5**,** 214.

WONG, W. & SCHLICHTER, L. C. 2004. Differential recruitment of Kv1.4 and Kv4.2 to lipid rafts by PSD-95. *J Biol Chem,* 279**,** 444-52.

XIE, Z., BARSKI, O. A., CAI, J., BHATNAGAR, A. & TIPPARAJU, S. M. 2011. Catalytic reduction of carbonyl groups in oxidized PAPC by Kvbeta2 (AKR6). *Chem Biol Interact,* 191**,** 255-60.

VICENTE, R., ESCALADA, A., SOLER, C., GRANDE, M., CELADA, A., TAMKUN, M. M., SOLSONA, C. & FELIPE, A. 2005. Pattern of Kv beta subunit expression in macrophages depends upon proliferation and the mode of activation. *J Immunol,* 174**,** 4736-44.

YANG, E. K., ALVIRA, M. R., LEVITAN, E. S. & TAKIMOTO, K. 2001. Kvbeta subunits increase expression of Kv4.3 channels by interacting with their C termini. *J Biol Chem,* 276**,** 4839-44.

3.1.2. Contribution 2:

Oligomerization, affinity and location of Kvβ subfamily oligomers

Roig SR[1], Pérez-Verdaguer M[1], Vicente R[2], Zeug A[3], Ponimaskin E[3], Felipe A[1]

[1]Molecular Physiology Laboratory, Departament de Bioquímica i Biomedicina Molecular, Institut de Biomedicina (IBUB), Universitat de Barcelona, Avda. Diagonal 643, 08028 Barcelona, Spain
[2]Laboratory of Molecular Physiology and Channelopathies, Departament de Ciències Experimentals i de la Salut, Universitat Pompeu Fabra, Barcelona, Spain.
[3]Department of Cellular Neurophysiology, Hannover Medical School, Hannover, Germany.

ABSTRACT

The family Kvβ has the ability of modulate the Kv channels in several different aspects. Not only regulates their inactivation rate or the activation kinetics, but also it has been proved that they can contribute to their traffic. Kvβ subunits are involved in the proper folding of the Kv structure as well as they enhance the membrane targeting of some members. The crystal structure of Kv1.2 together with Kvβ2.1 demonstrated that those proteins are attaching the channels in a forth members composition. Moreover, it was published that in the absence of the Kv, Kvβ2.1, but not Kvβ1.1, is able to form tetramers. From those results, it was proposed that Kvβ1.1 activity on Kv channels will be controlled by interacting with Kvβ2.1 complexes. However, we demonstrate that the oligomeric capability is present in both subtypes and the affinity to form homo or heteroligomers is highly similar. Thus, the Kv modulation by this family is based exclusively on the expression level of each subunit. The present work also points out the presence of those complexes at the plasma membrane, moving Kvβ2.1 out of lipid raft microdomains.

Report of the PhD student participation

Oligomerization, affinity and location of Kvβ subfamily oligomers

Sara Raquel Roig Merino performed all the experiments and the data analysis of this article except the MATLAB program.

Antonio Felipe

PhD thesis director

INTRODUCTION

The heterogeneity of voltage-sensitive potassium currents *in vivo* is due to the mixture of not only α-conducting subunits, but also of β-modulating families. Changes in the expression of a given subunit can alter the composition and the physiological properties of the channelosomes present at a certain cell moment (Pongs and Schwarz, 2010).

Kvβ family is formed by four different encoding genes: Kvβ1, Kvβ2 and Kvβ3. Some of those can undergo alternative splicing events ending in different subtypes. Even they exhibit a 85% of similarity, several functional differences have been studied, mainly focused on their Kv modulating function (Kilfoil et al., 2013). Kvβ1 and Kvβ3 accelerate the fast inactivation of some Kv channels. A ball-and-chain mechanism, similar to Kv1.4 or Kv3.4, was proposed for such modulation (Leicher et al., 1996, Heinemann et al., 1995). On the other hand, Kvβ2 has been related to an increase of surface expression of the channels (Shi et al., 1996). Previous to the Kv1.2 crystallization in the presence of Kvβ2, biochemical evidences pointed out the presence of more than one beta subunit in a Kv channel formation (Parcej et al., 1992). At that moment, the research of the possible interaction among this family in the presence but also in the absence of α-subunits started.

Few investigation saw the light regarding the oligomeric formation of Kvβ family. By a yeast-two-hybrid model, Kvβ2 was observed to form homoligomeric and heteroligomeric compositions with Kvβ1, while the latter had not this capability (Xu et al., 1998). The complex formation was also solved by atomic force and electron microscopy showing a tetrameric structure. In the same study they also detected tripartite structures and speculate of a possible intermediate complex (van Huizen et al., 1999). Finally, the resolution of the Kvβ2 crystal structure leads finally to observe not only the macromolecular structure but also the orientation assumed (England et al., 1995b).

The previous mentioned studies developed in yeast-two-hybrid concluded that the molecular determinants at Kvβ2 for the oligomeric formation would be placed in both the core region and the N-terminal. Although both proteins share the vast majority of the C-terminal sequence, Kvβ1.1 was not presenting those interacting domains. Regarding Kv's physiology, they correlate the higher the expression of Kvβ1, the bigger the inactivation rate; and so, the model of $\alpha_4\beta_n$ (four α-subunits with a variable number of β-subunits) fitted with their results (Xu et al., 1998). Further studies of the same group presented that Kvβ2 was able to inhibit the Kvβ1-mediated inactivation of Kv channels. This effect requires the core part of the subunit, necessary not only for the homo and heteroligomerization but also for the interaction with the channel. They defended that the Kvβ2-modulation of Kvβ1 would not imply the constriction of the inhibiting ball function. It was concluded that Kvβ2 would preferably interact with the Kv channels in an already-formed tetrameric structure displacing Kvβ1 (Xu and Li, 1997). However, slightly later, other laboratory proposed the opposite: Kvβ1.2 has the ability of forming homoligomers as well as Kvβ2. Thereby, mixtures of both proteins with Kv channels induces intermediate inactivation patterns on Kv1.2(Accili et al., 1997a).

The new properties detected for Kvβ2.1, but not for Kvβ1.1 regarding its *lipid raft* presence, drive our research to solve the disjunctive presented in 90's century. The present work was focused in Kvβ1.1, the shortest subunit on the Kvβ1 subfamily, and Kvβ2.1. Our results support the possible Kvβ1.1 complex formation, stablishing tetramers, and demonstrate that the affinity to form homo and heteroligomers among the Kvβ family

is highly similar. Those results drive the Kv regulation back to the concentration theory: the more expressed Kvβ, the higher its presence at the channelosomes. Moreover, our results rapport the presence of homomeric complexes at the plasma membrane and the modulation of Kvβ2 *lipid raft* localization in the presence of Kvβ1.

MATERIALS AND METHODS

Expression plasmids. mKvβ1.1 and mKvβ2.1 were provided by M.M. Tamkun (Colorado State University). mKvβ1.1 and mKvβ2.1 were subcloned into pEYFP-N1 and pECFP-N1 (Clontech). mKvβ2.1CFP mutants were generated using the QuikChange and QuikChange lightning multi-site-directed mutagenesis kits (Stratagene). All constructs were verified using automated DNA sequencing.

Cell culture, *transfections and pharmacological treatments.* HEK-293 cells were cultured on DMEM (LONZA) containing 10% fetal bovine serum (FBS) supplemented with penicillin (10.000 U/ml), streptomycin (100 µg/ml) (GIBCO) and L-glutamine (4 mM).

For confocal imaging and co-immunoprecipitation experiments cells were seeded (70-80% of confluence), in 6-well dish containing poly-lysine-coated coverslips or 100mm dish, respectively, 24h before transfection with selected cDNAs. Lipotransfectina® (Attendbio Research) was used for transfection according to the supplier's instructions. The amount of transfected DNA was 4µg for a 100mm dish and 500ng for each well of a 6-well dish (for coverslip use). Next, 4-6h after transfection, the mixture was removed from the dishes and replaced with new fresh culture media. All the experiments were performed 24 h after transfection.

Protein extraction, co-immunoprecipitation and western blotting. Cells were washed twice in cold PBS and lysed on ice with lysis buffer (5 mM HEPES, 150 mM NaCl, 1% Triton X-100, pH 7.5) supplemented with 1 µg/ml aprotinin, 1 µg/ml leupeptin, 1 µg/ml pepstatin and 1 mM phenylmethylsulfonyl fluoride as protease inhibitors. Cells were next scrapped and transferred to a 1.5 ml tube. Then they were incubated for 20 min at the orbital, and spun for 20 min at 14000 rpm. The supernatant was transferred to a new tube and protein contents were determined by using the Bio-Rad Protein Assay (Bio-Rad).

For co-immunoprecipitation, 1000 µg of protein of each condition were separated and brought up to a volume of 500 ml with Lysis Buffer for IPs (NaCl 150 mM, HEPES 50 mM, Titron X-100 1%, pH 7.4), supplemented with protease inhibitors. Preclean was performed with 40 µl of protein A sepharose beads (GE Healthcare), in an orbital 1 h at 4ºC. Next, each sample was incubated with a small chromatography column (BioRad Micro spin Cromaotgraphy Columns), which contained 2.5 µg of anti-GFP antibody (Genescript) previously crosslinked to protein A sepharose beads, for 2h at room temperature, with continuous mixing in an orbital. Next, columns were centrifuged 30s at 1000g. The supernatant (SN) was kept and stored at -20ºC. Columns were washed four times with 500µl of lysis buffer and centrifugations of 30sec at 1000 g. Finally, elution was performed by incubation of the columns with 100µl of 0.2M glycine pH 2.5, and spun 30sec at 1000g.

The eluted proteins (IP) were prepared for western blot by adding 20µl of Loading Buffer (5x) and 5µl of 1M Tris-HCl pH 10.

Irreversible crosslinking of the antibody to the sepharose beads was performed after one hour of incubation at RT of the antibody with protein A sepharose beads, incubating the beads with 500ul of dimethyl pimelimidate (DMP, from Pierce) for 30 min at RT. Next columns, were washed four times with 500 µl of 1x TBS, four times with 500 µl of 0.2 M glycine pH 2.5 and three times more with 1x TBS. Once these steps are performed, the columns could be incubated with the protein lysates, in order to perform the immunoprecipitation, following the protocol described before.

Protein samples (50µg), supernatants and immunoprecipitates were boiled in Laemmli SDS loading buffer and separated on 10% SDS-PAGE. For the non-denaturalizing protocol there was no boiling step, and the SDS-PAGE gel was 8% acrylamide. Next, they were transferred to nitrocellulose membranes (Immobilon-P, Millipore) and blocked in 0.2% Tween-20-PBS supplemented with 5% dry milk, before immunoreaction. Filters were immunoblotted with antibodies against Kvß1.1 (1/1000, Neuromab), Kvß2.1 (1/1000, Neuromab), Clathrin (1/1000, BD Transduction) or Caveolin (1/1000, BD transduction). Finally, filters were washed with 0.05% Tween 20 PBS and incubated with horseradish peroxidase conjugated secondary antibodies (BioRad).

Confocal microscopy and image analysis. For confocal image acquisition cells were seeded on poly-lysine-coated coverslips, and 24h later were transfected. The next day, cells were quickly washed twice, fixed with paraformaldehyde 4% for 10 min, washed three times for 5min with PBS-K+. Finally, coverslips were mounted on microscope slides (Acefesa) with house Mowiol mounting media. Coverslips were let dry at RT at least one day before imaging.

For membrane surface labelling, Wheat Germ Agglutinin-Texas Red (WGA) (from Invitrogen) was used. Live cells (on ice) were quickly washed with PBS at 4°C and stained with a dilution of WGA-TexasRed (1/1500) in DMEM supplemented with 30 mM Hepes for 15min at 4°C. Subsequently, cells were quickly washed twice and fixed with 4% paraformaldehyde in PBS for 6 min. Next, cells were washed and mounted as described before. In order to detect EEA1 marker, after fixation, cells were further permeabilized with 0.1% Triton X-100 for 20min. After 60min incubation with blocking solution (10% goat serum, 5% non-fat powdered milk and 0.05% Triton X-100) primary mouse anti-EEA1 (1:500) antibody was added 2h at RT (BD Transduction Laboratories) in 10% goat serum and 0.05% Triton X-100. Next, fixed cells were incubated with secondary goat anti-mouse antibody conjugated with Cyanine 5, for 1 hour at room temperature and further mounted as previously described.

The Fluorescence Resonance Energy Transfer (FRET) via acceptor photobleaching technique was measured in discrete ROI (Region of Interest). Fluorescent proteins from fixed cells were excited with the 458 nm or the 514 nm lines using low excitation intensities. Next, 475 to 495 nm bandpass and >530 nm longpass emission filters were applied. The YFP protein was bleached using maximum laser power. We obtained approximately 80% of acceptor intensity bleaching. After photobleaching, images of the donors and acceptors were taken. The FRET efficiency was calculated using the equation

$[(F_{CFPafter} - F_{CFPbefore})/F_{CFPbefore}]*100$, where $F_{CFPafter}$ was the fluorescence of the donor after bleaching and $F_{CFPbefore}$ was the fluorescence before bleaching. The loss of fluorescence as a result of the scans was corrected by measuring the CFP intensity in the unbleached part of the cell.

All images were acquired with a Leica TCS SL laser scanning confocal spectral microscope (Leica Microsystems), equipped with an Argon and Helium-Neon lasers. All experiments were done with a 63x oil-immersion objective lens NA 1.32. All offline image analysis was done using Image J software.

Plasma membrane lawns preparations. Plasma membrane lawns (PML) are membrane sheets obtained by an osmotic shock. HEK-293 cells were seeded in poli-D-lysine treated glass coverslips. Twenty-four hours after transfection they were cooled on ice for five minutes and washed twice in PBS. Next, incubated during five minutes in KHMgE buffer (70mM KCl, 30mM HEPES, 5mM MgCl2, 3mM EGTA, pH 7.5) diluted three times and then, gently washed with non-diluted KHMgE to induce the hypotonic shock. Bursted cells were removed from the coverslip by intensively pipetting up and down. After two washes with KHMgE buffer only membrane sheets remain attached. Preparations were fixed and mounted as previously described.

Lipid-raft isolation. Low density triton-insoluble complexes were isolated as previously described (Martens et al. 2000) from HEK293 cells transiently transfected with either Kvß1.1CFP, Kvß2.1CFP or both. Cells were homogenised in 1 ml of 1% Triton X-100, and sucrose was added to a final concentration of 40%. A 5-30% linear sucrose gradient was layered on top and further centrifuged (390.000g) for 20-22h at 4ºC in a Beckman SW41 rotor. Gradient fractions (1ml) were collected from the top and analysed by western blotting.

Spectral Lux-FRET Analysis in Living cells. HEK-293 cells were cotransfected with plasmid DNAs encoding for Kvβ1.1 or Kvβ2.1 fused with CFP and YFP. Two methods were applied: the measurement by the spectrofluorometer (Fluorolog; Horiba Jobin Yvon, Edison, NJ) and by the LSM780-Meta confocal microscope (Carl Zeiss, Jena, Germany).

Regarding the first method, twenty-four hours after transfection, cells were resuspended in phosphate-buffered saline. All measurements were performed in 5-mm pathway quartz cuvettes using a spectrofluorometer (Fluorolog; Horiba Jobin Yvon, Edison, NJ) equipped with a xenon lamp (450 W, 950 V). The cell suspension was stirred with a magnetic nucleus and the temperature was maintained at 37°C during the experiment. For calibration measurements, cells were cotransfected with plasmid encoding a single fluorophore-tagged Kvβ1.1 or Kvβ2.1. During the time-course experiments, two emission spectra were obtained for each time point by exciting at 458 and 488 nm with 5 nm of spectral resolution for excitation and emission, respectively, and 0.5 s integration time. The spectral contributions from light scattering and nonspecific fluorescence of the cells were taken into account by subtracting the emission spectra of nontransfected cells (background) from each measured spectra. Before the measurements, the

spectrofluorometer was calibrated for the xenonlamp spectrum and Raman scattering peak position. To determine apparent FRET efficiency for Kvβ1.1 and Kvβ2.1, we used a method described in detail by Ponimaskin's laboratory. This allows for a calculation of the total concentration ratio [At]/[Dt] of donor and acceptor, a donor molar fraction xD =[Dt]/([Dt][At]) as well as the apparent FRET efficiencies EfD and EfA, where fD =[DA]/[Dt] and fA= [DA]/[At] are the fractions of donors and acceptors in complexes, respectively (Wlodarczyk et al., 2008). A model characterizing apparent FRET efficiency, EfD, as a function of donor mole fraction, xD, for oligomeric structures has been developed previously (Veatch and Stryer, 1977):

$$Ef_D = E(1 - {x_d}^{n-1}) \quad (1)$$

Fitting this model to experimental data allows for the estimation of the true transfer efficiency, E, and also provides information about the number of units, n, interacting in the oligomeric complex. This model has been slightly augmented for use with EfA (Meyer et al., 2006):

$$Ef_A = \frac{x_d}{1 - x_d}(1 - {x_d}^{n-1}) \quad (2)$$

Considering the second method, the microscope was equipped with a 40×/1.3 numerical aperture oil-immersion objective at 512 × 512 pixels. The 458 nm line of a 40-mW argon laser was used at 15% power. Fluorescence emission was acquired from individual cells over 14 λ channels, in 10.7-nm steps, ranging from 475 to 625 nm. For each measurement, a series of eight images was acquired over a duration of 124 s. Cells were transfected on glass coverslips and twenty-four hours after transfection, the measurements started. Reference spectra were obtained from images of cells expressing only KvβCFP or YFP acquired with the acquisition settings mentioned above. From the obtained data, formulae one and two were also calculated.

From the results obtained in all the conditions assessed, the oligomerization model applied was previously described by Ponimaskin's group, by which the values of the total FRET efficiency, the basic subunit formation and the affinity constants are extracted (Renner et al., 2012).

RESULTS

Kvß1.1 and Kvß2.1 are able to homo and heteroligomerise.

The majority of papers published related to the Kvß family has been focused on the control that they exert on the regulated channels. Some others have been orientated on its function as aldoketoreductases and the modulation of the α-subunits due to this ability. Just few groups invested their time, by 90's century, to address their investigations on the putative oligomeric formation of Kvßs. Two different papers saw the light specifying that Kvß2, but not Kvß1, has the ability to form complexes. Kvß1 would be controlling the channel activity only depending on its concentration and Kvß2, by trapping Kvß1 in those complexes, could impair its function on the α-subunits (Xu and Li, 1997, Xu et al., 1998).

By electron microscopy they also inferred a prevalent tetrameric composition of the Kvß2 complexes (van Huizen et al., 1999). Slightly later, other group defended the opposite: both members can form complexes (Accili et al., 1997a).

The distinct location stablished for Kvß2 in the previous results leads to consider the possible presence of this subunit in complexes at the plasma membrane. To test the results obtained in yeast-two-hybrid, immunoprecipitation assays were performed in HEK cells transfected with: Kvß2.1 - Kvß2.1, Kvß2.1 - Kvß1.1 or Kvß1.1 – Kvß1.1.

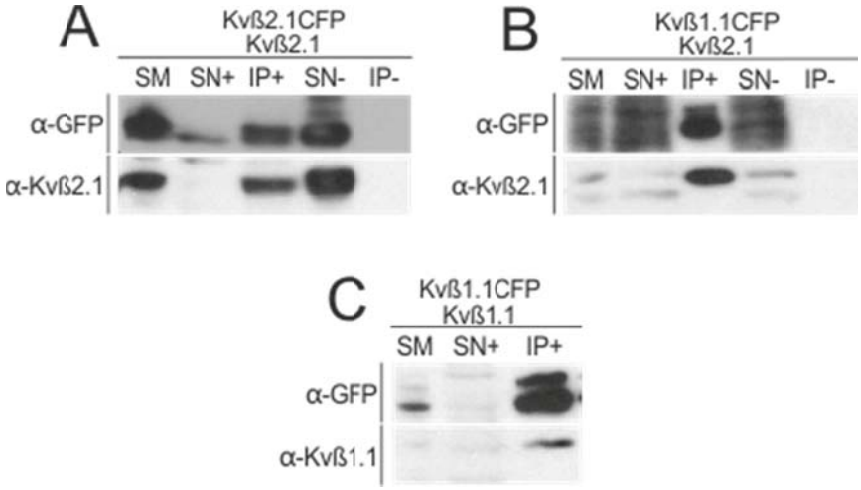

Figure 25. Not only Kvß2.1 but also Kvß1.1 can form oligomers. A. Immunoprecipitation assay against Kvß2.1CFP in the presence of Kvß2.1 untagged. B. Immunoprecipitation assay against Kvß1.1CFP in the presence of Kvß2.1 untagged. C. Immunoprecipitation assay against Kvß1.1GFP in the presence of Kvß1.1 untagged. Western blot using α-GFP antibody and α-Kvß2.1 antibody. SM: starting material. SN+: supernatant of the precipitation. IP+: Immunoprecipitation in the presence of the antibody.

The detection of complexes was achieved implementing immunoprecipitation assays. Surprisingly, not only for the conditions with Kvß2.1 cotransfection (figure 25A-B), but also in those with Kvß1.1 subunit only, significant coimmunoprecipitation was detected (figure 25C). Those homomeric structures could be formed by some mammal proteins that were not present in the yeast-two-hybrid technique, explaining the different results achieved. To solve this disjunctive, experiments of energy transference (figure 26A-D) were performed. In order to apply the technique FRET acceptorphotobleaching, each pair of proteins were tagged with CFP (figure 26A) or YFP (figure 26B) and used as donor and acceptor fluorophores respectively. A portion of the positive colocalisation regions (figure 26C) were subject to the acceptor bleach (square on figure 26D). By analysing and correcting the donor images captured, FRET transference values were obtained as well as the FRET images.

The conditions CFP-YFP and Kv1.3CFP-Kv1.3YFP were used as a negative and positive controls achieving values of 2,44% ± 0,64 and 16,35% ± 1,67% respectively (figure 26E).

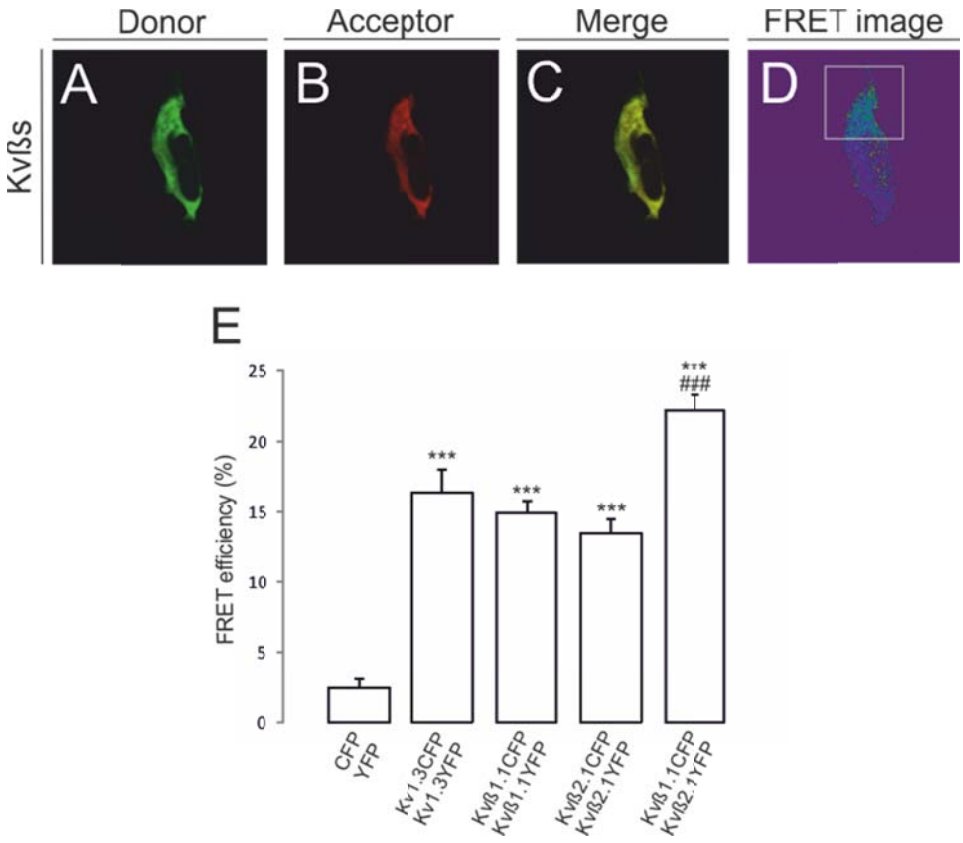

Figure 26. Kvß1.1 and Kvß2.1 have the ability for homo and heteroligomerizate. A. Representative image of a donor transfection, B. Representative image of an acceptor transfection, C. Merge of channels A and B, yellow meaning colocalisation. D. FRET image obtained on the relationship donor pre-bleach versus donor post-bleach after the acceptor photobleaching. E. FRET efficiency quantification. ***, p<0.001 compared with the negative condition. ###, p<0.001 compared with the previous two conditions

The values obtained for the pairs Kvß2.1CFP/ Kvß2.1YFP and Kvß1.1CFP/ Kvß1.1YFP were 13,44% ± 1,04 and 14,93% ± 0,84% respectively. Those are significantly different from the negative condition ensuring the capability of Kvß1.1 for forming complexes without auxiliary subunits. When Kvß1.1CFP/ Kvß2.1YFP was analysed, the FRET values achieved an 22,16% ± 1,12 and it was significantly different from the two previous conditions. FRET mesurements can present differences due to several different causes such as the dipole moment or the molecular distance. Thereby, it is not inferable that this significance is because that interaction presents more preference to be formed, but an affinity issue cannot be discarded.

Affinity for homo and heteroligomerization are equal

In order to solve the affinity of those complexes, it was implemented the technique lux-FRET. Designed by the Ponimaskin's lab, and based in the FRET sensitized emission technique, it can decipher the apparent FRET efficiency not only of the acceptor but also of the donor. From those values, it is calculable a theoretical FRET efficiency, the stoichiometry of the basic unit and the affinity constants (Wlodarczyk et al., 2008). Those experiments were performed firstly in cell suspensions, transfected with different molar ratio of the donor, and measured by a Fluorolog®.

Considering the condition Kvß1.1CFP/ Kvß1.1YFP, the model in figure 27A shows the possible interactions among those proteins. All FRET techniques are just able to detect the complexes formed by the combination of Kvß1.1CFP/ Kvß1.1YFP (orange square in figure 27A). In the lux-FRET technique, the apparent FRET efficiency of the donor (EfD) is reaching lower levels while increasing the donor molar fraction (continuous line in figure 27B). The case of the apparent FRET efficiency of the acceptor (EfA) is the opposite: the higher the donor molar fraction, the bigger the levels of this value (lashed line in figure 27B). As

Regarding the Kvß1.1CFP/ Kvß1.1YFP experiment, the percentage of FRET efficiency value was 30,2%, and the basic unit would be a complex formed by two subunits (N=1.933). For Kvß2.1CFP/ Kvß2.1YFP (figure 27C), the plot exhibits a similar pattern (figure 27D). Calculations brought a 22,3% of FRET efficiency and also a basic unit of two members (N=2,093).

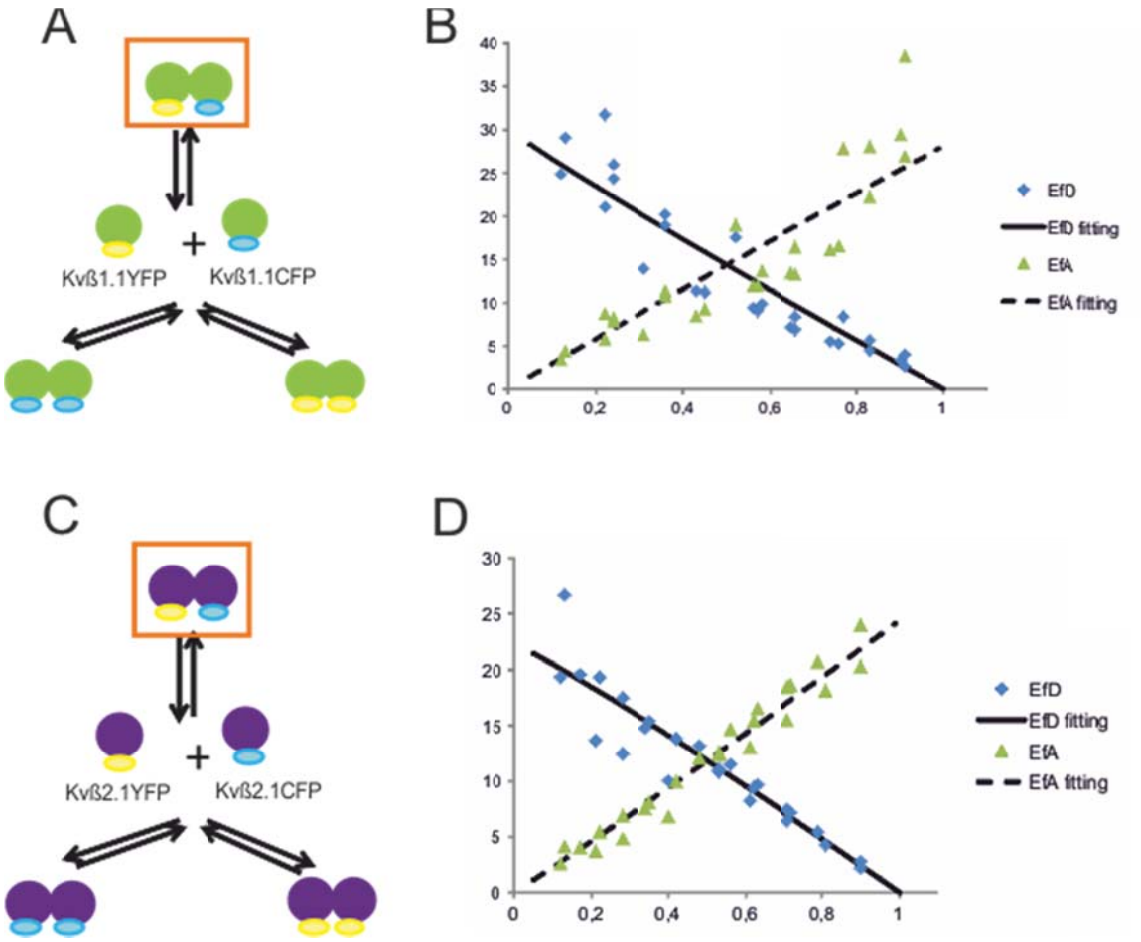

Figure 27. Kvß1.1/ Kvß1.1 and Kvß2.1/ Kvß2.1 complexes are exhibiting high FRET values and a basic unit of two proteins complex. A. Schematic representation of possible interactions under a Kvß1.1CFP/ Kvß1.1YFP cotransfection. B. Plot of EfD (blue squares), EfD fitting (continuous line), EfA (green triangles), EfA fitting (lashed line) versus the donor molar ratio. C. Schematic representation of possible interactions under a Kvß1.1CFP/ Kvß1.1YFP cotransfection. E. Plot of EfD (blue squares), EfD fitting (continuous line), EfA (green triangles), EfA fitting (lashed line) versus the donor molar ratio.

Once stablished the values for those two conditions, heteromultimeric compositions were analysed: Kvß1.1CFP/ Kvß2.1YFP and its reverse Kvß2.1CFP/ Kvß1.1YFP. Considering Kvß1.1CFP/ Kvß2.1YFP (figure 28A), the plot presents a shift to the lower donor molar ratios due to a slightly lower expression of Kvß1.1CFP compared with Kvß2.1YFP (figure 28B). Howcever the calculations return us a FRET efficiency of 32,5% and a basic unit of two proteins (N=1,88). On the other hand, Kvß2.1CFP/ Kvß1.1YFP exhibited a shift in the opposite direction due to the same effect of different level expressions. It presents also a value suggesting a basic unit of two (N=1,99) and a FRET of 30,4%.

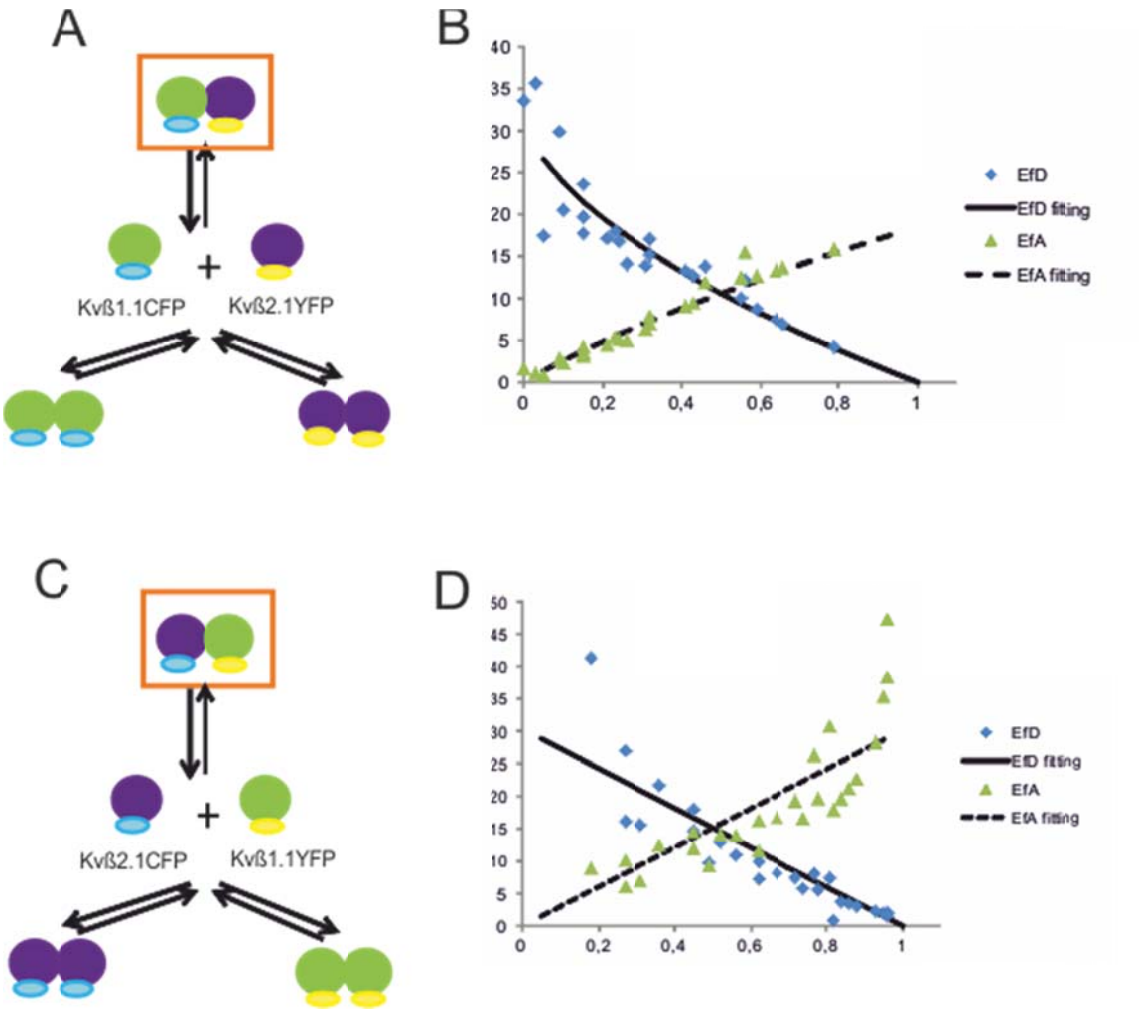

Figure 28. Kvß1.1/ Kvß2.1 complexes are exhibiting high FRET values and a basic unit of two proteins complex. A. Schematic representation of possible interactions under a Kvß1.1CFP/ Kvß2.1YFP cotransfection. B. Plot of EfD (blue squares), EfD fitting (continuous line), EfA (green triangles), EfA fitting (lashed line) versus the donor molar ratio. C. Schematic representation of possible interactions under a Kvß2.1CFP/ Kvß1.1YFP cotransfection. E. Plot of EfD (blue squares), EfD fitting (continuous line), EfA (green triangles), EfA fitting (lashed line) versus the donor molar ratio.

In order to confirm those results with the lux-FRET technique, but switching the measurement equip, they were performed on a spectral microscope. To assess different molar ratios of the same conditions, the transfection was slightly changed. The mixture of both plasmids with the transfecting vector were done separately and applied on the same

coverslip. Since the Lipofectamine® has an extraordinary rate of transfection, it is highly probable that both will be introduced in a same cell (figure 29A) but exhibiting a different donor/acceptor ratio (figure 29B). From one selected region of interest (ROI), the Ponimaskin's MATLab program calculate several different parameters plotting and returning them to the investigator such as the acceptor intensity (figure 29C) or the EfA (figure 29D) relativized by each photon counted. The measurement of the EfA and EfD for each ROI was finally plotted against the donor molar fraction and the maximum projection for both values was emitted in an image. Then, at a glance, different donor molar ratios are exhibiting different EfA and EfD (figure 29E-F).

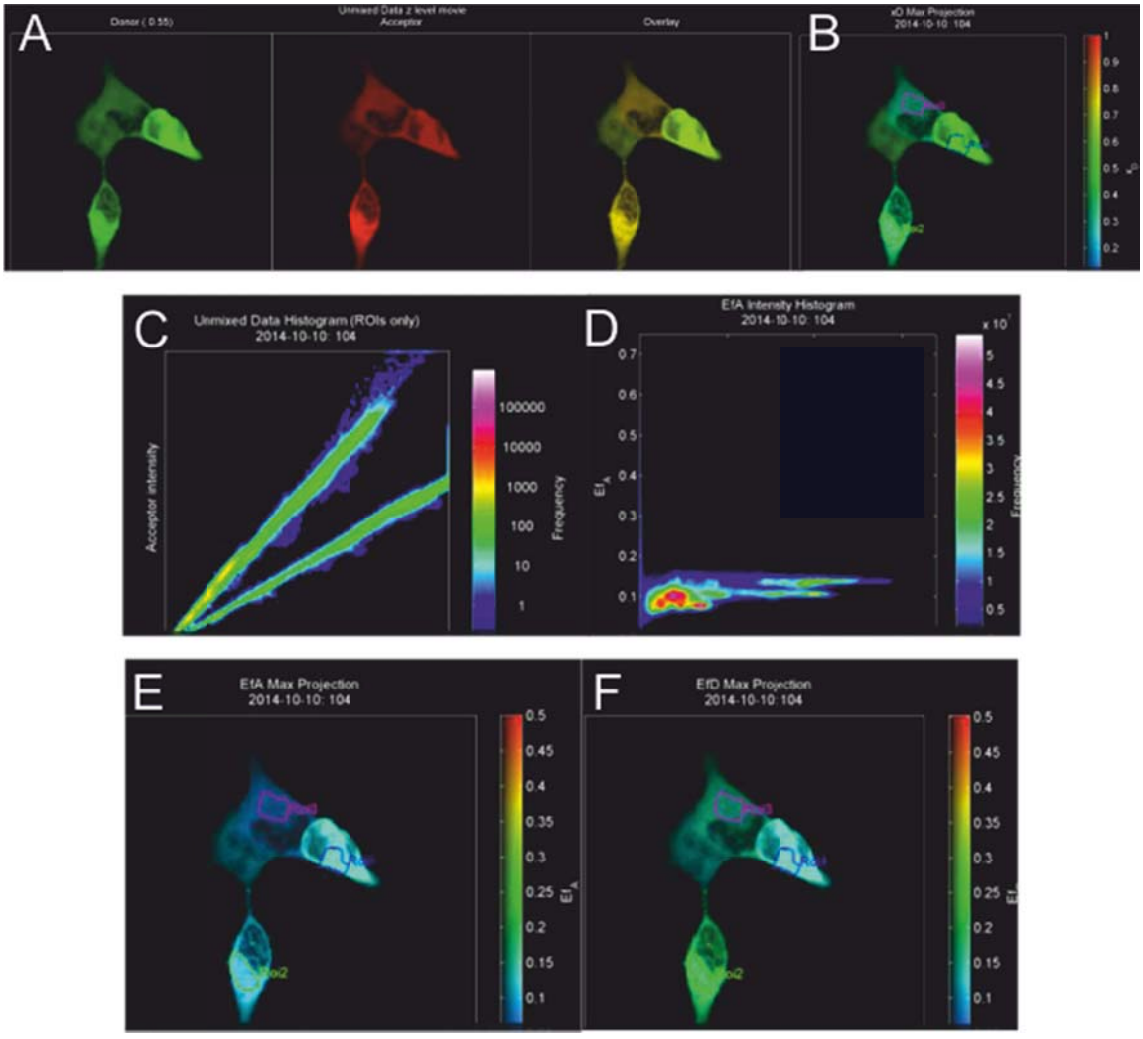

Figure 29. Representative image of a lux-FRET experiment on the spectral microscope. A. Representative image of different cells expressing variable amounts of donor and acceptor, leading a non-uniform merge channel. B. Donor molar ratio image of A pannel. C. Acceptor intensity by photon count image of ROIs in B. D. EfD by photon count image of ROIs in D. E. EfD maximum projection image of pannel A. F EfA maximum projection image of pannel A.

The plots obtained for the four conditions are showing a similar pattern (figure 30) than those obtained in the Fluorolog® previously. The calculations performed for the FRET efficiency included two different variants: the first considering that the two lines are

independent and the second that are dependent. Since the EfD and the EfA are tightly dependent, we assume the second calculation as the proper one.

For the pair Kvß1.1CFP/ Kvß1.1YFP (figure 30A), the value obtained was 47.1%, while for Kvß2.1CFP/ Kvß2.1YFP is 41.4%. In the case of Kvß1.1CFP/ Kvß2.1YFP, this value achieved a 44% while for Kvß2.1CFP/ Kvß1.1YFP it reaches the 51.6% being the highest scored. The calculations for the basic unit of the complexes formed were 2.1, 2.09, 2.17 and 2.03 respectively, pointing a dimer as the basic subunit.

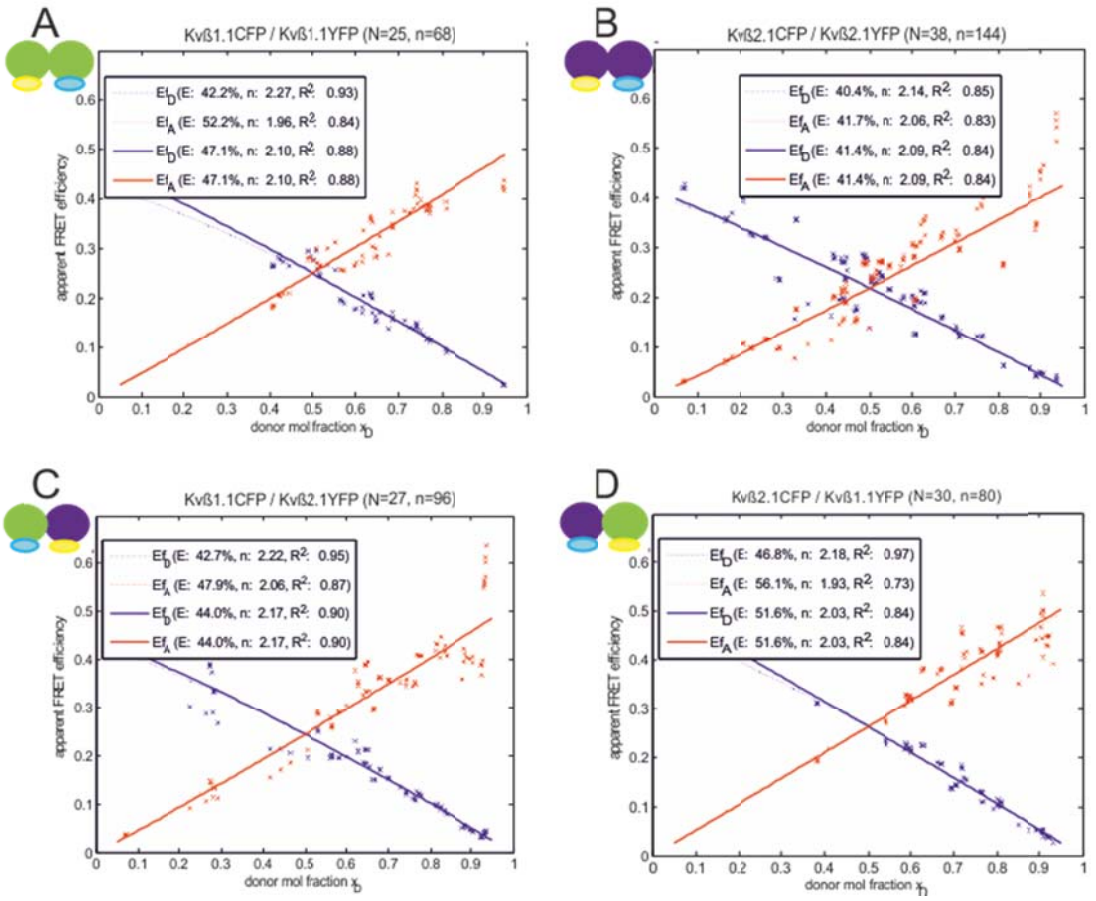

Figure 30. Results obtained with a spectral microscope are similar to the Fluorolog® mesurements. A. Plot of a Kvß1.1CFP/ Kvß1.1YFP EfD (blue crosses), EfD fitting (continuous blue line), EfA (red crosses), EfA fitting (red line) versus the donor molar ratio. B. Plot of a Kvß2.1CFP/ Kvß2.1YFP EfD (blue crosses), EfD fitting (continuous blue line), EfA (red crosses), EfA fitting (red line) versus the donor molar ratio. C. Plot of a Kvß1.1CFP/ Kvß2.1YFP EfD (blue crosses), EfD fitting (continuous blue line), EfA (red crosses), EfA fitting (red line) versus the donor molar ratio. D. Plot of a Kvß2.1CFP/ Kvß1.1YFP EfD (blue crosses), EfD fitting (continuous blue line), EfA (red crosses), EfA fitting (red line) versus the donor molar ratio.

The affinity constant measurement is based in the model presented at figure 31A. As it shows, the mixture between a donor and an acceptor presents the possibility of building three different kinds of complexes. Those will be formed in a bigger or lower extend depending on the affinity constants. This model was implemented for solving the affinity between Kvß1.1/Kvß2.1 (figure 31B). However, this system requires the evaluation of homomeric formations first. Posteriorly, the different affinity constants could be defined by using the formula in figure 31C. Our obtained data on the previous experiments was

concomitant with the plot on figure 31D. This was theoretically developed considering a condition in which all three affinity constants in the model are equal. The absence of tilted ends in our plots is due to the absence of differences in the affinity. Opposite to the data presented by Ponimaskin's laboratory, in which they could describe a different preference for the 5-HT oligomerization among the different families, Kvß1.1 and Kvß2.1 presents the same affinity homo and heteroligomerize (Renner et al., 2012).

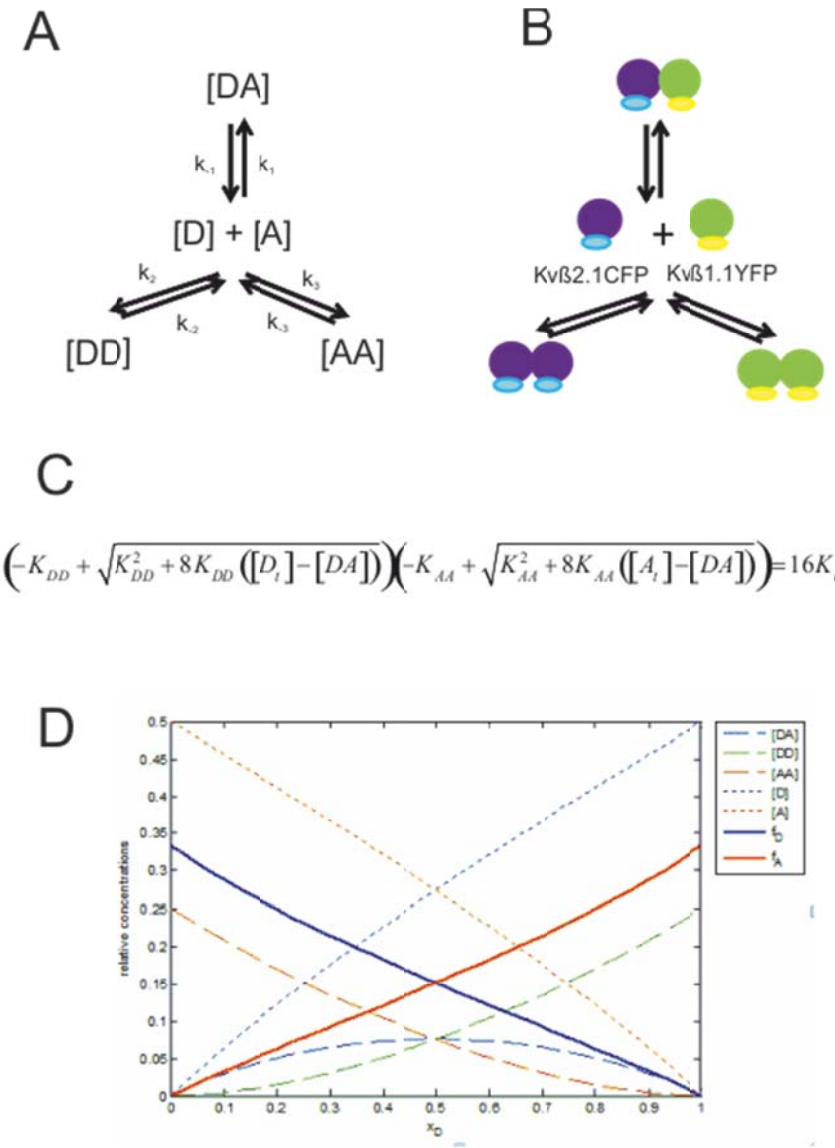

Figure 31. The Kvß1.1 and Kvß2.1 can form homo and heteromeric complexes with the same affinity. A. Model of interaction between donor and acceptor proteins. B. Model of Kvß1.1 and Kvß2.1 oligomerization. C. Formula implemented in Ponimaskin's laboratory MATLAB program to find the affinity constants model. D. Plot of the different parameters [DA], [DD], [AA], [D], [A], fD and fA depending on the donor molar fraction when a model presents the same affinity for forming the three different complexes. [DA], concentration of donor-acceptor complexes. [DD], concentration of donor-donor complexes. [AA], concentration of acceptor-acceptor complexes. [D], donor concentration, [A], acceptor concentration. fD, apparent donor efficiency. fA, apparent acceptor efficiency.

Kvß1.1 and Kvß2.1 form tetramers by dimer oligomerization

The basic unit for oligomerization was stablished in two members for all the conditions. This result implies that there are two different possibilities for the complex dynamics. On

one hand, Kvßs can be forming dimers (figure 32A), but on the other hand, this dimers could be oligomerizing to form tetrameric structures (figure 32B). The results are also indicating that there are no trimeric compositions, showing that in case of the option B, the tetrameric composition is due to a dimeric oligomerization.

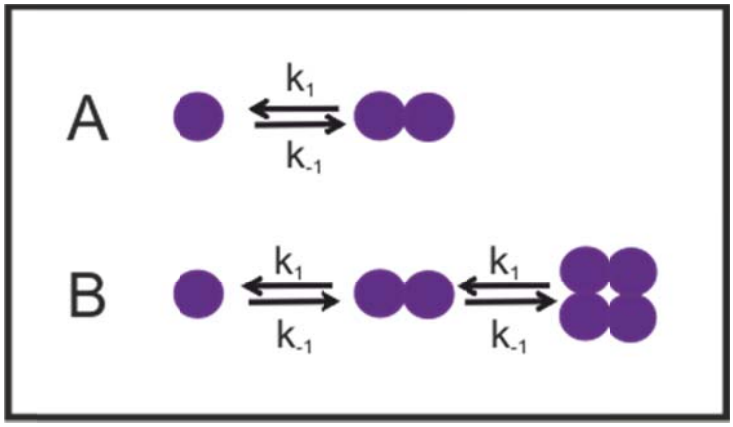

Figure 32. Scheme representing both putative options for Kvß oligomerization. A. Kvß could be forming dimers. B. Kvß could be forming dimeric and tetrameric structures by dimeric association. Purple balls mean Kvß subunits.

It was previously described that Kvß2.1 forms tetramers in the absence of the α-subunit. To check the possible stoichiometry of Kvß1.1, and to confirm the result obtained by atomic force microscopy several years ago, semi-denaturalising technique was implemented to HEK cell transfected with Kvß1.1CFP and Kvß2.1CFP. In this process, proteins are extracted without denaturalising agents and no boiling process is applied. The samples were loaded in the classical SDS-gels to allowing the proteins to run depending on their weight.

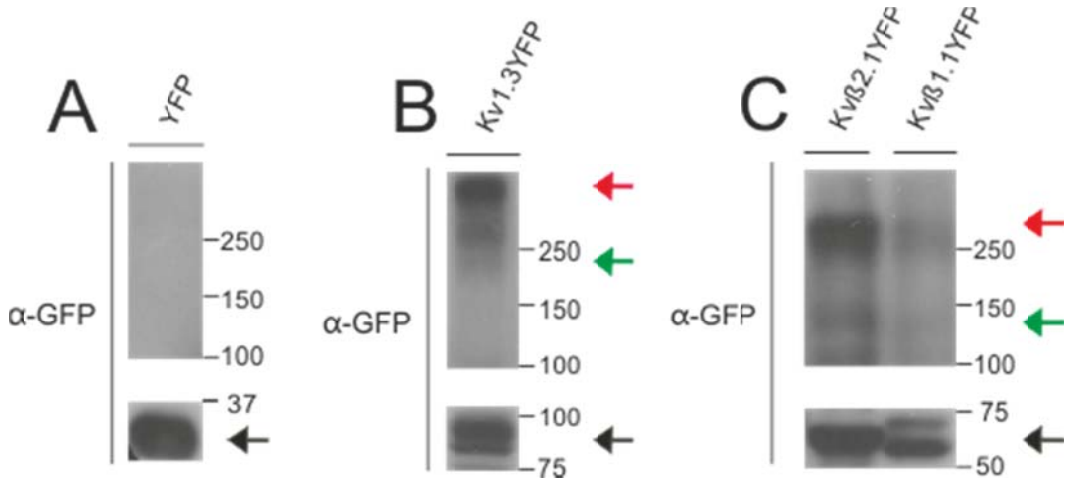

Figure 33. Both Kvß1.1 and Kvß2.1 form dimeric and tetrameric structures. A. Semi-denaturalising western blot of YFP transfected cells. B. Semi-denaturalising western blot of Kv1.3YFP transfected cells. C. Semi-denaturalising western blot of Kvß1.1YFP and Kvß2.1YFP transfected cells. Black arrow indicates monomeric forms. Green arrow indicates dimeric forms. Red arrow indicates tetrameric forms.

Monomeric structures were detected in all four conditions, but unlike YFP transfected cells (figure 33A), dimeric and tetrameric were also inferred in Kv1.3YFP (figure 33B), Kvß1.1YFP and Kvß2.1YFP lines. The channel, acting as a control for testing the technique, presents a band between 75KDa and 100KDa concomitant with the sum of 58.5 KDa of rKv1.3 and 27KDa of the YFP. It is detectable a tiny band surrounding the dimer weight (171KDa) and a bigger one at the possible tetrameric molecular weight (342KDa).

The hKvß1.1 and mKvß2.1 molecular weight are 44 and 41 KDa respectively, so the monomeric signal is placed around 71KDa and 68 KDa respectively (black arrow on figure 33C). The dimeric forms are predicted to weight 142 and 136KDa, while the tetrameric would weight 284KDa and 272 KDa. We can detect bands between 100 and 150KDa (green arrow on figure 33C), as well as just right up the 250KDa (red arrow on figure 33C). Confirming the lux-FRET prediction for the basic unit, no signal can be detected in a possible trimeric composition (213 and 204KDa respectively). Taken together, the two techniques are showing that both Kvß1.1 and Kvß2.1 can form tetramers by a dimeric interaction (figure 32B).

Oligomeric compositions are also membrane-associated

Regarding the localisation of Kvß1.1 and Kvß2.1 at membrane microdomains such as *lipid raft*, the possible polarised oligomerization was confronted. The data obtained and showed in figure 26 was mainly from the Kvßs occupying the intracellular space. In order to isolate those proteins that trafficked to the plasma membrane, FRET acceptorphotobleaching technique was applied to the plasma membrane loans purification.

The CFP-YFP condition, used as a negative control, was measured in a whole cell configuration due to its absence at the membrane (figure 33A-C). The positive control for the FRET experiment was Kv1.3CFP-Kv1.3YFP, since the molecular conformation that reaches the membrane is the tetramer (figure 33D-F). Kvß1.1CFP-Kvß1.1YFP (figure 33 G-I) and Kvß2.1CFP-Kvß2.1YFP (figure 33J-L) are all present at the plasma membrane purification as well as each pair exhibits a high colocalization (figure 33I,L). The analysis of the FRET acceptorfotobleahing showed positive values for both conditions (figure 33M) pointing out that they are trafficking to the plasma membrane in a multimeric conformation.

From the previous results it is extractable that the affinity homo and heteromultimerise is the same and they can occupy membrane localizations in a complex configuration. Since Kvß2.1, but not Kvß1.1, traffics to *lipid raft* microdomains, under coexpression the localisation of the complexes remained unknown. To decipher the question, low-buoyancy membrane fractions purification was performed.

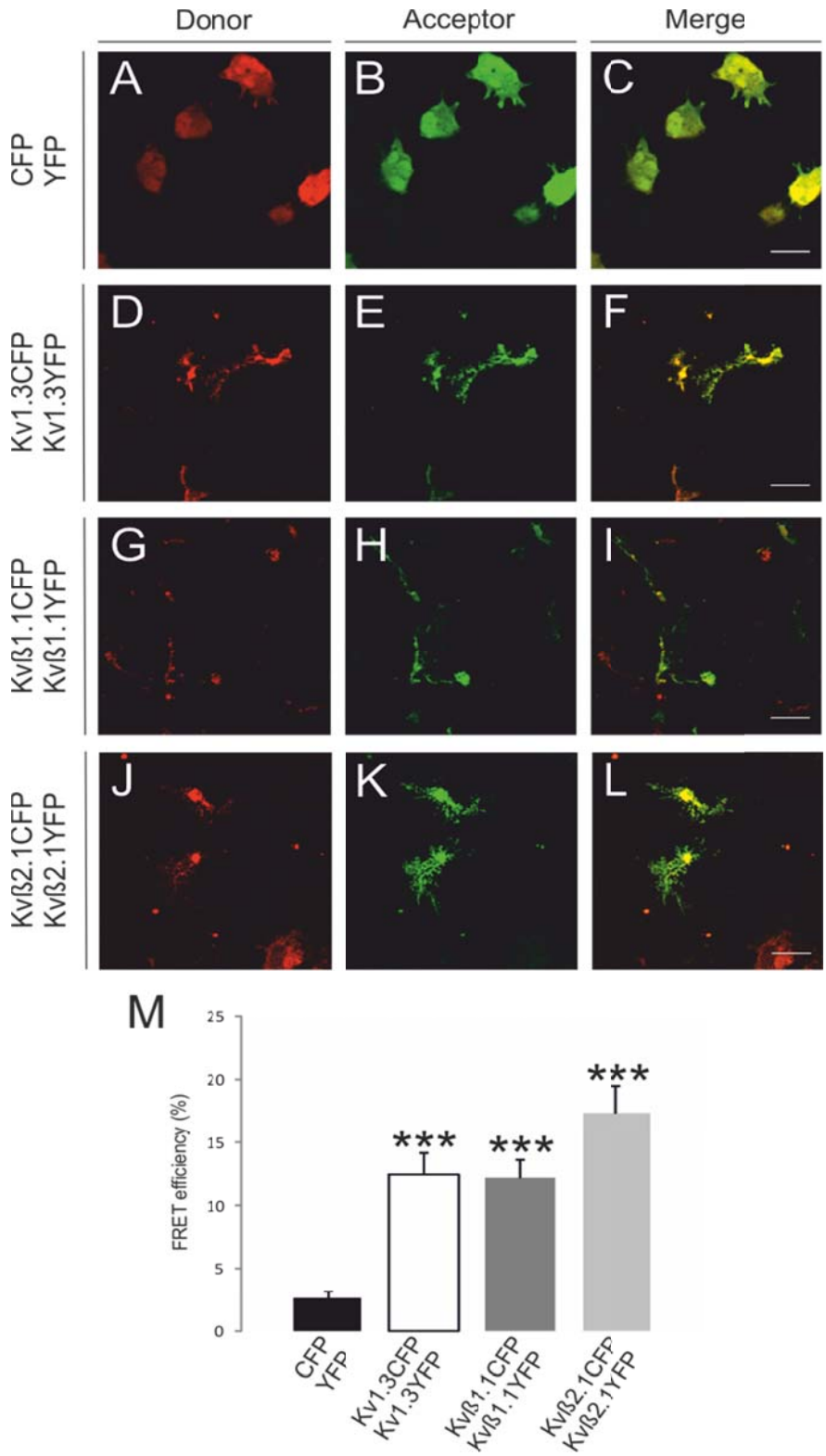

Figure 34. Both Kvß1.1 and Kvß2.1 are complexed in the plasma membrane targets. A-C. CFP – YFP transfected cells were used as negative controls. A. CFP. B. YFP. C. Merge, yellow means colocalisation. D-F. Kv1.3CFP-Kv1.3YFP plasma membrane loans purification. D. Kv1.3CFP. E. Kv1.3YFP. C. Merge, yellow means colocalisation. G-I. Kvß1.1CFP- Kvß1.1YFP plasma membrane loans purification. G. Kvß1.1CFP. H. Kvß1.1YFP. I. Merge, yellow means colocalisation. J-L. Kvß2.1CFP- Kvß2.1YFP plasma membrane loans purification. J. Kvß2.1CFP. K Kvß2.1YFP. L. Merge, yellow means colocalisation. M. FRET efficiency quantification. ***p<0.05, versus CFP-YFP condition.

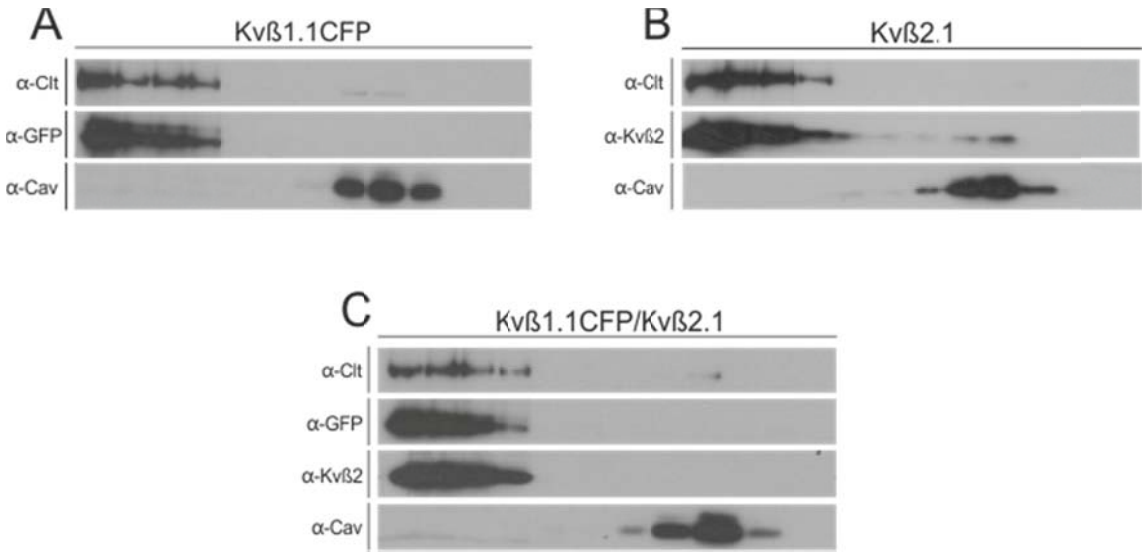

Figure 35. Kvß1.1CFP shifts out Kvß2.1 from lipid raft domains. A: Western blotting of lipid raft fractions of Kvß1.1CFP. B: Western blotting of lipid raft fractions of Kvß2.1. C: Western blotting of lipid raft fractions of Kvß1.1 and Kvß2.1CFP cotransfection.

A described in the previous contribution, while Kvß1.1 is not present in those domains (figure 35A), Kvß2.1 exhibits a partial localisation in *lipid raft* (figure 35B). When both subunits are coexpressed, Kvß2.1 is no longer able to traffic to those microdomains (figure 35C). Thereby, Kvß1.1 is controlling Kvß2.1 membrane localization shifting out its targeting.

DISCUSSION

The composition and stoichiometry of the α-β complex ultimately determine the kinetic and gating of the potassium channels as well as their cell traffic and distribution (Pongs and Schwarz, 2010). In this contribution we have applied several different techniques to solve the question on Kvß oligomers that remained opened. We have demonstrated for the first time that, indeed, both Kvß1.1 and Kvß2.1 can form complexes in intact cells. Actually, they present a similarity of 85%, and the supposed regions involved in the oligomerization are highly conserved for both. The homomeric composition for Kvß2 was previously described using yeast-two-hybrid system as well as size exclusion chromatography (Xu et al., 1998, van Huizen et al., 1999). Those complexes were also observed by atomic force microscopy. Although Kvß1 was found not to present this ability, other laboratories found that Kvß1.2 presented complex formation (Accili et al., 1997a).

One putative explanation for the negative yeast-two-hybrid result of Kvß1.1 was a possible lower affinity for oligomerize or a protein-mediated complexation. However, we have described that Kvß1.1 presents an innate capability of interaction. Due to those results, that laboratory proposed a possible regulation of the α-subunits depending on their oligomerization ability. Thereby, since only Kvß2 was already exhibiting tetrameric

formation, upon its increased expression, homomeric complexes were supposed to displace Kvß1 impairing its function (Xu and Li, 1997). However, our contribution shows that Kvß2.1 and Kvß1.1 can form heteroligomers in the absence of the Kv channel and without affinity differences compared with homoligomers. Thus, the governing force for forming the different complex compositions is the concentration of both species. Moreover, the Kv control will just depend on the expression level of every Kvß subunit. Many other proteins exhibit oligomeric composition control depending on the amount of each partner. For instance, ZIP1/ZIP2/ZIP3 are stablishing hetero and homodimers depending in the expression level which is under control by different insults (Gong et al., 1999, Croci et al., 2003). Because it has been demonstrated that two different subunits can govern one unique channel, by the fine-tuning Kvß concentrations, there is a putative mosaic of derivative currents (Pongs and Schwarz, 2010).

This study is contributing also to the dynamic formation of Kvß complexes. The oligomerization could occur in several different ways. By lux-FRET technique it is obtainable the basic subunit formation of the complexes (Renner et al., 2012). Combining the information of the lux-FRET and the non-denaturalising results we have defined the dynamic composition of Kvß oligomers. To achieve the tetrameric composition Kvßs are passing through two different steps: firstly the dimeric establishment and then a dimer dimerization assembly to form the final configuration. Even it was observable by AFM and EM some supposed trimeric structures, our results can only be fitted to this dynamism (van Huizen et al., 1999). Our finding is concomitant with the process that Kv channels undergo to form a conducting entity (Hille, 2001).

On the previous contribution, we demonstrate a clear difference between Kvß1.1 and Kvß2.1. Even both are exhibiting a membrane targeting, the microdomains occupied are different. While Kvß1.1 is associated with the β-actin cytoskeleton, Kvß2.1 is partially placed in lipid raft due to post-translational changes (Nakahira et al., 1998). The present contribution demonstrates that in those particular domains, Kvßs are already forming complexes. They are classified as aldoketoreductases and cellular changes on the redox state can be sensed (Kilfoil et al., 2013). The different distribution of the Kvß throughout the cell surface could ensure the detection of the redox changes in different microdomains. Moreover, the differential affinity for the cofactor NADPH determines some different detection abilities among distinct environment (Tipparaju et al., 2007). As discussed previously, the interaction of Kvß2 or Kvß1.1 with several different other proteins such as PKC or ZIP1/ZIP2/ZIP3 drives to the idea that the localization of this subfamily can act as a possible signalling platform (Gong et al., 1999). Since the combination of both proteins is shifting the location, also the interactors of one or the other will be controlled directly by their total amount in the cell. Thereby, it is tempting to speculate that upon different insults or cell-cycle-dependent changes, Kvßs protein expression would be regulated enhancing a specific localization of them and their partners.

REFERENCES

ACCILI, E. A., KIEHN, J., WIBLE, B. A. & BROWN, A. M. 1997a. Interactions among inactivating and noninactivating Kvbeta subunits, and Kvalpha1.2, produce potassium currents with intermediate inactivation. *J Biol Chem,* 272**,** 28232-6.

CROCI, C., BRANDSTATTER, J. H. & ENZ, R. 2003. ZIP3, a new splice variant of the PKC-zeta-interacting protein family, binds to GABAC receptors, PKC-zeta, and Kv beta 2. *J Biol Chem,* 278**,** 6128-35.

ENGLAND, S. K., UEBELE, V. N., SHEAR, H., KODALI, J., BENNETT, P. B. & TAMKUN, M. M. 1995b. Characterization of a voltage-gated K+ channel beta subunit expressed in human heart. *Proc Natl Acad Sci U S A,* 92**,** 6309-13.

GONG, J., XU, J., BEZANILLA, M., VAN HUIZEN, R., DERIN, R. & LI, M. 1999. Differential stimulation of PKC phosphorylation of potassium channels by ZIP1 and ZIP2. S*cience,* 285**,** 1565-9.

HILLE, B. 2001. Ion channels of excitable membranes. *Sinauerassociates, Sunderland, Mass.. Great Britain, 2001.*

HEINEMANN, S. H., RETTIG, J., GRAACK, H. R. & PONGS, O. 1996. Functional characterization of Kv channel beta-subunits from rat brain. *J Physiol,* 493 (Pt 3)**,** 625-33.

KILFOIL, P. J., TIPPARAJU, S. M., BARSKI, O. A. & BHATNAGAR, A. 2013. Regulation of ion channels by pyridine nucleotides. *Circ Res,* 112**,** 721-41.

LEICHER, T., ROEPER, J., WEBER, K., WANG, X. & PONGS, O. 1996. Structural and functional characterization of human potassium channel subunit beta 1 (KCNA1B). *Neuropharmacology,* 35**,** 787-95.

NAKAHIRA, K., MATOS, M. F. & TRIMMER, J. S. 1998. Differential interaction of voltage-gated K+ channel beta-subunits with cytoskeleton is mediated by unique amino terminal domains. *J Mol Neurosci,* 11**,** 199-208.

PARCEJ, D. N., SCOTT, V. E. & DOLLY, J. O. 1992. Oligomeric properties of alpha-dendrotoxin-sensitive potassium ion channels purified from bovine brain. *Biochemistry,* 31**,** 11084-8.

PONGS, O. & SCHWARZ, J. R. 2010. Ancillary subunits associated with voltage-dependent K+ channels. *Physiol Rev,* 90**,** 755-96.

RENNER, U., ZEUG, A., WOEHLER, A., NIEBERT, M., DITYATEV, A., DITYATEVA, G., GORINSKI, N., GUSEVA, D., ABDEL-GALIL, D., FROHLICH, M., DORING, F., WISCHMEYER, E., RICHTER, D. W., NEHER, E. & PONIMASKIN, E. G. 2012. Heterodimerization of serotonin receptors 5-HT1A and 5-HT7 differentially regulates receptor signalling and trafficking. *J Cell Sci,* 125**,** 2486-99.

SHI, G., NAKAHIRA, K., HAMMOND, S., RHODES, K. J., SCHECHTER, L. E. & TRIMMER, J. S. 1996. Beta subunits promote K+ channel surface expression through effects early in biosynthesis. *Neuron,* 16**,** 843-52.

TIPPARAJU, S. M., LIU, S. Q., BARSKI, O. A. & BHATNAGAR, A. 2007. NADPH binding to beta-subunit regulates inactivation of voltage-gated K(+) channels. *Biochem Biophys Res Commun,* 359**,** 269-76

VAN HUIZEN, R., CZAJKOWSKY, D. M., SHI, D., SHAO, Z. & LI, M. 1999. Images of oligomeric Kv beta 2, a modulatory subunit of potassium channels. *FEBS Lett,* 457**,** 107-11.

WLODARCZYK, J., WOEHLER, A., KOBE, F., PONIMASKIN, E., ZEUG, A. & NEHER, E. 2008. Analysis of FRET signals in the presence of free donors and acceptors. *Biophys J,* 94**,** 986-1000.

XU, J. & LI, M. 1997. Kvbeta2 inhibits the Kvbeta1-mediated inactivation of K+ channels in transfected mammalian cells. *J Biol Chem,* 272**,** 11728-35.

XU, J., YU, W., WRIGHT, J. M., RAAB, R. W. & LI, M. 1998. Distinct functional stoichiometry of potassium channel beta subunits. *Proc Natl Acad Sci U S A,* 95**,** 1846-51.

3.1.3. Contribution 3:

Kv1.3 lipid raft location and endocytosis modulation by Kvß family.

Roig SR[1], Pérez-Verdaguer M[1], Vicente R[2], Felipe A[1]

[1]Molecular Physiology Laboratory, Departament de Bioquímica i Biomedicina Molecular, Institut de Biomedicina (IBUB), Universitat de Barcelona. Barcelona, Spain
[2]Laboratory of Molecular Physiology and Channelopathies, Departament de Ciències Experimentals i de la Salut, Universitat Pompeu Fabra, Barcelona, Spain.

ABSTRACT

Kv1.3 channel is involved in several different and highly relevant functions in nervous and immune system. The absence of the proper fine-tunning of its function has been related to some autoimmunitary diseases such as lupus eritromatous or psoriasis. The properties of a channel current, such as Kv1.3, are the result of the different components of the complete channelosome. Other Kv subunits as well as β modulators can modify the response of Kv1.3. However, not only the current features but also the trafficking and cell localisation can be controlled by those other proteins. Thus, the deep comprehension of the role performed by Kvß subunits on Kv1.3 is necessary. On one hand it will allow us to understand the physiology and pathophysiology of the Kv1.3-missfunction derived effects. On the other hand, they are possible therapeutic targets in a future to influence the channel. The present contribution characterise the electrophysiological functions of Kvßs on Kv1.3, as well as their role in its general turnover. Kvß1.1 enhances the C-type inactivation, and both Kvß1.1 and Kvß2.1 control the membrane targeting in non-lipid raft localisations by competing with caveolin. Kvß2 can counteract the PMA-mediated internalisation of the channel, by impairing its ubiquitination. Thus, new controlling roles are described for Kvßs to Kv1.3 channelosome.

Report of the PhD student participation

Kv1.3 lipid raft location and endocytosis modulation by Kvß family

Sara Raquel Roig Merino performed all the experiments and the data analysis of this article except Kvß cloning.

Antonio Felipe

PhD thesis director

INTRODUCTION

Voltage-gated potassium channels are involved in controlling repolarization and resting membrane potential. Not only in excitable but also in non-excitable tissues are implicated in important cellular functions (Hille, 2001). The mammalian Kv1 family (*Shaker)* comprises 8 members (Kv1.1 – Kv1.8) which are controlling nerve and muscle physiology. The third member, Kv1.3 is mainly expressed in central nervous system and immune system cells (Gutman et al., 2005).

In the immune system, Kv1.3 is the voltage gated potassium channel more expressed. The effects on their physiology have been under intense investigation. Its presence in the immunological synapse was determined and it is widely accepted that plays a central role mediating the activation and proliferation transduction signal (Panyi et al., 2004, Cahalan and Chandy, 2009). While Kv1.3 activation in T cells seems to be involved in proliferation, channel inhibition would be related with apoptosis (Leonard et al., 1992, Szabo et al., 1996). The dual role of Kv1.3 in lymphocyte physiology highlights the importance of a fine activity regulation in the cell. Moreover, Kv1.3 alterations are related to automimmune pathologies like multiple sclerosis, type-I diabetes and rheumatoid arthritis, among others (Beeton and Chandy, 2005, Toldi et al., 2010, Nicolaou et al., 2010).

Ion channels subcellular localization is essential for their proper cell physiology (Martens et al., 2004). Once they target the plasma membrane, different locations are possible since it is not a homogeneous compartment (Brown and London, 1998). Lipid raft microdomains, which are enriched with highly packed sphingolipids and cholesterol, are likely to act as specific membrane platforms where several proteins, including ion channels, converge with signaling molecules, thereby regulating cellular responses (Dart, 2010). Those subcellular domains have been directly related with the capability of T and B cells for the activation. The BCR or the TCR-CD3 are relocated to them upon the presence of an activated antigen presenting cell (Varshney et al., 2016). Kv1.3 has been also detected in those domains colocalising with those receptors (Panyi et al., 2004). Moreover, defective temporal and spatial Kv1.3 redistribution in the IS are related to abnormal T cell physiology in systemic lupus erythematosus (Nicolaou et al., 2007).

Caveolae are specific omega-shaped lipid raft microdomains responsible for multiple cell functions such as cell signaling, mechanosensing or lipotoxicity protection (Shvets et al., 2014). Our laboratory has recently published the interaction between Kv1.3 and caveolin and the molecular determinants governing this association. This protein presents the capability of determining the localization of Kv1.3 at lipid raft microdomains (Perez-Verdaguer et al., 2016a). Actually, it has been described in $CD8^+$ T cell subsets that caveolin is the driving force for the polarization of the synapsis and the proper activation response (Tomassian et al., 2011). Concomitantly, caveolin-1-deficient mice are more susceptible to defective macrophage activity and inflammatory responses (Bucci et al., 2000, Medina et al., 2007).

Kvß accessory subunit family has been reported to be expressed in T cells presenting a control in its level depending on different stimuli (Autieri et al., 1997). This regulation has been detected also in macrophages where Kv1.3 channel is also expressed (Vicente et al., 2005). While the electrophysiology properties of Kv1.3 in the presence of the Kvß family were assessed some years ago, little is known about the possible alteration of the Kv1.3 cellular distribution when they are coexpressed (McCormack et al., 1999). Considering the

new distribution of Kvß2 previously reported (contribution 1), and the oligomerization process described (oligomerization 2), the putative traffic modulation on Kv1.3 was analysed.

Thus, the present work stablishes the electrophysiological properties of Kv1.3 currents on HEK cells, as well as the impairment of lipid raft microdomains targeting upon Kvß presence. Moreover, they are able to counteract the internalization of the channels by PKC activation through PMA treatment. So, Kvß are fine tuning the localisation of Kv1.3 channel.

MATERIAL AND METHODS

Expression plasmids. rKv1.3 in pRcCMV was provided by T.C. Holmes (New York University). It was subcloned into pEYFP-C1 and pECFP-C1 (Clontech) to preserve normal channel behavior (Vicente et al., 2008). mKvβ1.1 and mKvβ2.1 were provided by M.M. Tamkun (Colorado State University). mKvβ1.1 and mKvβ2.1 were subcloned into pEYFP-N1 and pECFP-N1 (Clontech). All constructs were verified using automated DNA sequencing.

Cell culture, *transfections and pharmacological treatments.* HEK-293 cells were cultured on DMEM (LONZA) containing 10% fetal bovine serum (FBS) supplemented with penicillin (10.000 U/ml), streptomycin (100 µg/ml) (GIBCO) and L-glutamine (4 mM).

For confocal imaging and co-immunoprecipitation experiments cells were seeded (70-80% of confluence), in 6-well dish containing poly-lysine-coated coverslips or 100mm dish, respectively, 24h before transfection with selected cDNAs. Lipotransfectina® (Attendbio Research) was used for transfection according to the supplier's instructions. The amount of transfected DNA was 4µg for a 100mm dish and 500ng for each well of a 6-well dish (for coverslip use). Next, 4-6h after transfection, the mixture was removed from the dishes and replaced with new fresh culture media. All the experiments were performed 24 h after transfection.

For patch-clamp experiments, HEK-293 cells were plated in a 35-mm dish and transfected with 300 ng of DNA using FuGene HD® according to the supplier's instructions.

In some specific experiments, twenty-four hours HEK transfected cells were incubated with 1µM PMA for 30min at 37ºC.

Electrophysiology. Transfected HEK-293 cells were accutased 24h after transfection and re-plated on 35mm glass-bottom dishes coated with Matrigel (BD Biosciences). After 1-2h, cells were extensively washed with whole-cell external recording solution, containing the following (in mM): 150 NaCl, 5 KCl, 10 $CaCl_2$, 2 $MgCl_2$, 10 glucose, and 10 HEPES, pH 7.4). Transfected HEK-293 cells were selected using an Olympus FV1000 confocal microscope equipped with spectral detectors and SIM scanner. Whole-cell K^+ currents in HEK-293 were recorded at room temperature (RT) using an Axopatch 200B and an EPC-10 (HEKA), respectively, and the appropriate software was used for data recording and analysis. Ionic currents were capacitance and series resistance compensated by 80–90%, sampled at 10

kHz (Digidata 1440; Molecular Devices), and filtered at 2.9 kHz. Patch electrodes of 2-4 MΩ were fabricated in a P-97 puller (Sutter Instruments Co.) from borosilicate glass (outer diameter 1.2 mm and inner diameter 0.94 mm; Clark Electromedical Instruments Co.) Electrodes for HEK cells were filled with a solution containing the following (in mM): 4 NaCl, 150 KCl, 1 $MgCl_2$, 0.5 EGTA, 5 ATP(K), and 10 HEPES, pH 7.4. HEK cells were clamped to a holding potential of –80 mV. To evoke voltage-gated currents, cells were stimulated with 250 ms square pulses ranging from –80 to +80 mV in 10 mV steps. All recordings were routinely subtracted for leak currents.

Protein extraction, co-immunoprecipitation and western blotting. Cells were washed twice in cold PBS and lysed on ice with lysis buffer (5 mM HEPES, 150 mM NaCl, 1% Triton X-100, pH 7.5) supplemented with 1 µg/ml aprotinin, 1 µg/ml leupeptin, 1 µg/ml pepstatin and 1 mM phenylmethylsulfonyl fluoride as protease inhibitors. Cells were next scrapped and transferred to a 1.5 ml tube. Then they were incubated for 20 min at the orbital, and spun for 20 min at 14000 rpm. The supernatant was transferred to a new tube and protein contents were determined by using the Bio-Rad Protein Assay (Bio-Rad).

For co-immunoprecipitation, 1000 µg of protein of each condition were separated and brought up to a volume of 500 ml with Lysis Buffer for IPs (NaCl 150 mM, HEPES 50 mM, Titron X-100 1%, pH 7.4), supplemented with protease inhibitors. Preclean was performed with 40 µl of protein A sepharose beads (GE Healthcare), in an orbital 1 h at 4ºC. Next, each sample was incubated with a small chromatography column (BioRad Micro spin Cromaotgraphy Columns), which contained 2.5 µg of anti-GFP antibody (Genescript) previously crosslinked to protein A sepharose beads, for 2h at room temperature, with continuous mixing in an orbital. Next, columns were centrifuged 30s at 1000g. The supernatant (SN) was kept and stored at -20ºC. Columns were washed four times with 500µl of lysis buffer and centrifugations of 30sec at 1000 g. Finally, elution was performed by incubation of the columns with 100µl of 0.2M glycine pH 2.5, and spun 30sec at 1000g. The eluted proteins (IP) were prepared for western blot by adding 20µl of Loading Buffer (5x) and 5µl of 1M Tris-HCl pH 10.

Irreversible crosslinking of the antibody to the sepharose beads was performed after one hour of incubation at RT of the antibody with protein A sepharose beads, incubating the beads with 500ul of dimethyl pimelimidate (DMP, from Pierce) for 30 min at RT. Next columns, were washed four times with 500 µl of 1x TBS, four times with 500 µl of 0.2 M glycine pH 2.5 and three times more with 1x TBS. Once these steps are performed, the columns could be incubated with the protein lysates, in order to perform the immunoprecipitation, following the protocol described before.

Protein samples (50µg), supernatants and immunoprecipitates were boiled in Laemmli SDS loading buffer and separated on 10% SDS-PAGE. Next, they were transferred to nitrocellulose membranes (Immobilon-P, Millipore) and blocked in 0.2% Tween-20-PBS supplemented with 5% dry milk, before immunoreaction. Filters were immunoblotted with antibodies against Kv1.3 (1/500, Neuromab), Kvß1.1 (1/1000, Neuromab), Kvß2.1 (1/1000, Neuromab), Clathrin (1/1000, BD Transduction) or Caveolin (1/1000, BD transduction). Finally, filters were washed with 0.05% Tween 20 PBS and incubated with horseradish peroxidase conjugated secondary antibodies (BioRad).

Confocal microscopy and image analysis. For confocal image acquisition cells were seeded on poly-lysine-coated coverslips, and 24h later were transfected. The next day, cells were quickly washed twice, fixed with paraformaldehyde 4% for 10 min, washed three times for 5min with PBS-K+. Finally, coverslips were mounted on microscope slides (Acefesa) with house Mowiol mounting media. Coverslips were let dry at RT at least one day before imaging.

For membrane surface labelling, Wheat Germ Agglutinin-Texas Red (WGA) (from Invitrogen) was used. Live cells (on ice) were quickly washed with PBS at 4°C and stained with a dilution of WGA-TexasRed (1/1500) in DMEM supplemented with 30 mM Hepes for 15min at 4°C. Subsequently, cells were quickly washed twice and fixed with 4% paraformaldehyde in PBS for 6 min. Next, cells were washed and mounted as described before. In order to detect EEA1 marker, after fixation, cells were further permeabilized with 0.1% Triton X-100 for 20min. After 60min incubation with blocking solution (10% goat serum, 5% non-fat powdered milk and 0.05% Triton X-100) primary mouse anti-EEA1 (1:500) antibody was added 2h at RT (BD Transduction Laboratories) in 10% goat serum and 0.05% Triton X-100. Next, fixed cells were incubated with secondary goat anti-mouse antibody conjugated with Cyanine 5, for 1 hour at room temperature and further mounted as previously described.

All images were acquired with a Leica TCS SL laser scanning confocal spectral microscope (Leica Microsystems), equipped with an Argon and Helium-Neon lasers. All experiments were done with a 63x oil-immersion objective lens NA 1.32. All offline image analysis was done using Image J software. A pixel by pixel colocalization study by using JACoP (Just Another Colocalization Plugin) was used. Manders split coefficients were further obtained which are proportional to the amount of fluorescence of the colocalizing pixels in each colour channel.

Lipid-raft isolation. Low density, Triton-insoluble complexes were isolated as previously described (Martens et al. 2000) from HEK293 cells transiently transfected with the specified combinations among Kv1.3YFP, Kvß1.1CFP and Kvß2.1. Cells were homogenised in 1 ml of 1% Triton X-100, and sucrose was added to a final concentration of 40%. A 5-30% linear sucrose gradient was layered on top and further centrifuged (390.000g) for 20-22h at 4ºC in a Beckman SW41 rotor. Gradient fractions (1ml) were collected from the top and analysed by western blotting.

Ubiquitination assay. Cells were washed twice in cold PBS and frozen at -80ºC for at least one night. On ice, cells were lysed 20min on ice with 2mL of lysis buffer (50mM HEPES, 150mM NaCl, 1% Triton X-100, 10% Glicerol, pH 7.5) supplemented with 0.0125g NEM, 0.2mM MG132, 1mM EGTA 1mM EDTA, 20mM NaF, 1% NaOV, 2mM DTT, 1µg/ml aprotinin, 1µg/ml leupeptin, 1µg/ml pepstatin and 1mM phenylmethylsulfonyl fluoride as protease inhibitors. After scrapping the cells, they were centrifuge at 14.000gs for 15min. Co-immunoprecipitation assay was performed as previously described.

RESULTS

Kvßs in HEK cells modulate Kv1.3 differently than in Xenopus oocytes

The modulation exerted on the Kv1 family by the Kvß subunits has been studied focused mainly in the electrophysiological changes generated. Modifications on them have been successfully related, also, to their aldoketoreductase activity (Kilfoil et al., 2013). Specifically considering Kv1.3, it was described that both Kvß2 and Kvß1 family were able to increase the current of this channel. It was also stablished that, after a *Xenopus oocyte* injection of both Kv1.3 and Kvß1, there was not a fast inactivation on this channel (McCormack et al., 1999). However, it is widely accepted that some results can vary depending on the cell line used to develop the experiments. Actually, it was described that *Xenopus oocytes* expresses endogenous Kv channels (Blumenthal and Kaczmarek, 1994).

Since our cellular model is HEK293, we moved to analyse the effect of Kvß proteins in this mammal environment. Thus, our studies on the Kvß control of Kv1.3 started by characterising the current control in HEK cells. Representative traces of the elicited currents are presented for Kv1.3YFP (figure 1A), as well as the cotransfections of Kv1.3YFP/ Kvß2.1CFP (figure 1B) and Kv1.3 YFP/ Kvß1.1CFP (figure 1C). The current density analysis showed that while Kvß2.1 (figure 1D black square) does not increase the Kv1.3 current (figure 1D white rhombus), Kvß1.1 had this specific ability (figure 1D grey triangle). When measured the current density at 50mV, this difference is statistically relevant compared with Kv1.3 and Kv1.3/ Kvß2.1 (figure 1E). To detect possible modifications on the Kv1.3 gating, currents were normalised by the highest value and it was inferable that both Kvß1.1 and Kvß2.1 produce a depolarizing shift for the opening voltage. Thereby, they both can enhance the channel opening at more negative voltage values (figure 1F). Moreover, even Kvß1.1 does not exert the typical fast closing described; it can increase the C-type inactivation for Kv1.3 (figure 1G). The obtainment of those results that differ from the previous published studies, leaded us to implement other techniques to ensure our results as well as reconsider other already-assumed Kvß capabilities on controlling Kv subunits.

Firstly, the association of the Kv1.3 channel with Kvß1.1 (figure 2A) and Kvß2.1 (figure 2B) subunits was checked by coimmunoprecipitation assays. Confocal microscopy experiments were assumed to assert our previous electrophysiological data. The evaluation of the Kv1.3 membrane proportion returned the same value for it alone (figure 2C-F) or coexpressed with Kvß1.1 (figure 2G-K). However, cotransfection with Kvß2.1 (figure 2L-P) leads to a decrease of this percentage (figure 2Q). This effect was not due to a decrease on the total channel expression, since no significant differences on fluorescence level were observed among conditions (figure 2R).

Thus, while electrophysiological recordings are exhibiting an increase of current with Kvß1.1, this modulation is not observable by colocalization experiments. On the other hand, Kvß2.1 is not exerting any depletion of the channel current, but microscopy results revealed a diminution of Kv1.3 at cell surface. The combination of data from both figures is just explainable by a higher amount of the Kv1.3 intracellular staining when it is cotransfected with Kvß subunits. This pattern is detectable at the profile of Kv1.3 in the presence of Kvß1.1 (figure 2K) or Kvß2.1 (figure 2P). Concomitantly, it was previously described that Kvß can function as a chaperon interacting with the channel at early stages of its pathway and allowing the proper folder (Pongs and Schwarz, 2010). However, our

results demonstrated that just the Kvß1.1 is able to enhance the traffic to the plasma membrane.

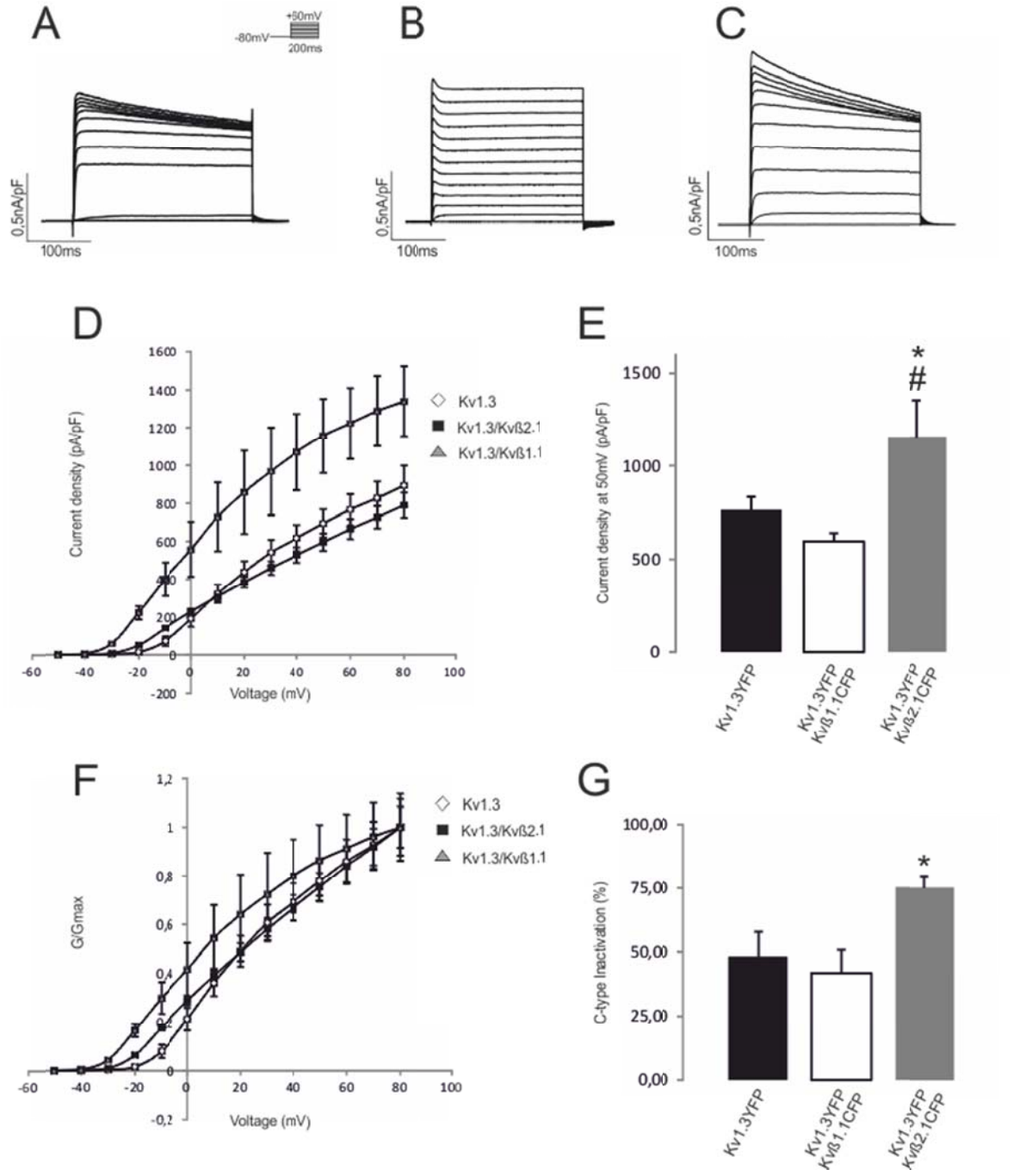

Figure 1. Characterization of Kv1.3 electrophysiological properties in the presence of the Kvß subunits. A-C. Voltage-dependent K^+ currents elicited in HEK cells transfected with Kv1.3YFP, Kv1.3YFP/Kvß2.1CFP and Kv1.3YFP/Kvß1.1CFP. A: Kv1.3YFP. B: Kv1.3YFP/ Kvß2.1CFP. C: Kv1.3YFP/Kvß1.1CFP. Cells were held at -80mV and pulse potentials were applied as indicated. D: Current density *vs* voltage plot of outward K^+ currents. White rombos, Kv1.3YFP; black square, Kv1.3YFP+ Kvß2.1CFP; grey triangle, Kv1.3YFP/ Kvß1.1CFP. Values are mean±SE (n=4-6 independent cells). E: Current density at 50mV. F: Steady-state activation of outward K^+ currents on Kv1.3YFP, Kv1.3YFP/Kvß2.1CFP and Kv1.3YFP/Kvß1.1CFP. White rombos, Kv1.3YFP; black square, Kv1.3YFP+ Kvß2.1CFP; grey triangle, Kv1.3YFP/ Kvß1.1CFP. Values are mean±SE (n=4-6 independent cells). G: Percentage of C-type inactivation. *p<0.05 compared with Kv1.3YFP. #p<0.05 compared with Kv1.3YFP/Kvß2.1CFP.

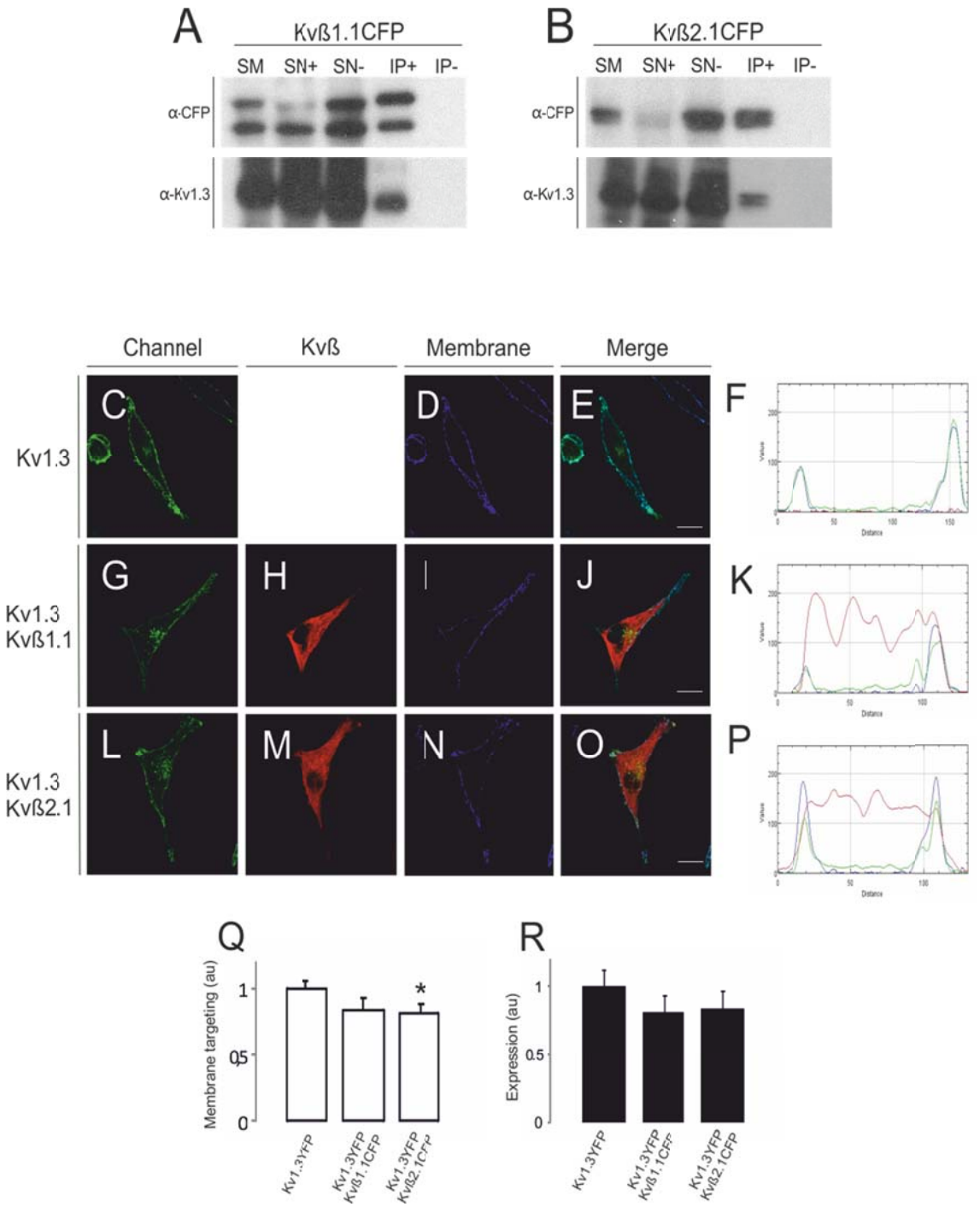

Figure 2. A-B. Kvß1.1CFP and Kvß2.1CFP can form complexes with Kv1.3. A: Immunoprecipitation of Kvß1.1CFP in the presence of Kv1.3HA. B: Immunoprecipitation of Kvß2.1CFP in the presence of Kv1.3HA. SM: staring material. SN+: supernatant collected after immunoprecipitation in presence of antibody. SN-: supernatant collected after immunoprecipitation in absence of antibody. IP+: immunoprecipitation in the presence of antibody. IP-: immunoprecipitation in the absence of antibody. C-R. Kvß1.1CFP and Kvß2.1CFP increases the presence of Kv1.3YFP intracellularly. C-F: Kv1.3YFP membrane colocalisation. C: Kv1.3YFP. D: membrane marker. E: merge of channels, turquoise means colocalization. F: pixel-by-pixel analysis of ROI in E. G-K. Kv1.3YFP membrane colocalization in presence of Kvß1.1CFP. G: Kv1.3YFP. H: Kvß1.1CFP. I: membrane marker. J: merge of channels, white means triple colocalization. K:pixel-by-pixel analysis of ROI in J. L-P. Kv1.3YFP membrane colocalization in presence of Kvß2.1CFP. L: Kv1.3YFP. M: Kvß2.1CFP. N: membrane marker. O: merge channels, white means colocalization. P: pixel-by-pixel-analysis of ROI in O. Q: Quantification of membrane colocalization using Mander's coefficiency. *p<0.05 compared with Kv1.3YFP. R: Intensity quantification of Kv1.3YFP.

Kvßs undergo non-lipid raft Kv1.3 distribution

Several years ago it was described that Kv1.3 can traffic to lipid raft microdomains, which in turn are closely related with the formation of immunological synapses (Vicente et al., 2008, Tomassian et al., 2011). Considering the new ability previously described for Kvß2.1, the relationship stablished with Kvß1.1 and the consequences on the final localization of both proteins, the effect on Kv1.3 submembrane localization was analysed.

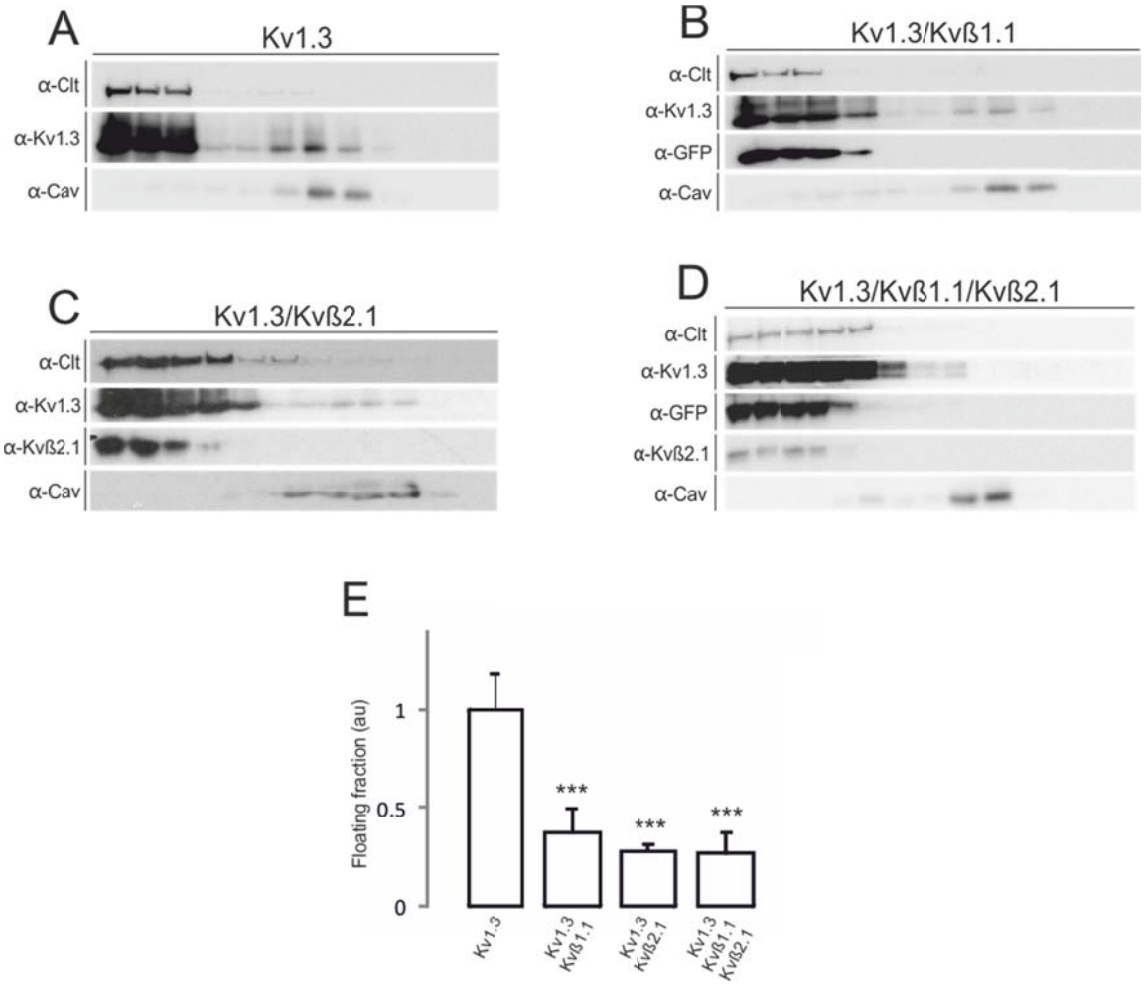

Figure 3. Kv1.3 is decreased in lipid raft domains when coexpressed with Kvß1.1 and Kvß2.1. A: Western blotting of lipid raft fractions of Kv1.3YFP. B: Western blotting of lipid raft fractions of Kv1.3YFP/Kvß1.1CFP. C: Western blotting of lipid raft fractions of Kv1.3YFP/Kvß2.1. D: Western blotting of lipid raft fractions of Kv1.3YFP/Kvß1.1CFP/Kvß2.1 E. Quantification of the flotability in all conditions relativized by the total amount of expression.

The association of Kvßs, known also long ago, has never been demonstrated as a putative modulator for this location. While Kv1.3 was present in those domains (figure 3A), the cotransfection with Kvß1.1 (figure 3B) as well as Kvß2.1 (figure 3C) leaded to a decrease in the detection of the channel in *lipid raft*. The coexpression of both subunits in a proportion 1:1 exerted the same effect (figure 3D). The three conditions are significantly different from the wild type expression (figure 3E). Considering that both Kvß have this effect on the channel, the specific trafficking property of Kvß2.1 is unlikely to be involved.

The binding domain among α and ß subunits was biochemically defined at the N-terminus of Kv1 channels, close to the tetramerization interacting domain for this family (T1).

Specifically for Kv1.3, the Kvß Binding Domain (ßBD) would be placed at the amino acids among 135-151 positions in the protein sequence (orange square on figure 4) (Sewing et al., 1996). Even though, the obtaining of the Kv1.2/ Kvß2.1 crystal structure allowed MacKinnon's laboratory to localise the contact interface among M-70 to Y-80 amino acids of the channel, corresponding to M-87 to Y-97 positions in Kv1.3 sequence (green square on figure 4) (Long et al., 2005). Moreover, some studies have reported also possible associations with some parts of the C-terminus (Sokolova et al., 2003).

Our laboratory has recently published the interaction of Kv1.3 with caveolin, acting as a driving force for placing the channel to lipid raft microdomains. We demonstrated that there is a molecular determinant for this association placed in the N-terminus of the channel, so called Caveolin Binding Domain (CBD). The CBD is formed by the amino acids among the 166-174 protein positions (yellow square in figure 4) (Perez-Verdaguer et al., 2016a). The ßBD defined from the crystal structure is 80 residues far the CBD. Regarding the possible molecular volume of either Kvß or caveolin and the position of their interacting sequences, it is likely to consider a possible competence for the N-terminus of the channel. Thereby, when all three proteins are expressed together, a diminution of Kv1.3 presence at the *lipid raft* microdomains could be a possible consequence .

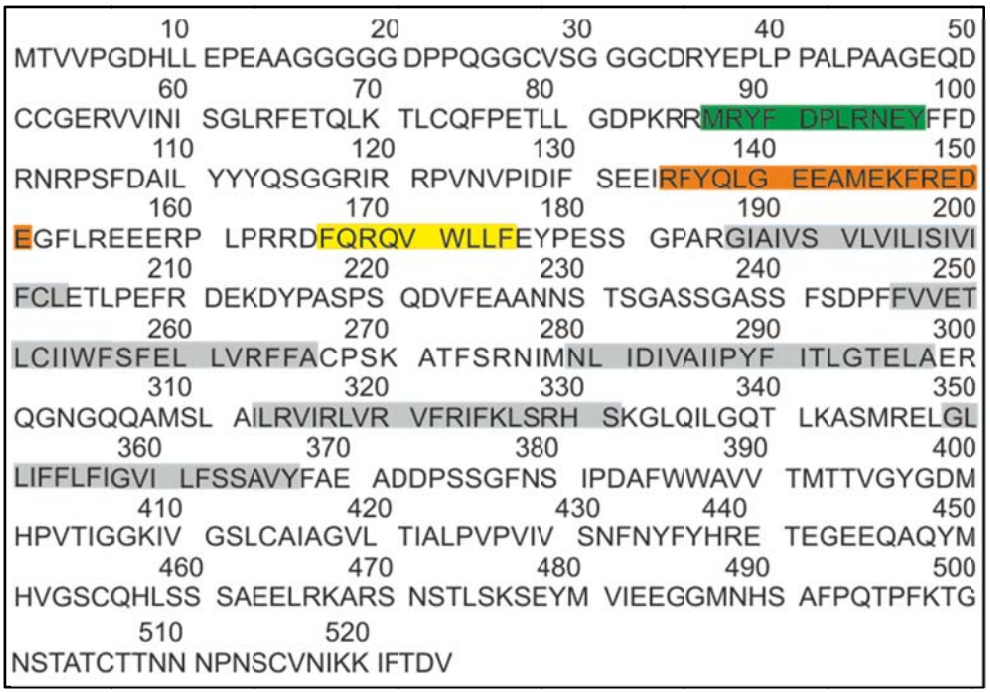

Figure 4. Rat Kv1.3 aminoacid sequence. Kvβ binding domain highlighted in orange; caveolin binding domain, in yellow; transmembrane domains, in grey.

To address this question, as shown in figure 5, the immunoprecipitation of transfected caveolin was addressed. As previously described, caveolin and Kv1.3 can form oligomers, contrary to the negative interaction between caveolin and Kvß2.1 (figure 5 and first contribution). Upon triple cotransfection, caveolin and Kv1.3 can interact but there are no tripartite complexes: caveolin and Kvß2.1 cannot interact with the same channel. (IP+ third lane figure 5). Thereby, our results confirmed a stearic competence for the Kv interacting region.

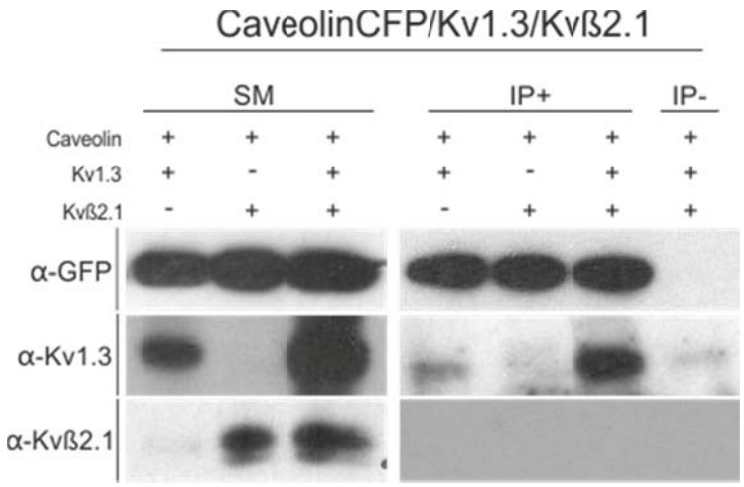

Figure 5. Caveolin and Kvβ2.1 compete for the interaction with Kv1.3. Immunoprecipitation assay against CaveolinCFP. Western blot using α-GFP antibody, α-Kv1.3 and α- Kvβ2.1 antibody. SM: starting material. IP+: Immunoprecipitation in the presence of the antibody. IP-: Immunoprecipitation in the absence of the antibody.

Kvßs counteracts partially PMA-induced Kv1.3 internalization

The amount of Kv1.3 at the cell surface, where it develops its major functions, is controlled not only by the trafficking but also trhough the recycling of the channel. Previous data from the laboratory defined that under PMA treatment, the channel undergoes exit of the lipid raft domains and internalization to endosomal particles. Summing up the results concerning Kvß2.1, two hypotheses are plausible. On one hand, regarding the internalization PMA-dependent of Kvß2.1, it is tempting to speculate that the endocytosis of the channel would be exacerbated. On the other hand, since it is impairing the *lipid raft* channel targeting, it is also possible that the PMA effect would be counteracted.

Kv1.3, mainly expressed at the cell surface, shows a low colocalization pattern (figure 6A-C) with the early endosome marker (EEA-1). This is highly increased when the cells are treated for 30 minutes with PMA (figure 6O), exhibiting a dramatic intracellular punctuate pattern (figure 6D-F). From previous results, we do know that Kvß2.1 increases the colocalization with the marker after the same treatment (figure 6O and contribution 1).

Upon coexpression with Kvß2.1, Kv1.3 presents a similar colocalization with EEA-1 than alone (figure 6G-J). When PMA was added, the channel is also undergoing internalization increasing this colocalization level (figure K-N). Even this phenomenon is significantly higher than the condition without any treatment, the level achieved by the Kv1.3/Kvß2.1 in the presence of PMA is hardly lower than Kv1.3 alone. Actually, it is still detectable some channel signal at the cell surface (figure 6K) upon coexpression and PMA.

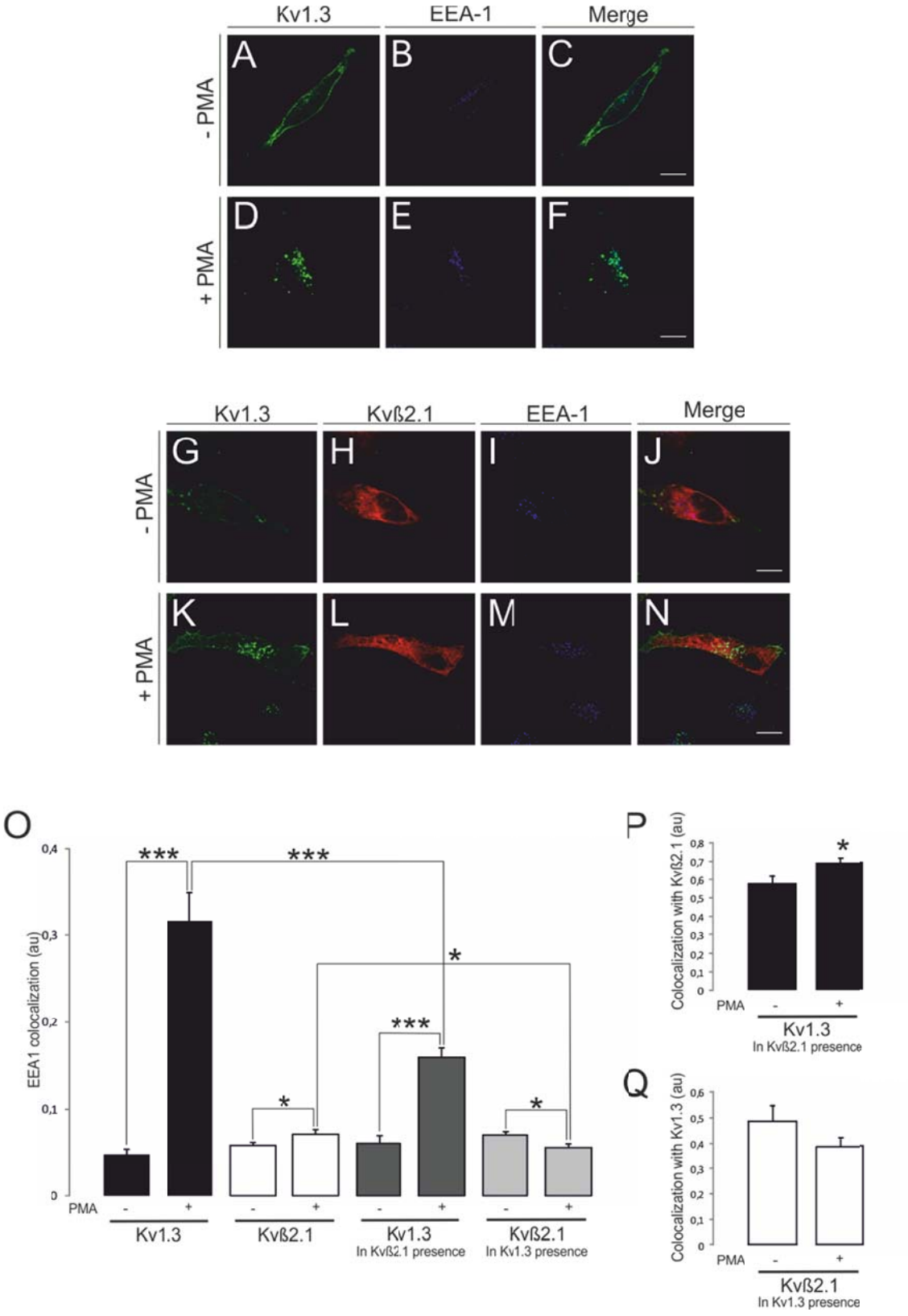

Figure 6. PMA-dependent internalization of Kv1.3 is partially impaired by Kvβ2.1. A-C. Kv1.3 colocalization with early endosomes marker (EEA-1). A: Kv1.3YFP. B: EEA-1 marker. C: merge channels, turquoise means colocalization. D-F: Kv1.3YFP colocalization with EEA-1 after treating the cells with PMA. D: Kv1.3YFP. E: EEA-1 marker. F: merge channels, turquoise means colocalization. G-J: Kv1.3 colocalization with early endosomes marker (EEA-1) in the presence of Kvβ2.1. G: Kv1.3YFP. H: Kvβ2.1CFP. I: EEA-1 marker. J: merge channels, white means triple colocalization. K-N: Kv1.3 colocalization with early endosomes marker (EEA-1) in the presence of Kvβ2.1 and PMA. K: Kv1.3YFP. L: Kvβ2.1CFP. M: EEA-1 marker. N: merge channels, white means triple colocalization. O: Quantification of colocalization with EEA-1 using Mander's

coefficiency. *p<0.05; ***p<0.001. P: Quantification of Kv1.3 colocalization with Kvβ2.1 in the absence and in the presence of PMA. Q: Quantification of Kvβ2.1 colocalization with Kv1.3 in the absence and in the presence of PMA.

Kvß2.1 is also changing its behaviour. While increasing the colocalisation level with EEA-1 after PMA treatment, this decreases when coexpressed with Kv1.3 (figure 6O). Thereby, both proteins are able to impair partially the internalization pattern under PMA stimulation.

The analysis of the colocalization between Kv1.3 and Kvß2.1 revealed that, while there are no relevant changes in Kvß2.1 (figure 6Q), Kv1.3 increase the colocalization with the subunit under PMA treatment (figure 6P). Since Kvß2.1 main localization is the cytoplasm, it is not surprising that an increase in internalization is accompanied with a higher colocalization with a cytosolic protein.

Since both proteins are behaving differently when they are expressed alone or accompanied, one possible explanation would be a partial dissociation of the complexes under PMA treatment, and once separated, act as lonely proteins.

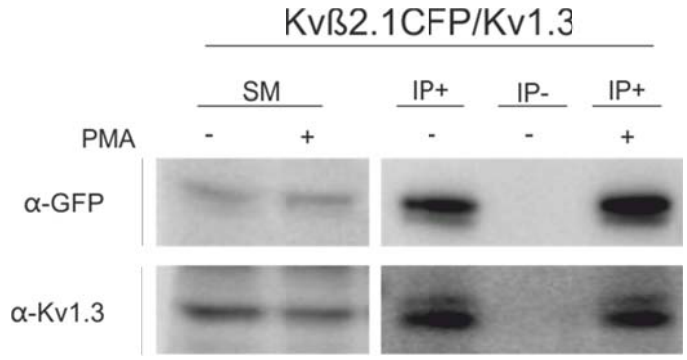

Figure 7.. Kvβ2.1/Kv1.3 complexes are not disrupted under PMA treatment. Immunoprecipitation assay against Kvβ2.1CFP. Western blot using α-GFP antibody and α-Kv1.3. SM: starting material. IP+: Immunoprecipitation in the presence of the antibody. IP-: Immunoprecipitation in the absence of the antibody.

To analyse the interaction, immunoprecipitation of Kvß2.1 in the presence or the absence of PMA was performed. As it is observable in figure 7, there were no changes in the interaction between Kvß2.1 and Kv1.3 upon PMA treatment.

Other possible hypothesis considered was that Kvß2.1could be impairing partially the process of Kv1.3 vesiculation. Previous results of the laboratory showed that PMA endocytosis is mediated by the ubiquitination of the channel. The treatment of cells expressing only Kv1.3 with this compound leaded to a massive detection of ubiquitinated channel. The quantification revealed a high and significant increase (figure 8A, C). This raise was also detected for Kv1.3/Kvß2.1 cotransfection (figure 8B). However, upon quantification of different experiments, this condition presents the tendency to be lower than the Kv1.3 alone (figure 8C).

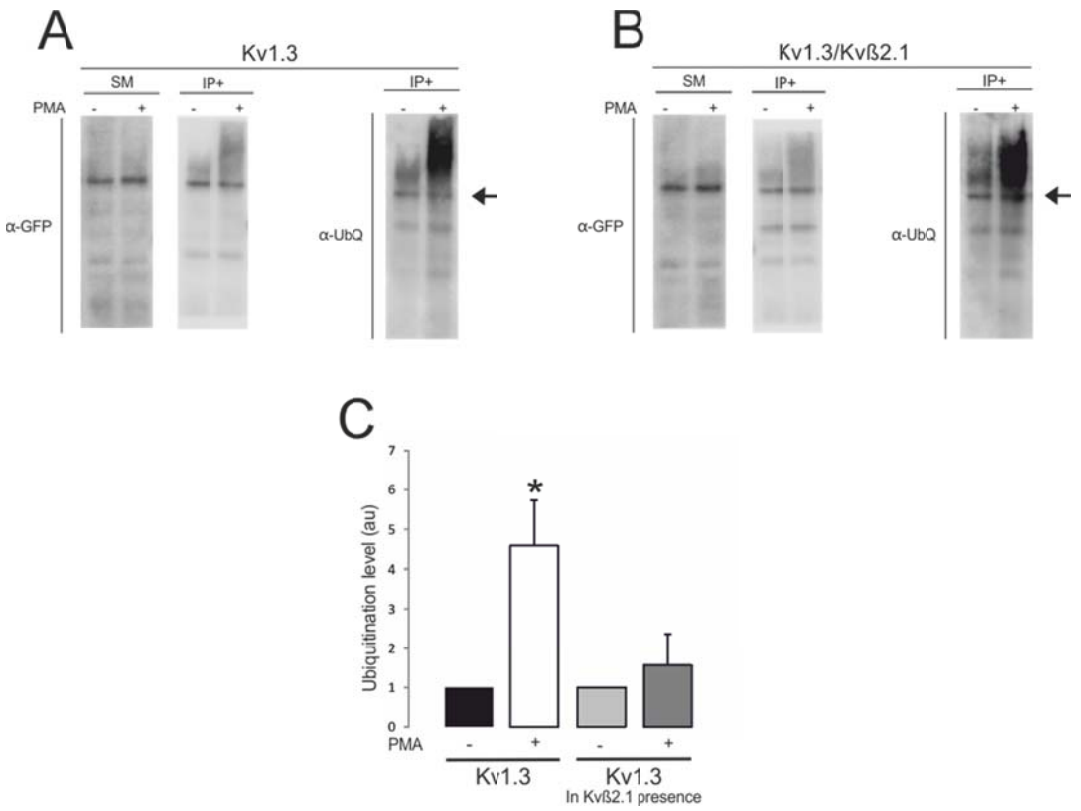

Figure 8. Kvß2.1 slightly impairs the PMA-dependent ubiquitination of the channel. Immunoprecipitation of Kv1.3 in the absence or the presence of Kvß2.1 and PMA. Immunoblot using α-GFP and α-Ubiquitin antibody. SM: starting material. IP+: immunoprecipitation in the presence of GFP antibody. Arrow indicates Kv1.3YFP.

DISCUSSION

The present work shows the regulation of Kvß1.1 and Kvß2.1 on Kv1.3 channel: from the electrophysiological properties to the trafficking modulation. Previous studies revealed that both Kvß1.1 and Kvß2.1 were exerting and enhancement on the current density (McCormack et al., 1999). No additional features were determined for Kvß2.1 but a small initial inactivation component on Kv1.3 current was observed upon coexpression with Kvß1.1. The kinetic properties analysed in this contribution revealed that both subunits are shifting the activation towards hyperpolarising voltages, similar to the effect on Kv1.5 (Heinemann et al., 1996). Moreover, Kvß1.1 exerts indeed an increased degree of C-type inactivation. However, contrary to the previous investigations, just Kvß1.1 was observed to increase the current density of the channel (Shi et al., 1996, McCormack et al., 1999). Previous controversies have been taking place due to the elected expression system. Functional Kv1.5 properties were not properly stablished due to the use of L-cell line that expresses Kvß2.1 endogenously (Uebele et al., 1996). Furthermore, it was published that *Xenopus oocytes* synthesize KCNE peptides endogenously, which could have modulates the Kv1.3 transfected (Anantharam et al., 2003). Competition among auxiliary subunits in *Xenopus oocytes* cannot be, thus, discarded as a part of the obtained results.

Kv1.3 is a channel that presents a good traffic to the plasma membrane without any auxiliary subunit help (Vicente et al., 2008). Recently our laboratory has published the

export signals present in the sequence that encodes this behavior (Martinez-Marmol et al., 2013). The present results suggest that Kvß1.1 could exhibit some additional signatures to traffic to the plasma membrane in the additional N-terminus segment. Similarly, by interacting with 14-3-3, SAC1 export from the ER is stimulated (Bajaj Pahuja et al., 2015). On the other hand, the ability of Kvß1.1 to interact with the actin cytoskeleton could be influencing the traffic of the channel (Nakahira et al., 1998). Kvß2.1 subunit is presenting a slight but significant reduction in the Kv1.3 proportion at the plasma membrane. The images obtained from the coexpression exhibit a higher staining in a Golgi-like compartment. Since the interaction among the proteins is known to happen at the ER compartment and enhance the mature glycosylation of other channels, it is tempting to speculate that Kvß2.1 is mediating a slightly slower processing of the channel (Nagaya and Papazian, 1997, Shi et al., 1996). Similar to the combination with *Shaker* and Kv1.5, the role exerted by Kvß2.1 is different than the kinetic modulation or the traffic enhancement of its partners (Accili et al., 1997b).

The present work exhibited a new level of control on Kv1 channels. Both Kvß1.1 and Kvß2.1 have the ability of impairing the Kv1.3 traffic to lipid raft microdomains. The alteration on the proper subcellular localization of those has been related with some diseases (Dart, 2010). It is the case of Kv1.3 and lupus eritomatoeus or the estrogen receptor and Alzheimer disease. Misslocalization of both proteins has been detected in both mentioned illnesses (Nicolaou et al., 2007, Canerina-Amaro et al., 2017). Thus, the control on the traffic to lipid raft microdomains is highly relevant, and Kvßs are a cellular mechanism to reduce this presence. Since the interaction of Kvß/Kv channels is taking placed at the endoplasmic reticulum, the destiny of them it is decided early in the secretory pathway.

Even the recent and unique characteristics of Kvß2.1, the molecular determinants underlying this Kv1.3 misslocalization effect were shared with Kvß1.1. We have recently published that the traffic of Kv1.3 to lipid raft microdomains is governed by caveolin. This protein detects a highly hydrophobic sequence placed at the N-terminus of the channel and enhances this specific localization (Perez-Verdaguer et al., 2016a). The principal Kvß interacting sequence is also located at this channel region. The results of this contribution showed that Kvßs were masking the CBD by interacting with their molecular determinant on Kv1.3. Similarly, 14-3-3 is able to coat a specific motif in TASK1 and TASK3 which is important for the COPI binding (Mathie et al., 2010). Moreover, in contribution 5, our results define a hiding event on Kv1.3 export signals by KCNE4 (Sole et al., 2016).

Regarding the Kvß expression regulation by different insults, and considering the new role stablished for them, one could speculate that Kvß presence can be translated as a preventing signal. The activation stimuli on T-cells imply the opening of Kv1.3 placed at lipid raft microdomains (Panyi et al., 2004, Varshney et al., 2016). The increase in the Kvß expression would lead to localization of the newly synthesised channel out of those domains. Thus, the signal could not be sustained due to the arrival of more Kv1.3. Since there are no possible tripartite complexes, electrophysiological properties of Kv1.3 at *lipid raft* would resemble to those obtained in presence of cholesterol (Hajdu et al., 2003). However, Kvß effect is not a complete inhibiting signal of the activity, since the channel will be present at the plasma membrane. Whether Kv1.3 can be recruited to those submembrane regions upon new insults, it remains unknown.

Finally, we have determined that Kvß is counteracting partially the PMA endocyting effect. The control on the channels function can be exerted not only on the traffic to the membrane, but also influencing the turnover. Actually, our group has recently published an EGF-dependent modulation of the Kv1.3 endocytosis (Martinez-Marmol et al., 2016). However, it is not the unique pathway to mediate the channel endocytosis. From previous laboratory results, it is known that the PKC activation leads to an internalisation of the channel, posterior to the exit from lipid raft microdomains. Lately, it has been published that the human organic anionic transporter 1 can undergo ubiquitination dependent on the activity of PKC (Xu et al., 2016a). The effect on Kv1.3 is also due to the ubiquitination of the channel at some lysines yet to be deciphered. Since the crystal structure is exhibiting a close contact between Kvß and both N and C terminus, a masking event on the sequence for the ubiquitination transference or the interaction with the ubiquitin ligase can be hypothesised (Gulbis et al., 1999). Thus, Kvß could be impairing the excess of Kv1.3 at lipid raft microdomains and diminishing the immunosuppression derived from PMA treatment. Thereby, as we previously mentioned. It is tempting to speculate that Kvß family are protective proteins of the immune system health.

REFERENCES

ACCILI, E. A., KIEHN, J., YANG, Q., WANG, Z., BROWN, A. M. & WIBLE, B. A. 1997b. Separable Kvbeta subunit domains alter expression and gating of potassium channels. *J Biol Chem,* 272**,** 25824-31.

ANANTHARAM, A., LEWIS, A., PANAGHIE, G., GORDON, E., MCCROSSAN, Z. A., LERNER, D. J. & ABBOTT, G. W. 2003. RNA interference reveals that endogenous Xenopus MinK-related peptides govern mammalian K+ channel function in oocyte expression studies. *J Biol Chem,* 278**,** 11739-45.

AUTIERI, M. V., BELKOWSKI, S. M., CONSTANTINESCU, C. S., COHEN, J. A. & PRYSTOWSKY, M. B. 1997. Lymphocyte-specific inducible expression of potassium channel beta subunits. *J Neuroimmunol,* 77**,** 8-16.

BAJAJ PAHUJA, K., WANG, J., BLAGOVESHCHENSKAYA, A., LIM, L., MADHUSUDHAN, M. S., MAYINGER, P. & SCHEKMAN, R. 2015. Phosphoregulatory protein 14-3-3 facilitates SAC1 transport from the endoplasmic reticulum. *Proc Natl Acad Sci U S A,* 112**,** E3199-206.

BEETON, C. & CHANDY, K. G. 2005. Potassium channels, memory T cells, and multiple sclerosis. *Neuroscientist,* 11**,** 550-62.

BLUMENTHAL, E. M. & KACZMAREK, L. K. 1994. The minK potassium channel exists in functional and nonfunctional forms when expressed in the plasma membrane of Xenopus oocytes. *J Neurosci,* 14**,** 3097-105.

BROWN, D. A. & LONDON, E. 1998. Structure and origin of ordered lipid domains in biological membranes. *J Membr Biol,* 164**,** 103-14.

BUCCI, M., GRATTON, J. P., RUDIC, R. D., ACEVEDO, L., ROVIEZZO, F., CIRINO, G. & SESSA, W. C. 2000. In vivo delivery of the caveolin-1 scaffolding domain inhibits nitric oxide synthesis and reduces inflammation. *Nat Med,* 6**,** 1362-7.

CAHALAN, M. D. & CHANDY, K. G. 2009. The functional network of ion channels in T lymphocytes. *Immunol Rev,* 231**,** 59-87.

CANERINA-AMARO, A., HERNANDEZ-ABAD, L. G., FERRER, I., QUINTO-ALEMANY, D., MESA-HERRERA, F., FERRI, C., PUERTAS-AVENDANO, R. A., DIAZ, M. & MARIN, R.

2017. Lipid raft ER signalosome malfunctions in menopause and Alzheimer's disease. *Front Biosci (Schol Ed),* 9**,** 111-126.

DART, C. 2010. Lipid microdomains and the regulation of ion channel function. *J Physiol,* 588**,** 3169-78.

GULBIS, J. M., MANN, S. & MACKINNON, R. 1999. Structure of a voltage-dependent K+ channel beta subunit. *Cell,* 97**,** 943-52.

GUTMAN, G. A., CHANDY, K. G., GRISSMER, S., LAZDUNSKI, M., MCKINNON, D., PARDO, L. A., ROBERTSON, G. A., RUDY, B., SANGUINETTI, M. C., STUHMER, W. & WANG, X. 2005. International Union of Pharmacology. LIII. Nomenclature and molecular relationships of voltage-gated potassium channels. *Pharmacol Rev,* 57**,** 473-508.

HAJDU, P., VARGA, Z., PIERI, C., PANYI, G. & GASPAR, R., JR. 2003. Cholesterol modifies the gating of Kv1.3 in human T lymphocytes. *Pflugers Arch,* 445**,** 674-82.

HILLE, B. 2001. Ion channels of excitable membranes. *Sinauerassociates, Sunderland, Mass.. Great Britain, 2001.*

HEINEMANN, S. H., RETTIG, J., GRAACK, H. R. & PONGS, O. 1996. Functional characterization of Kv channel beta-subunits from rat brain. *J Physiol,* 493 (Pt 3)**,** 625-33.

KILFOIL, P. J., TIPPARAJU, S. M., BARSKI, O. A. & BHATNAGAR, A. 2013. Regulation of ion channels by pyridine nucleotides. *Circ Res,* 112**,** 721-41.

LEONARD, R. J., GARCIA, M. L., SLAUGHTER, R. S. & REUBEN, J. P. 1992. Selective blockers of voltage-gated K+ channels depolarize human T lymphocytes: mechanism of the antiproliferative effect of charybdotoxin. *Proc Natl Acad Sci U S A,* 89**,** 10094-8LONG, S. B., CAMPBELL, E. B. & MACKINNON, R. 2005. Crystal structure of a mammalian voltage-dependent Shaker family K+ channel. *Science,* 309**,** 897-903.

MCCORMACK, T., MCCORMACK, K., NADAL, M. S., VIEIRA, E., OZAITA, A. & RUDY, B. 1999. The effects of Shaker beta-subunits on the human lymphocyte K+ channel Kv1.3. *J Biol Chem,* 274**,** 20123-6.

MARTENS, J. R., KWAK, Y. G. & TAMKUN, M. M. 1999. Modulation of Kv channel alpha/beta subunit interactions. *Trends Cardiovasc Med,* 9**,** 253-8.

MARTINEZ-MARMOL, R., PEREZ-VERDAGUER, M., ROIG, S. R., VALLEJO-GRACIA, A., GOTSI, P., SERRANO-ALBARRAS, A., BAHAMONDE, M. I., FERRER-MONTIEL, A., FERNANDEZ-BALLESTER, G., COMES, N. & FELIPE, A. 2013. A non-canonical di-acidic signal at the C-terminus of Kv1.3 determines anterograde trafficking and surface expression. *J Cell Sci,* 126**,** 5681-91.

MATHIE, A., REES, K. A., EL HACHMANE, M. F. & VEALE, E. L. 2010. Trafficking of neuronal two pore domain potassium channels. *Curr Neuropharmacol,* 8**,** 276-86.

MEDINA, F. A., COHEN, A. W., DE ALMEIDA, C. J., NAGAJYOTHI, F., BRAUNSTEIN, V. L., TEIXEIRA, M. M., TANOWITZ, H. B. & LISANTI, M. P. 2007. Immune dysfunction in caveolin-1 null mice following infection with Trypanosoma cruzi (Tulahuen strain). *Microbes Infect,* 9**,** 325-33.

NAGAYA, N. & PAPAZIAN, D. M. 1997. Potassium channel alpha and beta subunits assemble in the endoplasmic reticulum. *J Biol Chem,* 272**,** 3022-7.

NAKAHIRA, K., MATOS, M. F. & TRIMMER, J. S. 1998. Differential interaction of voltage-gated K+ channel beta-subunits with cytoskeleton is mediated by unique amino terminal domains. *J Mol Neurosci,* 11**,** 199-208.

NICOLAOU, S. A., NEUMEIER, L., TAKIMOTO, K., LEE, S. M., DUNCAN, H. J., KANT, S. K., MONGEY, A. B., FILIPOVICH, A. H. & CONFORTI, L. 2010. Differential calcium signaling and Kv1.3 trafficking to the immunological synapse in systemic lupus erythematosus. *Cell Calcium,* 47**,** 19-28.

PANYI, G., VAMOSI, G., BACSO, Z., BAGDANY, M., BODNAR, A., VARGA, Z., GASPAR, R., MATYUS, L. & DAMJANOVICH, S. 2004. Kv1.3 potassium channels are localized in the immunological synapse formed between cytotoxic and target cells. *Proc Natl Acad Sci U S A,* 101**,** 1285-90.

PEREZ-VERDAGUER, M., CAPERA, J., MARTINEZ-MARMOL, R., CAMPS, M., COMES, N., TAMKUN, M. M. & FELIPE, A. 2016a. Caveolin interaction governs Kv1.3 lipid raft targeting. *Sci Rep,* 6**,** 22453.

SHI, G., NAKAHIRA, K., HAMMOND, S., RHODES, K. J., SCHECHTER, L. E. & TRIMMER, J. S. 1996. Beta subunits promote K+ channel surface expression through effects early in biosynthesis. *Neuron,* 16**,** 843-52.

SHVETS, E., LUDWIG, A. & NICHOLS, B. J. 2014. News from the caves: update on the structure and function of caveolae. *Curr Opin Cell Biol,* 29**,** 99-106.

SOKOLOVA, O., ACCARDI, A., GUTIERREZ, D., LAU, A., RIGNEY, M. & GRIGORIEFF, N. 2003. Conformational changes in the C terminus of Shaker K+ channel bound to the rat Kvbeta2-subunit. *Proc Natl Acad Sci U S A,* 100**,** 12607-12.

SOLE, L., ROIG, S. R., VALLEJO-GRACIA, A., SERRANO-ALBARRAS, A., MARTINEZ-MARMOL, R., TAMKUN, M. M. & FELIPE, A. 2016. The C-terminal domain of Kv1.3 regulates functional interactions with the KCNE4 subunit. *J Cell Sci,* 129**,** 4265-4277.

SZABO, I., GULBINS, E., APFEL, H., ZHANG, X., BARTH, P., BUSCH, A. E., SCHLOTTMANN, K., PONGS, O. & LANG, F. 1996. Tyrosine phosphorylation-dependent suppression of a voltage-gated K+ channel in T lymphocytes upon Fas stimulation. *J Biol Chem,* 271**,** 20465-9.

TOLDI, G., VASARHELYI, B., KAPOSI, A., MESZAROS, G., PANCZEL, P., HOSSZUFALUSI, N., TULASSAY, T. & TRESZL, A. 2010. Lymphocyte activation in type 1 diabetes mellitus: the increased significance of Kv1.3 potassium channels. *Immunol Lett,* 133**,** 35-41.

TOMASSIAN, T., HUMPHRIES, L. A., LIU, S. D., SILVA, O., BROOKS, D. G. & MICELI, M. C. 2011. Caveolin-1 orchestrates TCR synaptic polarity, signal specificity, and function in CD8 T cells. *J Immunol,* 187**,** 2993-3002.

UEBELE, V. N., ENGLAND, S. K., CHAUDHARY, A., TAMKUN, M. M. & SNYDERS, D. J. 1996. Functional differences in Kv1.5 currents expressed in mammalian cell lines are due to the presence of endogenous Kv beta 2.1 subunits. *J Biol Chem,* 271**,** 2406-12.

VARSHNEY, P., YADAV, V. & SAINI, N. 2016. Lipid rafts in immune signalling: current progress and future perspective. *Immunology,* 149**,** 13-24.

VICENTE, R., ESCALADA, A., SOLER, C., GRANDE, M., CELADA, A., TAMKUN, M. M., SOLSONA, C. & FELIPE, A. 2005. Pattern of Kv beta subunit expression in macrophages depends upon proliferation and the mode of activation. *J Immunol,* 174**,** 4736-44.

VICENTE, R., VILLALONGA, N., CALVO, M., ESCALADA, A., SOLSONA, C., SOLER, C., TAMKUN, M. M. & FELIPE, A. 2008. Kv1.5 association modifies Kv1.3 traffic and membrane localization. *J Biol Chem,* 283**,** 8756-64.

XU, D., WANG, H., ZHANG, Q. & YOU, G. 2016a. Nedd4-2 but not Nedd4-1 is critical for protein kinase C-regulated ubiquitination, expression, and transport activity of human organic anion transporter 1. *Am J Physiol Renal Physiol,* 310**,** F821-31.

3.2. CHAPTER 2: Kv1.3 TRAFFIC REGULATION MECHANISM BY KCNE4

3.2.1. Contribution 4:

Published in Journal of Cell Science. 2013 Dec 15;126(Pt 24):5681-91.

A non-canonical di-acidic signal at the C-terminus of Kv1.3 determines anterograde trafficking and surface expression

Martínez-Mármol R[1], Pérez-Verdaguer M[1], Roig SR[1], Vallejo-Gracia A[1], Gotsi P[1], Serrano-Albarrás A[1], Bahamonde MI[2], Ferrer-Montiel A[3], Fernández-Ballester G[3], Comes N[1], Felipe A[1].

[1] Molecular Physiology Laboratory, Departament de Bioquı´mica i Biologia Molecular, Institut de Biomedicina (IBUB), Universitat de Barcelona. Barcelona, Spain

[2] Institute for Bioengineering of Catalonia. L' Hospitalet de Llobregat, Barcelona, Spain

[3] Instituto de Biologı´a Molecular y Celular, Universidad Miguel Hernández. Elche, Spain.

ABSTRACT

Impairment of Kv1.3 expression at the cell membrane in leukocytes and sensory neuron contributes to the pathophysiology of autoimmune diseases and sensory syndromes. Molecular mechanisms underlying Kv1.3 channel trafficking to the plasma membrane remain elusive. We report a novel non-canonical di-acidic signal (E483/484) at the C-terminus of Kv1.3 essential for anterograde transport and surface expression. Notably, homologous motifs are conserved in neuronal Kv1 and Shaker channels. Biochemical analysis revealed interactions with the Sec24 subunit of the coat protein complex II. Disruption of this complex retains the channel at the endoplasmic reticulum. A molecular model of the Kv1.3-Sec24a complex suggests salt-bridges between the di-acidic E483/484 motif in Kv1.3 and the di-basic R750/752 sequence in Sec24. These findings identify a previously unrecognized motif of Kv channels essential for their expression on the cell surface. Our results contribute to our understanding of how Kv1 channels target to the cell membrane, and provide new therapeutic strategies for the treatment of pathological conditions.

Report of the PhD student participation

A non-canonical di-acidic signal at the C-terminus of Kv1.3 determines anterograde trafficking and surface expression

Published in Journal of Cell Science, Impact Factor (2013): 5.91

Sara Raquel Roig Merino performed the Kv1.1 and Shaker experiments, the immunoprecipitation of Kv1.3 with Sec24D and the phylogenetic analysis of the species and sequences at supplemental figure 4.

Figures 1, 2, 3 and 6 were included on Ramón Martínez Marmol thesis, previous to the publication of the paper.

Antonio Felipe

PhD thesis director

A non-canonical di-acidic signal at the C-terminus of Kv1.3 determines anterograde trafficking and surface expression

Ramón Martínez-Mármol[1], Mireia Pérez-Verdaguer[1], Sara R. Roig[1], Albert Vallejo-Gracia[1], Pelagia Gotsi[1], Antonio Serrano-Albarrás[1], María Isabel Bahamonde[2], Antonio Ferrer-Montiel[3], Gregorio Fernández-Ballester[3], Núria Comes[1] and Antonio Felipe[1,*]

[1]Molecular Physiology Laboratory, Departament de Bioquímica i Biologia Molecular, Institut de Biomedicina (IBUB), Universitat de Barcelona, Av. Diagonal 643, E-08028 Barcelona, Spain
[2]Institute for Bioengineering of Catalonia (IBEC), Feixa Llarga s/n, 08907 L' Hospitalet de Llobregat, Barcelona, Spain
[3]Instituto de Biología Molecular y Celular, Universidad Miguel Hernández, Av. de la Universidad s/n, 03202 Elche, Alicante, Spain
*Author for correspondence (afelipe@ub.edu)

Accepted 29 September 2013
Journal of Cell Science 126, 5681–5691

doi: 10.1242/jcs.134825

Summary

Impairment of Kv1.3 expression at the cell membrane in leukocytes and sensory neuron contributes to the pathophysiology of autoimmune diseases and sensory syndromes. Molecular mechanisms underlying Kv1.3 channel trafficking to the plasma membrane remain elusive. We report a novel non-canonical di-acidic signal (E483/484) at the C-terminus of Kv1.3 essential for anterograde transport and surface expression. Notably, homologous motifs are conserved in neuronal Kv1 and Shaker channels. Biochemical analysis revealed interactions with the Sec24 subunit of the coat protein complex II. Disruption of this complex retains the channel at the endoplasmic reticulum. A molecular model of the Kv1.3–Sec24a complex suggests salt-bridges between the di-acidic E483/484 motif in Kv1.3 and the di-basic R750/752 sequence in Sec24. These findings identify a previously unrecognized motif of Kv channels essential for their expression on the cell surface. Our results contribute to our understanding of how Kv1 channels target to the cell membrane, and provide new therapeutic strategies for the treatment of pathological conditions.

Key words: Forward-traffic motifs, Lymphocytes, Neurons, Plasma membrane, Voltage-dependent K^+ channels

Introduction

Voltage-dependent potassium channels (Kv) control the resting membrane potential in mammalian cells (Hille, 2001). In this context, the Kv1.3 channel participates in the activity of sensory neurons and also controls the activation and proliferation of leukocytes (Vicente et al., 2003; Rivera et al., 2005; Cahalan and Chandy, 2009; Cavallin et al., 2010; Gazula et al., 2010). Therefore, Kv1.3 is considered to be a fundamental pharmacological target for diseases related to the nervous and immune systems (Koeberle and Schlichter, 2010; Villalonga et al., 2010; Conforti, 2012).

Kv1.3 signaling relies on the number of channels at the cell surface. Unlike other leukocytic channels, such as Kv1.5, Kv1.3 is very dynamic and is highly expressed on the cell surface, similar to the neuronal Kv1.4 (Manganas and Trimmer, 2000; Vicente et al., 2008). Many studies address the specific signatures responsible for the intracellular retention and membrane targeting of ion channels (Misonou and Trimmer, 2004). C-terminal sequences are essential for the expression of functional Kv channels. Human diseases such as juvenile epilepsy, Jervell and Lange-Nielsen syndrome, Romano–Ward syndrome and episodic ataxia are associated with mutations in the C-terminus of Kv7.2, Kv7.1, Kv11.1 and Kv1.1, respectively (Curran et al., 1995; Neyroud et al., 1997; Biervert et al., 1998; Manganas et al., 2001a; Rea et al., 2002). Therefore, the molecular determinants responsible for the intracellular retention and surface expression of Kv channels are of considerable importance.

The surface expression is determined by the balance between ERR (endoplasmic reticulum retention) and FT (forward trafficking) signals (Misonou and Trimmer, 2004). RxR (x being any amino acid) signatures and similar highly positively charged motifs are very powerful ERR elements. In contrast, a VxxSL sequence is an efficient FT motif for the expression of Kv channels at the cell membrane (Misonou and Trimmer, 2004; Zhu et al., 2003). Analysis of Kv1.3 revealed that neither ERR nor FT canonical signatures are present in the protein. Therefore, the molecular determinants and the mechanisms responsible for Kv1.3 cell surface targeting remain largely unknown. Because deficient Kv1.3 expression has been associated with several autoimmune diseases and an irregular sensory physiology (Rivera et al., 2005; Nicolaou et al., 2007; Marks et al., 2009), the identification of these signatures is essential.

In the present study, we aimed to characterize the molecular determinants and cellular machinery responsible for Kv1.3 cell surface targeting. We have identified a Y^{479}MVIEE^{484} cluster at the C-terminus of the channel that was responsible for efficient Kv1.3 forward trafficking. This domain is highly conserved in neuronal isoforms of the Kv1 family. The di-acidic (E483/484) motif within the Y^{479}MVIEE^{484} cluster was the main determinant for Kv1.3 surface expression. This motif interacts with the coat

protein complex II (COPII) to trigger ER-to-Golgi anterograde transport to the plasma membrane. This study identifies a novel signal in Kv channels that contributes to our understanding of the mechanisms underlying ion channel trafficking and the ability of cells to fine-tune cellular responses.

Results

The C-terminal domain is necessary for effective Kv1.3 membrane surface targeting

The location of Kv1.3 has important consequences for cellular physiology (Panyi et al., 2004; Rivera et al., 2005). Unlike Kv1.5, Kv1.3 efficiently targets to membranes (Vicente et al., 2008). Kv1.3 was found to be at the plasma membrane (supplementary material Fig. S1A–C), whereas Kv1.5 was predominantly intracellular (supplementary material Fig. S1E–G). In addition, Kv1.3 currents were twofold higher than those of Kv1.5 under similar conditions (supplementary material Fig. S1D,H). This distribution is similar to that observed in other neuronal channels. Thus, Kv1.1 (supplementary material Fig. S2A–C) and Kv1.5 exhibited equivalent intracellular retention. In contrast, Kv1.4 (supplementary material Fig. S2D–F) and Kv1.3 exhibited analogous plasma membrane-associated patterns.

Several molecular determinants influence the localization of Kv1 channels in mammalian neurons. An ERR signature is present within the Kv1.1 pore, a FT motif (VxxSL) can be found at the C-terminus of Kv1.4. A P-loop sequence analysis (supplementary material Fig. S2G) indicates that neither Kv1.3 nor Kv1.5 contained the amino acids responsible for the intracellular retention of Kv1.1 (A352, E353, S369 and Y379) (Manganas et al., 2001b; Zhu et al., 2001). Furthermore, an analysis of C-termini demonstrated that the Kv1.4 FT signature (V^{619}KESL^{623}) was less functionally robust in Kv1.5 (L^{638}RRSL^{642}) and absent in Kv1.3 (supplementary material Fig. S2H) (Li et al., 2000; Zhu et al., 2003; Steele et al., 2007).

To identify the motifs involved in Kv1.3 trafficking, Kv1.3/Kv1.5 chimeras were generated. Fig. 1 shows that a Kv1.3 with the Kv1.5 N-terminal (Fig. 1E–H) targeted to the membrane in a similar way to the Kv1.3 wild-type channels (Fig. 1A–D). However, when the C-terminus of Kv1.3 was replaced by that of Kv1.5 (Fig. 1I–L), the channel was retained intracellularly in a pattern similar to the Kv1.5 wild-type channel (Fig. 1M–P). These results indicated that the C-terminus of Kv1.3 is responsible for targeting Kv1.3 to the membrane. The reciprocal chimeras did not exhibit greater Kv1.5 surface expression, suggesting that the Kv1.3 element is not sufficient for normal Kv1.5 membrane surface expression and that potent ERR signatures must exist in Kv1.5.

To further study whether the Kv1.3 C-terminus was sufficient to promote membrane targeting, we generated a Kv1.3 lacking the complete C-terminus (93 residues). Unlike Kv1.3 (supplementary material Fig. S3A,B), Kv1.3(F433X) mistargeted the membrane surface and evoked no K^+ currents (supplementary material Fig. S3C,D). In addition, whereas Kv1.3 was highly expressed at the membrane and colocalized with the Golgi apparatus (supplementary material Fig. S3E–G), Kv1.3(F433X) remained at the ER (supplementary material Fig. S3H–J). Therefore, the Kv1.3 C-terminus contains signals that are essential for the proper delivery of the channels to the cell surface.

A di-acidic signature is sufficient to promote Kv1.3 localization at the cell membrane

To identify the Kv1.3 C-terminal signature responsible for targeting, we generated step-wise truncated channel proteins. We generated Kv1.3 channels lacking the final 34 (F492X), 39

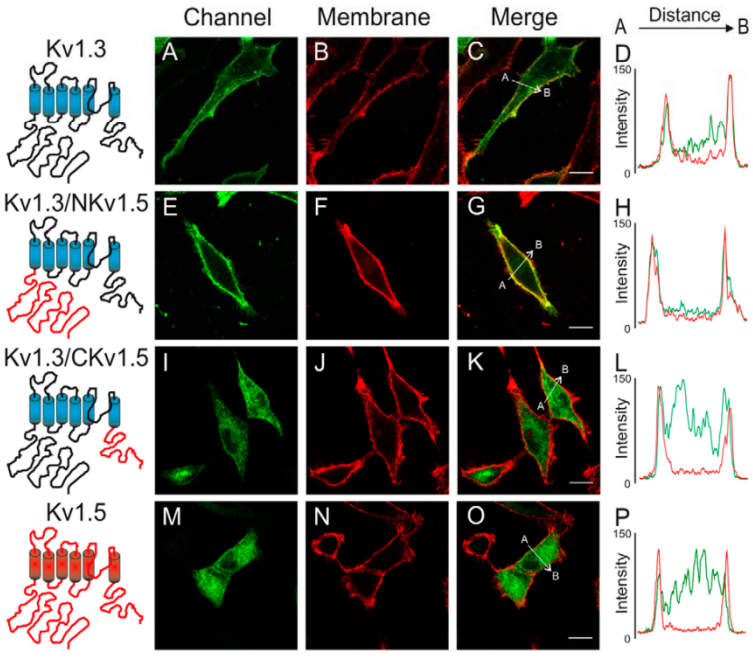

Fig. 1. The C-terminus of Kv1.5 impairs Kv1.3 membrane surface targeting. Confocal images demonstrate the distinct cellular distributions of the Kv1.3/Kv1.5 chimeras. Schematic diagrams of the channels are shown on the left. Kv1.3 is shown as blue transmembrane domains and black loops; Kv1.5 is shown as red transmembrane domains and red loops. (A–D) Kv1.3 is robustly expressed at the membrane surface. (A,E,I,M) Channel, (B,F,J,N) wheat germ agglutinin (WGA) staining of the plasma membrane, (C,G,K,O) merged image and (D,H,L,P) histogram showing the results of the pixel-by-pixel analysis of the section indicated by the arrow in the merged image. (E–H) Kv1.3/NKv1.5 colocalizes with WGA. (I–L) Kv1.3/CKv1.5 shows little colocalization with WGA. (M–P) Kv1.5 does not colocalize with WGA. Unlike A–H, little colocalization between the channels and WGA was observed in I–P. Although the Kv1.5 N-terminus did not mistarget the Kv1.3 channel to the surface, the C-terminal domain of Kv1.5 impaired the plasma membrane expression of Kv1.3. In all panels: green, channel; red, WGA; yellow, colocalization. Scale bars: 10 μm.

(M487X), 43 (E483X), 48 (E478X), 84 (E442X) and 93 (F433X, the entire C-terminus) residues (Fig. 2A). The progressive removal of residues from the Kv1.3 C-terminus yielded proteins that gradually decreased in size and that displayed altered glycosylation (Fig. 2B). Remarkably, the deletion of up to 39 residues at the far end of the C-terminus (wt, F492X and M487X) led to two major bands on western blots corresponding to mature glycosylated and immature non-glycosylated channels. The further removal of four or more amino acids (E483X, E478X, E442X and F433X) fully abolished channel glycosylation.

Fig. 2G,H shows that F492X and M487X were localized at the membrane. The distribution of M487X (Fig. 2I) was similar to that of the Kv1.3wt (see supplementary material Fig. S1A–D). In contrast, the deletion of four additional residues in the E483X channel severely impaired the surface expression (Fig. 2E,F). Kv1.3 mutants with further truncations (E478X and E442X) exhibited similar properties (Fig. 2C,D). Analysis of the Kv1.3 proteins and the membrane marker overlay revealed that less than 40% of the E483X channels were at the membrane. This membrane expression was similar to that observed for the Kv1.3 mutants with more severe truncations (Fig. 2J).

K^+ currents evoked by Kv1.3wt, F492X, E483X and F433X channels substantiated these observations (Fig. 2K,M). Although M487X currents were similar to those generated by Kv1.3wt, E483X currents were 85% lower than those evoked by the wt and M487F channels. Furthermore, E483X-evoked currents were similar to those obtained with F433X, which has no C-terminus (Fig. 2K,M). The *I–V* plots and similar half-activation voltages (26.1±1.8, 25.1±3.1, 32.2±0.7, 26.91±1.2 mV for Kv1.3, F433X, E483X and M487X, respectively) demonstrated that the deletion of the 43 amino acids at the C-terminus impaired Kv1.3 surface expression (Fig. 2L).

YxxΦ motifs (Φ being hydrophobic residues) are responsible in many proteins for endocytosis and/or transport in the early secretory pathway (Lai and Jan, 2006; Schwegmann-Wessels et al., 2004). Fig. 3A is a pictorial representation of the YMVIEE motif, which may be a FT signal for Kv1.3. Interestingly, although both the M487X and E483X mutants contain the YMVI motif, M487X targeted to the cell surface, whereas E483X remained intracellular. This suggests that the absence of E483/484 in the E483X mutant is crucial for channel trafficking. To further define the Kv1.3 FT signature, we performed an alanine-scanning mutagenesis analysis of the YMVIEE cluster. No single- or double-alanine mutants, with the exception of those with an altered di-acidic E483E484 signature, exhibited impaired channel–membrane colocalization (Fig. 3H). However, the E483E484 to A483/484 substitution triggered intracellular retention (Fig. 3B–D,H). Intriguingly, a variety of mutations from VIEE to AAAA partially restored membrane expression (Fig. 3H). Because di-isoleucin motifs increase the intracellular retention, we generated a hydrophobic cluster by changing E483E484 to I483/484. The YMVIII mutation had severe consequences, and channels remained mostly intracellular, with the membrane colocalization 80% lower than that of Kv1.3wt (Fig. 3E–H). Although the YxxΦ was preserved in Kv1.3(YMVIAA) and Kv1.3(YMVIII) no apparent colocalization with EEA1 (early endosome-associated protein 1) was found (not shown).

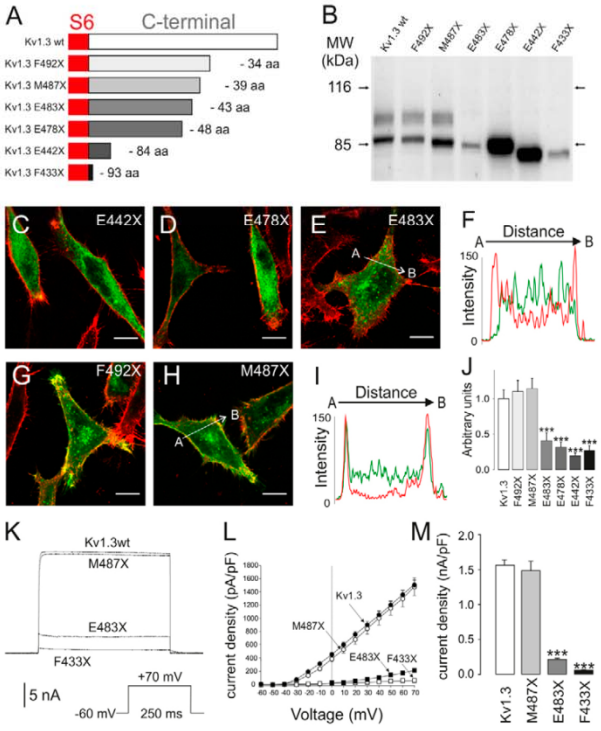

Fig. 2. Sequential Kv1.3 C-terminal domain truncation experiments reveal an important signaling element for membrane targeting and protein maturation. Kv1.3–YFP C-terminal truncations reveal an amino acid motif between M487 and E483 that participates in the anterograde transport, maturation and surface expression of Kv1.3. This motif has an important influence on cellular excitability. (A) A schematic diagram of the Kv1.3 C-terminal truncations. Red shows the position of the S6 transmembrane domain; the gradation from white to black represents the steady loss of residues. (B) Western blot analysis demonstrating that the progressive removal of amino acids reduces protein size and maturation. (C–E,G,H) Confocal images demonstrate that the sequential removal of residues split the channels into two categories. E442X (C), E478X (D) and E483X (C) are retained intracellularly in a pattern similar to F433X, which lacks the entire C-terminal domain, whereas, similar to Kv1.3wt, F492X (G) and M487X (H), which lack 34 and 39 aa, respectively, are targeted to the plasma membrane. (F,I) Histograms of the pixel-by-pixel analysis of the section indicated by the arrow in E (E483X) and H (M487X). Color code: green in all panels, channel; red, membrane; colocalization in yellow. Scale bars: 10 μm. (J) Membrane surface expressions of the truncated mutants. Pixel-by-pixel intensities from the confocal images were analyzed using ImageJ software. They were then compared with the relative intensity of the Kv1.3wt channel at the plasma membrane using a WGA overlay. Values are the means ± s.e.m. of at least 20 cells. (K–M) Sequential removal of residues from the Kv1.3 C-terminus severely impairs K^+ currents. (K) Representative traces. (L) Current–voltage dependence (pA/pF) of truncated mutants. (M) Current density (nA/pF). The cells were held at −60 mV, and currents were elicited by a single depolarizing pulse of 250 msecond duration to +70 mV (K and M) or similar depolarizing pulses in 10 mV steps (L). Values are the means ± s.e.m. of at least 10 cells. ***P<0.001 versus Kv1.3wt (Student's t-test).

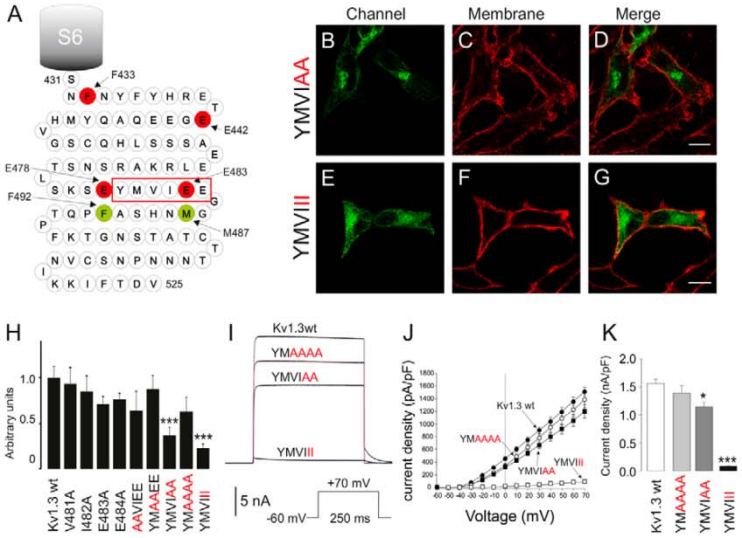

Fig. 3. Site-directed mutagenesis studies on the Y^{479}MVIEE^{484} motif. (A) Schematic diagram of the Kv1.3 C-terminal domain. The residues in green did not confer any harmful stops. In contrast, the amino acids in red conferred severe truncations. The S6 transmembrane domain is represented as a gray barrel. The YMVIEE cluster is indicated by the red box. (B–D) Confocal images demonstrating an impaired surface expression conferred by the substitution of E483/484 to Ala (YMVIAA). (E–G) Changes to I483/484 (YMVIII) almost abolished membrane targeting. Green, channel; red, WGA; merge, colocalization in yellow. Scale bars: 10 μm. (H) Membrane surface expression of mutated channels. Pixel-by-pixel intensities from the confocal images were analyzed using ImageJ software. Next, the results were compared with the relative intensity of the Kv1.3–YFP wt at the plasma membrane using a WGA overlay. Values are the means ± s.e.m. of at least 20 cells. Although ~50% of the YMVIAA mutant channels were expressed at the plasma membrane, YMVIII inhibited more than 70% of the surface expression. (I,J) Ala-scanning mutagenesis and Ile replacement of Glu at the YMVIEE motif impair K^+ currents. (I) Representative traces. (J) Current–voltage dependence (pA/pF) of mutants. (K) Current density (nA/pF). The cells were held at −60 mV, and currents were elicited by a single depolarizing pulse of 250 msecond duration to +70 mV (I,K) or similar depolarizing pulses in 10 mV steps (J). Values are the means ± s.e.m. of at least 10 cells. *P<0.05, ***P<0.001 versus Kv1.3wt (Student's t-test). Mutations are indicated in red.

As expected, E483/484 mutations generated reduced K^+ currents (Fig. 3I,K). The I–V plots and similar half-activation voltages (26.1±1.8, 24.2.±2.2, 28.8±2.3, 32.0±0.4 mV for Kv1.3, YMVAAAA, YMVIAA and YMVIII, respectively) demonstrated that the di-acidic E483/484 within the YMVIEE cluster at the C-terminus of Kv1.3 is a previously unrecognized FT signal that is responsible for channel trafficking to the cell surface.

Because Kv1.3 is important in sensory neurons (Rivera et al., 2005; Cavallin et al., 2010; Gazula et al., 2010) and leukocyte physiology (Vicente et al., 2003; Cahalan and Chandy, 2009) we analyzed the di-acidic E483/484 in neurons and lymphocytes. Rat embryo hippocampal neurons and Jurkat T-lymphocytes were transfected with Kv1.3wt and Kv1.3(I483/484). Whereas Kv1.3wt targeted to membranes and axons in neurons (Fig. 4A–C), Kv1.3 (I483/484) missed the axonal targeting and remained intracellular (Fig. 4D–F). Similarly, Kv1.3(I483/484) impaired the membrane surface expression in human T-lymphocytes (Fig. 4G,H). These observations further support that the E483/484 motif is essential for the delivery of the channels to the cell surface in neurons and lymphocytes.

Di-acidic signatures are present in neuronal Kv1 and Shaker channels

Is the YMVIEE motif conserved within the Kv1 and Shaker channels? We constructed a phylogenetic tree by comparing their C-terminal domains. Supplementary material Fig. S4 demonstrates that Kv1.1, Kv1.2 and Kv1.3 (neuronal channels) were in close proximity. Then, the distances enlarged (Kv1.5<Kv1.4=Kv1.6<Shaker=Kv1.7<Kv1.8). The proximity between Kv1.7 and Shaker channels is supported by Kv1.7 members from lizard (*Anolis carolinensis*) and a primitive coelacanth fish (*Latimeria chalumnae*) included in the Shaker cluster. Curiously, fish Kv1.7 members (*Tetraodon nigroviridis, Gasterosteus aculeatus* and *Takifugu rubripes*) are within the Kv1.8 cluster. Our data showed that most neuronal channels shared structural domains at the C-terminus (supplementary material Table S1). Therefore, we searched for YMVIEE motifs in Kv1 and Shaker subfamilies (Swiss-Prot, http://www.uniprot.org/). Similar YMVIEE signatures were present in neuronal Kv1.1 (YMEIEE), Kv1.2 (YMEIQE) and Kv1.4 (YLEMEE) (supplementary material Fig. S4B–E). Shakers exhibit a structurally homologous MDLDD consensus (supplementary material Fig. S4F). Notably, Kv1.5, a cardiac close relative of Kv1.1–Kv1.3, does not have the cluster, suggesting that this motif is restricted to neuronal Kv1 (supplementary material Table S1).

We analyzed Shaker and Kv1.1 channels to evaluate whether the di-acidic signature represents a general FT motif. Although Shaker wt (D532/533) partially targeted to the membrane (Fig. 5A–D), the mutant I532/533 showed a 60% reduction in membrane surface colocalization (Fig. 5E–H). Concomitantly, the Shaker mutant I532/533 exhibited K^+ currents 50% lower

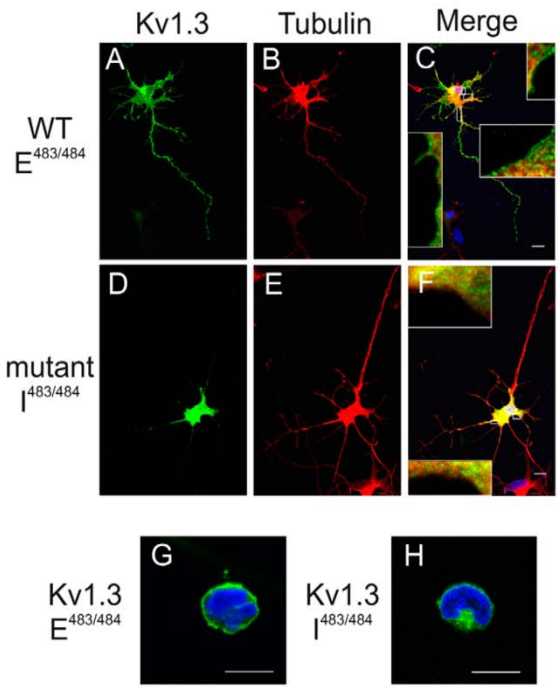

Fig. 4. The di-acidic E483/484 motif is important for axonal targeting and lymphocyte membrane surface expression. Hippocampal neurons from E17 rat embryos and Jurkat T-cells were cultured and transfected with Kv1.3wt (E483/484) and Kv1.3 mutant (E483/484I). (A–C) Kv1.3 wt targeted to axons. (A) Kv1.3 E483/484. (B) Neuron-specific class III-tubulin staining. (C) Merged image. (D–F) Kv1.3 (I483/484) mistargeted neuronal axons. (D) Kv1.3 mutant (I483/484). (E) Neuron-specific class III-tubulin. (F) merged image. Insets show enlarged views of the boxed regions. Scale bars: 10 µm. (G,H) The Kv1.3 mutant (I483/484) did not reach any membrane surface in human Jurkat T-lymphocytes. (G) Jurkat cell expressing Kv1.3 (E483/484). (H) Jurkat cell expressing Kv1.3 (I483/484). Scale bars: 5 µm. DAPI staining (in blue) was performed to highlight nuclei.

than Shaker wt (not shown). However, a P506 in the Kv1.4 pore, absent in Kv1.1 (A352), acts as a membrane surface expression motif (Manganas et al., 2001b). Unlike Kv1.4 (see supplementary material Fig. S2), Kv1.1 was intracellularly retained (Fig. 5I–L). However, the Kv1.1(A352P) mutation triggered a twofold increase in plasma membrane expression (Fig. 5M–P). Noteworthy, the additional mutation of the di-acidic motif in the A352P mutant (A352P/$E^{458/459}$I) increased the channel retention by 50% (Fig. 5O–Q) and prevented the plasma membrane expression. In this vein, although the Kv1.2 channel also distributes intracellularly (Manganas and Trimmer, 2000), when we replaced the YMEIQE motif of Kv1.2 with YMVIEE, the Kv1.2(YMVIEE) mutant membrane targeting rose twofold (not shown). Collectively, these findings indicate that the newly identified di-acidic signature is a FT motif in mammalian neuronal Kv1.1, Kv1.2 and Shaker channels.

COPII-dependent mechanism of Kv1.3 anterograde transport

The secretory pathway of ion channels is uncertain. Whereas CFTR and hERG channels use COPII-coated vesicles to exit the ER, Kv4.2 exits independently of COPII (Wang et al., 2004; Hasdemir et al., 2005; Delisle et al., 2009). We, therefore, questioned whether COPII was involved in Kv1.3 anterograde transport.

COPII vesicles include Sec23/Sec24 and Sec13/Sec31 heterodimers and Sar1 (Zanetti et al., 2012). Transfected Kv1.3wt cells were treated with brefeldin A for 24 hours, which resulted in Kv1.3 ER retention (Fig. 6A–F). Furthermore, inhibiting Sec13 recruitment by H89 increased Kv1.3 intracellular retention (Fig. 6G,H). The role of COPII was further supported by using the Sar1(H79G), which is a GTP-locked mutant that is a dominant negative and prevents the forward delivery of cargo proteins to the Golgi (Ward et al., 2001). Sar1(H79G) and Kv1.3 colocalized intracellularly (Fig. 6I–K) and were retained at the ER (Fig. 6L–O). Therefore, a COPII-dependent mechanism mediated the delivery of Kv1.3 to the cell surface.

We next analyzed association between COPII and the FT signature of the Kv1.3 C-terminus. Kv1.3wt showed little colocalization with Sec24D in cells co-transfected with both proteins (Fig. 7A–C). Similarly, the Kv1.3(E483X) mutant showed almost no colocalization with endogenous COPII vesicles (Fig. 7H–J). However, Sar1(H79G) triggered a notable Kv1.3-Sec24D-Sar1(H79G) intracellular colocalization (Fig. 7D–G). Furthermore, the presence of Sar1(H79G) increased the amount of Kv1.3 co-immunoprecipitated with Sec24D only when the Kv1.3 C-terminus was not disrupted (Fig. 7H). Sec24D did not significantly associate with E483X in the presence of Sar1(H79G), as revealed by the absence of Förster resonance energy transfer (FRET). However, Sar1(H79G) expression triggered FRET between Kv1.3wt and Sec24D. Therefore, alterations of the di-acidic E483/484 motif impairs molecular interactions between the channel and Sec24D (Fig. 7I).

To further understand the Kv1.3–Sec24 interaction at the molecular level, we used molecular modeling techniques. The transmembrane domain and the majority of the Kv1.3 N-terminus were homology modeled by using the Kv1.2 channel (PDB code 2R9R). The C-terminal domain shared significant similarity (~58%) with the nucleotide-binding domain of the reticulocyte-binding protein Py235 (3HGF) and the zinc-binding domain from neural zinc finger factor-1 (1PXE). Therefore, we used these proteins for building a molecular model of the Kv1.3 C-terminal region. The i-Tasser online server estimated a normalized Z-score of 0.92. Supplementary material Fig. S5A–C shows the side, top and bottom views of the full-length Kv1.3 model. In all three views, the YMVIEE cluster (depicted in red) in the C-terminus was accessible for protein–protein interactions. Fig. 8A–D shows a detailed view of the Kv1.3 C-terminal domain. The YMVIEE motif is a surface-exposed loop between two short alpha helices (Fig. 8A,B). Remarkably, the location of the E483/484 sequence suggested that this signature could easily establish saline bonds (Fig. 8B) with proteins such as Sec24. We next analyzed the docking of the Sec24a protein (PDB code 3EGD) to the Kv1.3 C-terminus in the model (Fig. 8C–E). Notably, Sec24a binds to vesicular stomatitis virus glycoprotein (VSVG). VSVG contains a characteristic YTDIEM cluster that is similar to the YMVIEE motif in Kv1.3. The main difference is that instead of the DxE signature in VSVG there is a VxE sequence in Kv1.3. Thus, the Asp is replaced by a hydrophobic residue. This change does not impact the interactions that are possible with either protein. As depicted in the model, I482 in Kv1.3 interacts with L498, L808 and V748 in Sec24a. In contrast, E483 in Kv1.3 establishes saline

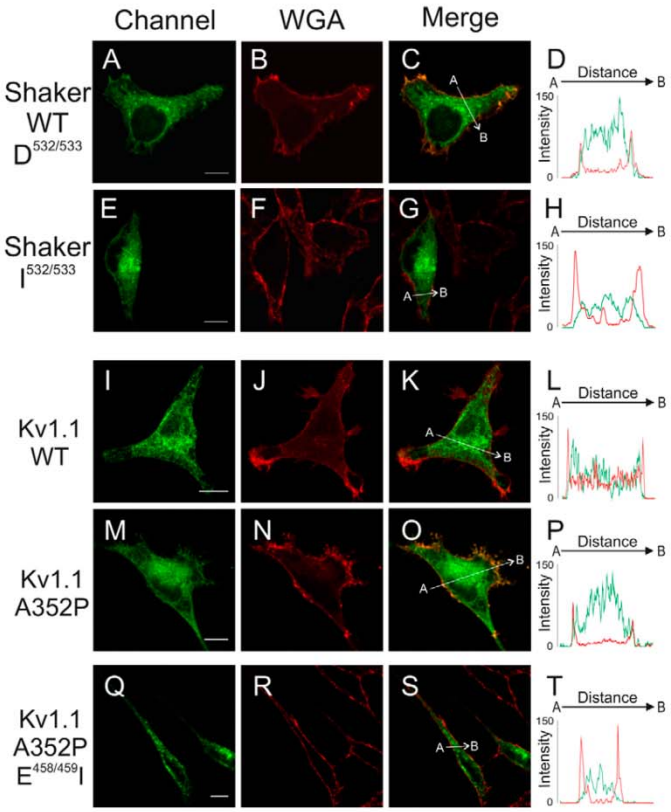

Fig. 5. Analysis of di-acidic elements in Shaker and Kv1.1 channels. (A–H) Shaker H4 wt D532/533 was mutated to I532/533 and membrane surface expression studied. (A–D) Shaker wt (D532/533) partially targeted to plasma membrane. (E–H) The I532/533 mutation impaired Shaker plasma membrane expression by 60% (*P<0.05 versus wt, Student's t-test). (I–T) The di-acidic E458/459 motif contributed to the Kv1.1 surface expression. (I–L) Kv1.1 wt was retained intracellularly. (M–P) Kv1.1(A352P) increased plasma membrane localization (**P<0.01 versus Kv1.1wt, Student's t-test). (Q–T) the triple mutant Kv1.1(A352P, E458/459I) restored the intracellular retention back to that of Kv1.1 wt (**P<0.01 versus A352P, Student's t-test). (D,H,L,P,T) Channel and WGA histograms. Pixel-by-pixel intensities from the confocal images were analyzed using ImageJ software. They were then compared with the relative intensity of the wt channels at the plasma membrane using the WGA overlay. Color code: green in all panels, channel; red, membrane WGA; yellow, colocalization in merged panels. Scale bars: 10 µm.

bonds with R752 and Y437 in Sec24a (Fig. 8D). The complex is further stabilized by the interactions of V497 and E484 in Kv1.3 with L773 and R750 in Sec24a, respectively (Fig. 8D). Note that the DxE signature that is responsible for Sec24a binding is replaced by the di-acidic E483/484 motif in the Kv1.3 C-terminus. Supporting this idea, I483/484 mutations in the di-acidic motif (YMVIII) fully disrupted the formation of saline bonds and prevented the binding of Sec24a to Kv1.3 (Fig. 8E). However, additional conformational changes should not be discounted.

Discussion

Kv1.3-mediated signaling is determined by the channel abundance at the cell surface. Thus, appropriate cellular trafficking and localization are crucial for the physiological roles of the Kv1.3 channels in sensory neurons and leukocytes. Alterations in these patterns are associated with autoimmune diseases and irregular axonal targeting (Rivera et al., 2005; Nicolaou et al., 2007; Steele et al., 2007; Tóth et al., 2009). Cumulative evidence suggests that the C-terminus of Kv channels plays crucial roles in their functionality as it contains domains implicated in protein trafficking to the cell surface, as well as ER retention (Curran et al., 1995; Neyroud et al., 1997; Biervert et al., 1998; Manganas et al., 2001a; Rea et al., 2002). Therefore, uncovering these signals is pivotal for understanding the molecular mechanisms underlying channel trafficking and surface expression in physiological and pathophysiological conditions. Furthermore, this knowledge is fundamental for the development of therapeutic approaches to treat human diseases caused by dysfunctional channel expression.

The most salient contribution of this study is the identification of the Y^{479}MVIEE^{484} motif as a molecular determinant of the anterograde transport and membrane targeting of Kv1.3 channels. In particular, the di-acidic E483/484 signature within this motif is crucial for forward channel trafficking, as evidenced by the loss of channel transport to the cell surface upon its deletion or mutation. Analysis of the underlying mechanism involved in trafficking reveals that Kv1.3 traffics to the cell surface by a COPII-dependent pathway through interaction with Sec24. In fact, Kv1.3 traffics efficiently through the Golgi apparatus en route to the cell surface (Vicente et al., 2008). A molecular model of the Kv1.3–Sec24 complex suggests salt bridges between the E483/484 di-acidic signature at the Y^{479}MVIEE^{484} motif of the channel and a di-basic R750/752 signature in Sec24. Taken together, these findings unveil a novel trafficking signal in the Kv1.3 C-terminus that appears to underlie the high expression of this channel in the plasma membrane.

Notably, this mechanism appears conserved because this signature is also present in neuronal Kv1 and Shaker subfamilies. However, unlike Kv1.3, the presence of this di-acidic motif in neuronal Kv1 channels does not suffice to efficiently trigger their surface expression as these channels display a significant ER location. This lower trafficking efficiency in Kv1.1 and Shaker, as compared with Kv1.3, arises

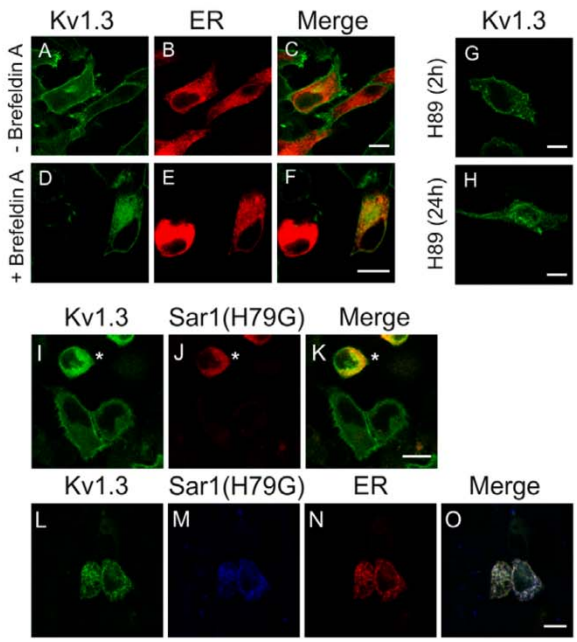

Fig. 6. Interfering with the COPII machinery impairs Kv1.3 trafficking and membrane surface targeting. (A–F) HEK-293 cells transiently transfected with Kv1.3-YFP and pDsRed-ER were treated in the absence (−) or the presence (+) of 10 µg/ml brefeldrin A. (A–C) Kv1.3 did not colocalize with ER. (D–F) The presence of brefeldrin A triggered protein retention in the ER. Green, Kv1.3; red, pDsRed–ER; merge, yellow colocalization in merged panels. (G,H) The presence of 100 µg/ml H89 for 2 hours did not modify Kv1.3 membrane expression, but treatment for 24 hours resulted in the intracellular retention of the channel. (I–O) Expression of the constitutively active Sar1(H79G) dominant-negative GTPase also triggers the retention of Kv1.3 in the ER. (I–K) Kv1.3 and Sar1(H79G) colocalize. (I) Kv1.3 in green, (J) Sar1(H79G) in red, (K) colocalization in yellow. Note that the top cell marked with an asterisk co-expresses both proteins. The bottom cells, which do not express Sar1(H79G), target the Kv1.3 channels to the membrane. (L–O) The presence of Sar1(H79G) confines Kv1.3 at the ER. (L) Kv1.3 in green, (M) Sar1(H79G) in blue, (N) pDsRed–ER in red, (O) merged image, with white indicating triple colocalization. Scale bars: 10 µm.

most probably from a balance between this FT element and ERR motifs coexisting in their structures. Indeed, positive and negative FT elements have been characterized in several Kv1 channels. Whereas the A352 residue within the Kv1.1 pore inhibits trafficking (Manganas et al., 2001b; Zhu et al., 2001), an equivalent P505 in Kv1.4 favors surface expression (Li et al., 2000; Manganas et al., 2001b; Zhu et al., 2001). The A352P substitution in Kv1.1 causes enhanced currents and surface expression compared with wild-type Kv1.1 (Manganas et al., 2001b). However, these elements are not sufficient for the targeting of Kv1.4 to the cell membrane. In fact, the surface expression of Kv1.4(YLEMII) mutant did not apparently change (not shown). Therefore, the Kv1.4 requires the crucial contribution of the VxxSL signature in the channel C-terminus (Li et al., 2000; Zhu et al., 2003). This FT motif is absent in Kv1.3. Kv1.3 contains several dibasic ERR elements, including RxR ($R^{86}MR^{88}$, $R^{101}NR^{103}$ and $R^{118}IR^{120}$) in the N-terminus, KKxx ($K^{519}KIF^{522}$) in the C-terminus, and P^{374} in the P-loop. However, mutation or deletion of these putative signals gave rise to inconclusive results and our data indicated that the Kv1.3 C-terminus must contain new and potent molecular FT determinants that act as signals for anterograde transport. This tenet was supported by the findings that Kv1.3(F433X) and the Kv1.3/Kv1.5 C-terminal chimera were not trafficked to the cell surface, suggesting that there are no FT sequences in the N-terminus or that inhibitory elements, such as the previously mentioned dibasic residues in this domain, act as dominant signals in the absence of the Kv1.3 C-terminus. Thus, the channel abundance at the cell surface is determined by the balance and strength of FT and ERR signals present in intracellular domains of the channels (Misonou and Trimmer, 2004).

A question that emerges is how this newly identified atypical di-acidic trafficking motif interacts with Sec24 to drive channel export from the ER to the plasma membrane. To address this question we modeled the complex formed by the Kv1.3 C-terminus and Sec24. In the absence of an atomic structure for the C-terminus of Kv1.3, we created a model that fulfilled all the structure–function available information and that was compatible with the reported density map at 23 Å-resolution of the Shaker channel (Sokolova et al., 2001; Sokolova et al., 2003). Thereafter, this model was docked into the atomic structure of the Sec24 protein, and energy minimized to have a picture of the complex. Although models have to be interpreted with caution, they represent very useful and testable tools for understanding molecular events. The proposed molecular model of the Kv1.3 channel suggests that its C-terminal domain can accommodate the four consecutive short alpha helices holding a water-exposed loop containing the YMVIEE motif, which is involved in Sec24 binding. Furthermore, the model highlights that the di-acidic motif forms salt bridges with two basic amino acids in the Sec24 protein and the hydrophobic residues contribute to stabilize the interaction of the complex. Notably, it has been reported that three consecutive hydrophobic residues ($V^{569}MI^{571}$) at the C-terminus of the GABA-1 transporter are responsible for exporting the protein from the endoplasmic reticulum–Golgi intermediate compartment (ERGC) (Farhan et al., 2008). Mutations in this motif are predicted to disrupt or destabilize the protein complex inhibiting COPII assembly and channel trafficking. Thus, the $Y^{479}MVI^{482}$ motif in Kv1.3 is also a hydrophobic domain that may play a similar role. In addition, the E483/484 di-acidic signature following this motif probably compensates for the absence of a canonical DxE and stabilizes the protein–protein interactions of Kv1.3 with its interacting partners, such as Sec24. In support of this tenet, clusters of acidic residues (e.g. ELETEEEE or EEEEDSE) act as post-Golgi surface-promoting signals in Kir channels without an obvious consensus sequence (Ma et al., 2002).

The identification of the molecular determinants responsible for normal channel function is essential for understanding their roles in health and disease. For example, in cystic fibrosis (CF) the CF transmembrane conductance regulator (CFTR) F508 mutant is misprocessed and intracellularly retained (Kartner et al., 1992). The forward trafficking of CFTR from the ER to the Golgi apparatus is dependent on COPII coat assembly in mammalian cells (Wang et al., 2004; Tsigelny et al., 2005). COPII proteins mediate the anterograde transport of cargo proteins to the cell membrane through the recognition of certain di-leucine and di-acidic motifs (Zanetti et al., 2012). For instance, the transport of the CFTR channel to the plasma membrane depends on a DxD

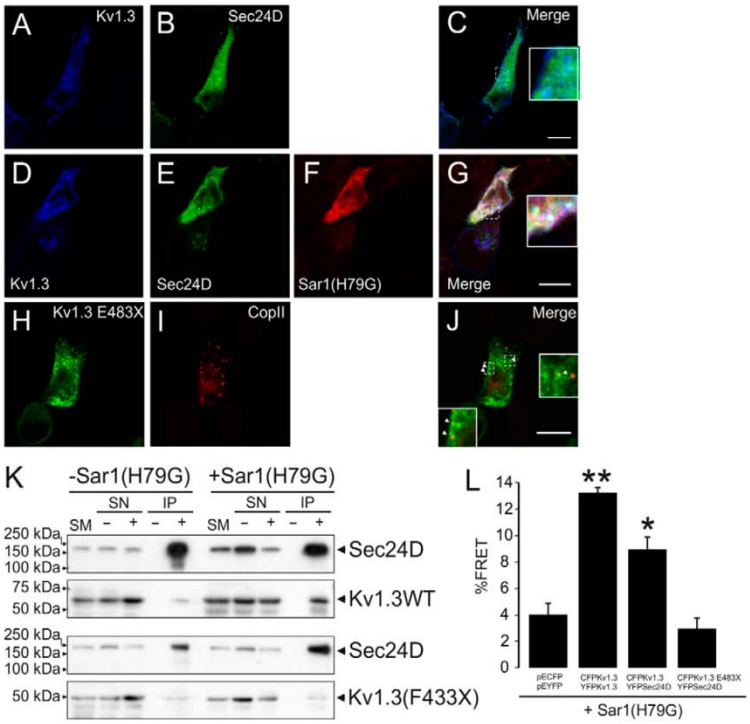

Fig. 7. Kv1.3 colocalizes with Sec24D in the presence of Sar1(H79G) and interacts with COPII as long as the di-acidic E483/484 motif is intact. (A–C) Kv1.3–CFP and Sec24D–YFP showed limited colocalization. (D–G) The presence of Sar1(H79G) triggered Kv1.3 ER-retention and colocalization with Sec24D. (A,D) Kv1.3, (B,E) Sec24D, (F) Sar1(H79G), (C,G) merged images. White indicates triple colocalization. (H–J) Kv1.3-YFP(E483X), which lacks the di-acidic E483/484 motif, barely colocalizes with endogenous COPII. (H) Kv1.3(E483X), (I) COPII, (J) merged image. Insets, Enlarged views of COPII vesicles marked with the arrowheads. Scale bars: 10 µm. (K,L) Kv1.3 interacts with COPII via the C-terminal domain. (K) HEK cells were transiently transfected with Kv1.3-HA, Kv1.3(F433X)-HA and Sec24D-YFP in the presence (+) or the absence (−) of Sar1(H79G). Cell extracts were immunoprecipitated against YFP (Sec24D). Filters were blotted against HA (Kv1.3) and YFP (Sec24D). Sar1(H79G) expression notably increases the abundance of Kv1.3wt, but not Kv1.3(F433X), which co-immunoprecipitated with Sec24D–YFP. SM, starting material; SN, supernatant; IP, immunoprecipitate; +, presence of anti-GFP antibody; −, absence of anti-GFP antibody. (L) FRET experiments demonstrating the molecular interactions between Kv1.3–CFP and Sec24D–YFP in the presence of Sar1(H79G). Histogram shows the FRET efficiency of different combinations. Negative controls, cells expressing CFP and YFP; positive controls, cells expressing Kv1.3–CFP and Kv1.3–YFP. The E483X–CFP mutant shows no FRET with Sec24D–YFP indicating that no physical interactions take place in the absence of the E483/484 motif. *P<0.05; **P<0.01 versus CFP or YFP (n=10, Student's t-test).

signature in the C-terminus of the protein (Wang et al., 2004). This DxD signature and other neighboring residues accelerate ER export. These signals have also been identified in the vesicular stomatitis virus glycoprotein (VSVG) (Nishimura and Balch, 1997). The YTDIEM motif present in the VSVG is similar to that in the CFTR channel (YKDAD) (Sevier et al., 2000; Wang et al., 2004). Similarly, a congenital hyperinsulinism disease is caused by the E282K mutation of a DxE trafficking motif in the inward rectifying potassium channel Kir6.2 (Sivaprasadarao et al., 2007). This mutation disrupts a DxE motif and prevents the channel from assembling into COPII through complexing with Sec24. Lack of formation of this complex results in the retention of the protein in the ER and in a decrease in the number of Kir6.2 channels at the cell surface, which accounts for the disease phenotype (Sivaprasadarao et al., 2007; Taneja et al., 2009).

In summary, we reported the identification of a previously unrecognized FT protein motif (YMVIEE) in the C-terminus of Kv1.3, which is highly homologous in most neuronal Kv1 and Shaker subfamilies. This domain is essential for COPII-mediated anterograde transport and the expression of the channel into the plasma membrane. Accordingly, alteration of the integrity of this novel molecular determinant of Kv1.3 trafficking gives rise to impaired channel expression, which may give rise to disease. The functioning of ion channels depends on both the activity control and the regulation of their abundance at the cell surface. Therefore, our data will help to understand pathologies associated to Kv1.3 such as autoimmune diseases, sensory neuron physiology, insulin resistance, obesity, hypertension and cancer. Thus, identifying the molecular determinants of Kv1.3 channel trafficking are of considerable interest and can aid to our understanding of channel function under physiological and pathological conditions. Furthermore, our findings point to Kv1.3 trafficking as a pharmacological target for drug development.

Materials and Methods

Expression plasmids and site-directed mutagenesis

Rat Kv1.3 in pRcCMV was provided by T.C. Holmes (New York University, NY). Rat Kv1.1 and Kv1.4 in pGEM7 and human Kv1.5 in pBK constructs were from M. M. Tamkun (Colorado State University, CO). Channels were subcloned into

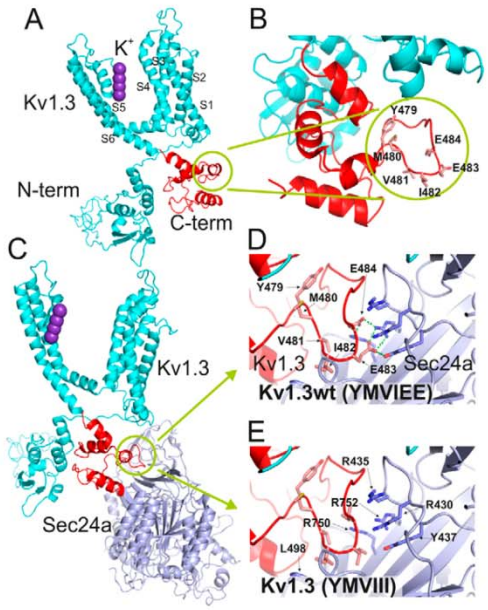

Fig. 8. Molecular dynamics simulation of the Kv1.3 C-terminal domain. (A–C) Molecular model of the Kv1.3 C-terminal domain. (A) A model of one Kv1.3 monomer is shown to highlight the surface-exposed loop structure. S1–S6 transmembrane domains (in cyan) and K^+ ions (in purple) are depicted for reference. The condensed C-terminal domain (in red), which contains four short alpha helices, is located on the side of the N-terminus (in cyan). (B) A detailed view of the surface-exposed YMVIEE loop structure. (C) Molecular recognition of the Kv1.3 C-terminus and the Sec24a subunits of COPII. The YMVIEE loop structure is circled in green. (D,E) Two views of the Kv1.3 C-terminus bound to Sec24d. Docking simulation identified potential sites of interaction between Sec24a and the YMVIEE motif of Kv1.3. Saline and hydrogen bonds are formed between E483/484 in Kv1.3 and R752, R750 and Y437 in Sec24a. These bonds are depicted by the green dashed lines. (D) YMVIEE in the Kv1.3 wt channels. (E) YMVIII in the Kv1.3 mutant channel illustrates the absence of interactions.

pEYFP-C1 and pECFP-C1 (Clontech). Constructs were verified by sequencing. The rKv1.3, externally tagged with HA between S3 and S4, was from D. B. Arnold (University of Southern California, CA). The pEYFP-Sec24D and the HA-Sar1(H79G) were from T. H. Ward (The London School of Hygiene and Tropical Medicine, UK) and R. Pepperkok (EMBL, Heidelberg, Germany), respectively. All Kv1.3 mutants and Kv1.3/Kv1.5 chimeras were generated in the pEYFP-Kv1.3, Kv1.3HA and pEYFP-Kv1.5 channels. Golgi (pECFP–Golgi) and ER (pDsRed–ER) markers were from Clontech. The Shaker H4 channel in pQBI25-fC3 was used for this study. All Shaker constructs, including the one referred to as 'wild type', contained a deletion of residues 6–46 to remove fast inactivation (Hoshi et al., 1990).

Kv1.3–Kv1.5 chimeras were generated by inserting *Bgl*II and *Eco*RI sites in the N- and C-terminal domains of the channels, respectively. Select restriction sites, truncations and single and multiple Kv1.1, Kv1.3 and Shaker mutants were generated using the QuikChange and QuikChange multi-site-directed mutagenesis kits (Stratagene). All mutations were verified using automated DNA sequencing.

Cell culture and transient transfections

HEK-293 cells were grown in DMEM containing 10% FBS and 100 U/ml penicillin and streptomycin. For the confocal analyses, cells cultured in the same medium were plated on poly-lysine-coated coverslips. Transient transfection was performed using MetafecteneTM Pro (Biontex) at nearly 80% confluency. Jurkat T-lymphocytes were cultured in RPMI culture medium, containing 10% FBS and supplemented with 10 U/ml penicillin and streptomycin and 2 mM L-glutamine. Transient transfection was performed by electroporation (Bio-Rad). Twenty-four hours after transfection, cells were washed in phosphate-buffered saline (PBS; without K^+), fixed with 4% paraformaldehyde in PBS for 10 minutes and mounted with Aqua Poly/Mount (Polysciences). In some experiments, Kv1.3-transfected cells were treated with 10 μg/ml brefeldin A (an inhibitor of a GTP–GDP exchange enzyme that impairs the release of ADP-ribosylating factor and COPII from the Golgi apparatus) and 100 μg/ml H89 (a selective protein kinase A inhibitor that prevents the recruitment of COPII to the ER export sites through Sec13-mediated mechanisms).

Dissociated and explant cultures of neurons

The hippocampus of E17 rat embryos was dissected out to obtain primary neuronal cultures. All animal experiments were performed according to approved guidelines. After trypsin–EDTA (0.05% trypsin, 0.53 mM EDTA, 12 minutes; Invitrogen) and DNase1 (100 U/ml, 10 minutes; Roche Diagnostics) treatments, tissue was dissociated by gentle stirring. 50,000 cells were cultured for 3 days onto poly-L-lysine-coated dishes in neurobasal medium containing L-glutamine, penicillin and streptomycin and B27 supplement (Invitrogen). Thirty-six hours after plating, neurons were transfected with pEYFP-Kv1.3 or pEYFP-Kv1.3YMVIII using Lipofectamine 2000 (Invitrogen). Hippocampal neurons were immunostained with an antibody against neuron-specific class III β-tubulin (clone TUJ-1; 1:4000; Sigma), followed by Alexa Fluor 568 secondary antibody (1:500; Molecular Probes) were processed as above.

Protein extraction, co-immunoprecipitation and western blot analysis

Cells, washed in cold PBS, were lysed on ice with NHG solution (1% Triton X-100, 10% glycerol, 50 mmol/l HEPES pH 7.2, 150 mmol/l NaCl) supplemented with 1 μg/ml aprotinin, 1 μg/ml leupeptin, 1 μg/ml pepstatin and 1 mM phenylmethylsulfonyl fluoride to inhibit proteases. Homogenates were centrifuged at 16,000 ***g*** for 15 minutes, and the protein content was measured using the Bio-Rad Protein Assay.

The samples were precleared with 30 μl of protein-G–Sepharose beads for 2 hours at 4℃ with gentle mixing as part of the co-immunoprecipitation procedures. The beads were then removed by centrifugation at 1000 ***g*** for 30 seconds at 4℃. Samples were incubated overnight with the desired antibody (4 ng/μg protein) at 4℃ with gentle agitation. Thirty microliters of protein-G–Sepharose were then added to each sample and they were incubated for 4 hours at 4℃. The beads were removed by centrifugation at 1000 ***g*** for 30 seconds at 4℃, washed four times in NHG, and resuspended in 80 μl SDS sample buffer.

Protein samples (50 μg) and immunoprecipitates were boiled in Laemmli SDS loading buffer and separated by 10% SDS-PAGE. Next, the samples were transferred to nitrocellulose membranes (Immobilon-P, Millipore) and blocked in 5% dry milk supplemented with 0.05% Tween 20 in PBS before the immunoreaction. The filters were then immunoblotted with antibodies against HA (1/200, Sigma) and GFP (1/1000, Roche).

Confocal microscopy and FRET

Staining with wheat germ agglutinin (WGA–Texas Red®; Invitrogen) to label the plasma membrane was performed under non-permeabilized conditions. Cells were washed with PBS and stained for 30 minutes at 4℃. Next, cells were washed and fixed with 4% paraformaldehyde in PBS for 10 minutes. To detect the COPII protein, cells were further permeabilized using 0.1% Triton X-100 for 10 minutes. After a 60 minute incubation with a blocking solution (10% goat serum, 5% non-fat dry milk, PBS), the cells were treated with an anti-COPII polyclonal antibody (1:250; ABR) in 10% goat serum, 0.05% Triton X-100 and again incubated for 1 hour. Then, the cells were further incubated for 45 minutes with an Alexa-Fluor-555 antibody (1:500; Molecular probes). All experiments were performed at room temperature.

The acceptor photobleaching technique was applied to measure the Förster resonance energy transfer (FRET). Fluorescent proteins from fixed cells were excited with the 458 nm or the 514 nm lines using low excitation intensities. Next, 475–495 nm bandpass and >530 nm longpass emission filters were applied. The YFP protein in half of each cell was bleached using maximum laser power. We obtained ~80% of acceptor intensity bleaching. After photobleaching, images of the donors and acceptors were taken. The FRET efficiency was calculated using the equation $[(F_{\text{CFPafter}}-F_{\text{CFPbefore}})/F_{\text{CFPbefore}}]\times 100$, where F_{CFPafter} was the fluorescence of the donor after bleaching and $F_{\text{CFPbefore}}$ was the fluorescence before bleaching. The loss of fluorescence as a result of the scans was corrected by measuring the CFP intensity in the unbleached part of the cell. FRET values were expressed as the mean and standard error of more than 15 cells for each group. Cells were examined with a 63× oil immersion objective on a Leica TCS SL laser scanning confocal microscope. All offline image analyses were performed using a Leica confocal microscope, ImageJ software and Sigmaplot.

Electrophysiology

Whole-cell currents were recorded using the patch–clamp technique in the whole-cell configuration with a HEKA EPC10 amplifier (HEKA Elektronik). PatchMaster software (HEKA) was used for data acquisition. A stimulation frequency of 50 kHz and a filter at 10 kHz was used. The capacitance and series resistance compensation were optimized. In most experiments, we obtained an

80% compensation of the effective access resistance. Micropipettes were made from borosilicate glass capillaries (Harvard Apparatus) using a P-97 puller (Sutter Instrument) and fire polished. Pipettes had a resistance of 2–4 MΩ when filled with a solution containing (in mM): 120 KCl, 1 $CaCl_2$, 2 $MgCl_2$, 10 HEPES, 10 EGTA, 20 D-glucose (pH 7.3 and 280 mOsm/l). The extracellular solution contained (in mM): 120 NaCl, 5.4 KCl, 2 $CaCl_2$, 1 $MgCl_2$, 10 HEPES and 25 D-glucose (pH 7.4 and 310 mOsm/l). Cells were clamped at a holding potential of −60 mV. To evoke voltage-gated currents, all cells were stimulated with 250-msecond square pulses ranging from −60 to +70 mV in 10 mV steps. The peak amplitude (pA) was normalized using the capacitance values (pF). Data analysis was performed using FitMaster (HEKA) and Sigma Plot 10.0 software (Systat Software). All recordings were performed at room temperature.

Kv1.3 channel modeling

The protein was modeled using high-resolution templates of remote or close homologs available from the Protein Data Bank (http://www.rcsb.org/pdb). The transmembrane domain and the N-terminus (except the first 49 amino acids) were modeled with the Kv1.2 potassium channel (PDB code 2R9R). The C-terminus and the remaining 49 amino acids from the N-terminus were modeled with 3HGF (nucleotide binding domain of the reticulocyte binding protein Py235) and 1PXE (zinc-binding domain from neural zinc finger factor-1) codes, respectively. This procedure has been outlined on the i-Tasser online server (http://zhanglab.ccmb.med.umich.edu/I-TASSER/). We then performed multiple sequence alignment using CLUSTALW (Thompson et al., 1994) from the European Bioinformatics Institute site (http://www.ebi.ac.uk). The homology modeling was performed using the Swiss-Model Protein Modeling Server (Schwede et al., 2003) on the ExPASy Molecular Biology website (http://kr.expasy.org/) under the *Project Mode*. Structure visualization and modifications were made using Yasara v11.6.16 (Krieger et al., 2002) and DeepView v4 (Guex and Peitsch, 1997). The orientation and optimization of the side chains were carried out in two steps. First, the residues showing van der Waals clashes were selected and fitted with the 'Quick and Dirty' algorithm (DeepView). Second, the models were energy minimized. This process involved an initial short steepest descent minimization to remove bumps. Next, we performed a simulated annealing minimization. In this procedure, the simulation cell was slowly cooled towards 0K by downscaling the atom velocities. The entire system was subject to an equilibration process before the molecular dynamics simulation. The equilibration consisted of an initial minimization of the fixed backbone atoms. Next, the restrained carbon alpha atoms were minimized and a short molecular dynamics (10 pseconds) minimization was performed. The goal of the latter step was to reduce the initial incorrect contacts and to fill the empty cavities. Finally, under periodic boundary conditions in the three coordinate directions, the full system was simulated at 310°K for 0.5 nseconds. All dynamic simulations were performed using Yasara (Krieger et al., 2002) with the force field AMBER03 (Duan et al., 2003). The cut-off used for long-range interactions was set at 10 Å.

The resulting model was used to test for docking with the Sec24a structure (Mancias and Goldberg, 2008). This structure was extracted from the mammalian COPII-coat protein complex Sec23a/Sec24a/Sec22 bound to the transport signal sequence of the vesicular stomatitis virus glycoprotein (PDB code 3EGD) (Mancias and Goldberg, 2008). A local docking procedure was accomplished using AutoDock 4 (Morris et al., 2008). In this procedure, a total of 100 flexible docking runs were set and clustered around the YMVIEE motif in the C-terminus of the Kv1.3 channel. The binding energy of the docked complexes was obtained by calculating the energy between the channel and the transport protein at infinite distance and then subtracting the energy of the whole complex. The energy in each cluster was stored, analyzed, and applied to select the most likely orientation of the interacting proteins. The energy of the model and the docking complexes were tested using FoldX (Guerois et al., 2002; Schymkowitz et al., 2005) on the CRG site: http://foldx.crg.es. The force field of FoldX allowed us to evaluate the properties of the structure. Such parameters as the atomic contact map, the accessibility of the atoms and residues, the backbone dihedral angles, the hydrogen bonds and the electrostatic networks of the protein were assessed. In addition, the model was evaluated using PROCHECK to show the residues in the allowed regions of the Ramachandran plots (Laskowski et al., 1996). The final molecular graphic representations were created using PyMOL v1.4.1 (http://www.pymol.org/).

Acknowledgements

The authors thank Drs A. Bidon-Chanal and F. J. Luque (IBUB, Universitat de Barcelona) for their help in molecular modeling simulations. The English editorial assistance of the American Journal Experts and Pilar Aguado-Jimenez is also acknowledged.

Author contributions

A.F. conceived and supervised the study and wrote the manuscript. R.M.M., M.P.V., S.R.R., A.V.G., P.G., A.S.A., M.I.B. and N.C. conducted experiments. A.F.M. and G.F.B. performed the phylogenic analysis and the channel modeling. All authors contributed to data analysis, interpretation and commented on the manuscript.

Funding

This work was supported by the Ministerio de Economia y Competitividad (MINECO), Spain [grant numbers BFU2011-23268 to A.F., BFU2009-08346 to A.F.M., PROMETEO2010/046 to A.F.M. and CSD2008-00005 to A.F. and A.F.M.]. R.M.M., M.P.V., S.R.R. and A.V.G. hold fellowships from the MINECO. N.C. was supported by the Juan de la Cierva program (MINECO).

Supplementary material available online at
http://jcs.biologists.org/lookup/suppl/doi:10.1242/jcs.134825/-/DC1

References

Biervert, C., Schroeder, B. C., Kubisch, C., Berkovic, S. F., Propping, P., Jentsch, T. J. and Steinlein, O. K. (1998). A potassium channel mutation in neonatal human epilepsy. *Science* **279**, 403-406.

Cahalan, M. D. and Chandy, K. G. (2009). The functional network of ion channels in T lymphocytes. *Immunol. Rev.* **231**, 59-87.

Cavallin, M. A., Powell, K., Biju, K. C. and Fadool, D. A. (2010). State-dependent sculpting of olfactory sensory neurons is attributed to sensory enrichment, odor deprivation, and aging. *Neurosci. Lett.* **483**, 90-95.

Conforti, L. (2012). The ion channel network in T lymphocytes, a target for immunotherapy. *Clin. Immunol.* **142**, 105-106.

Curran, M. E., Splawski, I., Timothy, K. W., Vincent, G. M., Green, E. D. and Keating, M. T. (1995). A molecular basis for cardiac arrhythmia: HERG mutations cause long QT syndrome. *Cell* **80**, 795-803.

Delisle, B. P., Underkofler, H. A., Moungey, B. M., Slind, J. K., Kilby, J. A., Best, J. M., Foell, J. D., Balijepalli, R. C., Kamp, T. J. and January, C. T. (2009). Small GTPase determinants for the Golgi processing and plasmalemmal expression of human ether-a-go-go related (hERG) K+ channels. *J. Biol. Chem.* **284**, 2844-2853.

Duan, Y., Wu, C., Chowdhury, S., Lee, M. C., Xiong, G., Zhang, W., Yang, R., Cieplak, P., Luo, R., Lee, T. et al. (2003). A point-charge force field for molecular mechanics simulations of proteins based on condensed-phase quantum mechanical calculations. *J. Comput. Chem.* **24**, 1999-2012.

Farhan, H., Reiterer, V., Kriz, A., Hauri, H. P., Pavelka, M., Sitte, H. H. and Freissmuth, M. (2008). Signal-dependent export of GABA transporter 1 from the ER-Golgi intermediate compartment is specified by a C-terminal motif. *J. Cell Sci.* **121**, 753-761.

Gazula, V. R., Strumbos, J. G., Mei, X., Chen, H., Rahner, C. and Kaczmarek, L. K. (2010). Localization of Kv1.3 channels in presynaptic terminals of brainstem auditory neurons. *J. Comp. Neurol.* **518**, 3205-3220.

Guerois, R., Nielsen, J. E. and Serrano, L. (2002). Predicting changes in the stability of proteins and protein complexes: a study of more than 1000 mutations. *J. Mol. Biol.* **320**, 369-387.

Guex, N. and Peitsch, M. C. (1997). SWISS-MODEL and the Swiss-PdbViewer: an environment for comparative protein modeling. *Electrophoresis* **18**, 2714-2723.

Hasdemir, B., Fitzgerald, D. J., Prior, I. A., Tepikin, A. V. and Burgoyne, R. D. (2005). Traffic of Kv4 K+ channels mediated by KChIP1 is via a novel post-ER vesicular pathway. *J. Cell Biol.* **171**, 459-469.

Hille, B. (2001). *Ion Channels of Excitable Membranes*. Sunderland, MA: Sinauer.

Hoshi, T., Zagotta, W. N. and Aldrich, R. W. (1990). Biophysical and molecular mechanisms of Shaker potassium channel inactivation. *Science* **250**, 533-538.

Kartner, N., Augustinas, O., Jensen, T. J., Naismith, A. L. and Riordan, J. R. (1992). Mislocalization of delta F508 CFTR in cystic fibrosis sweat gland. *Nat. Genet.* **1**, 321-327.

Koeberle, P. D. and Schlichter, L. C. (2010). Targeting K(V) channels rescues retinal ganglion cells in vivo directly and by reducing inflammation. *Channels (Austin)* **4**, 337-346.

Krieger, E., Koraimann, G. and Vriend, G. (2002). Increasing the precision of comparative models with YASARA NOVA—a self-parameterizing force field. *Proteins* **47**, 393-402.

Lai, H. C. and Jan, L. Y. (2006). The distribution and targeting of neuronal voltage-gated ion channels. *Nat. Rev. Neurosci.* **7**, 548-562.

Laskowski, R. A., Rullmannn, J. A., MacArthur, M. W., Kaptein, R. and Thornton, J. M. (1996). AQUA and PROCHECK-NMR: programs for checking the quality of protein structures solved by NMR. *J. Biomol. NMR* **8**, 477-486.

Li, D., Takimoto, K. and Levitan, E. S. (2000). Surface expression of Kv1 channels is governed by a C-terminal motif. *J. Biol. Chem.* **275**, 11597-11602.

Ma, D., Zerangue, N., Raab-Graham, K., Fried, S. R., Jan, Y. N. and Jan, L. Y. (2002). Diverse trafficking patterns due to multiple traffic motifs in G protein-activated inwardly rectifying potassium channels from brain and heart. *Neuron* **33**, 715-729.

Mancias, J. D. and Goldberg, J. (2008). Structural basis of cargo membrane protein discrimination by the human COPII coat machinery. *EMBO J.* **27**, 2918-2928.

Manganas, L. N. and Trimmer, J. S. (2000). Subunit composition determines Kv1 potassium channel surface expression. *J. Biol. Chem.* **275**, 29685-29693.
Manganas, L. N., Akhtar, S., Antonucci, D. E., Campomanes, C. R., Dolly, J. O. and Trimmer, J. S. (2001a). Episodic ataxia type-1 mutations in the Kv1.1 potassium channel display distinct folding and intracellular trafficking properties. *J. Biol. Chem.* **276**, 49427-49434.
Manganas, L. N., Wang, Q., Scannevin, R. H., Antonucci, D. E., Rhodes, K. J. and Trimmer, J. S. (2001b). Identification of a trafficking determinant localized to the Kv1 potassium channel pore. *Proc. Natl. Acad. Sci. USA* **98**, 14055-14059.
Marks, D. R., Tucker, K., Cavallin, M. A., Mast, T. G. and Fadool, D. A. (2009). Awake intranasal insulin delivery modifies protein complexes and alters memory, anxiety, and olfactory behaviors. *J. Neurosci.* **29**, 6734-6751.
Misonou, H. and Trimmer, J. S. (2004). Determinants of voltage-gated potassium channel surface expression and localization in Mammalian neurons. *Crit. Rev. Biochem. Mol. Biol.* **39**, 125-145.
Morris, G. M., Huey, R. and Olson, A. J. (2008). Using AutoDock for ligand-receptor docking. *Curr. Protoc. Bioinformatics* **24**, 8.14.1–8.14.40.
Neyroud, N., Tesson, F., Denjoy, I., Leibovici, M., Donger, C., Barhanin, J., Fauré, S., Gary, F., Coumel, P., Petit, C. et al. (1997). A novel mutation in the potassium channel gene KVLQT1 causes the Jervell and Lange-Nielsen cardioauditory syndrome. *Nat. Genet.* **15**, 186-189.
Nicolaou, S. A., Szigligeti, P., Neumeier, L., Lee, S. M., Duncan, H. J., Kant, S. K., Mongey, A. B., Filipovich, A. H. and Conforti, L. (2007). Altered dynamics of Kv1.3 channel compartmentalization in the immunological synapse in systemic lupus erythematosus. *J. Immunol.* **179**, 346-356.
Nishimura, N. and Balch, W. E. (1997). A di-acidic signal required for selective export from the endoplasmic reticulum. *Science* **277**, 556-558.
Panyi, G., Vámosi, G., Bacsó, Z., Bagdány, M., Bodnár, A., Varga, Z., Gáspár, R., Mátyus, L. and Damjanovich, S. (2004). Kv1.3 potassium channels are localized in the immunological synapse formed between cytotoxic and target cells. *Proc. Natl. Acad. Sci. USA* **101**, 1285-1290.
Rea, R., Spauschus, A., Eunson, L. H., Hanna, M. G. and Kullmann, D. M. (2002). Variable K(+) channel subunit dysfunction in inherited mutations of KCNA1. *J. Physiol.* **538**, 5-23.
Rivera, J. F., Chu, P. J. and Arnold, D. B. (2005). The T1 domain of Kv1.3 mediates intracellular targeting to axons. *Eur. J. Neurosci.* **22**, 1853-1862.
Schwede, T., Kopp, J., Guex, N. and Peitsch, M. C. (2003). SWISS-MODEL: An automated protein homology-modeling server. *Nucleic Acids Res.* **31**, 3381-3385.
Schwegmann-Wessels, C., Al-Falah, M., Escors, D., Wang, Z., Zimmer, G., Deng, H., Enjuanes, L., Naim, H. Y. and Herrler, G. (2004). A novel sorting signal for intracellular localization is present in the S protein of a porcine coronavirus but absent from severe acute respiratory syndrome-associated coronavirus. *J. Biol. Chem.* **279**, 43661-43666.
Schymkowitz, J., Borg, J., Stricher, F., Nys, R., Rousseau, F. and Serrano, L. (2005). The FoldX web server: an online force field. *Nucleic Acids Res.* **33**, W382-W388.
Sevier, C. S., Weisz, O. A., Davis, M. and Machamer, C. E. (2000). Efficient export of the vesicular stomatitis virus G protein from the endoplasmic reticulum requires a signal in the cytoplasmic tail that includes both tyrosine-based and di-acidic motifs. *Mol. Biol. Cell* **11**, 13-22.
Sivaprasadarao, A., Taneja, T. K., Mankouri, J. and Smith, A. J. (2007). Trafficking of ATP-sensitive potassium channels in health and disease. *Biochem. Soc. Trans.* **35**, 1055-1059.
Sokolova, O., Kolmakova-Partensky, L. and Grigorieff, N. (2001). Three-dimensional structure of a voltage-gated potassium channel at 2.5 nm resolution. *Structure* **9**, 215-220.
Sokolova, O., Accardi, A., Gutierrez, D., Lau, A., Rigney, M. and Grigorieff, N. (2003). Conformational changes in the C terminus of Shaker K+ channel bound to the rat Kvbeta2-subunit. *Proc. Natl. Acad. Sci. USA* **100**, 12607-12612.
Steele, D. F., Zadeh, A. D., Loewen, M. E. and Fedida, D. (2007). Localization and trafficking of cardiac voltage-gated potassium channels. *Biochem. Soc. Trans.* **35**, 1069-1073.
Taneja, T. K., Mankouri, J., Karnik, R., Kannan, S., Smith, A. J., Munsey, T., Christesen, H. B., Beech, D. J. and Sivaprasadarao, A. (2009). Sar1-GTPase-dependent ER exit of KATP channels revealed by a mutation causing congenital hyperinsulinism. *Hum. Mol. Genet.* **18**, 2400-2413.
Thompson, J. D., Higgins, D. G. and Gibson, T. J. (1994). CLUSTAL W: improving the sensitivity of progressive multiple sequence alignment through sequence weighting, position-specific gap penalties and weight matrix choice. *Nucleic Acids Res.* **22**, 4673-4680.
Tóth, A., Szilágyi, O., Krasznai, Z., Panyi, G. and Hajdú, P. (2009). Functional consequences of Kv1.3 ion channel rearrangement into the immunological synapse. *Immunol. Lett.* **125**, 15-21.
Tsigelny, I., Hotchko, M., Yuan, J. X. and Keller, S. H. (2005). Identification of molecular determinants that modulate trafficking of DeltaF508 CFTR, the mutant ABC transporter associated with cystic fibrosis. *Cell Biochem. Biophys.* **42**, 41-53.
Vicente, R., Escalada, A., Coma, M., Fuster, G., Sánchez-Tilló, E., López-Iglesias, C., Soler, C., Solsona, C., Celada, A. and Felipe, A. (2003). Differential voltage-dependent K+ channel responses during proliferation and activation in macrophages. *J. Biol. Chem.* **278**, 46307-46320.
Vicente, R., Villalonga, N., Calvo, M., Escalada, A., Solsona, C., Soler, C., Tamkun, M. M. and Felipe, A. (2008). Kv1.5 association modifies Kv1.3 traffic and membrane localization. *J. Biol. Chem.* **283**, 8756-8764.
Villalonga, N., David, M., Bielańska, J., González, T., Parra, D., Soler, C., Comes, N., Valenzuela, C. and Felipe, A. (2010). Immunomodulatory effects of diclofenac in leukocytes through the targeting of Kv1.3 voltage-dependent potassium channels. *Biochem. Pharmacol.* **80**, 858-866.
Wang, X., Matteson, J., An, Y., Moyer, B., Yoo, J. S., Bannykh, S., Wilson, I. A., Riordan, J. R. and Balch, W. E. (2004). COPII-dependent export of cystic fibrosis transmembrane conductance regulator from the ER uses a di-acidic exit code. *J. Cell Biol.* **167**, 65-74.
Ward, T. H., Polishchuk, R. S., Caplan, S., Hirschberg, K. and Lippincott-Schwartz, J. (2001). Maintenance of Golgi structure and function depends on the integrity of ER export. *J. Cell Biol.* **155**, 557-570.
Zanetti, G., Pahuja, K. B., Studer, S., Shim, S. and Schekman, R. (2012). COPII and the regulation of protein sorting in mammals. *Nat. Cell Biol.* **14**, 20-28.
Zhu, J., Watanabe, I., Gomez, B. and Thornhill, W. B. (2001). Determinants involved in Kv1 potassium channel folding in the endoplasmic reticulum, glycosylation in the Golgi, and cell surface expression. *J. Biol. Chem.* **276**, 39419-39427.
Zhu, J., Watanabe, I., Gomez, B. and Thornhill, W. B. (2003). Trafficking of Kv1.4 potassium channels: interdependence of a pore region determinant and a cytoplasmic C-terminal VXXSL determinant in regulating cell-surface trafficking. *Biochem. J.* **375**, 761-768.

SUPLEMENTAL FIGURES

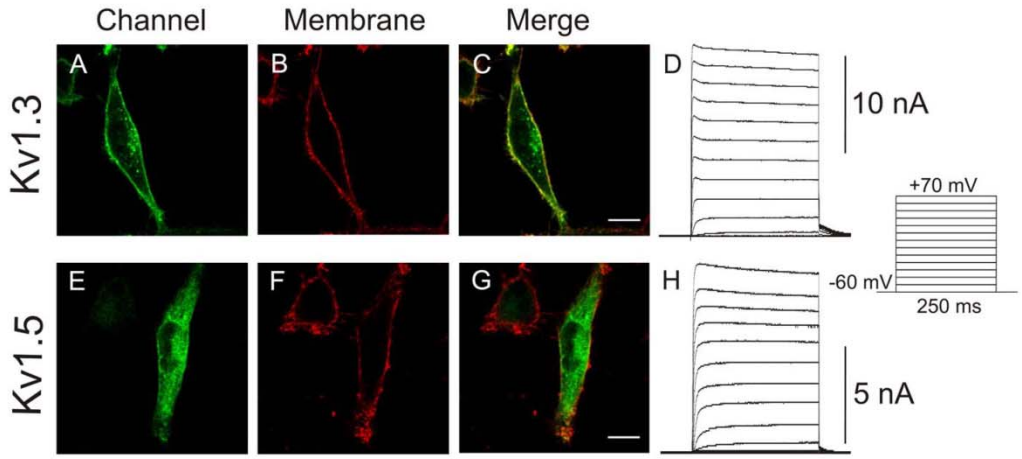

Fig. S1. Kv1.3 and Kv1.5 exhibit distinct cellular distributions and evoke different current intensities. HEK-293 cells were transiently transfected with either Kv1.3-YFP (A-D) or Kv1.5-YFP (E-H). (A-C) Kv1.3 is robustly expressed at the membrane surface. (A) Kv1.3, (B) WGA and (C) merge panels show colocalization (yellow). (E-G) Kv1.5 is mainly retained intracellularly. (E) Kv1.5, (F) WGA and (G) merge panel. Green, channels; red, WGA. Bars represent 10 μm. (D and H) Representative traces of K^+ currents from Kv1.3 (D) and Kv1.5 cells (H). The cells were held at –60 mV, and currents were elicited by depolarizing pulses in 10 mV steps (250 ms duration) from -60 to +70 mV.

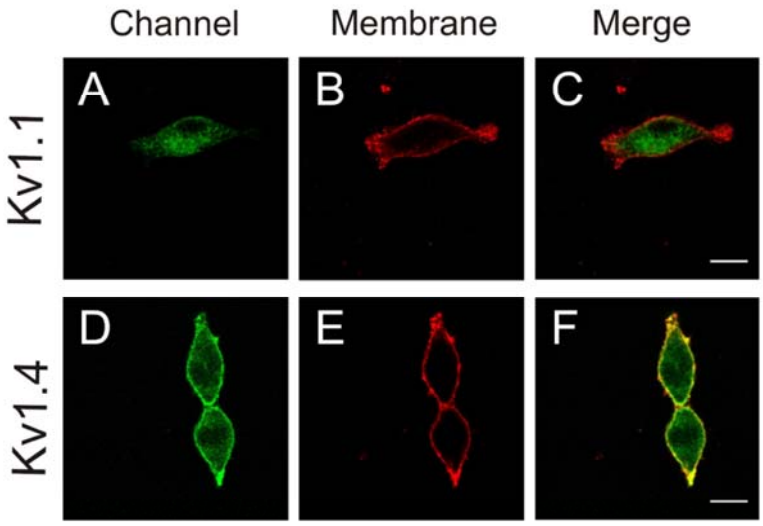

G

```
hKv1.1_loopP      346 FAEAEEAESHFSSIPDAFWWAVVSMTTVGYGDMYPVTIGGK
rKv1.3_loopP      368 ....DDPS.G.N..........T.........H.......
hKv1.4_loopP      498 ....D.PTT..Q..........T.........K.I.V...
hKv1.5_loopP      454 ....DNQGT.............T.........R.I.V...
```

H

```
hKv1.4_Cterm      562 SNFNYFYHRETENEEQTQLTQNAVSC---PYLPSNL-LKKFRSSTSSSLG
hKv1.1_Cterm      409 ............G...A..LH--..S---.N.A.DS-DLSR...STI.--
rKv1.3_Cterm      431 ............G...A.Y-MHVG..---QH.S.SA--EEL.KAR.N.TL
hKv1.5_Cterm      517 ...........DH..PAV.KEEQGTQSQG.G.DRGV-QR.V-.GSRG.FC

hKv1.4_Cterm      608 DKSEYLEMEEG-VKESLCGKEEKCQGKGDDSETDKNN---CSNAKAV---
hKv1.1_Cterm      451 -....M.I..D-MNN.IAHYRQANIRT.NCTA..Q-.---.V.KSKL---
rKv1.3_Cterm      475 S....MVI...GMNH.AFPQTPFKT.NSTATC.TN..PNS.V.I.KI---
hKv1.5_Cterm      565 KAGGT..NADS-ARRGS.-PL...NV.AK-.NV.LRR---SLY.LCLDTS
```

Fig. S2. Kv1.1 and Kv1.4 exhibit distinct cellular distributions and have different trafficking motifs. (A-F) HEK-293 cells were transiently transfected with either Kv1.1-YFP (A-C) or Kv1.4-YFP (D-F). (A-C) Kv1.1 shows notable intracellular retention. (A) Kv1.1, (B) WGA and (C) merge panel. (D-F) Kv1.4 is efficiently targeted to the membrane surface. (D) Kv1.4, (F) WGA and (G) merge panels show colocalization (yellow). Green, channels; red, WGA. Bars represent 10 µm. (G) Detailed sequence analysis of the P-loop in several Kv1 channels. Dots represent identical residues. Characters in red represent elements identified as ERR motifs in Kv1.1. (H) C-terminus sequence analysis of several Kv1 channels. Dots represent identical residues. Characters in red represent elements identified as FT signals. Dashes indicate amino acid gaps.

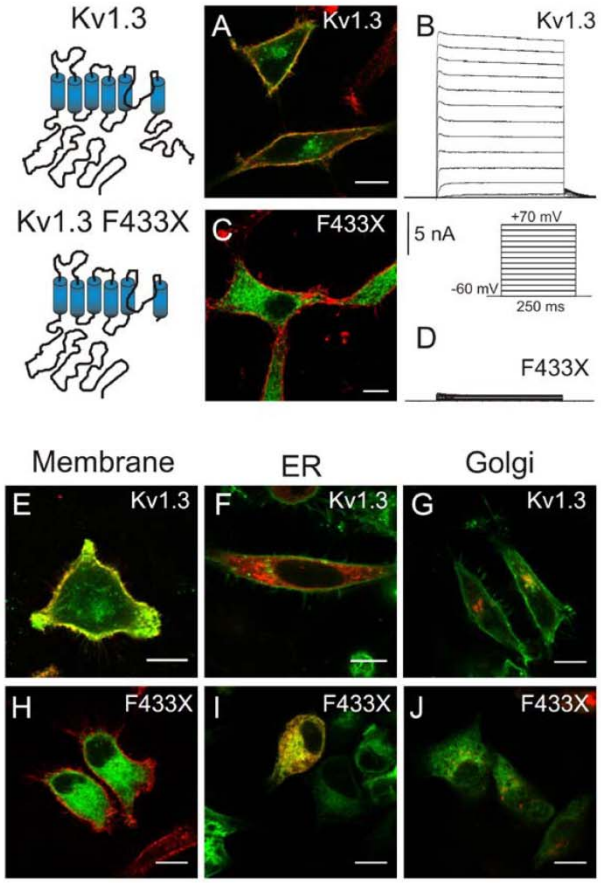

Fig. S3. The C-terminus of Kv1.3 is essential for anterograde transport and channel membrane surface targeting. Confocal images demonstrating that the deletion of the Kv1.3-YFP C-terminus (Kv1.3F433X) causes retention in the ER. Representative diagrams of the Kv1.3 channels are shown on the left. (A and B) Kv1.3 was mostly targeted to the membrane surface and generated important K^+ currents. (A) Kv1.3 colocalizes with WGA. (B) K^+ currents. (C and D) The F433X truncation, which generates a channel with no C-terminal domain, was mainly retained intracellular and evoked minimal currents. (C) F433X shows limited colocalization with WGA. (D) F433X currents are almost abolished. (E-J) Kv1.3wt and F433X are localized in distinct cellular patterns. (E-G) The Kv1.3wt is targeted to the membrane and colocalizes with the Golgi apparatus. (E) Channel and WGA colocalization, (F) channel and pDsRed-ER colocalization and (G) channel and pECFP-Golgi colocalization. (H-J) F433X showed little membrane colocalization and remained in the ER. (H) Channel and WGA colocalization, (I) channel and pDsRed-ER colocalization and (J) channel and pECFP-Golgi colocalization. Color code: Green in all panels, channel; Red, membrane (A, C, E and H), ER (F and I) and Golgi (G and J); Yellow shows colocalization. Bars represent 10 μm.

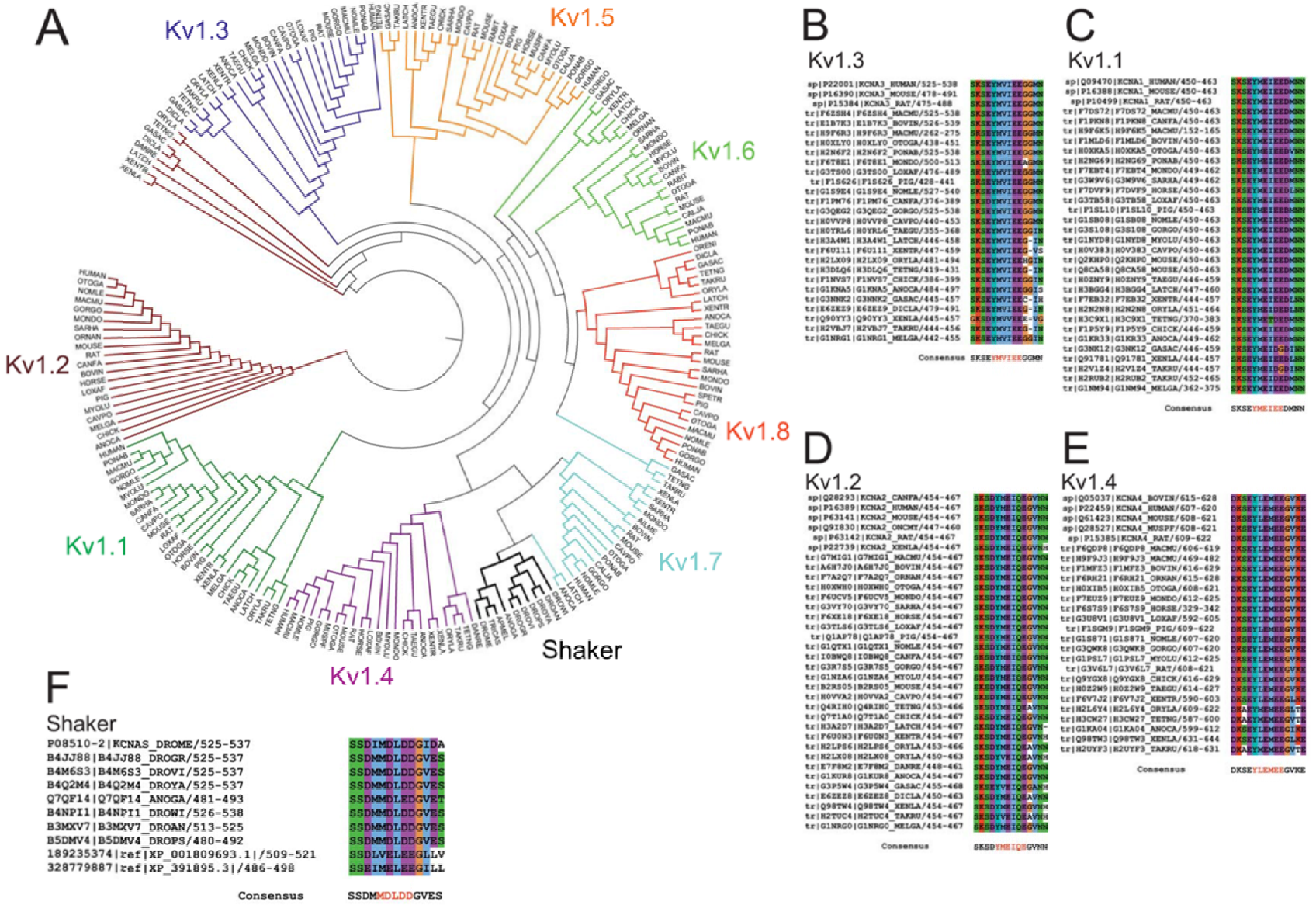
A
Kv1.3
Kv1.5
Kv1.6
Kv1.8
Kv1.7
Shaker
Kv1.4
Kv1.1
Kv1.2
B
Kv1.3
C
Kv1.1
D
Kv1.2
E
Kv1.4
F
Shaker
P08510-2|KCNAS_DROME/525-537 SSDIMDLDDGIDA
B4JJ88|B4JJ88_DROGR/525-537 SSDMMDLDDGVES
B4M6S3|B4M6S3_DROVI/525-537 SSDMMDLDDGVES
B4Q2M4|B4Q2M4_DROYA/525-537 SSDMMDLDDGVES
Q7QF14|Q7QF14_ANOGA/481-493 SSDMMDLEDGVET
B4NPI1|B4NPI1_DROWI/526-538 SSDMMDLDDGVES
B3MXV7|B3MXV7_DROAN/513-525 SSDMMDLDDGVES
B5DMV4|B5DMV4_DROPS/480-492 SSDMMDLDDGVES
189235374|ref|XP_001809693.1|/509-521 SSDLVELEEGLLV
328779887|ref|XP_391895.3|/486-498 SSEIMELEEGILL
Consensus SSDMMDLDDGVES

Fig. S4. Phylogenetic tree and sequence analysis of C-terminal domain of Kv1 and Shaker channels. The sequences for Kv potassium channels and *Shaker* families were retrieved in fasta format from UniProt (http://www.uniprot.org/) knowledgebase (UniProtKB) using the field gene name (GN) implemented in the advanced search. A wide set of channels belonging to different species were selected, although discarding redundant sequences. The C-terminus were extracted from the whole sequences and used to generate the phylogenetic tree. The program JalView v2.6.1 (Waterhouse et al., 2009) was used to edit and display the protein sequences. The automatic multiple sequence alignment of C-terms was made with ClustalW (Thompson et al., 1994) using default parameters implemented in the Web Service of JalView. ClustalW alignments were manually examined and found to be highly accurate. Thus, no manual adjustments were made except for the elimination of proteins that appeared to be truncated or otherwise incorrectly annotated. Phylogenetic analyses were performed in MEGA4 v4.0.1 (Tamura et al., 2007), using the Neighbor-Joining method (Saitou and Nei, 1987) and 1,000 bootstrap replicates for each analysis (Felsenstein, 1996). (A) Phylogenetic tree. Color code: Kv1.1, dark green; Kv1.2, brown; Kv1.3, dark blue; Kv1.4, purple; Kv1.5, orange; Kv1.6, light green; Kv1.7, light blue; Kv1.8, red; black, Shaker. (B) Kv1.3 C-terminal YMVIEE motif ClustalW alignment. Note that all Kv1.3 members conserved the YMVIEE motif in red as a consensus. (C-F) Only channel subfamilies that presented a motif similar to that observed in Kv1.3 (YMVIEE) are shown. (C) Kv1.1 (YMEIEE). (D) Kv1.2 (YMEIQE). (E) Kv1.4 (YLEMEE). (F) Shaker (MDLDD). Only the four amino acids before and after the motif are shown for simplicity. In all cases the conserved motif is highlighted in red. (B-F) The UniProt number is provided for all sequences at the right. AILME, *Ailuropoda melanoleuca*; ANOCA, *Anolis carolinensis*; ANOGA, *Anopheles gambiae*; APMEL, *Apis mellifera*; BOVIN, *Bos Taurus*; CALJA, *Callithrix jacchus*, CANFA, *Canis familiaris*; CAVPO, *Cavia porcellus*; CHICK, *Gallus gallus*; DANRE, *Danio rerio*; DICLA, *Dicentrarchus labrax*; DROAN, *Drosophila ananassae*; DROGR, *Drosophila grimshawi*; DROME, *Drosophila melanogaster*; DROPS; *Drosophila pseudoobscura*; DROVI, *Drosophila virilis*; DROWI, *Drosophila willistoni*; DROYA, *Drosophila yakuba*; GASAC, *Gasterosteus aculeatus*; GORGO, *Gorilla gorilla*; HORSE, *Equus caballus*; HUMAN, *Homo sapiens*; LATCH, *Latimeria chalumnae*; LOXAF, *Loxodonta Africana*; MACMU, *Macaca mulatta*; MELGA, *Meleagris gallopavo*; MONDO, *Monodelphis domestica*; MOUSE, *Mus musculus*; MUSPF, *Mustela putorius furo*; MYOLU, *Myotis lucifugus*; NOMLE, *Nomascus leucogenys*; ONCMY, *Oncorhynchus mykiss*; ORENI, *Oreochromis niloticus*; ORNAN, *Ornithorhynchus anatinus*, ORYLA; *Oryzias latipes*, OTOGA, *Otolemur garnettii*, PIG, *Sus scrofa*. PONAB, *Pongo abelii*; RABIT, *Oryctolagus cuniculus*; RAT; *Rattus norvegicus*; SARHA, *Sarcophilus harrisii*; SPETR, *Spermophilus tridecemlineatus*; TAEGU, *Taeniopygia guttata*; TAKRU, *Takifugu rubripes*; TETNG, *Tetraodon nigroviridis*; TRICA, *Tribolium castaneum*; XENLA, *Xenopus laevis*; XENTR, *Xenopus tropicalis*.

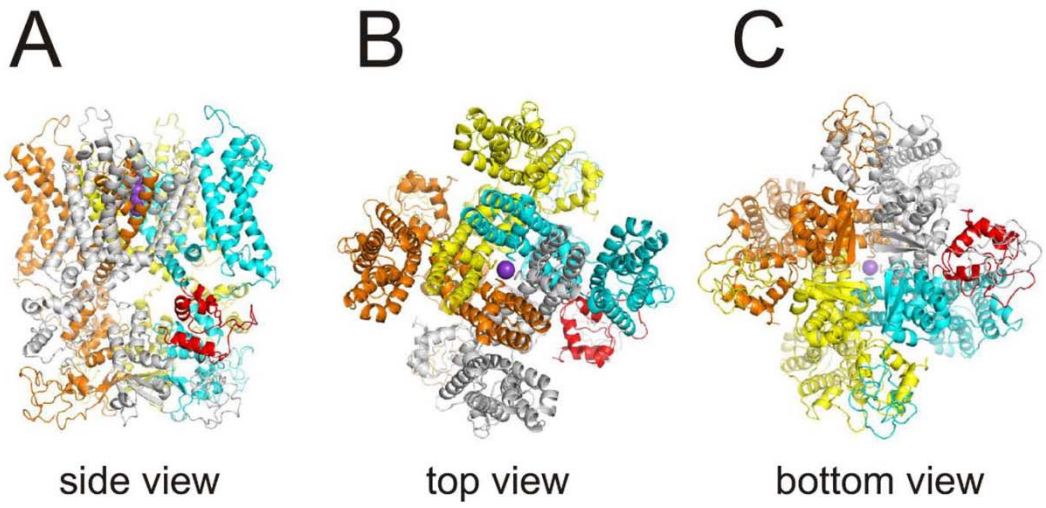

Fig. S5. Molecular model of the Kv1.3 channel. The four monomers of the tetrameric channel are shown in different colors (orange, yellow, blue and grey). However, the C-terminal domain of the blue monomer is shown in red to visualize the surface-exposed loop structure. (A) Side view, (B) top view, (C) bottom view. K^+ ions are depicted in purple for reference.

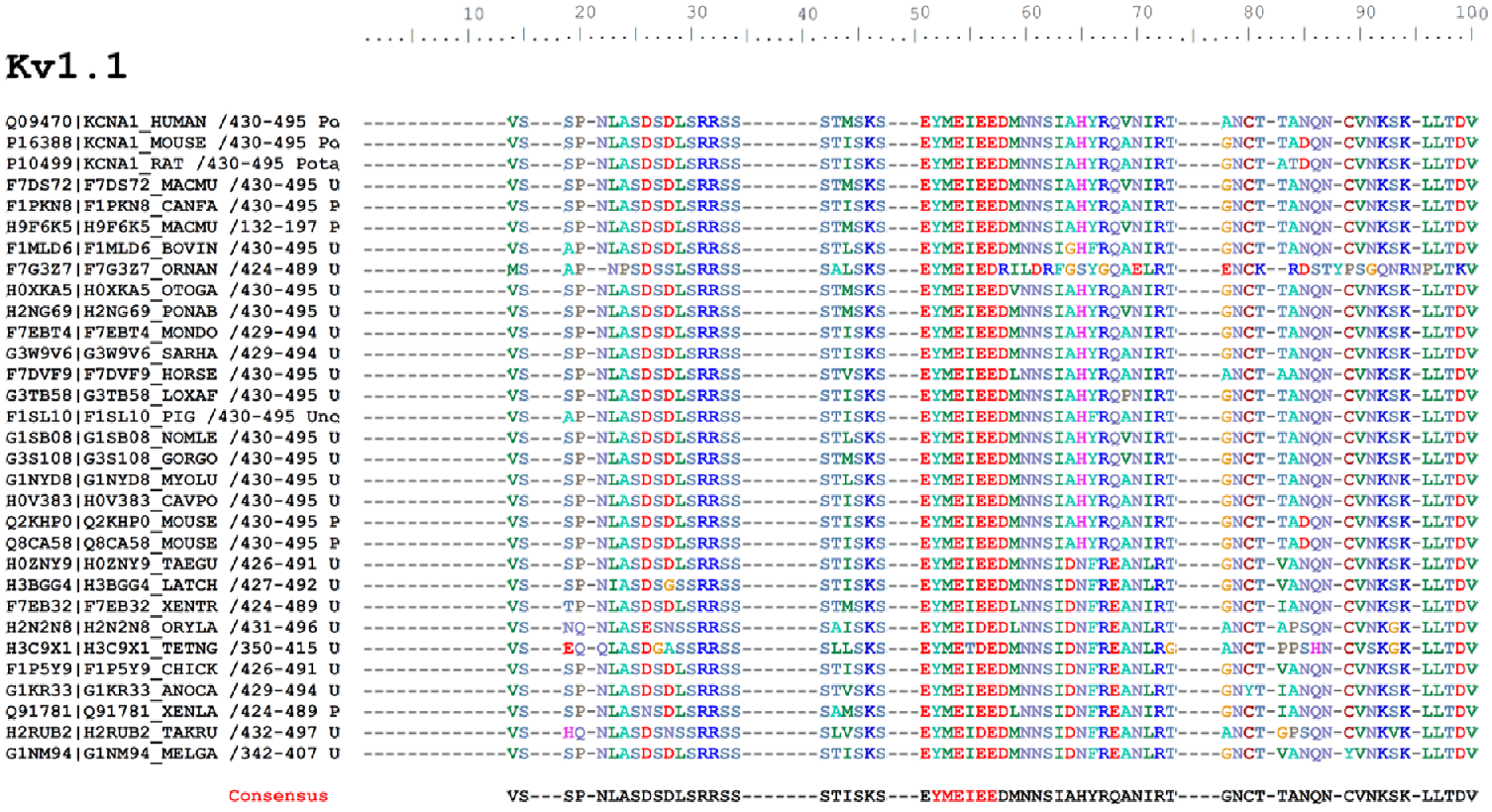
10 20 30 40 50 60 70 80 90 100
Kv1.1
Q09470|KCNA1_HUMAN /430-495 Po
P16388|KCNA1_MOUSE /430-495 Po
P10499|KCNA1_RAT /430-495 Pota
F7DS72|F7DS72_MACMU /430-495 U
F1PKN8|F1PKN8_CANFA /430-495 P
H9F6K5|H9F6K5_MACMU /132-197 P
F1MLD6|F1MLD6_BOVIN /430-495 U
F7G3Z7|F7G3Z7_ORNAN /424-489 U
H0XKA5|H0XKA5_OTOGA /430-495 U
H2NG69|H2NG69_PONAB /430-495 U
F7EBT4|F7EBT4_MONDO /429-494 U
G3W9V6|G3W9V6_SARHA /429-494 U
F7DVF9|F7DVF9_HORSE /430-495 U
G3TB58|G3TB58_LOXAF /430-495 U
F1SL10|F1SL10_PIG /430-495 Unc
G1SB08|G1SB08_NOMLE /430-495 U
G3S108|G3S108_GORGO /430-495 U
G1NYD8|G1NYD8_MYOLU /430-495 U
H0V383|H0V383_CAVPO /430-495 U
Q2KHP0|Q2KHP0_MOUSE /430-495 P
Q8CA58|Q8CA58_MOUSE /430-495 P
H0ZNY9|H0ZNY9_TAEGU /426-491 U
H3BGG4|H3BGG4_LATCH /427-492 U
F7EB32|F7EB32_XENTR /424-489 U
H2N2N8|H2N2N8_ORYLA /431-496 U
H3C9X1|H3C9X1_TETNG /350-415 U
F1P5Y9|F1P5Y9_CHICK /426-491 U
G1KR33|G1KR33_ANOCA /429-494 U
Q91781|Q91781_XENLA /424-489 P
H2RUB2|H2RUB2_TAKRU /432-497 U
G1NM94|G1NM94_MELGA /342-407 U
Consensus
VS---SP-NLASDSDLSRRSS-------STISKS---EYMEIEEDMNNSIAHYRQANIRT----GNCT-TANQN-CVNKSK-LLTDV
Kv1.2
Q28293|KCNA2_CANFA /419-499 Po
P16389|KCNA2_HUMAN /419-499 Po
P63141|KCNA2_MOUSE /419-499 Po
Q9I830|KCNA2_ONCMY /414-494 Po
P63142|KCNA2_RAT /419-499 Pota
P22739|KCNA2_XENLA /419-499 Po
G7MIG1|G7MIG1_MACMU /419-499 P
A6H7J0|A6H7J0_BOVIN /419-499 K
RETEGEEQAQYLQVT---SCPKIP-SSPDLKKSR-----SASTISKS---DYMEIQEGVNNSNEDFREENLKT----ANCT-LANTN-YVNI-TKMLTDV

```
F7A2Q7|F7A2Q7_ORNAN /419-499 U  RETEGEEQAQYLQVT---SCPKIP-SSPDLKKSR-----SASTISKS---DYMEIQEGVNNSNEDFREENLKT----ANCT-LANTN-YVNI-TKMLTDV
H0XWH0|H0XWH0_OTOGA /419-499 U  RETEGEEQAQYLQVT---SCPKIP-SSPDLKKSR-----SASTISKS---DYMEIQEGVNNSNEDFREENLKT----ANCT-LANTN-YVNI-TKMLTDV
F6UCV5|F6UCV5_MONDO /419-499 U  RETEGEEQAQYLQVT---SCPKIP-SSPDLKKSR-----SASTISKS---DYMEIQEGVNNSNEDFREENLKT----ANCT-LANTN-YVNI-TKMLTDV
G3VY70|G3VY70_SARHA /419-499 U  RETEGEEQAQYLQVT---SCPKIP-SSPDLKKSR-----SASTISKS---DYMEIQEGVNNSNEDFREENLKT----ANCT-LANTN-YVNI-TKMLTDV
F6XE18|F6XE18_HORSE /419-499 U  RETEGEEQAQYLQVT---SCPKIP-SSPDLKKSR-----SASTISKS---DYMEIQEGVNNSNEDFREENLKT----ANCT-LANTN-YVNI-TKMLTDV
G3TLS6|G3TLS6_LOXAF /419-499 U  RETEGEEQAQYLQVT---SCPKIP-SSPDLKKSR-----SASTISKS---DYMEIQEGVNNSNEDFREENLKT----ANCT-LANTN-YVNI-TKMLTDV
Q1AP78|Q1AP78_PIG /419-499 Pot  RETEGEEQAQYLQVT---SCPKIP-SSPDLKKSR-----SASTISKS---DYMEIQEGVNNSNEDFREENLKT----ANCT-LANTN-YVNI-TKMLTDV
G1QTX1|G1QTX1_NOMLE /419-499 U  RETEGEEQAQYLQVT---SCPKIP-SSPDLKKSR-----SASTISKS---DYMEIQEGVNNSNEDFREENLKT----ANCT-LANTN-YVNI-TKMLTDV
I0BWQ8|I0BWQ8_CANFA /419-499 P  RETEGEEQAQYLQVT---SCPKIP-SSPDLKKSR-----SASTISKS---DYMEIQEGVNNSNEDFREENLKT----ANCT-LANTN-YVNI-TKMLTDV
G3R7S5|G3R7S5_GORGO /419-499 U  RETEGEEQAQYLQVT---SCPKIP-SSPDLKKSR-----SASTISKS---DYMEIQEGVNNSNEDFREENLKT----ANCT-LANTN-YVNI-TKMLTDV
G1NZA6|G1NZA6_MYOLU /419-499 U  RETEGEEQAQYLQVT---SCPKIP-SSPDLKKSR-----SASTISKS---DYMEIQEGVNNSNEDFREENLKT----ANCT-LANTN-YVNI-TKMLTDV
B2RS05|B2RS05_MOUSE /419-499 P  RETEGEEQAQYLQVT---SCPKIP-SSPDLKKSR-----SASTISKS---DYMEIQEGVNNSNEDFREENLKT----ANCT-LANTN-YVNI-TKMLTDV
H0VVA2|H0VVA2_CAVPO /419-499 U  RETEGEEQAQYLQVT---SCPKIP-SSPDLKKSR-----SASTISKS---DYMEIQEGVNNSNEDFREENLKT----ANCT-LANTN-YVNI-TKMLTDV
Q4RIH0|Q4RIH0_TETNG /419-498 C  RETEGEEQAQYLQVN----VAKTD-SAEELKKSR-----SDSTISKS---DYMEIQEAVNNSNEDFQEENLKT----ANCT-LANTN-YVNI-TKMLTDV
Q7T1A0|Q7T1A0_CHICK /419-499 S  RETEGEEQAQYLQVT---SCPKIP-SSPDLKKSR-----SASTISKS---DYMEIQEGVNNSNEDFREENLKT----ANCT-LANTN-YVNI-TKMLTDV
H3A2D7|H3A2D7_LATCH /419-498 U  RETEGEEQAQCLQVT---SCPKIP-SSPELKKSR-----SASTISKS---DYMEIQEGVN-SNEDFREENLKT----TNCT-LANTN-YVHI-TKMLTDV
F6U0N3|F6U0N3_XENTR /419-499 U  RETEGEEQAQYLQVT---SCPKIP-SSPDLQKSR-----SASTLSKS---DYMEIQEGVNHSNEDFREKNLKT----ANCT-LGNTN-YVNI-TKMLTDV
H2LPS6|H2LPS6_ORYLA /419-498 U  RETEGEEQAQFLQVN----VPKTD-SAEDLKKSR-----SGSTISKS---DYMEIQEAVNNSNEDFQEENLKT----ANCT-LANTN-YVNI-TKMLTDV
E7F8M2|E7F8M2_DANRE /414-493 U  RETEGEEQAQYLQVN----VPKAD-SQEELKGSR-----SGSTISKS---DYMEIQEGVNNSNEDFQEENLKT----ANCT-LANTN-YVKI-TMMLKRY
G1KUR8|G1KUR8_ANOCA /419-499 U  RETEGEEQAQYLQVT---SCPKIP-SSPDLKKSR-----SASTISKS---DYMEIQEGVNNSNEDFREENLKT----ANCT-LANTN-YVNI-TKMLTDV
G3NNJ8|G3NNJ8_GASAC /415-494 U  RETEGEEQAQYLQVN----VAKAD-SSEELKKSR-----SGSTISKS---DYMEIQEAVNNSREEIQEENLKT----ANCT-LANTN-YVNI-TKMLTDV
E6ZEZ8|E6ZEZ8_DICLA /416-495 P  RETEGEEQAQYLQVN----VPKAD-SAEELKKSR-----SGSTISKS---DYMEIQEAVNNSNEDFQEENLKT----ANCT-LANTN-YVNI-TKMLTDV
Q98TW4|Q98TW4_XENLA /419-499 K  RETEGGEQAQYLQVT---SCPKIP-SSPDLQKSR-----SASTLSKS---DYMEIQEGVNHSNEDFREKNLKT----ANCT-LGNTN-YVNI-TKMLTDV
H2TUC4|H2TUC4_TAKRU /415-499 U  RETEGEEQAQYLNIP---SVPKAS-SADELKKSGGRCR-SSSTLSKS---DYVEIQEAVNHSMEDFRPEGVKR----GNCT-LANTN-YVNI-TKRRTDV
G1NRG0|G1NRG0_MELGA /419-499 U  RETEGEEQAQYLQVT---SCPKIP-SSPDLKKSR-----SASTISKS---DYMEIQEGVNNSNEDFREENLKT----ANCT-LANTN-YVNI-TKMLTDV

                       Consensus RETEGEEQAQYLQVT---SCPKIP-SSPDLKKSR-----SASTISKS---DYMEIQEGVNNSNEDFREENLKT----ANCT-LANTN-YVNI-TKMLTDV
```

Kv1.3

```
P22001|KCNA3_HUMAN /489-575 Po  RETEGEEQSQYMHVG---SCQHLSSSAEELRKAR-----SNSTLSKS---EYMVIEEGGMNHSA-FPQTPFKTGNSTATCTTNNNPNSCVNI-KKIFTDV
P16390|KCNA3_MOUSE /442-528 Po  RETEGEEQAQYMHVG---SCQHLSSSAEELRKAR-----SNSTLSKS---EYMVIEEGGMNHSA-FPQTPFKTGNSTATCTTNNNPNSCVNI-KKIFTDV
P15384|KCNA3_RAT /439-525 Pota  RETEGEEQAQYMHVG---SCQHLSSSAEELRKAR-----SNSTLSKS---EYMVIEEGGMNHSA-FPQTPFKTGNSTATCTTNNNPNSCVNI-KKIFTDV
F6ZSH4|F6ZSH4_MACMU /489-575 P  RETEGEEQAQYMHVG---SCQHLSSSAEELRKAR-----SNSTLSKS---EYMVIEEGGMNHSA-FPQTPFKTGNSTATCTTNNNPNSCVNI-KKIFTDV
E1B7K3|E1B7K3_BOVIN /490-576 U  RETEGEEQAQCLHVG---SCQHLSPSAEELRKAR-----SNSTLSKS---EYMVIEEGGMNHSA-FPQAPFKTGNSTATCTTNNNPNSCVNI-KKIFTDV
H9F6R3|H9F6R3_MACMU /226-312 P  RETEGEEQAQYMHVG---SCQHLSSSAEELRKAR-----SNSTLSKS---EYMVIEEGGMNHSA-FPQTPFKTGNSTATCTTNNNPNSCVNI-KKIFTDV
H0XLY0|H0XLY0_OTOGA /402-488 U  RETEGEEQAQYMHVG---SCQHLSSSAEELRKAR-----SNSTLSKS---EYMVIEEGGMNHST-FPQTPFKTGNSTATCTTNNNPNSCVNI-KKIFTDV
H2N6F2|H2N6F2_PONAB /489-575 U  RETEGEEQAQYMHVG---SCQHLSSSAEELRKAR-----SNSTLSKS---EYMVIEEGGMNHSA-FPQTPFKTGNSTATCTTNNNPNSCVNI-KKIFTDV
F6T8E1|F6T8E1_MONDO /464-550 U  RETEGEEQAQYMHVG---SCQHLSSSVEELRKAR-----SNSTLSKS---EYMVIEEAGMNHST-FPPAPFKTGNSTATCTTNNNPNSCVNI-KKIFTDV
G3TS00|G3TS00_LOXAF /440-526 U  RETEGEEQAQYMHVG---SCQHLSSSAEELRKAR-----SNSTLSKS---EYMVIEEGGMNHSA-FPQTPFKTGNSTATCTTNNNPNSCVSI-KKIFTDV
F1S626|F1S626_PIG /392-478 Unc  RETEGEEQAQYMHVG---SCQHLSSSAEELRKAR-----SNSTLSKS---EYMVIEEGGMNHSA-FPQTPFKTGNSTATCTTNNNPNSCVNI-KKIFTDV
G1S9E4|G1S9E4_NOMLE /491-577 U  RETEGEEQAQYMHVG---SCQHLSSSAEELRKAR-----SNSTLSKS---EYMVIEEGGMNHSA-FPQTPFKTGNSTATCTTNNNPNSCVNI-KKIFTDV
F1PM76|F1PM76_CANFA /340-426 U  RETEGEEQAQYMHVG---SCQHLSSSAEELRKAR-----SNSTLSKS---DYMVIEEGGMNHSA-FPQTPFKTGNSTATCTTNNNPNSCVNI-KKIFTDV
G3QEG2|G3QEG2_GORGO /489-575 U  RETEGEEQAQYMHVG---SCQHLSSSAEELRKAR-----SNSTLSKS---EYMVIEEGGMNHSA-FPQTPFKTGNSTATCTTNNNPNSCVNI-KKIFTDV
H0VVP8|H0VVP8_CAVPO /404-490 U  RETEGEEQAQYMHVG---SCQHLSSSAEELRKAR-----SNSTLSKS---EYMVIEEGGMNHST-FPQTPFKTGNSTATCTTNNNPNSCVNI-KKIFTDV
H0YRL6|H0YRL6_TAEGU /320-400 U  RETEGEEQAQYMHVG---SCQHLS-SSEEMKKAR-----SNSTLSKS---EYMVIEEGGINHSA-FKQAAFKAGN----CTTTNNPN-CVNI-KKIFTDV
H3A4W1|H3A4W1_LATCH /411-489 U  RETEGEEQAQYLHVG---SCQHLSS-TEDLKKTR-----SSSSLSKS---EYMVIEEGINNSAF-KQ-PNFKTGN-----CTTNN-QNCVNI-KKIFTDV
F6U111|F6U111_XENTR /412-490 U  RETEGEEQAQYLHVG---SCQHLS-SNEDLKKAR-----SNSSLSKS---EYMVIEEG-VSPGP-FKQPAFKTGN----CTT--NNPNCVNI-KKIFTDV
H2LX09|H2LX09_ORYLA /446-525 U  RETEGEEQAQYLHVG---SCQPLAD-TEELRKTR-----SSSSLSKS---EYMVIEEHGINSAF-KQQPNFPT-------TTQNNSQNCVNISKKIFTDV
```

```
H3DLQ6|H3DLQ6_TETNG /385-457 U  RETEGEEQPQYVHTG---SCEHLP--AEALRRSC-----SSSSLSKS---EYMVIEEG-INSAF-KQ-PNF---------STENT-QNCVNI-KKMFTDV
F1NVS7|F1NVS7_CHICK /351-431 U  RETEGEEQAQYMHVG---SCQHLS-STEEMRKAR-----SNSTLSKS---EYMVIEEGGINHSA-FKQAAFKTGN----CTTTNNPN-CVNI-KKIFTDV
G1KNA5|G1KNA5_ANOCA /449-529 U  RETEGEEQAQYMHVG---SCQHLS-STEELRKAR-----SNSTISKS---EYMVIEEGGISNSA-FKQAAFKTGN----CTAVNNPN-CVNI-KKIFTDV
G3NNK2|G3NNK2_GASAC /411-483 U  RETDGEETPQYVHTS---SCEHLP--TEELRRSC-----SSTSLSKS---EYMVIEEC-IHSAF-KQ-PNF---------STENN-QNCVNI-TKIFTDV
E6ZEZ9|E6ZEZ9_DICLA /445-517 P  RETDGEEHPQYVHTS---SCEHLP--SEELRRSC-----SSSSLSKS---EYMVIEEG-INSAF-KQ-PNF---------TTENN-QNCVNI-KKIFTDV
Q90YY3|Q90YY3_XENLA /412-485 S  RETEGEEQAQYMHVG---SCQ--S-SNEDVKKTQ-----SNSSLGKS---DYMVVEEE-VGPGP------FKTGN----CTTANNNPNCVNI-KKIFTDV
H2VBJ7|H2VBJ7_TAKRU /410-482 U  RETDGEEQPQYVHTG---SCEHLP--SEELRRSC-----SSSSLSKS---EYMVIEEG-INSTF-KQ-PNF---------NTENN-QNCVNI-KKMFTDV
G1NRG1|G1NRG1_MELGA /407-487 U  RETEGEEQAQYMHVG---SCQHLS-STEEMRKAR-----SNSTLSKS---EYMVIEEGGINHSA-FKQAAFKTGN----CTTTNNPN-CVNI-KKIFTDV

                                 Consensus RETEGEEQAQYMHVG---SCQHLSSSAEELRKAR-----SNSTLSKS---EYMVIEEGGMNHSAFPQTPFKTGNSTATCTTNNGNPNSCVNI-KKIFTDV
```

Kv1.4

```
Q05037|KCNA4_BOVIN /577-660 Po  RETEN-EEQTQLTQN-AVSCPYLPSNLLKKFRSSTS-----SSLGDK--SEYLEMEEGVKESLCAK-EKCQGK----GDDSETDKNN-VSNA-KAVETDV
P22459|KCNA4_HUMAN /569-653 Po  RETEN-EEQTQLTQN-AVSCPYLPSNLLKKFRSSTS-----SSLGDK--SEYLEMEEGVKESLCAKEEKCQGK----GDDSETDKNN-CSNA-KAVETDV
Q61423|KCNA4_MOUSE /570-654 Po  RETEN-EEQTQLTQN-AVSCPYLPSNLLKKFRSSTS-----SSLGDK--SEYLEMEEGVKESLCGKEEKCQGK----GDESETDKNN-CSNA-KAVETDV
Q28527|KCNA4_MUSPF /570-654 Po  RETEN-EEQTQLTQN-AVSCPYLPSNLLKKFRSSTS-----SSLGDK--SEYLEMEEGVKESLCAKEGKCQGK----GDDSETDKNN-CSNA-KAVETDV
P15385|KCNA4_RAT /571-655 Pota  RETEN-EEQTQLTQN-AVSCPYLPSNLLKKFRSSTS-----SSLGDK--SEYLEMEEGVKESLCGKEEKCQGK----GDDSETDKNN-CSNA-KAVETDV
F6QDP8|F6QDP8_MACMU /568-652 U  RETEN-EEQTQLTQN-AVSCPYLPSNLLKKFRSSTS-----SSLGDK--SEYLEMEEGVKESLCAKEEKCQGK----GDDSETDKNN-CSNA-KAVETDV
H9F9J3|H9F9J3_MACMU /431-515 P  RETEN-EEQTQLTQN-AVSCPYLPSNLLKKFRSSTS-----SSLGDK--SEYLEMEEGVKESLCAKEEKCQGK----GDDSETDKNN-CSNA-KAVETDV
F1MFZ3|F1MFZ3_BOVIN /578-661 P  RETEN-EEQTQLTQN-AVSCPYLPSNLLKKFRSSTS-----SSLGDK--SEYLEMEEGVKESLCAK-EKCQGK----GDDSETDKNN-CSNA-KAVETDV
F6RH21|F6RH21_ORNAN /577-661 U  RETEN-EEQTQLTQN-AVSCPYLPSNLLKKFRSSTS-----SSLGEK--SEYLEMEEGVKESLCAKEEKCQGK----GRGSETAKKN-CANA-KAVETDV
H0XIB5|H0XIB5_OTOGA /570-654 U  RETEN-EEQTQLTQN-AVSCPYLPSNLLKKFRSSTS-----SSLGDK--SEYLEMEEGVKESLCAKEEKCQGK----GDESETDKNN-CSNA-KAVETDV
F7EUZ9|F7EUZ9_MONDO /574-658 U  RETEN-EEQTQMTQN-AVSCPYLPSNLLKKFRSSTS-----SSLGDK--SEYLEMEEGVKESLCAKEEKCQGK----GDESETEKNN-CTNA-KTVETDV
F6S7S9|F6S7S9_HORSE /291-375 U  RETEN-EEQTQLTQN-AVSCPYLPSNLLKKFRSSTS-----SSLGDK--SEYLEMEEGVKESLCAKEEKCQGK----EDDSETDKNN-CSNV-KAVETDV
G3U8V1|G3U8V1_LOXAF /554-638 U  RETEN-EEQTQLTQN-AVSCPYLPSNLLKKFRSSTS-----SSLGDK--SEYLEMEEGVKESLCAKEEKCQGK----GDDSETDKNN-CSNV-KAVETDV
F1SGM9|F1SGM9_PIG /571-654 Unc  RETEN-EEQTQLTQN-AVSCPYLPSNLLKKFRSSTS-----SSLGDK--SEYLEMEEGVKESLCAK-EKCQGK----GDDSETDKNN-CSNA-KAVETDV
G1S871|G1S871_NOMLE /569-652 U  RETEN-EEQTQLTQN-AVSCPYLPSNLLKKFRSSTS-----SSLGDK--SEYLEMEEGVKESLCAK-EKCQGK----GDDSETDKNN-CSNA-KAVETDV
G3QWK8|G3QWK8_GORGO /569-653 U  RETEN-EEQTQLTQN-AVSCPYLPSNLLKKFRSSTS-----SSLGDK--SEYLEMEEGVKESLCAKEDKCQGK----GDDSETDKNN-CSNA-KAVETDV
G3S8C4|G3S8C4_GORGO /553-637 U  RETEN-EEQTQLTQN-AVSCPYLPSNLLKKFRSSTS-----SSLGDK--SEYLEMEEGVKESLCAKEDKCQGK----GDDSETDKNN-CSNA-KAVETDV
G1PSL7|G1PSL7_MYOLU /574-657 U  RETEN-EEQTQLTQN-AVSCPYIPSNLLKKFRSSTS-----SSLGDK--SEYLEMEEGVKESLCAK-EKCQGK----GDDSETDKNN-CSNA-KAVETDV
G3V6L7|G3V6L7_RAT /570-654 Pot  RETEN-EEQTQLTQN-AVSCPYLPSNLLKKFRSSTS-----SSLGDK--SEYLEMEEGVKESLCGKEEKCQGK----GDDSETDKNN-CSNA-KAVETDV
Q9YGX8|Q9YGX8_CHICK /578-662 P  RETEN-EEQTQLMQN-AVSCPYLPTNLLKKFRSSSS-----SSTEDK--SEYLEMEEGVKESLCVKEKKSQDT----GNSSESEKKN-CVNS-NSVETDV
H0Z2W9|H0Z2W9_TAEGU /576-660 U  RETEN-EEHTQMMQN-AVSCPYLPTNLLKKFRSASS-----SSTEDK--SEYLEMEEGVKESLCVKETKSQDT----GNSSESEKKN-CVNS-NSVETDV
F6V7J2|F6V7J2_XENTR /552-636 U  RETDN-EEQTQLTQS-SSSCPYLPTNLLKKLRSSTS-----SSLQDK--SEYLEMEEGLKESLCIKDKASEGT----GNGNETIKYN-CVNL-KILETDV
H2L6Y4|H2L6Y4_ORYLA /569-654 U  RETDNNEDQTPVVESMPPGCPYFPD-FLRKFKGSPSG----SSLGDK--AEYMEMEEGLTESLCGLD-KSPSK----GNGTDISRKN-STNS-KSIQTDV
F1Q929|F1Q929_DANRE /411-497 U  RETDN-EDQAPAVEQPPPGCPYFPD-FLRKFKGSPSG----SSLGDKA-AEYMEMEEGVTESLCGGDTQSPSR----GNGTDLGGKN-SSHS-RTLQTDV
H3CW27|H3CW27_TETNG /548-632 U  RETDN-EDQAPVVESVPPGCPYFPD-FLRKFKGSPSG----SSLGDK--AEYMEMEEGVTESLCGLD-KSPSK----GNGTDIGRRN-STNS-KSIQTDV
G1KA04|G1KA04_ANOCA /562-645 U  RETDN-EEQTQLTQN-AVSCPYLPT-IIKKFRSSSS-----SSTEDK--SEYLEMEEGIKESLCVKEKKCQVT----GNGNETAKQN-CVNA-KSVETDV
Q98TW3|Q98TW3_XENLA /593-677 K  RETDN-EEQTQLTQS-SSSCPYLPTNLLKKLRSSTS-----SSLQDK--SEYLEMEEGLKESLCVKDKAIEGT----GNGNETIKYN-CVSL-KILETDV
H2UYF3|H2UYF3_TAKRU /579-663 U  RETDN-EDQAPVVESVPPVCPYFPD-FLRKFKSSPSG----SSLGDK--AEYMEMEEGVTESLCGLD-KSPSK----GNGTDIGRRN-STNS-KSIQTDV
H2UYF5|H2UYF5_TAKRU /527-610 U  RETDN-EDQAPVVESVPPVCPYFPD-FLRKFKSSPSG----SSLGDK--AEYMEMEEGVTESLCGLD-KSPSK----GNGTDIGRRN-STNS-KSIQTD-
H2UYF4|H2UYF4_TAKRU /568-652 U  RETDN-EDQAPVVESVPPVCPYFPD-FLRKFKSSPSG----SSLGDK--AEYMEMEEGVTESLCGLD-KSPSK----GNGTDIGRRN-STNS-KSIQTDV

                                 Consensus RETEN-EEQTQLTQNVAVSCPYLPSNLLKKFRSSTS-----SSLGDK--SEYLEMEEGVKESLCAKEEKCQGK----GDDSETDKNN-CSNA-KAVETDV
```

Kv1.5

```
P22460|KCNA5_HUMAN /530-613 Po  ------EEPAVLKEE-QGTQSQGPGLDRGVQRKV---SGSRGSFCKAG--GTLENADSARRGSCPLEKCNVKA----KSNVDLRRSLYALCLDTSRETDL
Q61762|KCNA5_MOUSE /519-602 Po  ------EEQAALKEE-QGIQRRESGLDTGGQRKV---SCSKASFCKTG--GPLESTDSIRRGSCPLEKCHLKA----KSNVDLRRSLYALCLDTSRETDL
```

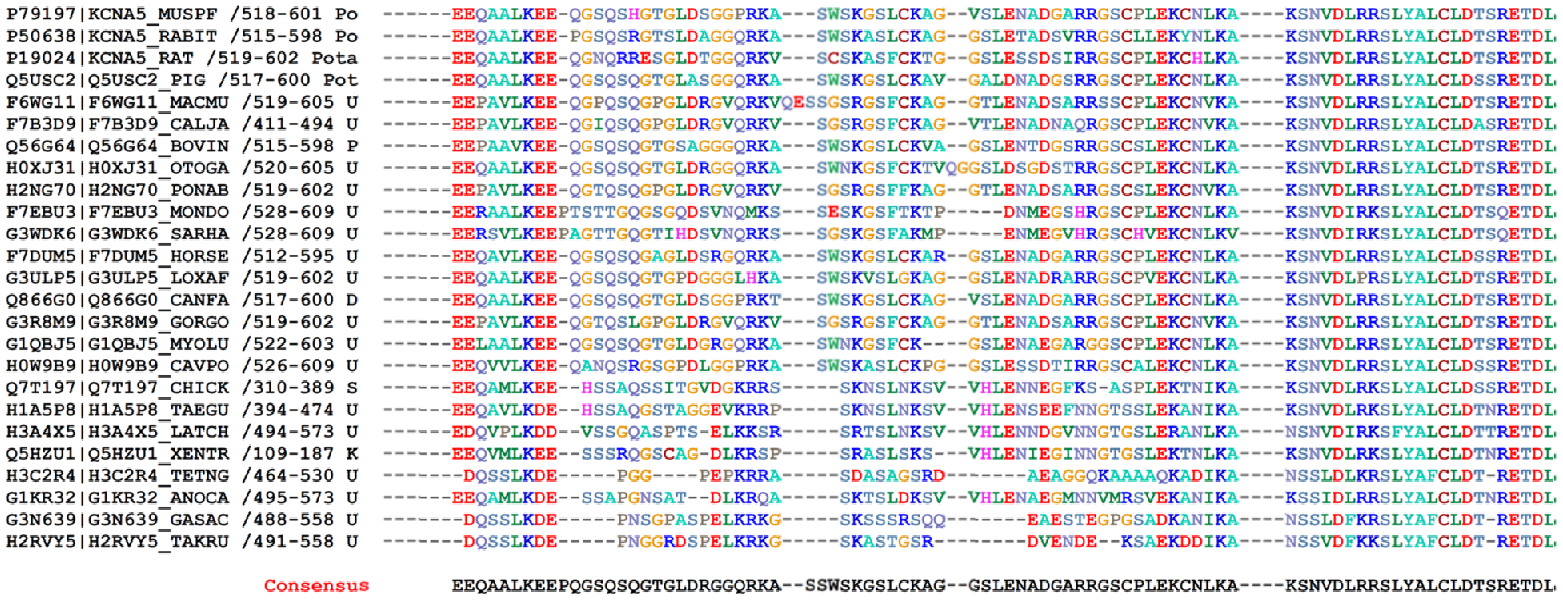
P79197|KCNA5_MUSPF /518-601 Po
P50638|KCNA5_RABIT /515-598 Po
P19024|KCNA5_RAT /519-602 Pota
Q5USC2|Q5USC2_PIG /517-600 Pot
F6WG11|F6WG11_MACMU /519-605 U
F7B3D9|F7B3D9_CALJA /411-494 U
Q56G64|Q56G64_BOVIN /515-598 P
H0XJ31|H0XJ31_OTOGA /520-605 U
H2NG70|H2NG70_PONAB /519-602 U
F7EBU3|F7EBU3_MONDO /528-609 U
G3WDK6|G3WDK6_SARHA /528-609 U
F7DUM5|F7DUM5_HORSE /512-595 U
G3ULP5|G3ULP5_LOXAF /519-602 U
Q866G0|Q866G0_CANFA /517-600 D
G3R8M9|G3R8M9_GORGO /519-602 U
G1QBJ5|G1QBJ5_MYOLU /522-603 U
H0W9B9|H0W9B9_CAVPO /526-609 U
Q7T197|Q7T197_CHICK /310-389 S
H1A5P8|H1A5P8_TAEGU /394-474 U
H3A4X5|H3A4X5_LATCH /494-573 U
Q5HZU1|Q5HZU1_XENTR /109-187 K
H3C2R4|H3C2R4_TETNG /464-530 U
G1KR32|G1KR32_ANOCA /495-573 U
G3N639|G3N639_GASAC /488-558 U
H2RVY5|H2RVY5_TAKRU /491-558 U
Consensus

Kv1.6

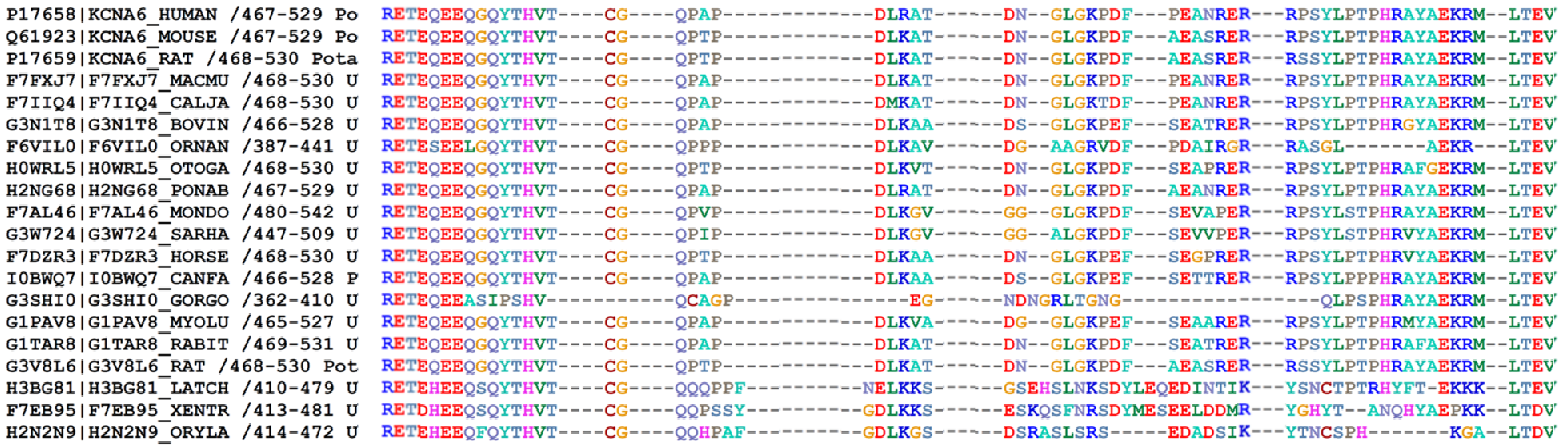
P17658|KCNA6_HUMAN /467-529 Po
Q61923|KCNA6_MOUSE /467-529 Po
P17659|KCNA6_RAT /468-530 Pota
F7FXJ7|F7FXJ7_MACMU /468-530 U
F7IIQ4|F7IIQ4_CALJA /468-530 U
G3N1T8|G3N1T8_BOVIN /466-528 U
F6VIL0|F6VIL0_ORNAN /387-441 U
H0WRL5|H0WRL5_OTOGA /468-530 U
H2NG68|H2NG68_PONAB /467-529 U
F7AL46|F7AL46_MONDO /480-542 U
G3W724|G3W724_SARHA /447-509 U
F7DZR3|F7DZR3_HORSE /468-530 U
I0BWQ7|I0BWQ7_CANFA /466-528 P
G3SHI0|G3SHI0_GORGO /362-410 U
G1PAV8|G1PAV8_MYOLU /465-527 U
G1TAR8|G1TAR8_RABIT /469-531 U
G3V8L6|G3V8L6_RAT /468-530 Pot
H3BG81|H3BG81_LATCH /410-479 U
F7EB95|F7EB95_XENTR /413-481 U
H2N2N9|H2N2N9_ORYLA /414-472 U

```
H2LFC3|H2LFC3_ORYLA /410-479 U  RENEEEENVQHVHVT----CGLVEQQPYTGEGDSIR-----SNLSLS------QTESYQESDDL--------------ETLTHPSTNQSDAYVGKLTDV
E1C6I6|E1C6I6_CHICK /443-513 U  RETDNEEQCQYTHVT----CG----QQQSLF----------SEPKKG------NSNQSLSKSEFFEVEDLESMK---YSNFIPPGNQGYKEKKM--LTEV
G3PSY5|G3PSY5_GASAC /409-448 U  RETEGEEQFRYTHVT----CG----QQQ--F----------GELERS------DSGSSLSKL-----DHRD----------------------------
G3NK16|G3NK16_GASAC /410-478 U  RENEDEENVLYVHVT----CGQ-QQQPSSRECDSIK-----SDQSPS------KTESSQGSDDL--------------EALTYPNITPVETYVARLTDV
G1NS10|G1NS10_MELGA /403-473 U  RETDNEEQCQYTHVT----CG----QQQSPF----------SEPKKG------DSNQSLSKSEFLEVEDLESMK---YSNFIPPGNQGYKEKKM--LTEV

                      Consensus  RETEQEEQGQYTHVT----CGQQQSPFPAP-----------DLKAT------DN--GLGKPDFSEAEDLDRER---RPSYLPTPHRAYAEKRM--LTEV
```

Kv1.7

```
Q96RP8|KCNA7_HUMAN /403-456 Po  RETEGEEAGMFSHVD----M-----QPCGP--------------LEG------KANGGLVDGEV--------------PELPPPLWAPPGKHL--VTEV
Q17ST2|KCNA7_MOUSE /436-489 Po  RETEGEEAGMYSHVD----T-----QPCGT--------------LEG------KANGGLVDSEV--------------PELLPPLWPPAGKHM--VTEV
B2RU13|B2RU13_HUMAN /403-456 P  RETEGEEAGMFSHVD----T-----QPCGP--------------LEG------KANGGLVDGEV--------------PELPPPLWAPPGKHL--VTEV
F7HJ15|F7HJ15_CALJA /403-456 U  RETEGEEAGMYSHVD----T-----QPCGP--------------LEG------KANGGLVDSEV--------------PELPPPLWAPPGKHL--VTEV
F7HJ21|F7HJ21_CALJA /404-457 U  RETEGEEAGMYSHVD----T-----QPCGP--------------LEG------KANGGLVDSEV--------------PELPPPLWAPPGKHL--VTEV
E1B9N0|E1B9N0_BOVIN /451-504 U  RETDDEEAGMYSHVD----T-----QPCGP--------------LEG------KVNGGLVDPEV--------------SELPPPLWAPPGKHM--VTEV
H0WHY5|H0WHY5_OTOGA /435-488 U  RETEGEEAGMFSHVD----T-----QPCGT--------------LEG------KANGGLVDGEM--------------PELPPPLWAPPAKHL--VTEV
H2NZL4|H2NZL4_PONAB /406-459 U  RETEGEEAGMFSHVD----T-----QPCGP--------------LEG------KANGGLVDREV--------------PEHPPPLWAPPGKPL--VTEV
F6TVP3|F6TVP3_MONDO /420-463 U  RETEGEDMGRYRHVA----T-----QPCCPP-----------EAPEG------KANG-LVGG-----------------------------SGKHL--VTEV
G3VJD1|G3VJD1_SARHA /224-267 U  RETEGEDTGRYRHVA----T-----QPCCPP-----------ETPEG------KANG-LVGG-----------------------------SGKHL--VTEV
G1QYA8|G1QYA8_NOMLE /401-454 U  RETEGEEAGMFSHVD----T-----QPCGP--------------LEG------KANGGLVDGEV--------------PELPPPLWAPPGKHL--VTEV
G3RD08|G3RD08_GORGO /315-368 U  RETEGEEAGMFSHVD----T-----QPCGP--------------LEG------KANGGLVDGEV--------------PELPPPLWAPPGKHL--VTEV
G1M7F1|G1M7F1_AILME /320-373 U  RETEGEDGGMYSHVD----T-----QPCGP--------------LEG------KVNGGLMDGEM--------------PELPPPLWAPPGKHM--VTEV
D4A810|D4A810_RAT /436-489 Pot  RETEGEEAGMYSHVD----T-----QPCGT--------------LEG------KANGGLVDSEV--------------PELLPPLWAPSGKHM--VTEV
H0W9I3|H0W9I3_CAVPO /401-454 U  RETEGEEAGMYSHVD----T-----QPCIN--------------LED------KVNGGLVDGEV--------------PELPPPLWAPPGKHL--VTEV
H3B809|H3B809_LATCH /413-491 U  RETECEDQTQYTHVT----TCPYVPPPSPKMQSITG----KSTEAEE------DFMDSLCAPLQ---TDHMDSF---YTTDSGNLQSSQQ-QQKPLVTQV
F7DT93|F7DT93_XENTR /416-489 U  RETECSDIGQYNHVG----SCPNGPPHTPKIKGKDK-------SPTI------SKLRNTYTNSK---ANFLDGL---GPADDRQLISGQS---SHLITEV
H3CM69|H3CM69_TETNG /385-464 U  RETECEDRTEYTHVK----TSLWDNEDEERFEQEEREEGDRCPE-NY------YPVEGICSPLN---GTLLGGL---CTGQN---REGNMHQREPLVTQV
G3NZC4|G3NZC4_GASAC /382-425 U  RETECVEHTEYSPVQ----AGAWEDEGRDVEE-EDG-------DADY------FAVEGSCSP-----------------------------------
Q98TW2|Q98TW2_XENLA /416-489 K  RETECSDIGQYDHVG----SCPNSPPLTPKTKGKDK-------SPMI------SKLRNIVTNSK---AEFLDGL---GPADDRQLVPGQP---SHLITEV
H2UA67|H2UA67_TAKRU /380-456 U  RETECEDRTEYTHVK----TSLWDNEDSEREELEQE---NRCPE-DY------YPTDGICSPLN---GTLLGGL---CTGQN---KEGNMYLREPLVTQV

                      Consensus  RETEGEEAGMYSHVD----T-----QPCGPEE-EG-------ELEG------KANGGLVDGEV------L--L-----PELPPPLWAPPGKHL--VTEV
```

Kv1.8

```
Q7T199|KCA10_CHICK /462-516 Po  -----VSNFNYFYHR----------ETENEEKQ---------ILPGE----VERILNSVVTGNDSMESLNKTN----GGYPRDKAKK----------
Q16322|KCA10_HUMAN /457-511 Po  -----VSNFNYFYHR----------ETENEEKQ---------NIPGE----IERILNSVGSRMGSTDSLNKTN----GGCSTEKSRK----------
F7HL26|F7HL26_MACMU /457-511 U  -----VSNFNYFYHR----------ETENEEKQ---------NIPSE----IERILNGVGSRMGSTDSLSKTN----GGCSTEKSRK----------
F1N0E8|F1N0E8_BOVIN /458-512 U  -----VSNFNYFYHR----------ETENEEKQ---------SIPGE----INKLLNSAGSRMGSTDSLSKTN----GSCSTEKSRK----------
F7A2P0|F7A2P0_ORNAN /372-418 U  -----VSNFNYFYHR----------ETENEEKQ---------SQQGE----MDRILTT-----GSPQPRKYRD----SSGQGKP----------
H0XQS6|H0XQS6_OTOGA /457-511 U  -----VSNFNYFYHR----------ETENEEKR---------NIPGE----IDKILNSVGSRTGSTDSLTKTN----GGCSTEKSRK----------
H2N6F4|H2N6F4_PONAB /458-512 U  -----VSNFNYFYHR----------ETENEEKQ---------NIPGE----IERILNSVGSRMGSTDSLNKTS----GGCSTEKSRK----------
F6UCT6|F6UCT6_MONDO /458-512 U  -----VSNFNYFYHR----------ETENEEKQ---------NIPGE----TDKLLASVISGMGSTDSLNKTN----GGCSREKSRK----------
G3VP89|G3VP89_SARHA /459-513 U  -----VSNFNYFYHR----------ETENEEKQ---------TIPGE----TDKLLASVISGMGSMDSLSKKN----GSCSGEKSRK----------
I3LK48|I3LK48_PIG /361-415 Unc  -----VSNFNYFYHR----------ETENEEKQ---------IIPGE----IDKILNSVGSRRGSTDSLSKTN----SGCSAEKSRK----------
G1S9E3|G1S9E3_NOMLE /457-511 U  -----VSNFNYFYHR----------ETENEEKQ---------NIPGE----IERILNSVGSRMGSTDSLNKSN----GGCSTKKSRK----------
G3QZB3|G3QZB3_GORGO /457-511 U  -----VSNFNYFYHR----------ETENEEKQ---------NIPGE----IERILNSVGSRMGSTDSLNKTN----GGCSTEKSRK----------
G1QCV0|G1QCV0_MYOLU /458-513 U  -----VSNFNYFYHR----------ETQKEERQK--------NMPQE----INKMAPSVDSRMGSADSLSKTN----GGCSAEPSLE---------
B2RQA1|B2RQA1_MOUSE /457-511 P  -----VSNFNYFYHR----------ETENEEKP---------NIPGE----LDKILNSMGSRMGSTESLNKTN----GSCSAEKSRK----------
```

Shaker

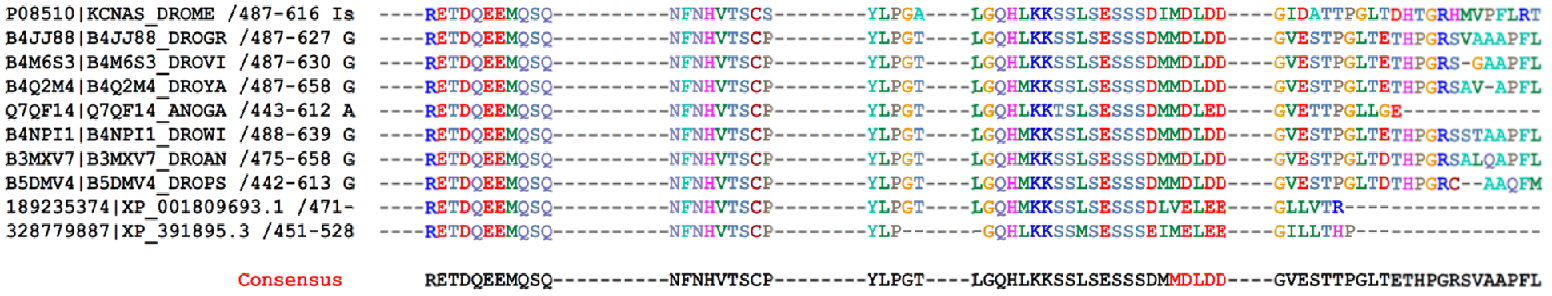

Table S1. FASTA format for Kv1 and Shaker channels. Only the 100 first amino acids which contain full Kv1.1-Kv1.8, but not Shaker, C-terminal domain are depicted for simplicity. Consensus sequences are indicated. The FT element containing the di-acidic motif is highlighted in red. The UniProt number is provided. Species are described in the legend to Supplementary Fig. S4.

3.2.2. Contribution 5:

Published in Journal of Cell Science. 2016 Nov 15;129(22):4265-4277.

The C-terminal domain of Kv1.3 regulates functional interactions with the KCNE4 subunit

Laura Solé[1,2*], Sara R. Roig[1*], Albert Vallejo-Gracia[1], Antonio Serrano-Albarrás[1], Ramón Martínez-Mármol[1,3], Michael M. Tamkun[2] and Antonio Felipe[1].

[1] Molecular Physiology Laboratory, Departament de Bioquı´mica i Biologia Molecular, Institut de Biomedicina (IBUB), Universitat de Barcelona. Barcelona, Spain
[2] Department of Biomedical Sciences, Colorado State University. Fort Collins, USA.
[3] Clem Jones Centre for Ageing Dementia Research, Queensland Brain Institute, The University of Queensland. Brisbane, Australia.

ABSTRACT

Impairment of Kv1.3 expression at the cell membrane in leukocytes and sensory neuron contributes to the pathophysiology of autoimmune diseases and sensory syndromes. Molecular mechanisms underlying Kv1.3 channel trafficking to the plasma membrane remain elusive. We report a novel non-canonical di-acidic signal (E483/484) at the C-terminus of Kv1.3 essential for anterograde transport and surface expression. Notably, homologous motifs are conserved in neuronal Kv1 and Shaker channels. Biochemical analysis revealed interactions with the Sec24 subunit of the coat protein complex II. Disruption of this complex retains the channel at the endoplasmic reticulum. A molecular model of the Kv1.3-Sec24a complex suggests salt-bridges between the di-acidic E483/484 motif in Kv1.3 and the di-basic R750/752 sequence in Sec24. These findings identify a previously unrecognized motif of Kv channels essential for their expression on the cell surface. Our results contribute to our understanding of how Kv1 channels target to the cell membrane, and provide new therapeutic strategies for the treatment of pathological conditions.

Report of the PhD student participation

The C-terminal domain of Kv1.3 regulates functional interactions with the KCNE4 subunit

Published in Journal of Cell Science, Impact Factor (2016): 5.33

Sara Raquel Roig Merino performed dendritic immunofluorescence in figure 1, colocalization images and FRET acceptorphotobleaching experiments in figure 2, western blot quantification in figure 5, and all experimental data from figures 6, 7 and 8

Figures 3, 4 and 5 were included on Laura Solé thesis, previous to the publication of the paper.

Antonio Felipe

PhD thesis director

© 2016. Published by The Company of Biologists Ltd | Journal of Cell Science (2016) 129, 4265-4277 doi:10.1242/jcs.191650

RESEARCH ARTICLE

The C-terminal domain of Kv1.3 regulates functional interactions with the KCNE4 subunit

Laura Solé[1,2,*], Sara R. Roig[1,*], Albert Vallejo-Gracia[1], Antonio Serrano-Albarrás[1], Ramón Martínez-Mármol[1,3], Michael M. Tamkun[2] and Antonio Felipe[1,‡]

ABSTRACT

The voltage-dependent K^+ channel Kv1.3 (also known as KCNA3), which plays crucial roles in leukocytes, physically interacts with KCNE4. This interaction inhibits the K^+ currents because the channel is retained within intracellular compartments. Thus, KCNE subunits are regulators of K^+ channels in the immune system. Although the canonical interactions of KCNE subunits with Kv7 channels are under intensive investigation, the molecular determinants governing the important Kv1.3– KCNE4 association in the immune system are unknown. Our results suggest that the tertiary structure of the C-terminal domain of Kv1.3 is necessary and sufficient for such an interaction. However, this element is apparently not involved in modulating Kv1.3 gating. Furthermore, the KCNE4-dependent intracellular retention of the channel, which negatively affects the activity of Kv1.3, is mediated by two independent and additive mechanisms. First, KCNE4 masks the YMVIEE signature at the C-terminus of Kv1.3, which is crucial for the surface targeting of the channel. Second, we identify a potent endoplasmic reticulum retention motif in KCNE4 that further limits cell surface expression. Our results define specific molecular determinants that play crucial roles in the physiological function of Kv1.3 in leukocytes.

KEY WORDS: Potassium channels, Trafficking, Channelosome, Intracellular retention

INTRODUCTION

Voltage-dependent K^+ (Kv) channels are crucial for the cardiac action potential and propagation of the nerve impulse. In addition, Kv channels play important roles in many cellular processes such as maintenance of the resting membrane potential, regulation of cell volume and proliferation (Hille, 2001). Kv currents present substantial variability and functional versatility in tissues, which is achieved by heterooligomerization and by post-translational modifications that regulate their activity. The Kv1.3 channel (also known as KCNA3), which plays important roles in the immune system response, is not an exception. Kv1.3 controls leukocyte physiology by modulating the membrane potential and driving force for Ca^{2+} entry through Ca^{2+} release-activated Ca^{2+} channels (I_{CRAC}). Indeed, pharmacological blockade of Kv1.3 inhibits the immune response *in vivo*, and aberrant surface expression of Kv1.3 is linked to the development of autoimmune diseases (Chandy et al., 2004). For example, T-effector memory cells from patients with multiple sclerosis and other autoimmune dysfunctions present an elevated number of Kv1.3 channels at the cell membrane (Varga et al., 2010). In addition, systemic lupus erythematosus cells display an abnormal surface distribution of channels (Nicolaou et al., 2007). By contrast, immunosuppression can be related to an impairment of the cell surface expression of Kv1.3 (Villalonga et al., 2010). In summary, the pharmacological regulation of Kv1.3 activity and localization is of enormous clinical interest.

Kv1.3 heterooligomeric associations also modulate physiological responses by governing both the number and the spatial distribution of surface channels (Vicente et al., 2008). Assembly with Kv1.5 (also known as KCNA5) modulates channel behavior, and heterotetrameric channels with different stoichiometries might form in mononuclear phagocytes, such as macrophages and dendritic cells, thereby fine-tuning cellular responses (Felipe et al., 2010). In addition, co-assembly with accessory subunits, such as Kvβ (also known as KCNAB) or KCNE subunits, generates further functional diversity that affects both channel gating kinetics and trafficking (Sole et al., 2009; Vicente et al., 2005). In this context, KCNE4 efficiently regulates Kv1.3 activity by promoting its retention within the endoplasmic reticulum (ER), thereby impairing its surface expression (Sole et al., 2009). Specifically, KCNE4, which is present in the immune system, might act as a very powerful dominant-negative regulatory subunit of Kv1.3 channels in leukocytes (Sole and Felipe, 2010). Although the T1 domain of the channel, located at the N-terminus, is the molecular determinant involved in the interaction with Kvβ subunits (Gulbis et al., 2000), nothing is known about the domains involved in this physiologically relevant Kv1.3–KCNE4 association, which, by controlling channel surface expression, could have an enormous influence on the immunological response.

KCNE subunits are single-transmembrane-domain proteins that canonically associate with Kv7 channels (McCrossan and Abbott, 2004). KCNE4 is the most divergent member of the KCNE family (KCNE1–KCNE5) and plays a dominant-negative role for numerous K^+ channels, such as Kv7.1 (KCNQ1), Kv1.1 (KCNA1), Kv1.3, Kv4.2 (KCND2) and $K_{Ca}1.1$ (KCNMA1) (McCrossan and Abbott, 2004). Although residues from the S6 domain of Kv7.1 are necessary for KCNE4-dependent inhibition of channel gating, the physical association itself involves the Kv7.1 channel C-terminus (Vanoye et al., 2009). Structural features are quite different among different K^+ channel families, and surprisingly, no studies have addressed the interactions of KCNE4 with other K^+ channels. Because KCNE4 exerts important influences over Kv1.3 that could modulate the immune response (Sole et al., 2009), we aimed to decipher the molecular determinants

[1]Molecular Physiology Laboratory, Departament de Bioquímica i Biomedicina Molecular, Institut de Biomedicina (IBUB), Universitat de Barcelona, Avda. Diagonal 643, Barcelona 08028, Spain. [2]Department of Biomedical Sciences, Colorado State University, Fort Collins, CO 80523, USA. [3]Clem Jones Centre for Ageing Dementia Research, Queensland Brain Institute, The University of Queensland, Brisbane, Queensland 4072, Australia.
*These authors contributed equally to this work

‡Author for correspondence (afelipe@ub.edu)

A.F., 0000-0002-7294-6431

Received 30 April 2016; Accepted 29 September 2016

Journal of Cell Science

Journal of Cell Science (2016) 129, 4265-4277 doi:10.1242/jcs.191650

in Kv1.3 that are involved in the association with KCNE4. Our data suggest that the tertiary topology of the C-terminal domain of Kv1.3 is the structural element responsible for the interaction with KCNE4. Although this domain is sufficient to transfer the physical association capability to other Kv channels, such as Kv1.5, it is not involved in the control of the Kv1.3 gating. A major consequence of this association is the decrease in functional channels at the surface owing to massive intracellular retention. In this context, we demonstrate that KCNE4 masks the recently identified forward di-acidic trafficking motif at the C-terminus of Kv1.3, thereby impairing the plasma membrane targeting. In addition, an ER retention motif in KCNE4 further participates in the intracellular retention of the Kv1.3–KCNE4 complex, which, in turn, can alter the immunological response.

RESULTS

Kv1.3 and KCNE4 associate in CY15 dendritic cells

Kv1.3 and KCNE4 are present in leukocytes, and KCNE4 modulates the surface expression of the functional complex at the plasma membrane (Sole et al., 2009). Therefore, we first investigated whether a functional heterooligomeric complex is present in immune system cells. Leukocytes, which express a limited repertoire of K^+ channels, exhibit important differences among cell lineages. Therefore, we analyzed the voltage-dependent K^+ currents in both Jurkat T-cells and CY15 dendritic cells (Fig. 1A–D). Depolarizing pulses elicited K^+ currents that resembled those from Kv1.3 channels in Jurkat T-cells and CY15 cells (Fig. 1A,B), although both cell types slightly differed in the slow C-type inactivation. To elucidate whether these macroscopic currents were indeed conducted by Kv1.3, biophysical and pharmacological properties, such as the cumulative inactivation and the inhibition by margatoxin (MgTx), were analyzed. Cumulative inactivation was obtained by applying a train of 15 depolarizing voltage steps of 250 ms from −80 to +60 mV once every second (Fig. 1C,D). We found that K^+ currents were sensitive to MgTx in both cell lines (Fig. 1E). Thus K^+ currents in T-lymphocytes and dendritic cells are indeed mostly conducted by Kv1.3. However, Kv currents in CY15 dendritic cells showed less cumulative inactivation than in T-lymphocytes (34±2% and 66±8%, mean±s.e.m., respectively). In addition, 1 and 10 nM MgTx

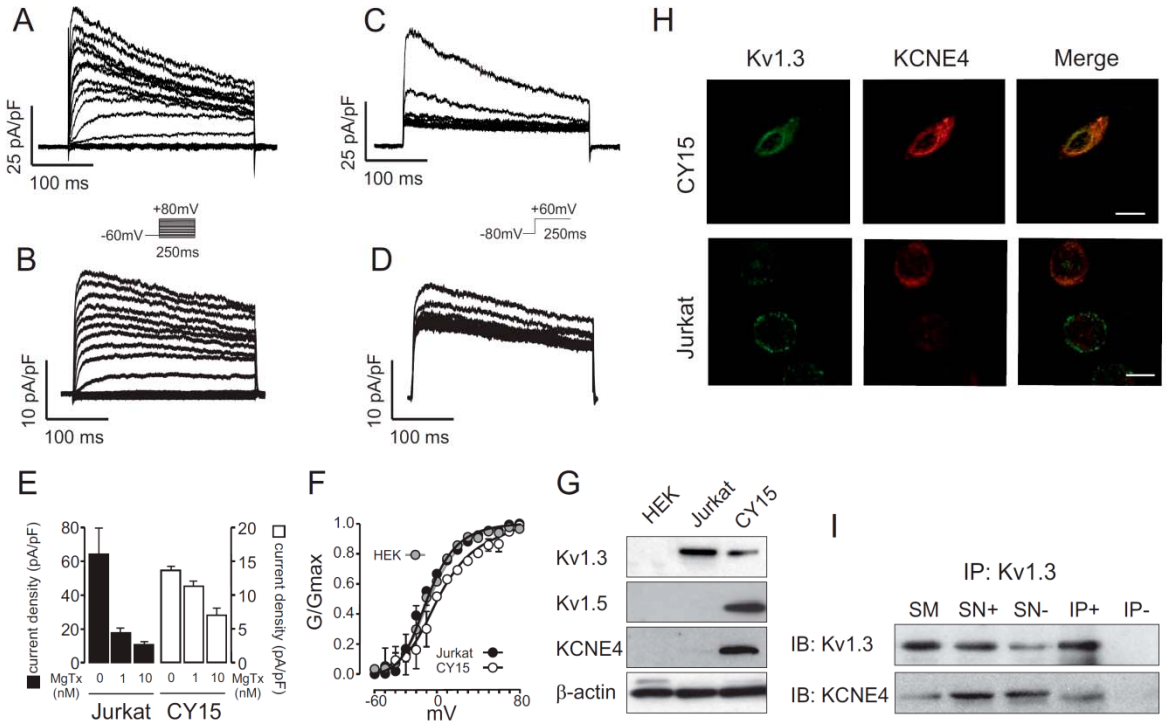

Fig. 1. Kv1.3 and KCNE4 form functional channels in leukocytes. Endogenous expression of Kv1.3 and KCNE4 was analyzed in human Jurkat T-lymphocytes and mouse CY15 dendritic cells. Endogenous voltage-dependent K^+ currents were elicited in Jurkat (A) and CY15 cells (B). Cells were held at −60 mV, and pulse potentials were applied as indicated. Cumulative inactivation of K^+ currents was elicited in Jurkat (C) and CY15 cells (D) by a train of 15 depolarizing 250 ms pulses ranging from −80 mV to +60 mV once every 1 s. (E) K^+ currents elicited in Jurkat (left axis) and CY15 cells (right axis) at the peak current density (+80 mV) in the presence or the absence of 1 and 10 nM MgTx. Black bars, Jurkat T-cells; white bars, CY15 dendritic cells. Values are shown as the mean±s.e.m. (n=6–8 cells/group). (F) Steady-state activation of outward K^+ currents. Gray circles, HEK-293 cells transfected with Kv1.3; black circles, Jurkat cells; white circles, CY15 cells. Values are shown as the mean±s.e.m. (n=4–6 independent cells). (G) Protein expression of Kv1.3, Kv1.5 and KCNE4 in leukocytes as determined by western blotting. HEK-293 cells were used as a negative control. Notably, although Jurkat and CY15 dendritic cells express both Kv1.3 and KCNE4, the abundance of KCNE4 and Kv1.5 is much lower in T-cells and was barely detected. (H) Representative confocal images of Kv1.3 and KCNE4 in Jurkat T-lymphocytes and CY15 dendritic cells. Scale bars: 10 µm. (I) KCNE4 co-immunoprecipitates with Kv1.3 in dendritic cells. Western blots from Kv1.3 and KCNE4 co-immunoprecipitation. Lysates were immunoprecipitated for Kv1.3 (IP: Kv1.3). Upper panel: Kv1.3 immunoblot (IB: Kv1.3). Lower panel: KCNE4 immunoblot (IB: KCNE4). SM, starting material (input); IP+, immunoprecipitation in the presence of the anti-Kv1.3 antibody; IP−, immunoprecipitation in the absence of the anti-Kv1.3 antibody; SN+, supernatant from the IP+; SN−, supernatant from the IP−.

Journal of Cell Science (2016) 129, 4265-4277 doi:10.1242/jcs.191650

inhibited Kv currents in Jurkat lymphocytes (72±7% and 83±4%, respectively) more potently than in CY15 cells (17±8% and 49±7%, respectively). Steady-state activation indicated that whereas Jurkat T-cells displayed a similar $V_{0.5}$ (voltage for half maximal activation) to HEK-293 cells transfected with Kv1.3 (−11.9±1.9 and −15.1±2.3 mV, mean±s.e.m., respectively), the half-activation voltage shifted to depolarizing potentials in CY15 cells (0.20±3.3 mV) (Fig. 1F). Other mononuclear phagocytes, such as macrophages, exhibit similar biophysical and pharmacological alterations owing to the presence of heterotetrameric Kv1.3–Kv1.5 channels (Villalonga et al., 2007). Indeed, unlike Jurkat T-lymphocytes, but similar to human dendritic cells (Zsiros et al., 2009), mouse CY15 cells express Kv1.5 (Fig. 1G). Furthermore, although Jurkat and CY15 cells both had substantial levels of Kv1.3, the amount of KCNE4 was much higher in dendritic cells (Fig. 1G). Further immunocytochemistry studies showed that Kv1.3 and KCNE4 colocalized in Jurkat T-cells to a lesser extent. Furthermore, unlike in T-cells, Kv1.3 was mostly retained intracellularly in CY15 cells (Fig. 1H). Our results suggest that, unlike in Jurkat cells, when the expression of KCNE4 is abundant in dendritic cells, Kv1.3 remains mostly intracellularly, further supporting observations from HEK-293 cells and Raw 264.7 macrophages (Sole et al., 2009). To gain insight regarding whether a Kv1.3–KCNE4 association might participate in this phenotype, we performed co-immunoprecipitation studies that demonstrated, for the first time, that Kv1.3 and KCNE4 interact in CY15 dendritic cells (Fig. 1I).

Our data indicate that Kv1.3 and KCNE4 form oligomeric channels in leukocytes. This association alters the channel behavior, thereby leading to physiological consequences. To explore the molecular determinants involved in the Kv1.3–KCNE4 interaction, we further validated and extended our results in HEK-293 cells (Fig. 2). As previously reported (Sole et al., 2009), KCNE4 inhibits Kv1.3 currents when expressed in HEK-293 cells, and this is associated with an intracellular retention of the channel. Although Kv1.3 was efficiently targeted to the membrane surface, KCNE4, similar to Kv1.5, exhibited a marked intracellular phenotype (Fig. 2A–C). As mentioned above, the presence of KCNE4 caused the intracellular retention of Kv1.3 (Fig. 2D). However, although Kv1.5 and KCNE4 shared an intracellular location, their colocalization was clearly minor (Fig. 2E). Kv1.5 and KCNE4 are present in macrophages and dendritic cells, and whether these two subunits associate is an open debate. Grunnet et al. (2003) have demonstrated that KCNE4 does not modulate Kv1.5, whereas Abbott and co-workers (Crump et al., 2016) found a Kv1.5–KCNE4 association relevant to heart physiology. To elucidate this issue, we elicited voltage-dependent K^+ currents in HEK-293 cells transfected with Kv1.3 and Kv1.5 in the presence or the absence of KCNE4 (Fig. 2F–I). In line with what we and others previously found (Grunnet et al., 2003), the presence of KCNE4 inhibited Kv1.3 but did not modulate Kv1.5 (Fig. 2J). To further explore any putative association, we assessed fluorescence resonance energy transfer (FRET) for Kv1.3 and Kv1.5 with KCNE4 in HEK-293 cells under the same conditions (Fig. 2K). Our results show that although Kv1.3 and KCNE4 triggered significant positive values, indicating a molecular association, the co-expression of Kv1.5 and KCNE4 produced no significant energy transfer, further supporting the electrophysiological (Fig. 2H,I) and confocal (Fig. 2E) studies. Our results indicate that, in our conditions, as in similar previous observations in oocytes (Grunnet et al., 2003), there is no association between KCNE4 and Kv1.5 in HEK-293 cells. This was further confirmed by co-immunoprecipitation experiments (see below).

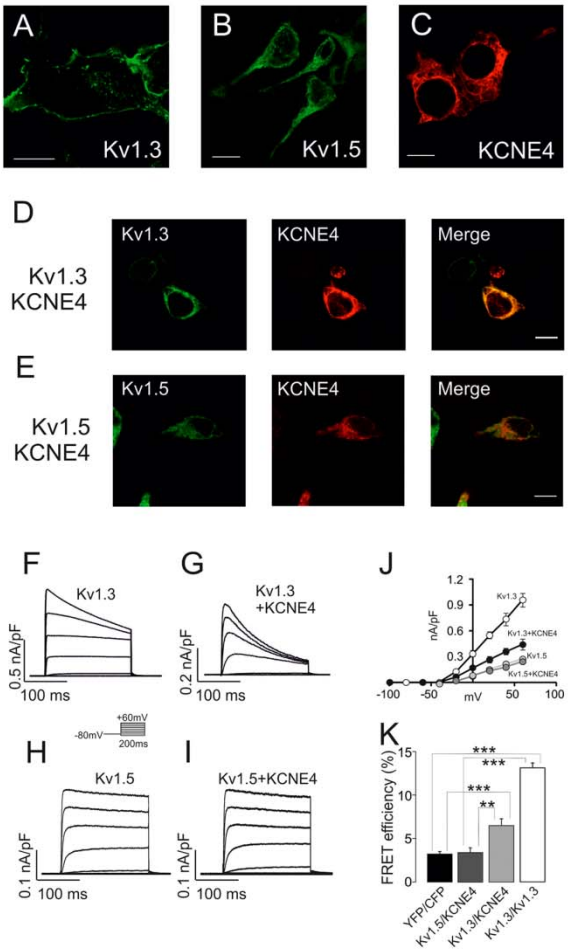

Fig. 2. Kv1.3, but not Kv1.5, associates with KCNE4 in HEK-293 cells. KCNE4 modulates Kv1.3 trafficking and activity. HEK-293 cells were transfected with Kv1.3–YFP or Kv1.5–YFP in the presence or absence of KCNE4–CFP. Confocal images of (A) Kv1.3–YFP, (B) Kv1.5–YFP and (C) KCNE4–CFP. (D) HEK-293 cells co-transfected with Kv1.3 and KCNE4. (E) Kv1.5 and KCNE4. Color code: green, channels; red, KCNE4; yellow in merge panels shows colocalization. Scale bars: 10 µm. Voltage-dependent K^+ currents were elicited in HEK-293 cells transfected with Kv1.3 (F,G) and Kv1.5 (H,I) in the absence (F,H) or the presence (G,I) of KCNE4. Cells were held at −80 mV, and pulse potentials were applied as indicated. (J) Current density versus voltage plot of outward K^+ currents. White circles, Kv1.3; black circles, Kv1.3+KCNE4; light gray circles, Kv1.5; dark gray circles, Kv1.5+KCNE4. Values are shown as the mean±s.e.m. (n=6–10 independent cells). (K) Molecular association of Kv1.3 and Kv1.5 with KCNE4 as measured by FRET efficiency (%). HEK-293 cells were transfected with Kv1.3–YFP and Kv1.5–YFP in the presence of KCNE4–CFP. YFP–CFP and Kv1.3–YFP or Kv1.3–CFP were used as negative and positive controls, respectively. Values are shown as the mean±s.e.m. (n>25 independent cells). $^{**}P$<0.01; $^{***}P$<0.001 (Student's t-test).

The C-terminus of Kv1.3 is required for KCNE4 association

Our data show that KCNE4 controls the channel behavior of Kv1.3 but not of Kv1.5. However, the structural motifs involved in this association are completely unknown. We first checked whether the intracellular N- and C-terminal domains of Kv1.3 are involved in the KCNE4 association. To that end, we constructed mutant

Journal of Cell Science (2016) 129, 4265-4277 doi:10.1242/jcs.191650

channels lacking the N-terminus (Kv1.3ΔN) or the C-terminus (Kv1.3ΔC) of Kv1.3 (Fig. S1A,B). Because KCNE4 alters the cellular distribution of Kv1.3 in HEK-293 (Fig. 2D) and dendritic cells (Fig. 1H), we wondered whether the trafficking of Kv1.3 mutants was altered in the presence of KCNE4. Unlike wild-type Kv1.3 (Kv1.3 wt; Fig. 2A), Kv1.3ΔN and Kv1.3ΔC showed a markedly intracellular distribution (Fig. S1A,B) in the absence of KCNE4. Whereas KCNE4 triggered an important intracellular retention of Kv1.3 wt (Fig. 3A–C), the distribution of Kv1.3ΔN (Fig. 3D–F) and Kv1.3ΔC (Fig. 3G–I) was not apparently altered. However, an extensive pixel-by-pixel analysis illustrated that, although there was not a significant decrease in the colocalization of Kv1.3ΔN versus Kv1.3 wt with KCNE4, Kv1.3ΔC–KCNE4 colocalization decreased by ~26% (P<0.001 versus Kv1.3, n=25) (Fig. 3J). To further decipher which Kv1.3 domain was involved in the KCNE4 association, co-immunoprecipitation experiments were performed in HEK-293 cells co-transfected with KCNE4 in the presence of Kv1.3, Kv1.3ΔN and Kv1.3ΔC (Fig. 3K,L). KCNE4 co-immunoprecipitated with Kv1.3 (Fig. 3K, bottom panel) and with Kv1.3ΔN (Fig. 3L, bottom panel) but not with Kv1.3ΔC (Fig. 3L, bottom panel). These results suggest that the C-terminal domain of Kv1.3 is required for interaction with KCNE4.

The removal of important intracellular domains, such as the N- and C-termini, triggers major structural changes and impairs the trafficking of Kv1.3 (Martinez-Marmol et al., 2013). Therefore, we further analyzed the involvement of the Kv1.3 C-terminal domain in the KCNE4 interaction by using chimeric Kv1.3–Kv1.5 channels. We used Kv1.5 because this channel, which is also expressed in macrophages and dendritic cells, is not associated with KCNE4 (Grunnet et al., 2003; Vicente et al., 2006; Zsiros et al., 2009, and see Fig. 2). Chimeric channels were obtained by replacing the N- and C-terminal domains of Kv1.5 with those of Kv1.3 (Kv1.3NKv1.5 and Kv1.3CKv1.5, respectively) and vice versa. We first studied the cellular distribution of the chimeras (Fig. S1C–F). Similar to Kv1.3 wt (Fig. 4A–C), the targeting of the Kv1.3NKv1.5 chimera to the plasma membrane was impaired by the presence of KCNE4

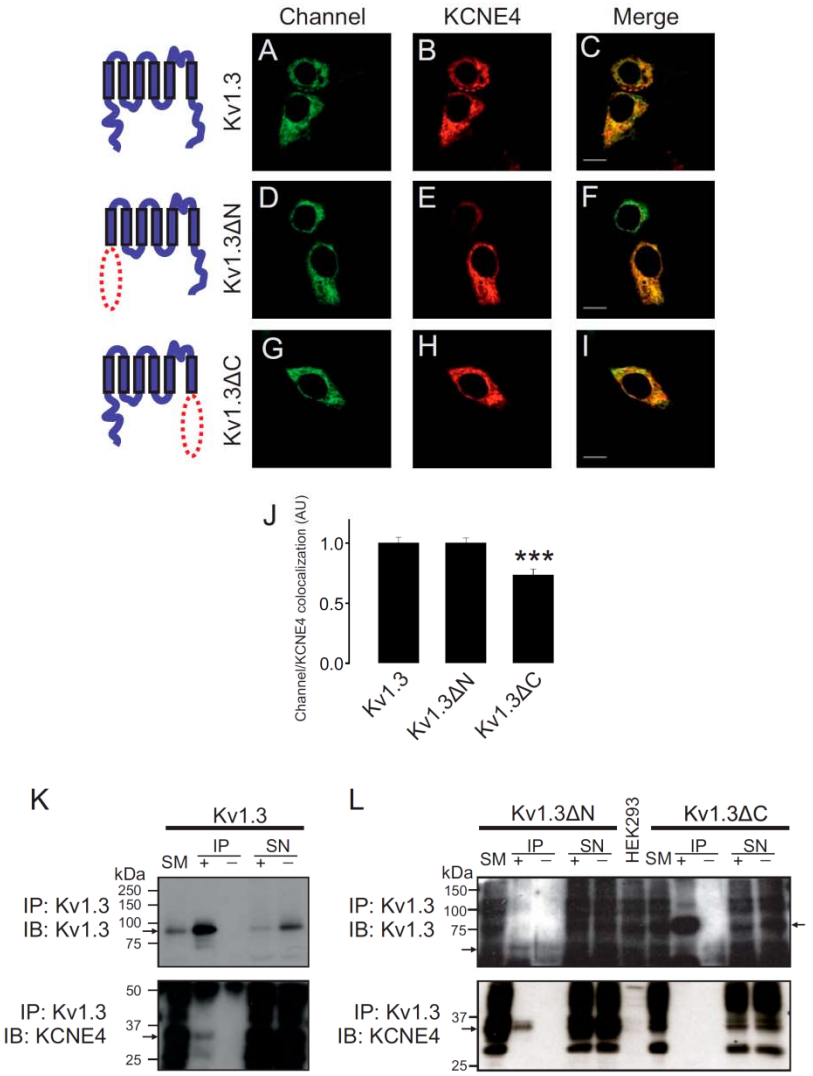

Fig. 3. KCNE4 associates with the Kv1.3 C-terminal domain. HEK-293 cells were transfected with Kv1.3–YFP channels and KCNE4. (A–I) Confocal images from HEK-293 cells transfected with wt and mutant Kv1.3–YFP channels and KCNE4–CFP. (A,D,G) Kv1.3–YFP, Kv1.3ΔN–YFP and Kv1.3ΔC–YFP channels in green. (B,E,H) Cellular distribution of KCNE4–CFP in red. (C,F,I) Merged images show colocalization in yellow. Scale bars: 10 µm. Note that in all cases, Kv1.3 is mostly intracellular. Representative cartoons of different Kv1.3 channels are shown at the left of their respective images. The red dotted ellipse highlights the deleted domain. (J) Histogram representing the relative colocalization between Kv1.3 channels and KCNE4. Results in arbitrary units (A.U.) are the mean±s.e.m. of a pixel-by-pixel analysis on 25–40 cells. ***P<0.001 vs Kv1.3 (Student's t-test). (K,L) Representative western blots from Kv1.3–YFP, Kv1.3ΔN–YFP and Kv1.3ΔC–YFP co-immunoprecipitation. (K) Kv1.3–YFP immunoprecipitation against GFP (IP: Kv1.3). Upper panel: GFP immunoblot (IB: Kv1.3). Lower panel: KCNE4–HA immunoblot (IB: KCNE4). Kv1.3–YFP and KCNE4–HA are indicated with arrows. (L) Immunoprecipitation against GFP for Kv1.3ΔN–YFP (left side) and Kv1.3ΔC–YFP (right side). The top panel corresponds to the immunoblotting against GFP (IB: Kv1.3), in which Kv1.3ΔN–YFP and Kv1.3ΔC–YFP are indicated by arrows. The bottom panel represents immunoblotting against KCNE4–HA (IB: KCNE4). KCNE4–HA is indicated with an arrow. SM, starting material (input); IP+, immunoprecipitation in the presence of the anti-GFP antibody; IP–, immunoprecipitation in the absence of the anti-GFP antibody; SN+, supernatant from the IP+; SN–, supernatant from the IP–. Note that the anti-GFP antibody used recognizes YFP.

Journal of Cell Science (2016) 129, 4265-4277 doi:10.1242/jcs.191650

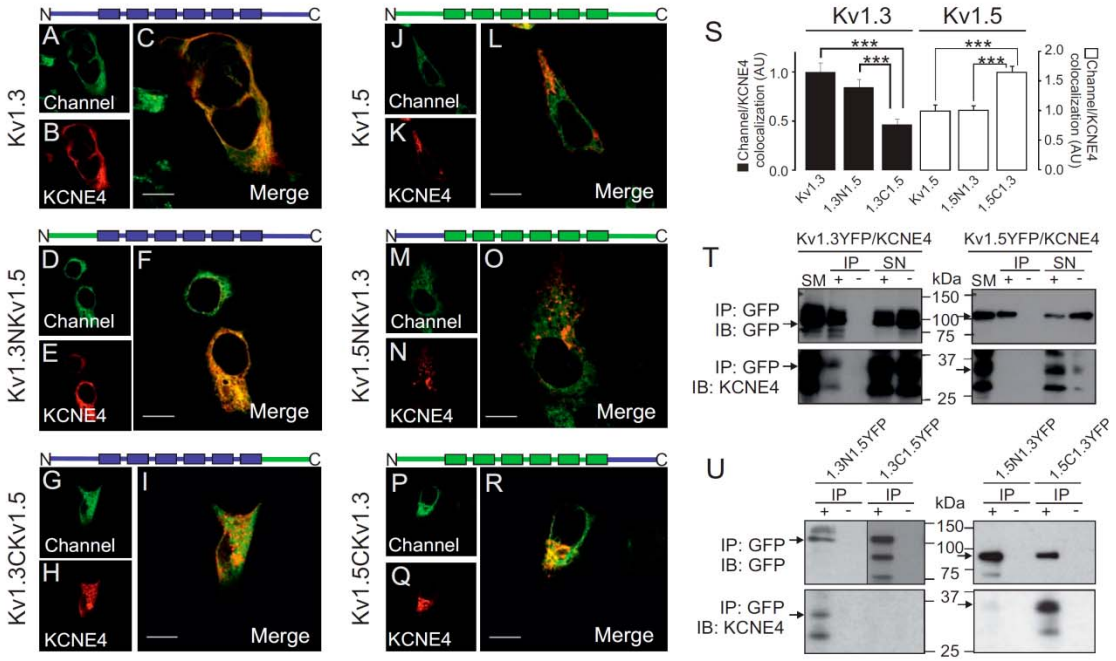

Fig. 4. The C-terminus of Kv1.3, but not Kv1.5, is necessary and sufficient for the association with KCNE4. Confocal images from HEK-293 cells transfected with Kv1.3–YFP (A–C), Kv1.3NKv1.5–YFP (D–F) and Kv1.3CKv1.5–YFP (G–I) in the presence of KCNE4–CFP. All Kv1.3 channels presented an intracellular distribution, but the colocalization of Kv1.3CKv1.5 with KCNE4–CFP is 40% lower than that with Kv1.3 or Kv1.3NKv1.5. HEK-293 cells were also transfected with Kv1.5–YFP (J–L), Kv1.5NKv1.3 (M–O) and Kv1.5CKv1.3 (P–R) in the presence of KCNE4. Although all Kv1.5 channels were distributed intracellularly, notable colocalization was only observed between KCNE4 and Kv1.5CKv1.3. Cartoons on top of panels represent chimeric channels with the N- and C-terminal domains, and six transmembrane domains (boxes). Blue, Kv1.3 domains; green, Kv1.5 domains. Color code in confocal images: green, channels; red, KCNE4; yellow, colocalization in merge panels. Scale bars: 10 µm. (S) Histogram representing the relative colocalization between Kv1.3 and Kv1.5 channels and chimeras and KCNE4. Results are mean±s.e.m. (n=25–30 independent cells). Black columns represent Kv1.3 and Kv1.3–Kv1.5 chimeras (1.3N1.5 and 1.3C1.5). White columns represent Kv1.5 and Kv1.5–Kv1.3 chimeras (1.5N1.3 and 1.5C1.3). ***P<0.001 (Student's t-test). (T) Western blots for Kv1.3–YFP and Kv1.5–YFP with KCNE4–HA co-immunoprecipitation. Left panels: Kv1.3–YFP immunoprecipitation against GFP (IP: GFP). Right panels: Kv1.5–YFP immunoprecipitation against GFP (IP: GFP). Upper panels: Kv1.3–YFP and Kv1.5–YFP immunoblots (IB: GFP). Lower panels: KCNE4–HA immunoblots (IB: KCNE4). YFP channels and KCNE4–HA are marked with arrows. (U) Western blots for Kv1.3–Kv1.5–YFP and Kv1.5–Kv1.3–YFP chimeras with KCNE4–HA co-immunoprecipitation. Left panels: immunoprecipitation against GFP of Kv1.3NKv1.5–YFP and Kv1.3CKv1.5–YFP (IP: GFP). Right panels: immunoprecipitation against GFP for Kv1.5NKv1.3–YFP and Kv1.5CKv1.3–YFP (IP: GFP). Top panels correspond to the immunoblotting against Kv1.3 and Kv1.5 chimeras (IB: GFP), where channels are denoted by an arrow. Bottom panels correspond to the immunoblotting against KCNE4–HA (IB: KCNE4). KCNE4–HA is marked with an arrow, and co-immunoprecipitates with Kv1.3NKv1.5–YFP and Kv1.5CKv1.3–YFP. SM, starting material (input); IP+, immunoprecipitation in the presence of the anti-GFP antibody; IP–, immunoprecipitation in the absence of the anti-GFP antibody; SN+, supernatant from the IP+; SN–, supernatant from the IP–. Note that the anti-GFP antibody used recognizes YFP.

(Fig. 4D–F). KCNE4 and Kv1.3CKv1.5 both showed intracellular retention, but their distribution patterns were different (Fig. 4G–I). A pixel-by-pixel analysis (Fig. 4S) showed that Kv1.3CKv1.5 colocalization with KCNE4 was reduced by more than 50% compared to Kv1.3 wt (P<0.001, Student's t-test, n=30).

Although the C-terminus of Kv1.3 is required for the KCNE4 interaction, we next wanted to know whether this domain was sufficient for the association with the regulatory subunit. We generated Kv1.5 chimeras where the N- or C-terminus was replaced with the corresponding domain from Kv1.3 (Kv1.5NKv1.3 and Kv1.5CKv1.3, respectively). Kv1.5 and both the Kv1.5–Kv1.3 chimeras presented a low level of cell surface targeting both with and without KCNE4 (Fig. 4J–R; Fig. S1E,F, respectively). However, Kv1.5CKv1.3 showed higher colocalization with KCNE4 than Kv1.5NKv1.3 or Kv1.5 wt (P<0.001 vs Kv1.5 +KCNE4, n=30) (Fig. 4S). This higher colocalization suggests that the C-terminus of Kv1.3 is both necessary and sufficient for the interaction with KCNE4.

To further address the role of the Kv1.3 C-terminus in the interaction with KCNE4, we performed co-immunoprecipitation experiments. Unlike Kv1.3 (Fig. 4T, left panels), Kv1.5 did not co-immunoprecipitate with KCNE4 (Fig. 4T, right panels). Although Kv1.3NKv1.5 co-immunoprecipitated with KCNE4, no significant co-immunoprecipitation of Kv1.3CKv1.5 with KCNE4 was observed (Fig. 4U, left panels). Furthermore, KCNE4 co-immunoprecipitated with Kv1.5CKv1.3 but not with either Kv1.5NKv1.3 or Kv1.5 (Fig. 4T,U, right panels). Thus, both the intracellular localization and the immunoprecipitation results support a role for the C-terminal domain of Kv1.3 in the association with KCNE4.

The C-terminal domain of Kv1.3 is not involved in modulating the Kv1.3 current density

Evidence collected during almost two decades suggests that structural domains implicated in the canonical interactions of Kv7 channels with KCNE peptides are not related to the modulation of

Journal of Cell Science (2016) 129, 4265-4277 doi:10.1242/jcs.191650

gating, although this area is still under intensive investigation (Liin et al., 2015; Wrobel et al., 2012). Because Kv1.3 is structurally different from Kv7 channels, we investigated whether the C-terminus-based association between Kv1.3 and KCNE4 modulated the channel current density. To that end, we performed patch-clamp experiments using HEK-293 cells transfected with Kv1.3, Kv1.5 and the Kv1.3–Kv1.5 chimeras in the presence and the absence of KCNE4 (Fig. S2). KCNE4 inhibited Kv1.3 and Kv1.3NKv1.5 currents by ∼50%. However, as previously described (Grunnet et al., 2003), K^+ currents from Kv1.5 were not affected (see also Fig. 2J–I). Similarly, the Kv1.3CKv1.5 chimera and the other Kv1.5 constructs containing Kv1.3 intracellular domains (Kv1.5NKv1.3 and Kv1.5CKv1.3) were also not inhibited by the presence of KCNE4. Considering that Kv1.5CKv1.3 efficiently co-immunoprecipitated with KCNE4 (Fig. 4U), our data suggest that the C-terminal domain of the Kv1.3 physically interacts with KCNE4 but does not cause an alteration of the current density. Therefore, similar to Kv7 channels, additional research is required to fully understand the mechanism underlying channel modulation.

The structural conformation of the Kv1.3 C-terminal domain is responsible for the association with KCNE4

To gain further insights about the C-terminal Kv1.3 motif implicated in the KCNE4 interaction, we generated Kv1.3 mutants with stop codons sequentially introduced (Fig. 5). Fig. 5A shows a schematic representation of the truncated Kv1.3

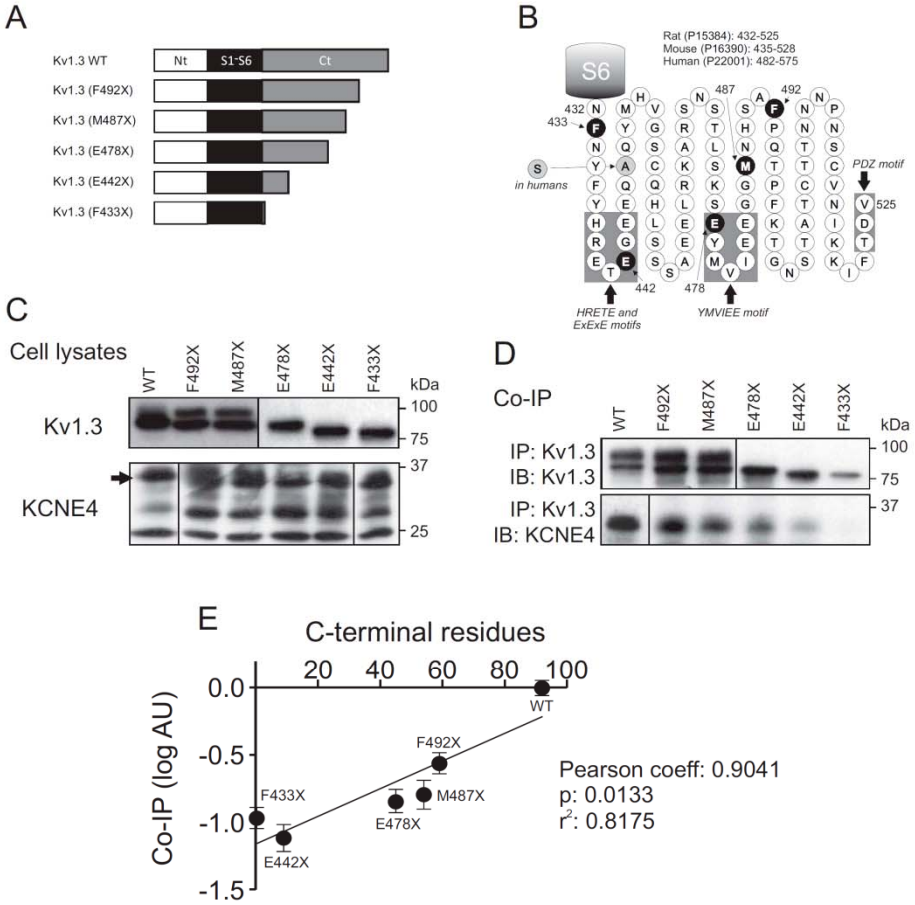

Fig. 5. The structure of the Kv1.3 C-terminal domain mediates the association with KCNE4. HEK-293 cells were transfected with Kv1.3 wt, various Kv1.3 truncated mutants and KCNE4. (A) Scheme representing Kv1.3 wt and the different C-terminus truncation mutants. Bars indicate the N-terminus in white (Nt), the S1–S6 transmembrane domains in black and the C-terminal domain in gray (Ct). (B) Schematic diagram of the Kv1.3 C-terminal domain highlighting some important forward trafficking signatures and the distal PDZ motif. The residues in black indicate the truncations. A unique change (A to S) between human and rodents is indicated in gray. The S6 transmembrane domain is represented as a gray barrel. The HRETE, ExExE, YMVIEE and the PDZ motifs are indicated by gray boxes. The SwissProt number, as well as the number of residues in the C-terminus, for rat, mouse and humans is also indicated. (C) Cell lysates. Immunoprecipitation of Kv1.3–YFP C-terminus mutants with anti-GFP antibody. Top panels show the immunoblot against GFP (Kv1.3). Bottom panels show the immunoblot against KCNE4 (arrow). (D) Co-immunoprecipitation (Co-IP). Cell lysates (as in C) were immunoprecipitated with anti-GFP antibody (IP Kv1.3) and immunoblotted against Kv1.3 (IB: Kv1.3, top panel) and KCNE4 (IP: KCNE4, bottom panel). Note that the anti-GFP antibody used recognizes YFP. (E) Plot of the remaining number of C-terminal residues in the Kv1.3 C-terminus truncated mutants versus the co-immunoprecipitation of KCNE4. Values (mean±s.e.m., n=4) are calculated as the logarithm (log) of co-immunoprecipitation in arbitrary units (AU) standardized to the maximum level (scored as 1) of the co-immunoprecipitation of KCNE4 with Kv1.3 wt from D. Values followed a notable linear correlation (r^2=0.8175) which yielded a statistical significant (P=0.0133) Pearson's coefficient (0.9041).

channels. Fig. 5B shows the C-terminus of Kv1.3, highlighting the mutations and the main forward trafficking and associative motifs. As previously described (Martinez-Marmol et al., 2013), the progressive removal of residues from the Kv1.3 C-terminus yielded proteins that gradually decreased in size and that displayed altered glycosylation (Fig. 5C,D). Co-immunoprecipitation analysis of the channels in the presence of KCNE4 demonstrated that the association of KCNE4 with Kv1.3 decreased concomitantly with increasingly severe truncations of the C-terminal domain (Fig. 5C,D). Our results indicate that no specific region of the Kv1.3 C-terminus is involved in the KCNE4 interaction. Instead, the shorter the C-terminus, the greater the reduction in KCNE4 co-immunoprecipitation that was observed (Fig. 5E). The correlation was notable (r^2=0.8175), yielding a Pearson coefficient of 0.9041, which is statistically significant (P=0.0133). Therefore, our data suggest that rather than a specific motif, the conformational tertiary structure of the Kv1.3 C-terminal domain is responsible for the KCNE4 association.

Structural motifs responsible for the KCNE4-mediated Kv1.3 ER retention

The binding of KCNE4 to Kv1.3 triggers massive ER retention that, in turn, downregulates cell surface expression (Sole et al., 2009). Our data indicate that KCNE4 interacts with Kv1.3 through the structural conformation of its C-terminal domain. This region contains several forward trafficking elements, including the potent YMVIEE motif (Fig. 5B), which is crucial in the COPII-dependent forward trafficking of Kv1.3 to the cell surface (Martinez-Marmol et al., 2013). Therefore, we wondered whether the KCNE4 interaction impairs these events. In fact, KCNE4 hindered the interaction of Sec24D, an element of the COPII machinery, with Kv1.3 (Fig. 6). In the presence of Sar1(H79G), which leads to the retention of the channel in the ER due to constitutively active GTPase activity, Kv1.3 co-immunoprecipitated with Sec24D. KCNE4, which also causes localization of Kv1.3 to the ER, impeded this association (Fig. 6A,B). To further analyze this mechanism, we performed FRET experiments addressing the potential interaction between Kv1.3 and Sec24D (Fig. 6C–G). Kv1.3 colocalized with KCNE4 and Sec24D in discrete locations. Staining for the three proteins identified two (positive and negative) FRET region of interest (ROI) populations, increasing the variability of the results (Fig. 6G). However, elevated levels of KCNE4 correlated with negative FRET values for Kv1.3 and Sec24D in discrete ROIs (Fig. 6H). This indicates that the Kv1.3–Sec24D interaction decreased when KCNE4 was abundant. Our results suggest that KCNE4 and Sec24 competed for the association with Kv1.3, further supporting the idea that the C-terminal domain of the channel is involved in that interaction.

To gain insights into whether the KCNE4 masking of the YMVIEE motif at the C-terminal domain of Kv1.3 was entirely responsible for the observed ER retention, we analyzed the intracellular localization of a Kv1.3 mutant, in which residues E483 and E484 had both been replaced with I (hereafter referred to as $E^{483/484}I$), and which exhibits poor cell membrane targeting due to an impaired association with COPII (Martinez-Marmol et al., 2013). KCNE4 was co-expressed with Kv1.3 wt and Kv1.3 ($E^{483/484}I$) channels (Fig. 7). Whereas KCNE4 retained the Kv1.3 wt intracellularly (Fig. 7A–G), KCNE4 did not alter the intracellular expression pattern of Kv1.3 ($E^{483/484}I$) (Fig. 7H–N). However, the surface expression analysis indicated that KCNE4 triggered a stronger ER retention of both Kv1.3 and Kv1.3 ($E^{483/484}I$) channels than upon mutating the Kv1.3 forward trafficking motif alone (Fig. 7O). Therefore, other ER retention motifs (ERRMs) within KCNE4 might be involved in preventing forward trafficking of Kv1.3. Basic elements, such as RxR and KKxx, are important ERRMs (Gao et al., 2014; Zerangue et al., 1999), and KCNE4 does contain a positively charged signature (K^{110}SKRREKKSS^{119}) within its C-terminal domain (Fig. 8A). Thus, we investigated whether this motif further enhances ER retention of the Kv1.3–KCNE4 channelosome. We mutated several basic residues of the ERRM signature to alanine residues in order to disrupt putative canonical and recurrent signals (Fig. 8A). When expressed alone, the KCNE4 (KSAAREAKSS) mutant [denoted KCNE4(ERRM)] showed twice the cell surface targeting observed with the wt KCNE4 (Fig. 8B–G,P). In addition, when Kv1.3 was co-expressed with KCNE4(ERRM), the channel reached the membrane more efficiently than with KCNE4 wt (Fig. 8H–O). These data are summarized in Fig. 8P. Thus, it appears that KCNE4 retains the Kv1.3 channelosome within the cell by two independent, but complementary, mechanisms: (1) through a KCNE4 interaction with the C-terminus of Kv1.3, which hinders the di-acidic forward trafficking signature, and (2) by providing potent ERRMs to the complex.

DISCUSSION

KCNE4 is a regulatory subunit that modulates the cell surface abundance and the spatial localization of Kv1.3 channels. Both proteins are present in leukocytes and form heterooligomeric channels (Sole and Felipe, 2010; Sole et al., 2009, 2013). In the present work, we analyzed the molecular determinants in Kv1.3 that participate in the Kv1.3–KCNE4 interaction. Our data suggest that the tertiary structural conformation of the C-terminal domain of Kv1.3 is responsible for the association with KCNE4. However, other domains, which are yet to be characterized, are responsible for the gating modulation. Furthermore, we also demonstrated that two independent, but complementary, mechanisms collectively participate in the intracellular retention of the Kv1.3–KCNE4 channelosome. Overall, our results shed light onto the mechanisms that control Kv1.3 surface expression, which is closely linked to immune cell activation. In addition, our data illustrate how differing tissue-specific oligomeric associations configure both functional and trafficking heterogeneity.

Regulatory subunits, such as KCNE and Kvβ subunits, modulate Kv subcellular distribution (Kanda and Abbott, 2012; Roura-Ferrer et al., 2010; Shi et al., 1996). For instance, Kvβ2.1 (also known as KCAB2) stabilizes Kv1 channels at the cell surface (Shi et al., 1996), and KCNE1 participates in the Kv7.1 plasma membrane location (Kanda and Abbott, 2012; Roura-Ferrer et al., 2010). In contrast, KCNE4 impairs Kv1.3 surface targeting, triggering dramatic consequences for the channel function (Sole et al., 2009). Kv1.3 is crucial for the immune response, and an alteration in its membrane abundance can be responsible for both physiological changes and pathological conditions. For instance, the number of Kv1.3 channels increases during T-lymphocyte activation (Varga et al., 2010). Similarly, macrophages elevate Kv1.3 at the plasma membrane during activation and proliferation (Vicente et al., 2003). Furthermore, Kv1.3 channels are targeted to raft microdomains under specific insults (Vicente et al., 2008). However, exacerbated surface expression or altered spatial localization is related to autoimmune diseases (Chandy et al., 2004; Nicolaou et al., 2007; Varga et al., 2010). In contrast, immunosuppression decreases Kv1.3, triggering similar effects to those of channel blockers (Chandy et al., 2004; Villalonga et al., 2010). Therefore, the control of functional Kv1.3 channels at the cell surface is crucial for appropriate cell responses. In addition, KCNE4 expression is tightly

Journal of Cell Science (2016) 129, 4265-4277 doi:10.1242/jcs.191650

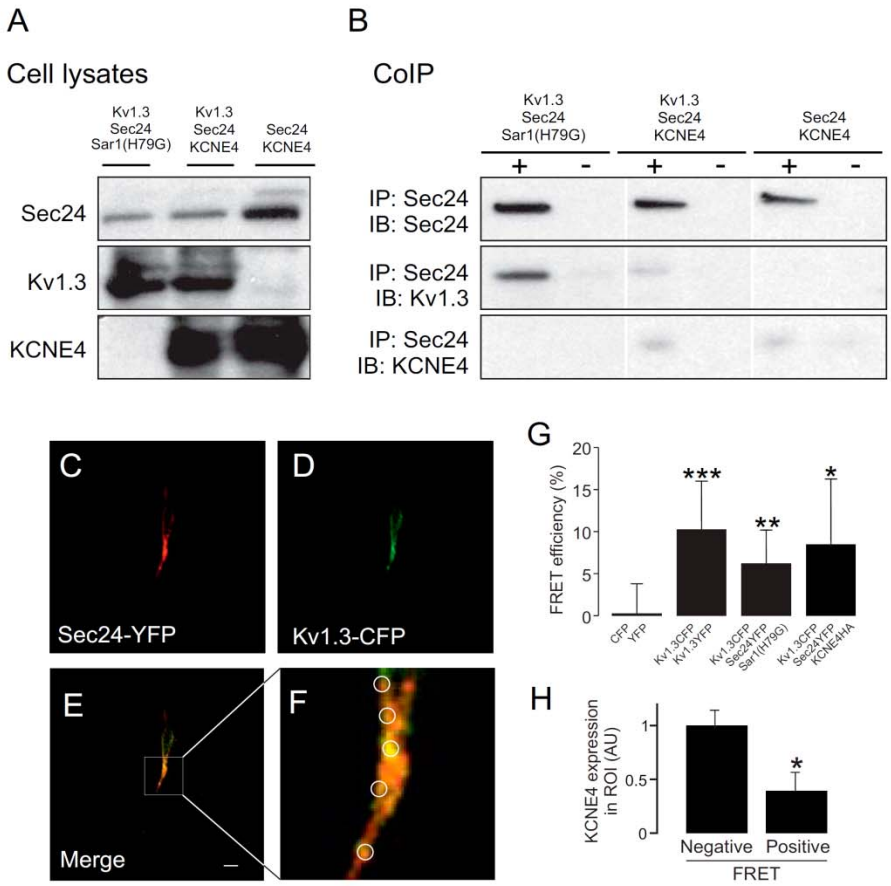

Fig. 6. KCNE4 interacts with the C-terminal domain of Kv1.3, thereby impairing the association with the COPII anterograde trafficking mechanism. HEK-293 cells were transfected with Kv1.3 in the presence or the absence of KCNE4, Sec24D–YFP and Sar1(H79G)–HA. (A,B) Co-immunoprecipitation of Kv1.3 and Sec24D in the presence or the absence of KCNE4. (A) Expression of Sec24D, Kv1.3 and KCNE4 in starting materials (cell lysates). (B) Co-immunoprecipitations. Samples were immunoprecipitated (+IP) against Sec24D–YFP and immunoblotted (IB) against GFP (Sec24D), Kv1.3 and KCNE4. Sar1 (H79G) and KCNE4 expression led to the retention of Kv1.3 in the ER. Note that KCNE4 notably impaired the association between Kv1.3 and Sec24D. In addition, KCNE4 showed a slight co-immunoprecipitation with Sec24. Note that the anti-GFP antibody used recognizes YFP. (C–H) Molecular interaction between Kv1.3 and Sec24D in the presence or the absence of KCNE4. (C–F) A representative FRET experiment for Kv1.3 and Sec24D in the presence of KCNE4. (C) Sec24D–YFP (red) in the acceptor panel. (D) Kv1.3–CFP (green) in the donor panel. (E) Colocalization is shown in yellow. (F) Magnification of the boxed area in E. Circles highlight some ROIs. Scale bar: 10 µm. (G) FRET efficiency of the Kv1.3–Sec24D interaction in the presence or the absence of Sar1(H79G) and KCNE4. YFP and CFP, and Kv1.3–CFP and Kv1.3–YFP pairs were used as negative and positive controls, respectively. Note that although FRET values between Kv1.3 and Sec24D were positive, the presence of KCNE4 triggered a larger variability. (H) Relative KCNE4 expression in arbitrary units (AU) in FRET-positive or FRET-negative ROIs. Considering the FRET between Kv1.3 and Sec24D, two types of ROI were observed. When ROI triggered clearly positive FRET, KCNE4 expression was low. However, in ROIs with no relevant FRET values, KCNE4 expression was higher. Values are shown as the mean±s.e.m. of n>30 cells. *P<0.05; **P<0.01; ***P<0.001 (Student's t-test).

regulated in leukocytes (Sole et al., 2013). In this scenario, the association with KCNE4, by controlling the number and spatial localization of surface Kv1.3, would be essential. Kv1.3 is considered a multi-pharmacological target because channel alterations are present in the onset of numerous pathologies, including sensory discrimination, autoimmune diseases, type II diabetes, obesity and cancer (Perez-Verdaguer et al., 2016b). Considering the variety of functions in which Kv1.3 participates (i.e. activation, proliferation and apoptosis), it is tempting to speculate that this diversity is achieved by a variety of complementary subunit associations that govern channel localization and function.

Our present data suggest that it is the folded structural conformation of the Kv1.3 C-terminus, rather than specific signatures, that is important for the KCNE4 association. Although KCNE peptides bind to Kv7 isoforms through interactions with the C-terminal domain (Wrobel et al., 2012; Zheng et al., 2010), nothing was known previously about their association with other Kv channels. Structural elements are quite different among Kv families (Hille, 2001). For example, the Kv7 family as well as the EAG superfamily contain tetramerization domains at their C-termini (Hausammann and Grutter, 2013; Jenke et al., 2003; Schwake et al., 2006), whereas Kv1–Kv6 channels contain their tetramerization domains, named T1, at the N-terminus (Li et al., 1992). The T1 domain and nearby structures participate in associations with Kvβ subunits and caveolin (Gulbis et al., 2000; Perez-Verdaguer et al., 2016a). However, the C-terminus of Kv1 channels does contain

Journal of Cell Science (2016) 129, 4265-4277 doi:10.1242/jcs.191650

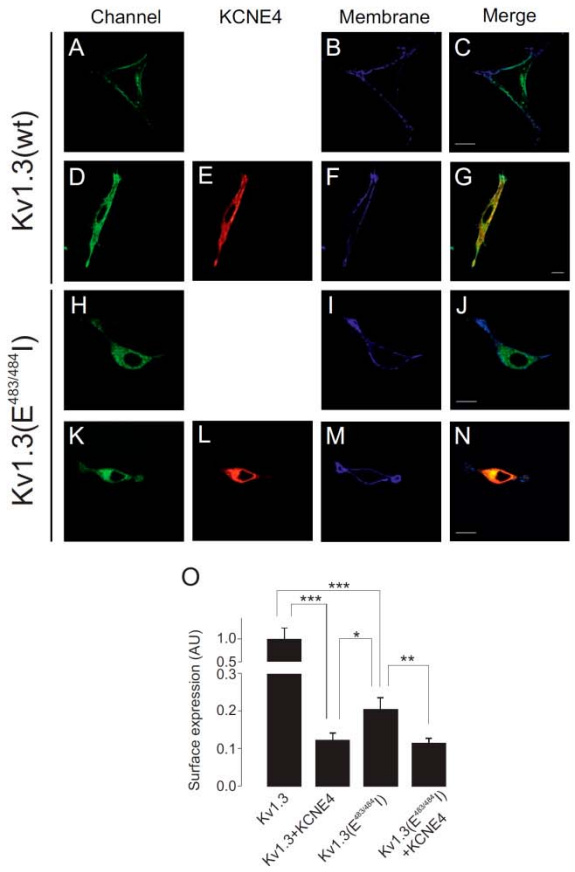

Fig. 7. The KCNE4 interaction further aggravated the intracellular retention of the Kv1.3($E^{483/484}$I) mutant. HEK-293 cells were transfected with Kv1.3wt, Kv1.3($E^{483/484}$I) and KCNE4. Membrane surface labeling was performed using WGA as described in the Materials and Methods. (A–G) Representative confocal images of Kv1.3 wt in the absence (A–C) or the presence (D–G) of KCNE4. (H–N) Representative confocal images of Kv1.3 ($E^{483/484}$I) in the absence (H–J) or the presence (K–N) of KCNE4. (A,D,H,K) Kv1.3 channels in green. (E,L) KCNE4 in red. (B,F,I,M) WGA membrane staining in blue. (C,G,J,N) Color code in merged panels: Kv1.3 channels and KCNE4 colocalization, yellow; channels and membrane, cyan; triple colocalization, white. Scale bars: 10 µm. (O) Kv1.3 membrane surface expression in arbitrary units (AU) in a pixel-by-pixel analysis. Values are shown as the mean±s.e.m. of n>25 cells. *P<0.05; **P<0.01; ***P<0.001 (Student's t-test).

important elements for their trafficking and localization. A PDZ domain, which interacts with PSD proteins, such as PSD95 or SAP-97, is positioned at the very distal part of the channel (Szilagyi et al., 2013; Tiffany et al., 2000). In addition, forward trafficking motifs, such as VxxSL, HRETE or YMVIEE, are also located within this intracellular region (Li et al., 2000; Martinez-Marmol et al., 2013; Zhu et al., 2007). However, there was little information about the interactions of this C-terminal domain with ancillary partners (Misonou and Trimmer, 2004). The COPII machinery is responsible for a di-acidic interaction within the C-terminal domain of the Kv1.3 channel (Martinez-Marmol et al., 2013; Spear et al., 2015). Our new data suggest that the interaction between KCNE4 and the Kv1.3 C-terminal domain masks this motif and triggers a marked ER retention, which impairs membrane targeting. Furthermore, this association does not function alone, as the strong intracellular phenotype is further ensured by a strong ERRM in KCNE4.

KCNE peptides control the surface abundance of Kv7 channels. Whereas KCNE1 increases the Kv7.1 membrane staining, KCNE4, similar to our observations for Kv1.3, reduces Kv7.1 surface expression and lipid raft localization (Roura-Ferrer et al., 2010). The balance between forward trafficking and ER retention signals is crucial for the membrane targeting and function (Misonou and Trimmer, 2004). In two-pore-domain background K^+ channels (K_{2P} channels), the influence of protein–protein interactions on sorting decisions is crucial. The adaptor protein 14-3-3 interacts with TASK-1 and TASK-3 (also known as KCNK3 and KCNK9, respectively) to mask a retention signal in the C-terminus of the channels, which is important for the COPI binding (Mathie et al., 2010). In fact, 14-3-3 promotes plasma membrane expression of several ion channels, such as Cav2.2 (also known as CACNA1B) (Liu et al., 2015). The effect of KCNE4 would be the opposite; by interacting with the C-terminus of Kv1.3, the ancillary peptide would hide a di-acidic forward trafficking motif important for COPII anterograde traffic. By contrast, the adaptor protein p11 (also known as protein S100-A10), which interacts with TASK-1, carries a di-lysine retention signal that retains the channel at the ER (Mathie et al., 2010). KCNE4 association also provides a strong ERRM to Kv1.3. Unlike TASK channels, the KCNE4 mechanism can be considered to be redundant and effective. Several forward trafficking signals have been identified in the C-terminal domain of Kv1.3. Thus, the HRETE motif, its alternative ExExE extension and the YMVIEE cluster containing a di-acid motif promote anterograde transport through the COPII-mediated early secretory pathway (Martinez-Marmol et al., 2013; Spear et al., 2015). However, the interaction of KCNE4 with the fully folded C-terminal domain fine-tunes cell surface expression by both masking forward trafficking signals and providing an ER retention signal.

Furthermore, our results suggest that motifs involved in the association are not responsible for the gating control, as KCNE regulatory subunits can bind to channels without modifying their kinetics (McCrossan and Abbott, 2004; Wrobel et al., 2012). In this context, KCNE4, although it associates with Kv7.4 (also known as KCNQ4), does not modulate the channel activity. However, the transfer of the S6 domain from Kv7.1 to Kv7.4 leads to inhibition, whereas transferring the S6 domain from Kv7.4 to Kv7.1 prevents inhibition by KCNE4 (Vanoye et al., 2009). This effect is due to a dipeptide domain (KT, amino acids 326–327) preceding the S6 segment. Neither Kv1.3 nor Kv1.5 contains such an element. Although Kv1.1–Kv1.6 channels possess a lysine residue in this position, this residue cannot support the KCNE4 modulation because it is specific for only Kv1.3 and Kv1.1 (Grunnet et al., 2003; Sole et al., 2009). The C-terminus and S5–S6 domains of Kv7.1 are required for modulation by KCNE1 and KCNE3 (Melman et al., 2004). Evidence supports the idea that the C-terminus of Kv7.1 acts by anchoring and correctly positioning the regulatory subunit (Manderfield et al., 2009; Vanoye et al., 2009). Furthermore, multiple interactions have been described between the KCNE and the gating machinery of Kv7.1, such as residues S1, S4, S5 and S6 (Chouabe et al., 2000; Franqueza et al., 1999; Melman et al., 2004; Nakajo and Kubo, 2007; Panaghie et al., 2006; Xu et al., 2008). Our data indicate that, similar to the Kv7.1–KCNE interaction, the C-terminus of Kv1.3 plays a role in anchoring KCNE4 to the complex, but that additional interactions modulate channel gating.

Our results are physiologically relevant because KCNE4 and Kv1.3 associate in antigen-presenting cells. Kv1.3 channels

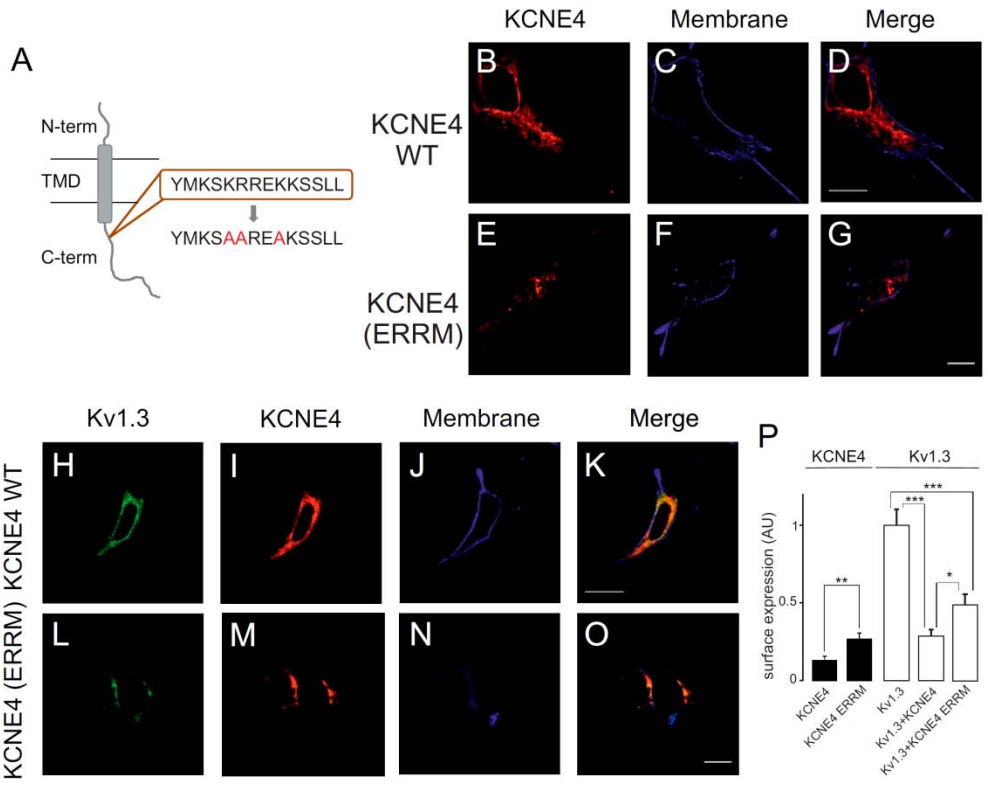

Fig. 8. The disruption of the ERRM of KCNE4 only partially counteracted the intracellular retention of Kv1.3. HEK-293 cells were transfected with Kv1.3–YFP, KCNE4–CFP and the KCNE4(ERRM)–CFP mutant. (A) Cartoon illustrating the ERRM in the C-terminal domain of KCNE4. Positive residues (R and K) in the wild-type ERRM (brown box) were mutated to alanine residues to disrupt the motif. N-term, N-terminal extracellular domain; C-term, C-terminal intracellular domain; TMD, transmembrane domain. (B–G) Confocal images of KCNE4 wt (B–D) and the KCNE4(ERRM) mutant (E–G). (B,E) KCNE4. (C,F) Membrane staining with WGA. (D,G) Merge channel. (H–O) Representative images of Kv1.3 in the presence of KCNE4 (H–K) and KCNE4(ERRM) (L–O). (H,L) Kv1.3 in green; (I,M) KCNE4 in red; (J,N) membrane in blue; (K,O) merge. Note that although Kv1.3 colocalization with KCNE4 showed marked intracellular retention in all cases, the channel reached the surface better in the presence of KCNE4(ERRM). Scale bars: 10 µm. (P) Pixel-by-pixel analysis of the relative membrane surface expression, in arbitrary units (AU), of KCNE4 (black bars) and Kv1.3 (white bars). Note that KCNE4(ERRM) showed double the KCNE4 membrane surface expression. Furthermore, Kv1.3 reached the cell surface more efficiently in the presence of KCNE4(ERRM) than with KCNE4. Values are shown as the mean±s.e.m. (n>25 cells). *P<0.05; **P<0.01; ***P<0.001 (Student's t-test).

participate in the immune response and, through a variable KCNE4 interaction, dendritic cells and macrophages might be able to precisely modulate their cell physiology. This work highlights some of the mechanisms by which interacting proteins might govern the intracellular trafficking and surface abundance of ion channels involved in the immune response.

MATERIALS AND METHODS

Expression plasmids, chimeric channels and site-directed mutagenesis

Rat (r)Kv1.3 in pRcCMV was provided by Todd C. Holmes (New York University, NY). Mouse (m)KCNE4 in pSGEM was from Michael Sanguinetti (University of Utah, Salt Lake City, UT). piRES-EGFP-hKCNE4-HA was obtained from Alfred L. George (Northwestern University Feinberg School of Medicine, Chicago, IL). Human (h)Kv1.5 has been extensively analyzed in our laboratory. rKv1.3 and hKv1.5 were subcloned into pEYFP-C1 and pECFP-C1 (Clontech) to preserve normal channel behavior. mKCNE4 was introduced in pECFP-N1 (Clontech). rKv1.3–YFP, mKCNE4–CFP and hKCNE4–HA constructs were previously described (Sole et al., 2009). Kv1.3–CFP, Kv1.5–YFP, Kv1.3–Kv1.5 chimeras and Kv1.3 mutants and truncations have been analyzed previously (Martinez-Marmol et al., 2013). Kv1.3–YFP and KCNE4–CFP mutants were generated using the QuikChange and QuikChange multi-site-directed mutagenesis kits (Stratagene). All constructs and mutants were verified using automated DNA sequencing. The pEYFP-Sec24D and the HA-Sar1(H79G) were from Theresa H. Ward (The London School of Hygiene & Tropical Medicine, London, UK) and Rainer Pepperkok (EMBL, Heidelberg, Germany), respectively.

Cell culture

HEK-293 cells, Jurkat human T-lymphocytes and CY15 mouse dendritic cells were cultured in Dulbecco's modified Eagle's medium (DMEM) and RPMI culture medium, respectively (LONZA), supplemented with 10% fetal bovine serum (FBS), 10,000 U/ml penicillin, 100 µg/ml streptomycin and 2 mM L-glutamine (GIBCO).

For patch-clamp experiments, trypsinized HEK-293 cells from a confluent 100-mm dish were electroporated with 1 µg of DNA using a Bio-Rad Genepulser Xcell (Bio-Rad) with a 0.2-cm-gap cuvette and a single 110 V and 25 ms pulse. Transfected cells were then plated on a 50-mm dish.

For confocal imaging and co-immunoprecipitation experiments, cells were seeded (70–80% confluence), in six-well dishes containing poly-lysine-coated coverslips or in 100-mm dishes, respectively, 24 h before transfection with selected cDNAs. Metafectene PRO (Biontex) was used for transfection according to the supplier's instructions. The amount of transfected DNA was 500 ng per well of a six-well dish and 4 µg for a

Journal of Cell Science (2016) 129, 4265-4277 doi:10.1242/jcs.191650

100-mm dish. Next, 4–6 h after transfection, the mixture was removed from the dishes and replaced with fresh culture medium. All the experiments were performed 24 h after transfection.

Electrophysiology

Transfected HEK-293 cells were trypsinized 24 h after electroporation and re-plated on 35-mm glass-bottom dishes coated with Matrigel (BD Biosciences). After 2–4 h, cells were extensively washed with whole-cell external recording solution, containing the following (in mM): 150 NaCl, 5 KCl, 10 $CaCl_2$, 2 $MgCl_2$, 10 glucose and 10 HEPES, pH 7.4. Transfected HEK-293 cells were selected using an Olympus FV1000 confocal microscope equipped with spectral detectors and SIM scanner. Whole-cell K^+ currents in HEK-293, Jurkat and CY15 cells were recorded at room temperature using an Axopatch 200B and an EPC-10 (HEKA), respectively, and the appropriate software was used for data recording and analysis. Ionic currents were capacitance- and series-resistance-compensated by 80–90%, sampled at 10 kHz (Digidata 1440; Molecular Devices) and filtered at 2.9 kHz. Patch electrodes of 2–4 MΩ were fabricated in a P-97 puller (Sutter Instruments Co.) from borosilicate glass (outer diameter 1.2 mm and inner diameter 0.94 mm; Clark Electromedical Instruments Co.). Electrodes for HEK-293 cells were filled with a solution containing the following (in mM): 4 NaCl, 150 KCl, 1 $MgCl_2$, 0.5 EGTA, 5 ATP(K) and 10 HEPES, pH 7.4. HEK-293 cells were clamped to a holding potential of −80 mV. Electrodes for CY15 and Jurkat cells were filled with a solution containing the following (in mM): 84 K-aspartate, 36 KCl, 10 KH_2PO_4, 6 K_2ATP, 5 HEPES, 5 EGTA, 3 $MgCl_2$, pH 7.2. The extracellular solution contained (in mM): 136 NaCl, 4 KCl, 1.8 $CaCl_2$, 1 MgCl2, 10 HEPES and 10 D-glucose, pH 7.4. CY15 and Jurkat cells were clamped to a holding potential of −60 mV. To evoke voltage-gated currents, all cells were stimulated with 250-ms square pulses ranging from −80 to +80 mV in 10 mV steps. The normalized G/G_{max} versus the voltage curve was fitted using Boltzmann's equation: $G/G_{max}=1/(1+\exp(V_{0.5}-V/k))$, where $V_{0.5}$ is the voltage at which the current is half-activated, and k is the slope factor of the activation curve. Cumulative inactivation of K^+ currents was elicited in Jurkat and CY15 cells by a train of 15 depolarizing 250-ms pulses from −80 mV to +60 mV once every 1 s. All recordings were routinely subtracted for leak currents.

Protein extraction, co-immunoprecipitation and western blotting

Cells were washed twice in cold PBS and lysed on ice with lysis solution (1% Triton X-100, 10% glycerol, 50 mM HEPES, 150 mM NaCl, pH 7.2) supplemented with 1 µg/ml aprotinin, 1 µg/ml leupeptin, 1 µg/ml pepstatin and 1 mM phenylmethylsulfonyl fluoride as protease inhibitors. Homogenates were centrifuged at 12,000 ***g*** for 10 min, and the supernatant was collected. Protein content was determined using the Bio-Rad Protein Assay (Bio-Rad).

For co-immunoprecipitation, 1 mg of protein was brought up to 500 µl of lysis buffer for immunoprecipitation (in NaCl 150 mM, HEPES 50 mM, Titron X-100 1%, pH 7.4, supplemented with protease inhibitors). Samples were precleared with 50 µl of protein-G–Sepharose beads for 2 h at 4°C with gentle mixing. Next, each sample was incubated in a small chromatography column (BioRad Micro Bio-Spin Chromatography Columns), which contained 2.5 µg of the desired antibody previously crosslinked to protein-A or -G–Sepharose beads, for 1 h at room temperature with gentle mixing. Columns were centrifuged for 30 s at 1000 ***g***. The supernatant was kept and stored at −20°C. Columns were washed four times with 500 µl of lysis buffer and centrifugations of 30 s at 1000 ***g***. Finally, for elution, the columns were incubated with 100 µl of 0.2 M glycine pH 2.5 and spun for 30 s at 1000 ***g***. The eluted proteins were prepared by adding 20 µl of SDS Laemmli SDS loading buffer (5×) and 5 µl of 1 M Tris-HCl pH 10, and the preparations were boiled and separated on 10% SDS-PAGE gels. Next, they were transferred to nitrocellulose membranes (Immobilon-P; Millipore) and blocked in 0.05% Tween-20 in PBS supplemented with 5% dried milk before immunoreaction. Filters were immunoblotted with antibodies against HA (1:1000, cat. no. H 6908; Sigma), GFP (1:1000, cat. no. 11 814 460 001; Roche), Kv1.3 (1:200, cat. no. 75-009; NeuroMab), Kv1.5 (1:500, cat. no. APC-004; Alomone) and KCNE4 (1:500, cat. no. 18289-1-AP; Proteintech). Anti-β-actin antibody was used as a loading control (1:50,000, cat. no. A5441; Sigma).

Irreversible crosslinking of the antibody to the Sepharose beads was performed after an incubation of the antibody with protein-A or -G–Sepharose beads for 1 h at room temperature. The beads were then incubated with 500 µl of 5.2 mg/ml of dimethyl pimelimidate (Pierce) for 30 min at room temperature by gentle mixing. The beads were then washed four times with 500 µl of 1× TBS, four times with 500 µl of 0.2 M glycine pH 2.5 and three times more with 1× TBS. Once these steps were performed, the columns were incubated with the protein lysates in order to perform the immunoprecipitation as described above.

Immunocytochemistry

Jurkat and CY15 cells were cultured on 20×20 mm poly-lysine-coated glass coverslips for up to 24 h. Cells were fixed in methanol (−20°C) for 15 min at room temperature, washed twice in PBS without K^+ (denoted PBS-K^+, wash buffer) for 5 min to rehydrate cells, and blocked and permeabilized for 1 h with blocking buffer (PBS-K^+ containing 0.05% Triton X-100, 5% non-fat milk, 10% bovine serum albumin). Cells were subsequently incubated with rabbit anti-KCNE4 (1:100, cat. no. 18289-1-AP; Proteintech) for 2 h, and unbound antibody was removed with wash buffer. Coverslips were exposed to Cy3-conjugated goat anti-rabbit-IgG secondary antibody (1:200, Molecular Probes) for 1 h. After washing to remove unbound secondary antibody, CY15 cells were blocked again for 1 h in blocking buffer. CY15 cells were incubated with anti-Kv1.3 (1:50, cat. no. 75-009; NeuroMab) at 4°C overnight, washed, and then exposed to Cy5-conjugated goat anti-mouse-IgG (1:200, Molecular Probes) for 1 h. After removing unbound secondary antibody, coverslips were mounted with Mowiol (Calbiochem) and examined with a confocal laser-scanning fluorescent microscope.

Confocal microscopy and image analysis

For confocal image acquisition, cells were seeded on poly-lysine-coated coverslips and transfected 24 h later. The next day, cells were quickly washed twice, fixed with 10% paraformaldehyde for 10 min, and washed three times for 5 min with PBS-K^+. Finally, coverslips were mounted on microscope slides (Acefesa) with Mowiol. Preparations were dried at room temperature before imaging.

For membrane surface labeling under non-permeabilized conditions, wheat germ agglutinin conjugated to Texas Red (WGA–Texas Red®, Invitrogen) was used. Live cells (on ice) were quickly washed with PBS at 4°C and stained with a dilution of WGA–TexasRed (1:1500) in DMEM supplemented with 30 mM HEPES for 15 min at 4°C. Cells were washed twice and fixed with 4% paraformaldehyde in PBS for 10 min. Next, cells were washed and mounted as described above.

The fluorescence resonance energy transfer (FRET) was achieved by an acceptor photobleaching technique and was measured in discrete ROIs. Fluorescent proteins from fixed cells were excited with the 458 nm or the 514 nm lines using low excitation intensities. Next, 475- to 495-nm bandpass and >530-nm longpass emission filters were applied. The YFP was bleached using maximum laser power. We obtained ~80% of acceptor intensity bleaching. After photobleaching, images of the donors and acceptors were taken. The FRET efficiency was calculated using the equation $[(F_{CFPafter}-F_{CFPbefore})/F_{CFPbefore}]\times100$, where $F_{CFPafter}$ was the fluorescence of the donor after bleaching and $F_{CFPbefore}$ was the fluorescence before bleaching. The loss of fluorescence as a result of the scans was corrected by measuring the CFP intensity in an unbleached part of the cell.

All images were acquired with a Leica TCS SL laser-scanning confocal spectral microscope (Leica Microsystems), equipped with argon and helium-neon lasers. All the experiments were performed with a 63× oil-immersion objective lens, NA 1.32. All offline image analysis was performed using Image J and SigmaPlot software. A pixel-by-pixel colocalization analysis was performed using JACoP (Just Another Colocalization Plugin). Manders split coefficients, which are proportional to the amount of fluorescence of the colocalizing pixels in each color channel, were obtained. Thus, although the spatial resolution of the light microscope is limited by the wavelength of the light (less than 200 nm), our data were exhaustively corroborated by the rest of the above-mentioned techniques such as FRET, co-immunoprecipitation and electrophysiological recording.

Acknowledgements
Authors thank the Centres Científics i Tecnològics de la Universitat de Barcelona (CCiTUB) for confocal microscopy experiments. The English editorial assistance of the American Journal Experts is also acknowledged.

Competing interests
The authors declare no competing or financial interests.

Author contributions
A.F. and M.M.T. conceived and supervised the present study. R.R.-M. provide reagents and tools. L.S., S.R.R., A.S.-A. and A.V.-G. performed the experiments and analyzed the data. A.F. and L.S. wrote the manuscript. All authors contributed to the interpretation and commented on the manuscript.

Funding
Supported by the Ministerio de Economía y Competitividad (MINECO), Spain (BFU2014-54928-R and BFU2015-70067-REDC) and Fondo Europeo de Desarrollo Regional (FEDER). This work was also supported by the National Institutes of Health (R01GM84136, R01GM084136S1 and R01GM109888-01 to M.M.T.). L.S., S.R.R. and A.V.-G. hold a fellowship from the Ministerio de Economía y Competitividad (MINECO) and A.S.-A. from Generalitat de Catalunya. R.M.-M. was supported by the Juan de la Cierva program (MINECO). Deposited in PMC for release after 12 months.

Supplementary information
Supplementary information available online at
http://jcs.biologists.org/lookup/doi/10.1242/jcs.191650.supplemental

References

Chandy, K. G., Wulff, H., Beeton, C., Pennington, M., Gutman, G. A. and Cahalan, M. D. (2004). K^+ channels as targets for specific immunomodulation. *Trends Pharmacol. Sci.* **25**, 280-289.

Chouabe, C., Neyroud, N., Richard, P., Denjoy, I., Hainque, B., Romey, G., Drici, M.-D., Guicheney, P. and Barhanin, J. (2000). Novel mutations in KvLQT1 that affect Iks activation through interactions with Isk. *Cardiovasc. Res.* **45**, 971-980.

Crump, S. M., Hu, Z., Kant, R., Levy, D. I., Goldstein, S. A. N. and Abbott, G. W. (2016). Kcne4 deletion sex- and age-specifically impairs cardiac repolarization in mice. *FASEB J.* **30**, 360-369.

Felipe, A., Soler, C. and Comes, N. (2010). Kv1.5 in the immune system: the good, the bad, or the ugly? *Front. Physiol.* **1**, 152.

Franqueza, L., Lin, M., Splawski, I., Keating, M. T. and Sanguinetti, M. C. (1999). Long QT syndrome-associated mutations in the S4-S5 linker of KvLQT1 potassium channels modify gating and interaction with minK subunits. *J. Biol. Chem.* **274**, 21063-21070.

Gao, C., Cai, Y., Wang, Y., Kang, B.-H., Aniento, F., Robinson, D. G. and Jiang, L. (2014). Retention mechanisms for ER and Golgi membrane proteins. *Trends Plant Sci.* **19**, 508-515.

Grunnet, M., Rasmussen, H. B., Hay-Schmidt, A., Rosenstierne, M., Klaerke, D. A., Olesen, S.-P. and Jespersen, T. (2003). KCNE4 is an inhibitory subunit to Kv1.1 and Kv1.3 potassium channels. *Biophys. J.* **85**, 1525-1537.

Gulbis, J. M., Zhou, M., Mann, S. and MacKinnon, R. (2000). Structure of the cytoplasmic beta subunit-T1 assembly of voltage-dependent K+ channels. *Science* **289**, 123-127.

Hausammann, G. J. and Grutter, M. G. (2013). Chimeric hERG channels containing a tetramerization domain are functional and stable. *Biochemistry* **52**, 9237-9245.

Hille, B. (2001). *Ion Channels of Excitable Membranes*. Sunderland, MA: Sinauer.

Jenke, M., Sanchez, A., Monje, F., Stuhmer, W., Weseloh, R. M. and Pardo, L. A. (2003). C-terminal domains implicated in the functional surface expression of potassium channels. *EMBO J.* **22**, 395-403.

Kanda, V. A. and Abbott, G. W. (2012). KCNE regulation of K+ channel trafficking - a Sisyphean Task? *Front. Physiol.* **3**, 231.

Li, M., Jan, Y. N. and Jan, L. Y. (1992). Specification of subunit assembly by the hydrophilic amino-terminal domain of the Shaker potassium channel. *Science* **257**, 1225-1230.

Li, D., Takimoto, K. and Levitan, E. S. (2000). Surface expression of Kv1 channels is governed by a C-terminal motif. *J. Biol. Chem.* **275**, 11597-11602.

Liin, S. I., Barro-Soria, R. and Larsson, H. P. (2015). The KCNQ1 channel - remarkable flexibility in gating allows for functional versatility. *J. Physiol.* **593**, 2605-2615.

Liu, F., Zhou, Q., Zhou, J., Sun, H., Wang, Y., Zou, X., Feng, L., Hou, Z., Zhou, A., Zhou, Y. et al. (2015). 14-3-3tau promotes surface expression of Cav2.2 (alpha1B) Ca2+ channels. *J. Biol. Chem.* **290**, 2689-2698.

Manderfield, L. J., Daniels, M. A., Vanoye, C. G. and George, A. L., Jr. (2009). KCNE4 domains required for inhibition of KCNQ1. *J. Physiol.* **587**, 303-314.

Martinez-Marmol, R., Perez-Verdaguer, M., Roig, S. R., Vallejo-Gracia, A., Gotsi, P., Serrano-Albarras, A., Bahamonde, M. I., Ferrer-Montiel, A., Fernandez-Ballester, G., Comes, N. et al. (2013). A non-canonical di-acidic signal at the C-terminus of Kv1.3 determines anterograde trafficking and surface expression. *J. Cell Sci.* **126**, 5681-5691.

Mathie, A., Rees, K. A., El Hachmane, M. F. and Veale, E. L. (2010). Trafficking of neuronal two pore domain potassium channels. *Curr. Neuropharmacol.* **8**, 276-286.

McCrossan, Z. A. and Abbott, G. W. (2004). The MinK-related peptides. *Neuropharmacology* **47**, 787-821.

Melman, Y. F., Um, S. Y., Krumerman, A., Kagan, A. and McDonald, T. V. (2004). KCNE1 binds to the KCNQ1 pore to regulate potassium channel activity. *Neuron* **42**, 927-937.

Misonou, H. and Trimmer, J. S. (2004). Determinants of voltage-gated potassium channel surface expression and localization in Mammalian neurons. *Crit. Rev. Biochem. Mol. Biol.* **39**, 125-145.

Nakajo, K. and Kubo, Y. (2007). KCNE1 and KCNE3 stabilize and/or slow voltage sensing S4 segment of KCNQ1 channel. *J. Gen. Physiol.* **130**, 269-281.

Nicolaou, S. A., Szigligeti, P., Neumeier, L., Lee, S. M., Duncan, H. J., Kant, S. K., Mongey, A. B., Filipovich, A. H. and Conforti, L. (2007). Altered dynamics of Kv1.3 channel compartmentalization in the immunological synapse in systemic lupus erythematosus. *J. Immunol.* **179**, 346-356.

Panaghie, G., Tai, K.-K. and Abbott, G. W. (2006). Interaction of KCNE subunits with the KCNQ1 K+ channel pore. *J. Physiol.* **570**, 455-467.

Perez-Verdaguer, M., Capera, J., Martinez-Marmol, R., Camps, M., Comes, N., Tamkun, M. M. and Felipe, A. (2016a). Caveolin interaction governs Kv1.3 lipid raft targeting. *Sci. Rep.* **6**, 22453.

Perez-Verdaguer, M., Capera, J., Serrano-Novillo, C., Estadella, I., Sastre, D. and Felipe, A. (2016b). The voltage-gated potassium channel Kv1.3 is a promising multitherapeutic target against human pathologies. *Expert Opin. Ther. Targets* **20**, 577-591.

Roura-Ferrer, M., Sole, L., Oliveras, A., Dahan, R., Bielanska, J., Villarroel, A., Comes, N. and Felipe, A. (2010). Impact of KCNE subunits on KCNQ1 (Kv7.1) channel membrane surface targeting. *J. Cell Physiol.* **225**, 692-700.

Schwake, M., Athanasiadu, D., Beimgraben, C., Blanz, J., Beck, C., Jentsch, T. J., Saftig, P. and Friedrich, T. (2006). Structural determinants of M-type KCNQ (Kv7) K+ channel assembly. *J. Neurosci.* **26**, 3757-3766.

Shi, G., Nakahira, K., Hammond, S., Rhodes, K. J., Schechter, L. E. and Trimmer, J. S. (1996). Beta subunits promote K^+ channel surface expression through effects early in biosynthesis. *Neuron* **16**, 843-852.

Sole, L. and Felipe, A. (2010). Does a physiological role for KCNE subunits exist in the immune system? *Commun. Integr. Biol.* **3**, 166-168.

Sole, L., Roura-Ferrer, M., Perez-Verdaguer, M., Oliveras, A., Calvo, M., Fernandez-Fernandez, J. M. and Felipe, A. (2009). KCNE4 suppresses Kv1.3 currents by modulating trafficking, surface expression and channel gating. *J. Cell Sci.* **122**, 3738-3748.

Sole, L., Vallejo-Gracia, A., Roig, S. R., Serrano-Albarras, A., Marruecos, L., Manils, J., Gomez, D., Soler, C. and Felipe, A. (2013). KCNE gene expression is dependent on the proliferation and mode of activation of leukocytes. *Channels* **7**, 85-96.

Spear, J. M., Koborssy, D. A., Schwartz, A. B., Johnson, A. J., Audhya, A., Fadool, D. A. and Stagg, S. M. (2015). Kv1.3 contains an alternative C-terminal ER exit motif and is recruited into COPII vesicles by Sec24a. *BMC Biochem.* **16**, 483.

Szilagyi, O., Boratko, A., Panyi, G. and Hajdu, P. (2013). The role of PSD-95 in the rearrangement of Kv1.3 channels to the immunological synapse. *Pflugers Arch.* **465**, 1341-1353.

Tiffany, A. M., Manganas, L. N., Kim, E., Hsueh, Y.-P., Sheng, M. and Trimmer, J. S. (2000). PSD-95 and SAP97 exhibit distinct mechanisms for regulating K(+) channel surface expression and clustering. *J. Cell Biol.* **148**, 147-158.

Vanoye, C. G., Welch, R. C., Daniels, M. A., Manderfield, L. J., Tapper, A. R., Sanders, C. R. and George, A. L., Jr. (2009). Distinct subdomains of the KCNQ1 S6 segment determine channel modulation by different KCNE subunits. *J. Gen. Physiol.* **134**, 207-217.

Varga, Z., Hajdu, P. and Panyi, G. (2010). Ion channels in T lymphocytes: an update on facts, mechanisms and therapeutic targeting in autoimmune diseases. *Immunol. Lett.* **130**, 19-25.

Vicente, R., Escalada, A., Coma, M., Fuster, G., Sanchez-Tillo, E., Lopez-Iglesias, C., Soler, C., Solsona, C., Celada, A. and Felipe, A. (2003). Differential voltage-dependent K^+ channel responses during proliferation and activation in macrophages. *J. Biol. Chem.* **278**, 46307-46320.

Vicente, R., Escalada, A., Soler, C., Grande, M., Celada, A., Tamkun, M. M., Solsona, C. and Felipe, A. (2005). Pattern of Kv beta subunit expression in macrophages depends upon proliferation and the mode of activation. *J. Immunol.* **174**, 4736-4744.

Vicente, R., Escalada, A., Villalonga, N., Texido, L., Roura-Ferrer, M., Martin-Satue, M., Lopez-Iglesias, C., Soler, C., Solsona, C., Tamkun, M. M. et al. (2006). Association of Kv1.5 and Kv1.3 contributes to the major voltage-dependent K^+ channel in macrophages. *J. Biol. Chem.* **281**, 37675-37685.

Vicente, R., Villalonga, N., Calvo, M., Escalada, A., Solsona, C., Soler, C., Tamkun, M. M. and Felipe, A. (2008). Kv1.5 association modifies Kv1.3 traffic and membrane localization. *J. Biol. Chem.* **283**, 8756-8764.

Villalonga, N., Escalada, A., Vicente, R., Sanchez-Tillo, E., Celada, A., Solsona, C. and Felipe, A. (2007). Kv1.3/Kv1.5 heteromeric channels compromise pharmacological responses in macrophages. *Biochem. Biophys. Res. Commun.* **352**, 913-918.

Villalonga, N., David, M., Bielanska, J., Vicente, R., Comes, N., Valenzuela, C. and Felipe, A. (2010). Immunomodulation of voltage-dependent K^+ channels in macrophages: molecular and biophysical consequences. *J. Gen. Physiol.* **135**, 135-147.

Wrobel, E., Tapken, D. and Seebohm, G. (2012). The KCNE tango - how KCNE1 interacts with Kv7.1. *Front. Pharmacol.* **3**, 142.

Xu, X., Jiang, M., Hsu, K.-L., Zhang, M. and Tseng, G.-N. (2008). KCNQ1 and KCNE1 in the IKs channel complex make state-dependent contacts in their extracellular domains. *J. Gen. Physiol.* **131**, 589-603.

Zerangue, N., Schwappach, B., Jan, Y. N. and Jan, L. Y. (1999). A new ER trafficking signal regulates the subunit stoichiometry of plasma membrane K(ATP) channels. *Neuron* **22**, 537-548.

Zheng, R., Thompson, K., Obeng-Gyimah, E., Alessi, D., Chen, J., Cheng, H. and McDonald, T. V. (2010). Analysis of the interactions between the C-terminal cytoplasmic domains of KCNQ1 and KCNE1 channel subunits. *Biochem. J.* **428**, 75-84.

Zhu, J., Gomez, B., Watanabe, I. and Thornhill, W. B. (2007). Kv1 potassium channel C-terminus constant HRETE region: arginine substitution affects surface protein level and conductance level of subfamily members differentially. *Mol. Membr. Biol.* **24**, 194-205.

Zsiros, E., Kis-Toth, K., Hajdu, P., Gaspar, R., Bielanska, J., Felipe, A., Rajnavolgyi, E. and Panyi, G. (2009). Developmental switch of the expression of ion channels in human dendritic cells. *J. Immunol.* **183**, 4483-4492.

J. Cell Sci. 129: doi:10.1242/jcs.191650: Supplementary information

Supplementary information

The carboxy terminal domain of Kv1.3 regulates functional interactions with the KCNE4 subunit

Laura Solé, Sara R. Roig, Albert Vallejo-Gracia, Antonio Serrano-Albarrás, Ramón Martínez-Mármol, Michael M. Tamkun, Antonio Felipe.

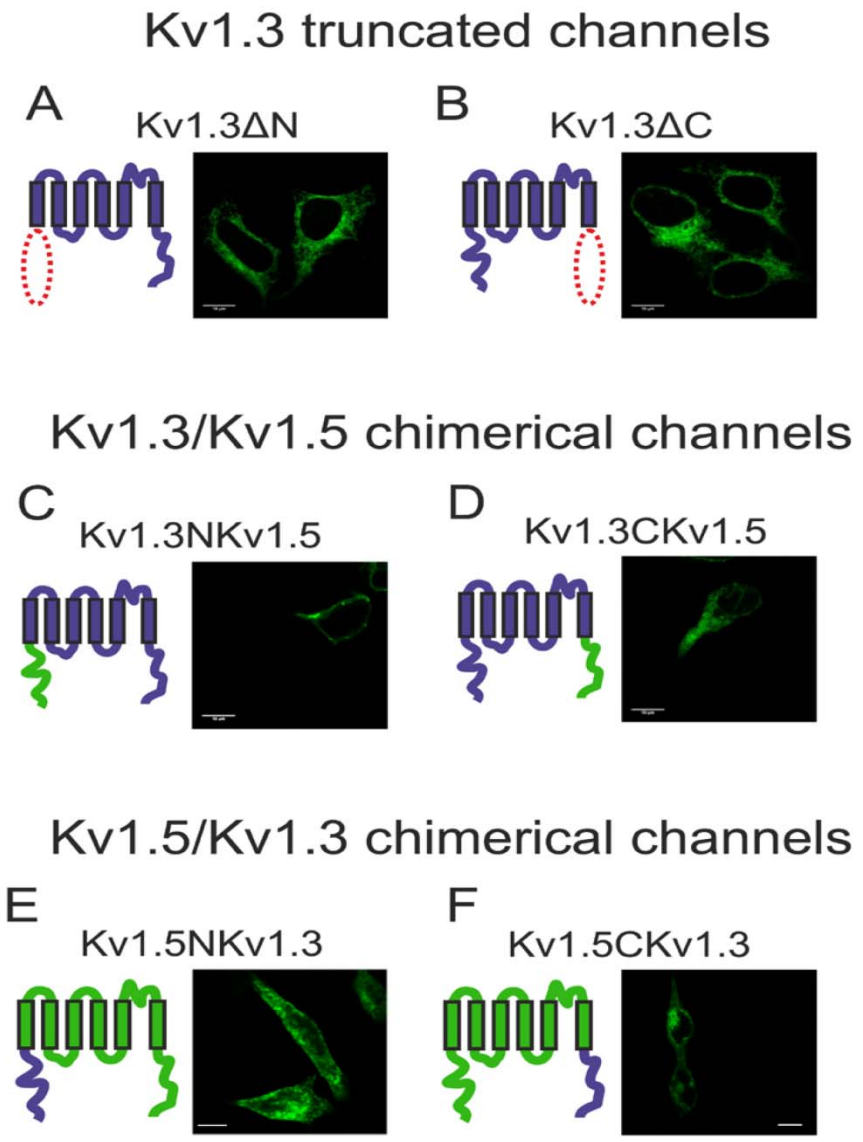

Fig. S1. *Intracellular distributions of Kv1.3 mutants, Kv1.3/Kv1.5 and Kv1.5/Kv1.3 chimeras used in this study.* HEK-293 cells were transfected with YFP-tagged mutants and chimeras. (A, B) In the Kv1.3 truncated channels, the lack of the C- and N-terminal domains is indicated with red dots. (C-F) Kv1.3 domains are colored in blue. Kv1.5 domains are shown in green. The left panels present schematic cartoons. The right panels show representative confocal images illustrating the intracellular distribution. Bars represent 10 μm.

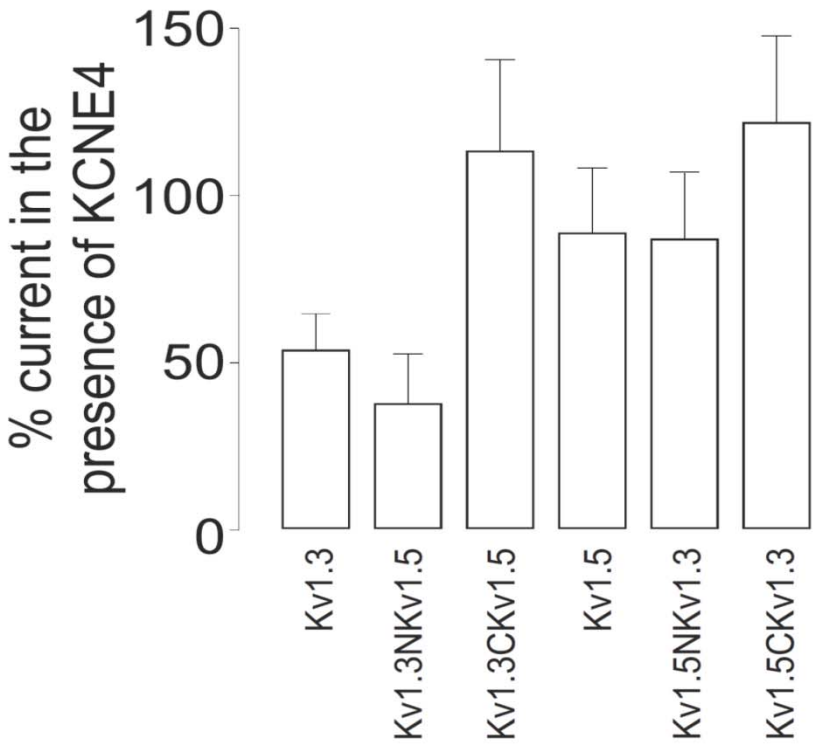

Fig. S2. *The C-terminal domain of Kv1.3 is necessary but not sufficient for the KCNE4-dependent inhibition of Kv1.3 currents.* HEK-293 cells were transfected with Kv1.3, Kv1.5, various Kv1.3 and Kv1.5 chimeras and KCNE4. Cells were held at -80 mV, and currents were elicited by a 200 ms depolarizing pulse to +60 mV. Relative KCNE4 inhibition was calculated based on the channel current in the absence vs. the presence of KCNE4. Note that currents were inhibited by approximately 50% only when the integrity of Kv1.3 was mostly preserved (Kv1.3 and Kv1.3NKv1.5). In contrast, although the Kv1.5CKv1.3 co-immunoprecipitated and co-localized with KCNE4 (see previous Fig. 4), the currents were not affected. Values are shown as the mean±SE of >10 cells.

3.2.3. Contribution 5:

Competence for KCNE4 C-terminus: molecular determinants of a multiprotein binding site

Roig SR[1*], Solé L[2*], Sastre D[1], Tamkun MM[2], Felipe A[1]

[1] Molecular Physiology Laboratory, Departament de Bioquímica i Biomedicina Molecular, Institut de Biomedicina (IBUB), Universitat de Barcelona. Barcelona, Spain

[2] Department of Biomedical Sciences, Colorado State University. Fort Collins, USA.

ABSTRACT

Kv1.3 is one of the leukocyte channels more expressed. Actions such as proliferation, activation and apoptosis are highly different in nature but all modulated by this channel. The fine tunning of its electrophyisiological features, traffic and subcellular function are, thus, crucial. Over expression of Kv1.3 has been linked to some autoimmune diseases such as lupus eritromatous or multiple sclerosis. KCNE subunits are promiscuous, single-spanning proteins that are expressed in immune system. Concretely KCNE4, is a member that exerts a dominant-negative function on the channel. The deeper knowledge of its function on Kv1.3 is extremely relevant. We previously described the channel molecular determinants implicated in the interaction, and the mechanism behind the KCNE4 impairment of Kv1.3 traffic. In the present work, we moved forward. We stablish the subunit specific region that mediates the interaction with the channel. This revealed to be a platform domain in which Kv1.3, Ca^{2+}/Calmodulin and KCNE itself competes for a complex formation. Moreover, this domain is impairing the traffic of the entity and, together with the retaining motif previously described, is generating the typical KCNE4 subcellular distribution. Each described feature are conditioning the final distribution and behavious or the Kv1.3 channel.

Report of the PhD student participation

Competence for KCNE4 C-terminus: molecular determinants of a multiprotein binding site

Sara Raquel Roig Merino performed all the experiments and the data analysis of figures 10 to 16.

Antonio Felipe

PhD thesis director

INTRODUCTION

Kv channels are key role proteins on maintaining the resting membrane potential and the repolarization process at excitable cells. However, several other functions have been linked to them, such as control of the cell-cycle progression, adhesion or cell volume. From the firstly-described *Shaker* family, eight isoforms were identified in mammals. Kv1.3, the third member, is mainly expressed in nervous and immune system (Hille, 2001). Actually, leukocytes present a limited repertoire of potassium channels and Kv1.3 is widely accept to be involved in highly important functions (Panyi, 2005). Activation in some of those cells implies the translocation of this channel to the immunological synapse where it would maintain the driving force for a sustained calcium signalling (Panyi et al., 2004). However, posterior studies related this specific entity with the apoptosis program (Bock et al., 2003, Szabo et al., 2008). Thus, this channel requires a refined control to enhance the proper cellular responses.

Several auxiliary subunits have been discovered to modulate highly diverse aspects on potassium currents characteristics. Electrophysiology, traffic, subcellular localization or lipid raft positioning are some changed features of the channelosomes. KCNE family is a promiscuous, small, single-spanning protein group within the auxiliary members described to accompany potassium channels (Pongs and Schwarz, 2010). Each member presented different tissue distribution, but all of them are found at immune system. Moreover, their level expression is modified depending on the cellular inputs, highlighting the importance of this family in macrophages, T and B cells (Sole et al., 2013). For instance, upon proliferation stimuli, KCNE1 increases while KCNE2 and KCNE4 diminishes (Sole and Felipe, 2010).

Our laboratory has extensively worked on KCNE4 peptide. This specific member is known to generate mainly dominant-negative functions on regulated Kv channels. For instance, upon coexpression with Kv1.1, Kv1.3, Kv2.1 and Kv7.1 this subunit generates a dramatic decrease of final potassium currents (Grunnet et al., 2003, Grunnet et al., 2002, David et al., 2015). The deepest knowledge of the KCNE4 abilities is about its combination with Kv7.1. This protein exerts inhibition of the current without altering the surface expression of the channel (Grunnet et al., 2002, Grunnet et al., 2005). Moreover, it enhances the absence of Kv7.1 at lipid raft microdomains (Roura-Ferrer et al., 2010). Further studies demonstrated that functional interactions between KCNE4 and Kv7.1 required the presence of Calmodulin. Actually, through a tetraleucine domain placed at the juxtamembrane C-terminus of the auxiliary subunit, KCNE4 can interact with Ca^{2+}/Calmodulin (Ciampa et al., 2011).

As previously mentioned, this KCNE member is also present at immune system, and studies from our group demonstrated a tight regulation through different insults. At some immune cell types, Kv1.3 is playing a central role in several processes. To understand the modulation of this channel by KCNE4 several studies were developed in our laboratory (Grunnet et al., 2003). Thus, it is inhibiting Kv1.3 by impairing its surface expression, lipid raft localization and modifying some electrophysiological properties (Sole et al., 2009). Moreover, at the previous contribution, we defined which are the specific molecular mechanisms involved in KCNE4 effects. Furthermore, the interacting interface of the channel with the auxiliary subunit was also defined (Sole et al., 2016). Actually, studies

developed about KCNE-Kv complexes have been focused mainly in determining the molecular interaction domains at the channel. Some oriented to the KCNE domain implicated, pointed out that it exists more than one interface of contact (Gage and Kobertz, 2004, Manderfield et al., 2009). However, other studies considered just one domain involved: or the C-terminal acting as an anchor or a transmembrane contact (Melman et al., 2004, Melman et al., 2002).

This present study moves towards to exactly understand the KCNE4 molecular determinants involved in the Kv1.3 channelosome formation. Moreover, we also describe the previous dimerization of the subunit in the absence of the channel exactly at the same domain. Finally, we infer a competition among those two proteins and calmodulin just in the presence of calcium. Considering the importance of this secondary messenger at the immune system where those proteins are expressed, this investigation is highly relevant and the starting point for further and necessary research.

MATERIALS AND METHODS

Expression plasmids and site-directed mutagenesis. rKv1.3 in pRcCMV was provided by T.C. Holmes (New York University). It was subcloned into pEYFP-C1 and pECFP-C1 (Clontech) to preserve normal channel behavior (Vicente et al., 2008). KCNE4-CFP, KCNE4-HA, KCNE2-CFP and KCNE2-HA constructs were previously described in Solé et al 2008 (Sole et al., 2009). Kv1.3-Kv1.5 chimeras and Kv1.3 mutants were described in Martínez-Marmo,l 2010 (Martínez-Mármol 2010). CaMYFP was obtained from Alvaro Villarroel (Universidad País Vasco-CSIC). The endoplasmic reticulum (pDsRed-ER) marker was obtained from Clontech. HA-Sar1H79G was provided by R. Pepperkok (EMBL).

NruI and MluI sites were introduced to mKCNE4CFP and hKCNE2CFP to remove their transmembrane and C-terminus. Next, transmembrane and C-terminal domains of KCNE2 and KCNE4 were obtained by PCR and subcloned to the respective plasmid, generating KCNE(4-2-4)-CFP (transmembrane domain of KCNE4 replaced for the KCNE2 one), KCNE(2-4-2)-CFP (transmembrane domain of KCNE2 replaced for the KCNE4 one), KCNE(4-4-2)-CFP (C-terminal domain of KCNE4 replaced for the KCNE2 one), and KCNE(2-2-4)-CFP (C-terminal domain of KCNE2 replaced for the KCNE4 one) chimeras.

HA-hKCNE4 C-terminal mutants were obtained by single site-directed mutagenesis (Stratagene), introducing stop codons at the positions Ser 68, Tyr 73, Val 96, Val 125, Val 140, Ser 151.

Mutants	Primers used for mutagenesis
HA-KCNE4_S68_stop	F: 5'- GGGAGAAGAAGTCCTGACTCCTGCTGCTGTAC -3' R: 5'- GTACAGCAGCAGGAGTCAGGACTTCTTCTCCC -3'
HA-KCNE4_Y73_stop	F: 5'- GCCTCCTGCTGCTGTAGAAAGACGAGGAGCG -3' R: 5'- CGCTCCTCGTCTTTCTACAGCAGCAGGAGGC -3'
HA-KCNE4_V96_stop	F: 5'- CGGGCCTGAGGTCGTAGCAGGTGCCCCTGATG -3'

	R: 5'- CATCAGGGGCACCTGCTACGACCTCAGGCCCG -3'
HA-KCNE4_V125_stop	F: 5'- CCATGGAAGGGGACAGCTAGAGCTCCGAGTCCTC -3' R: 5'- GAGGACTCGGAGCTCTAGCTGTCCCCTTCCATGG -3'
HA-KCNE4_V140_stop	F 5'- GCACCTCACCATTTAGGAGGAGGGGGCAGACGATG -3' R: 5'- CATCGTCTGCCCCCTCCTCCTAAATGGTGAGGTGC -3'
HA-KCNE4_S151_stop	F: 5'- GAGCTGGAGGAGACCTAGGAGACGCCCCTCAACG -3' R: 5'- CGTTGAGGGGCGTCTCCTAGGTCTCCTCCAGCTC -3'

The leucines from the tetra-leucine motif of KCNE4-CFP (Leu 69-72) were mutated to alanines by single-site directed mutagenesis, generating KCNE4(L69-72)-CFP (primers used: F: 5'-GAGAAGAAGTCCAGCGCTGCGGCGGCGTACAAAGACGAGGAG-3' and R: 5'CTCCTCGTCTTTGTACGCCGCCGCAGCGCTGGACTTCTTCTC-3').

The tetraleucine motif of KCNE4 was transferred to KCNE2CFP, by a two sequential single-site directed mutagenesis reactions. First, Asp 81, Pro 82 and Tyr 83 were mutated to a Ser and two Leu, respectively (KCNE2-LL-CFP). Next, His 84 and Gln 85 were mutated to two more Leu (KCNE2-LLLL-CFP). The primers used were:

F1:5'- CAAGAGACGGGAACACTCCAGTTCCTTATACCACCAGTACAGTACATTGTAG-3',

R1: 5'- CTACAATGTACTGGTGGTATAAGGAACTGGAGTGTTCCCGTCTCTTG -3',

F2: 5'- GAACACTCCAGTTCCTTATTACTCCTGTACATTGTAGAGGACTGGC-3'

R2: 5'- GCCAGTCCTCTACAATGTACAGGAGTAATAAGGAACTGGAGTGTTC-3'.

All constructs were verified by sequenciation.

Cell culture. HEK-293 cells were cultured on DMEM (LONZA) containing 10% fetal bovine serum (FBS) supplemented with penicillin (10.000 U/ml), streptomycin (100 µg/ml) (GIBCO) and L-glutamine (4 mM).

For patch-clamp experiments trypsinized cells from a confluent 100-mm dish were electroporated with 1 µg of DNA using a Bio-Rad Genepulser Xcell (Bio-Rad) with a 0.2-cmgap cuvette and a single 110 V / 25 ms pulse. Transfected cells were then plated on a 50 mm dish.

For confocal imaging and co-immunoprecipitation experiments cells were seeded (70/80 % of confluence), in 6-well dish containing poly-lysine-coated coverslips or 100 mm dish, respectively, 24 h before transfection with selected cDNAs. Metafectene PRO (Biontex) was used for transfection according to the supplier's instructions. The amount of transfected DNA was 4 ug for a 100 mm dish and 500 ng for each well of a 6-well dish (for coverslip use). Next, 4-6 h after transfection, the mixture was removed from the dishes and replaced with new fresh culture media. All the experiments were performed 24 h after transfection.

Electrophysiology experiments. Transfected HEK-293 cells were trypsinized 24 h after electroporation and re-plated on 35 mm glass-bottom dishes coated with Matrixgel (BD Biosciences). After 2-4 h, cells were extensively washed with whole-cell external recording solution, containing (in mM) 150 NaCl, 5 KCl, 10 CaCl2, 2 MgCl2, 10 glucose, and 10 HEPES, pH 7.4. Transfected HEK-293 cells were chosen by using an Olympus FV1000 confocal microscope equipped with spectral detectors and SIM scanner. Whole-cell K+ currents were recorded at room temperature (RT) using an Axopatch 200B amplifier (Molecular Devices).

Ionic currents were capacitance and series resistance compensated by 80–90%, sampled at 10 kHz (Digidata 1440; Molecular Devices), and filtered at 2 kHz. All recordings were performed with series resistance <5 MΩ and series resistance compensation of at least 80%. The pClamp8 software (Axon Instruments) was used for pulse generation and data acquired using an Axon Digidata A/D interface and subsequent analysis. Electrodes were made of borosilicate glass capillaries with filament (Sutter Instruments) using a Flaming-Brown (P-87) micropipette puller (Sutter Instruments) and fire polished. Pipettes had a resistance of 1.5-3 MΩ when filled with a solution containing (in mM): 4 NaCl, 150 KCl, 1 MgCl2, 0.5 EGTA, 5 ATP(K), and 10 HEPES, pH 7.4. Cells were clamped to a holding potential of –80 mV. To evoke voltage gated currents, all cells were stimulated with 200 millisecond square pulses ranging from –100 to +60 mV in 20 mV steps. All recordings were routinely subtracted for leak current

Protein extraction, co-immunoprecipitation and western blotting. Cells were washed twice in cold PBS and lysed on ice with lysis buffer (5 mM HEPES, 150 mM NaCl, 1% Triton X-100, pH 7.5) supplemented with 1 µg/ml aprotinin, 1 µg/ml leupeptin, 1 µg/ml pepstatin and 1 mM phenylmethylsulfonyl fluoride as protease inhibitors. Cells were next scrapped and transferred to a 1.5 ml tube. Then they were incubated for 20 min at the orbital, and spun for 20 min at 14000 rpm. The supernatant was transferred to a new tube and protein contents were determined by using the Bio-Rad Protein Assay (Bio-Rad).

For co-immunoprecipitation, 1000 µg of protein of each condition were separated and brought up to a volume of 500 ml with Lysis Buffer for IPs (NaCl 150 mM, HEPES 50 mM, Titron X-100 1%, pH 7.4), supplemented with protease inhibitors. Preclean was performed with 40 µl of protein A sepharose beads (GE Healthcare), in an orbital 1 h at 4ºC. Next, each sample was incubated with a small chromatography column (BioRad Micro spin Cromaotgraphy Columns), which contained 2.5 µg of anti-GFP antibody (Genescript) previously crosslinked to protein A sepharose beads, for 2h at room temperature, with continuous mixing in an orbital. Next, columns were centrifuged 30s at 1000g. The supernatant (SN) was kept and stored at -20ºC. Columns were washed four times with 500µl of lysis buffer and centrifugations of 30sec at 1000 g. Finally, elution was performed by incubation of the columns with 100µl of 0.2M glycine pH 2.5, and spun 30sec at 1000g. The eluted proteins (IP) were prepared for western blot by adding 20µl of Loading Buffer (5x) and 5µl of 1M Tris-HCl pH 10.

Irreversible crosslinking of the antibody to the sepharose beads was performed after one hour of incubation at RT of the antibody with protein A sepharose beads, incubating the beads with 500ul of dimethyl pimelimidate (DMP, from Pierce) for 30 min at RT. Next columns, were washed four times with 500 µl of 1x TBS, four times with 500 µl of 0.2 M

glycine pH 2.5 and three times more with 1x TBS. Once these steps are performed, the columns could be incubated with the protein lysates, in order to perform the immunoprecipitation, following the protocol described before.

In the experiments performed in presence of calcium or calcium chelators, the lysis buffer (extraction and IP) was further supplemented with 2 mM CaCl2, or 2 mM EGTA plus 2 mM EDTA, respectively.

Protein samples (50µg), supernatants and immunoprecipitates were boiled in Laemmli SDS loading buffer and separated on 10% SDS-PAGE. Next, they were transferred to nitrocellulose membranes (Immobilon-P, Millipore) and blocked in 0.2% Tween-20-PBS supplemented with 5% dry milk, before immunoreaction. Filters were immunoblotted with antibodies against Kv1.3 (1/500, Neuromab), HA (1/1000, Sigma), KCNE4 (1/800, Proteintech), GFP (1/1000, Roche) or Calmodulin (1/600, Millipore). Finally, filters were washed with 0.05% Tween 20 PBS and incubated with horseradish peroxidase conjugated secondary antibodies (BioRad).

DMP crosslinking protocol. Twenty-four hours transfected HEK cells were washed twice in cold PBS and lysed on ice with a lysis buffer that contains: 50mM boric acid, 100mM of potassium acetate, 2mM of magnesium clorur, 1mM of EGTA and 1% of triton at pH: 8,5. Half of protein was incubate with 5mM of DMP for one hour, while the other remained as a control. The reaction was stopped by adding 1mL of tris buffer 0,5M at pH: 6,8. Protein samples (50ug) were boiled in Laemmli SDS loading buffer and separated on 7% SDS-PAGE.

Kv1.3-KCNE4 complex modeling. Kv1.3 was modeled using high-resolution templates of remote or close homologs available from the Protein Data Bank (http://www.rcsb.org/pdb). The transmembrane domain and the N-terminus (except the first 49 amino acids) were modeled with the Kv1.2 potassium channel (PDB code 2R9R). The C-terminus and the remaining 49 amino acids from the N-terminus were modeled with 3HGF (nucleotide binding domain of the reticulocyte binding protein Py235) and 1PXE (zinc-binding domain from neural zinc finger factor-1) codes, respectively (Martínez-Mármol et al. 2013).

KCNE4 was modeled using high-resolution templates of homologs available from the Protein Data Bank (http://www.rcsb.org/pdb). The N-terminus, transmembrane domain and the proximal C-terminus (residues 1-98) were modeled with the KCNE1 (PDB code 2K21). The distal C-terminus (residues 99-170) were modeled with 3HTC, the best scored model (C-score [-5,2]= -3,96 y 0,29±0,09 (TM-score), 12,2±4,4Å (RMSD)) from i-Tasser modeling server (http://zhanglab.ccmb.med.umich.edu/I-TASSER/). Then, multiple sequence alignment was performed using CLUSTALW (Thompson et al., 1994) from the European Bioinformatics Institute site (http://www.ebi.ac.uk). The homology modeling was performed using the Swiss-Model Protein Modeling Server (Schwede et al. 2003) on the ExPASy Molecular Biology website (http://kr.expasy.org/) under the Project Mode. Structure visualization and modifications were made using Yasara v11.6.16 (Krieger et al. 2002) and DeepView v4 (Guex and Peitsch 1997). The orientation and optimization of the side chains were carried out in two steps. First, the residues showing van der Waals

clashes were selected and fitted with the "Quick and Dirty" algorithm (DeepView). Second, the models were energy minimized (Yasara). Briefly, this process involved an initial short steepest descent minimization to remove bumps, followed by a simulated annealing minimization. In this procedure, the simulation cell was slowly cooled towards 0K by downscaling the atom velocities. The entire system was subjected to an equilibration process before the molecular dynamics simulation. The equilibration consisted of an initial minimization of the fixed backbone atoms. Next, the restrained carbon alpha atoms were minimized and a short molecular dynamics (10 ps) minimization was performed. The goal of the latter step was to reduce the initial incorrect contacts and to fill the empty cavities. Finally, under periodic boundary conditions in the three coordinate directions, the full system was simulated at 310ºK for 0.5 ns. All dynamic simulations were performed using Yasara (Krieger et al., 2002) with the force field AMBER03 (Duan et al. 2003). The cutoff used for long-range interactions was set at 10 Å. In addition, the model was evaluated using PROCHECK to show the residues in the allowed regions of the Ramachandran plots (Laskowsky et al. 1996). The final molecular graphic representations were created using PyMOL v1.4.1 (http://pymorl.org/).

The resulting models were used to search for plausible docking interactions between Kv1.3 and Kcne4. The docking process was set in a three-step procedure: (i) Docking the Nterminus and the transmembrane domains of KCNE4. The docking model available for KCNE1-Kv7.1 complex in the open state (Kang et al 2008) was used as template to align the transmembrane regions of Kcne4 (fragment 1-62) on Kv1.3. This docking locates both proteins in the membrane context and restricts the possible conformations of their cytosolic domains. (ii) Docking the interacting regions. To accomplish the docking of the cytosolic regions between Kv1.3 and Kcne4, we isolated the C-terminus of Kv1.3 (region 439-525) as well as the putative interacting region of Kcne4 (amino acids 63 to 81, containing the leucines 69-72). The fragments were sent to GRAMM server (http://vakser.bioinformatics.ku.edu/resources/gramm/grammx/), for protein-protein docking. The docking solutions were filtered by interaction energy and by complementarity/compatibility with the transmembrane regions. The binding energy of the docked complexes was obtained by calculating the energy between the C-terminus of Kv1.3 and the KCNE4 fragment at infinite distance and then subtracting the energy of the whole complex. The energy in each cluster was stored, analyzed, and applied to select the most likely orientation of the interacting proteins. The energy of the model and the docking complexes were tested using FoldX (Guerois et al. 2002; Schymkowitz et al. 2005) on the CRG site: http://foldx.crg.es. The force field of FoldX allowed us to evaluate the properties of the structure. Such parameters as the atomic contact map, the accessibility of the atoms and residues, the backbone dihedral angles, the hydrogen bonds and the electrostatic networks of the protein were assessed. (iii) Connection of the KCNE4 domains. The best docking solution of the step (ii) was merged with the complex obtained in step (i). Finally the distal Cterminus of KCNE4 (fragment 82-170) was joined to obtain the full Kv1.3-KCNE4 complex.

Confocal microscopy and image analysis. For confocal image acquisition cells were seeded on poly-lysine-coated coverslips, and 24h later were transfected. The next day, cells were quickly washed twice, fixed with paraformaldehyde 4% for 10 min, washed three times for 5min with PBS-K+. Finally, coverslips were mounted on microscope slides (Acefesa) with

house Mowiol mounting media. Coverslips were let dry at RT at least one day before imaging.

For membrane surface labelling, Wheat Germ Agglutinin-Texas Red (WGA) (from Invitrogen) was used. Live cells (on ice) were quickly washed with PBS at 4°C and stained with a dilution of WGA-TexasRed (1/1500) in DMEM supplemented with 30 mM Hepes for 15min at 4°C. Subsequently, cells were quickly washed twice and fixed with 4% paraformaldehyde in PBS for 6 min. Next, cells were washed and mounted as described before.

The Fluorescence Resonance Energy Transfer (FRET) via acceptor photobleaching technique was measured in discrete ROI (Region of Interest). Fluorescent proteins from fixed cells were excited with the 458 nm or the 514 nm lines using low excitation intensities. Next, 475 to 495 nm bandpass and >530 nm longpass emission filters were applied. The YFP protein was bleached using maximum laser power. We obtained approximately 80% of acceptor intensity bleaching. Posteriorly, images of the donors and acceptors were taken. The FRET efficiency was calculated using the equation $[(F_{CFPafter} - F_{CFPbefore})/F_{CFPbefore}]*100$, where $F_{CFPafter}$ was the fluorescence of the donor after bleaching and $F_{CFPbefore}$ was the fluorescence before bleaching. The loss of fluorescence as a result of the scans was corrected by measuring the CFP intensity in the unbleached part of the cell.

All images were acquired with a Leica TCS SL laser scanning confocal spectral microscope (Leica Microsystems), equipped with an Argon and Helium-Neon lasers. All experiments were done with a 63x oil-immersion objective lens NA 1.32. All offline image analysis was done using Image J software. A pixel by pixel colocalization study by using JACoP (Just Another Colocalization Plugin) was used. Manders split coefficients were further obtained which are proportional to the amount of fluorescence of the colocalizing pixels in each colour channel.

RESULTS

C-terminus of KCNE4 is involved in Kv1.3 association

KCNE4 is a dominant negative peptide that exerts a reduction on Kv1.3 presence at the cell surface (Sole et al., 2009). Two mechanisms are promoting this effect: the masking of Kv1.3 export signal and the transferring of a retention motif to the channelosome (Sole et al., 2016). This subunit interacts with the channel through the C-terminal domain of the conducting protein. However, none is known about the part of KCNE4 implicated in this process.

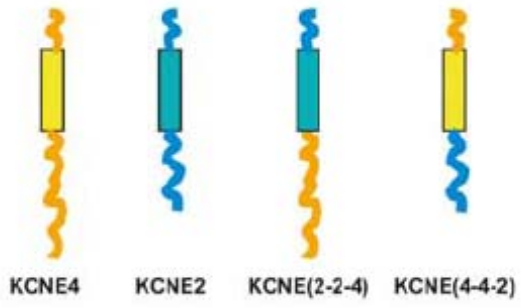

Figure 1. Scheme of the KCNE4-KCNE2 chimeras. KCNE4 domains are coloured in orange, while KCNE2 is coloured in blue. B. Anti-CFP

In order to explore this specific issue, quimeric proteins were developed using KCNE4 and KCNE2, the latter as a non-interacting peptide (Sole et al., 2009). It was initially explored the possibility that the interaction could rely on the same part than with the KCNQ family. Thus, the C-terminal domain of KCNE2 was transferred to KCNE4 leading the chimera KCNE(4-4-2), and the reverse peptide was also generated so called KCNE(2-2-4) (figure 1)

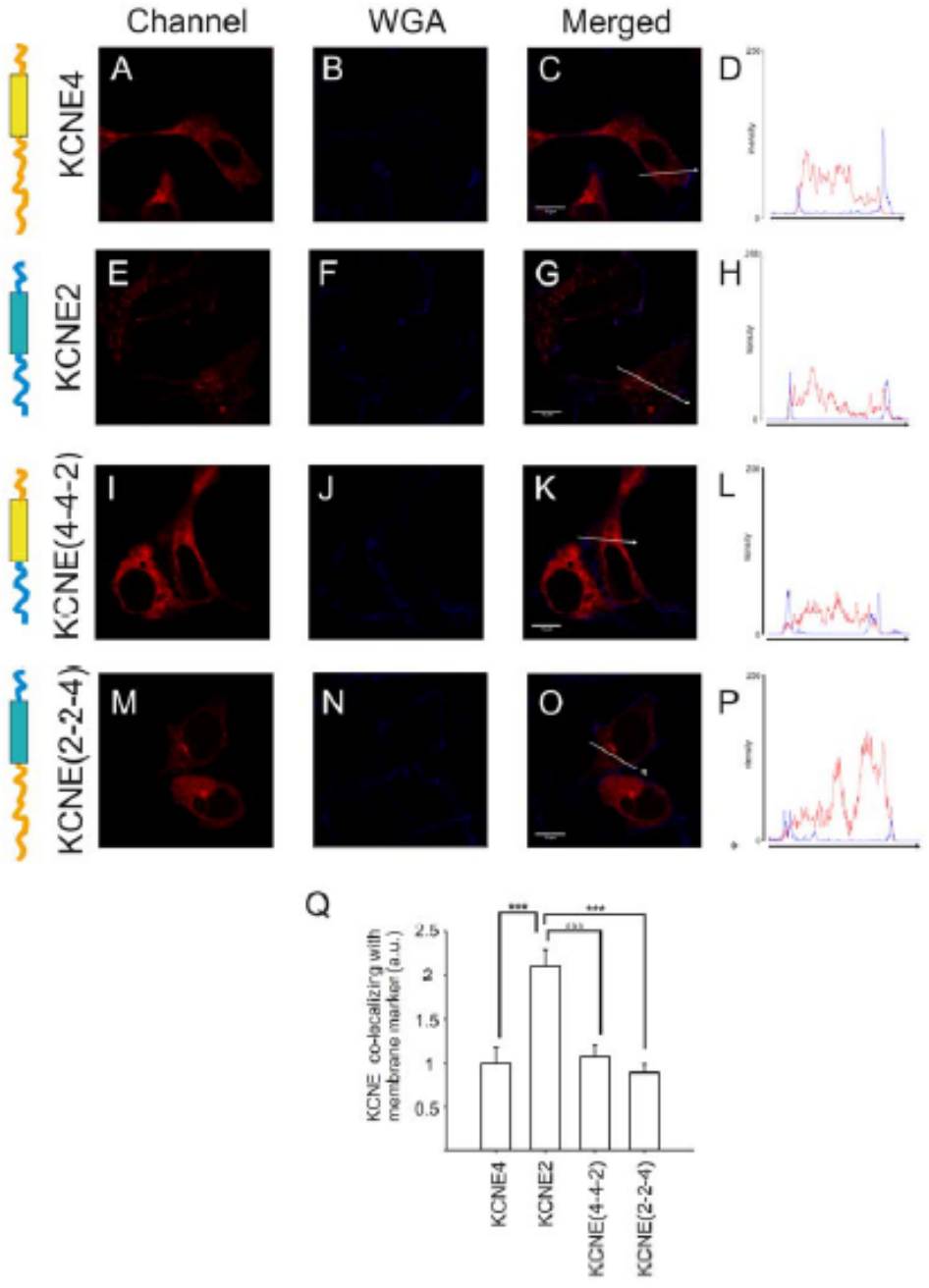

Figure 2. Membrane localization of chimeric KCNE proteins with WGA overlay. Confocal images from HEK-293 transfected cells. A-D: KCNE4 mainly presented intracellular distribution. A: KCNE4CFP. B: membrane marker. C: merged image. D: histogram of the pixel by pixel analysis of the section indicated by the arrow in D. E-H: KCNE2 shows better co-localization with the membrane marker. E: KCNE2CFP. F: membrane marker. G: merged image, pink highlights partial co-localization. H:

pixel by pixel analysis of the section indicated by the arrow in G. I-L: KCNE(4-4-2) also shows intracellular distribution. I: KCNE(4-4-2)CFP. J: membrane marker. K: merged image. L: pixel by pixel analysis of the section indicated by the arrow in K. M-P: KCNE(2-2-4) remains intracellular. M: KCNE(2-2-4)CFP. N: membrane marker. O: merged image. P: pixel by pixel

analysis of the section indicated by the arrow in O. Q: Quantification of the membrane expression of KCNE4, KCNE2, KCNE(4-4-2) and KCNE(2-2-4). Data was compared with the relative intensity of KCNE4 at the plasma membrane (determined by co-localization with the membrane marker). Values are the mean ± of 20-27 cells. ***, p<0.001 vs KCNE2 and KCNE4 (Student's t-test). Scale bars: 10 μm.

Firstly, KCNE proteins and chimeras were expressed in HEK cells and non-deleterous phenotype was detectable. In figure 2 there are representative images of the distribution for KCNE4 (A-D), KCNE2 (E-H). KCNE(4-4-2) (I-K) and KCNE(2-2-4) (M-P). Similar to KCNE4 (figure 2A-D) distribution, and contrary to KCNE2 (figure 1E-H), both KCNE(4-4-2) and KCNE(2-2-4) exhibit an intracellular distribution (figure 2Q).

To decipher the implication of this domain in the final complex formation, immunoprecipitations of those newly-generated proteins were performed in the presence of Kv1.3 (figure 2). KCNE4, as well as KCNE(2-2-4), showed a coimmunoprecipitation band corresponding to the channel, while KCNE2 and KCNE(4-4-2) do not. Thereby, it is only detectable Kv1.3 where the C-terminal of KCNE4 is present.

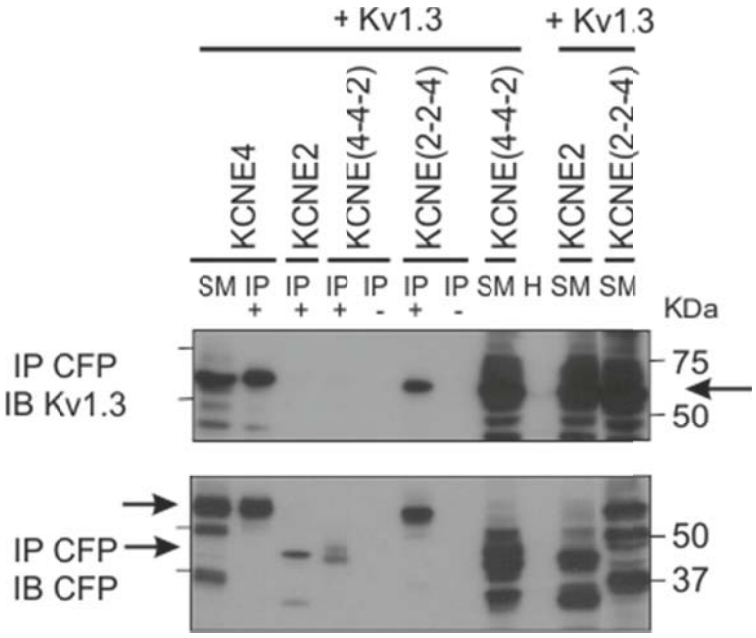

Figure 3. Immunoprecipitation of the C-terminus KCNE2KCNE4CFP chimeras in the presence of HA-Kv1.3. Anti-CFP was used to immunoprecipitate KCNEsCFP peptides. Top panel: Immunoblot against Kv1.3. Bottom panel: immunoblot against CFP. SM: starting material, IP+: immunoprecipitated in presence of CFP antibody, IP-: immunoprecipitated in absence of CFP antibody. H: Sham-transfected HEK.293 cells.

The membrane targeting of Kv1.3 upon the presence of each peptide was analysed. KCNE4 (figure 4E-I) generates a massive retention of the channel (figure 4A-D), while KCNE2 do not modify its traffic (figure 4J-N). Those results are similar to the previously published (Sole et al., 2009). Although the KCNE(4-4-2) exerts an intracellular retention of the channel (figure 4O-S), a higher degree of the Kv1.3 at the plasma membrane was observed. Moreover, there is a decrease in the colocalization between both proteins when compared with Kv1.3-KCNE4 results (figure 4Y-Z). On the other hand, KCNE(2-2-4) generates a

dramatic impairment of the Kv1.3 traffic to the plasma membrane (figure 4T-W) and both proteins increased the colocalization reaching similar levels to those resumed for Kv1.3-KCNE4 (figure 4Y-Z).

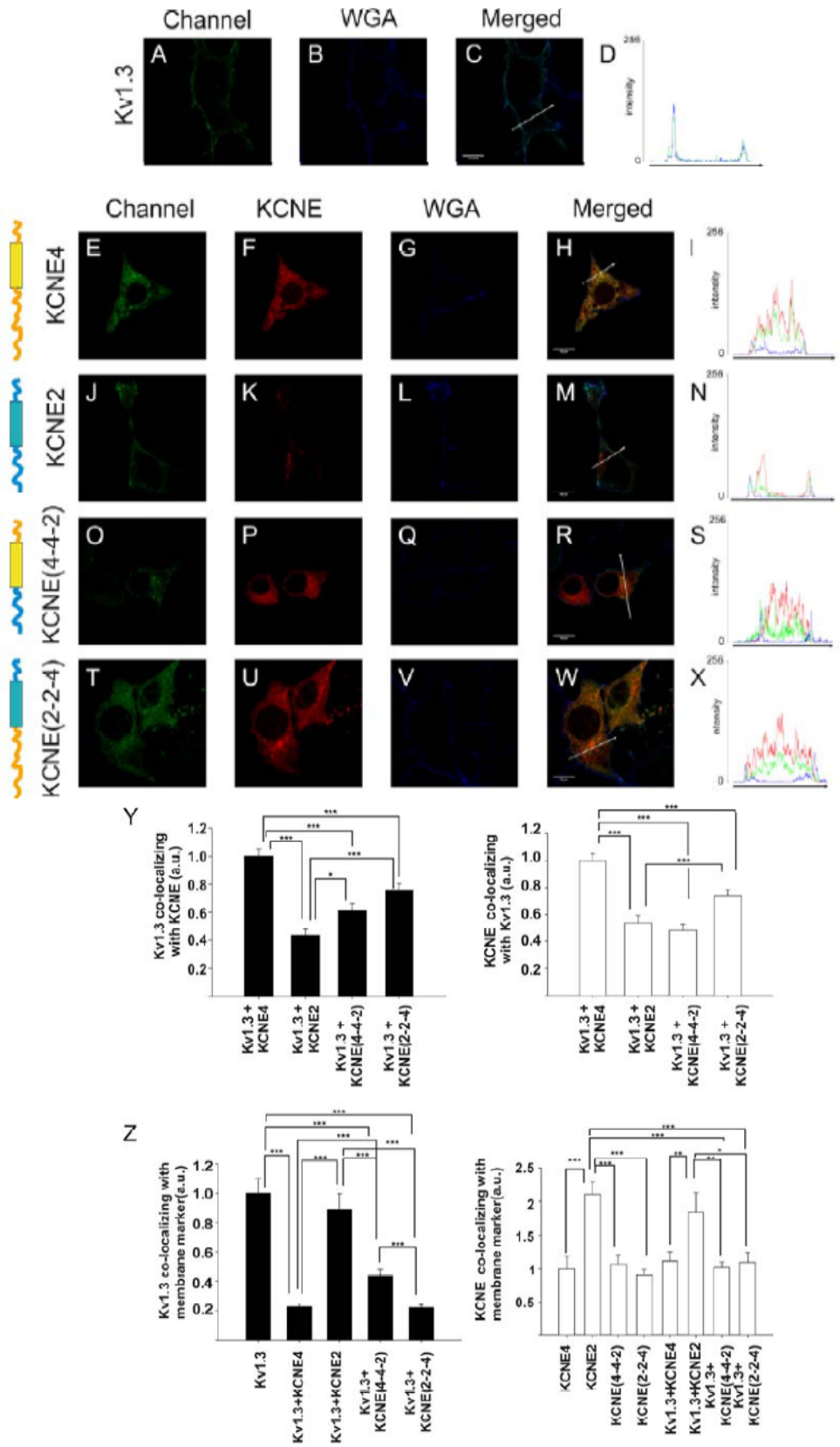

Figure 4. Distribution of Kv1.3 in the presence of chimeric KCNE proteins. Confocal images from transfected HEK-293 cells. A-D: Kv1.3 targeted to membrane surface. A: Kv1.3YFP, B: WGA, C: merged image, D: pixel by pixel analysis of the section indicated by the arrow in D. E-I: Kv1.3 and KCNE4 co-localized intracellular. E: Kv1.3 YFP. F.:KCNE4CFP. G: membrane marker. H: merged image, yellow means co-localization with Kv1.3 and KCNE4 and white triple colocalization with membrane marker. I: pixel by pixel analysis of the section indicated by the arrow in H. J-N: KCNE2 and Kv1.3 co-localized at the plasma membrane. J: Kv1.3YFP. K: KCNE2CFP. L: membrane marker. M: merged image. N: pixel by pixel analysis of the section indicated by the arrow in M. O-S: KCNE(4-4-2) and Kv1.3 did not share the same distribution, although both partially localized intracellularly. O: Kv1.3YFP. P: KCNE(4-4-2)CFP. Q: membrane marker. R: merged image. S: pixel by pixel analysis of the section indicated by the arrow in R. T-X: KCNE(2-2-4) mainly co-localized intracellularly with Kv1.3. T: Kv1.3YFP. U: KCNE(2-2-4)CFP. V: membrane marker. W: merged image. X: pixel by pixel analysis of the section indicated by the arrow in W. Y: Quantification of the relative amount of Kv1.3 that co-localizes with KCNE (left graph), and the amount of KCNE that co-localizes with Kv1.3 (right graph). Z: Quantification of membrane expression of Kv1.3 under different conditions (left graph), and the relative membrane expression of the KCNE peptides (right graph). Values are the mean ± of 24-35 cells. *, $p<0.05$; **,$p< 0.01$; ***, $p<0.001$ (Student's t-test). Scale bars: 10 μm.

Considering our previous data, the interaction domain could not coincide with the specific region that exerts the electrophysiological modulation. Patch-clamp studies of the channel and the different chimeras were carried out and representative traces are showed in figure 5: Kv1.3 (A), Kv1.3-KCNE4(B), Kv1.3-KCNE2(C), Kv1.3-KCNE(4-4-2) (D), KCNE(2-2-4) (E). Only KCNE4 modulated Kv1.3 (2545.15±241.37 pA/pF, n=21 vs 1368.01±277.32 pA/pF, n=12, in the absence and the presence of KCNE4, respectively, ** $p<0.01$, Student's t-test). KCNE2, KCNE4-4-2 and KCNE2-2-4 showed similar values to Kv1.3 (2993.92±435.89 pA/pFa, n=9; 2408.75±786.37 pA/pFa, n=11; 2540.96±410.61, n=10, respectively), which suggests that while KCNE2-2-4 associated with the channel, did not inhibit its current (figure 5G).

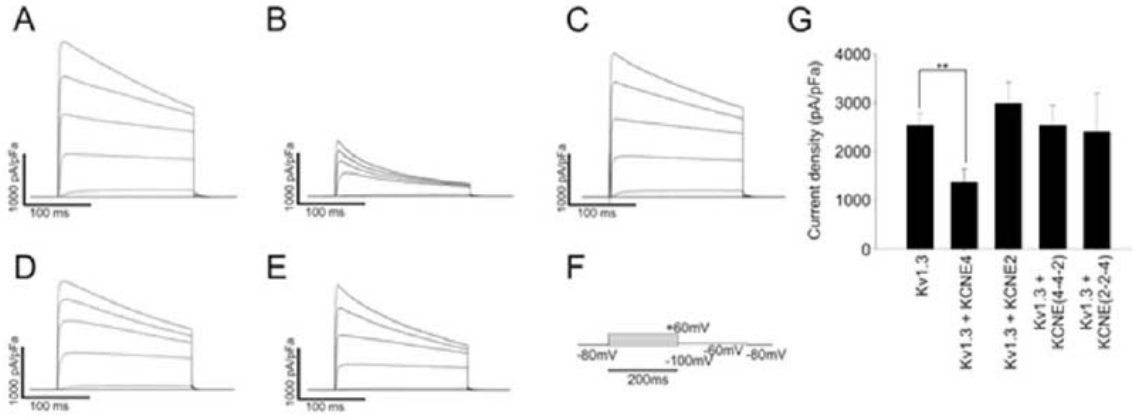

Figure 5. Representative traces from transfected HEK-293 cells with: A: Kv1.3, B: Kv1.3+KCNE4, C: Kv1.3+KCNE2, D: Kv1.3+KCNE(4-4-2) and E: Kv1.3+KCNE(2-2-4). F: Pulse protocol. Cells were voltage clamped at –80 mV and current traces were elicited by 200 millisecond voltage steps to potentials ranging from –100 mV to +60 mV in 20-mV increments. G: Current densities. **, $p< 0.01$, (Student's t-test).

Summing up, the C-terminal domain is implicated in the channelosome formation; even it is not able to exert gating changes. Moreover, a partial interaction is happening between KCNE(4-4-2) and the channel, since it is partially imposing KCNE4 effects. Since some residues in the transmembrane segment of KCNE1 and KCNE3 were determined to exert

gating modulation on Kv7.1. chimeras shifting the transmembrane domain were designed (Melman et al., 2002, Melman et al., 2001). Thus, KCNE(2-4-2) presents both soluble domains of KCNE2 with KCNE4 transmembrane segment, and KCN(4-2-4) it is the reverse chimera.

Upon coexpression with the channel, pull-downed KCNE4 and KCNE(4-2-4) were accompanied by Kv1.3. However, KCNE2 did not drag the channel. The chimera KCNE(2-4-2), which transmembrane segment comes from KCNE4, presented a coimmunoprecipitation faint band of channel. Thus, it is clear that also some residues of this part can enhance the channelosome formation (figure 6).

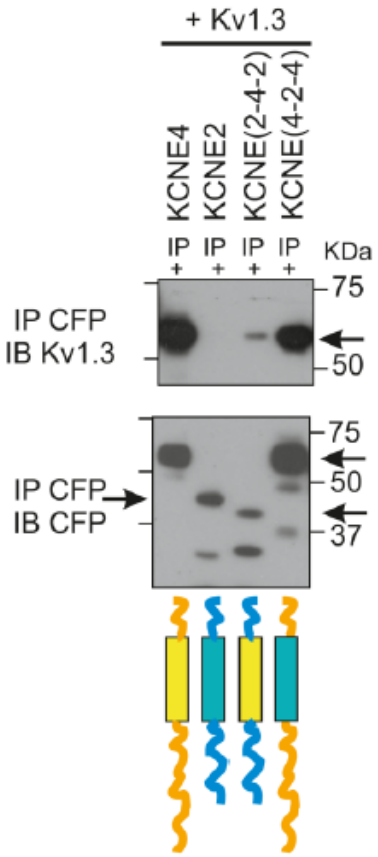

Figure 6. Some residues at the KCNE4 transmembrane motif also act as minor determinants in the interaction with Kv1.3. Immunoprecipation against CFP of transfected HEK-293 cells with Kv1.3HA and KCNE4CFP, KCNE2CFP, KCNE(2-4-2)CFP or KCNE(4-2-4). . Schemes of the diferent chimeras are also shown. KCNE4 domains are colored in orange, while KCNE2 domains are colored in blue. Top panel: immunoblot against Kv1.3. Bottom panel: immunoblot against CFP. IP+: immunoprecipitation in presence of anti-CFP antibody.

Mapping the C-terminus of KCNE4

KCNE4 C-terminus is the longest and diverse within the KCNE family. Once we determined that is in this region where the main interacting ability is placed, the exact location of this domain was explored. To assess this question, sequentially cropped C-terminal mutants were designed at different positions (figure 7A).

Immunoprecipitation assays were performed pulling-down Kv1.3CFP and coimmunoprecipitation presence was observed for: KCNE4, KCNE_S151STOP, KCNE_V140STOP, KCNE_V125STOP and KCNE_V96STOP. At longer exposures of the western blot membranes, KCNE_Y73STOP can be also detected. However, KCNE_S68STOP

lost the ability to form complexes. Thus, among the amino acids of those latter positions the major interacting interface is located (figure 7B).

Between serine-68 and tyrosine-73, there is a tetraleucine motif (69-72) that could be the responsible signature for this associating capability. Therefore, we mutated these four residues to alanines (KCNE4(L69-72A)CFP). In addition, two or four leucines were incorporated into the KCNE2 C-terminus at the homologous position (KCNE2-LL-CFP and KCNE2-LLLL-CFP, respectively) (figure 8A)

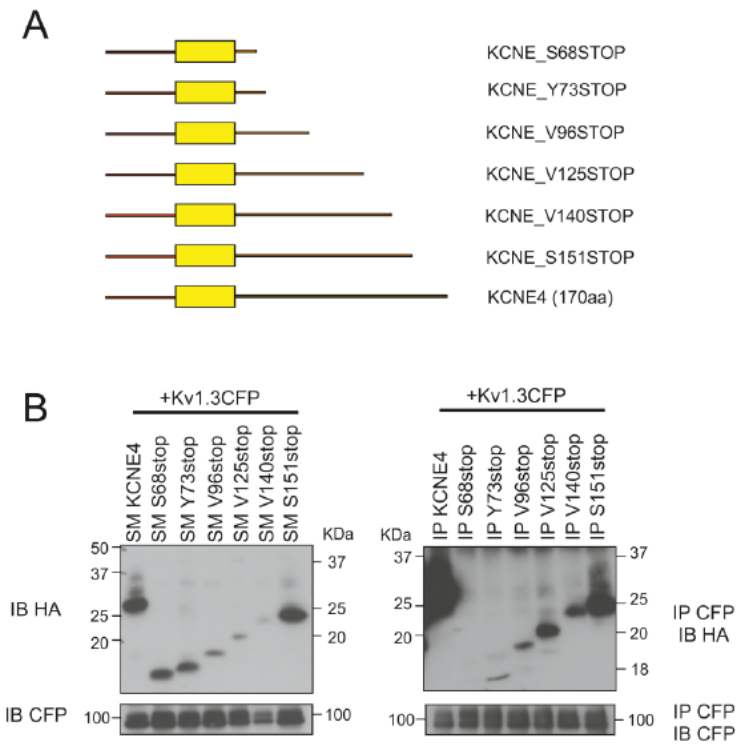

Figure 7. KCNE4 C-terminal domain mutants. A: Scheme from the KCNE4 C-terminus Stop codon mutants, indicating the amino acid which has been replaced for a stop codon, and its position. Mutants were performed by single-site directed mutagenesis from HAhKCNE4. B: Coimmunoprecipitation of KCNE4 Cterminus Stop mutants. Left panel: starting materials from transiently transfected HEK-293 cells lysates. Right panel: Immunoprecipitated samples. Top panel: immunoblot against HA. Bottom panel: immunoblot against CFP. SM: starting material. IP: immunoprecipitation.

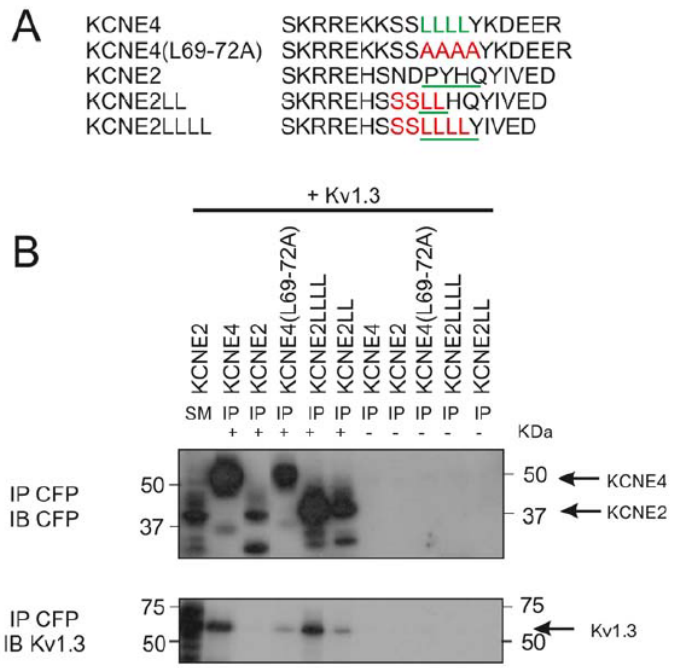

Figure 8. Role of a tetra-leucine motif in KCNE4 C-terminal domain A: Proximal sequence of the C-terminus of KCNE4, KCNE2, KCNE4(L69-72A), KCNE2LL and KCNE2LLLL peptides. The tetra-leucine motif is depicted in green. Mutations are highlighted in red. The green underlined amino acids represent the homologous region of the tetra-leucine motif. B: The tetraleucine motif is involved in KCNE4-Kv1.3 interaction. Immunoprecipitation of KCNECFP mutants and Kv1.3HA, against CFP. Top panel: immunoblot against CFP. Bottom panel: immunoblot against Kv1.3. SM: Starting material. IP+: Immunoprecipitated in presence of CFP antibody. IP-: Immunoprecipitated in absence of CFP antibody

Immunoprecipitation experiments against CFP were performed in transfected cells with all the mutants and Kv1.3. The channel effectively coimmunoprecitated with KCNE4CFP, but in the case of KCNE4(L6972A)CFP the level of coimmunoprecipitation decreased (Fig. 8B). On the other hand, while KCNE2 is a non-interacting protein for Kv1.3, the presence of two leucines (KCNE2LLCFP) led to the association of the two proteins. Moreover, when the complete signal was transferred to this subunit, the level of co-immunoprecipitation triggered a notable increase. These experiments confirmed that the tetra-leucine motif of KCNE4 is playing a central role for anchoring to the channel. Furthermore, this domain is sufficient to transfer this capability to other KCNE members.

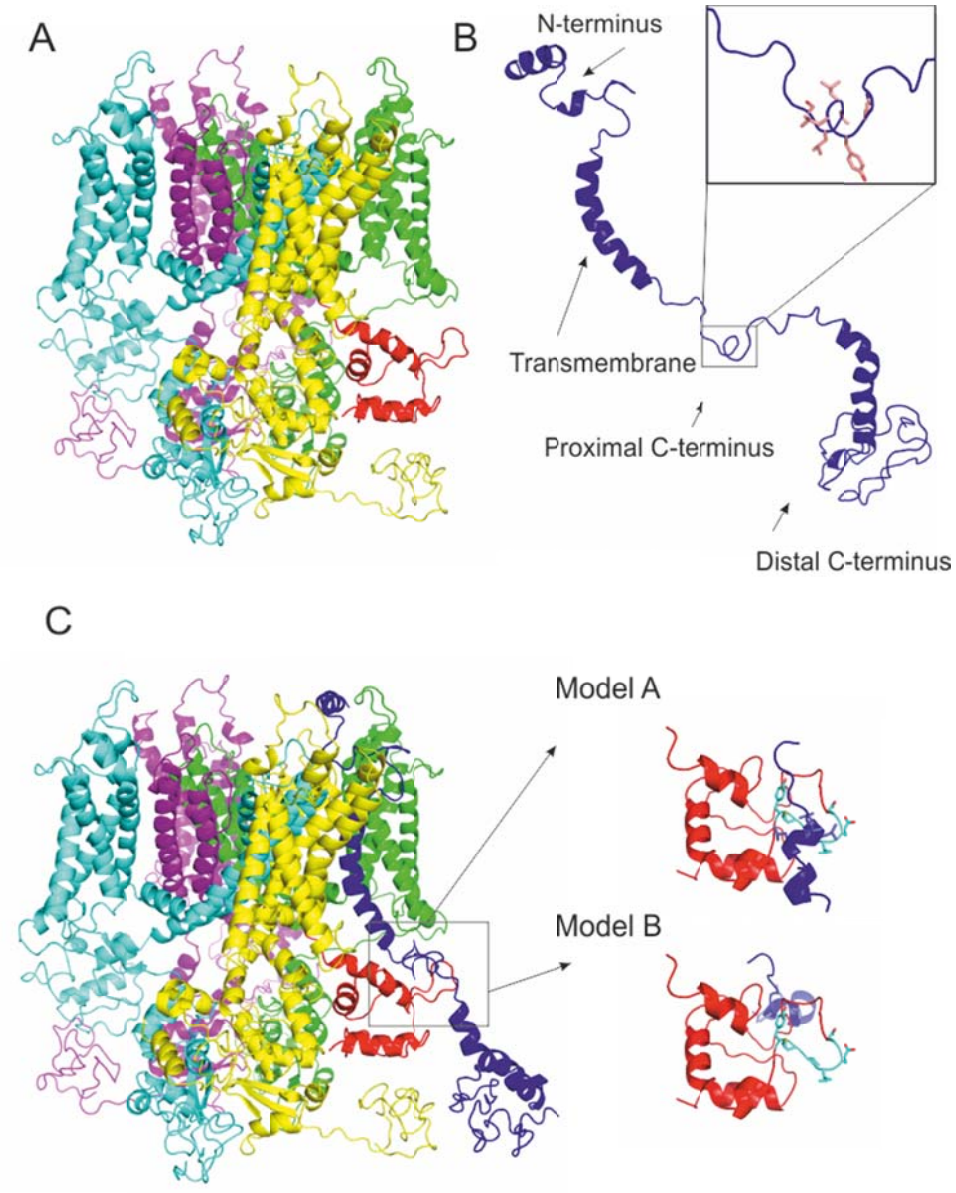

Figure 9. Molecular modeling of the Kv1.3-KCNE4 complex. A: Modeling of Kv1.3. Each subunit of the tetramer is differentially colored (cyan, pink, green and yellow). The C-terminus of the yellow subunit is colored in red. B: Molecular modeling of KCNE4 (blue). An enlargementof the tetra-leucine motif in the proximal KCNE4 C-terminus is shown. C: Docking of the Kv1.3-KCNE4 complex. Two models are equally possible, regarding the configuration of Kv1.3 and KCNE4 C-terminus. Model A involves amino acids from 474 to 484 of Kv1.3 and Leucines 69 and 72 of KCNE4. Model B involves residues 490 to 500 of Kv1.3 and Leucines 69, and 72 of KCNE4.

Implementing as a template the structural model of Sanders and collaborators of Kv7.1-KCNE1 complex (Kang et al. 2008), and considering our previous results, we used molecular dynamics modelling in order to obtain a putative model of the Kv1.3-KCNE4 complex (figure 9). KCNE4 (in blue) lies in a cleft between two Kv1.3 subunits, near S1 of one subunit and the S6 helix from another one, similar to the interaction described for the Kv7.1-KCNE1 open state. Thereby, it points out the possibility of interacting through the transmembrane domain of the auxiliary subunit.

But the more relevant part of this modelling considering our research, is regarding the position of the C-terminus of KCNE4. After an extensive docking analysis, we suggest two possible conformations. The first model considered (Model A) involves a hydrophobic pocket formed by L474, S477, M480, V481, I482, E484. Amino acids from 480 to 484 are a portion of the exhibiting motif previously described (Martinez-Marmol et al., 2013). The L69 and L72 coming from KCNE4 sequence seem to be the two principal aminoacids playing the main role in the interaction. Thereby, the tetraleucine motif would exert the masking effect on the export of the channel. In the second model (Model B), the residues implicated are F492-G500 of Kv1.3 and L69, L70 and perhaps L72 of KCNE4.

Oligomerization capability of KCNE4 resides also at tetraleucine motif

Few studies are relating the leucine rich domains with the capability to form homoligomers. For instance, upon activation of the toll-like receptors, their leucine-rich domains allow the dimerization (Berglund et al., 2015). Since there is a high similarity with the previous domain, implicated in the interaction with Kv1.3, we decided to check the possibility of oligomer formation.

Two different techniques were implemented to assess the answer. Comimunoprecipitation assay in HEK cells transfected with KCNE4CFP and KCNE4HA was assumed. Pull-down of KCNE4CFP leaded to the detection of a partner complexed: KCNE4HA (figure 10A). Moreover, FRET technique was performed for the pair KCNE4CFP/KCNE4YFP (figure 10B-D). CFP/YFP and Kv1.3CFP/Kv1.3YFP were used as positive and negative controls of the technique. KCNE1CFP/KCNE1YFP was also included as a negative condition of the specific experiment. It was previously described that this subunit is not forming any complex when expressed alone. Positive FRET values were obtained for both Kv1.3 and KCNE4 condition, while KCNE1 was not statistically distinguishable from the negative control (figure 10E). Thereby, KCNE4, different from other KCNE peptides, has the capability of forming oligomers.

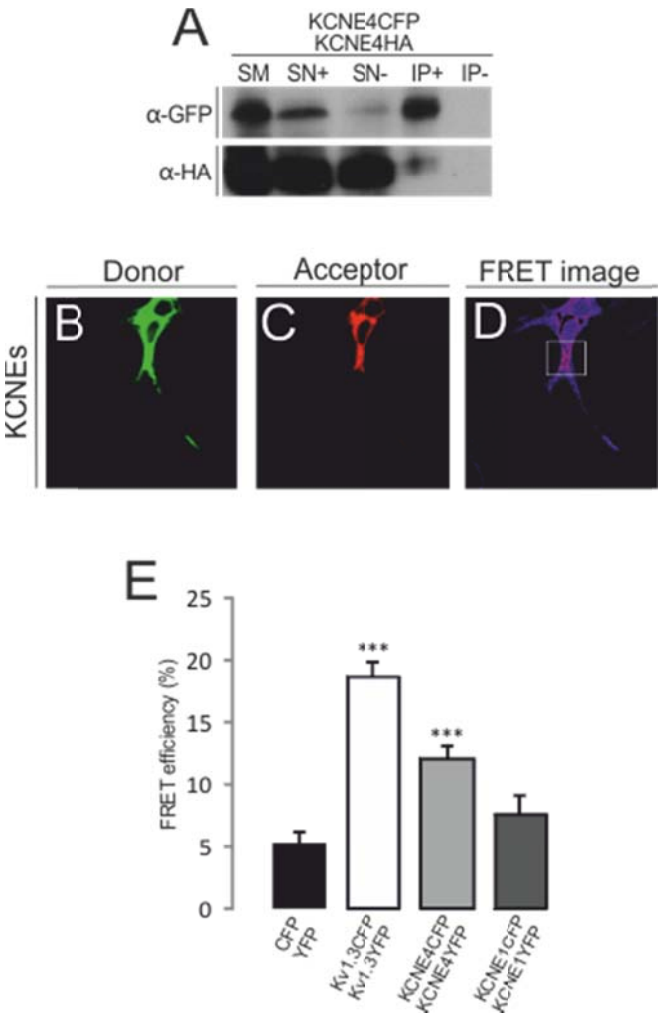

Figure 10. KCNE4 is able to form homoligomers. A. Immunoprecipitation assay against KCNE4CFP in the presence of KCNE4HA. Top panel: Immunoblot against CFP. Bottom panel: immunoblot against HA. SM: starting material. SN+: supernatant of the precipitation in the presence of antibody. SN-: supernatant of the precipitation in the absence of antibody. IP+: Immunoprecipitation in the presence of the antibody. IP-: Immunoprecipitation in the absence of the antibody. B-E.: Homoligomerization detected by FRET acceptorphotobleaching technique. B: Representative image of a donor transfection. C: Representative image of an acceptor transfection. D: FRET image obtained on the relationship donor pre-bleach versus donor post-bleach after the acceptor photobleaching. E: FRET efficiency quantification. Values are the mean of 20-30 cells. ***, $p<0.001$ compared with the negative conditions (Student's t-test).

The possible stoichiometry of this protein is completely unknown since no other KCNE member has been demonstrated to form complexes. Moreover, as mentioned before, KCNE1 oligomerization was discarded some years ago by bleaching-steps technique (Nakajo et al., 2010). To approach to the answer, DMP crosslinking and western blot analysis was performed. This compound generates covalent bounds with proteins that are not exceeding the 9,2Ă distance. Thereby, it allows a current protein extraction, boiling and loading in gels to perform typical western blot of HEK cells transfected with the condition of interest. Complexes can then be identified by weight without taking into

account other variables. Mock, CFP, Kv1.3CFP and KCNE4CFP conditions were transfected, and after the protein extraction, a portion was treated with DMP. Mock and CFP were used as negative controls. In Kv1.3CFP lines it is detectable that, upon DMP treatment, the monomer weight decreases, while the tetramer increases (figure 11 red arrows). Similarly, KCNE4 monomer molecular weight presents a lower signal when exposed at DMP, and a band pattern appears at dimerization predicted level (figure 11 yellow arrows). No further bands were obtained in this last condition. Thereby, KCNE4 is forming, most probably dimers when oligomerisation occurs.

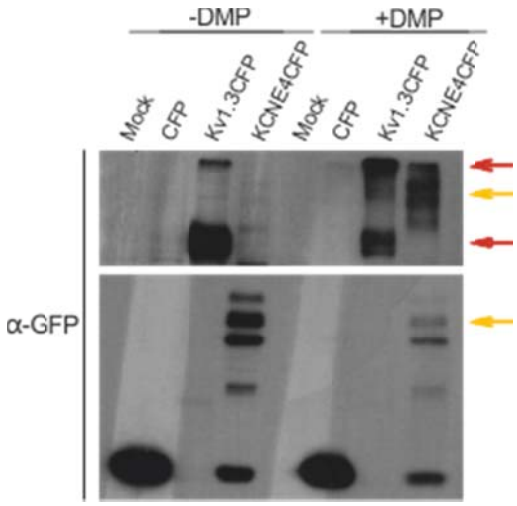

Figure 11. Dimerization of KCNE4 as the major macromolecular conformation. Protein extraction non-treated (-DMP) and treated (+DMP) with this crosslinker. Immunoblot against CFP. Lower yellow arrow, KCNE4 monomer molecular weight. Lower red arrow, Kv1.3 monomer molecular weight. Upper yellow arrow, KCNE4 dimer molecular weight. Upper red arrow, Kv1.3 tetramer molecular weight.

Immunoprecipitation assays were performed. While HA-tagged KCNE4 is forming complexes with KCNE4CFP, the mutant KCNE4(L69-72A)CFP exhibits a strong decrease in this ability (figure 12A arrow). It is detectable a small portion of KCNE4(L69-72A)HA, pointing to other possible interfaces involved, but the major interacting domain is the tetraleucine motif. FRET acceptorphotobleaching technique was implemented to confirm the previous results (figure 12B). CFP/YFP and Kv1.3CFP/Kv1.3YFP were used as negative and positive controls respectively. Even reaching significantly positive values, the condition KCNE4(L69-72A)CFP/KCNE4YFP presents a reduction of around 40% of FRET efficiency. Similar to the determinants involved in the interaction with the channel, the induction of this capacity by transferring this domain was tested. Thus, upon coexpression on HEK cells, immunoprecipitation of KCNE4CFP, KCNE4(L69-72A)CFP, KCNE2 and KCNE2LLLL were performed in the presence of KCNE4HA. Compared with KCNE4 wild type and the tetraleucine motif, a completely negative interaction is observed for the combination with KCNE2. Upon transference of this signal to KCNE2, the capacity of forming complexes with KCNE4 is detectable (figure 12C arrow).

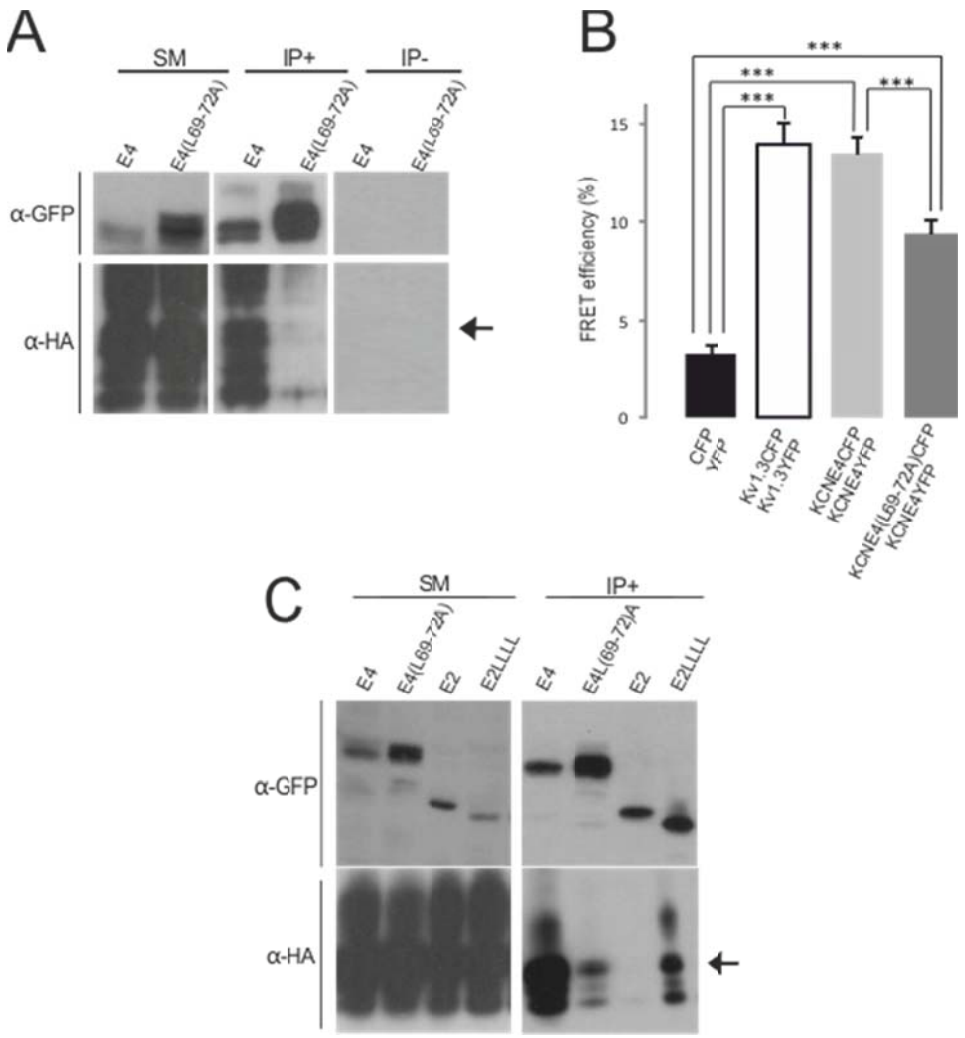

Figure 12. KCNE4 oligomerization ability is placed at the tetraleucine domain and it is transferable. A. Immunoprecipitation assay against KCNE4CFP and KCNE4(L69-72A)CFP in the presence of KCNE4(L69-72)AHA. Top panel: Immunoblot against CFP. Bottom panel: immunoblot against HA. SM: starting material. IP+: Immunoprecipitation in the presence of the antibody. IP-: Immunoprecipitation in the absence of the antibody. Arrow indicates KCNE4HA band. B. FRET efficiency quantification. Values are the mean of 20-30 cells. ***, $p<0.001$ compared with negative condition or KCNE4 wild type (Student's t-test). A. Immunoprecipitation assay against KCNE4CFP, KCNE4(L69-72A)CFP, KCNE2 and KCNE2LLLLCFP in the presence of KCNE4HA. Top panel: Immunoblot against CFP. Bottom panel: immunoblot against HA. SM: starting material. IP+: Immunoprecipitation in the presence of the antibody. Arrow indicates KCNE4HA band.

KCNE4 is, thus, able to form oligomers, probably dimers, using the same interface described for calmodulin and Kv1.3 interaction. Thus, the complex could be impaired upon the presence of those two partners (figure 13A). To analyse this hypothesis, FRET efficiency levels between KCNE4CFP and KCNE4YFP were analysed, when transfected without or with untagged calmodulin and Kv1.3. CFP/YFP and Kv1.3CFP/Kv1.3YFP were used as negative and positive controls (figure 13B). Compared with the transfection of just KCNE4, the presence of calmodulin and Kv1.3 is impairing partially the formation of those complexes or disrupting the already-formed oligomers. However, the efficacy to influence

on the interaction is different. While calmodulin was transfected in a ratio 1:1 with KCNE4 to produce a significant effect, Kv1.3 was in a 1:3 relation. Thus, although both proteins can exert a similar disruption, the efficiency is higher for Kv1.3.

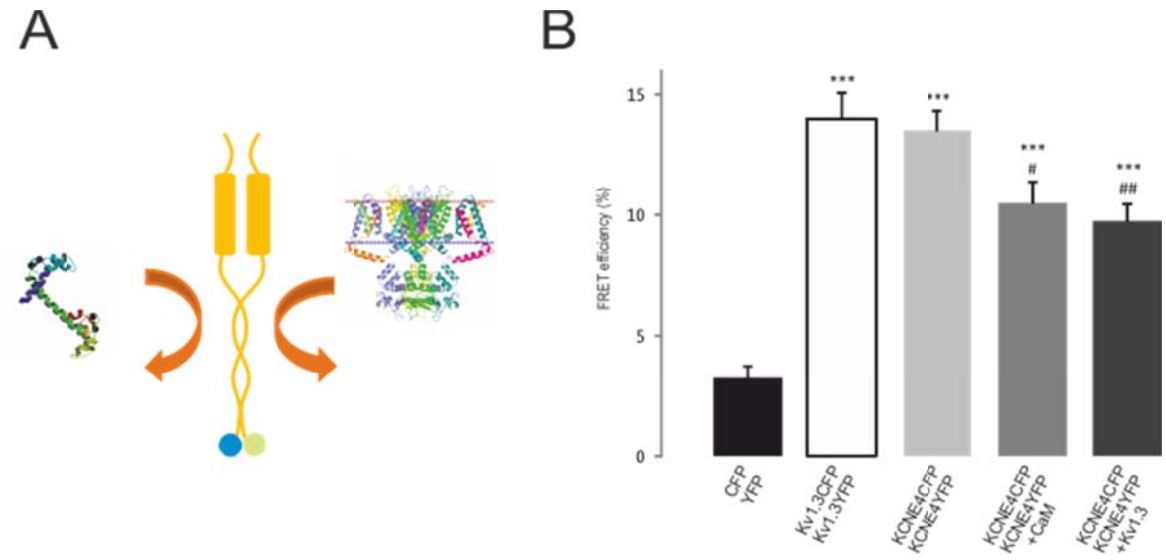

Figure 13. Calmodulin and Kv1.3 presence impair the dimerization process of KCNE4. A. Schematic representation of the possible competence with the dimer KCNE4CFP/KCNE4YFP. B. FRET efficiency quantification of KCNE4CFP/KCNE4YFP in the presence of untagged calmodulin and Kv1.3. Values are the mean of 20-30 cells. ***, $p<0.001$ compared with the negative control. #, $p<0.05$. ##, $p<0.01$ compared with solely KCNE4CFP/KCNEYFP (Student's t-test).

Calmodulin controls COPII-dependent KCNE4 traffic through the tetraleucine motif

Calmodulin is a highly studied transmitter of the calcium signalling in the cell physiology. Upon an increase in this specific ion, calmodulin is interacting with four of its ions and changing dramatically the conformation. Moreover, several proteins has been determined to interact and response to calcium-calmodulin complexes. Considering ion channels physiology it is known to enhance the traffic of Kv7 channels by interacting at a specific domain of their N-terminus (Liu and Devaux, 2014). Thereby, the traffic of KCNE4 was investigated coexpressed with exogenous calmodulin.

Upon coexpression of calmodulin-YFP and KCNE4, two different cell populations were identified. Compared with the KCNE4 solely expressed (figure 14A-C), some were presenting the typical KCNE4 ER pattern (figure 14H-K), but some others exhibit membrane staining (figure 14D-G). All the images were obtained using the same parameters of laser intensity and photo-multiplication. Thus, a study of both calmodulin and KCNE4 intensities were calculated and plotted against the localization of KCNE4 at the endoplasmic reticulum. As shown in figure 13L, the higher the ratio KCNE4/Calmodulin; the lower the colocalization of KCNE4 and ER marker (figure 14L). Thus, calmodulin presence is directly proportional to ER exit by KCNE4. Concomitantly with figure 13, the ratio 1:1 among those two proteins is the possible threshold for the disruption.

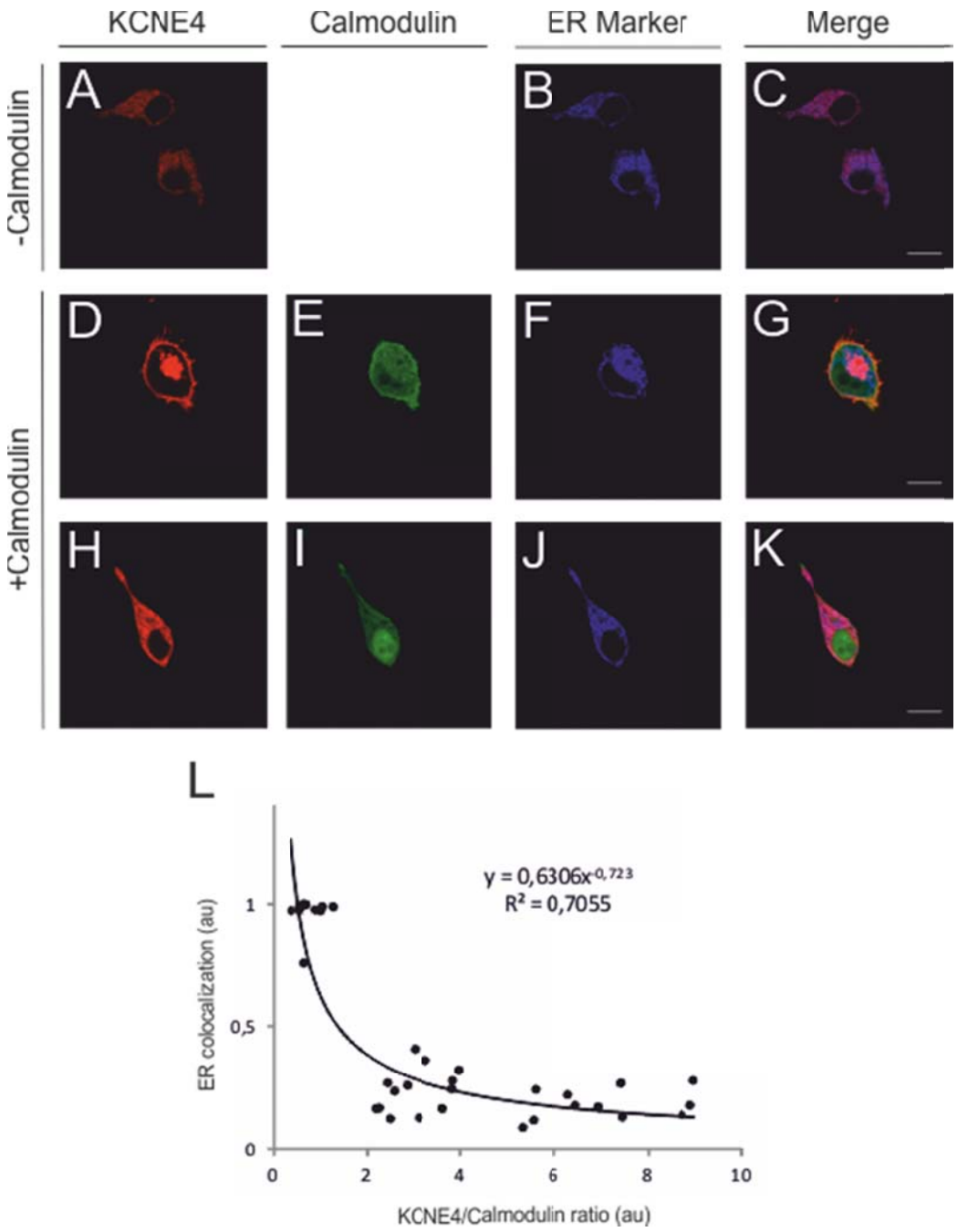

Figure 14. KCNE4 ER colocalization in the presence or the absence of calmodulin. A-C. KCNE4 colocalization with ER marker. A: KCNE4. B: ER marker. C: merge of channels, purple means colocalization. D-K: Two populations can be found upon cotransfection with calmodulin. D: KCNE4 distribution type 1. E: Calmodulin. F: ER marker. G: merge of channels, white means triple colocalization. H: KCNE4 distribution type 2. I: Calmodulin. J: ER marker. K: merge of channels. Purple means colocalization between KCNE4 and ER marker. Yellow means colocalization between KCNE4 and calmodulin. White or soft pink means triple colocalization. L: ER colocalization of KCNE4 plotted against the KCNE4/Calmodulin ratio. Potential regression curve is fitting with the data. Formula and R^2 calculation are specified. Values were obtained from 20-30cells. Scale bars: 10 μm.

In the previous contribution it was described a highly positive domain that retains KCNE4 at the endoplasmic reticulum. To further confirm the implication of the tetraleucine motif

in the KCNE4 traffic, membrane colocalization analysis of the mutant KCNE4(L69-72A)CFP was analyzed and compared with KCNE4ERRM. Compared with the typical ER retention pattern of KCNE4 (figure 15A-C) both KCNE4(L69-72A)CFP (figure 15D-F) and KCNE4(ERRM) (figure 15G-I) present a higher colocalization signal at the cell surface. We decided to mutate both signals in a unique protein in order to dissect if the signals were impairing different traffic ways. This new peptide, so called KCNE4(RM&L), was neither present in the ER compartment but at the cell surface. Quantification of this traffic showed that all three mutants are significantly more present at the plasma membrane than KCNE4 wild type (figure 15Y). Even the tendency to exit the ER compartment is bigger for KCNE4(RM&L), the membrane staining is not statistically different. Thereby, KCNE retention motif and tetraleucine domain are driving the exit through the same mechanism.

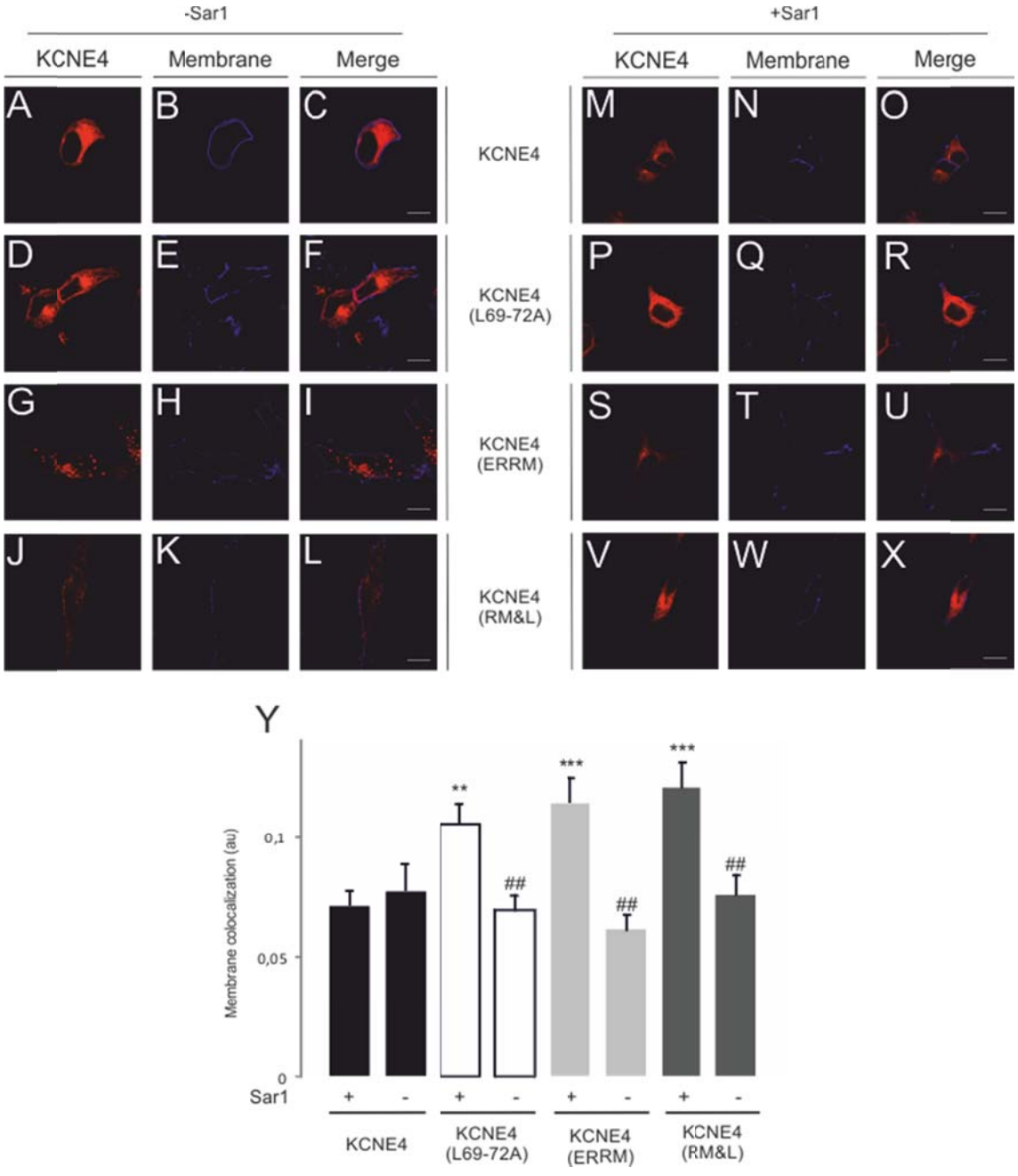

Figure 15. KCNE4 peptides traffic to the plasma membrane through a COPII-dependent mechanism. A-C. KCNE4 colocalization with membrane marker. A: KCNE4. B: membrane marker. C: merge of channels. D-F: KCNE4(L69-72A)

increases its colocalization with the membrane marker. D: KCNE4(L69-72A). E: membrane marker. F: merge of channels. G-I: KCNE4(ERRM) presents higher colocalization with the membrane marker. G: KCNE4(ERRM). H: membrane marker. I: merge of channels. J-L: KCNE4(RM&L) exhibits the highest membrane colocalization. J: KCNE4(RM&L). K: membrane marker. L: merge of channels. M-O. KCNE4 colocalization with membrane marker in the presence of Sar1-H79G. M: KCNE4. N: membrane marker. O: merge of channels. P-R: KCNE4(L69-72A) impairment of its colocalization with the membrane marker in the presence of Sar1-H79G. P: KCNE4(L69-72A). Q: membrane marker. R: merge of channels. S-U: KCNE4(ERRM) shows a fewer colocalization with the membrane marker in the presence of Sar1-H79G. S: KCNE4(ERRM). T: membrane marker. U: merge of channels. W-Y: KCNE4(RM&L) exhibits a lower membrane colocalization in the presence of Sar1-H79G. W: KCNE4(RM&L). X: membrane marker. Y: merge of channels. Purple means colocalization. Y: Quantification of membrane colocalization using Mander's coefficient. **, p<0,01; ***, p<0.001 compared with KCNE4 wild type. ##, p<0.01 compared with KCNE4(L69-72A), KCNE4(ERRM) and KCNE4(RM&L) for each condition. Values were obtained from 20-30cells. Scale bars: 10 μm.

To ensure which is the pathway that KCNE4 uses to traffic to the plasma membrane, Sar1-H79G was cotransfected with each peptide. This is an inactive mutant of the conventional secretory pathway. Thus, when it is coexpressed, COPII dependent ER-export traffic is impaired. KCNE4(L69-72A)CFP (figure 14P-R), KCNE4 (ERRM) (figure 14S-U) and KCNE4(RM&L) (figure 14V-X) switched back to the KCNE4 typical pattern. Moreover wild type protein was not affected by the presence of Sar1-H79G (figure 14M-O). Quantification of the three mutants revealed a significant reduction in membrane colocalization comparable to KCNE4 levels. Thereby, both signals are involved in the impairment of the KCNE4 traffic, while in its sequence it presents the ability for exiting by COPII dependent pathway.

The tetraleucine motif can interact with Calmodulin and Kv1.3 as well as controls the subcellular localization of KCNE4. Since all mutant proteins present an enhanced traffic to the plasma membrane and the pathway involved is the same used by Kv1.3, the effect on the complete channelosome of these sequence alterations was investigated. Moreover, previous results from our laboratory suggest that some KCNE-Kv combinations can traffic to the plasma membrane using unconventional routes, while separately KCNE peptide travel through the conventional one. Thereby, the possible pathway for the channelosomes upon coexpression was also assessed.

Coexpression of KCNE4 and the mutants with Kv1.3 leaded to different effects on the channel. KCNE4 is impairing its distribution at the plasma membrane (figure 15A-D) as previously published by our laboratory (Sole et al., 2009). As described in the contribution 2, KCNE4 ERRM is able to rescue partially the traffic of the channel to the cell surface (figure 15I-L). Similarly but in a major extend, KCNE4(L69-72A) allows a higher membrane targeting of the channel (figure 15E-H). Since this mutant presents a partially impaired interaction, the behavior observed could be due to solely Kv1.3. However, when we analyzed the presence at the cell surface of KCNE4(L69-72A) in the presence or in the absence of Kv1.3 (figure 14Y and figure 15GG), this mutant significantly traffics more to the plasma membrane when Kv1.3 is present. Thus, it is likely to consider that effects are due to a non-masking Kv1.3 export signal event rather than a dissociation phenomenon. This conclusion is supported by the model A of the molecular dynamics, which places the interface interaction with the tetraleucine motif at the YMVIEE signal. The presence of both mutations in the same protein achieves the highest values of Kv1.3 presence at the cell surface. The absence of the retention motif and the tetraleucine domain stops the massive impairment of Kv1.3 (figure 15M-O).

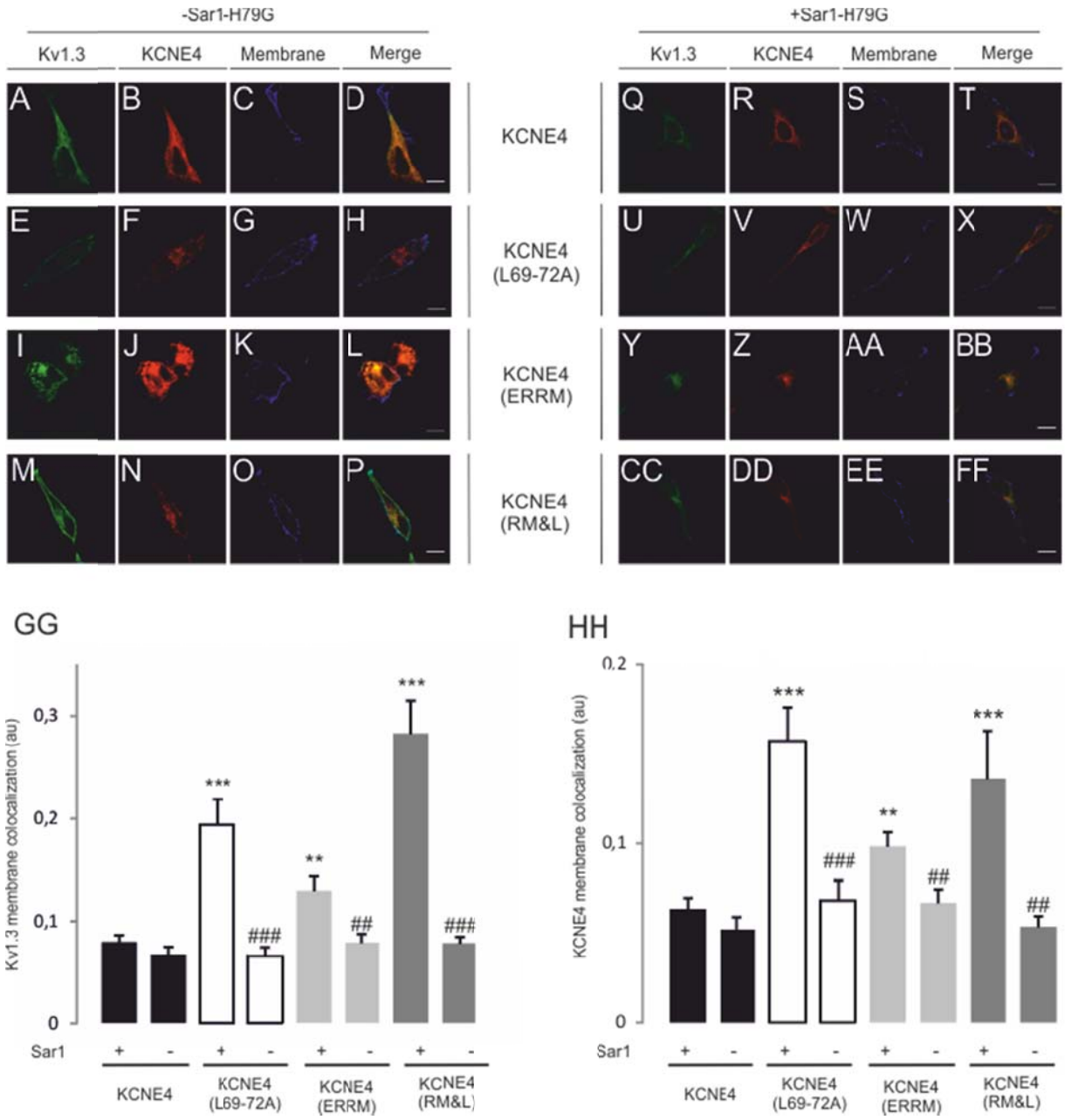

Figure 16. Kv1.3 targets the plasma membrane upon coexpression with KCNE4 mutants through COPII-dependent mechanism. A-D: Kv1.3 and KCNE4 membrane targeting. A: Kv1.3. B: KCNE4. C: membrane marker. D: merge of channels. E-H: Kv1.3 and KCNE4(L69-72A) are trafficking better to the plasma membrane. E: Kv1.3. F: KCNE4(L69-72A). G: membrane marker. H: merge of channels. I-L: Kv1.3 and KCNE4(ERRM) also target higher the membrane. I: Kv1.3. J: KCNE4(ERRM). K: membrane marker. L: merge of channels. M-P: Kv1.3 and KCNE4(RM&L) similar distribution to the other mutants. M: Kv1.3. N: KCNE4(RM&L). O: membrane marker. P: merge of channels. Q-T: Kv1.3 and KCNE4 membrane targeting in the presence of Sar1-H79G. Q: Kv1.3. R: KCNE4. S: membrane marker. T: merge of channels. U-X: Kv1.3 and KCNE4(L69-72A) impair their traffic in the presence of Sar1-H79G. U: Kv1.3. V: KCNE4(L69-72A). W: membrane marker. X: merge of channels. Y-BB: Kv1.3 and KCNE4(ERRM) decrease the membrane staining upon Sar1-H79G coexpression. Y: Kv1.3. Z: KCNE4(ERRM). AA: membrane marker. BB: merge of channels. CC-FF: Kv1.3 and KCNE4(RM&L) diminution of traffic in the presence of Sar1-H79G. CC: Kv1.3. DD: KCNE4(RM&L). EE: membrane marker. FF: merge of channels. Yellow means colocalization between Kv1.3 and KCNE4. Purple, colocalization between KCNE4 and the membrane marker. Aquamarine, colocalization between Kv1.3 and the membrane marker. White, triple colocalization. GG: Quantification of Kv1.3 membrane colocalization using Mander's coefficient. HH: Quantification of KCNE4 membrane colocalization using Mander's coefficient.**, p<0,01; ***, p< 0,001 compared with KCNE4 wild type. ##, p<0,01; ###, p<0,001 compared with KCNE4(L69-72A), KCNE4(ERRM) and KCNE4(RM&L) for each condition. Values were obtained from 20-30cells. Scale bars: 10 µm.

Excepting KCNE4 (figure 15Q-T), the coexpression of Sar1-H79G generates a retention at the ER on KCNE4(L69-72) (figure 15U-X), KCNE4(ERRM) (figure 15Y-BB) and KCNE4(RM&L) (figure 15CC-FF) . Levels of surface expression are significantly different from those obtained without the Sar1-H79G in each condition. Moreover, they are similar to KCNE4 wild type condition. Thus, channelosomes that do not present or the retention or the tetraleucine motif, are exiting the ER compartment through the conventional secretory pathway (figure 14GG).

The analysis of the KCNE4 peptides behavior revealed some supporting information. As mentioned before, the absence of the tetraleucine motif and the coexpression with Kv1.3 generates a higher membrane targeting of KCNE4(L69-72A). However, KCNE4(ERRM) kept the same distribution. Both mutations in the same peptide do not lead to a significantly different cell surface expression than the tetraleucine motif (figure 15HH). Thereby, upon coexpression with the channel, the masking effect on the export signal seems to have a deeper effect than the retention motif. However, both control the exit from the ER avoiding the COPII mechanism.

Tango of KCNE4, Kv1.3 and Calmodulin

The role of KCNE4 on Kv1.3 is to exert dominant-negative effects of its membrane functions, while calmodulin can generate an enhancement of KCNE4 traffic. Both Calmodulin and Kv1.3 require KCNE4 tetraleucine motif intact, since the interaction domain is shared. Thereby, it could be inferred a putative competence for this domain leading an impossible tripartite complex. On the other hand, since the transmembrane domain can interact also with Kv1.3, channelosome formation with the three peptides could also be contemplated.

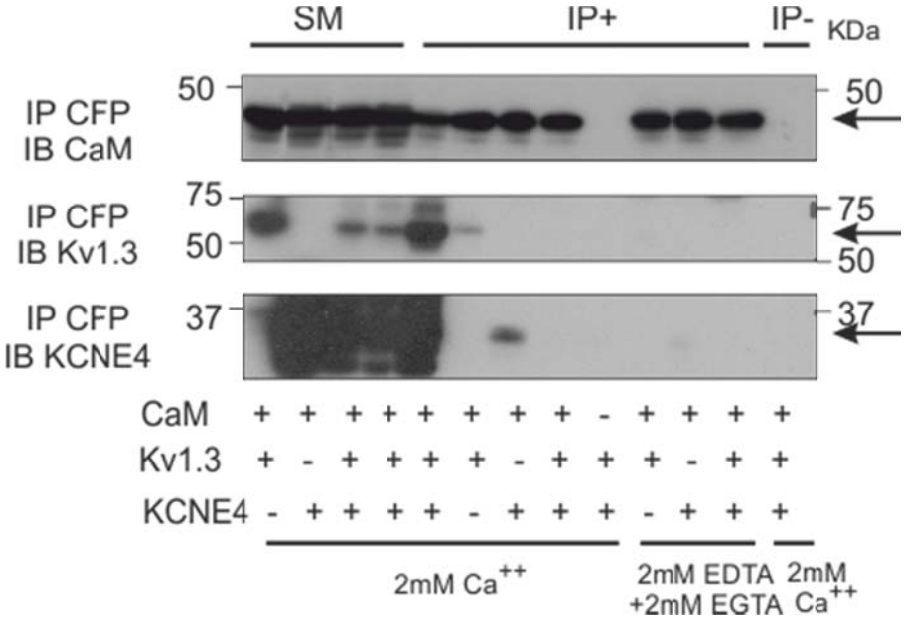

Figure 16. Kv1.3 and KCNE4 coimmunoprecipated with CaM. Immunoprecipitation against CFP of HEK-293 cells transfected with the indicated proteins (+), in the presence of 2 mM Ca2+ and 2 mM EDTA plus 2 mM EGTA. Top panel: Immunoblot against CaM. Center panel: Immunoblot against: Kv1.3. Bottom panel: immunoblot against KCNE4.

To solve this question, immunoprecipitation assays of calmodulinYFP were performed in the presence of KCNE4, Kv1.3 or both proteins. All the conditions were split in two in order to incubate them with calcium or EDTA/EGTA mixture. Thus, the calcium-dependence of an interaction can be observed.

As previously described, Calmodulin can interact with KCNE4 in the presence of calcium, but not EDTA/EGTA (Ciampa et al., 2011). Surprisingly, Kv1.3 can be also detected in those specific conditions associated with calmodulin. However, upon triple coexpression, neither KCNE4 nor Kv1.3 is detectable coimmunoprecipitating (figure 16). Thereby, a competence phenomenon for KCNE4 tetraleucine domain is taking place once all three proteins are expressed together.

DISCUSSION

The present work describes intensively the KCNE4 domain implicated in the interaction with Kv1.3. A tetraleucine motif at the juxtamembrane domain of KCNE4 C-terminus is mediating the complex. Few evidences are known in the interacting interface of the KCNE family. It was described that KCNE1 transmembrane domain is involved in the interaction, while the C-terminal was modulating the properties of Kv7.1 (Tapper and George, 2000) . Posteriorly, exactly the opposite data was defended by another group. While the cytoplasmic domain is anchoring the channel, the transmembrane is modulating the electrophysiological signature (Melman et al., 2001). Further research leaded to a bipartite theory: both C-terminus and transmembrane domains were mediating the interaction. For modulation, the KCNE transmembrane sequence is either active or passive in basal activation. In the case of KCNE3, the transmembrane domain is active and overrides the C-terminus. Conversely, the KCNE1 transmembrane domain is passive and reveals a C-terminal modulation of K7.1 (Gage and Kobertz, 2004). Within this scenario, KCNE4-Kv1.3 combination resembles to KCNE3: a cytoplasmic domain involved in the anchoring, while it is not modulating the channel features. The tetraleucine motif was shown not only to be necessary but sufficient to transfer the ability of forming complexes. However, no current modifications are derived from the entire domain. Contrarily, other studies focused on KCNE4 pointed out that modulation of Kv7.1 currents needs the C-terminal domain, even it is not sufficient (Manderfield et al., 2009). Thereby, Kv1.3 and Kv7.1 do not share the same KCNE4 regulating mechanisms.

Dileucine motifs have been identified as mediators in functions as promoting the endocytosis, protein-protein interactions or basolateral trafficking (Govers et al., 1998, Xu et al., 2016b, Wang et al., 2007, de la Fuente-Ortega et al., 2015). Few are known relating those domains to dimerization capability. Leucine enriched domains has been implicated as mediators in the physiology of the Toll-like receptors enhancing the oligomerization state upon stimulation (Berglund et al., 2015). However, those domains mainly imply a leucine residue every three other amino acids (Afzal et al., 2013). As presented in this work, the tetraleucine signal is the main part of the protein able to generate those dimers, and it is sufficient to transfer this capability. Moreover, we have demonstrated that they are acting as trafficking impairments. The mutation of this signal, as well as the previous analysed retention signal, allows KCNE4 to target the plasma membrane (Sole et al., 2016). Several publications have related the traffic of other proteins with those specific residues. Contrarily to our results, the mutation to alanine of a dileucine motif in the organic soluble

transporter impairs its membrane localization (Xu et al., 2016b). However, other publications pointed out an opposite role. For instance, acid sensing ion channels present a double dileucine motif (LLDLL) and when mutated, those enhance their the presence at the plasma membrane (Wu et al., 2016). Moreover, the mutation of a dileucine determinant at the carboxyl terminal sequence of the LHβ subunit generates an increased trafficking and exocytosis (Jablonka-Shariff and Boime, 2011). Our results showed that the masking of this specific signal, thus, enhances its traffic to the plasma membrane. Calmodulin, upon calcium stimuli, can interact with KCNE4 specifically at this domain (Ciampa et al., 2011). Concomitantly, when both proteins are coexpressed, Calmodulin partially impairs the dimerization and promotes KCNE4 export through COPII mechanism. Thereby, it is likely to speculate that this implicates a masking of the leucine motif. Similar mechanism was proposed for E-cadherin endocytosis. A dileucine motif in the juxtamembrane cytoplasmic domain is required for E-cadherin endocytosis. When mutated, this protein can no longer be internalized. An interactor, p-120, is able to interact and mask this signal and thus reducing the endocytosis (Miyashita and Ozawa, 2007). Thereby, KCNE4 final targeting can be controlled by calcium stimulus. Furthermore, the previous data show that KCNE4 sequence presents specific signals to traffic to the plasma membrane through COPII mechanism. Even the glycosylation modification was described for those proteins, the specific trafficking mechanism was not previously dissected (Malaby and Kobertz, 2013). However, the balance of exiting and staying signals is highly displaced to the retention ones. Considering that some authors defend that the assembly of KCNE and Kv channels can happen at the cell surface, calmodulin could be controlling the already-synthesized channels by trafficking KCNE4 (Vanoye et al., 2010).

The channelosome formation with Kv1.3 generates a massive retention of the channel at the ER compartment (Sole et al., 2009). As described in the previous contribution, this is due to two different mechanisms: the masking of the YMVIEE signal of the channel and the addition of retention signals coming from KCNE4 (Sole et al., 2016). The absence of the tetraleucine motif generates also an increased presence of Kv1.3 at the plasma membrane. Even the interaction driving force is absent; at a cellular level they remained together through the transmembrane domain. Changes in KCNE4(L69-72A) distribution upon coexpression with Kv1.3 revealed this association. If we consider the first model proposed in the molecular dynamics data, the absence on the tetraleucine motif would leave the YMVIEE signal not covered and thus generating the recognition by Sec24. Thereby, our data is pointing that the tetraleucine motif is the responsible of the export signal covering. Thus, both tetraleucine motif and the retention signal are involved in controlling the exit of the channelosome through the COPII-dependent mechanism. As shown in the first contribution, it is the mechanism used by Kv1.3 to reach the cell membrane (Martinez-Marmol et al., 2013).

Finally, we demonstrate that Kv1.3, KCNE4 and Calmodulin are in a tight relationship. However, no tripartite complexes are able to be formed. Contrary to Kv7.1, Kv1.3 does not need calmodulin to interact with KCNE4 (Ciampa et al., 2011). Considering Kv1.3 and Calmodulin, although previous investigations described a negative interaction, we have shown a possible complex formed by those two proteins (Fanger et al., 1999). Actually, previous studies revisited the effect of calcium on Kv1.3 current and a dependent reduction of Kv1.3 current in megacariocytes and also COS-7 transfected cells was observed (Martínez-Pinna et al. 2012). However, further studies need to be performed to

discard a tripartite complex mediated by an associated kinase (for instance CaMKII) (Chang et al., 2001). Taking all results in consideration, the present work is highly relevant regarding the importance of all three proteins at the immune system. Further research is imperative to understand the regulation of all three entities and the role of each on the physiology of their partners.

REFERENCES

AFZAL, A. J., SROUR, A., GOIL, A., VASUDAVEN, S., LIU, T., SAMUDRALA, R., DOGRA, N., KOHLI, P., MALAKAR, A. & LIGHTFOOT, D. A. 2013. Homo-dimerization and ligand binding by the leucine-rich repeat domain at RHG1/RFS2 underlying resistance to two soybean pathogens. *BMC Plant Biol,* 13**,** 43.

BERGLUND, N. A., KARGAS, V., ORTIZ-SUAREZ, M. L. & BOND, P. J. 2015. The role of protein-protein interactions in Toll-like receptor function. *Prog Biophys Mol Biol,* 119**,** 72-83.

BOCK, J., SZABO, I., GAMPER, N., ADAMS, C. & GULBINS, E. 2003. Ceramide inhibits the potassium channel Kv1.3 by the formation of membrane platforms. *Biochem Biophys Res Commun,* 305**,** 890-7.

CIAMPA, E. J., WELCH, R. C., VANOYE, C. G. & GEORGE, A. L., JR. 2011. KCNE4 juxtamembrane region is required for interaction with calmodulin and for functional suppression of KCNQ1. *J Biol Chem,* 286**,** 4141-9.

CHANG, M. C., KHANNA, R. & SCHLICHTER, L. C. 2001. Regulation of Kv1.3 channels in activated human T lymphocytes by Ca(2+)-dependent pathways. *Cell Physiol Biochem,* 11**,** 123-34.

DAVID, J. P., STAS, J. I., SCHMITT, N. & BOCKSTEINS, E. 2015. Auxiliary KCNE subunits modulate both homotetrameric Kv2.1 and heterotetrameric Kv2.1/Kv6.4 channels. *Sci Rep,* 5**,** 12813.

DE LA FUENTE-ORTEGA, E., GRAVOTTA, D., PEREZ BAY, A., BENEDICTO, I., CARVAJAL-GONZALEZ, J. M., LEHMANN, G. L., LAGOS, C. F. & RODRIGUEZ-BOULAN, E. 2015. Basolateral sorting of chloride channel 2 is mediated by interactions between a dileucine motif and the clathrin adaptor AP-1. *Mol Biol Cell,* 26**,** 1728-42.

FANGER, C. M., GHANSHANI, S., LOGSDON, N. J., RAUER, H., KALMAN, K., ZHOU, J., BECKINGHAM, K., CHANDY, K. G., CAHALAN, M. D. & AIYAR, J. 1999. Calmodulin mediates calcium-dependent activation of the intermediate conductance KCa channel, IKCa1. *J Biol Chem,* 274**,** 5746-54.

GAGE, S. D. & KOBERTZ, W. R. 2004. KCNE3 truncation mutants reveal a bipartite modulation of KCNQ1 K+ channels. *J Gen Physiol,* 124**,** 759-71.

GOVERS, R., VAN KERKHOF, P., SCHWARTZ, A. L. & STROUS, G. J. 1998. Di-leucine-mediated internalization of ligand by a truncated growth hormone receptor is independent of the ubiquitin conjugation system. *J Biol Chem,* 273**,** 16426-33.

GRUNNET, M., JESPERSEN, T., RASMUSSEN, H. B., LJUNGSTROM, T., JORGENSEN, N. K., OLESEN, S. P. & KLAERKE, D. A. 2002. KCNE4 is an inhibitory subunit to the KCNQ1 channel. *J Physiol,* 542**,** 119-30.

GRUNNET, M., OLESEN, S. P., KLAERKE, D. A. & JESPERSEN, T. 2005. hKCNE4 inhibits the hKCNQ1 potassium current without affecting the activation kinetics. *Biochem Biophys Res Commun,* 328**,** 1146-53.

GRUNNET, M., RASMUSSEN, H. B., HAY-SCHMIDT, A., ROSENSTIERNE, M., KLAERKE, D. A., OLESEN, S. P. & JESPERSEN, T. 2003. KCNE4 is an inhibitory subunit to Kv1.1 and Kv1.3 potassium channels. *Biophys J,* 85**,** 1525-37.

HILLE, B. 2001. Ion channels of excitable membranes. *Sinauerassociates, Sunderland, Mass.. Great Britain, 2001.*

JABLONKA-SHARIFF, A. & BOIME, I. 2011. A dileucine determinant in the carboxyl terminal sequence of the LHbeta subunit is implicated in the regulated secretion of lutropin from transfected GH3 cells. *Mol Cell Endocrinol,* 339**,** 7-13.

LIU, W. & DEVAUX, J. J. 2014. Calmodulin orchestrates the heteromeric assembly and the trafficking of KCNQ2/3 (Kv7.2/3) channels in neurons. *Mol Cell Neurosci,* 58**,** 40-52.

MALABY, H. L. & KOBERTZ, W. R. 2013. Molecular determinants of co- and post-translational N-glycosylation of type I transmembrane peptides. *Biochem J,* 453**,** 427-34.

MANDERFIELD, L. J., DANIELS, M. A., VANOYE, C. G. & GEORGE, A. L., JR. 2009. KCNE4 domains required for inhibition of KCNQ1. *J Physiol,* 587**,** 303-14.

MARTINEZ-MARMOL, R., PEREZ-VERDAGUER, M., ROIG, S. R., VALLEJO-GRACIA, A., GOTSI, P., SERRANO-ALBARRAS, A., BAHAMONDE, M. I., FERRER-MONTIEL, A., FERNANDEZ-BALLESTER, G., COMES, N. & FELIPE, A. 2013. A non-canonical di-acidic signal at the C-terminus of Kv1.3 determines anterograde trafficking and surface expression. *J Cell Sci,* 126**,** 5681-91.

MELMAN, Y. F., DOMENECH, A., DE LA LUNA, S. & MCDONALD, T. V. 2001. Structural determinants of KvLQT1 control by the KCNE family of proteins. *J Biol Chem,* 276**,** 6439-44.

MELMAN, Y. F., KRUMERMAN, A. & MCDONALD, T. V. 2002. A single transmembrane site in the KCNE-encoded proteins controls the specificity of KvLQT1 channel gating. *J Biol Chem,* 277**,** 25187-94.

MELMAN, Y. F., UM, S. Y., KRUMERMAN, A., KAGAN, A. & MCDONALD, T. V. 2004. KCNE1 binds to the KCNQ1 pore to regulate potassium channel activity. *Neuron,* 42**,** 927-37.

MIYASHITA, Y. & OZAWA, M. 2007. Increased internalization of p120-uncoupled E-cadherin and a requirement for a dileucine motif in the cytoplasmic domain for endocytosis of the protein. *J Biol Chem,* 282**,** 11540-8.

NAKAJO, K., ULBRICH, M. H., KUBO, Y. & ISACOFF, E. Y. 2010. Stoichiometry of the KCNQ1 - KCNE1 ion channel complex. *Proc Natl Acad Sci U S A,* 107**,** 18862-7.

PANYI, G. 2005. Biophysical and pharmacological aspects of K+ channels in T lymphocytes. *Eur Biophys J,* 34**,** 515-29.

PANYI, G., VAMOSI, G., BACSO, Z., BAGDANY, M., BODNAR, A., VARGA, Z., GASPAR, R., MATYUS, L. & DAMJANOVICH, S. 2004. Kv1.3 potassium channels are localized in the immunological synapse formed between cytotoxic and target cells. *Proc Natl Acad Sci U S A,* 101**,** 1285-90.

PONGS, O. & SCHWARZ, J. R. 2010. Ancillary subunits associated with voltage-dependent K+ channels. *Physiol Rev,* 90**,** 755-96.

ROURA-FERRER, M., SOLE, L., OLIVERAS, A., DAHAN, R., BIELANSKA, J., VILLARROEL, A., COMES, N. & FELIPE, A. 2010. Impact of KCNE subunits on KCNQ1 (Kv7.1) channel membrane surface targeting. *J Cell Physiol,* 225**,** 692-700.

SOLE, L. & FELIPE, A. 2010. Does a physiological role for KCNE subunits exist in the immune system? *Commun Integr Biol,* 3**,** 166-8.

SOLE, L., ROIG, S. R., VALLEJO-GRACIA, A., SERRANO-ALBARRAS, A., MARTINEZ-MARMOL, R., TAMKUN, M. M. & FELIPE, A. 2016. The C-terminal domain of Kv1.3 regulates functional interactions with the KCNE4 subunit. *J Cell Sci,* 129**,** 4265-4277.

SOLE, L., ROURA-FERRER, M., PEREZ-VERDAGUER, M., OLIVERAS, A., CALVO, M., FERNANDEZ-FERNANDEZ, J. M. & FELIPE, A. 2009. KCNE4 suppresses Kv1.3 currents by modulating trafficking, surface expression and channel gating. *J Cell Sci,* 122**,** 3738-48.

SOLE, L., VALLEJO-GRACIA, A., ROIG, S. R., SERRANO-ALBARRAS, A., MARRUECOS, L., MANILS, J., GOMEZ, D., SOLER, C. & FELIPE, A. 2013. KCNE gene expression is dependent on the proliferation and mode of activation of leukocytes. *Channels (Austin),* 7**,** 85-96.

SZABO, I., BOCK, J., GRASSME, H., SODDEMANN, M., WILKER, B., LANG, F., ZORATTI, M. & GULBINS, E. 2008. Mitochondrial potassium channel Kv1.3 mediates Bax-induced apoptosis in lymphocytes. *Proc Natl Acad Sci U S A,* 105**,** 14861-6.

TAPPER, A. R. & GEORGE, A. L., JR. 2000. MinK subdomains that mediate modulation of and association with KvLQT1. *J Gen Physiol,* 116**,** 379-90.

VANOYE, C. G., WELCH, R. C., TIAN, C., SANDERS, C. R. & GEORGE, A. L., JR. 2010. KCNQ1/KCNE1 assembly, co-translation not required. *Channels (Austin),* 4**,** 108-14.

WANG, Q., ZHU, F. & WANG, Z. 2007. Identification of EGF receptor C-terminal sequences 1005-1017 and di-leucine motif 1010LL1011 as essential in EGF receptor endocytosis. *Exp Cell Res,* 313**,** 3349-63.

WU, J., LENG, T., JING, L., JIANG, N., CHEN, D., HU, Y., XIONG, Z. G. & ZHA, X. M. 2016. Two di-leucine motifs regulate trafficking and function of mouse ASIC2a. *Mol Brain,* 9**,** 9.

XU, S., SOROKA, C. J., SUN, A. Q., BACKOS, D. S., MENNONE, A., SUCHY, F. J. & BOYER, J. L. 2016. A Novel Di-Leucine Motif at the N-Terminus of Human Organic Solute Transporter Beta Is Essential for Protein Association and Membrane Localization. *PLoS One,* 11**,** e0158269.

3.3. CHAPTER 3: HETEROLIGOMERIC FORMATION OF Kv1.3 CHANNELOSOME

3.3.1. Contribution 1:

Short letter.

KCNE4 effects are dominant on Kv1.3-Kvß2.1 complexes

Roig SR[1], Solé L[2], Vicente R[3], Felipe A[1]

[1]Molecular Physiology Laboratory, Departament de Bioquímica i Biomedicina Molecular, Institut de Biomedicina (IBUB), Universitat de Barcelona, Barcelona, Spain

[2]Department of Biomedical Sciences, Colorado State University. Fort Collins, USA.

[3]Laboratory of Molecular Physiology and Channelopathies, Departament de Ciències Experimentals i de la Salut, Universitat Pompeu Fabra, Barcelona, Spain.

ABSTRACT

Voltage-gated potassium channels are key proteins in highly different processes of the cellular physiology. Kv1.3 has been described to be a player in activation and proliferation of T-cells, as well as in apoptosis. The *in vivo* constitution of those proteins is not as solely conducting entities but as channelosomes coupling auxiliary subunits. Several different families have been described to modulate Kv channels. They can alter from the electrophysiology to the traffic or the subcellular localization, controlling the final function. KCNE4 is a Kv1.3 regulator with a dominant-negative effect by impairing its traffic to the plasma membrane. Kvβ2.1, also a channel partner, determines the specific submembrane fractions presence. Moreover, Kvβ2.1 can partially counteract the PMA-dependent endocytosis of Kv1.3. Both can exert changes in the electrophysiological properties of this specific channel. All three proteins share the expression in similar tissues. Therefore, the present work analysed the possibility of tripartite complexes and their putative effects on the final channel physiology. They can build macromolecular conducting entities that behave highly similar to KCNE4-Kv1.3 complexes. However, electrophysiology recordings exhibit slight differences due to the presence of Kvβ2.1. This work represents a step further to comprehend the possible channelosome combinations in native cells.

Report of the PhD student participation

KCNE4 effects are dominant on Kv1.3-Kvß2.1 complexes

Sara Raquel Roig Merino performed all the experiments and the data analysis of this article except the KCNE4-Kv1.3 chimera.

Antonio Felipe

PhD thesis director

INTRODUCTION

Kv channels are highly important proteins involved in several different cellular functions. *In vivo* studies showed that rarely are acting as solely conducting entities, but as multiprotein complexes. The partners of a channelosome are known as β or auxiliary subunits. From their discovery, a wide range of modifications induced by those peptides has been published. Electrophysiology modulations have been extensively studied in multicomplexes, but distribution, traffic and turnover are also affected features (Hille, 2001).

Mainly, studies are focused in the combination of Kv channels and a unique β-subunit. However, *in vivo* systems contain a vast number of auxiliary subunits. Therefore, complexes formed by a Kv channel and more than one modulator are physiologically relevant. Regarding KCNEs subfamily, some publications deciphered that, indeed, tripartite complexes were possible to be formed. Thus, from mouse brain Kv12.2 was isolated forming channelosomes with KCNE1 and KCNE3 (Clancy et al., 2009). Moreover, all members of the KCNE family have been reported to modulate channels integrated by Kv7.1-KCNE1 forming tripartite complexes (Lundquist et al., 2005, Wu et al., 2006). Considering the Kvβ family, few studies were designed to decipher the effects of a Kvβ mixture on the channel. For instance, intermediate modulation was detected on Kv1.2 upon the presence of Kvβ1.2 and Kvβ2 (Accili et al., 1997a).

Considering channelosomes formed by three different auxiliary families, it was published that KCNE4 requires calmodulin to interact and alter Kv7.1 (Ciampa et al., 2011). Previously, it was also described the possible complex formation among KChIP, DPPX and Kv4.2 building the combination to generate an I_A current in neurons (Seikel and Trimmer, 2009). Moreover, the I_{KS} complex can interact with Yotiao forming a tripartite channelosome (Abbott, 2016a). However, there is not massive research regarding this topic. The present work addressed the possible complex formation among Kv1.3, Kvβ2.1 and KCNE4. All three entities are expressed in similar tissues but there is not available information about their putative tripartite interaction (Vicente et al., 2005, Sole et al., 2009, Abbott, 2016b, Downen et al., 1999). Thereby, channelosome formation, electrophysiology consequences and traffic analysis of this specific combination were addressed. KCNE4 dominance was observed for the traffic, but partial Kvβ2.1 electrophysiological features were also identified. Studies that consider an atmosphere closer to *in vivo* systems are highly relevant to understand the variety of functions of a voltage-gated potassium channel such as Kv1.3.

MATERIALS AND METHODS

Expression plasmids and site-directed mutagenesis. rKv1.3 in pRcCMV was provided by T.C. Holmes (New York University). It was subcloned into pEYFP-C1 and pECFP-C1 (Clontech) to preserve normal channel behaviour (Vicente et al., 2008). KCNE4CFP was previously described (Sole et al., 2009). mKvβ2.1 was provided by M.M. Tamkun (Colorado State University). mKvβ2.1 was subcloned into pEYFP-N1 and pECFP-N1 (Clontech). All constructs were verified using automated DNA sequencing.

Cell culture, *transfections and pharmacological treatments.* HEK-293 cells were cultured on DMEM (LONZA) containing 10% fetal bovine serum (FBS) supplemented with penicillin (10.000 U/ml), streptomycin (100 µg/ml) (GIBCO) and L-glutamine (4 mM). Dendritic cells were cultured on RPMI (LONZA) containing 10% fetal bovine serum (FBS) supplemented with penicillin (10.000U/ml) and streptomycin (100ug/ml) (GIBCO).

For confocal imaging and co-immunoprecipitation experiments cells were seeded (70-80% of confluence), in 6-well dish containing poly-lysine-coated coverslips or 100mm dish, respectively, 24h before transfection with selected cDNAs. Lipotransfectina® (Attendbio Research) was used for transfection according to the supplier's instructions. The amount of transfected DNA was 4µg for a 100mm dish and 500ng for each well of a 6-well dish (for coverslip use). Next, 4-6h after transfection, the mixture was removed from the dishes and replaced with new fresh culture media. All the experiments were performed 24 h after transfection.

For patch-clamp experiments, HEK-293 cells were plated in a 35-mm dish and transfected with 300 ng of DNA using FuGene HD® according to the supplier's instructions.

Electrophysiology. Transfected HEK-293 cells were accutased 24h after transfection and re-plated on 35mm glass-bottom dishes coated with Matrigel (BD Biosciences). After 1-2h, cells were extensively washed with whole-cell external recording solution, containing the following (in mM): 150 NaCl, 5 KCl, 10 $CaCl_2$, 2 $MgCl_2$, 10 glucose, and 10 HEPES, pH 7.4). Transfected HEK-293 cells were selected using an Olympus FV1000 confocal microscope equipped with spectral detectors and SIM scanner. Whole-cell K^+ currents in HEK-293 were recorded at room temperature (RT) using an Axopatch 200B and an EPC-10 (HEKA), respectively, and the appropriate software was used for data recording and analysis. Ionic currents were capacitance and series resistance compensated by 80–90%, sampled at 10 kHz (Digidata 1440; Molecular Devices), and filtered at 2.9 kHz. Patch electrodes of 2-4 MΩ were fabricated in a P-97 puller (Sutter Instruments Co.) from borosilicate glass (outer diameter 1.2 mm and inner diameter 0.94 mm; Clark Electromedical Instruments Co.) Electrodes for HEK cells were filled with a solution containing the following (in mM): 4 NaCl, 150 KCl, 1 $MgCl_2$, 0.5 EGTA, 5 ATP(K), and 10 HEPES, pH 7.4. HEK cells were clamped to a holding potential of –80 mV. To evoke voltage-gated currents, cells were stimulated with 250 ms square pulses ranging from –80 to +80 mV in 10 mV steps. All recordings were routinely subtracted for leak currents.

Protein extraction, co-immunoprecipitation and western blotting. Cells were washed twice in cold PBS and lysed on ice with lysis buffer (5 mM HEPES, 150 mM NaCl, 1% Triton X-100, pH 7.5) supplemented with 1 µg/ml aprotinin, 1 µg/ml leupeptin, 1 µg/ml pepstatin and 1 mM phenylmethylsulfonyl fluoride as protease inhibitors. Cells were next scrapped and transferred to a 1.5 ml tube. Then they were incubated for 20 min at the orbital, and spun for 20 min at 14000 rpm. The supernatant was transferred to a new tube and protein contents were determined by using the Bio-Rad Protein Assay (Bio-Rad).

For co-immunoprecipitation, 1000 µg of protein of each condition were separated and brought up to a volume of 500 ml with Lysis Buffer for IPs (NaCl 150 mM, HEPES 50 mM, Titron X-100 1%, pH 7.4), supplemented with protease inhibitors. Preclean was

performed with 40 µl of protein A sepharose beads (GE Healthcare), in an orbital 1 h at 4ºC. Next, each sample was incubated with a small chromatography column (BioRad Micro spin Cromaotgraphy Columns), which contained 2.5 µg of anti-GFP antibody (Genescript) previously crosslinked to protein A sepharose beads, for 2h at room temperature, with continuous mixing in an orbital. Next, columns were centrifuged 30s at 1000g. The supernatant (SN) was kept and stored at -20ºC. Columns were washed four times with 500µl of lysis buffer and centrifugations of 30sec at 1000 g. Finally, elution was performed by incubation of the columns with 100µl of 0.2M glycine pH 2.5, and spun 30sec at 1000g. The eluted proteins (IP) were prepared for western blot by adding 20µl of Loading Buffer (5x) and 5µl of 1M Tris-HCl pH 10.

Irreversible crosslinking of the antibody to the sepharose beads was performed after one hour of incubation at RT of the antibody with protein A sepharose beads, incubating the beads with 500ul of dimethyl pimelimidate (DMP, from Pierce) for 30 min at RT. Next columns, were washed four times with 500 µl of 1x TBS, four times with 500 µl of 0.2 M glycine pH 2.5 and three times more with 1x TBS. Once these steps are performed, the columns could be incubated with the protein lysates, in order to perform the immunoprecipitation, following the protocol described before.

Protein samples (50µg), supernatants and immunoprecipitates were boiled in Laemmli SDS loading buffer and separated on 10% SDS-PAGE. Next, they were transferred to nitrocellulose membranes (Immobilon-P, Millipore) and blocked in 0.2% Tween-20-PBS supplemented with 5% dry milk, before immunoreaction. Filters were immunoblotted with antibodies against Kv1.3 (1/500, Neuromab), Kvß2.1 (1/1000, Neuromab) or GFP (1/500, Roche). Finally, filters were washed with 0.05% Tween 20 PBS and incubated with horseradish peroxidase conjugated secondary antibodies (BioRad).

Confocal microscopy and image analysis. For confocal image acquisition cells were seeded on poly-lysine-coated coverslips, and 24h later were transfected. The next day, cells were quickly washed twice, fixed with paraformaldehyde 4% for 10 min, washed three times for 5min with PBS-K+. Finally, coverslips were mounted on microscope slides (Acefesa) with house Mowiol mounting media. Coverslips were let dry at RT at least one day before imaging.

For membrane surface labelling, Wheat Germ Agglutinin-Texas Red (WGA) (from Invitrogen) was used. Live cells (on ice) were quickly washed with PBS at 4°C and stained with a dilution of WGA-TexasRed (1/1500) in DMEM supplemented with 30 mM Hepes for 15min at 4°C. Subsequently, cells were quickly washed twice and fixed with 4% paraformaldehyde in PBS for 6 min. Next, cells were washed and mounted as described before. In order to detect Kv1.3 (1/100, Neuromab), KCNE4 (1/100, Proteintech), Kvβs (1/100) after fixation, cells were further permeabilized with 0.1% Triton X-100 for 20min. After 60min incubation with blocking solution (10% goat serum, 5% non-fat powdered milk and 0.05% Triton X-100) primary antibodies were added O/N at 4ºC in 10% goat serum and 0.05% Triton X-100. Next day, after washing the cells, they were incubated with secondary goat anti-mouse or goat anti-rabbit antibody conjugated with Cyanine 5, for 2 hours at room temperature and further mounted as previously described.

The Fluorescence Resonance Energy Transfer (FRET) via acceptor photobleaching technique was measured in discrete ROI (Region of Interest). Fluorescent proteins from fixed cells were excited with the 458 nm or the 514 nm lines using low excitation intensities. Next, 475 to 495 nm bandpass and >530 nm longpass emission filters were applied. The YFP protein was bleached using maximum laser power. We obtained approximately 80% of acceptor intensity bleaching. After photobleaching, images of the donors and acceptors were taken. The FRET efficiency was calculated using the equation $[(F_{CFPafter} - F_{CFPbefore})/F_{CFPbefore}]*100$, where $F_{CFPafter}$ was the fluorescence of the donor after bleaching and $F_{CFPbefore}$ was the fluorescence before bleaching. The loss of fluorescence as a result of the scans was corrected by measuring the CFP intensity in the unbleached part of the cell.

All images were acquired with a Leica TCS SL laser scanning confocal spectral microscope (Leica Microsystems), equipped with an Argon and Helium-Neon lasers. All experiments were done with a 63x oil-immersion objective lens NA 1.32. All offline image analysis was done using Image J software. A pixel by pixel colocalization study by using JACoP (Just Another Colocalization Plugin) was used. Manders split coefficients were further obtained which are proportional to the amount of fluorescence of the colocalizing pixels in each colour channel.

RESULTS

KCNE4, Kvß2.1 and Kv1.3 can form tripartite channelosomes

Kv1.3 is mainly expressed at nervous and immune system. At the latter tissue, the channel is playing high important roles in several cellular functions (Panyi, 2005). Moreover, the dysfunction of Kv1.3 has been related to autoimmune diseases (Beeton and Chandy, 2005, Beeton et al., 2011). In dendritic cells, we have previously described that express both Kv1.3 and KCNE4 (Sole et al., 2016). At figure 1A, not only Kv1.3 and KCNE4 are detectable in those cells, but also Kvß2.1. Immunofluorescence for detecting Kv1.3, KCNE4 and Kvßs exhibit the expected pattern. Kv1.3 is mainly intracellular, similar to KCNE4, and Kvßs antibody revealed a cytosolic staining (figure 1B).

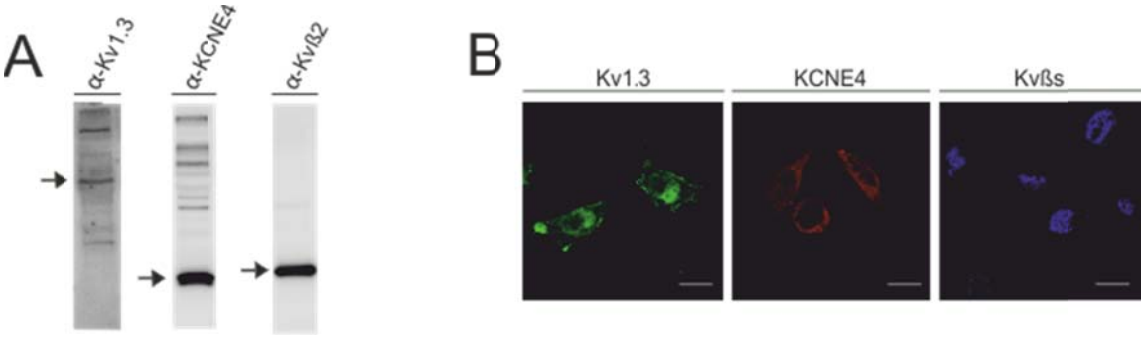

Figure 1. Kv1.3, KCNE4 and Kvßs are expressed at dendritic cells. A. Immunoblot detection of all three proteins at dendritic protein extraction. B. Immunofluorescence of dendritic cells to detect the channel, KCNE4 and Kvßs.

Since the expression of all three proteins share some locations, the possibility of forming tripartite complexes is plausible. Due to the already-mentioned importance of the channel in some functions, the fine-tunning of Kv1.3 can determine the final cellular decision. In order to ensure the presence of the three entities at the same channelosome, a previously described chimera was used (Solé, 2013). KCNE4 is attached to Kv1.3 through a flexible linker and the YFP protein (figure 2A). Immunoprecipitation assay in the presence of Kv1.3 was performed as a positive control, and coimmunoprecipitation was detected. Upon coexpression with Kvß2.1, the pull-down of the chimera was accompanied by the auxiliary subunit (figure 2B).

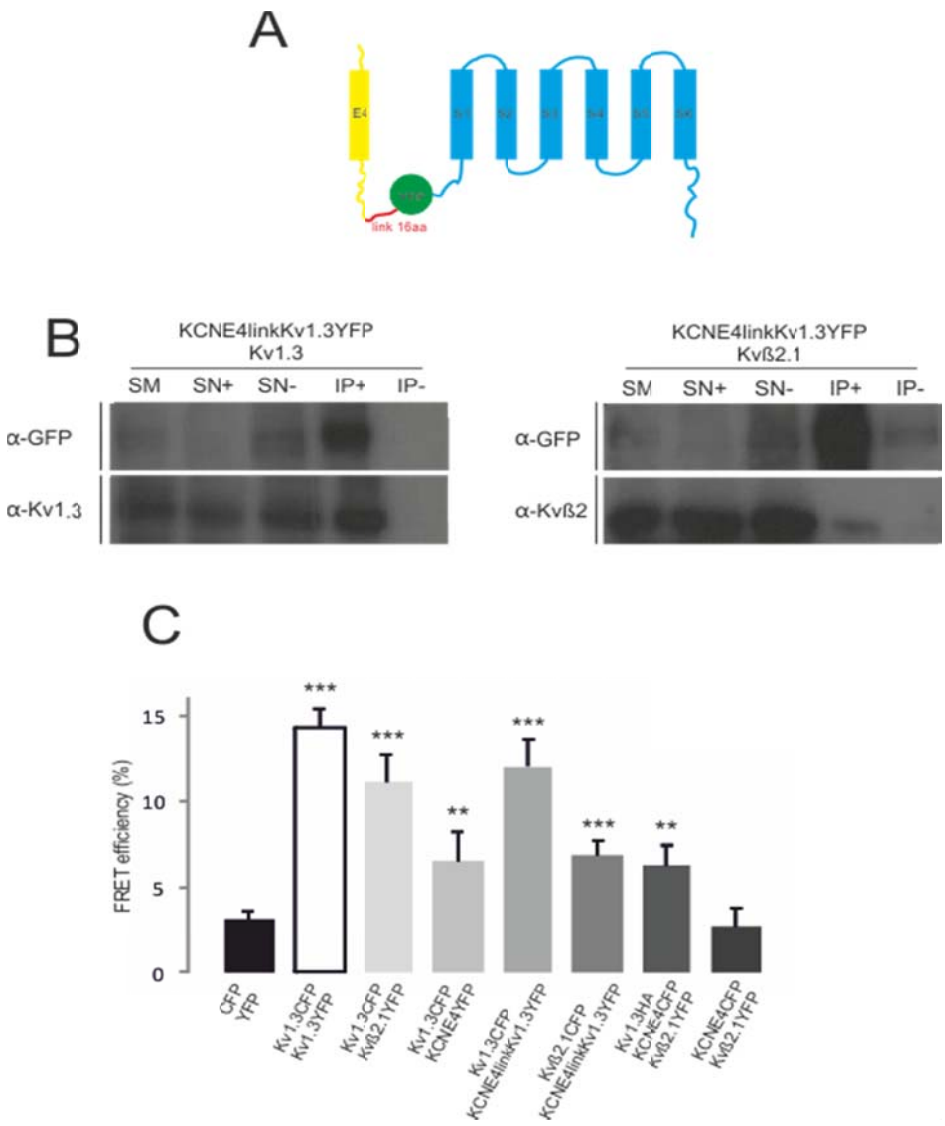

Figure 2. Tripartite complexes are formed by Kv1.3, KCNE4 and Kvß2.1. A. Scheme of KCNE4linkKv1.3YFP chimera. B. Coimmunoprecipitation of the chimera in the presence of Kv1.3 (left) and Kvß2.1 (right). Top panel: Immunoblot against CFP. Bottom panel: immunoblot against Kv1.3 (left) or Kvß2.1 (right). SM: starting material. SN+: supernatant of the precipitation in the presence of antibody. SN-: supernatant of the precipitation in the absence of antibody. IP+: Immunoprecipitation in the presence of the antibody. IP-: Immunoprecipitation in the absence of the antibody. C. FRET efficiency quantification. Values are the mean of 20-30 cells. **, $p<0.01$; ***, $p<0.001$ compared with the negative control (Student's t-test).

FRET experiments were performed to support the previous data. CFP/YFP and Kv1.3CFP/Kv1.3YFP were used as negative and positive conditions. Concomitant with

previous published data, significant values were obtained for Kv1.3CFP/Kvß2.1YFP and Kv1.3CFP/KCNE4YFP. Similar to the immunoprecipitation assay and as a specific control for the chimera, a condition was addressed cotransfecting Kv1.3CFP. We obtained positive FRET values for KCNE4linkKv1.3YFP in the presence of Kv1.3CFP and also Kvß2.1CFP. Thereby, tripartite channelosomes can be built. Moreover, the complex is formed even in the absence of the linker. Significant FRET values were obtained for the condition Kv1.3HA, KCNE4CFP and Kvß2.1YFP. Since upon Kvß2.1YFP and KCNE4CFP coexpression, the measurement was negative, the channelosome formation is due to the presence of Kv1.3 (figure 2C).

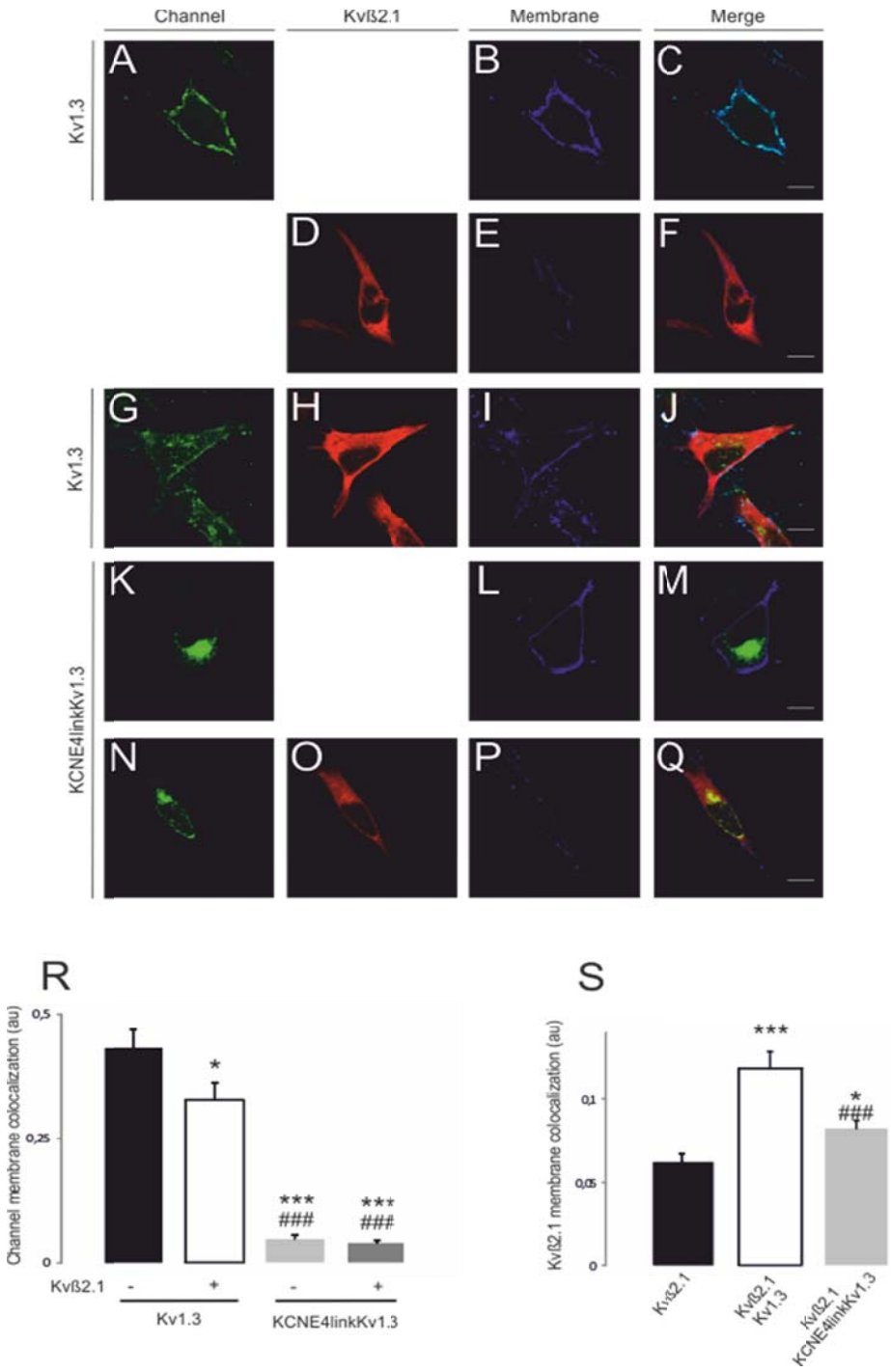

Figure 3. KCNE4 is dominant on Kv1.3 traffic upon coexpression with Kvß2.1. A-C: Kv1.3 membrane targeting. A: Kv1.3. B: Membrane marker. C: merge. D-F: Cellular distribution of Kvß2.1. D: Kvß2.1. E: Membrane marker. F: merge of channels. G-J:

Kv1.3 distribution in the presence of Kvß2.1. G: Kv1.3. H: Kvß2.1. I: Membrane marker. J: merge of channels. K-M: Chimera KCNE4linkKv1.3 traffic. K: KCNE4linkKv1.3YFP. L: Membrane marker. M: merge of channels. N-Q: Cellular distribution of KCNE4linkKv1.3 in the presence of Kvß2.1. N: KCNE4link Kv1.3. O: Kvß2.1. P: Membrane marker. Q: merge of channels. R: Quantification of channel membrane colocalization using Mander's coefficient. S: Quantification of Kvß2.1 membrane colocalization using Mander's coefficient *, $p<0.05$; ***, $p<0.001$ compared with Kv1.3 in the absence of Kvß2.1. ###, $p<0.001$ compared with Kvß2.1 in the presence of Kv1.3 (Student's T-test). Values were obtained from 20-30cells. Scale bars: 10 µm.

KCNE4 dominant-negative entity of tripartite channelosomes

Once the possibility of forming channelosomes was confirmed, effects on the traffic were analysed. Concomitantly, to ensure the stoichiometry of the complexes, KCNE4linkKv1.3YFP was used to describe the effects. While Kv1.3 alone presents a high staining at the plasma membrane (figure 3A-C); Kvß2.1 exhibits an intracellular location (figure 3D-F). As previously demonstrated, coexpression of both proteins does not increase the membrane targeting of the channel, but promotes the channel intracellular detection (figure 3G-J). KCNE4linkKv1.3YFP exhibits a highly retained pattern similar to the coexpression of KCNE4 and Kv1.3, concomitant with former data (Solé L, 2013) (figure 3K-M). Coexpression of Kvß2.1 with this chimera does not counteract the KCNE4 dominant negative effect on the channel (figure 3N-Q). Thus, the presence of the KCNE member impairs any effect of Kvß2.1 on the traffic (figure 3R). Considering Kvß2.1 distribution, its membrane staining is increased upon the presence of Kv1.3. However, the presence of KCNE4 at the channelosome, impairing Kv1.3 surface targeting, weaken the improved presence of Kvß2.1 at the cell surface (figure 3S). Summing up, KCNE4 is masking Kvß2.1 modulation on the channel by imposing its effect. Dose-effect need to be performed to identify the stoichiometry required to force KCNE4 volition.

Regarding the electrophysiological properties of the channel, both proteins have been described to alter some features. While KCNE4 reduces the current density and the cumulative inactivation; previous data on this dissertation showed that Kvß2.1 generates an activation shift towards more negative values. Electrophysiological recordings were obtained for Kv1.3 (figure 4A), Kv1.3 and Kvß2.1 (figure 4B), Kv1.3 and KCNE4 (figure 4C) and finally Kv1.3, Kvß2.1 and KCNE4 (figure 4D).

The measurement of the current density (figure 4E) showed that, different to Kv1.3 and Kv1.3-Kvß2.1 combination (rhombus and square in figure 4E), KCNE4 generates a great impairment of the channel current (triangle in figure 4E). Moreover, Kvß2.1 coexpression does not counteract this effect (cross in figure 4E). However, previous contributions in this dissertation demonstrated that Kvß2.1 promotes an earlier activation of the channel. Concomitantly, Kv1.3 current is significantly higher measured at -20mV when Kvß2.1 is coexpressed. This effect was not observed for the KCNE4 condition. However, even the tripartite formation does not reach the Kv1.3- Kvß2.1 level at -20mV, there is more current in the presence than in the absence of Kvß2.1 (figure 4F). However, when it is measured at 50mV, those conditions in which KCNE4 is cotransfected exhibit a dramatic decrease of total current density (figure 4G).

Concomitant with the traffic data, Kvß2.1 does not exert counteract KCNE4 effect on the Kv1.3. However, those channelosomes which succeed on reaching the cell surface present partially the activation feature typical from Kvß2.1.

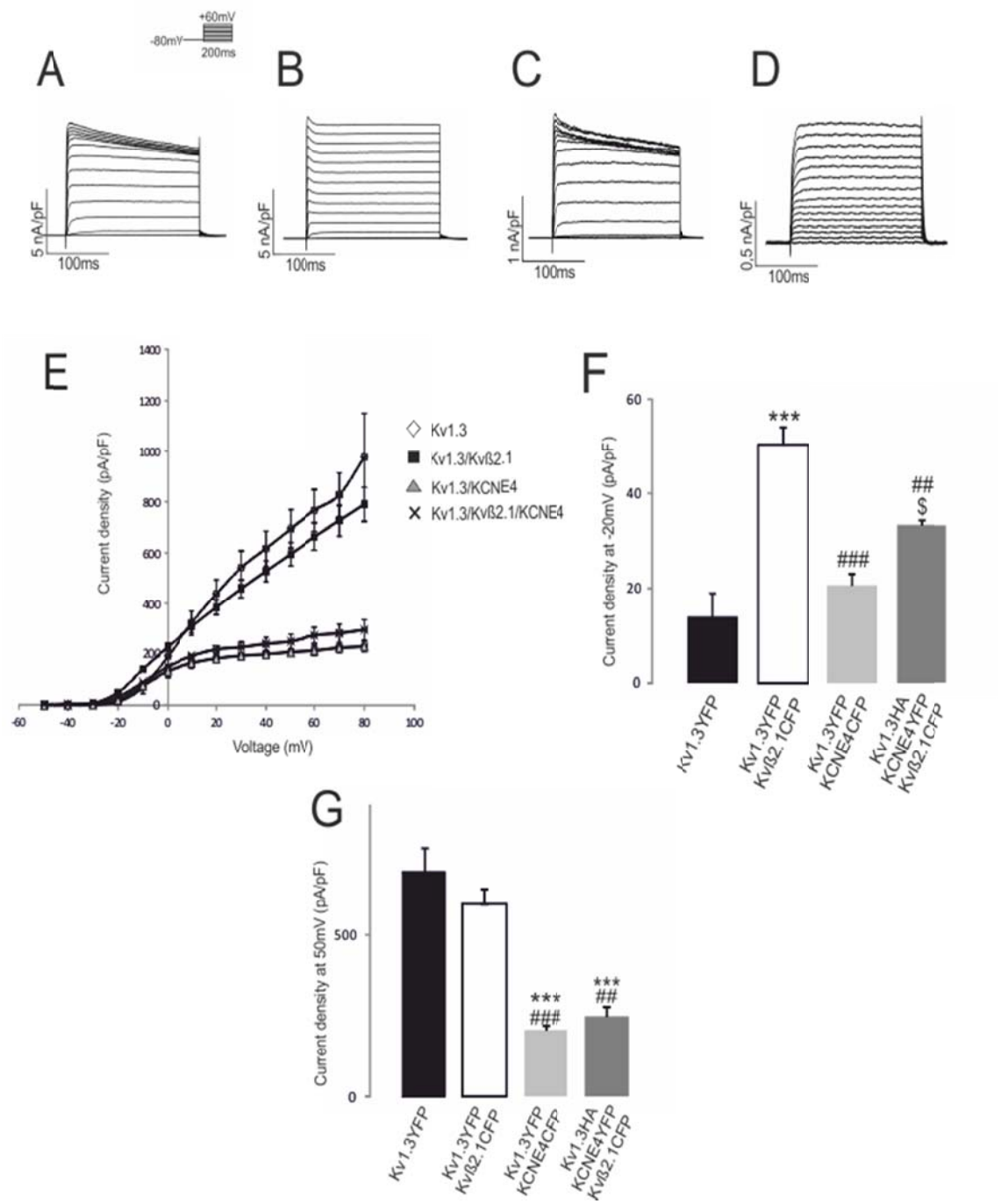

Figure 4. Characterization of Kv1.3-KCNE4- Kvß2.1 channelosome electrophysiological properties. *A*-C. Voltage-dependent K^+ currents elicited in HEK cells transfected with Kv1.3YFP, Kv1.3YFP/Kvß2.1CFP, Kv1.3YFP/KCNE4CFP and Kv1.3HA/KCNE4YFP/Kvß2.1CFP. A: Kv1.3YFP. B: Kv1.3YFP/ Kvß2.1CFP. C: Kv1.3YFP/KCNE4CFP. D: Kv1.3HA/KCNE4YFP/Kvß2.1CFP. Cells were held at -80mV and pulse potentials were applied as indicated. E: Current density *vs* voltage plot of outward K^+ currents. White **r**hombus, Kv1.3YFP; black square, Kv1.3YFP/Kvß2.1CFP; grey triangle, Kv1.3YFP/ KCNE4CFP; black cross, Kv1.3HA/KCNE**4**YFP/Kvß2.1CFP. Values are mean±SE (n=4-6, independent cells). F: Current density at -20mV. F: Current density at 5**0**mV. ***p<0.001 compared with Kv1.3YFP. ##p<0.01; ###p<0.001 compared with Kv1.3YFP/Kvß2.1CFP. $ p<0.05 compared with Kv1.3CFP/KCNE4YFP (Student's T-test).

DISCUSSION

Kv1.3 channel is expressed in several tissues but mainly in nervous and immune system. Several different publications have related this specific voltage-gated potassium channel with a wide variety of functions. Upon T-cell activation, it is present at the immunological synapse enforcing the signalling pathway (Panyi et al., 2004, Toth et al., 2009). Actually, improper relocation of the channel has been related with lupus erythematosus (Nicolaou et al., 2007). It was also described that it is involved in proliferation of leukocytes (Beeton and Chandy, 2005). Further publications located the molecular determinants involved in this function (Jimenez-Perez et al., 2016). However, other studies pointed Kv1.3 as a key protein in apoptosis, not only involving those channels present at the cell surface, but also the mitochondrial partition (Bock et al., 2003, Szabo et al., 2008). Thus, Kv1.3 regulation can determine some highly diverse cellular consequences.

Concomitant with our results on dendritic cells, previous studies pointed out that both KCNE4 and Kvß2.1 are, indeed, sharing tissue expression with Kv1.3: they are located in brain and immune system (Abbott, 2016a, Pongs and Schwarz, 2010). In some immune system cells, their level exhibited a regulation upon different insults (Sole et al., 2009, Sole and Felipe, 2010, Vicente et al., 2005, Autieri et al., 1997). Thereby, the formation and functional consequence of a channelosome formed by those three entities was a relevant issue. We initially demonstrated that a tripartite complex was possible. Actually, both proteins are interacting with different parts of the channel (Pongs and Schwarz, 2010, Sole et al., 2016). Moreover, we observed that there is not a direct association between Kvß2.1 and KCNE4. Contrary to KCNE4, calmodulin and Kv7.1, Kv1.3 is the central entity that possesses the ability to interact with the β-subunits (Ciampa et al., 2011).

The present study concluded that KCNE4 acts as a dominant subunit on the channel distribution and the current density, when coexpressed with Kvß2.1. Similarly, KCNE4 was previously described to perform its negative functions on Kv7.1 even upon KCNE1 cotransfection. Thus, the I_{KS} current was dramatically affected by the presence of this entity (Lundquist et al., 2005). However, a partial opening at more negative values was observed, modulation previously described of Kvß2.1 on Kv1.3. Thus, final currents are the result of non-equal mixture of features transferred from both proteins. Whether these multiprotein complexes can include more actors, is an opened question. The scenario considered is a step further to conceive the *natural* channelosomes, but farther research needs to be performed in this direction.

REFERENCES

ABBOTT, G. W. 2016a. KCNE1 and KCNE3: The yin and yang of voltage-gated K(+) channel regulation. *Gene,* 576**,** 1-13.

ABBOTT, G. W. 2016b. KCNE4 and KCNE5: K(+) channel regulation and cardiac arrhythmogenesis. *Gene,* 593**,** 249-60.

ACCILI, E. A., KIEHN, J., WIBLE, B. A. & BROWN, A. M. 1997. Interactions among inactivating and noninactivating Kvbeta subunits, and Kvalpha1.2, produce potassium currents with intermediate inactivation. *J Biol Chem,* 272**,** 28232-6.

AUTIERI, M. V., BELKOWSKI, S. M., CONSTANTINESCU, C. S., COHEN, J. A. & PRYSTOWSKY, M. B. 1997. Lymphocyte-specific inducible expression of potassium channel beta subunits. *J Neuroimmunol,* 77**,** 8-16.

BEETON, C. & CHANDY, K. G. 2005. Potassium channels, memory T cells, and multiple sclerosis. *Neuroscientist,* 11**,** 550-62.

BEETON, C., PENNINGTON, M. W. & NORTON, R. S. 2011. Analogs of the sea anemone potassium channel blocker ShK for the treatment of autoimmune diseases. *Inflamm Allergy Drug Targets,* 10**,** 313-21.

BOCK, J., SZABO, I., GAMPER, N., ADAMS, C. & GULBINS, E. 2003. Ceramide inhibits the potassium channel Kv1.3 by the formation of membrane platforms. *Biochem Biophys Res Commun,* 305**,** 890-7.

CIAMPA, E. J., WELCH, R. C., VANOYE, C. G. & GEORGE, A. L., JR. 2011. KCNE4 juxtamembrane region is required for interaction with calmodulin and for functional suppression of KCNQ1. *J Biol Chem,* 286**,** 4141-9.

CLANCY, S. M., CHEN, B., BERTASO, F., MAMET, J. & JEGLA, T. 2009. KCNE1 and KCNE3 beta-subunits regulate membrane surface expression of Kv12.2 K(+) channels in vitro and form a tripartite complex in vivo. *PLoS One,* 4**,** e6330.

DOWNEN, M., BELKOWSKI, S., KNOWLES, H., CARDILLO, M. & PRYSTOWSKY, M. B. 1999. Developmental expression of voltage-gated potassium channel beta subunits. *Brain Res Dev Brain Res,* 117**,** 71-80.

HILLE, B. 2001. Ion channels of excitable membranes. *Sinauerassociates, Sunderland, Mass.. Great Britain, 2001.*

JIMENEZ-PEREZ, L., CIDAD, P., ALVAREZ-MIGUEL, I., SANTOS-HIPOLITO, A., TORRES-MERINO, R., ALONSO, E., DE LA FUENTE, M. A., LOPEZ-LOPEZ, J. R. & PEREZ-GARCIA, M. T. 2016. Molecular Determinants of Kv1.3 Potassium Channels-induced Proliferation. *J Biol Chem,* 291**,** 3569-80.

LUNDQUIST, A. L., MANDERFIELD, L. J., VANOYE, C. G., ROGERS, C. S., DONAHUE, B. S., CHANG, P. A., DRINKWATER, D. C., MURRAY, K. T. & GEORGE, A. L., JR. 2005. Expression of multiple KCNE genes in human heart may enable variable modulation of I(Ks). *J Mol Cell Cardiol,* 38**,** 277-87.

NICOLAOU, S. A., SZIGLIGETI, P., NEUMEIER, L., LEE, S. M., DUNCAN, H. J., KANT, S. K., MONGEY, A. B., FILIPOVICH, A. H. & CONFORTI, L. 2007. Altered dynamics of Kv1.3 channel compartmentalization in the immunological synapse in systemic lupus erythematosus. *J Immunol,* 179**,** 346-56.

PANYI, G. 2005. Biophysical and pharmacological aspects of K+ channels in T lymphocytes. *Eur Biophys J,* 34**,** 515-29.

PANYI, G., VAMOSI, G., BACSO, Z., BAGDANY, M., BODNAR, A., VARGA, Z., GASPAR, R., MATYUS, L. & DAMJANOVICH, S. 2004. Kv1.3 potassium channels are localized in the immunological synapse formed between cytotoxic and target cells. *Proc Natl Acad Sci U S A,* 101**,** 1285-90.

PONGS, O. & SCHWARZ, J. R. 2010. Ancillary subunits associated with voltage-dependent K+ channels. *Physiol Rev,* 90**,** 755-96.

SEIKEL, E. & TRIMMER, J. S. 2009. Convergent modulation of Kv4.2 channel alpha subunits by structurally distinct DPPX and KChIP auxiliary subunits. *Biochemistry,* 48**,** 5721-30.

SOLE, L. & FELIPE, A. 2010. Does a physiological role for KCNE subunits exist in the immune system? *Commun Integr Biol,* 3**,** 166-8.

SOLE, L., ROIG, S. R., VALLEJO-GRACIA, A., SERRANO-ALBARRAS, A., MARTINEZ-MARMOL, R., TAMKUN, M. M. & FELIPE, A. 2016. The C-terminal domain of Kv1.3 regulates functional interactions with the KCNE4 subunit. *J Cell Sci,* 129**,** 4265-4277.

SOLE, L., ROURA-FERRER, M., PEREZ-VERDAGUER, M., OLIVERAS, A., CALVO, M., FERNANDEZ-FERNANDEZ, J. M. & FELIPE, A. 2009. KCNE4 suppresses Kv1.3 currents by modulating trafficking, surface expression and channel gating. *J Cell Sci,* 122**,** 3738-48.

SZABO, I., BOCK, J., GRASSME, H., SODDEMANN, M., WILKER, B., LANG, F., ZORATTI, M. & GULBINS, E. 2008. Mitochondrial potassium channel Kv1.3 mediates Bax-induced apoptosis in lymphocytes. *Proc Natl Acad Sci U S A,* 105**,** 14861-6.

TOTH, A., SZILAGYI, O., KRASZNAI, Z., PANYI, G. & HAJDU, P. 2009. Functional consequences of Kv1.3 ion channel rearrangement into the immunological synapse. *Immunol Lett,* 125**,** 15-21.

VICENTE, R., ESCALADA, A., SOLER, C., GRANDE, M., CELADA, A., TAMKUN, M. M., SOLSONA, C. & FELIPE, A. 2005. Pattern of Kv beta subunit expression in macrophages depends upon proliferation and the mode of activation. *J Immunol,* 174**,** 4736-44.

VICENTE, R., VILLALONGA, N., CALVO, M., ESCALADA, A., SOLSONA, C., SOLER, C., TAMKUN, M. M. & FELIPE, A. 2008. Kv1.5 association modifies Kv1.3 traffic and membrane localization. *J Biol Chem,* 283**,** 8756-64.

WU, D. M., JIANG, M., ZHANG, M., LIU, X. S., KOROLKOVA, Y. V. & TSENG, G. N. 2006. KCNE2 is colocalized with KCNQ1 and KCNE1 in cardiac myocytes and may function as a negative modulator of I(Ks) current amplitude in the heart. *Heart Rhythm,* 3**,** 1469-80.

4. SUMMARY

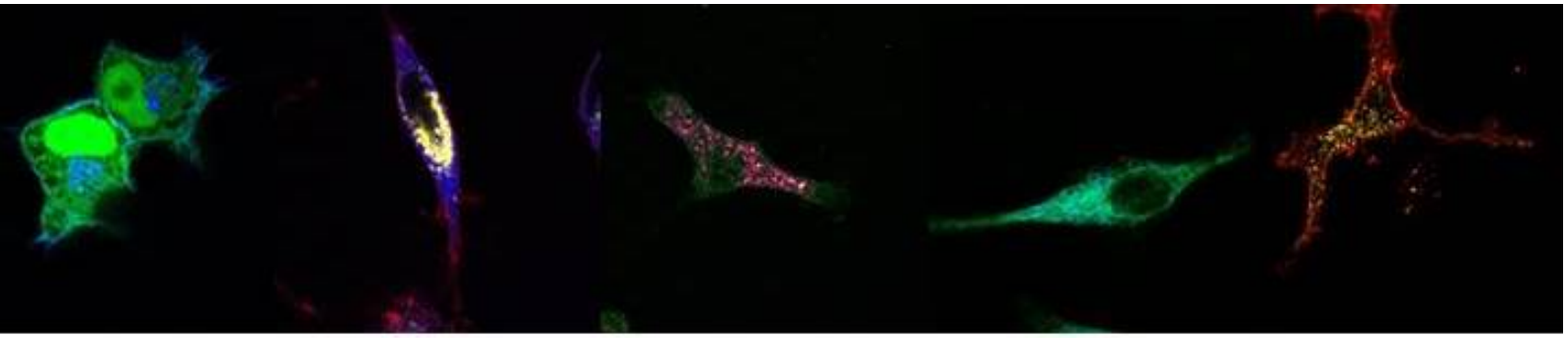

4. SUMMARY

Voltage-gated potassium channels are proteins that allow the flux of potassium ions across the plasma membrane in response to a voltage stimulus. Those proteins were initially described in nervous system as the repolarization entities posterior to a depolarization. However, several different roles have been discovered to be enhanced, mediated or influenced by those entities. Cell cycle progression, homeostasis, proliferation or activation and apoptosis program are some of those functions.

Kv1.3 is the third member of the first family of voltage-gated potassium channels in humans. This specific entity is mainly expressed in nervous and immune system. It has been associated with the repolarization of neurons, the activation and proliferation of leukocytes and apoptosis. Moreover, its dysfunctionality has been related to some autoimmune disease. The fine-tunning of the channel is highly relevant to control the final cell decision. The subunits that accompany the channel were classically named as β-subunits. Several different families have been described to modulate some channel features. Kvβ family are cytoplasmic proteins that can enhance the traffic to the plasma membrane and promote a switch towards negative voltages of the channel activation. However, few are known about alternative locations and Kv1.3 modulation. KCNE family are single spanning proteins highly promiscuous that modulate several different Kvα-subunits. Depending on the KCNE subtype, the effect on the channels can present different natures. This dissertation is focused on KCNE4 member, a peptide which generally negatively regulates Kv channels.

This thesis described the positioning of Kvβ2.1, but not Kvβ1.1, in specific regions of the plasma membrane: lipid raft microdomains. Those are considered as signalling platforms at the plasma membrane highly relevant for several cellular processes. The possible mechanism that drives Kvβ2.1 is the palmitoylation of its amino acidic sequence; even other causes are not discarded. Proliferation signals are enhancing this localization while PMA treatment generates the opposite effect. This protein, as well as its partner Kvβ1.1, can form homo and heteroligomers. Their affinity and stoichiometry was addressed. Furthermore, multiprotein complexes were detected at membrane associated environments. Traffic and electrophysiological consequences on the channel were analysed upon coexpression with those subunits. Kv1.3 was removed from lipid raft microdomains and Kvβs prevented partially its PMA-dependent internalization.

The molecular determinants involved in the Kv1.3 traffic to the plasma membrane were localised at the C-terminal domain. Previous results from the laboratory determined that KCNE4 is impairing the traffic of the channel. This thesis deciphered the molecular mechanisms involved in this effect concluding a bipartite system: (i) the masking of Kv1.3 export signal and (ii) the transference of a retention signal to the channelosome. Moreover, the specific domains of Kv1.3 and KCNE4 implicated in their interaction were mapped and pointed out to the C-terminal regions of both peptides. KCNE4 was also found to form oligomers and present several signals for its retention at the endoplasmic reticulum.

Finally, the combination of both subunits (Kvβ2.1 and KCNE4) with the channel revealed a dominance of KCNE4 effects, but an electrophysiological function of Kvβ2.1 on Kv1.3 kept

preserved. Thus, the present thesis brought light to the comprehension of Kv1.3 channelosome.

5. GENERAL DISCUSSION

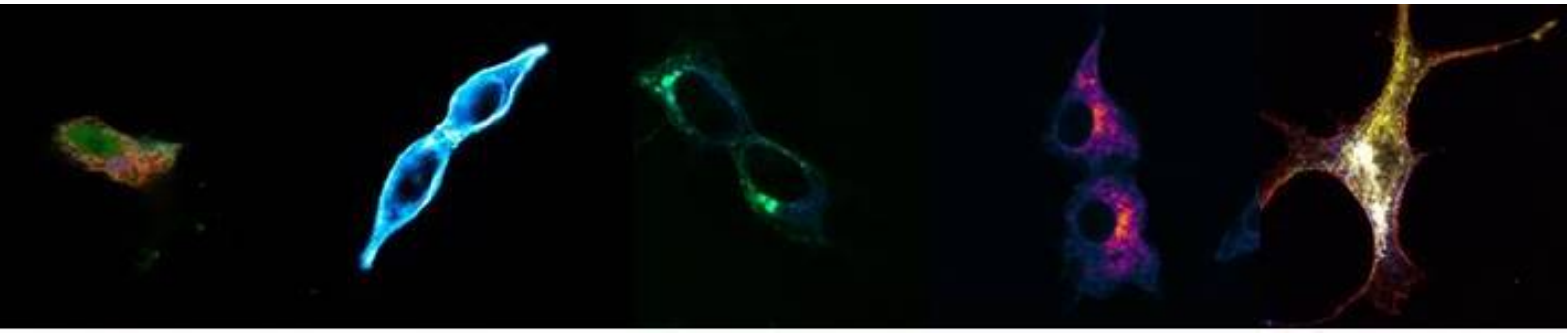

5. GENERAL DISCUSSION

Voltage-gated potassium channels were initially described to mediate a highly relevant role in excitable cells: the repolarization. Posterior to a depolarization stimulus of a neuron, the opening of those entities enables the recuperation of the resting voltage at the membrane. Even their voltage-dependent nature, several other functions have been reported also in non-excitable cells. Secretion, cell volume, homeostasis, proliferation, activation or apoptosis are mediated by Kv channels (Hille, 2001).

It is widely accepted that voltage-gated potassium channels are rarely acting as solely entities, but as multiprotein complexes (Gutman et al., 2005). Auxiliary subunits are accompanying the channel and regulating their properties. From one unique conducting protein, a wide range of final current and cell distribution can be obtained by the combination of those modulators (Pongs and Schwarz, 2010). Firstly, Kvβ family was identified. They are soluble proteins, attached to the N-terminus of the channels and depending on the subtype can exert fast-inactivation or increased membrane targeting (Scott et al., 1994, Li et al., 2006). From this starting point, several other families were discovered. Their protein nature is divers: KCNEs are single-spanning transmembrane proteins as well as DPPX, while KChIP and KchAP are soluble. Other molecules, not classified as auxiliary subunits can also interfere in the channels physiology such as Calmodulin, PKC and PKA (Pongs and Schwarz, 2010).

This dissertation is focused in the Kv1.3 channelosome. This α-subunit is mainly expressed in nervous and immune system (Gutman et al., 2005). Previous research on leukocyte physiology demonstrated that Kv1.3 is playing a major role in activation, proliferation and apoptosis (Szabo et al., 2008, Panyi et al., 2004). Those three processes have been considered as opposite cellular decisions by some authors. Thus, the involvement of a unique protein in such diverse functions could imply a different company for each cellular moment (Li et al., 2006). The present thesis aimed to bring light to the modulation roles in the Kv1.3 channel by two auxiliary subunits: Kvβ2.1 and KCNE4.

Firstly, innate features of Kvβ2.1 were analysed in the absence of the channel. The comprehension of its natural behaviour paves the way to understand their final function. We detected Kvβ2.1, but not Kvβ1.1, in lipid raft microdomains. These specific platforms are involved in exocytosis, internalization, migration or proliferation (Sonnino and Prinetti, 2013). It is widely accepted that they are also overcoming the distance between proteins involved in the same signaling pathway (Sonnino and Prinetti, 2013, Patel et al., 2008). Apart from Kv channels, Kvβ2.1 has been described to interact with other proteins. For instance, EB-1 transport Kvβ2.1 to axonal environments independently from Kv channels (Gu et al., 2006). Moreover, they dissociates after a phosphorylation CDK-dependent (Vacher et al., 2011, Vacher and Trimmer, 2011). However, CDK is not the unique kinase that interacts with Kvβ2.1, but also different subtypes of PKC as well as ZIP1, ZIP2 and ZIP3 proteins (Gong et al., 1999, Croci et al., 2003, Liu et al., 2003). Thereby, it is tempting to speculate that Kvβ2.1 presence at lipid raft can drive all its interactors at those locations.

We have described that Kvβ2.1 is palmitoylated and this modification is the major driving force for lipid raft targeting. Palmitoylation of soluble proteins has been proposed as a

membrane targeting mechanism (Chamberlain et al., 2013, Smotrys and Linder, 2004). SNAP-25, a SNARE protein, develops its major role at the cell surface mediating the fusion of adjacent membranes. However, it does not present any transmembrane domain. A palmitoylation modification allows it to occupy this specific location (Greaves et al., 2010). Moreover, H-Ras and N-Ras are the example further studied of cytosolic proteins that target the plasma membrane. It was demonstrated that they are trafficking by the conventional secretory pathway once they are palmitoylated (Linder and Deschenes, 2007). However, there is a substantial difference with Kvβ2.1. While those proteins are known to develop specific functions membrane-dependent, which is the role of Kvβ2.1 at lipid raft microdomains?

Since Kvβ2.1 was described and its high expression in brain channelosomes was observed, vast efforts were invested to decipher its specific functions. Compared with its family relatives, Kvβ2.1 does not present the ball-and-chain domain able to close open state channels (Rhodes et al., 1996). It was observed that the combination with concrete channels enhance their expression at the plasma membrane upon interaction early in the secretory pathway (Nagaya and Papazian, 1997, Shi et al., 1996). This effect was extensive to channels as Kv4.3, TRPV1 and TREK1 (Yang et al., 2001, Bavassano et al., 2013, Kisselbach et al., 2012). However, the knock out mice for this protein do not revealed a dramatic phenotype compared with the trafficking importance previously given to this subunit (McCormack et al., 2002). Posteriorly, it was described that some patients lacking Kvβ2.1 were presenting abnormal electroencephalogram or infantile epilepsy (Heilstedt et al., 2001). This latter phenotype could be explained by the initially proposed chaperone role. Thus, functions of Kvβ2.1 are still controversial and several contributions discussed the existence of a yet-not-discovered role of this protein (McCormack et al., 2002, Connor et al., 2005) .

From a natural selection point of view, the lipidic modification and traffic to a concrete subcellular domain need to have a specific reason behind. Kvβ2.1 was classified within the AKR family, and the reduction ability was tested. Compared with other members it is a slow enzyme to complete the entire turnover, but its rate for the hydride transfer is fast enough to consider it as a sensor of the redox state in the cell (Tipparaju et al., 2008, Xie et al., 2011). The data published determined that Kvβ2.1 in physiological conditions would be interacting with NADPH (Kilfoil et al., 2013). However, conditions leading to a decrease in the concentration of NADPH and an increase in NAD (e.g. hypoxia and oxidative stress) may result in changes in the Kvβ-nucleotide complex (Coppock et al., 2001, Ishii et al., 2013). Thus, it is tempting to speculate that the particular localization of Kvβ2.1 is due to the necessity of a redox sensor at lipid raft microdomains. Actually, a it has been reported the presence of redox signalling platforms at lipid raft microdomains (Jin et al., 2011). For instance, eNOS and NADPH oxidase (NOX) have been located at lipid raft microdomains (Patel and Insel, 2009). Mechanistic studies have revealed that interleukin-8 (IL-8) sequentially regulates the assembly of NOX in lipid rafts in neutrophils and prepares the oxidant response to bacterial peptides. This generates the production of O_2^- in the extracellular media, provoking the respiratory burst (Guichard et al., 2005). Both enzymes would generate a decrease in the local amount of NADPH which could be sensed by Kvβ2.1. Whether the sensing is transmitted to their interactors need to be further investigated as a hypothesis for Kvβ2.1 alternative functions.

It was also described for Kvβ2.1 that it is able of catalysing oxPAC, an specific component of mmLDL. The production of oxPAC can be linked to the exposition of those particles to oxidant environments. It has been proved that oxPAC can enhance the generation of ROS in neutrophils as well as the release of active granule enzymes lysozyme and beta-glucuronidase (Kopprasch et al., 1998). Moreover, they can be detected by CD36 scavenger receptor and PAFR (platelet-activating factor receptor) on macrophages provoking the activation of cytokine gene transcription (Rios et al., 2012). However, in order to generate those effects, CD36 and PAFR need to be emplaced at the same lipid raft microdomain (Rios et al., 2013). Previous results from our laboratory exhibited that Kvβ2.1 expression is under specific regulation in macrophages: while M-CSF and LPS generates an increase at 24h after treatment, TNF-α do not modify the levels (Vicente et al., 2005). Concomitantly, Kvβ2.1 increases its lipid raft presence when the proliferation was induced in HEK-293 cells. Thereby, upon determined stimulus, Kvβ2.1 expression is increased and translocated to those microdomains. Thus, the close proximity to the reception platform of oxLDL allows us to consider Kvβ2.1 location as a detoxification enzyme. Actually, the prolongated exposure to oxLDL generates an inhibition of cholesterol-dependent plasma membrane platforms (Brameshuber et al., 2016). Kvβ2.1-dependent oxLDL reduction would act as a lipid raft integrity protector. Moreover, PMA-treatment generated exactly the opposite consequence to activation on Kvβ2.1. Whether both stimuli mediate these effects by increasing the palmitoylation of Kvβ2.1 remains unknown. Moreover, the presence of PSD95 counteracts the PMA-dependent endocytosis without interacting with Kvβ2.1. A possible masking of PKC domains need to be further analysed.

The present thesis determined that, contrary to previous data, Kvβ1.1 is also able to form complexes (Xu and Li, 1997). Since the techniques implemented were different in nature, a weaker affinity between Kvβ1.1 could be the explanation. However, we determine that the affinity of forming homoligomers of Kvβ2.1 and Kvβ1.1 and heteroligomers is the same. This allows inferring that the control of the members in each complex is exclusively dose-dependent (Xu et al., 1998). The same behaviour was described for Kvβ1.2 and Kvβ2 modulation of Kv1.2 (Accili et al., 1997a). Similar to Kvβ2.1, Kvβ1.1 is building a tetrameric structures through dimeric oligomerization (van Huizen et al., 1999). Those multiprotein structures are localized also at the membrane. However, Kvβ1.1 diminishes the Kvβ2.1 lipid raft distribution. Thus, Kvβ1.1 could be negatively affecting the putative functions of Kvβ2.1 at those microdomains.

Previous reported effects of Kvβs on Kv1.3 channel showed an increased amount of current (McCormack et al., 1999). However, our results exhibited a different scenario. Kvβ1.1, but not Kvβ2.1 generates a higher current density. This controversy can be due to different cellular models used. *Xenopus oocytes e*xhibit some endogenous auxiliary subunits that could interfere in the result (Anantharam et al., 2003). However, HEK 293 cells are expressing neither channels nor modulators. We detected an increase in channel intracellular staining concomitant with the chaperon effect and the early interaction in the secretory pathway (Nagaya and Papazian, 1997, Shi et al., 1996). However, further experiments have to be assessed to clearly demonstrate this effect.

Recently, our laboratory has published the caveolin government on Kv1.3 lipid raft distribution. Both proteins interact through a Caveolin Binding Domain (CBD) at the N-terminus of the channel (Perez-Verdaguer et al., 2016a). Other groups demonstrated that caveolin is the responsible for the TCR-induced synaptic membrane raft polarity in $CD8^+$ T-

lymphocytes (Tomassian et al., 2011) It was also described that Kv1.3 is located at the immunological synapse formation at $CD8^+$ T-lymphocytes stimulating the activation pathway (Panyi et al., 2004, Cahalan and Chandy, 2009). Moreover, the spatial position of Kv1.3 is essential for its proper function (Nicolaou et al., 2007). We have showed that Kvβ2.1 and Kvβ1.1 impaired the channel lipid raft targeting by a competence with caveolin. Within this scenario, Kvβs could be buffering the arrival to lipid raft of newly-synthesized channels. Concomitantly, some publications show an upregulated expression of those proteins upon activation stimuli (Autieri et al., 1997). Different to KCNE4, Kvβs allow the channel to reach the membrane but avoiding those specific domains (Sole et al., 2009). Thus, they generate a milder effect on the total current. New approaches to decipher whether Kvβs are a terminator signal of Kv1.3 are highly interesting and necessary. Whether those channels can be laterally recruited upon new activation inputs remain also unknown.

Our laboratory has recently published the PMA-dependent endocytosis of the channel. Clathrin-coated pits mediate internalization after a lipid raft exit. This effect is due to ubiquitination of some residues. A similar route has been also described for other proteins such as dopamine receptor D3, GABAB or the human organic anionic transporter (Zhang et al., 2016, Lahaie et al., 2016, Xu et al., 2016a). We have demonstrated that Kvβ2.1 is capable to counteract partially the PMA effect on the channel internalization. Although not statistically relevant, a milder ubiquitination signal of the channel was detected, instead of blocking the ubiquitin ligase binding domain as described for other proteins (Wiener et al., 2012, Perez et al., 2015). Summing up, Kvβ2.1 is regulating the amount of channel at lipid raft microdomains and counteracting partially the immunosuppression derived from the PMA treatment. Thereby, Kvβ2.1 is smoothing different effects on Kv1.3 physiology.

Among Kv1 family, Kv1.3 reaches the plasma membrane in a higher extend. The balance between export and retention signals is defining the final targeting of the channels (Ma and Jan, 2002). Originally, it was described that a motif containing DxE and surrounding tyrosines were enabling the vesicular stomatitits glycoprotein to export from the ER (Sevier et al., 2000). Regarding ion channels, studies of the trafficking of the Kir family revealed an ER export signal, FCYENE, in Kir2.1 (Stockklausner et al., 2001). Mutations of this motif greatly reduced the steady-state surface density. Moreover, Kir3.1 is retained at the ER if it is expressed alone. However, heteroligomers with Kir3.2 or Kir3.4 efficiently exits the ER due to the presence of this exportation signal (Ma et al., 2002). Considering Kv1 channels, molecular determinants for the export and retention has been partially mapped. At the C-terminus of Kv1.4, VXXSL motif is promoting the exit from ER compartment. The absence of this specific sequence on Kv1.3 allowed us to search for another putative motif (Li et al., 2000). A C-terminal S6 motif, HRETE, was described to enhance the traffic of both Kv1.2 and Kv1.4 (Zhu et al., 2007). Even Kv1.3 also present this motif, the loss of its traffic appeared even when this domain was kept. Thereby, even a motif can promote a specific behaviour, it is the total combination that will determined the final distribution. We demonstrated that the signature YMVIEE was the main molecular determinant responsible for Kv1.3 export. This signature is highly conserved among Kv1 channels, but Kv1.5. Previously, Kv1.1 was demonstrated to present a retention motif in the pore sequence. The mutation of Kv1.1A352P leaded the channel to increase the traffic to the plasma membrane (Manganas et al., 2001). Upon mutating YMVIEE to the Kv1.1-

A352P, the original intracellular pattern was obtained. We thus demonstrated that YMVIEE is indeed an export signature in the balance of the channel trafficking.

We described that YMVIEE signature is recognized by Sec24D, the sorting entity of COPII dependent mechanism (Barlowe, 2003). Similarly, KAT1 potassium channel presents positive FRET values with Sec24 in specific regions of the ER: the ER exit sites. Moreover, CFTR protein presents a diacidic motif that interacts with Sec24 in order to exit the ER domain (Wang et al., 2004a). Sec24 presents different cargo sorting sites: A, B and C (Wendeler et al., 2007). The previously mentioned vesicular stomatitits virus glycoprotein exits the ER because it is identified by the B-site of Sec24a and Sec24b (Mancias and Goldberg, 2008). Further reports suggested that the B-site generally interacts with diacidic domains and that binding requires a glutamate at the final position (Mossessova et al., 2003). However, for the Kir1.1 and CFTR channels, an ExD and DxD motif was found to function as an ER export signal (Heusser and Schwappach, 2005, Wang et al., 2004a). This may be explained by more than one binding site for diacidic ER export motifs. Thus, our results showed that Sec24D recognises the YMVIEE signal, probably not trough the B-site, and Kv1.3 travels through the conventional secretory pathway.

KCNE4 was described to impair Kv1.3 current dramatically (Grunnet et al., 2003). Our laboratory pointed out that KCNE4 modify electrophysiology features decreasing the current density, slowing the activation, accelerating inactivation and increasing cumulative inactivation. Moreover, it generates a massive ER retention and lipid raft impairment (Sole et al., 2009). Both proteins are expressed in the immune system cells. Kv1.3 have a central role in the activation, proliferation and apoptosis of the leukocytes (Beeton and Chandy, 2005). KCNE4 expression is modulated by different insults in diverse immune cells (Sole et al., 2013). Our contribution showed that the final current on Jurkat T-cells and dendritic cells presented differences, and also the pattern of margatoxin dose-responses. Even both cell types express KCNE4, dendritic cells in a major extent. The immunocytochemistry corroborates that the more KCNE4 the higher the retention pattern of Kv1.3 and, moreover, they coimmunoprecipitate. To study the molecular determinants for the interaction, chimeras with Kv1.5 were used as negative controls. While other groups reported an interaction, our FRET results demonstrated that no direct physical association is held between Kv1.5 and KCNE4 (Crump et al., 2016). We found that the major interacting domain in Kv1.3 with KCNE4 is placed at the C-terminal. Similarly, they are implicated in KCNE1 and Kv7.1 combination (Haitin et al., 2009). There is not a specific region of Kv1.3 but the complete C-terminus of the channel. The entire conformation would be detected by KCNE4.

The final function of a channelosome is the reflection of the principal channels and the β-subunits accompanying (Pongs and Schwarz, 2010). Masking events are molecular mechanisms published to control Kv channels features in some specific combinations. Our previous contributions showed a masking of caveolin signals by Kvβ subunits, thus controlling a non-lipid raft distribution. SAP97 blocks the RXR ER retention signal of NMDA rectors (Hong et al., 2015). Similarly, the interaction of β-subunits to the linker I-II of Cav2.2 channel impairs its proteasomal degradation enhancing the membrane targeting (Waithe et al., 2011). Moreover, β3 auxiliary subunits mask the retention RRR signal of Nav1.8 channel promoting the exit of ER (Zhang et al., 2008). KChIP1, KChIP2 and KChIP3 generate an exit from the ER of KV4.2 channels (Shibata et al., 2003). Similarly to the examples, KCNE4 is masking the export signal of Kv1.3 for exit the ER, but it is not the

unique mechanism (Sole et al., 2016). The transference to the channelosome of retention signals is the second mechanism involved. The signals balance is then displaced to the retention motifs. Considering that Kv1.3 is trafficking efficiently to the plasma membrane, an inhibiting subunit is highly relevant. Kv1.3 is involved in the progression of many autoimmune diseases such as multiple sclerosis, diabetes mellitus, arthritis rheumatoid, etc. In fact, a specific overexpression and hyperactivity of Kv1.3 in T effector memory cells has been described as a possible cause of these diseases (Wulff et al., 2003, Rangaraju et al., 2009, Varga et al., 2010, Toldi et al., 2016, Perez-Verdaguer et al., 2016b). Moreover, it has been demonstrated the immunotherapeutic effect of the selective Kv1.3 deletion on Kv1.3 knock-out mice, which are resistant to experimental autoimmune encephalomyelitis (EAE) (Gocke et al., 2012). Therefore, it is tempting to speculate that KCNE4 enhancement could counteract the overexpression of Kv1.3 and thus providing new therapeutic approaches. To decipher each detail of this interaction is highly appropriate as well as the research to find an activator of KCNE4 expression

The interaction domain of KCNE4 with Kv1.3 was also determined and located at the C-terminus. Regarding KCNE proteins, it was proposed that this is the anchoring part of KCNE members to Kv7.1 (Melman et al., 2001). Concretely, KCNE4 interaction site with Kv7.1 was also published pointing to the C-terminal domain (Manderfield et al., 2009). However, other groups proposed also the transmembrane domain as the principal interaction domain (Tapper and George, 2000). We have described the specific signature for the interaction: a tetraleucin motif. However, our results showed that no changes in gating are exerted by the C-terminal. Other regions of the KCNE peptide need to be involved to generate the electrophysiological effects. Thus, considering the bipartite model proposed by Gage and Kobertz, KCNE4 could resemble the KCNE3 peptide: it would present an active transmembrane domain (Gage and Kobertz, 2004). KCNE4 does not have the amino acids described for KCNE3 nor KCNE1 at the transmembrane segment. Thereby, further researcher need to be performed in this direction to decipher the specific molecular determinants for the electrophysiological modulations.

To further decipher the molecular interactions between Kv1.3 and KCNE4 we performed molecular dynamics following a Kv7.1-KCNE1 structural model proposed by Kang et al (Kang et al. 2008). In our model, KCNE4 sits in a cleft between two adjacent Kv1.3 subunits. Some amino acids from the transmembrane domain of KCNE4 are in close proximity with some amino acids from the S1 and S6 Kv1.3 domains, similar to what has been described for the Kv7.1-KCNE1 complex. In addition, the tetra-leucine motif of KCNE4 may interact with several amino acids within a hydrophobic pocket of Kv1.3. It is interesting that one of the models correspond to the amino acids from the forward trafficking signal of Kv1.3 previously described in the dissertation (Martinez-Marmol et al., 2013). Thereby, it supports the masking effect of KCNE4 on Kv1.3.

The tetraleucine is the responsible signature of KCNE4 to interact with Kv1.3. Previous results described that it is also a Ca^{2+}/Calmodulin binding domain (Ciampa et al., 2011). Moreover, oligomerization of KCNE4 is mediated through this domain. Thus, a specific tetrad of amino acids becomes a protein interacting platform.

Leucine motifs have been studied and related to several functions such as endocytosis or protein-protein interactions (Govers et al., 1998, Xu et al., 2016b). Few studies determined that leucine can mediate oligomerization. However, publications were mainly considering

the leucine-reach domains: repeated spaced leucines (Afzal et al., 2013). We have demonstrated that it mediates the oligomerization and it is sufficient to transfer the ability. The absence of this domain in other KCNE members allows us to hypothesize that they can not form oligomers. Indeed, another group published that KCNE1 is a monomer entity within the cell (Nakajo et al., 2010). Through the non-denaturalising technique we could suppose that the major form is a dimer. Unpublished results of our laboratory, using bleaching steps technique, support this result. Multiprotein complexes have been published for other β-subunits. For instance, KChIP1, KChIP2.1 and KChIP2.2 can homo and heteroligomerize (Lin et al., 2004). Kvβ subunits form tetramers with similar affinity among the subtypes, as previously discussed. Moreover, DPPX exists primarily as homodimers even heterodimers are also possible. This transmembrane auxiliary subunit is speculated to interact with Kv4 as an already-formed dimer (Strop et al., 2004). Contrary, we demonstrated that the cotransfection of calmodulin and Kv1.3 leads to a partial impairment of the dimerization. Thereby, depending on the company, KCNE4 would be interacting with Ca^{2+}/Calmodulin, Kv1.3 or other KCNE4. Considering the dramatic effect on Kv1.3 traffic, the formation of the dimer could be understood as a threshold of blockage. Until Kv1.3 does not reach a proper concentration, KCNE4 would be not impairing its traffic.

KCNE4 coexpression with calmodulin leads to an increase of its cell surface targeting. Calmodulin, by its calcium binding ability, has been related to several different functions. For instance, its interaction with Rab3 limited the number of exocytotic events in MDCK cell (Coppola et al., 1999). However, it has been also demonstrated that it mediates the endosome fusion Ca^{2+}- dependent (Colombo et al., 1997). Regarding the Kv physiology, Kv7 members generally interact with calmodulin. Depending on calcium stimulus, calmodulin enhances the Kv7.2 exit from the ER and controls the expression at the plasma membrane (Etxeberria et al., 2008, Alaimo et al., 2009). Moreover, some epilepsy-causing mutations in Kv7.2 are affecting the specific interaction site for calmodulin (Ambrosino et al., 2015). Nonetheless, the molecular intricacies involved in this function remain unknown. Since, Calmodulin binding site is the tetraleucin motif, a masking event for the enhanced traffic was considered.

Several publications have related dileucine motifs with change in traffic patterns. Opposite to our results, hyperpolarization-activated cyclic nucleotide-gated 1 (HCN1) channels present a leucine-based ER export signal that traffic them to the plasma membrane of the inner segment in photoreceptors (Pan et al., 2015). At the carboxy-terminal domain of *ShaI* channels there is a dileucine rich domain that enhances its traffic to dendritic membrane (Rivera et al., 2003). Moreover, Kv7.1 and CLC-2 channels traffic to basolateral membranes due to the presence of a dileucine motif in their sequence (de la Fuente-Ortega et al., 2015, Jespersen et al., 2004). Actually, specific Sec24 isoforms has been determined to enable the exit from the ER compartment detecting a dileucine motif in their cargo proteins (Wendeler et al., 2007). However, the same signature has been implicated to impair the export of other proteins. Acid sensing ion channels present a double dileucine motif (LLDLL) that impairs its presence at the plasma membrane (Wu et al., 2016). For the G protein-coupled inwardly-rectifying potassium channels, the ER retention is defined by the presence of a dileucine motif (Diaz-Bello et al., 2013). Moreover, disruption of this signature in LHβ subunit generates an increased trafficking and exocytosis (Jablonka-Shariff and Boime, 2011). Concomitantly, our results showed that the tetraleucine motif is

impairing the traffic of KCNE4. The level of impairment is similar to the one described for the ER retention motif mutant. However, both proteins exhibited wild type membrane colocalization levels upon coexpression of Sar1. Taking together, these results imply that KCNE4 possess the necessary export signals to travel through COPII-dependent mechanism. However, the retention motifs are important enough to maintain it at endoplasmic reticulum. Upon disappearance of those motifs in KCNE4(ERRM) and KCNE4(L69-72A), the cell surface presence increased. The absence of summative or synergy effects in KCNE4(RM&L) could be due to that both impaired exactly the same route. Even redundant for trafficking, dileucine motif can form dimers, while not the retention signal. In KCNE4 sequence, just after the tetraleucin motif, there is a sequence YKDEE. This signal is highly similar to the diacidic signal in Kv1.3 (Martinez-Marmol et al., 2013). Thereby, the dimerization through tetraleucine-mediated could be masking this export signal. KCNE4(ERRM) and KCNE4(L69-72A) would be preventing the export by different mechanisms.

The complex formed by KCNE4-Kv1.3, if trafficking to the plasma membrane, it is also through a COPII-dependent mechanism. Even the absence of the major interacting interface in KCNE4(L69-72A), both proteins can still traffic together, at least partially. KCNE4(ERRM) was able to rescue partially the traffic of Kv1.3 to the plasma membrane as well as KCNE4(L69-72A). Thus, these results confirms the balance retention/export signals that govern ion channels trafficking (Barlowe, 2003). Considering the molecular model presented, the absence of the tetraleucine domain would leave the YMVIEE signal freer for interacting with Sec24. The total compute of retention/export signals would incorporate the YMVIEE previously masked. Since the traffic improvement is higher without tetraleucine than the ER retention motif, YMVIEE is a stronger motif in the balance. As previously commented, to decipher the specific intricacies of the complex Kv1.3 – KCNE4 is highly relevant considering the implication of the channel in the pathophysiology of some human autoimmune diseases (Perez-Verdaguer et al., 2016b).

We have also demonstrated that Kv1.3, KCNE4 and calmodulin can not form tripartite structures. It is exactly the opposite scenario that in Kv7.1 physiology. KCNE4 inhibition of Kv7.1 requires the interaction with Ca^{2+}/ calmodulin. However, the interaction between KCNE4 and Kv7.1 is not completely lost (Ciampa et al., 2011). Thus, other regions of contact are involved in the interaction Kv7.1-KCNE4. A dipeptide motif close to the S6 domain was determined as an important anchoring site in Kv7.1 where the KCNE4 C-terminus can interact (Vanoye et al., 2009, Manderfield et al., 2009). In the case of Kv1.3, the molecular determinants of the interaction are exactly the same. Thus, the complex formation is mutually exclusive. Final complexes will present Kv1.3-KCNE, KCNE4-Calmodulin or Kv1.3-calmodulin. Actually, we have also determined that Kv1.3 can associate with calmodulin and KCNE4 disrupts its association. It is not known yet the role of calmodulin on Kv1.3. It was proposed that Kv1.3 was inhibited by internal calcium in lymphoblasts. Kv1.3 currents were reduced in a Ca^{2+}- dependent manner by inhibiting calmodulin. The authors proposed that the inhibition may imply more than one mechanism, and they demonstrated a biochemical association with CaM kinase II (Chang et al., 2001). However, other authors did not find Kv1.3-calmodulin association (Fanger et al., 1999). Other groups defend that a calcium-dependent reduction of Kv1.3 inactivation is taking place in megakaryocytes and heterologous system (Martinez-Pinna et al., 2012).

Our results support a possible interaction. However it is not disposable that it is not direct but mediated by other proteins as CaM kinase II.

Several different auxiliary subunits have been described to modulate Kv channels. Moreover, most of them are sharing the expression at the same tissues. Thus, in *in vivo* systems, a recently-formed channel would be sharing space with the diversity of expressed auxiliary subunits. Thereby, the final characteristics of a specific channelosome will be defined by its partners. For instance, Kv4.2 channels recapitulate the voltage-dependent inactivation kinetics of A-type potassium channels when it is coexpressed with DPPX and KChIP proteins (Amarillo et al., 2008). This specific type of current can present some minor electrophysiological differences. These are due to different channelosomes, and the precise composition of channel and auxiliary subunits underlie tissue and regional variability of those currents (Jerng et al., 2005). It was determined that the IKs complex, responsible of the slower delayed rectifier current, it is formed by Kv7.1, KCNE1 and the AKAP Yotiao (Kurokawa et al., 2004). Concomitantly, we detected Kv1.3-KCNE4-Kvβ2.1 presence in dendritic cells and heterologous system showed a trimeric composition. The analysis of the electrophysiological features revealed a dominant KCNE4 effect on the current density. Actually, it was previously described that KCNE4 was exerting a dominant negative effect on Kv7.1-KCNE1 current (Manderfield and George, 2008). Similarly, KCNE2 exerts a decrease in IKs activity when coexpressed (Wu et al., 2006). However, in our experiments, higher currents were obtained at more negative potentials compared with Kv1.3-KCNE4. Thus, Kvβ partial modulation can be inferred. Thereby, Kv1.3 final currents exhibit a mixture non-equivalent of the effects of both proteins. Our traffic results support the dominance of KCNE4. There is not a rescued Kv1.3 membrane staining by Kvβ2.1. Similarly, SAP97 effects are dominant on Kv4.2 traffic generating its clustering at the plasma membrane even in the company of KChIP or DPP-6. Furthermore, the presence of SAP97 enables CaM kinase II phosphorylation of the channel (El-Haou et al., 2009). Opposite to the other KChIPs1-3, KChIP4 is able to negatively affect the trafficking effects of DPPX-S on Kv4.2 channels (Seikel and Trimmer, 2009). Thereby, a specific combination of α-subunits, β partners, modulators, kinases and stimulus will finally define the current, traffic and function of a channelosome.

6. Conclusions

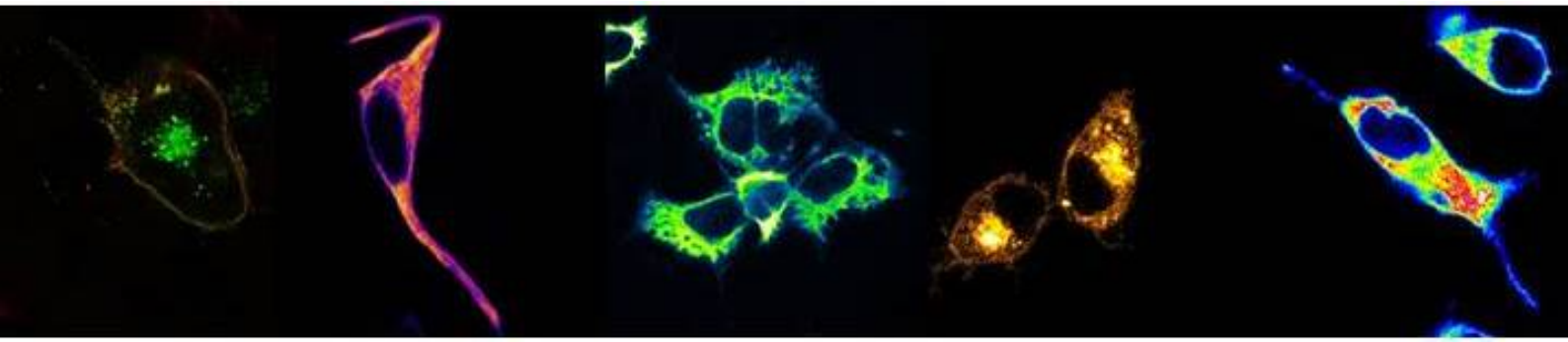

6. CONCLUSIONS

1. Kvβ2.1 is located at lipid raft microdomains because undergoes posttraductional palmitoylation modification. Proliferation stimuli enhance this location while PMA treatment mediates the endocytosis of the protein. This PMA effect is counteracted by PSD95. Both Kvβ1.1 and Kvβ2.1 form homo and heterotetramers with the same affinity located also at membrane associated regions.

2. Kvβ1.1, but not Kvβ2.1, increase the Kv1.3 current, and both generates a left shift in the activation curve. They impair the channel lipid raft targeting and partially counteract the PMA-dependent endocytosis.

3. Kv1.3 presents a highly conserved diacidic export signal at the C-terminus. The interaction with KCNE4 is placed at this cytoplasmic domain causing a massive impairment of the Kv1.3 traffic. This phenotype is induced by masking of the diacidic export signal and transferring retention motifs present on KCNE4 sequence.

4. KCNE4 tetraleucine motif, placed at the C-terminus, is governing the association with Kv1.3. Moreover, it regulates KCNE4 traffic; enhances the dimerization of the subunit and associates with Calmodulin. The competence for the interacting interface defines the impossibility to form trimeric complexes.

5. The formation of Kv1.3 channelosomes with Kvβ2.1 and KCNE4 is possible. KCNE4 exerts a dominant effect on Kv1.3 traffic and current density even in the presence of Kvβ2.1.

7. References

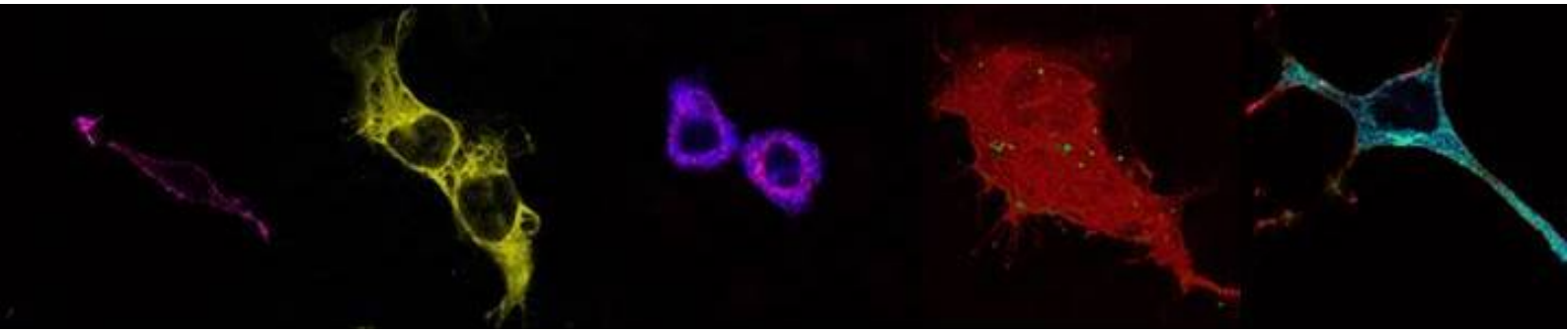

7. REFERENCES

ABBOTT, G. W. 2015. The KCNE2 K(+) channel regulatory subunit: Ubiquitous influence, complex pathobiology. *Gene,* 569**,** 162-72.

ABBOTT, G. W. 2016a. KCNE1 and KCNE3: The yin and yang of voltage-gated K(+) channel regulation. *Gene,* 576**,** 1-13.

ABBOTT, G. W. 2016b. KCNE4 and KCNE5: K(+) channel regulation and cardiac arrhythmogenesis. *Gene,* 593**,** 249-60.

ABBOTT, G. W. 2016c. Novel exon 1 protein-coding regions N-terminally extend human KCNE3 and KCNE4. *FASEB J,* 30**,** 2959-69.

ABBOTT, G. W. 2016d. Regulation of human cardiac potassium channels by full-length KCNE3 and KCNE4. *Sci Rep,* 6**,** 38412.

ABBOTT, G. W., BUTLER, M. H., BENDAHHOU, S., DALAKAS, M. C., PTACEK, L. J. & GOLDSTEIN, S. A. 2001. MiRP2 forms potassium channels in skeletal muscle with Kv3.4 and is associated with periodic paralysis. *Cell,* 104**,** 217-31.

ABBOTT, G. W. & GOLDSTEIN, S. A. 1998. A superfamily of small potassium channel subunits: form and function of the MinK-related peptides (MiRPs). *Q Rev Biophys,* 31**,** 357-98.

ABBOTT, G. W. & GOLDSTEIN, S. A. 2001. Potassium channel subunits encoded by the KCNE gene family: physiology and pathophysiology of the MinK-related peptides (MiRPs). *Mol Interv,* 1**,** 95-107.

ABBOTT, G. W., SESTI, F., SPLAWSKI, I., BUCK, M. E., LEHMANN, M. H., TIMOTHY, K. W., KEATING, M. T. & GOLDSTEIN, S. A. 1999. MiRP1 forms IKr potassium channels with HERG and is associated with cardiac arrhythmia. *Cell,* 97**,** 175-87.

ACCILI, E. A., KIEHN, J., WIBLE, B. A. & BROWN, A. M. 1997a. Interactions among inactivating and noninactivating Kvbeta subunits, and Kvalpha1.2, produce potassium currents with intermediate inactivation. *J Biol Chem,* 272**,** 28232-6.

ACCILI, E. A., KIEHN, J., YANG, Q., WANG, Z., BROWN, A. M. & WIBLE, B. A. 1997b. Separable Kvbeta subunit domains alter expression and gating of potassium channels. *J Biol Chem,* 272**,** 25824-31.

ACCILI, E. A., KURYSHEV, Y. A., WIBLE, B. A. & BROWN, A. M. 1998. Separable effects of human Kvbeta1.2 N- and C-termini on inactivation and expression of human Kv1.4. *J Physiol,* 512 (Pt 2)**,** 325-36.

AFZAL, A. J., SROUR, A., GOIL, A., VASUDAVEN, S., LIU, T., SAMUDRALA, R., DOGRA, N., KOHLI, P., MALAKAR, A. & LIGHTFOOT, D. A. 2013. Homo-dimerization and ligand binding by the leucine-rich repeat domain at RHG1/RFS2 underlying resistance to two soybean pathogens. *BMC Plant Biol,* 13**,** 43.

ALAIMO, A., GOMEZ-POSADA, J. C., AIVAR, P., ETXEBERRIA, A., RODRIGUEZ-ALFARO, J. A., ARESO, P. & VILLARROEL, A. 2009. Calmodulin activation limits the rate of KCNQ2 K+ channel exit from the endoplasmic reticulum. *J Biol Chem,* 284**,** 20668-75.

ALKA, K., DOLLY, J. O., RYAN, B. J. & HENEHAN, G. T. 2014. New inhibitors of the Kvbeta2 subunit from mammalian Kv1 potassium channels. *Int J Biochem Cell Biol,* 55**,** 35-9.

ALKA, K., RYAN, B. J., DOLLY, J. O. & HENEHAN, G. T. 2010. Substrate profiling and aldehyde dismutase activity of the Kvbeta2 subunit of the mammalian Kv1 potassium channel. *Int J Biochem Cell Biol,* 42**,** 2012-8.

AMARILLO, Y., DE SANTIAGO-CASTILLO, J. A., DOUGHERTY, K., MAFFIE, J., KWON, E., COVARRUBIAS, M. & RUDY, B. 2008. Ternary Kv4.2 channels recapitulate voltage-dependent inactivation kinetics of A-type K+ channels in cerebellar granule neurons. *J Physiol,* 586**,** 2093-106.

AMBROSINO, P., ALAIMO, A., BARTOLLINO, S., MANOCCHIO, L., DE MARIA, M., MOSCA, I., GOMIS-PEREZ, C., ALBERDI, A., SCAMBIA, G., LESCA, G., VILLARROEL, A., TAGLIALATELA, M. & SOLDOVIERI, M. V. 2015. Epilepsy-causing mutations in Kv7.2 C-terminus affect binding and functional modulation by calmodulin. *Biochim Biophys Acta,* 1852**,** 1856-66.

ANANTHARAM, A., LEWIS, A., PANAGHIE, G., GORDON, E., MCCROSSAN, Z. A., LERNER, D. J. & ABBOTT, G. W. 2003. RNA interference reveals that endogenous Xenopus MinK-related peptides govern mammalian K+ channel function in oocyte expression studies. *J Biol Chem,* 278**,** 11739-45.

ANGELO, K., JESPERSEN, T., GRUNNET, M., NIELSEN, M. S., KLAERKE, D. A. & OLESEN, S. P. 2002. KCNE5 induces time- and voltage-dependent modulation of the KCNQ1 current. *Biophys J,* 83**,** 1997-2006.

APPENZELLER-HERZOG, C. & HAURI, H. P. 2006. The ER-Golgi intermediate compartment (ERGIC): in search of its identity and function. *J Cell Sci,* 119**,** 2173-83.

ARIAS, C., GUIZY, M., DAVID, M., MARZIAN, S., GONZALEZ, T., DECHER, N. & VALENZUELA, C. 2007. Kvbeta1.3 reduces the degree of stereoselective bupivacaine block of Kv1.5 channels. *Anesthesiology,* 107**,** 641-51.

ARNESTAD, M., CROTTI, L., ROGNUM, T. O., INSOLIA, R., PEDRAZZINI, M., FERRANDI, C., VEGE, A., WANG, D. W., RHODES, T. E., GEORGE, A. L., JR. & SCHWARTZ, P. J. 2007. Prevalence of long-QT syndrome gene variants in sudden infant death syndrome. *Circulation,* 115**,** 361-7.

AUTIERI, M. V., BELKOWSKI, S. M., CONSTANTINESCU, C. S., COHEN, J. A. & PRYSTOWSKY, M. B. 1997. Lymphocyte-specific inducible expression of potassium channel beta subunits. *J Neuroimmunol,* 77**,** 8-16.

BAHRING, R., MILLIGAN, C. J., VARDANYAN, V., ENGELAND, B., YOUNG, B. A., DANNENBERG, J., WALDSCHUTZ, R., EDWARDS, J. P., WRAY, D. & PONGS, O. 2001. Coupling of voltage-dependent potassium channel inactivation and oxidoreductase active site of Kvbeta subunits. *J Biol Chem,* 276**,** 22923-9.

BAJAJ PAHUJA, K., WANG, J., BLAGOVESHCHENSKAYA, A., LIM, L., MADHUSUDHAN, M. S., MAYINGER, P. & SCHEKMAN, R. 2015. Phosphoregulatory protein 14-3-3 facilitates SAC1 transport from the endoplasmic reticulum. *Proc Natl Acad Sci U S A,* 112**,** E3199-206.

BALSE, E., STEELE, D. F., ABRIEL, H., COULOMBE, A., FEDIDA, D. & HATEM, S. N. 2012. Dynamic of ion channel expression at the plasma membrane of cardiomyocytes. *Physiol Rev,* 92**,** 1317-58.

BARHANIN, J., LESAGE, F., GUILLEMARE, E., FINK, M., LAZDUNSKI, M. & ROMEY, G. 1996. K(V)LQT1 and lsK (minK) proteins associate to form the I(Ks) cardiac potassium current. *Nature,* 384**,** 78-80.

BARLOWE, C. 2003. Signals for COPII-dependent export from the ER: what's the ticket out? *Trends Cell Biol,* 13**,** 295-300.

BARROS, F., DOMINGUEZ, P. & DE LA PENA, P. 2012. Cytoplasmic domains and voltage-dependent potassium channel gating. *Front Pharmacol,* 3**,** 49.

BAS, T., GAO, G. Y., LVOV, A., CHANDRASEKHAR, K. D., GILMORE, R. & KOBERTZ, W. R. 2011. Post-translational N-glycosylation of type I transmembrane KCNE1 peptides: implications for membrane protein biogenesis and disease. *J Biol Chem,* 286**,** 28150-9.

BAVASSANO, C., MARVALDI, L., LANGESLAG, M., SARG, B., LINDNER, H., KLIMASCHEWSKI, L., KRESS, M., FERRER-MONTIEL, A. & KNAUS, H. G. 2013. Identification of voltage-gated K(+) channel beta 2 (Kvbeta2) subunit as a novel interaction partner of the pain transducer Transient Receptor Potential Vanilloid 1 channel (TRPV1). *Biochim Biophys Acta,* 1833**,** 3166-75.

BAYCIN-HIZAL, D., GOTTSCHALK, A., JACOBSON, E., MAI, S., WOLOZNY, D., ZHANG, H., KRAG, S. S. & BETENBAUGH, M. J. 2014. Physiologic and pathophysiologic consequences of altered sialylation and glycosylation on ion channel function. *Biochem Biophys Res Commun,* 453**,** 243-53.

BEETON, C. & CHANDY, K. G. 2005. Potassium channels, memory T cells, and multiple sclerosis. *Neuroscientist,* 11**,** 550-62.

BEETON, C., PENNINGTON, M. W. & NORTON, R. S. 2011. Analogs of the sea anemone potassium channel blocker ShK for the treatment of autoimmune diseases. *Inflamm Allergy Drug Targets,* 10**,** 313-21.

BENDAHHOU, S., MARIONNEAU, C., HAUROGNE, K., LARROQUE, M. M., DERAND, R., SZUTS, V., ESCANDE, D., DEMOLOMBE, S. & BARHANIN, J. 2005. In vitro molecular interactions and distribution of KCNE family with KCNQ1 in the human heart. *Cardiovasc Res,* 67**,** 529-38.

BERGLUND, N. A., KARGAS, V., ORTIZ-SUAREZ, M. L. & BOND, P. J. 2015. The role of protein-protein interactions in Toll-like receptor function. *Prog Biophys Mol Biol,* 119**,** 72-83.

BEZANILLA, F. 2008. Ion channels: from conductance to structure. *Neuron,* 60**,** 456-68.

BHATNAGAR, A. 1995. Electrophysiological effects of 4-hydroxynonenal, an aldehydic product of lipid peroxidation, on isolated rat ventricular myocytes. *Circ Res,* 76**,** 293-304.

BIGGIN, P. C., ROOSILD, T. & CHOE, S. 2000. Potassium channel structure: domain by domain. *Curr Opin Struct Biol,* 10**,** 456-61.

BLUMENTHAL, E. M. & KACZMAREK, L. K. 1994. The minK potassium channel exists in functional and nonfunctional forms when expressed in the plasma membrane of Xenopus oocytes. *J Neurosci,* 14**,** 3097-105.

BLUNCK, R., CORDERO-MORALES, J. F., CUELLO, L. G., PEROZO, E. & BEZANILLA, F. 2006. Detection of the opening of the bundle crossing in KcsA with fluorescence lifetime spectroscopy reveals the existence of two gates for ion conduction. *J Gen Physiol,* 128**,** 569-81.

BOCK, J., SZABO, I., GAMPER, N., ADAMS, C. & GULBINS, E. 2003. Ceramide inhibits the potassium channel Kv1.3 by the formation of membrane platforms. *Biochem Biophys Res Commun,* 305**,** 890-7.

BOWLBY, M. R., FADOOL, D. A., HOLMES, T. C. & LEVITAN, I. B. 1997. Modulation of the Kv1.3 potassium channel by receptor tyrosine kinases. *J Gen Physiol,* 110**,** 601-10.

BRAMESHUBER, M., SEVCSIK, E., ROSSBOTH, B. K., MANNER, C., DEIGNER, H. P., PEKSEL, B., PETER, M., TOROK, Z., HERMETTER, A. & SCHUTZ, G. J. 2016. Oxidized Phospholipids Inhibit the Formation of Cholesterol-Dependent Plasma Membrane Nanoplatforms. *Biophys J,* 110**,** 205-13.

BROWN, D. A. & LONDON, E. 1998. Structure and origin of ordered lipid domains in biological membranes. *J Membr Biol,* 164**,** 103-14.

BUCCI, M., GRATTON, J. P., RUDIC, R. D., ACEVEDO, L., ROVIEZZO, F., CIRINO, G. & SESSA, W. C. 2000. In vivo delivery of the caveolin-1 scaffolding domain inhibits nitric oxide synthesis and reduces inflammation. *Nat Med,* 6**,** 1362-7.

BUDNIK, A. & STEPHENS, D. J. 2009. ER exit sites--localization and control of COPII vesicle formation. *FEBS Lett,* 583**,** 3796-803.

BUTLER, D. M., ONO, J. K., CHANG, T., MCCAMAN, R. E. & BARISH, M. E. 1998. Mouse brain potassium channel beta1 subunit mRNA: cloning and distribution during development. *J Neurobiol,* 34**,** 135-50.

CAHALAN, M. D. & CHANDY, K. G. 2009. The functional network of ion channels in T lymphocytes. *Immunol Rev,* 231**,** 59-87.

CAMPOMANES, C. R., CARROLL, K. I., MANGANAS, L. N., HERSHBERGER, M. E., GONG, B., ANTONUCCI, D. E., RHODES, K. J. & TRIMMER, J. S. 2002. Kv beta subunit oxidoreductase activity and Kv1 potassium channel trafficking. *J Biol Chem,* 277**,** 8298-305.

CANERINA-AMARO, A., HERNANDEZ-ABAD, L. G., FERRER, I., QUINTO-ALEMANY, D., MESA-HERRERA, F., FERRI, C., PUERTAS-AVENDANO, R. A., DIAZ, M. & MARIN, R. 2017. Lipid raft ER signalosome malfunctions in menopause and Alzheimer's disease. *Front Biosci (Schol Ed),* 9**,** 111-126.

CIAMPA, E. J., WELCH, R. C., VANOYE, C. G. & GEORGE, A. L., JR. 2011. KCNE4 juxtamembrane region is required for interaction with calmodulin and for functional suppression of KCNQ1. *J Biol Chem,* 286**,** 4141-9.

CLANCY, S. M., CHEN, B., BERTASO, F., MAMET, J. & JEGLA, T. 2009. KCNE1 and KCNE3 beta-subunits regulate membrane surface expression of Kv12.2 K(+) channels in vitro and form a tripartite complex in vivo. *PLoS One,* 4**,** e6330.

COLEMAN, S. K., NEWCOMBE, J., PRYKE, J. & DOLLY, J. O. 1999. Subunit composition of Kv1 channels in human CNS. *J Neurochem,* 73**,** 849-58.

COLOMBO, M. I., BERON, W. & STAHL, P. D. 1997. Calmodulin regulates endosome fusion. *J Biol Chem,* 272**,** 7707-12.

COLLINS, B. M., DAVIS, M. J., HANCOCK, J. F. & PARTON, R. G. 2012. Structure-based reassessment of the caveolin signaling model: do caveolae regulate signaling through caveolin-protein interactions? *Dev Cell,* 23**,** 11-20.

COMES, N., BIELANSKA, J., VALLEJO-GRACIA, A., SERRANO-ALBARRAS, A., MARRUECOS, L., GOMEZ, D., SOLER, C., CONDOM, E., RAMON, Y. C. S., HERNANDEZ-LOSA, J., FERRERES, J. C. & FELIPE, A. 2013. The voltage-dependent K(+) channels Kv1.3 and Kv1.5 in human cancer. *Front Physiol,* 4**,** 283.

CONNOR, J. X., MCCORMACK, K., PLETSCH, A., GAETA, S., GANETZKY, B., CHIU, S. Y. & MESSING, A. 2005. Genetic modifiers of the Kv beta2-null phenotype in mice. *Genes Brain Behav,* 4**,** 77-88.

COPPOCK, E. A., MARTENS, J. R. & TAMKUN, M. M. 2001. Molecular basis of hypoxia-induced pulmonary vasoconstriction: role of voltage-gated K+ channels. *Am J Physiol Lung Cell Mol Physiol,* 281**,** L1-12.

COPPOLA, T., PERRET-MENOUD, V., LUTHI, S., FARNSWORTH, C. C., GLOMSET, J. A. & REGAZZI, R. 1999. Disruption of Rab3-calmodulin interaction, but not other effector interactions, prevents Rab3 inhibition of exocytosis. *EMBO J,* 18**,** 5885-91.

COUET, J., LI, S., OKAMOTO, T., IKEZU, T. & LISANTI, M. P. 1997. Identification of peptide and protein ligands for the caveolin-scaffolding domain. Implications for the interaction of caveolin with caveolae-associated proteins. *J Biol Chem,* 272**,** 6525-33.

CROCI, C., BRANDSTATTER, J. H. & ENZ, R. 2003. ZIP3, a new splice variant of the PKC-zeta-interacting protein family, binds to GABAC receptors, PKC-zeta, and Kv beta 2. *J Biol Chem,* 278**,** 6128-35.

CRUMP, S. M., HU, Z., KANT, R., LEVY, D. I., GOLDSTEIN, S. A. & ABBOTT, G. W. 2016. Kcne4 deletion sex- and age-specifically impairs cardiac repolarization in mice. *FASEB J,* 30**,** 360-9.

CHAMBERLAIN, L. H., LEMONIDIS, K., SANCHEZ-PEREZ, M., WERNO, M. W., GORLEKU, O. A. & GREAVES, J. 2013. Palmitoylation and the trafficking of peripheral membrane proteins. *Biochem Soc Trans,* 41**,** 62-6.

CHANDA, B., ASAMOAH, O. K., BLUNCK, R., ROUX, B. & BEZANILLA, F. 2005. Gating charge displacement in voltage-gated ion channels involves limited transmembrane movement. *Nature,* 436**,** 852-6.

CHANDRASEKHAR, K. D., BAS, T. & KOBERTZ, W. R. 2006. KCNE1 subunits require co-assembly with K+ channels for efficient trafficking and cell surface expression. *J Biol Chem,* 281**,** 40015-23.

CHANG, M. C., KHANNA, R. & SCHLICHTER, L. C. 2001. Regulation of Kv1.3 channels in activated human T lymphocytes by Ca(2+)-dependent pathways. *Cell Physiol Biochem,* 11**,** 123-34.

CHAPALAMADUGU, K. C., PANGULURI, S. K., BENNETT, E. S., KOLLIPUTI, N. & TIPPARAJU, S. M. 2015. High level of oxygen treatment causes cardiotoxicity with arrhythmias and redox modulation. *Toxicol Appl Pharmacol,* 282**,** 100-7.

CHAROLLAIS, J. & VAN DER GOOT, F. G. 2009. Palmitoylation of membrane proteins (Review). *Mol Membr Biol,* 26**,** 55-66.

CHEN, H., KIM, L. A., RAJAN, S., XU, S. & GOLDSTEIN, S. A. 2003. Charybdotoxin binding in the I(Ks) pore demonstrates two MinK subunits in each channel complex. *Neuron,* 40**,** 15-23.

CHEN, J., ZHENG, R., MELMAN, Y. F. & MCDONALD, T. V. 2009. Functional interactions between KCNE1 C-terminus and the KCNQ1 channel. *PLoS One,* 4**,** e5143.

CHEN, L., JEFFRIES, O., ROWE, I. C., LIANG, Z., KNAUS, H. G., RUTH, P. & SHIPSTON, M. J. 2010. Membrane trafficking of large conductance calcium-activated potassium channels is regulated by alternative splicing of a transplantable, acidic trafficking motif in the RCK1-RCK2 linker. *J Biol Chem,* 285**,** 23265-75.

CHI, V., PENNINGTON, M. W., NORTON, R. S., TARCHA, E. J., LONDONO, L. M., SIMS-FAHEY, B., UPADHYAY, S. K., LAKEY, J. T., IADONATO, S., WULFF, H., BEETON, C. & CHANDY, K. G. 2012. Development of a sea anemone toxin as an immunomodulator for therapy of autoimmune diseases. *Toxicon,* 59**,** 529-46.

CHO, K. O., HUNT, C. A. & KENNEDY, M. B. 1992. The rat brain postsynaptic density fraction contains a homolog of the Drosophila discs-large tumor suppressor protein. *Neuron,* 9**,** 929-42.

CHOI, B. H. & HAHN, S. J. 2010. Kv1.3: a potential pharmacological target for diabetes. *Acta Pharmacol Sin,* 31**,** 1031-5.

CHUNG, D. Y., CHAN, P. J., BANKSTON, J. R., YANG, L., LIU, G., MARX, S. O., KARLIN, A. & KASS, R. S. 2009. Location of KCNE1 relative to KCNQ1 in the I(KS) potassium channel by disulfide cross-linking of substituted cysteines. *Proc Natl Acad Sci U S A,* 106**,** 743-8.

DART, C. 2010. Lipid microdomains and the regulation of ion channel function. *J Physiol,* 588**,** 3169-78.

DAVID, J. P., STAS, J. I., SCHMITT, N. & BOCKSTEINS, E. 2015. Auxiliary KCNE subunits modulate both homotetrameric Kv2.1 and heterotetrameric Kv2.1/Kv6.4 channels. *Sci Rep,* 5**,** 12813.

DAVID, M., MACIAS, A., MORENO, C., PRIETO, A., MARTINEZ-MARMOL, R., VICENTE, R., GONZALEZ, T., FELIPE, A., TAMKUN, M. M. & VALENZUELA, C. 2012. Protein kinase C (PKC) activity regulates functional effects of Kvbeta1.3 subunit on KV1.5 channels: identification of a cardiac Kv1.5 channelosome. *J Biol Chem,* 287**,** 21416-28.

DE LA FUENTE-ORTEGA, E., GRAVOTTA, D., PEREZ BAY, A., BENEDICTO, I., CARVAJAL-GONZALEZ, J. M., LEHMANN, G. L., LAGOS, C. F. & RODRIGUEZ-BOULAN, E. 2015. Basolateral sorting of chloride channel 2 is mediated by interactions between a dileucine motif and the clathrin adaptor AP-1. *Mol Biol Cell,* 26**,** 1728-42.

DECHER, N., GONZALEZ, T., STREIT, A. K., SACHSE, F. B., RENIGUNTA, V., SOOM, M., HEINEMANN, S. H., DAUT, J. & SANGUINETTI, M. C. 2008. Structural determinants

of Kvbeta1.3-induced channel inactivation: a hairpin modulated by PIP2. *EMBO J,* 27**,** 3164-74.

DECHER, N., KUMAR, P., GONZALEZ, T., RENIGUNTA, V. & SANGUINETTI, M. C. 2005. Structural basis for competition between drug binding and Kvbeta 1.3 accessory subunit-induced N-type inactivation of Kv1.5 channels. *Mol Pharmacol,* 68**,** 995-1005.

DEDEK, K. & WALDEGGER, S. 2001. Colocalization of KCNQ1/KCNE channel subunits in the mouse gastrointestinal tract. *Pflugers Arch,* 442**,** 896-902.

DIAZ-BELLO, B., RANGEL-GARCIA, C. I., SALVADOR, C., CARRISOZA-GAYTAN, R. & ESCOBAR, L. I. 2013. The polarization of the G-protein activated potassium channel GIRK5 to the vegetal pole of Xenopus laevis oocytes is driven by a di-leucine motif. *PLoS One,* 8**,** e64096.

DIAZ-ROHRER, B. B., LEVENTAL, K. R., SIMONS, K. & LEVENTAL, I. 2014. Membrane raft association is a determinant of plasma membrane localization. *Proc Natl Acad Sci U S A,* 111**,** 8500-5.

DOI, K., SATO, T., KURAMASU, T., HIBINO, H., KITAHARA, T., HORII, A., MATSUSHIRO, N., FUSE, Y. & KUBO, T. 2005. Meniere's disease is associated with single nucleotide polymorphisms in the human potassium channel genes, KCNE1 and KCNE3. *ORL J Otorhinolaryngol Relat Spec,* 67**,** 289-93.

DOUGLASS, J., OSBORNE, P. B., CAI, Y. C., WILKINSON, M., CHRISTIE, M. J. & ADELMAN, J. P. 1990. Characterization and functional expression of a rat genomic DNA clone encoding a lymphocyte potassium channel. *J Immunol,* 144**,** 4841-50.

DOWNEN, M., BELKOWSKI, S., KNOWLES, H., CARDILLO, M. & PRYSTOWSKY, M. B. 1999. Developmental expression of voltage-gated potassium channel beta subunits. *Brain Res Dev Brain Res,* 117**,** 71-80.

DOYLE, D. A., MORAIS CABRAL, J., PFUETZNER, R. A., KUO, A., GULBIS, J. M., COHEN, S. L., CHAIT, B. T. & MACKINNON, R. 1998. The structure of the potassium channel: molecular basis of K+ conduction and selectivity. *Science,* 280**,** 69-77.

EL-HAOU, S., BALSE, E., NEYROUD, N., DILANIAN, G., GAVILLET, B., ABRIEL, H., COULOMBE, A., JEROMIN, A. & HATEM, S. N. 2009. Kv4 potassium channels form a tripartite complex with the anchoring protein SAP97 and CaMKII in cardiac myocytes. *Circ Res,* 104**,** 758-69.

ENGLAND, S. K., UEBELE, V. N., KODALI, J., BENNETT, P. B. & TAMKUN, M. M. 1995a. A novel K+ channel beta-subunit (hKv beta 1.3) is produced via alternative mRNA splicing. *J Biol Chem,* 270**,** 28531-4.

ENGLAND, S. K., UEBELE, V. N., SHEAR, H., KODALI, J., BENNETT, P. B. & TAMKUN, M. M. 1995b. Characterization of a voltage-gated K+ channel beta subunit expressed in human heart. *Proc Natl Acad Sci U S A,* 92**,** 6309-13.

ETXEBERRIA, A., AIVAR, P., RODRIGUEZ-ALFARO, J. A., ALAIMO, A., VILLACE, P., GOMEZ-POSADA, J. C., ARESO, P. & VILLARROEL, A. 2008. Calmodulin regulates the trafficking of KCNQ2 potassium channels. *FASEB J,* 22**,** 1135-43.

FADOOL, D. A. 1998. Tyrosine phosphorylation downregulates a potassium current in rat olfactory bulb neurons and a cloned Kv1.3 channel. *Ann N Y Acad Sci,* 855**,** 529-32.

FADOOL, D. A., TUCKER, K., PERKINS, R., FASCIANI, G., THOMPSON, R. N., PARSONS, A. D., OVERTON, J. M., KONI, P. A., FLAVELL, R. A. & KACZMAREK, L. K. 2004. Kv1.3 channel gene-targeted deletion produces "Super-Smeller Mice" with altered glomeruli, interacting scaffolding proteins, and biophysics. *Neuron,* 41**,** 389-404.

FALK, T., KILANI, R. K., STRAZDAS, L. A., BORDERS, R. S., STEIDL, J. V., YOOL, A. J. & SHERMAN, S. J. 2003. Developmental regulation of the A-type potassium-channel

current in hippocampal neurons: role of the Kvbeta 1.1 subunit. *Neuroscience,* 120**,** 387-404.

FANGER, C. M., GHANSHANI, S., LOGSDON, N. J., RAUER, H., KALMAN, K., ZHOU, J., BECKINGHAM, K., CHANDY, K. G., CAHALAN, M. D. & AIYAR, J. 1999. Calmodulin mediates calcium-dependent activation of the intermediate conductance KCa channel, IKCa1. *J Biol Chem,* 274**,** 5746-54.

FOLCO, E. J., LIU, G. X. & KOREN, G. 2004. Caveolin-3 and SAP97 form a scaffolding protein complex that regulates the voltage-gated potassium channel Kv1.5. *Am J Physiol Heart Circ Physiol,* 287**,** H681-90.

GAGE, S. D. & KOBERTZ, W. R. 2004. KCNE3 truncation mutants reveal a bipartite modulation of KCNQ1 K+ channels. *J Gen Physiol,* 124**,** 759-71.

GIESE, K. P., STORM, J. F., REUTER, D., FEDOROV, N. B., SHAO, L. R., LEICHER, T., PONGS, O. & SILVA, A. J. 1998. Reduced K+ channel inactivation, spike broadening, and after-hyperpolarization in Kvbeta1.1-deficient mice with impaired learning. *Learn Mem,* 5**,** 257-73.

GOCKE, A. R., LEBSON, L. A., GRISHKAN, I. V., HU, L., NGUYEN, H. M., WHARTENBY, K. A., CHANDY, K. G. & CALABRESI, P. A. 2012. Kv1.3 deletion biases T cells toward an immunoregulatory phenotype and renders mice resistant to autoimmune encephalomyelitis. *J Immunol,* 188**,** 5877-86.

GONG, J., XU, J., BEZANILLA, M., VAN HUIZEN, R., DERIN, R. & LI, M. 1999. Differential stimulation of PKC phosphorylation of potassium channels by ZIP1 and ZIP2. *Science,* 285**,** 1565-9.

GONZALEZ, T., NAVARRO-POLANCO, R., ARIAS, C., CABALLERO, R., MORENO, I., DELPON, E., TAMARGO, J., TAMKUN, M. M. & VALENZUELA, C. 2002. Assembly with the Kvbeta1.3 subunit modulates drug block of hKv1.5 channels. *Mol Pharmacol,* 62**,** 1456-63.

GOVERS, R., VAN KERKHOF, P., SCHWARTZ, A. L. & STROUS, G. J. 1998. Di-leucine-mediated internalization of ligand by a truncated growth hormone receptor is independent of the ubiquitin conjugation system. *J Biol Chem,* 273**,** 16426-33.

GREAVES, J., PRESCOTT, G. R., GORLEKU, O. A. & CHAMBERLAIN, L. H. 2010. Regulation of SNAP-25 trafficking and function by palmitoylation. *Biochem Soc Trans,* 38**,** 163-6.

GRISSMER, S., DETHLEFS, B., WASMUTH, J. J., GOLDIN, A. L., GUTMAN, G. A., CAHALAN, M. D. & CHANDY, K. G. 1990. Expression and chromosomal localization of a lymphocyte K+ channel gene. *Proc Natl Acad Sci U S A,* 87**,** 9411-5.

GRUNNET, M., JESPERSEN, T., RASMUSSEN, H. B., LJUNGSTROM, T., JORGENSEN, N. K., OLESEN, S. P. & KLAERKE, D. A. 2002. KCNE4 is an inhibitory subunit to the KCNQ1 channel. *J Physiol,* 542**,** 119-30.

GRUNNET, M., OLESEN, S. P., KLAERKE, D. A. & JESPERSEN, T. 2005. hKCNE4 inhibits the hKCNQ1 potassium current without affecting the activation kinetics. *Biochem Biophys Res Commun,* 328**,** 1146-53.

GRUNNET, M., RASMUSSEN, H. B., HAY-SCHMIDT, A., ROSENSTIERNE, M., KLAERKE, D. A., OLESEN, S. P. & JESPERSEN, T. 2003. KCNE4 is an inhibitory subunit to Kv1.1 and Kv1.3 potassium channels. *Biophys J,* 85**,** 1525-37.

GRUPE, A., SCHROTER, K. H., RUPPERSBERG, J. P., STOCKER, M., DREWES, T., BECKH, S. & PONGS, O. 1990. Cloning and expression of a human voltage-gated potassium channel. A novel member of the RCK potassium channel family. *EMBO J,* 9**,** 1749-56.

GU, C., ZHOU, W., PUTHENVEEDU, M. A., XU, M., JAN, Y. N. & JAN, L. Y. 2006. The microtubule plus-end tracking protein EB1 is required for Kv1 voltage-gated K+ channel axonal targeting. *Neuron,* 52**,** 803-16.

GU, Y. & GU, C. 2010. Dynamics of Kv1 channel transport in axons. *PLoS One,* 5**,** e11931.

GUBITOSI-KLUG, R. A., MANCUSO, D. J. & GROSS, R. W. 2005. The human Kv1.1 channel is palmitoylated, modulating voltage sensing: Identification of a palmitoylation consensus sequence. *Proc Natl Acad Sci U S A,* 102**,** 5964-8.

GUICHARD, C., PEDRUZZI, E., DEWAS, C., FAY, M., POUZET, C., BENS, M., VANDEWALLE, A., OGIER-DENIS, E., GOUGEROT-POCIDALO, M. A. & ELBIM, C. 2005. Interleukin-8-induced priming of neutrophil oxidative burst requires sequential recruitment of NADPH oxidase components into lipid rafts. *J Biol Chem,* 280**,** 37021-32.

GULBINS, E., SZABO, I., BALTZER, K. & LANG, F. 1997. Ceramide-induced inhibition of T lymphocyte voltage-gated potassium channel is mediated by tyrosine kinases. *Proc Natl Acad Sci U S A,* 94**,** 7661-6.

GULBIS, J. M., MANN, S. & MACKINNON, R. 1999. Structure of a voltage-dependent K+ channel beta subunit. *Cell,* 97**,** 943-52.

GULBIS, J. M., ZHOU, M., MANN, S. & MACKINNON, R. 2000. Structure of the cytoplasmic beta subunit-T1 assembly of voltage-dependent K+ channels. *Science,* 289**,** 123-7.

GUTMAN, G. A., CHANDY, K. G., GRISSMER, S., LAZDUNSKI, M., MCKINNON, D., PARDO, L. A., ROBERTSON, G. A., RUDY, B., SANGUINETTI, M. C., STUHMER, W. & WANG, X. 2005. International Union of Pharmacology. LIII. Nomenclature and molecular relationships of voltage-gated potassium channels. *Pharmacol Rev,* 57**,** 473-508.

HAITIN, Y., WIENER, R., SHAHAM, D., PERETZ, A., COHEN, E. B., SHAMGAR, L., PONGS, O., HIRSCH, J. A. & ATTALI, B. 2009. Intracellular domains interactions and gated motions of I(KS) potassium channel subunits. *EMBO J,* 28**,** 1994-2005.

HAJDU, P., VARGA, Z., PIERI, C., PANYI, G. & GASPAR, R., JR. 2003. Cholesterol modifies the gating of Kv1.3 in human T lymphocytes. *Pflugers Arch,* 445**,** 674-82.

HANADA, T., LIN, L., CHANDY, K. G., OH, S. S. & CHISHTI, A. H. 1997. Human homologue of the Drosophila discs large tumor suppressor binds to p56lck tyrosine kinase and Shaker type Kv1.3 potassium channel in T lymphocytes. *J Biol Chem,* 272**,** 26899-904.

HILLE, B. 2001. Ion channels of excitable membranes. *Sinauerassociates, Sunderland, Mass.. Great Britain, 2001.*

HEGINBOTHAM, L., LU, Z., ABRAMSON, T. & MACKINNON, R. 1994. Mutations in the K+ channel signature sequence. *Biophys J,* 66**,** 1061-7.

HEILSTEDT, H. A., BURGESS, D. L., ANDERSON, A. E., CHEDRAWI, A., THARP, B., LEE, O., KASHORK, C. D., STARKEY, D. E., WU, Y. Q., NOEBELS, J. L., SHAFFER, L. G. & SHAPIRA, S. K. 2001. Loss of the potassium channel beta-subunit gene, KCNAB2, is associated with epilepsy in patients with 1p36 deletion syndrome. *Epilepsia,* 42**,** 1103-11.

HEINEMANN, S. H., RETTIG, J., GRAACK, H. R. & PONGS, O. 1996. Functional characterization of Kv channel beta-subunits from rat brain. *J Physiol,* 493 (Pt 3)**,** 625-33.

HEINEMANN, S. H., RETTIG, J., WUNDER, F. & PONGS, O. 1995. Molecular and functional characterization of a rat brain Kv beta 3 potassium channel subunit. *FEBS Lett,* 377**,** 383-9.

HEUSSER, K. & SCHWAPPACH, B. 2005. Trafficking of potassium channels. *Curr Opin Neurobiol,* 15**,** 364-9.

HOLLAND, S. M., COLLURA, K. M., KETSCHEK, A., NOMA, K., FERGUSON, T. A., JIN, Y., GALLO, G. & THOMAS, G. M. 2016. Palmitoylation controls DLK localization, interactions and activity to ensure effective axonal injury signaling. *Proc Natl Acad Sci U S A,* 113**,** 763-8.

HONG, X., AVETISYAN, M., RONILO, M. & STANDLEY, S. 2015. SAP97 blocks the RXR ER retention signal of NMDA receptor subunit GluN1-3 through its SH3 domain. *Biochim Biophys Acta,* 1853**,** 489-99.

HOOG, S. S., PAWLOWSKI, J. E., ALZARI, P. M., PENNING, T. M. & LEWIS, M. 1994. Three-dimensional structure of rat liver 3 alpha-hydroxysteroid/dihydrodiol dehydrogenase: a member of the aldo-keto reductase superfamily. *Proc Natl Acad Sci U S A,* 91**,** 2517-21.

ISHII, T., WARABI, E., SIOW, R. C. & MANN, G. E. 2013. Sequestosome1/p62: a regulator of redox-sensitive voltage-activated potassium channels, arterial remodeling, inflammation, and neurite outgrowth. *Free Radic Biol Med,* 65**,** 102-16.

JABLONKA-SHARIFF, A. & BOIME, I. 2011. A dileucine determinant in the carboxyl terminal sequence of the LHbeta subunit is implicated in the regulated secretion of lutropin from transfected GH3 cells. *Mol Cell Endocrinol,* 339**,** 7-13.

JACKSON, L. P. 2014. Structure and mechanism of COPI vesicle biogenesis. *Curr Opin Cell Biol,* 29**,** 67-73.

JEFFRIES, O., GEIGER, N., ROWE, I. C., TIAN, L., MCCLAFFERTY, H., CHEN, L., BI, D., KNAUS, H. G., RUTH, P. & SHIPSTON, M. J. 2010. Palmitoylation of the S0-S1 linker regulates cell surface expression of voltage- and calcium-activated potassium (BK) channels. *J Biol Chem,* 285**,** 33307-14.

JENSEN, D. & SCHEKMAN, R. 2011. COPII-mediated vesicle formation at a glance. *J Cell Sci,* 124**,** 1-4.

JENSEN, M. O., JOGINI, V., BORHANI, D. W., LEFFLER, A. E., DROR, R. O. & SHAW, D. E. 2012. Mechanism of voltage gating in potassium channels. *Science,* 336**,** 229-33.

JERNG, H. H., KUNJILWAR, K. & PFAFFINGER, P. J. 2005. Multiprotein assembly of Kv4.2, KChIP3 and DPP10 produces ternary channel complexes with ISA-like properties. *J Physiol,* 568**,** 767-88.

JERVELL, A. & LANGE-NIELSEN, F. 1957. Congenital deaf-mutism, functional heart disease with prolongation of the Q-T interval and sudden death. *Am Heart J,* 54**,** 59-68.

JESPERSEN, T., RASMUSSEN, H. B., GRUNNET, M., JENSEN, H. S., ANGELO, K., DUPUIS, D. S., VOGEL, L. K., JORGENSEN, N. K., KLAERKE, D. A. & OLESEN, S. P. 2004. Basolateral localisation of KCNQ1 potassium channels in MDCK cells: molecular identification of an N-terminal targeting motif. *J Cell Sci,* 117**,** 4517-26.

JEZ, J. M., BENNETT, M. J., SCHLEGEL, B. P., LEWIS, M. & PENNING, T. M. 1997. Comparative anatomy of the aldo-keto reductase superfamily. *Biochem J,* 326 (Pt 3)**,** 625-36.

JIANG, M., XU, X., WANG, Y., TOYODA, F., LIU, X. S., ZHANG, M., ROBINSON, R. B. & TSENG, G. N. 2009. Dynamic partnership between KCNQ1 and KCNE1 and influence on cardiac IKs current amplitude by KCNE2. *J Biol Chem,* 284**,** 16452-62.

JIANG, Y., LEE, A., CHEN, J., RUTA, V., CADENE, M., CHAIT, B. T. & MACKINNON, R. 2003. X-ray structure of a voltage-dependent K+ channel. *Nature,* 423**,** 33-41.

JIMENEZ-PEREZ, L., CIDAD, P., ALVAREZ-MIGUEL, I., SANTOS-HIPOLITO, A., TORRES-MERINO, R., ALONSO, E., DE LA FUENTE, M. A., LOPEZ-LOPEZ, J. R. & PEREZ-GARCIA, M. T. 2016. Molecular Determinants of Kv1.3 Potassium Channels-induced Proliferation. *J Biol Chem,* 291**,** 3569-80.

JIN, S., ZHOU, F., KATIRAI, F. & LI, P. L. 2011. Lipid raft redox signaling: molecular mechanisms in health and disease. *Antioxid Redox Signal,* 15**,** 1043-83.

JINDAL, H. K., FOLCO, E. J., LIU, G. X. & KOREN, G. 2008. Posttranslational modification of voltage-dependent potassium channel Kv1.5: COOH-terminal palmitoylation modulates its biological properties. *Am J Physiol Heart Circ Physiol,* 294**,** H2012-21.

JING, J., PERETZ, T., SINGER-LAHAT, D., CHIKVASHVILI, D., THORNHILL, W. B. & LOTAN, I. 1997. Inactivation of a voltage-dependent K+ channel by beta subunit. Modulation

by a phosphorylation-dependent interaction between the distal C terminus of alpha subunit and cytoskeleton. *J Biol Chem,* 272**,** 14021-4.

JOW, F., ZHANG, Z. H., KOPSCO, D. C., CARROLL, K. C. & WANG, K. 2004. Functional coupling of intracellular calcium and inactivation of voltage-gated Kv1.1/Kvbeta1.1 A-type K+ channels. *Proc Natl Acad Sci U S A,* 101**,** 15535-40.

KANDA, V. A., LEWIS, A., XU, X. & ABBOTT, G. W. 2011. KCNE1 and KCNE2 inhibit forward trafficking of homomeric N-type voltage-gated potassium channels. *Biophys J,* 101**,** 1354-63.

KANG, C., TIAN, C., SONNICHSEN, F. D., SMITH, J. A., MEILER, J., GEORGE, A. L., JR., VANOYE, C. G., KIM, H. J. & SANDERS, C. R. 2008. Structure of KCNE1 and implications for how it modulates the KCNQ1 potassium channel. *Biochemistry,* 47**,** 7999-8006.

KEYNES, R. D. & ELINDER, F. 1999. The screw-helical voltage gating of ion channels. *Proc Biol Sci,* 266**,** 843-52.

KILFOIL, P. J., TIPPARAJU, S. M., BARSKI, O. A. & BHATNAGAR, A. 2013. Regulation of ion channels by pyridine nucleotides. *Circ Res,* 112**,** 721-41.

KIM, K. 2016. Cargo trafficking from the trans-Golgi network towards the endosome. *Biol Cell,* 108**,** 205-18.

KIM, S. J., AO, Z., WARNOCK, G. & MCINTOSH, C. H. 2013. Incretin-stimulated interaction between beta-cell Kv1.5 and Kvbeta2 channel proteins involves acetylation/deacetylation by CBP/SirT1. *Biochem J,* 451**,** 227-34.

KISSELBACH, J., SCHWEIZER, P. A., GERSTBERGER, R., BECKER, R., KATUS, H. A. & THOMAS, D. 2012. Enhancement of K2P2.1 (TREK1) background currents expressed in Xenopus oocytes by voltage-gated K+ channel beta subunits. *Life Sci,* 91**,** 377-83.

KONI, P. A., KHANNA, R., CHANG, M. C., TANG, M. D., KACZMAREK, L. K., SCHLICHTER, L. C. & FLAVELLA, R. A. 2003. Compensatory anion currents in Kv1.3 channel-deficient thymocytes. *J Biol Chem,* 278**,** 39443-51.

KOPPRASCH, S., LEONHARDT, W., PIETZSCH, J. & KUHNE, H. 1998. Hypochlorite-modified low-density lipoprotein stimulates human polymorphonuclear leukocytes for enhanced production of reactive oxygen metabolites, enzyme secretion, and adhesion to endothelial cells. *Atherosclerosis,* 136**,** 315-24.

KOSOLAPOV, A. & DEUTSCH, C. 2003. Folding of the voltage-gated K+ channel T1 recognition domain. *J Biol Chem,* 278**,** 4305-13.

KREMER, W., WEYAND, M., WINKLMEIER, A., SCHREIER, C. & KALBITZER, H. R. 2013. 1.2 A X-ray structure of the renal potassium channel Kv1.3 T1 domain. *Protein J,* 32**,** 533-42.

KUROKAWA, J., MOTOIKE, H. K., RAO, J. & KASS, R. S. 2004. Regulatory actions of the A-kinase anchoring protein Yotiao on a heart potassium channel downstream of PKA phosphorylation. *Proc Natl Acad Sci U S A,* 101**,** 16374-8.

KURYSHEV, Y. A., WIBLE, B. A., GUDZ, T. I., RAMIREZ, A. N. & BROWN, A. M. 2001. KChAP/Kvbeta1.2 interactions and their effects on cardiac Kv channel expression. *Am J Physiol Cell Physiol,* 281**,** C290-9.

KWAK, Y. G., HU, N., WEI, J., GEORGE, A. L., JR., GROBASKI, T. D., TAMKUN, M. M. & MURRAY, K. T. 1999. Protein kinase A phosphorylation alters Kvbeta1.3 subunit-mediated inactivation of the Kv1.5 potassium channel. *J Biol Chem,* 274**,** 13928-32.

LAHAIE, N., KRALIKOVA, M., PREZEAU, L., BLAHOS, J. & BOUVIER, M. 2016. Post-endocytotic Deubiquitination and Degradation of the Metabotropic gamma-Aminobutyric Acid Receptor by the Ubiquitin-specific Protease 14. *J Biol Chem,* 291**,** 7156-70.

LARSSON, H. P., BAKER, O. S., DHILLON, D. S. & ISACOFF, E. Y. 1996. Transmembrane movement of the shaker K+ channel S4. *Neuron,* 16**,** 387-97.

LEBLANC, N. 2010. Kv3.4, a key signalling molecule controlling the cell cycle and proliferation of human arterial smooth muscle cells. *Cardiovasc Res,* 86**,** 351-2.

LEICHER, T., ROEPER, J., WEBER, K., WANG, X. & PONGS, O. 1996. Structural and functional characterization of human potassium channel subunit beta 1 (KCNA1B). *Neuropharmacology,* 35**,** 787-95.

LEITINGER, N., WATSON, A. D., FAULL, K. F., FOGELMAN, A. M. & BERLINER, J. A. 1997. Monocyte binding to endothelial cells induced by oxidized phospholipids present in minimally oxidized low density lipoprotein is inhibited by a platelet activating factor receptor antagonist. *Adv Exp Med Biol,* 433**,** 379-82.

LEONARD, R. J., GARCIA, M. L., SLAUGHTER, R. S. & REUBEN, J. P. 1992. Selective blockers of voltage-gated K+ channels depolarize human T lymphocytes: mechanism of the antiproliferative effect of charybdotoxin. *Proc Natl Acad Sci U S A,* 89**,** 10094-8.

LEVIN, G., CHIKVASHVILI, D., SINGER-LAHAT, D., PERETZ, T., THORNHILL, W. B. & LOTAN, I. 1996a. Phosphorylation of a K+ channel alpha subunit modulates the inactivation conferred by a beta subunit. Involvement of cytoskeleton. *J Biol Chem,* 271**,** 29321-8.

LEVIN, G., PERETZ, T., CHIKVASHVILLI, D., JING, J. & LOTAN, I. 1996b. Deletion of the N-terminus of a K+ channel brings about short-term modulation by cAMP and beta 1-adrenergic receptor activation. *J Mol Neurosci,* 7**,** 269-76.

LEVITE, M., CAHALON, L., PERETZ, A., HERSHKOVIZ, R., SOBKO, A., ARIEL, A., DESAI, R., ATTALI, B. & LIDER, O. 2000. Extracellular K(+) and opening of voltage-gated potassium channels activate T cell integrin function: physical and functional association between Kv1.3 channels and beta1 integrins. *J Exp Med,* 191**,** 1167-76.

LEVY, D. I., CEPAITIS, E., WANDERLING, S., TOTH, P. T., ARCHER, S. L. & GOLDSTEIN, S. A. 2010. The membrane protein MiRP3 regulates Kv4.2 channels in a KChIP-dependent manner. *J Physiol,* 588**,** 2657-68.

LEVY, D. I., WANDERLING, S., BIEMESDERFER, D. & GOLDSTEIN, S. A. 2008. MiRP3 acts as an accessory subunit with the BK potassium channel. *Am J Physiol Renal Physiol,* 295**,** F380-7.

LEVY, M., JING, J., CHIKVASHVILI, D., THORNHILL, W. B. & LOTAN, I. 1998. Activation of a metabotropic glutamate receptor and protein kinase C reduce the extent of inactivation of the K+ channel Kv1.1/Kvbeta1.1 via dephosphorylation of Kv1.1. *J Biol Chem,* 273**,** 6495-502.

LEWIS, A., MCCROSSAN, Z. A. & ABBOTT, G. W. 2004. MinK, MiRP1, and MiRP2 diversify Kv3.1 and Kv3.2 potassium channel gating. *J Biol Chem,* 279**,** 7884-92.

LI, D., TAKIMOTO, K. & LEVITAN, E. S. 2000. Surface expression of Kv1 channels is governed by a C-terminal motif. *J Biol Chem,* 275**,** 11597-602.

LI, Y., UM, S. Y. & MCDONALD, T. V. 2006. Voltage-gated potassium channels: regulation by accessory subunits. *Neuroscientist,* 12**,** 199-210.

LIAO, T., WANG, L., HALM, S. T., LU, L., FYFFE, R. E. & HALM, D. R. 2005. K+ channel KVLQT1 located in the basolateral membrane of distal colonic epithelium is not essential for activating Cl- secretion. *Am J Physiol Cell Physiol,* 289**,** C564-75.

LIN, Y. L., CHEN, C. Y., CHENG, C. P. & CHANG, L. S. 2004. Protein-protein interactions of KChIP proteins and Kv4.2. *Biochem Biophys Res Commun,* 321**,** 606-10.

LINDER, M. E. & DESCHENES, R. J. 2007. Palmitoylation: policing protein stability and traffic. *Nat Rev Mol Cell Biol,* 8**,** 74-84.

LIU, S. Q., JIN, H., ZACARIAS, A., SRIVASTAVA, S. & BHATNAGAR, A. 2001. Binding of pyridine coenzymes to the beta-subunit of the voltage sensitive potassium channels. *Chem Biol Interact,* 130-132**,** 955-62.

LIU, S. Q., YIN, J. & BHATNAGAR, A. 2003. Protein kinase C-dependent phosphorylation of the beta-subunit of the voltage-sensitive potassium channels (Kvbeta2). *Chem Biol Interact,* 143-144**,** 597-604.

LIU, W. & DEVAUX, J. J. 2014. Calmodulin orchestrates the heteromeric assembly and the trafficking of KCNQ2/3 (Kv7.2/3) channels in neurons. *Mol Cell Neurosci,* 58**,** 40-52.

LONG, S. B., CAMPBELL, E. B. & MACKINNON, R. 2005. Crystal structure of a mammalian voltage-dependent Shaker family K+ channel. *Science,* 309**,** 897-903.

LORINCZI, E., GOMEZ-POSADA, J. C., DE LA PENA, P., TOMCZAK, A. P., FERNANDEZ-TRILLO, J., LEIPSCHER, U., STUHMER, W., BARROS, F. & PARDO, L. A. 2015. Voltage-dependent gating of KCNH potassium channels lacking a covalent link between voltage-sensing and pore domains. *Nat Commun,* 6**,** 6672.

LUNDQUIST, A. L., MANDERFIELD, L. J., VANOYE, C. G., ROGERS, C. S., DONAHUE, B. S., CHANG, P. A., DRINKWATER, D. C., MURRAY, K. T. & GEORGE, A. L., JR. 2005. Expression of multiple KCNE genes in human heart may enable variable modulation of I(Ks). *J Mol Cell Cardiol,* 38**,** 277-87.

LUNDQUIST, A. L., TURNER, C. L., BALLESTER, L. Y. & GEORGE, A. L., JR. 2006. Expression and transcriptional control of human KCNE genes. *Genomics,* 87**,** 119-28.

MA, D. & JAN, L. Y. 2002. ER transport signals and trafficking of potassium channels and receptors. *Curr Opin Neurobiol,* 12**,** 287-92.

MA, D., ZERANGUE, N., RAAB-GRAHAM, K., FRIED, S. R., JAN, Y. N. & JAN, L. Y. 2002. Diverse trafficking patterns due to multiple traffic motifs in G protein-activated inwardly rectifying potassium channels from brain and heart. *Neuron,* 33**,** 715-29.

MA, K. J., LI, N., TENG, S. Y., ZHANG, Y. H., SUN, Q., GU, D. F. & PU, J. L. 2007. Modulation of KCNQ1 current by atrial fibrillation-associated KCNE4 (145E/D) gene polymorphism. *Chin Med J (Engl),* 120**,** 150-4.

MACKINNON, R. 2003. Potassium channels. *FEBS Lett,* 555**,** 62-5.

MACVINISH, L. J., GUO, Y., DIXON, A. K., MURRELL-LAGNADO, R. D. & CUTHBERT, A. W. 2001. Xe991 reveals differences in K(+) channels regulating chloride secretion in murine airway and colonic epithelium. *Mol Pharmacol,* 60**,** 753-60.

MALABY, H. L. & KOBERTZ, W. R. 2013. Molecular determinants of co- and post-translational N-glycosylation of type I transmembrane peptides. *Biochem J,* 453**,** 427-34.

MANCIAS, J. D. & GOLDBERG, J. 2008. Structural basis of cargo membrane protein discrimination by the human COPII coat machinery. *EMBO J,* 27**,** 2918-28.

MANDERFIELD, L. J., DANIELS, M. A., VANOYE, C. G. & GEORGE, A. L., JR. 2009. KCNE4 domains required for inhibition of KCNQ1. *J Physiol,* 587**,** 303-14.

MANDERFIELD, L. J. & GEORGE, A. L., JR. 2008. KCNE4 can co-associate with the I(Ks) (KCNQ1-KCNE1) channel complex. *FEBS J,* 275**,** 1336-49.

MANGANAS, L. N., WANG, Q., SCANNEVIN, R. H., ANTONUCCI, D. E., RHODES, K. J. & TRIMMER, J. S. 2001. Identification of a trafficking determinant localized to the Kv1 potassium channel pore. *Proc Natl Acad Sci U S A,* 98**,** 14055-9.

MARKS, D. R. & FADOOL, D. A. 2007. Post-synaptic density perturbs insulin-induced Kv1.3 channel modulation via a clustering mechanism involving the SH3 domain. *J Neurochem,* 103**,** 1608-27.

MARTENS, J. R., KWAK, Y. G. & TAMKUN, M. M. 1999. Modulation of Kv channel alpha/beta subunit interactions. *Trends Cardiovasc Med,* 9**,** 253-8.

MARTENS, J. R., O'CONNELL, K. & TAMKUN, M. 2004. Targeting of ion channels to membrane microdomains: localization of KV channels to lipid rafts. *Trends Pharmacol Sci,* 25**,** 16-21.

MARTINEZ-MARMOL, R., COMES, N., STYRCZEWSKA, K., PEREZ-VERDAGUER, M., VICENTE, R., PUJADAS, L., SORIANO, E., SORKIN, A. & FELIPE, A. 2016. Unconventional EGF-induced ERK1/2-mediated Kv1.3 endocytosis. *Cell Mol Life Sci,* 73**,** 1515-28.

MARTINEZ-MARMOL, R., PEREZ-VERDAGUER, M., ROIG, S. R., VALLEJO-GRACIA, A., GOTSI, P., SERRANO-ALBARRAS, A., BAHAMONDE, M. I., FERRER-MONTIEL, A., FERNANDEZ-BALLESTER, G., COMES, N. & FELIPE, A. 2013. A non-canonical di-acidic signal at the C-terminus of Kv1.3 determines anterograde trafficking and surface expression. *J Cell Sci,* 126**,** 5681-91.

MATHIE, A., REES, K. A., EL HACHMANE, M. F. & VEALE, E. L. 2010. Trafficking of neuronal two pore domain potassium channels. *Curr Neuropharmacol,* 8**,** 276-86.

MATZNER, N., ZEMTSOVA, I. M., NGUYEN, T. X., DUSZENKO, M., SHUMILINA, E. & LANG, F. 2008. Ion channels modulating mouse dendritic cell functions. *J Immunol,* 181**,** 6803-9.

MCCORMACK, K., CONNOR, J. X., ZHOU, L., HO, L. L., GANETZKY, B., CHIU, S. Y. & MESSING, A. 2002. Genetic analysis of the mammalian K+ channel beta subunit Kvbeta 2 (Kcnab2). *J Biol Chem,* 277**,** 13219-28.

MCCORMACK, T., MCCORMACK, K., NADAL, M. S., VIEIRA, E., OZAITA, A. & RUDY, B. 1999. The effects of Shaker beta-subunits on the human lymphocyte K+ channel Kv1.3. *J Biol Chem,* 274**,** 20123-6.

MCCROSSAN, Z. A., LEWIS, A., PANAGHIE, G., JORDAN, P. N., CHRISTINI, D. J., LERNER, D. J. & ABBOTT, G. W. 2003. MinK-related peptide 2 modulates Kv2.1 and Kv3.1 potassium channels in mammalian brain. *J Neurosci,* 23**,** 8077-91.

MCINTOSH, P., SOUTHAN, A. P., AKHTAR, S., SIDERA, C., USHKARYOV, Y., DOLLY, J. O. & ROBERTSON, B. 1997. Modification of rat brain Kv1.4 channel gating by association with accessory Kvbeta1.1 and beta2.1 subunits. *Pflugers Arch,* 435**,** 43-54.

MEDINA, F. A., COHEN, A. W., DE ALMEIDA, C. J., NAGAJYOTHI, F., BRAUNSTEIN, V. L., TEIXEIRA, M. M., TANOWITZ, H. B. & LISANTI, M. P. 2007. Immune dysfunction in caveolin-1 null mice following infection with Trypanosoma cruzi (Tulahuen strain). *Microbes Infect,* 9**,** 325-33.

MELKONIAN, K. A., OSTERMEYER, A. G., CHEN, J. Z., ROTH, M. G. & BROWN, D. A. 1999. Role of lipid modifications in targeting proteins to detergent-resistant membrane rafts. Many raft proteins are acylated, while few are prenylated. *J Biol Chem,* 274**,** 3910-7.

MELMAN, Y. F., DOMENECH, A., DE LA LUNA, S. & MCDONALD, T. V. 2001. Structural determinants of KvLQT1 control by the KCNE family of proteins. *J Biol Chem,* 276**,** 6439-44.

MELMAN, Y. F., KRUMERMAN, A. & MCDONALD, T. V. 2002. A single transmembrane site in the KCNE-encoded proteins controls the specificity of KvLQT1 channel gating. *J Biol Chem,* 277**,** 25187-94.

MELMAN, Y. F., UM, S. Y., KRUMERMAN, A., KAGAN, A. & MCDONALD, T. V. 2004. KCNE1 binds to the KCNQ1 pore to regulate potassium channel activity. *Neuron,* 42**,** 927-37.

MIGUEL-VELADO, E., PEREZ-CARRETERO, F. D., COLINAS, O., CIDAD, P., HERAS, M., LOPEZ-LOPEZ, J. R. & PEREZ-GARCIA, M. T. 2010. Cell cycle-dependent expression of Kv3.4 channels modulates proliferation of human uterine artery smooth muscle cells. *Cardiovasc Res,* 86**,** 383-91.

MIHIC, A., CHAUHAN, V. S., GAO, X., OUDIT, G. Y. & TSUSHIMA, R. G. 2011. Trafficking defect and proteasomal degradation contribute to the phenotype of a novel KCNH2 long QT syndrome mutation. *PLoS One,* 6**,** e18273.

MIYASHITA, Y. & OZAWA, M. 2007. Increased internalization of p120-uncoupled E-cadherin and a requirement for a dileucine motif in the cytoplasmic domain for endocytosis of the protein. *J Biol Chem,* 282**,** 11540-8.

MORALES, M. J., WEE, J. O., WANG, S., STRAUSS, H. C. & RASMUSSON, R. L. 1996. The N-terminal domain of a K+ channel beta subunit increases the rate of C-type inactivation from the cytoplasmic side of the channel. *Proc Natl Acad Sci U S A,* 93**,** 15119-23.

MORIN, T. J. & KOBERTZ, W. R. 2007. A derivatized scorpion toxin reveals the functional output of heteromeric KCNQ1-KCNE K+ channel complexes. *ACS Chem Biol,* 2**,** 469-73.

MORIN, T. J. & KOBERTZ, W. R. 2008. Counting membrane-embedded KCNE beta-subunits in functioning K+ channel complexes. *Proc Natl Acad Sci U S A,* 105**,** 1478-82.

MOSSESSOVA, E., BICKFORD, L. C. & GOLDBERG, J. 2003. SNARE selectivity of the COPII coat. *Cell,* 114**,** 483-95.

NADOLSKI, M. J. & LINDER, M. E. 2007. Protein lipidation. *FEBS J,* 274**,** 5202-10.

NAGAYA, N. & PAPAZIAN, D. M. 1997. Potassium channel alpha and beta subunits assemble in the endoplasmic reticulum. *J Biol Chem,* 272**,** 3022-7.

NAKAHIRA, K., MATOS, M. F. & TRIMMER, J. S. 1998. Differential interaction of voltage-gated K+ channel beta-subunits with cytoskeleton is mediated by unique amino terminal domains. *J Mol Neurosci,* 11**,** 199-208.

NAKAJO, K., ULBRICH, M. H., KUBO, Y. & ISACOFF, E. Y. 2010. Stoichiometry of the KCNQ1 - KCNE1 ion channel complex. *Proc Natl Acad Sci U S A,* 107**,** 18862-7.

NICKEL, W. & RABOUILLE, C. 2009. Mechanisms of regulated unconventional protein secretion. *Nat Rev Mol Cell Biol,* 10**,** 148-55.

NICOLAOU, S. A., NEUMEIER, L., TAKIMOTO, K., LEE, S. M., DUNCAN, H. J., KANT, S. K., MONGEY, A. B., FILIPOVICH, A. H. & CONFORTI, L. 2010. Differential calcium signaling and Kv1.3 trafficking to the immunological synapse in systemic lupus erythematosus. *Cell Calcium,* 47**,** 19-28.

NICOLAOU, S. A., SZIGLIGETI, P., NEUMEIER, L., LEE, S. M., DUNCAN, H. J., KANT, S. K., MONGEY, A. B., FILIPOVICH, A. H. & CONFORTI, L. 2007. Altered dynamics of Kv1.3 channel compartmentalization in the immunological synapse in systemic lupus erythematosus. *J Immunol,* 179**,** 346-56.

NICOLAS, M., DEMEMES, D., MARTIN, A., KUPERSHMIDT, S. & BARHANIN, J. 2001. KCNQ1/KCNE1 potassium channels in mammalian vestibular dark cells. *Hear Res,* 153**,** 132-45.

O'CONNELL, K. M. & TAMKUN, M. M. 2005. Targeting of voltage-gated potassium channel isoforms to distinct cell surface microdomains. *J Cell Sci,* 118**,** 2155-66.

O'NEILL, A. K., GALLEGOS, L. L., JUSTILIEN, V., GARCIA, E. L., LEITGES, M., FIELDS, A. P., HALL, R. A. & NEWTON, A. C. 2011. Protein kinase Calpha promotes cell migration through a PDZ-dependent interaction with its novel substrate discs large homolog 1 (DLG1). *J Biol Chem,* 286**,** 43559-68.

OGAWA, Y., HORRESH, I., TRIMMER, J. S., BREDT, D. S., PELES, E. & RASBAND, M. N. 2008. Postsynaptic density-93 clusters Kv1 channels at axon initial segments independently of Caspr2. *J Neurosci,* 28**,** 5731-9.

OHNO, S., ZANKOV, D. P., DING, W. G., ITOH, H., MAKIYAMA, T., DOI, T., SHIZUTA, S., HATTORI, T., MIYAMOTO, A., NAIKI, N., HANCOX, J. C., MATSUURA, H. & HORIE, M.

2011. KCNE5 (KCNE1L) variants are novel modulators of Brugada syndrome and idiopathic ventricular fibrillation. *Circ Arrhythm Electrophysiol,* 4**,** 352-61.

OLIVA, C., ESCOBEDO, P., ASTORGA, C., MOLINA, C. & SIERRALTA, J. 2012. Role of the MAGUK protein family in synapse formation and function. *Dev Neurobiol,* 72**,** 57-72.

OLIVER, D., LIEN, C. C., SOOM, M., BAUKROWITZ, T., JONAS, P. & FAKLER, B. 2004. Functional conversion between A-type and delayed rectifier K+ channels by membrane lipids. *Science,* 304**,** 265-70.

PAN, Y., LAIRD, J. G., YAMAGUCHI, D. M. & BAKER, S. A. 2015. An N-Terminal ER Export Signal Facilitates the Plasma Membrane Targeting of HCN1 Channels in Photoreceptors. *Invest Ophthalmol Vis Sci,* 56**,** 3514-21.

PAN, Y., LEVIN, E. J., QUICK, M. & ZHOU, M. 2012. Potentiation of the Kv1 family K(+) channel by cortisone analogues. *ACS Chem Biol,* 7**,** 1641-6.

PAN, Y., WENG, J., CAO, Y., BHOSLE, R. C. & ZHOU, M. 2008a. Functional coupling between the Kv1.1 channel and aldoketoreductase Kvbeta1. *J Biol Chem,* 283**,** 8634-42.

PAN, Y., WENG, J., KABALEESWARAN, V., LI, H., CAO, Y., BHOSLE, R. C. & ZHOU, M. 2008b. Cortisone dissociates the Shaker family K+ channels from their beta subunits. *Nat Chem Biol,* 4**,** 708-14.

PANAGHIE, G., TAI, K. K. & ABBOTT, G. W. 2006. Interaction of KCNE subunits with the KCNQ1 K+ channel pore. *J Physiol,* 570**,** 455-67.

PANYI, G. 2005. Biophysical and pharmacological aspects of K+ channels in T lymphocytes. *Eur Biophys J,* 34**,** 515-29.

PANYI, G., VAMOSI, G., BACSO, Z., BAGDANY, M., BODNAR, A., VARGA, Z., GASPAR, R., MATYUS, L. & DAMJANOVICH, S. 2004. Kv1.3 potassium channels are localized in the immunological synapse formed between cytotoxic and target cells. *Proc Natl Acad Sci U S A,* 101**,** 1285-90.

PARCEJ, D. N., SCOTT, V. E. & DOLLY, J. O. 1992. Oligomeric properties of alpha-dendrotoxin-sensitive potassium ion channels purified from bovine brain. *Biochemistry,* 31**,** 11084-8.

PATEL, H. H. & INSEL, P. A. 2009. Lipid rafts and caveolae and their role in compartmentation of redox signaling. *Antioxid Redox Signal,* 11**,** 1357-72.

PATEL, H. H., MURRAY, F. & INSEL, P. A. 2008. Caveolae as organizers of pharmacologically relevant signal transduction molecules. *Annu Rev Pharmacol Toxicol,* 48**,** 359-91.

PAULICK, M. G. & BERTOZZI, C. R. 2008. The glycosylphosphatidylinositol anchor: a complex membrane-anchoring structure for proteins. *Biochemistry,* 47**,** 6991-7000.

PAYET, M. D. & DUPUIS, G. 1992. Dual regulation of the n type K+ channel in Jurkat T lymphocytes by protein kinases A and C. *J Biol Chem,* 267**,** 18270-3.

PENNING, T. M. 2015. The aldo-keto reductases (AKRs): Overview. *Chem Biol Interact,* 234**,** 236-46.

PEREZ-GARCIA, M. T., LOPEZ-LOPEZ, J. R. & GONZALEZ, C. 1999. Kvbeta1.2 subunit coexpression in HEK293 cells confers O2 sensitivity to kv4.2 but not to Shaker channels. *J Gen Physiol,* 113**,** 897-907.

PEREZ-VERDAGUER, M., CAPERA, J., MARTINEZ-MARMOL, R., CAMPS, M., COMES, N., TAMKUN, M. M. & FELIPE, A. 2016a. Caveolin interaction governs Kv1.3 lipid raft targeting. *Sci Rep,* 6**,** 22453.

PEREZ-VERDAGUER, M., CAPERA, J., SERRANO-NOVILLO, C., ESTADELLA, I., SASTRE, D. & FELIPE, A. 2016b. The voltage-gated potassium channel Kv1.3 is a promising multitherapeutic target against human pathologies. *Expert Opin Ther Targets,* 20**,** 577-91.

PEREZ, J. M., CHIRIELEISON, S. M. & ABBOTT, D. W. 2015. An IkappaB Kinase-Regulated Feedforward Circuit Prolongs Inflammation. *Cell Rep,* 12**,** 537-44.

PERI, R., WIBLE, B. A. & BROWN, A. M. 2001. Mutations in the Kv beta 2 binding site for NADPH and their effects on Kv1.4. *J Biol Chem,* 276**,** 738-41.

PEROZ, D., DAHIMENE, S., BARO, I., LOUSSOUARN, G. & MEROT, J. 2009. LQT1-associated mutations increase KCNQ1 proteasomal degradation independently of Derlin-1. *J Biol Chem,* 284**,** 5250-6.

PICCINI, M., VITELLI, F., SERI, M., GALIETTA, L. J., MORAN, O., BULFONE, A., BANFI, S., POBER, B. & RENIERI, A. 1999. KCNE1-like gene is deleted in AMME contiguous gene syndrome: identification and characterization of the human and mouse homologs. *Genomics,* 60**,** 251-7.

PONGS, O., LEICHER, T., BERGER, M., ROEPER, J., BAHRING, R., WRAY, D., GIESE, K. P., SILVA, A. J. & STORM, J. F. 1999. Functional and molecular aspects of voltage-gated K+ channel beta subunits. *Ann N Y Acad Sci,* 868**,** 344-55.

PONGS, O. & SCHWARZ, J. R. 2010. Ancillary subunits associated with voltage-dependent K+ channels. *Physiol Rev,* 90**,** 755-96.

PUSCH, M. 1998. Increase of the single-channel conductance of KvLQT1 potassium channels induced by the association with minK. *Pflugers Arch,* 437**,** 172-4.

RANGARAJU, S., CHI, V., PENNINGTON, M. W. & CHANDY, K. G. 2009. Kv1.3 potassium channels as a therapeutic target in multiple sclerosis. *Expert Opin Ther Targets,* 13**,** 909-24.

RENNER, U., ZEUG, A., WOEHLER, A., NIEBERT, M., DITYATEV, A., DITYATEVA, G., GORINSKI, N., GUSEVA, D., ABDEL-GALIL, D., FROHLICH, M., DORING, F., WISCHMEYER, E., RICHTER, D. W., NEHER, E. & PONIMASKIN, E. G. 2012. Heterodimerization of serotonin receptors 5-HT1A and 5-HT7 differentially regulates receptor signalling and trafficking. *J Cell Sci,* 125**,** 2486-99.

RETTIG, J., HEINEMANN, S. H., WUNDER, F., LORRA, C., PARCEJ, D. N., DOLLY, J. O. & PONGS, O. 1994. Inactivation properties of voltage-gated K+ channels altered by presence of beta-subunit. *Nature,* 369**,** 289-94.

RHODES, K. J., MONAGHAN, M. M., BARREZUETA, N. X., NAWOSCHIK, S., BEKELE-ARCURI, Z., MATOS, M. F., NAKAHIRA, K., SCHECHTER, L. E. & TRIMMER, J. S. 1996. Voltage-gated K+ channel beta subunits: expression and distribution of Kv beta 1 and Kv beta 2 in adult rat brain. *J Neurosci,* 16**,** 4846-60.

RIOS, F. J., FERRACINI, M., PECENIN, M., KOGA, M. M., WANG, Y., KETELHUTH, D. F. & JANCAR, S. 2013. Uptake of oxLDL and IL-10 production by macrophages requires PAFR and CD36 recruitment into the same lipid rafts. *PLoS One,* 8**,** e76893.

RIOS, F. J., KOGA, M. M., FERRACINI, M. & JANCAR, S. 2012. Co-stimulation of PAFR and CD36 is required for oxLDL-induced human macrophages activation. *PLoS One,* 7**,** e36632.

RIVERA, J. F., AHMAD, S., QUICK, M. W., LIMAN, E. R. & ARNOLD, D. B. 2003. An evolutionarily conserved dileucine motif in Shal K+ channels mediates dendritic targeting. *Nat Neurosci,* 6**,** 243-50.

ROCKS, O., GERAUER, M., VARTAK, N., KOCH, S., HUANG, Z. P., PECHLIVANIS, M., KUHLMANN, J., BRUNSVELD, L., CHANDRA, A., ELLINGER, B., WALDMANN, H. & BASTIAENS, P. I. 2010. The palmitoylation machinery is a spatially organizing system for peripheral membrane proteins. *Cell,* 141**,** 458-71.

ROEPER, J., SEWING, S., ZHANG, Y., SOMMER, T., WANNER, S. G. & PONGS, O. 1998. NIP domain prevents N-type inactivation in voltage-gated potassium channels. *Nature,* 391**,** 390-3.

ROEPKE, T. K., KANDA, V. A., PURTELL, K., KING, E. C., LERNER, D. J. & ABBOTT, G. W. 2011. KCNE2 forms potassium channels with KCNA3 and KCNQ1 in the choroid plexus epithelium. *FASEB J,* 25**,** 4264-73.

ROEPKE, T. K., KONTOGEORGIS, A., OVANEZ, C., XU, X., YOUNG, J. B., PURTELL, K., GOLDSTEIN, P. A., CHRISTINI, D. J., PETERS, N. S., AKAR, F. G., GUTSTEIN, D. E., LERNER, D. J. & ABBOTT, G. W. 2008. Targeted deletion of kcne2 impairs ventricular repolarization via disruption of I(K,slow1) and I(to,f). *FASEB J,* 22**,** 3648-60.

ROEPKE, T. K., PURTELL, K., KING, E. C., LA PERLE, K. M., LERNER, D. J. & ABBOTT, G. W. 2010. Targeted deletion of Kcne2 causes gastritis cystica profunda and gastric neoplasia. *PLoS One,* 5**,** e11451.

ROURA-FERRER, M., SOLE, L., OLIVERAS, A., DAHAN, R., BIELANSKA, J., VILLARROEL, A., COMES, N. & FELIPE, A. 2010. Impact of KCNE subunits on KCNQ1 (Kv7.1) channel membrane surface targeting. *J Cell Physiol,* 225**,** 692-700.

SANGUINETTI, M. C., CURRAN, M. E., ZOU, A., SHEN, J., SPECTOR, P. S., ATKINSON, D. L. & KEATING, M. T. 1996. Coassembly of K(V)LQT1 and minK (IsK) proteins to form cardiac I(Ks) potassium channel. *Nature,* 384**,** 80-3.

SARASTE, J., DALE, H. A., BAZZOCCO, S. & MARIE, M. 2009. Emerging new roles of the pre-Golgi intermediate compartment in biosynthetic-secretory trafficking. *FEBS Lett,* 583**,** 3804-10.

SCOTT, V. E., PARCEJ, D. N., KEEN, J. N., FINDLAY, J. B. & DOLLY, J. O. 1990. Alpha-dendrotoxin acceptor from bovine brain is a K+ channel protein. Evidence from the N-terminal sequence of its larger subunit. *J Biol Chem,* 265**,** 20094-7.

SCOTT, V. E., RETTIG, J., PARCEJ, D. N., KEEN, J. N., FINDLAY, J. B., PONGS, O. & DOLLY, J. O. 1994. Primary structure of a beta subunit of alpha-dendrotoxin-sensitive K+ channels from bovine brain. *Proc Natl Acad Sci U S A,* 91**,** 1637-41.

SCHROEDER, B. C., WALDEGGER, S., FEHR, S., BLEICH, M., WARTH, R., GREGER, R. & JENTSCH, T. J. 2000. A constitutively open potassium channel formed by KCNQ1 and KCNE3. *Nature,* 403**,** 196-9.

SCHROEDER, R. J., AHMED, S. N., ZHU, Y., LONDON, E. & BROWN, D. A. 1998. Cholesterol and sphingolipid enhance the Triton X-100 insolubility of glycosylphosphatidylinositol-anchored proteins by promoting the formation of detergent-insoluble ordered membrane domains. *J Biol Chem,* 273**,** 1150-7.

SCHULTZ, D., LITT, M., SMITH, L., THAYER, M. & MCCORMACK, K. 1996. Localization of two potassium channel beta subunit genes, KCNA1B and KCNA2B. *Genomics,* 31**,** 389-91.

SCHULZE-BAHR, E., WANG, Q., WEDEKIND, H., HAVERKAMP, W., CHEN, Q., SUN, Y., RUBIE, C., HORDT, M., TOWBIN, J. A., BORGGREFE, M., ASSMANN, G., QU, X., SOMBERG, J. C., BREITHARDT, G., OBERTI, C. & FUNKE, H. 1997. KCNE1 mutations cause jervell and Lange-Nielsen syndrome. *Nat Genet,* 17**,** 267-8.

SEIKEL, E. & TRIMMER, J. S. 2009. Convergent modulation of Kv4.2 channel alpha subunits by structurally distinct DPPX and KChIP auxiliary subunits. *Biochemistry,* 48**,** 5721-30.

SESTI, F., ABBOTT, G. W., WEI, J., MURRAY, K. T., SAKSENA, S., SCHWARTZ, P. J., PRIORI, S. G., RODEN, D. M., GEORGE, A. L., JR. & GOLDSTEIN, S. A. 2000. A common polymorphism associated with antibiotic-induced cardiac arrhythmia. *Proc Natl Acad Sci U S A,* 97**,** 10613-8.

SEVIER, C. S., WEISZ, O. A., DAVIS, M. & MACHAMER, C. E. 2000. Efficient export of the vesicular stomatitis virus G protein from the endoplasmic reticulum requires a signal in the cytoplasmic tail that includes both tyrosine-based and di-acidic motifs. *Mol Biol Cell,* 11**,** 13-22.

SEWING, S., ROEPER, J. & PONGS, O. 1996. Kv beta 1 subunit binding specific for shaker-related potassium channel alpha subunits. *Neuron,* 16**,** 455-63.

SHAMOTIENKO, O. G., PARCEJ, D. N. & DOLLY, J. O. 1997. Subunit combinations defined for K+ channel Kv1 subtypes in synaptic membranes from bovine brain. *Biochemistry,* 36**,** 8195-201.

SHAW, A. S. & FILBERT, E. L. 2009. Scaffold proteins and immune-cell signalling. *Nat Rev Immunol,* 9**,** 47-56.

SHI, G., NAKAHIRA, K., HAMMOND, S., RHODES, K. J., SCHECHTER, L. E. & TRIMMER, J. S. 1996. Beta subunits promote K+ channel surface expression through effects early in biosynthesis. *Neuron,* 16**,** 843-52.

SHIBATA, R., MISONOU, H., CAMPOMANES, C. R., ANDERSON, A. E., SCHRADER, L. A., DOLIVEIRA, L. C., CARROLL, K. I., SWEATT, J. D., RHODES, K. J. & TRIMMER, J. S. 2003. A fundamental role for KChIPs in determining the molecular properties and trafficking of Kv4.2 potassium channels. *J Biol Chem,* 278**,** 36445-54.

SHVETS, E., LUDWIG, A. & NICHOLS, B. J. 2014. News from the caves: update on the structure and function of caveolae. *Curr Opin Cell Biol,* 29**,** 99-106.

SMOTRYS, J. E. & LINDER, M. E. 2004. Palmitoylation of intracellular signaling proteins: regulation and function. *Annu Rev Biochem,* 73**,** 559-87.

SOKOLOVA, O., ACCARDI, A., GUTIERREZ, D., LAU, A., RIGNEY, M. & GRIGORIEFF, N. 2003. Conformational changes in the C terminus of Shaker K+ channel bound to the rat Kvbeta2-subunit. *Proc Natl Acad Sci U S A,* 100**,** 12607-12.

SOLE, L. & FELIPE, A. 2010. Does a physiological role for KCNE subunits exist in the immune system? *Commun Integr Biol,* 3**,** 166-8.

SOLE, L., ROIG, S. R., VALLEJO-GRACIA, A., SERRANO-ALBARRAS, A., MARTINEZ-MARMOL, R., TAMKUN, M. M. & FELIPE, A. 2016. The C-terminal domain of Kv1.3 regulates functional interactions with the KCNE4 subunit. *J Cell Sci,* 129**,** 4265-4277.

SOLE, L., ROURA-FERRER, M., PEREZ-VERDAGUER, M., OLIVERAS, A., CALVO, M., FERNANDEZ-FERNANDEZ, J. M. & FELIPE, A. 2009. KCNE4 suppresses Kv1.3 currents by modulating trafficking, surface expression and channel gating. *J Cell Sci,* 122**,** 3738-48.

SOLE, L., VALLEJO-GRACIA, A., ROIG, S. R., SERRANO-ALBARRAS, A., MARRUECOS, L., MANILS, J., GOMEZ, D., SOLER, C. & FELIPE, A. 2013. KCNE gene expression is dependent on the proliferation and mode of activation of leukocytes. *Channels (Austin),* 7**,** 85-96.

SONNINO, S. & PRINETTI, A. 2013. Membrane domains and the "lipid raft" concept. *Curr Med Chem,* 20**,** 4-21.

SPLAWSKI, I., SHEN, J., TIMOTHY, K. W., LEHMANN, M. H., PRIORI, S., ROBINSON, J. L., MOSS, A. J., SCHWARTZ, P. J., TOWBIN, J. A., VINCENT, G. M. & KEATING, M. T. 2000. Spectrum of mutations in long-QT syndrome genes. KVLQT1, HERG, SCN5A, KCNE1, and KCNE2. *Circulation,* 102**,** 1178-85.

STOCKKLAUSNER, C., LUDWIG, J., RUPPERSBERG, J. P. & KLOCKER, N. 2001. A sequence motif responsible for ER export and surface expression of Kir2.0 inward rectifier K(+) channels. *FEBS Lett,* 493**,** 129-33.

STROP, P., BANKOVICH, A. J., HANSEN, K. C., GARCIA, K. C. & BRUNGER, A. T. 2004. Structure of a human A-type potassium channel interacting protein DPPX, a member of the dipeptidyl aminopeptidase family. *J Mol Biol,* 343**,** 1055-65.

STRUTZ-SEEBOHM, N., SEEBOHM, G., FEDORENKO, O., BALTAEV, R., ENGEL, J., KNIRSCH, M. & LANG, F. 2006. Functional coassembly of KCNQ4 with KCNE-beta- subunits in Xenopus oocytes. *Cell Physiol Biochem,* 18**,** 57-66.

SUZUKI, T., DU, F., TIAN, Q. B., ZHANG, J. & ENDO, S. 2008. Ca2+/calmodulin-dependent protein kinase IIalpha clusters are associated with stable lipid rafts and their formation traps PSD-95. *J Neurochem,* 104**,** 596-610.

SWANSON, R., MARSHALL, J., SMITH, J. S., WILLIAMS, J. B., BOYLE, M. B., FOLANDER, K., LUNEAU, C. J., ANTANAVAGE, J., OLIVA, C., BUHROW, S. A. & ET AL. 1990. Cloning and expression of cDNA and genomic clones encoding three delayed rectifier potassium channels in rat brain. *Neuron,* 4**,** 929-39.

SZABO, I., BOCK, J., GRASSME, H., SODDEMANN, M., WILKER, B., LANG, F., ZORATTI, M. & GULBINS, E. 2008. Mitochondrial potassium channel Kv1.3 mediates Bax-induced apoptosis in lymphocytes. *Proc Natl Acad Sci U S A,* 105**,** 14861-6.

SZABO, I., BOCK, J., JEKLE, A., SODDEMANN, M., ADAMS, C., LANG, F., ZORATTI, M. & GULBINS, E. 2005. A novel potassium channel in lymphocyte mitochondria. *J Biol Chem,* 280**,** 12790-8.

SZABO, I., GULBINS, E., APFEL, H., ZHANG, X., BARTH, P., BUSCH, A. E., SCHLOTTMANN, K., PONGS, O. & LANG, F. 1996. Tyrosine phosphorylation-dependent suppression of a voltage-gated K+ channel in T lymphocytes upon Fas stimulation. *J Biol Chem,* 271**,** 20465-9.

SZABO, I., ZORATTI, M. & GULBINS, E. 2010. Contribution of voltage-gated potassium channels to the regulation of apoptosis. *FEBS Lett,* 584**,** 2049-56.

SZILAGYI, O., BORATKO, A., PANYI, G. & HAJDU, P. 2013. The role of PSD-95 in the rearrangement of Kv1.3 channels to the immunological synapse. *Pflugers Arch,* 465**,** 1341-53.

SZUL, T. & SZTUL, E. 2011. COPII and COPI traffic at the ER-Golgi interface. *Physiology (Bethesda),* 26**,** 348-64.

TAI, K. K. & GOLDSTEIN, S. A. 1998. The conduction pore of a cardiac potassium channel. *Nature,* 391**,** 605-8.

TAKUMI, T., OHKUBO, H. & NAKANISHI, S. 1988. Cloning of a membrane protein that induces a slow voltage-gated potassium current. *Science,* 242**,** 1042-5.

TAMKUN, M. M., O'CONNELL K, M. & ROLIG, A. S. 2007. A cytoskeletal-based perimeter fence selectively corrals a sub-population of cell surface Kv2.1 channels. *J Cell Sci,* 120**,** 2413-23.

TAPPER, A. R. & GEORGE, A. L., JR. 2000. MinK subdomains that mediate modulation of and association with KvLQT1. *J Gen Physiol,* 116**,** 379-90.

TEMPLE, J., FRIAS, P., ROTTMAN, J., YANG, T., WU, Y., VERHEIJCK, E. E., ZHANG, W., SIPRACHANH, C., KANKI, H., ATKINSON, J. B., KING, P., ANDERSON, M. E., KUPERSHMIDT, S. & RODEN, D. M. 2005. Atrial fibrillation in KCNE1-null mice. *Circ Res,* 97**,** 62-9.

TENG, S., MA, L., ZHEN, Y., LIN, C., BAHRING, R., VARDANYAN, V., PONGS, O. & HUI, R. 2003. Novel gene hKCNE4 slows the activation of the KCNQ1 channel. *Biochem Biophys Res Commun,* 303**,** 808-13.

TINEL, N., DIOCHOT, S., BORSOTTO, M., LAZDUNSKI, M. & BARHANIN, J. 2000. KCNE2 confers background current characteristics to the cardiac KCNQ1 potassium channel. *EMBO J,* 19**,** 6326-30.

TIPPARAJU, S. M., BARSKI, O. A., SRIVASTAVA, S. & BHATNAGAR, A. 2008. Catalytic mechanism and substrate specificity of the beta-subunit of the voltage-gated potassium channel. *Biochemistry,* 47**,** 8840-54.

TIPPARAJU, S. M., LI, X. P., KILFOIL, P. J., XUE, B., UVERSKY, V. N., BHATNAGAR, A. & BARSKI, O. A. 2012. Interactions between the C-terminus of Kv1.5 and Kvbeta regulate pyridine nucleotide-dependent changes in channel gating. *Pflugers Arch,* 463**,** 799-818.

TIPPARAJU, S. M., LIU, S. Q., BARSKI, O. A. & BHATNAGAR, A. 2007. NADPH binding to beta-subunit regulates inactivation of voltage-gated K(+) channels. *Biochem Biophys Res Commun,* 359**,** 269-76.

TIPPARAJU, S. M., SAXENA, N., LIU, S. Q., KUMAR, R. & BHATNAGAR, A. 2005. Differential regulation of voltage-gated K+ channels by oxidized and reduced pyridine nucleotide coenzymes. *Am J Physiol Cell Physiol,* 288**,** C366-76.

TOLDI, G., MUNOZ, L., HERRMANN, M., SCHETT, G. & BALOG, A. 2016. The effects of Kv1.3 and IKCa1 channel inhibition on cytokine production and calcium influx of T lymphocytes in rheumatoid arthritis and ankylosing spondylitis. *Immunol Res,* 64**,** 627-31.

TOLDI, G., VASARHELYI, B., KAPOSI, A., MESZAROS, G., PANCZEL, P., HOSSZUFALUSI, N., TULASSAY, T. & TRESZL, A. 2010. Lymphocyte activation in type 1 diabetes mellitus: the increased significance of Kv1.3 potassium channels. *Immunol Lett,* 133**,** 35-41.

TOMASSIAN, T., HUMPHRIES, L. A., LIU, S. D., SILVA, O., BROOKS, D. G. & MICELI, M. C. 2011. Caveolin-1 orchestrates TCR synaptic polarity, signal specificity, and function in CD8 T cells. *J Immunol,* 187**,** 2993-3002.

TORRES, Y. P., MORERA, F. J., CARVACHO, I. & LATORRE, R. 2007. A marriage of convenience: beta-subunits and voltage-dependent K+ channels. *J Biol Chem,* 282**,** 24485-9.

TOTH, A., SZILAGYI, O., KRASZNAI, Z., PANYI, G. & HAJDU, P. 2009. Functional consequences of Kv1.3 ion channel rearrangement into the immunological synapse. *Immunol Lett,* 125**,** 15-21.

TRISTANI-FIROUZI, M. & SANGUINETTI, M. C. 1998. Voltage-dependent inactivation of the human K+ channel KvLQT1 is eliminated by association with minimal K+ channel (minK) subunits. *J Physiol,* 510 (Pt 1)**,** 37-45.

TSAKADZE, N. L., SRIVASTAVA, S., AWE, S. O., ADEAGBO, A. S., BHATNAGAR, A. & D'SOUZA, S. E. 2003. Acrolein-induced vasomotor responses of rat aorta. *Am J Physiol Heart Circ Physiol,* 285**,** H727-34.

TU, L. & DEUTSCH, C. 1999. Evidence for dimerization of dimers in K+ channel assembly. *Biophys J,* 76**,** 2004-17.

TU, L., WANG, J., HELM, A., SKACH, W. R. & DEUTSCH, C. 2000. Transmembrane biogenesis of Kv1.3. *Biochemistry,* 39**,** 824-36.

TUCKER, K., CAVALLIN, M. A., JEAN-BAPTISTE, P., BIJU, K. C., OVERTON, J. M., PEDARZANI, P. & FADOOL, D. A. 2010. The Olfactory Bulb: A Metabolic Sensor of Brain Insulin and Glucose Concentrations via a Voltage-Gated Potassium Channel. *Results Probl Cell Differ,* 52**,** 147-57.

UEBELE, V. N., ENGLAND, S. K., CHAUDHARY, A., TAMKUN, M. M. & SNYDERS, D. J. 1996. Functional differences in Kv1.5 currents expressed in mammalian cell lines are due to the presence of endogenous Kv beta 2.1 subunits. *J Biol Chem,* 271**,** 2406-12.

UEBELE, V. N., ENGLAND, S. K., GALLAGHER, D. J., SNYDERS, D. J., BENNETT, P. B. & TAMKUN, M. M. 1998. Distinct domains of the voltage-gated K+ channel Kv beta 1.3 beta-subunit affect voltage-dependent gating. *Am J Physiol,* 274**,** C1485-95.

UPADHYAY, S. K., ECKEL-MAHAN, K. L., MIRBOLOOKI, M. R., TJONG, I., GRIFFEY, S. M., SCHMUNK, G., KOEHNE, A., HALBOUT, B., IADONATO, S., PEDERSEN, B., BORRELLI, E., WANG, P. H., MUKHERJEE, J., SASSONE-CORSI, P. & CHANDY, K. G. 2013. Selective Kv1.3 channel blocker as therapeutic for obesity and insulin resistance. *Proc Natl Acad Sci U S A,* 110**,** E2239-48.

UYSAL, S., VASQUEZ, V., TERESHKO, V., ESAKI, K., FELLOUSE, F. A., SIDHU, S. S., KOIDE, S., PEROZO, E. & KOSSIAKOFF, A. 2009. Crystal structure of full-length KcsA in its closed conformation. *Proc Natl Acad Sci U S A,* 106**,** 6644-9.

VACHER, H. & TRIMMER, J. S. 2011. Diverse roles for auxiliary subunits in phosphorylation-dependent regulation of mammalian brain voltage-gated potassium channels. *Pflugers Arch,* 462**,** 631-43.

VACHER, H., YANG, J. W., CERDA, O., AUTILLO-TOUATI, A., DARGENT, B. & TRIMMER, J. S. 2011. Cdk-mediated phosphorylation of the Kvbeta2 auxiliary subunit regulates Kv1 channel axonal targeting. *J Cell Biol,* 192**,** 813-24.

VAN HUIZEN, R., CZAJKOWSKY, D. M., SHI, D., SHAO, Z. & LI, M. 1999. Images of oligomeric Kv beta 2, a modulatory subunit of potassium channels. *FEBS Lett,* 457**,** 107-11.

VANOYE, C. G., WELCH, R. C., DANIELS, M. A., MANDERFIELD, L. J., TAPPER, A. R., SANDERS, C. R. & GEORGE, A. L., JR. 2009. Distinct subdomains of the KCNQ1 S6 segment determine channel modulation by different KCNE subunits. *J Gen Physiol,* 134**,** 207-17.

VANOYE, C. G., WELCH, R. C., TIAN, C., SANDERS, C. R. & GEORGE, A. L., JR. 2010. KCNQ1/KCNE1 assembly, co-translation not required. *Channels (Austin),* 4**,** 108-14.

VARGA, Z., HAJDU, P. & PANYI, G. 2010. Ion channels in T lymphocytes: an update on facts, mechanisms and therapeutic targeting in autoimmune diseases. *Immunol Lett,* 130**,** 19-25.

VARSHNEY, P., YADAV, V. & SAINI, N. 2016. Lipid rafts in immune signalling: current progress and future perspective. *Immunology,* 149**,** 13-24.

VEATCH, W. & STRYER, L. 1977. The dimeric nature of the gramicidin A transmembrane channel: conductance and fluorescence energy transfer studies of hybrid channels. *J Mol Biol,* 113**,** 89-102.

VICENTE, R., ESCALADA, A., SOLER, C., GRANDE, M., CELADA, A., TAMKUN, M. M., SOLSONA, C. & FELIPE, A. 2005. Pattern of Kv beta subunit expression in macrophages depends upon proliferation and the mode of activation. *J Immunol,* 174**,** 4736-44.

VICENTE, R., ESCALADA, A., VILLALONGA, N., TEXIDO, L., ROURA-FERRER, M., MARTIN-SATUE, M., LOPEZ-IGLESIAS, C., SOLER, C., SOLSONA, C., TAMKUN, M. M. & FELIPE, A. 2006. Association of Kv1.5 and Kv1.3 contributes to the major voltage-dependent K+ channel in macrophages. *J Biol Chem,* 281**,** 37675-85.

VICENTE, R., VILLALONGA, N., CALVO, M., ESCALADA, A., SOLSONA, C., SOLER, C., TAMKUN, M. M. & FELIPE, A. 2008. Kv1.5 association modifies Kv1.3 traffic and membrane localization. *J Biol Chem,* 283**,** 8756-64.

VIJAYABASKAR, M. S. & VISHVESHWARA, S. 2012. Insights into the fold organization of TIM barrel from interaction energy based structure networks. *PLoS Comput Biol,* 8**,** e1002505.

VILLALONGA, N., ESCALADA, A., VICENTE, R., SANCHEZ-TILLO, E., CELADA, A., SOLSONA, C. & FELIPE, A. 2007. Kv1.3/Kv1.5 heteromeric channels compromise pharmacological responses in macrophages. *Biochem Biophys Res Commun,* 352**,** 913-8.

WAITHE, D., FERRON, L., PAGE, K. M., CHAGGAR, K. & DOLPHIN, A. C. 2011. Beta-subunits promote the expression of Ca(V)2.2 channels by reducing their proteasomal degradation. *J Biol Chem,* 286**,** 9598-611.

WANG, K. W. & GOLDSTEIN, S. A. 1995. Subunit composition of minK potassium channels. *Neuron,* 14**,** 1303-9.

WANG, K. W., TAI, K. K. & GOLDSTEIN, S. A. 1996. MinK residues line a potassium channel pore. *Neuron,* 16**,** 571-7.

WANG, Q., ZHU, F. & WANG, Z. 2007. Identification of EGF receptor C-terminal sequences 1005-1017 and di-leucine motif 1010LL1011 as essential in EGF receptor endocytosis. *Exp Cell Res,* 313**,** 3349-63.

WANG, W., KIM, H. J., LEE, J. H., WONG, V., SIHN, C. R., LV, P., PEREZ FLORES, M. C., MOUSAVI-NIK, A., DOYLE, K. J., XU, Y. & YAMOAH, E. N. 2014. Functional significance of K+ channel beta-subunit KCNE3 in auditory neurons. *J Biol Chem,* 289**,** 16802-13.

WANG, X., MATTESON, J., AN, Y., MOYER, B., YOO, J. S., BANNYKH, S., WILSON, I. A., RIORDAN, J. R. & BALCH, W. E. 2004a. COPII-dependent export of cystic fibrosis transmembrane conductance regulator from the ER uses a di-acidic exit code. *J Cell Biol,* 167**,** 65-74.

WANG, X., ZHANG, J., BERKOWSKI, S. M., KNOWLEG, H., CHANDRAMOULY, A. B., DOWNENS, M. & PRYSTOWSKY, M. B. 2004b. Protein kinase C-mediated phosphorylation of Kv beta 2 in adult rat brain. *Neurochem Res,* 29**,** 1879-86.

WENDELER, M. W., PACCAUD, J. P. & HAURI, H. P. 2007. Role of Sec24 isoforms in selective export of membrane proteins from the endoplasmic reticulum. *EMBO Rep,* 8**,** 258-64.

WENG, J., CAO, Y., MOSS, N. & ZHOU, M. 2006. Modulation of voltage-dependent Shaker family potassium channels by an aldo-keto reductase. *J Biol Chem,* 281**,** 15194-200.

WIENER, R., ZHANG, X., WANG, T. & WOLBERGER, C. 2012. The mechanism of OTUB1-mediated inhibition of ubiquitination. *Nature,* 483**,** 618-22.

WILSON, D. K., BOHREN, K. M., GABBAY, K. H. & QUIOCHO, F. A. 1992. An unlikely sugar substrate site in the 1.65 A structure of the human aldose reductase holoenzyme implicated in diabetic complications. *Science,* 257**,** 81-4.

WILLIAMS, C. P., HU, N., SHEN, W., MASHBURN, A. B. & MURRAY, K. T. 2002. Modulation of the human Kv1.5 channel by protein kinase C activation: role of the Kvbeta1.2 subunit. *J Pharmacol Exp Ther,* 302**,** 545-50.

WILLIAMS, T. M. & LISANTI, M. P. 2004. The caveolin proteins. *Genome Biol,* 5**,** 214.

WLODARCZYK, J., WOEHLER, A., KOBE, F., PONIMASKIN, E., ZEUG, A. & NEHER, E. 2008. Analysis of FRET signals in the presence of free donors and acceptors. *Biophys J,* 94**,** 986-1000.

WONG, W. & SCHLICHTER, L. C. 2004. Differential recruitment of Kv1.4 and Kv4.2 to lipid rafts by PSD-95. *J Biol Chem,* 279**,** 444-52.

WU, D., DELALOYE, K., ZAYDMAN, M. A., NEKOUZADEH, A., RUDY, Y. & CUI, J. 2010a. State-dependent electrostatic interactions of S4 arginines with E1 in S2 during Kv7.1 activation. *J Gen Physiol,* 135**,** 595-606.

WU, D., PAN, H., DELALOYE, K. & CUI, J. 2010b. KCNE1 remodels the voltage sensor of Kv7.1 to modulate channel function. *Biophys J,* 99**,** 3599-608.

WU, D. M., JIANG, M., ZHANG, M., LIU, X. S., KOROLKOVA, Y. V. & TSENG, G. N. 2006. KCNE2 is colocalized with KCNQ1 and KCNE1 in cardiac myocytes and may function as a negative modulator of I(Ks) current amplitude in the heart. *Heart Rhythm,* 3**,** 1469-80.

WU, J., LENG, T., JING, L., JIANG, N., CHEN, D., HU, Y., XIONG, Z. G. & ZHA, X. M. 2016. Two di-leucine motifs regulate trafficking and function of mouse ASIC2a. *Mol Brain,* 9**,** 9.

WU, J., SHIMIZU, W., DING, W. G., OHNO, S., TOYODA, F., ITOH, H., ZANG, W. J., MIYAMOTO, Y., KAMAKURA, S., MATSUURA, H., NADEMANEE, K., BRUGADA, J., BRUGADA, P., BRUGADA, R., VATTA, M., TOWBIN, J. A., ANTZELEVITCH, C. & HORIE, M. 2010c. KCNE2 modulation of Kv4.3 current and its potential role in fatal rhythm disorders. *Heart Rhythm,* 7**,** 199-205.

WULFF, H., CALABRESI, P. A., ALLIE, R., YUN, S., PENNINGTON, M., BEETON, C. & CHANDY, K. G. 2003. The voltage-gated Kv1.3 K(+) channel in effector memory T cells as new target for MS. *J Clin Invest,* 111**,** 1703-13.

XIE, Z., BARSKI, O. A., CAI, J., BHATNAGAR, A. & TIPPARAJU, S. M. 2011. Catalytic reduction of carbonyl groups in oxidized PAPC by Kvbeta2 (AKR6). *Chem Biol Interact,* 191**,** 255-60.

XU, D., WANG, H., ZHANG, Q. & YOU, G. 2016a. Nedd4-2 but not Nedd4-1 is critical for protein kinase C-regulated ubiquitination, expression, and transport activity of human organic anion transporter 1. *Am J Physiol Renal Physiol,* 310**,** F821-31.

XU, J. & LI, M. 1997. Kvbeta2 inhibits the Kvbeta1-mediated inactivation of K+ channels in transfected mammalian cells. *J Biol Chem,* 272**,** 11728-35.

XU, J., YU, W., WRIGHT, J. M., RAAB, R. W. & LI, M. 1998. Distinct functional stoichiometry of potassium channel beta subunits. *Proc Natl Acad Sci U S A,* 95**,** 1846-51.

XU, S., SOROKA, C. J., SUN, A. Q., BACKOS, D. S., MENNONE, A., SUCHY, F. J. & BOYER, J. L. 2016b. A Novel Di-Leucine Motif at the N-Terminus of Human Organic Solute Transporter Beta Is Essential for Protein Association and Membrane Localization. *PLoS One,* 11**,** e0158269.

YANG, E. K., ALVIRA, M. R., LEVITAN, E. S. & TAKIMOTO, K. 2001. Kvbeta subunits increase expression of Kv4.3 channels by interacting with their C termini. *J Biol Chem,* 276**,** 4839-44.

YELLEN, G. 2002. The voltage-gated potassium channels and their relatives. *Nature,* 419**,** 35-42.

ZHANG, M., JIANG, M. & TSENG, G. N. 2001. minK-related peptide 1 associates with Kv4.2 and modulates its gating function: potential role as beta subunit of cardiac transient outward channel? *Circ Res,* 88**,** 1012-9.

ZHANG, M., WANG, Y., JIANG, M., ZANKOV, D. P., CHOWDHURY, S., KASIRAJAN, V. & TSENG, G. N. 2012. KCNE2 protein is more abundant in ventricles than in atria and can accelerate hERG protein degradation in a phosphorylation-dependent manner. *Am J Physiol Heart Circ Physiol,* 302**,** H910-22.

ZHANG, X., SUN, N., ZHENG, M. & KIM, K. M. 2016. Clathrin-mediated endocytosis is responsible for the lysosomal degradation of dopamine D3 receptor. *Biochem Biophys Res Commun,* 476**,** 245-51.

ZHANG, Z. N., LI, Q., LIU, C., WANG, H. B., WANG, Q. & BAO, L. 2008. The voltage-gated Na+ channel Nav1.8 contains an ER-retention/retrieval signal antagonized by the beta3 subunit. *J Cell Sci,* 121**,** 3243-52.

ZHOU, M., MORAIS-CABRAL, J. H., MANN, S. & MACKINNON, R. 2001. Potassium channel receptor site for the inactivation gate and quaternary amine inhibitors. *Nature,* 411**,** 657-61.

ZHU, J., GOMEZ, B., WATANABE, I. & THORNHILL, W. B. 2007. Kv1 potassium channel C-terminus constant HRETE region: arginine substitution affects surface protein level and conductance level of subfamily members differentially. *Mol Membr Biol,* 24**,** 194-205.